

VPH2022



virtual physiological human conference

**DIGITAL TWINS FOR PERSONALIZED
TREATMENT DEVELOPMENT AND
CLINICAL TRIALS**

6–9 September 2022, PORTO, PORTUGAL

ABSTRACT BOOK

Plenary Lectures 3
Sessions overview 7

1. Cardiovascular 1	7
2. Computational modeling in health and disease 1	15
3. In silico clinical trials 1	23
4. Medical device modelling 1	30
5. Computational tools and simulation in biomechanics 1	38
6. Computational modeling in health and disease 2	44
7. Clinical imaging, Image-based in-vivo analysis, Imaging and visualization	50
8. Medical device modeling 2	56
10. Computational modeling in health and disease 3	61
11. In silico trials for medical product development	69
12. Mathematical biomedical models 1	77
13. Cardiovascular 2	85
14. Multiscale modeling	93
15. Mechanobiology	101
16. Big data and machine learning	109
17. Computational tools and simulation in biomechanics 2	117
18. Reproductive and pregnancy modelling	122
19. In silico clinical trials 2	127
20. Cancer early detection and therapy	132
21. The role of exascale computing in Computational Biomedicine	137
22. Computational modeling in health and disease 4	141
23. Computational tools and simulation in biomechanics 3	147
24. Musculoskeletal biomechanics	153
25. Computational tools and simulation in biomechanics 4	156
26. Computational modeling in health and disease 5	150
27. Agent based models	164
28. Mathematical biomedical models 2	168

Poster sessions overview 177

1. Poster session 1	177
2. Poster session 2	191
3. Poster session 3	206
4. Poster session 4	221

Author Index 236

Plenary talk 1

Patient-specific models in tumor growth: integrating organoids and image-based biomarkers

José Manuel García-Aznar¹

1 University of Zaragoza, Zaragoza, Spain

1. Introduction

Cancer is normally recognized as a group of diseases characterized by its high complexity that induces an uncontrolled growth and spread of abnormal cells.

Despite the tremendous progress made, cancer incidence and mortality continue growing. Therefore, it is compulsory understanding how cancers develop, and how treatments should be delivered to maximise the therapeutic benefit for each individual patient.

Computational simulations can provide complementary information for advancing in the understanding of this complexity that contribute to the initiation and progression of tumours.

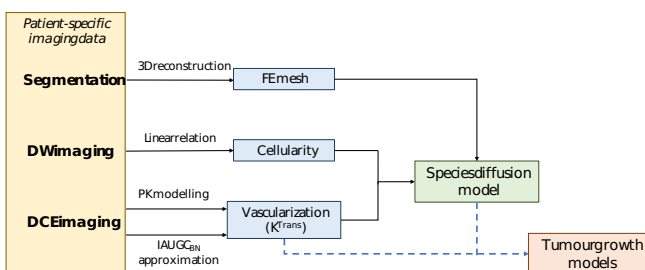
In this work, a computational approach is developed to mechanically link from patient tumour image-based biomarkers to macroscopic simulation of tumour growth.

2. Materials and Methods

A new methodology is proposed to build Finite Element-based models to simulate the tumour of one specific patient from image-based data.

Initially, from 2D segmentations of the tumour geometry a 3D volume is created, which will be the base for the construction of the FE mesh. As it is shown in Figure 1, a patient-specific model is constructed from dynamic contrast enhanced magnetic resonance imaging (DCE-MRI) and diffusion weighted imaging (DWI-MRI), which provide data about the spatial distribution of the vascular network [1] and the cellularity. Hence, we can simulate the transport of nutrients and oxygen within the whole tumour.

Next, we construct a biomechanical-based predictive model to simulate how tumour size and shape is going to progress, taking into account the



heterogenous distribution of the nutrients and the chemotherapy.

Figure 1: Scheme used to construct patient-specific models of tumours for the simulation of tumour growth.

3. Results

Preliminary results of the 3D distribution of nutrients in a real tumour can be seen in Figure 2.

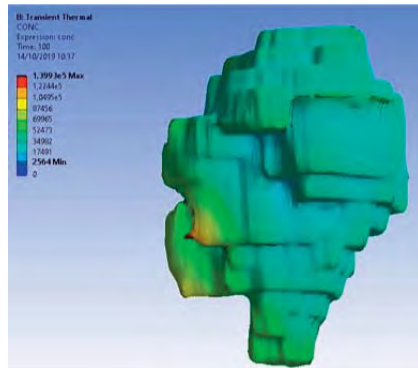


Figure 2: 3D nutrients map in a real geometry.

Further simulations are developed to predict how tumour is progressing.

4. Discussion and Conclusions

Although metabolism at the cellular scale has been modelled with different strategies [2], it has been challenging to link these cellular models to the macroscopic tissue scale. Recently, de Melo Quintela et al proposed an original spatial multiscale approach to connect both scales [3]. However, it is difficult to link with specific patient tumour metabolic measurements. In this work, a novel approach is proposed where cellular models are calibrated with multiple data from in-vitro experiments of tumour organoids [4,5].

5. References

1. Sainz-DeMena, et al. A finite element based optimization algorithm to include diffusion into the analysis of DCE-MRI. *Engineering with Computers* (2022): 1-17.
2. Bull & Byrne (2022). The hallmarks of mathematical oncology. *Proceedings of the IEEE*, 110(5), 523-540.
3. de Melo Quintela et al. A theoretical analysis of the scale separation in a model to predict solid tumour growth. *J Theor Biol* 547 (2022): 111173.
4. Plou et al From individual to collective 3D cancer dissemination: role of collagen concentration & TGF- β . *Sci Rep* 8.1 (2018):1-14.
5. Gonçalves & Garcia-Aznar. Extracellular matrix density regulates the formation of tumour spheroids through cell migration. *PLoS computational biology* 17.2 (2021): e1008764.

Acknowledgements:

The authors would like to thank the European Union's Horizon 2020 research and innovation programme under grant agreement No. 826494 (PRIMAGE) and the European Research Council (Grant no: 101018587, ICoMICS) for providing financial support to this project.

Plenary talk 2

Microstructure-informed in silico modeling of the human brain

Silvia Budday¹

¹ Friedrich-Alexander-University Erlangen-Nürnberg (FAU), Erlangen, Germany

1. Introduction

Brain tissue is not only one of the most important but also the arguably most complex and compliant tissue in the human body. While long underestimated, increasing evidence confirms that mechanics plays a critical role in modulating brain function and dysfunction [1]. Computational models based on nonlinear continuum mechanics can help understand the basic processes in the brain, e.g., during development, injury, and disease, and facilitate early diagnosis and treatment of neurological disorders [2].

2. Materials and Methods

By closely integrating biomechanical experiments on human brain tissue, microstructural analyses, continuum mechanics modeling, and finite element simulations, we develop computational models that capture both biological processes on the cellular scale and macroscopic loading and pathologies. We introduce the cell density as an additional field controlling the local tissue stiffness and brain growth during development, as illustrated in Figure 1 [3].

5. References

1. Budday S, Ovaert TC, Holzapfel GA, Steinmann P, Kuhl E. *Arch. Comput. Methods Eng.*; 27:1187-1230 (2020).
2. Goriely A, Geers MG, Holzapfel GA, Jayamohan J, Jérusalem A, Sivaloganathan S, Squier W, van Dommelen JA, Waters S, Kuhl E. *Biomech. Model. Mechanobiol.*; 14(5):931-65 (2015).
3. M. S. Zarzor, S. Kaessmair, P. Steinmann, I. Blümcke, S. Budday. *Brain Multiphys.*; 2: 100025 (2021).
4. S. Budday, M. Sarem, L. Starck, G. Sommer, J. Pfefferle, N. Phunchago, E. Kuhl, F. Paulsen, P. Steinmann, P.V. Shastri, and G.A. Holzapfel. *Acta Biomater.*; 104:53-65 (2020).
5. N. Reiter, B. Roy, F. Paulsen, and S. Budday. *J. Elas.*; 145:99–116 (2021).

Acknowledgements:

We gratefully acknowledge the funding by the Deutsche Forschungsgemeinschaft (DFG, German Research Foundation) through the grant BU 3728/1-1.

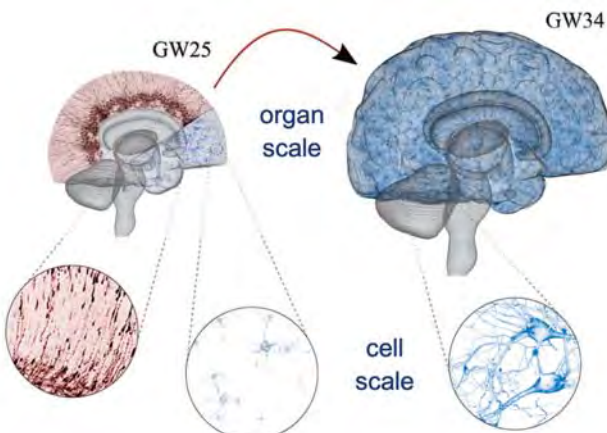


Figure 1: Nonlinear continuum mechanics framework to model the evolution of cell density, growth and associated cortical folding in the developing human brain [3].

3. Results

We demonstrate that our models are capable of capturing the evolution of cell density and cortical folding in the developing brain [3] as well as regional variations in tissue properties in the adult brain [4,5].

4. Discussion and Conclusions

In the future, those models can provide deeper insights into the behavior of the human brain under physiological and pathological conditions, and simulate progression of injury and disease.

Plenary talk 3**Contributions of myocardial hypertrophy and stiffening to right-ventricular remodelling in pulmonary arterial hypertension****Daniela Valdez-Jasso¹**

1 University of San Diego, San Diego, United States

Pulmonary arterial hypertension (PAH) is a disease of the pulmonary arterial vasculature and its remodeling, in which patient mortality is significantly associated with impaired right-ventricular (RV) function. The prognosis of patients with PAH is very poor with five-year survival <50%, and there are no available therapies to prevent right heart failure in PAH. PAH is two- to four-times more prevalent in women and pregnancy is a risk factor.

Using a sugen-hypoxia (SuHx) rat model, we investigated the systolic and diastolic chamber function during the progression of PAH. To distinguish the relative contributions of RV geometric remodeling from myocardial material remodeling to changes in RV function, a biomechanics model was fitted to measured RV pressure-volume relations and morphology. After an initial decrease in RV ejection fraction ($66\pm10\%$ to $44\pm6\%$, $p<0.01$), systolic function stabilized (subsequent 2% change in EF through the end of the study, $p>0.05$), despite progressive increases to RV end-systolic pressure. The model attributed these changes to RV myocardial hypertrophic wall-thickening, with only minor increases in myocyte force generating capacity at week 5. After RV systolic function stabilized, end-diastolic pressure increased significantly ($p<0.05$), with maintained RV diastolic volumes. Unlike end systole, RV end-diastolic volume was maintained due to stiffening of myocardium resting properties. These passive stiffness findings agree with previously identified increases in diastolic chamber and myocardial stiffening in both PAH animals and patients occurring before the onset of severe systolic dysfunction^{2,3}. While significant myocardial passive stiffness was found in this study, there was no evidence of changes in total collagen content ($p>0.05$) or collagen type I to III ratio ($p>0.05$). This points towards possible collagen matrix remodeling such as collagen fiber structure, tortuosity, or cross-linking, or changes in titin isoforms or phosphorylation. This progressive increase in RV myocardial passive stiffness that occurs after RV hypertrophy has stabilized systolic function may be a compensatory mechanism to delay or prevent RV dilation but may also eventually contribute to diastolic dysfunction.

Plenary talk 4

Kinetic modelling and network analysis of total-body PET data

Adriana Tavares¹

1 University of Edinburgh, Edinburgh, United Kingdom

1. Introduction

Non-invasive Positron Emission Tomography (PET) imaging is a powerful technique for *in vivo* quantification of specific molecular processes. It has served as a valuable biomarker for understanding the development and progression of a variety of diseases, as well as a companion biomarker in drug discovery programmes.

In the clinical setting, PET imaging with 18F-FDG, a glucose analogue, is the oncologist's workhorse for staging of cancer patients and for assessment of treatment efficacy. Over 1.2 million and 2 million PET scans are collected in Europe and the USA, respectively, in a single year. Depending on each country's specific cost-recovery model, each PET scan costs on average between £500-£1000 yielding an economic impact of £1.6-3.2 billion/year.

The future influence of PET imaging in research and clinical practice is set to increase further as novel molecular treatments will be introduced, while new clinical total-body PET scanners are disseminated, which will break critical barriers to wide use of PET imaging, including cost (by enabling the scanning of 5-6 times more patients per day) and radiation dose (by reducing the radiation dose by up to 40 times). Even more exciting are the prospects of using this novel and powerful PET technology to access, for the first time, continuous dynamic whole-body human PET datasets, which is currently only available for mice. This new feature will be invaluable for integrated systems biology analyses.

Our group is currently exploring the use of network analysis of whole-body PET images as means to derive a unique "molecular fingerprint". We have started our "molecular fingerprinting" research by looking into changes in the skeletal system in healthy and during cancer. This is because recent discoveries show the skeleton's role as an endocrine organ regulating whole-body glucose homeostasis. Consequently, we hypothesise that changes to bone function could influence whole-body health and diseases of different organ systems.

2. Materials and Methods

Total-body and whole-body 18F-FDG PET/ Computed Tomography (CT) scans of healthy human subjects and lung cancer patients respectively were analysed to measure bone glucose metabolism. Network analysis was used to determine connectivity between bones and how networks varied dependent on sex, age and disease severity/vital status.

3. Results

In healthy humans, individual bones had different glucose metabolism (higher in axial bones versus appendicular bones) and energy networks compared with mice as well as lung cancer patients (lower in cancer versus health). Measured bone glucose metabolism was sex-dependent in health (higher for females versus males) but not during disease. Network analysis of PET data clustered lung cancer patients into two main clusters that translated into a two-tiered survival plot.

4. Discussion and Conclusions

Data showed species and bone specific glucose metabolism differences. Sex-dependent differences in glucose metabolism in health disappear during disease. Network analysis has the potential to be used as a new approach to stratify patients based on PET bone glucose biomarker with ability to predict patient survival.

5. References

- Suchacki KF, Alcaide-Corral CA, Nimale S, Macaskill MG, Stimson RH, Farquharson C, Freeman TC and Tavares AAS. *Front. Med.* 2021; 8:740615
- Machtay M, Duan F, Siegel BA, Snyder BS, Gorelick JJ, Reddin JS, Munden R, Johnson DW, Wilf LH, DeNittis A, Sherwin N, Cho KH, Kim SK, Videtic G, Neumann DR, Komaki R, Macapinlac H, Bradley JD, Alavi A. *J Clin Oncol.* 2013; 31(30):3823-30

Acknowledgements:

The author would like to thank the Chan Zuckerberg Initiative (CZI) for providing financial support to this project. EXPLORER Total-Body PET data provided by Prof Cherry's group at UC Davis, US, as part of an ongoing collaboration with Dr Tavares' team at the University of Edinburgh.

1.1

A continuum model of a fibrin rich clot

Mohammad Rezaeimoghaddam¹, Janneke Cruts², Frank Gijzen², Frans van de Vosse¹

¹ Eindhoven University of Technology, Department of Biomedical Engineering, Netherlands

² Erasmus MC, Department of Biomedical Engineering, Rotterdam, Netherlands

1. Introduction

Excessive blood clot formation is a serious clinical condition leading to ischemic stroke and myocardial infarction. The aim of this study is to introduce a novel coupled scheme using a continuum model of thrombus formation together with the rheological changes of the blood clot as a viscoelastic material model.

2. Materials and Methods

The biochemical model of the fibrin rich clot is developed based on the framework presented earlier in Bouchnita et al. [1]. A system of coupled convection diffusion reaction (CDR) equations is needed to describe the passive transport of biomolecules and agonists. In this study, the concentrations of prothrombin, thrombin, antithrombin, factor IX and X, protein C, fibrinogen, fibrin and fibrin polymer are solved. The production or consumption of each agonist is incorporated into the source terms in the CDR equations. The computational domain consists of a 2D channel with a height of 60 μm and a length of 500 μm . The bottom wall serves as a surface flux boundary condition representing a portion of the tissue factor coated surface. The model is implemented into the computational fluid dynamics software FLUENT 2021 R1. The blood is considered as a Newtonian fluid, and fibrin polymer is considered as a viscoelastic material using the Oldroyd-B model [2]. Four additional scalar transport equations are used to represent the polymer contribution in the model. The value of the Deborah number is selected such that the elasticity dominates the stress field. The extra polymeric stresses are introduced as the source terms in the momentum equations.

3. Results

Thrombus development at $t=100\text{s}$ and $t=200\text{s}$ with colored velocity magnitude are given in Figure 1 (a-b).

The fibrin concentrations and scalar transport of τ_{yy} are demonstrated in Figure 2 (a-b).

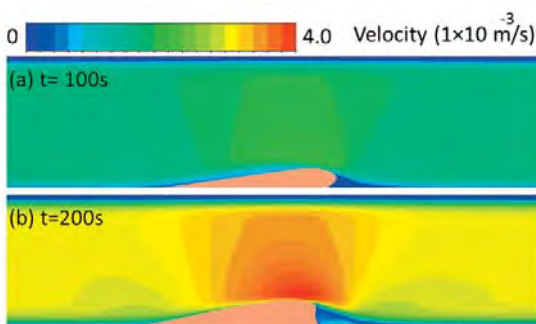


Figure 1: Spatial and temporal evolution of a clot.

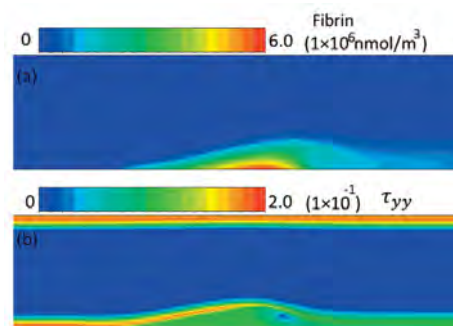


Figure 2: Visualization of (a) fibrin and (b) scalar τ_{xx} of the Oldroyd-B model, both at $t=200\text{s}$.

4. Discussion and Conclusions

A novel coupled continuum biochemical model to simulate fibrin rich clot has been developed. The kinetics of fibrin formation is shown to be highly related to alterations in local hemodynamics, shear forces and Deborah number.

5. References

- [1] A. Bouchnita et al. *Appl. Math. Lett.*, vol. 51, no. 2015, pp. 74–79, 2016.
- [2] A. Sequeira et al. *Math. Model. Nat. Phenom.*, vol. 9, no. 6, pp. 34–45, 2014.

Acknowledgements:

This work is supported by RegMed XB and powered by Health~Holland, top sector life sciences & health.

1.2

Advancing the physics and performance of blood flow simulations towards exascale

Jon McCullough¹, Ioannis Zacharoudiou¹, Sharp Lo¹, Peter Coveney^{1,2}

¹ University College London, Chemistry, London, United Kingdom

² University of Amsterdam, Institute for Informatics, Amsterdam, Netherlands

1. Introduction

This presentation will highlight developments towards simulating human-scale blood flow including representing elastic walls in 3D flow simulations. We will also discuss our efforts in porting our code to GPU architectures with a view towards utilising the first generation of exascale supercomputers. To conclude, we will discuss some of the outstanding challenges to be addressed.

2. Materials and Methods

In our work, we have used the open-source HemeLB code [1]. HemeLB is built upon the lattice Boltzmann method and, in combination with several memory optimisations, allows for highly scalable studies of macroscopic blood flow in complex and sparse vascular domains. In [2], we demonstrate how the conversion of the key algorithms of HemeLB to CUDA allow for a significant enhancement of the strong scaling performance of the code.

The choice of wall model in 3D blood flow simulations is often a choice between physical accuracy and computational performance. Rigid walls are simple to implement and, generally, fast to compute but lack physical realism. Introduction of elastic walls often demands coupling the fluid simulation to an explicit solid mechanics model – a computationally expensive process. In [3], we develop an LBM boundary condition that provides a wall slip velocity commensurate to that experienced at the simulation wall location if an elastic wall had stretched beyond it.

3. Results

We compare the results from our method to those with a rigid wall implementation by simulating flow through a cylinder according to the elastic walled Womersley flow equations. Whilst our method still has some error, it is significantly more accurate than the rigid wall approximation. We also identify that our method displays the same performance characteristics as the rigid wall model.

4. Discussion and Conclusions

Our work demonstrates how computationally efficient blood flow simulation can be combined with more physically realistic representations of the study domain. There remain many challenges ahead for achieving exascale performance for vascular simulations. On the technical side, these relate to aspects including geometry generation, data management, visualisation and code portability. On the physics side there remains the challenge of multiscale effects and coupling blood flow to the wider digital twin system of organ models.

5. References

1. <https://github.com/hemelb-codes>
2. I. Zacharoudiou et al, Pre-print (2022) DOI: 10.21203/rs.3.rs-1305290/v1
3. J. W. S. McCullough & P. V. Coveney, Sci. Rep., 11, 24260 (2021) DOI: 10.1038/s41598-021-03584-2

Acknowledgements:

We acknowledge funding from European Commission CompBioMed Centre of Excellence (Grant No. 675451 and 823712); UK Engineering and Physical Sciences Research Council for UK Consortium on Mesoscale Engineering Sciences (UKCOMES) (Grant No. EP/R029598/1); MRC for a Medical Bioinformatics grant (MR/L016311/1), and special funding from the UCL Provost. This work was supported by computing time on SuperMUC-NG (LRZ) and Summit (OLCF).

1.3

Arterial flows as social networks: a novel approach to disentangle hemodynamic complexity

Karol Calò¹, Diego Gallo¹, Andrea Guala², Stefania Scarsoglio¹, David A. Steinman³, Luca Ridolfi¹, Umberto Morbiducci¹

¹ PoliToBIOMed Lab, Politecnico di Torino, Torino, Italy

² Vall d'Hebron Institut de Recerca (VHIR), Barcelona, Spain

³ University of Toronto, Department of Mechanical & Industrial Engineering, Toronto, Canada

Corresponding author: umberto.morbiducci@polito.it

1. Introduction

Current approaches for deciphering the richness of information in cardiovascular flows are mainly based on visual evaluation or integral quantities. To disentangle complex arterial hemodynamics identifying coherent blood flow patterns, an approach modelling arterial flows as "social networks" is proposed [1]. The final aim is distilling the information emergent from blood flow topology into physio-pathological significance. The Complex Networks (CNs) are exploited to quantify the degree of dynamical similarity of correlated blood flow patterns, and the association with vascular geometric attributes is explored in silico and in vivo.

2. Materials and Methods

Like a social network made up of a set of dynamical units and social interactions among them, here arterial flows are modelled as a set of hemodynamic time-dependent signals interconnected based on the correlation between their dynamic behaviours (Fig. 1A). The pattern of connections between correlated fluid structures in a CN is called topology and it contains useful information on the level of organization of the investigated 4D flows. To extract such information, a series of CNs metrics can be computed to quantify, for example, (1) the degree of dynamical similarity of arterial structures, and (2) the anatomical propagation distance over which a hemodynamic signal maintains its coherence (i.e., correlation) inside the vessel. The presented approach has been successfully applied in a series of in silico and in vivo studies [1,2].

3. Results

Explanatory results of the application of CNs to study axial velocity features in computational models of healthy carotid bifurcation [1], and 4D flow MRI models of dilated thoracic aorta [2] are reported in Fig. 1B: the volume maps of CNs metrics, measuring topological and anatomical hemodynamic similarity allow to visualize coherent hemodynamic patterns and quantify the extent of their dynamical similarity within the fluid domain. From the distribution of the anatomical length of persistence of the hemodynamic correlation, regions where flow coherence is disrupted (e.g., by vascular geometric attributes, as in the carotid bulb [1] or in the ascending aorta [2]) or is maintained for a longer distance in the vasculature can be identified.

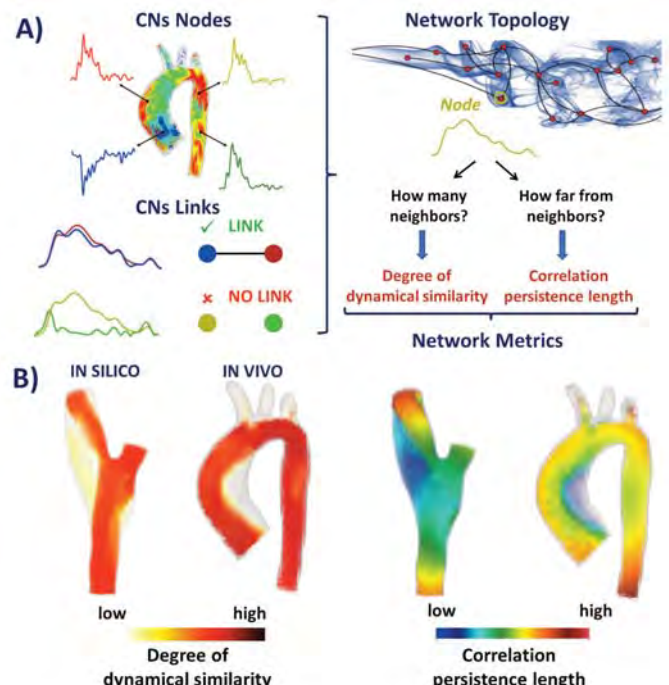


Figure 1: A) Schematic of the CNs approach. B) Explanatory results of coherent flow structures characterization using CNs.

4. Discussion and Conclusions

A new paradigm is introduced, which models arterial flows as social networks, providing a stronger quantitative definition of "coherent hemodynamic structures". CNs emerge as a powerful tool for identifying still poorly explored/hidden features of arterial hemodynamics.

5. References

1. Calò K et al, *IEEE Trans Biomed Eng*, 67(7) (2020).
2. Calò K et al, *Ann Biomed Eng*, 49(9) (2021).

1.4

Computational models for hemodynamic management in critically ill patients: a systematic review

Marijn Mulder¹, Libera Fresiello¹, Dirk Donker^{1,2}

¹ University of Twente, Cardiovascular and Respiratory Physiology, Technical Medical Center, Enschede, Netherlands

² University Medical Center Utrecht, Intensive Care Center, Utrecht, Netherlands

1. Introduction

Timely diagnosis of hemodynamic instability and differentiation of underlying aetiologies are all crucial for taking adequate treatment decisions in critically ill patients [1]. A promising methodology to support more personalised hemodynamic management in critical care is the use of computational physiological models. These mathematical descriptions of one or more physiological processes allow real-time medical simulations of patient-specific disease and treatment. This systematic literature review provides a comprehensive overview of current computational cardiovascular zero-dimensional (0D) models and their practical applicability in the intensive care unit.

2. Materials and Methods

Four databases (PubMed, Embase, Scopus and Web of Science) are searched for original papers on 0D cardiovascular models. The selection process is performed by two independent researchers, with a third researcher to resolve conflicts. Data on model characteristics and clinical applications is extracted from the included articles. Model quality is assessed by GRADE [2] and NASA [3] guidelines. The analysis was finalized in a narrative synthesis of the collected data from the included models, with a focus on model structure, clinical application and usability.

3. Results

A total of 9927 records were found in the four databases, after duplicate removal 5757 remained for screening. The analysis conducted revealed the following:

- Structure: the models ranged in complexity from simple models with only 3 compartments to detailed models with time- and pressure-varying parameters in more than 50 compartments.
- Application: the main clinical use described in the articles can be centred around volume status, vasoactive medication or temporary mechanical support.
- Usability: often, the quality of the models could not be assessed and the level of technology readiness did not reach higher than level 5.

4. Discussion and Conclusions

0D closed-loop computational models are well suited to simulate hemodynamic instability in critically ill patients in real-time. Essentially, they could aid in personalised monitoring, clinical decision making and therapeutic interventions and act as a patient's 'digital twin'. Yet, clinical personalisation of currently available models remains challenging, since only limited patient data are available and many input parameters demand for a best educated estimate. Therefore, reaching a perfect trade-off between model simplicity and clinically-relevant output is an ultimate goal. In this sense and despite of their abundant availability, most cardiovascular models lack proper validation and verification. Since this is essential for future clinical use in daily practice and the reliability of the models' output, there is an need for more dedicated guidelines to advance a well-structured clinical implementation. Current limitations and perspectives as deduced from this systemic review still point towards a significant, yet bridgeable gap between bench and bedside applications for computational cardiovascular models in critical care.

5. References

1. Ceconi M et al. Consensus on circulatory shock and hemodynamic monitoring. *Intensive Care Med.* 2014;40(12):1795-1815
2. Brozek JL et al. GRADE SERIES GRADE Guidelines 30: the GRADE approach to assessing the certainty of modeled evidenced, *J Clin Epidemiol.* 2021;129:138-150
3. National Aeronautics and Space Administration, Standard for models and simulations. NASA-STD-7009A W/Change 1, Published online 2016:1-72

Marijn Mulder, University of Twente, P.O. box 217, 7500 AE Enschede, the Netherlands, phone: +31 53 489 56 25, email: m.p.mulder-1@utwente.nl

1.5

Evaluating the risk of myocardial ischemia in patients with Kawasaki Disease using patient-specific simulations of coronary hemodynamics

Karthik Menon^{1,2}, Jongmin Seo³, Jane Burns⁴, Andrew Kahn⁴, Alison Marsden¹

1 Stanford University, Stanford, United States

2 Stanford Cardiovascular Institute, Stanford University, Stanford, United States

3 Kyung Hee University, Korea, Rep. of South

4 University of California San Diego, La Jolla, United States

*Corresponding author. Contact: karthikmenon@stanford.edu

1. Introduction

Kawasaki disease (KD) is a pediatric vasculitis that leads to the formation of coronary artery aneurysms (CAAs) in about 25% of untreated patients. It is the most common form of acquired heart disease in children in developed countries [1]. While hemodynamics associated with thrombosis – the main risk associated with CAAs – has been investigated previously [2-3], less is known about the myocardial ischemic risk due to abnormal blood flow in CAAs. Here, we use patient-specific blood flow simulations to retrospectively evaluate ischemic risk measured by prevalence of abnormal fractional flow reserve (FFR) in KD patients.

2. Materials and Methods

We perform 3D multiscale patient-specific simulations of coronary hemodynamics in 15 patients using CTA image-based models. Model construction and finite element simulations use the open-source SimVascular software [4], and 3D flows are coupled with closed-loop lumped parameter models for distal vasculature and systemic circulation. Model parameters are tuned to patient-specific clinical measurements using automated surrogate-based optimization [5]. Simulations at hyperemia are used to estimate FFR in coronary arteries of interest to evaluate ischemic risk.

3. Results

We find that arteries affected by CAAs are often associated with abnormal FFR as well as more severe slope in FFR. Fig. 1 shows results for a representative case. We see that the automated model tuning matches well with patient specific targets for coronary hemodynamics and that arteries with severe CAAs ('rca1' and 'lca2' in this case) show lower FFR. We also find that FFR slope is branch-dependent and correlates with CAA shape-related metrics.

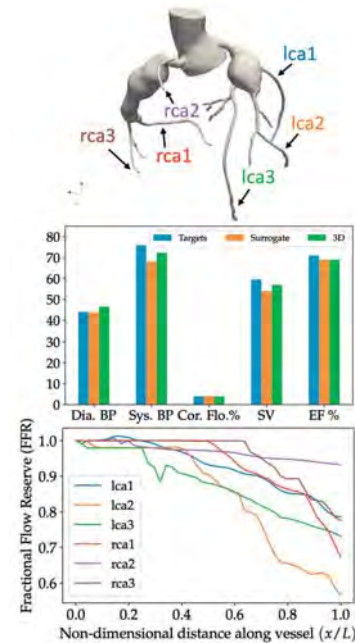


Figure 1: (Top) Model constructed from CTA images; (middle) Comparison of automated tuning with patient-specific targets; (bottom) Computed FFR along coronary branches.

4. Discussion and Conclusions

We evaluate the risk of myocardial ischemia associated with KD using patient-specific simulations of coronary hemodynamics, along with a tuning framework to match patient-specific clinical targets. Although thrombosis and luminal myofibroblastic proliferation are considered primary risks leading to myocardial infarction in patients with KD, we show that abnormal blood flow due to CAAs can also lead to severe FFR and is an additional risk factor that warrants further consideration.

5. References

1. B.W. McCrindle et al. *Circulation*, 135(17), 2017.
2. N. Grande Gutierrez et al. *Int. J. Cardiol.*, 281, pp. 15–21, 2019.
3. D. Sengupta et al. *Biomech. Model. Mechanobiol.*, 13(6), pp. 1261–1276, 2014.
4. A. Updegrove et al. *Ann. Biomed. Eng.*, 45 (3), pp. 525–541, 2017.
5. J.S. Tran et al. *Comput. Fluids*, 142, pp. 128–138, 2017.

1.6

Impact of coronary artery stenting on the wall shear stress topological skeleton features

Valentina Mazzi¹, Claudio Chiastra¹, Diego Gallo¹, Umberto Morbiducci¹

1 PoliToBIOMed Lab, Politecnico di Torino, Departement of Mechanical and Aerospace Engineering, Torino, Italy
 Corresponding author: umberto.morbiducci@polito.it

1. Introduction

It is well known that flow disturbances play a key role in processes leading to In-Stent Restenosis (ISR) in stented coronary arteries [1]. However, how local hemodynamics influence flow-related mechanisms underlying ISR is still not fully clarified. Aiming at bridging this gap of knowledge, a marked interest has recently emerged on Wall Shear Stress (WSS) Topological Skeleton (TS), because of its link with flow features (flow separation, recirculation) involved in vascular dysfunction [2]. The WSS TS is composed by fixed points, where WSS vanishes, and by contraction/expansion regions [2]. This study aims to investigate the role of WSS TS features in ISR process by analysing patient-specific and idealized computational fluid dynamics models of stented coronary arteries.

2. Materials and Methods

Patient-specific models of pathologic left anterior descending artery were considered. Details on stent design and computational settings are provided elsewhere [3]. Idealized models of stented vessels were built by varying the shape and thickness of the strut cross-section to investigate the stent design impact on WSS TS features. Based on a recently proposed Eulerian method [2], the divergence of the normalized WSS vector (DIVWSS) was used to identify contraction and expansion regions. In addition, to measure the amount of variation in WSS contraction and expansion action, the Topological Shear Variation Index (TSVI) [2]

$$TSVI = \left\{ \frac{1}{T} \int_0^T [\nabla \cdot (\tau_u) - \bar{\nabla} \cdot (\tau_u)]^2 dt \right\}^{1/2}, \quad (1)$$

where τ_u is the WSS unit vector and T is the cardiac cycle period, was computed.

3. Results

An example of cycle-average WSS TS and TSVI distribution on the surface of a patient-specific model treated with a Magmaris scaffold and idealized cases built based on the Magmaris design are presented in Fig. 1. In all models, WSS contraction regions (negative DIVWSS) were located upstream from the struts and WSS expansion regions (positive DIVWSS) were located downstream from the struts, with opposite DIVWSS in the stent malapposition region (Fig. 1A). The highest TSVI values were located at stent peaks and close to stent struts. Stent strut streamlining (e.g., trapezoidal vs. square strut shape) and decreased thickness (e.g., 80 vs. 150 μ m) reduced the TSVI median values (e.g., 375 m⁻¹ vs. 675 m⁻¹ for the cases (3) and (1) in Fig. 1B).

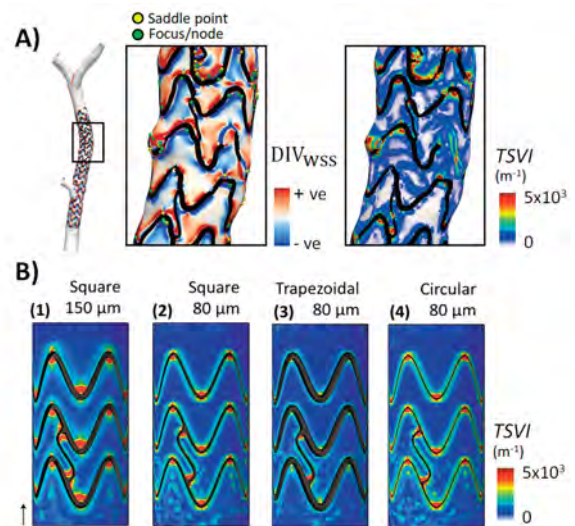


Figure 1: A) Cycle-average WSS TS and TSVI for a patient-specific case. B) TSVI for idealized cases.

4. Discussion and Conclusions

The findings of this analysis suggest that WSS TS features could represent a hemodynamic cue affecting ISR. More in detail, the exposure to high TSVI values could induce a recurring variation in intracellular and intercellular tension, impacting on the endothelium in terms of permeability and inflammatory response. Moreover, the WSS TS analysis could support stent design phase to improve the hemodynamic performance of a coronary stent. In conclusion, this approach might contribute to a deeper understanding of the hemodynamics-driven processes underlying ISR in coronary arteries.

5. References

1. Ng J et al, *Arterioscler Thromb Vasc Biol*; 37(12):2231-2242 (2017).
2. Mazzi V et al, *Mathematics*; 9(7):720 (2021).
3. Chiastra C et al, *J Biomech Eng*; 144(6) (2022).

1.7

Parametric aortic valve geometric modeling for subject-specific blood flow simulations using a resistive approach

Giorgia Pase¹, Emiel Brinkhuis¹, Tanja de Vries¹, Jiri Kosinka¹, Tineke Willem², Cristobal Bertoglio¹

¹ University of Groningen, Bernoulli Institute, Groningen, Netherlands

² University Medical Center Groningen, Department of Radiology, Groningen, Netherlands

1. Introduction

Cardiac valves simulation is one of the most complex tasks in cardiovascular modeling. Fluid-structure interaction is not only highly computationally demanding but also requires knowledge of the mechanical properties of the tissue [1]. Therefore, an alternative when the valve geometry is known is to include them as flow obstacles. This requires to prescribe the geometry (and its possible changes) in a simple way, but, at the same time, complex enough to reproduce pathological configurations.

2. Materials and Methods

The model consists in a generalization of the model from [2] such that surfaces can be constructed in a parametric way and distance functions to the valves can be computed for RIIS-based modeling. Doing so we aim to be capable of generating pathological geometries in a wide range of shapes. We will also detail our protocol on the extraction of the shape parameters from 3D CT images. We then propose an approach to generate resistive immersed implicit surfaces (RIIS, see also [3]) from the valvular geometry to incorporate them into fluid flow simulations. We assessed the capability of the model to generate a wide variety of shapes on a few open valve geometries coming from CT images before a transcatheter aortic valve intervention (TAVI). Examples of transvalvular blood flow simulations using resistive volumes are also included.

3. Results

Figure 1 shows a patient-specific example of the valve model, including a snapshot of the blood flow simulation, which was performed with a monolithic velocity-pressure coupling, backward Euler time discretization and P1bubble/P1 velocity/pressure finite elements.

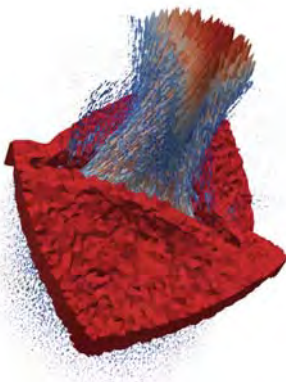


Figure 1: Flow obstacle representing the valve (red) and arrows representing the blood velocity field (blue: low velocities, red: high velocities).

4. Discussion and Conclusions

The new parametric model of the aortic valve allows to obtain patient-specific geometries that can be included into blood flow simulations using a resistive immersed implicit surface (RIIS) approach.

5. References

1. Astorino M et al., *Computer Methods in Applied Mechanics and Engineering*. 198: 3603-3612 (2009).
2. Haj-Ali R et al., *J Biomech*. 45(14):2392-2397 (2012).
3. Fedele M et al., *Biomech Model Mechanobiol*. 16(5):1779-1803 (2017).

Acknowledgements:

This work was partially funded by the European Research Council (ERC) under the European Union's Horizon 2020 research and innovation programme (grant 852544 – CardioZoom).

1.8

Simulating the hemodynamic effect of an edge-to-edge repair of mitral valve regurgitation using a lumped parameter model

Juliana Franz¹, Markus Reinthaler², Mario Kasner², Fabian Barbieri², Leonid Goubergrits¹

1 Charité - Universitätsmedizin Berlin, Institute of Computer-assisted Cardiovascular Medicine, Berlin, Germany

2 Charité - Universitätsmedizin Berlin, Department of Cardiology, Berlin, Germany

1. Introduction

Mitral valve regurgitation (MR) is one of the most prevalent valvular heart diseases in the western world. For severely symptomatic patients who are at high surgical risk, transcatheter edge-to-edge repair (TEER) can be a suitable treatment alternative to a surgical procedure [1]. The TEER device serves to reduce the regurgitant orifice area and thus the MR flow, but a sufficiently large diastolic mitral orifice area should remain to prevent mitral stenosis after treatment. We developed a patient-specific lumped parameter model of the cardiovascular system to simulate the hemodynamic effect of the TEER treatment in patients with MR.

2. Materials and Methods

A lumped parameter model and a personalisation workflow were developed to simulate patients with MR. The model equation describing the regurgitant valve flow rate as a function of the regurgitant orifice size and shape is based on [2]. The model is personalised using clinical measurements, including arterial blood pressure, left ventricular volume, mitral valve orifice area and left atrial pressure. To simulate the effect of the TEER device, the mitral orifice area is reduced and the model is re-personalised to match arterial pressures to pre-intervention values.

3. Results

Fig. 1 shows the personalised simulation results for a patient with MR and the predicted post-treatment hemodynamic outcome. The v-wave of the left atrial pressure is significantly reduced after the treatment. The deceleration time of the mitral valve E-wave is increased and peak flow rates are reduced. The mean transmитral pressure gradient during diastole increases from 0.5 mmHg to 1.9 mmHg post-intervention. The left ventricular pressure-volume loop after treatment shows a decreased left ventricular stroke volume.

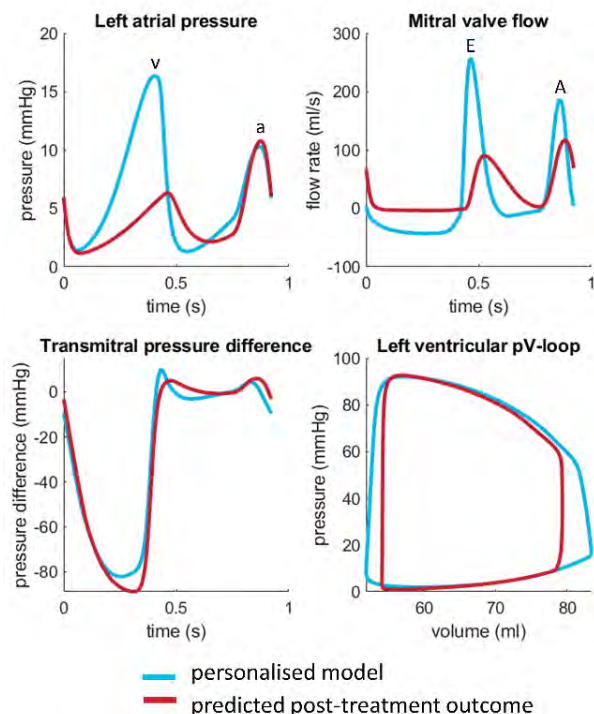


Figure 1: Personalised model results for a patient with MR and predicted outcome after TEER treatment.

4. Discussion and Conclusions

The presented model provides clinically relevant parameters to assess MR and to evaluate the effect of a TEER device on the patient's hemodynamics. In particular, the potential risk of mitral stenosis can be assessed with the simulated transmитmal pressure gradients. A significant advantage of the proposed model is its low computational cost. This allows for a fast evaluation of multiple treatment scenarios and their effects.

The simulation results are in qualitative agreement with clinical observations. A quantitative comparison between modelled and clinically measured values both pre- and post-intervention of several patients is needed to validate the model results.

5. References

- Otto CM et al., Circulation; 143:e72–e227 (2021).
- Franz J et al., Eng Appl Comput Fluid Mech; 15(1):1868-1884 (2021).

2.1

The 12 Labours Project: Digital Twins for Personalised Medicine

Julie Choisne¹, Thiranja Prasad Babarenda Gamage¹, Thor Besier¹, David Budgett¹, Leo Cheng¹, Alys Clark¹, Alex Dixon¹, Robert Gallichan¹, Simon Malpas¹, Martyn Nash¹, David Nickerson¹, Poul Nielsen¹, Andrew Taberner¹, Merryn Tawhai¹, Peter Hunter¹

¹ Auckland Bioengineering Institute, Auckland, New Zealand

Correspondence: j.choisne@auckland.ac.nz

1. Introduction

The overall goal for this 5 years project is to further develop the predictive modelling capability that we and our international partners have built in the Physiome Project [1,2], and to add personalised modelling to assist in the clinical diagnosis and treatment of a range of medical conditions.

2. Materials and Methods

The technology platforms are designed to support the development and clinical application of highly integrated multiscale digital twins (Figure 1).

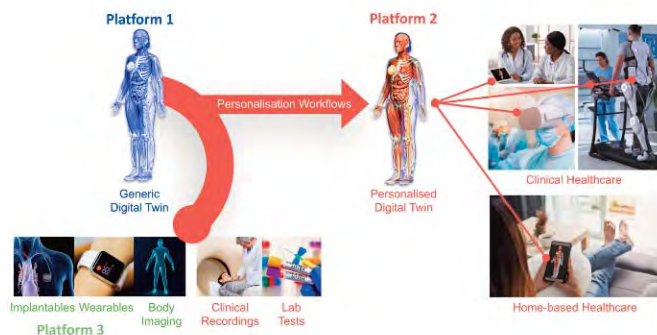


Figure 1: Workflow demonstrating the interaction between the platforms.

Platform 1: Develop the tools and databases needed to combine and link models across spatial and temporal scales.

Platform 2: Develop a cloud-based platform integrated with health IT systems for personalising Physiome models using patient specific data.

Platform 3: Develop an interface to connect wearable, implanted and home-based devices to the cloud-based platform to provide a continuous flow of data to update an individual personalised digital twin for diagnostic monitoring and predicting therapeutic outcomes.

We are using three exemplar projects (EPs) to demonstrate healthcare applications of multiscale biophysically based modelling, by combining multiscale models of multiple organ systems to address complex physiological questions; EP1: Pulmonary hypertension, EP2: Personalised rehabilitation of upper limb disorders and EP3: Control of organ function by the autonomic nervous system.

3. Results

In the first year, we have developed 1) a software platform for running personalised digital twins workflows along with a data management plan for encouraging best practices in data access and stewardship. Clinical pilot studies are being performed to test the platform using an existing clinical workflow [3]; 2) a workflow interfacing an implantable pressure sensor to monitor pressure within the body. ISO27001 and HL7 FHIR standards were used to ensure security and interoperability, and 3) a 36-cameras system to capture full body imaging to rapidly and accurately capture body surface geometry.

4. Discussion and Conclusions

The novelty of the 12 Labours project rely on the (i) creation of new multi-organ Physiome models that deal with complex physiological problems and (ii) application of these models to precision medicine and a new generation of wearable, implantable and home-based devices.

5. References

1. Osanlou M et al. *Front. Physiol.* 12; 2021. DOI: 10.3389/fphys.2021.693735
2. Hunter PJ, Borg TK. *Nature Reviews Mol Cell Biol*, 4(3):237-243 (2003).
3. Babarenda Gamage TP et al. *Interface focus*, 9; 2019

Acknowledgements:

Ministry of Business, Innovation and Employment's Catalyst Strategic Fund New Zealand and the Aotearoa fellowship.

2.2

Towards a patient-specific fetal cardiac growth model by using digital twin technology

Bettine van Willigen^{1,2}, M. B. van der Hout-van der Jagt^{1,2,3}, Wouter Huberts^{1,4}, Frans van de Vosse⁴

1 Eindhoven University of Technology, Cardiovascular Biomechanics, Biomedical Engineering, Eindhoven, Netherlands

2 Maxima MC Veldhoven, Obstetrics and Gynaecology, Veldhoven, Netherlands

3 Eindhoven University of Technology, Signal Processing Systems, Electrical Engineering, Eindhoven, Netherlands

4 Maastricht University, Department of Biomedical Engineering, Cardiovascular Research Institute Maastricht, Maastricht, Netherlands

1. Introduction

The Perinatal Life Support (PLS) consortium is developing a liquid-based incubator (PLS system) to increase chance of survival of extremely preterm infants (< 28 weeks of gestational age, GA) referred to as perinates [1]. To develop such a complex device, multidisciplinary knowledge must be integrated into one single system. Physiology-based mathematical models are used to support this integration by composing a digital twin Arielle of the PLS system and the growing perinate, allowing for computer simulations to predict the well-being of the perinate over time and its interaction with the device. Arielle is continuously updated based on data monitored by the PLS system. Since, during the GA from 24 to 28 weeks, the fetus grows from approximately 600 to 1100 grams [2], a simulation model of realistic fetal growth is of importance. This study focusses on fetal cardiac growth.

2. Materials and Methods

Each of the four cardiac chambers are described by an one fiber model (OFM) as proposed by [3] for the adult left ventricle. This model can describe the underlying phenomena of contraction by relating the cavity pressure p_{cav} to cavity volume V_{cav} , myocardial wall volume V_{wall} , and myocardial stress σ_f :

$$p_{cav}(t)=1/3 \sigma_f \ln(1+(V_{wall}/V_{cav})) \quad (1)$$

This model can simulate cardiac adaptation based on physiological principles. To simulate fetal cardiac growth, the adult geometric parameters and material characteristics are adapted based on known physiological principles [4,5]. The fetal cardiovascular system is described by [6]. For fetal growth, the scaling laws of [7] are used.

3. Results

Figure 1 and 2 show the results of Arielle (green) and literature data (black) consisting of the combined cardiac output (CCO), the right-to-left CO ratio (RCO/LCO), and E/A ratio of mitral (mv) and tricuspid valve (tv) over GA. The results show an increase of E/A ratio of both valves over GA and a right dominant heart, which corresponds with [8–14].

4. Discussion and Conclusions

This study shows that the fetal cardiac growth module of Arielle simulates growth realistically by adapting parameters on physiological principles. To make this model a digital twin, the next step is to couple model parameters to the fetal electrocardiogram allowing continuously updates of clinical data.

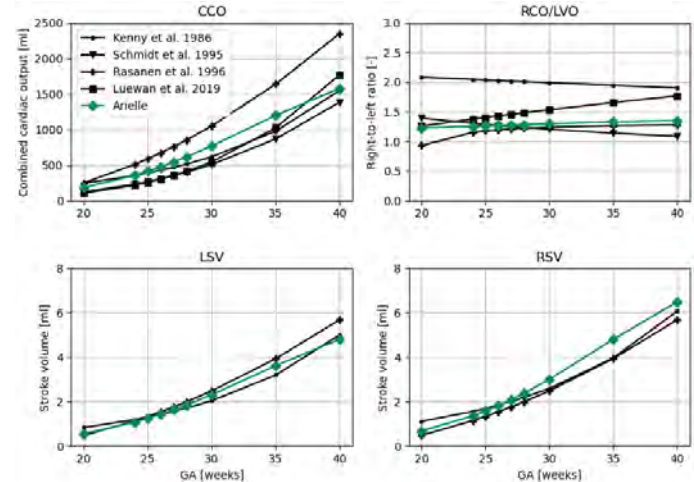


Figure 1: The simulated (Arielle, green) CCO, RCO/LCO ratio, and E/A ratio of mv and tv over GA compared with literature data (black) [8–14].

5. References

- [1] van der Hout-van der Jagt et al.(2022)
- [2] Alexander et al.(1996)
- [3] Bovendeerd et al.(2006)
- [4] Finnemore et al.(2015)
- [5] Abuhamad et al.(2015)
- [6] Yigit et al.(2015)
- [7] Yigit et al.(2019)
- [8] Kenny et al.(1986)
- [9] Schmidt et al.(1997)
- [10] Rasanen et al.(1996)
- [11] Luewan et al.(2020)
- [12] Zidere et al.(2021)
- [13] Fernández Pineda et al.(2000)
- [14] Carceller-Blanchard et al.(1993)

Acknowledgements

The authors would like to thank the European Union (Grant no: 863087) for providing financial support to this project.

2.3

Virtual cutaneous leishmaniasis patient: modeling the natural history of infection and preliminary assessment of drug efficacy using Universal Immune System Simulator (UISS)

Maria Adelaida Gomez¹, Giulia Russo², Valentina Di Salvatore², Avisa Maleki³, Elena Crispino⁴, Francesco Pappalardo²

1 Centro Internacional de Entrenamiento e Investigaciones Médicas, Cali, Colombia

2 University of Catania, Department of Drug and Health Sciences, Catania, Italy

3 University of Catania, Department of Mathematics and Computer Science, Catania, Italy

4 University of Catania, Department Of Biomedical and Biotechnological Sciences, Catania, Italy

1. Introduction

Cutaneous Leishmaniasis (CL) is a neglected infectious disease caused by protozoan parasites of the genus *Leishmania*, through the bite of Phlebotominae sandflies [1]. CL affects >1.5 million people annually and is endemic in 98 tropical and subtropical countries worldwide. There is no available vaccine. Drug treatments are unacceptably toxic, long and have a high rate of treatment failure (>25%). One of the critical challenges for drug development is the evaluation of toxicity profiles and efficacy throughout the sociodemographic diversity of the affected population. In-silico trials can be implemented as a support strategy in biomedical research with the aim to reduce, partially replace and refine in vitro experimental designs and in vivo testing.

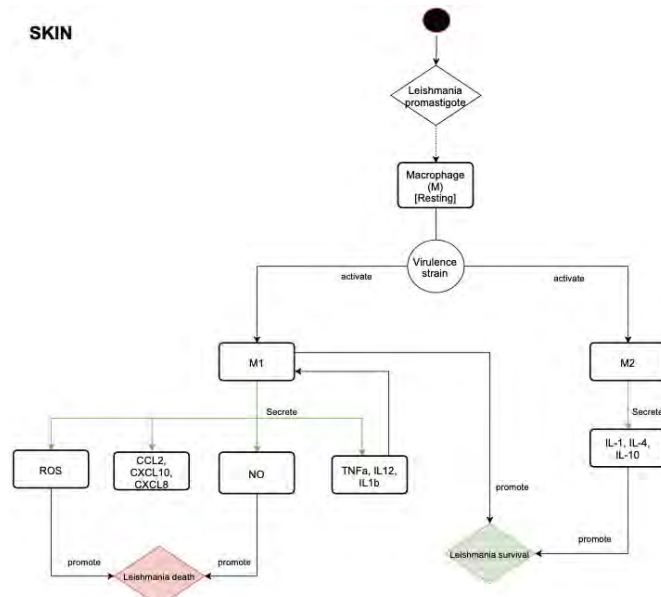


Figure 1: Conceptual Model of the initial stage of infection

2. Materials and Methods

Universal Immune System Simulator (UISS) [2] is a multi-compartment, polyclonal, stochastic patient-specific agent-based model able to predict the response of the human immune system to several disease [3], including CL. A clinical and sociodemographic database of >500 CL patients from Colombia was used as input to generate in silico patients. We will specifically evaluate the utility and implementability of the in silico clinical trial technology to model adult and pediatric CL patients, as a tool to optimize antileishmanial treatment regimens.

3. Results

This study aims at answering the following questions:

- Can the length of the therapeutic regimen be reduced from 20 to 10 days?
- Can we predict CL patients who will have treatment failure, as to provide personalized therapies for CL?

4. Discussion and Conclusions

Most available and approved treatments for CL are systemic, and demand long therapeutic schedules. The high costs, logistical and regulatory limitations, among others, impede the development of clinical trials throughout the range and diversity of affected CL patients. Computational approaches emerge as an alternative to overcome these gaps.

5. References

1. Murray et al., H. W., "Advances in leishmaniasis," *Lancet* 366(9496), 2005.
2. C. Curreli et al., "Verification of an agent-based disease model of human *Mycobacterium tuberculosis* infection," *Int. j. numer. method. biomed. eng.*, vol. 37, no. 7, Jul. 2021.
3. G. Russo et al., "A multi-step and multi-scale bioinformatic protocol to investigate potential SARS-CoV-2 vaccine targets," *Brief. Bioinform.*, Oct. 2021.

Acknowledgements:

The authors would like to thank the Department of Drug and Health Sciences, University of Catania, for partially funding the visiting activity of Dr. M. A. Gomez.

2.4

Simulating radiation-induced pulmonary fibrosis through personalised in silico modelling

Eleftherios Ioannou¹, Myrianthi Hadjicharalambous¹, Anastasia Malai², Chloe Symeonidou², Morfo Georgiou², Nicos Katodritis², Dimitrios Vomvas², Vasileios Vavourakis^{1,3}

¹ University of Cyprus, Mechanical & Manufacturing Engineering, Nicosia, Cyprus

² Bank of Cyprus Oncology Centre, Cyprus

³ University College London, Medical Physics & Biomedical Engineering, United Kingdom

1. Introduction

Pulmonary fibrosis (PF) is a serious chronic lung disease, caused by abnormal response to an injury in lung tissue. PF leads to the formation and accumulation of excess fibrous tissue, which reduces lung function resulting in breathing difficulties and eventually death. Fibrosis can occur as a side effect of external beam radiation treatment (RT) in the chest area in lung cancer or/and breast cancer patients. Staging and prognosis of radiation-induced lung damage remains elusive, mainly because of the highly heterogeneous course of the disease in cancer patients [1].

There is a clinical need to make reliable prognosis in radiation-induced PF development and to determine appropriate radiation dosage that minimizes the risk of fibrosis occurrence after RT.

exhibit the development of fibrosis in the lungs which follows clinically observed patterns that resemble irregular "honeycombing" patterns seen in widespread PF. In Figure 1, the RT dosage distribution and the tumour location (before treatment) is shown on the lung model. Also, fibrosis predictions following 6 and 12 months after treatment (blue) is compared against the clinically-evidenced PF (pink).

4. Discussion and Conclusions

Our results demonstrate the in silico model capacity to recapitulate PF progression exhibited in lung cancer patients who received RT as part of their treatment. Simulation results are in good agreement with clinical evidence, which highlights the potential of in silico towards improving RT planning and therapeutic outcomes.

5. References

1. Kolb M, Collard HR. Eur Res Rev (2014). DOI:10.1183/09059180.00002114
2. Vavourakis V, et al. PLOS ONE (2016). DOI:10.1371/journal.pone.0159766

Acknowledgements:

We would like to thank UCY for the financial support (LungSim project) and using the HPC facilities.

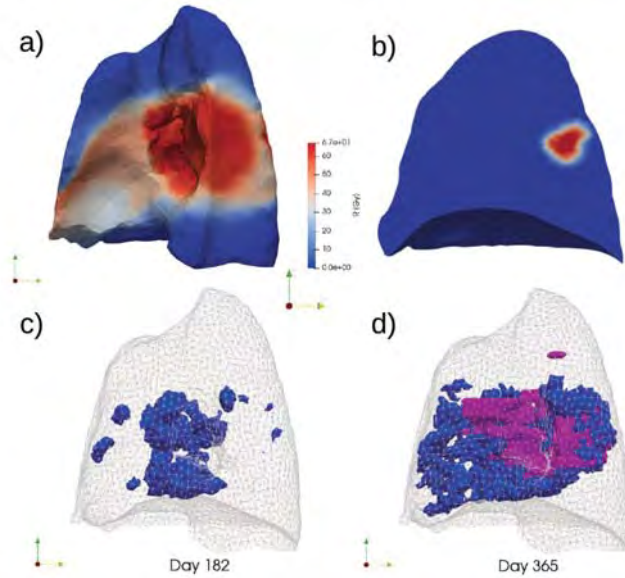


Figure 1: Model shows a) RT dosage distribution, b) initial tumour location; simulated fibrotic region c) 6 months and d) 12 months after therapy.

2. Materials and Methods

We present an in silico modelling procedure of tumour regression and radiation-induced PF that incorporates patient-specific information and enables high-fidelity description of fibrosis development. The model adopts a continuum-based formulation of 3 PDEs, which govern the evolution of carcinoma cells, fibroblasts, and lung tissue. The equations are discretised via FEM and solved using our in-house simulator [2].

3. Results

The model is informed after image processing CT scans of 10 lung cancer patients treated at BoCOC; the patients were diagnosed with PF several months after treatment. Structural information (HU), radiation dosage distributions and tumour position are used as initial conditions. Simulations

2.5

Personalized, automatized brain stimulation modelling partly explains intersubject behavioral response variability

Melanie Steiner¹, Esra Neufeld¹, Bryn Lloyd¹, Taylor Newton¹, Antonino Cassara¹, Katie Zhuang¹, Pedro Crespo-Valero¹, Silvia Farcito¹, Niels Kuster¹

1 ITIS Foundation

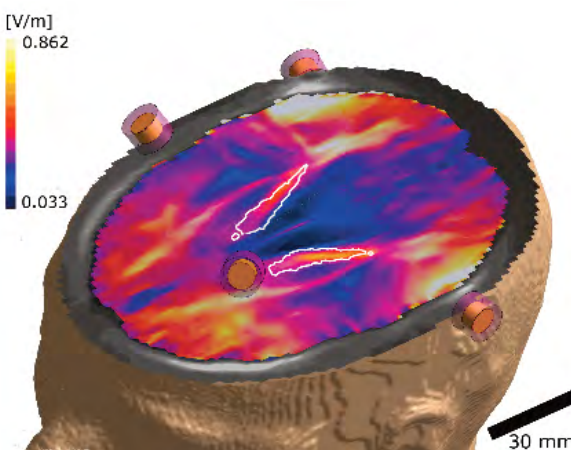
1. Introduction

Intersubject variability results in significant differences when applying transcranial brain stimulation conditions. Recent results have shown that accounting for anatomical and dielectric differences and their impact on electromagnetic exposure explains an important part of the differences in BOLD response. Hence, there is a need for means of efficiently generating personalized head models from patient image data that reproduce the anatomy in sufficient detail. However, existing solutions are time consuming, require significant manual (correction) work, are failure prone, frequently distinguish too few tissue classes, and can have tool-specific restrictions (e.g., constrained to onion-like tissue topologies). A new approach has been developed and benchmarked against a state-of-the-art reference tool in terms of segmentation accuracy metrics, as well as exposure metrics.

2. Methods

A convolutional neural network has been trained on labelled (16 tissues) multimodal image data from 20 subjects. For robustness, data augmentation was used, and an automatic post-processing process (clean-up, dura-insertion) was implemented.

The head model generation method was integrated in a comprehensive pipeline for personalized brain stimulation modelling. The pipeline takes patient image data, produces a segmentation, extracts surfaces, uses co-registered DTI image data to assign anisotropic, heterogeneous dielectric property maps, places electrodes according to the 10-10 system, simulates electromagnetic fields, and extracts EEG lead matrices. Exposure metrics are computed and can be used to optimize stimulation parameters. The pipeline is mostly automatized.



3. Results

The AI-based approach provides segmentations in a few minutes (reference tool: 2-10h) and is capable of distinguishing 17 (vs. 6) tissue classes. With the automatic clean-up, it achieves superior segmentation quality. Data augmentation is effective in increasing robustness and generalizing to different imaging protocols.

The automatized brain stimulation modelling platform was used to reproduce temporal interference brain stimulation sessions from a clinical trial involving 15 volunteers. It successfully explained 36% (R^2) of the behavioural response variability ($p=1.8\%$).

The impact of personalization factors on brain exposure prediction metrics (target exposure magnitude, coverage and selectivity, off-target stimulation) was systematically assessed.

4. Conclusions

The personalized head model generation method robustly produces superior model quality (number of distinguished tissue classes, accuracy), much faster. In a brain stimulation modelling pipeline, it demonstrated the predictive value of personalized exposure modelling, as well as the potential of personalized exposure optimization. The method can readily be retrained to deal with different imaging protocols and modalities.

Acknowledgement:

We gratefully acknowledge experimental data and insights contributed by the team of Prof. Hummel (EPFL).

2.6

Computational analysis of subject-specific muscle-driven ankle-foot kinematics

Armagan Can Yildiz¹, Animesh Ranjan^{1,2}, Okan Avcı¹, Oliver Röhrle^{1,2}

1 Fraunhofer Institute for Manufacturing Engineering and Automation, Biomechatronic Systems, Stuttgart, Germany

2 Institute for Modelling and Simulation of Biomechanical Systems (CBB), Stuttgart, Germany

1. Introduction

Orthopaedic foot diseases, such as cerebral palsy and muscle spasticity, occur as a result of neuromuscular imbalances. This leads to various levels of foot deformities, which require careful rehabilitation or even surgical intervention. Moreover, there is a general lack of physics-based objective metrics that can aid surgeons in the decision-making process. Concerning this, the structural modelling and analysis of musculoskeletal systems can provide better understanding of joint and soft tissue kinematics and can be used for clinical applications. However, there are currently no 3D simulation models of the shank-foot complex that can reliably be utilized in the evaluation of the muscle-driven ankle joint function. In the following study, we aim to develop a 3D continuum-mechanical human shank-foot model that use muscle activations to simulate the influence on ankle-foot kinematics.

2. Materials and Methods

The modelling process involves all of relevant muscles, tendons, ligaments and bones. The geometries are obtained from a subject-specific MRI data set. Herein, we derive the respective computational models and represent them as CAD geometries. From a functional point of view, we use, instead of relying on predefined rotation axes, an activation-driven approach to achieve anatomical ankle movements. While bones and cartilages provide articulation surfaces, the ligaments stabilize the ankle and restrict the movements that remain in a physiological range of motion.

The contractile properties of the muscles are modelled using a nonlinear, hyperelastic, transversely isotropic, constitutive law [1], wherein the muscle fibre orientations are obtained through a novel 3D steady-state thermal analysis approach. Numerical optimization methods are employed in the determination of pre-stretch values of the muscles using range of motion data measured by marker-based motion capture.

3. Results

The resulting finite element (FE) model can yield physiological foot kinematics based on sequence of shank-muscle activations.

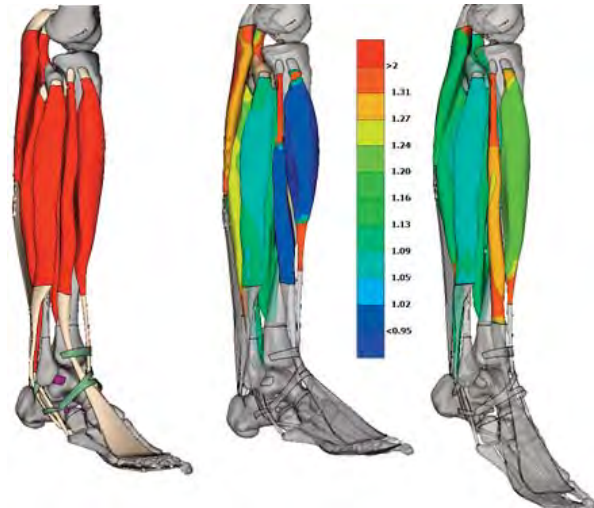


Figure 1: (left) Computational model (muscles: red, tendons: beige, retinaculum: green, ligaments: purple); fibre stretches of the muscles in dorsiflexion (middle) and plantarflexion (right).

4. Discussion and Conclusions

The developed virtual shank-foot model provides valuable information regarding the relationship between muscle physiology and foot kinematics. Readjustment of obtained pre-stretch values can be utilized to better understand the implications of orthopaedic foot surgeries such as tendinoplasty. Moreover, by the inclusion of subject-specific soft tissue properties, the model can be further extended for in-silico development of medical devices.

5. References

- Röhrle, O., Sprenger, M., and Schmitt, S. (2017). A two-muscle, continuum-mechanical forward simulation of the upper limb. *Biomechan. Model. Mechanobiol.* 16, 743–762.

Acknowledgements:

This work made possible by BMBF through the "Data-Integrated, 3D Muscle Modelling for Optimized Orthopaedic Surgery of the Foot" Project (01EC1907B/01EC1907D).

2.7

Subject-specific knee joint in musculoskeletal modelling : prediction of contact forces and moments during gait for two patients with total knee arthroplasty

Sacha Guitteny^{1,2}, Rachid Aissaoui³, Raphaël Dumas^{1,2}

1 Claude Bernard University Lyon 1, Villeurbanne, France

2 Université Gustave Eiffel Campus de Bron, Bron, France

3 École de technologie supérieure ÉTS, Génie des systèmes, Montréal, Canada

Email: raphael.dumas@univ-eiffel.fr

1. Introduction

Assessment of tibiofemoral contact loads is crucial in the follow-up of patients with total knee arthroplasty (TKA). Estimations from musculoskeletal models have been widely used but their customization is often limited to the scaling of musculoskeletal geometry or the adaption of muscle lines of action. This study presents subject-specific knee joint models with TKA kinematics and geometry of two patients and evaluates the predicted tibiofemoral contact forces and moments during gait.

2. Materials and Methods

This study uses kinematic data, ground reaction forces and moments and fluoroscopic measurements from two CAMS-Knee patients with instrumented TKAs (1M/1F, 77/80years, 103/66kg, 173/168cm) [1]. One patient (K3R) had a TKA implanted with large axial rotation relative to the bone segments. A musculoskeletal lower limb model was used [2] with spherical and universal hip and ankle joints, respectively. The tibiofemoral joint was modelled as prescribed contact point trajectories: either generic [3] or subject-specific (fluoroscopic measurements during squat [4]). The patellofemoral joint model was also generic [3] or subject-specific (axis of the implant's trochlea, patellar tendon insertion). Finally, cylinders fitted on the generic bone condyles or on the implant trochlea and condyles were added to wrap hamstrings, quadriceps and gastrocnemii muscles.

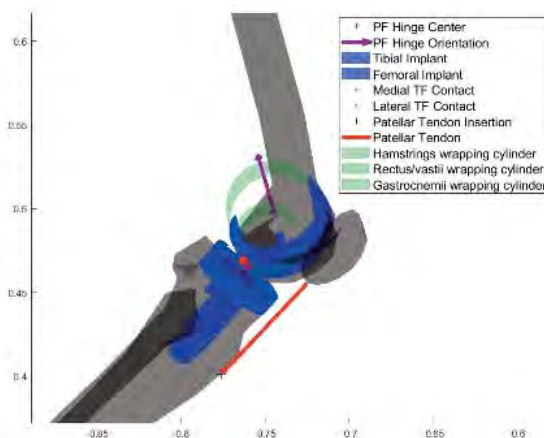


Figure 1: TKA knee subject-specific model

Static optimisation was applied to estimate tibiofemoral contact force and moments along with musculotendinous forces [5]. Predictions with generic (GE) and subject-specific (SP) models were compared to the instrumented implant measurements (Table1).

3. Results

Both models predict well the proximal-distal (PD) force and the abduction-adduction (AA) moment. The subject-specific models improve the predictions of medial-lateral (ML) force, internal-external rotation (IE) and flexion-extension (FE) moments for both patients compared to the generic model. The prediction of the anterior-posterior (AP) force was comparable between GE and SP models with different outcomes between subjects.

R²	AP	PD	ML	AA	IE	FE	
GE	K3R	0.4	0.94	0.01	0.79	0	0.42
	K7L	0.73	0.95	0.01	0.82	0.18	0.23
SP	K3R	0.59	0.93	0.24	0.77	0.13	0.66
	K7L	0.69	0.96	0.68	0.92	0.51	0.64
RMSE (in BW and BW*Height)							
GE	K3R	0.06	0.29	0.1	1.05	0.88	2.22
	K7L	0.06	0.5	0.17	2.01	0.73	0.68
SP	K3R	0.06	0.34	0.07	1.43	0.65	0.96
	K7L	0.05	0.46	0.06	0.92	0.71	0.43

Table 1: Predicted and measured contact loads (improvements with subject-specific knee joint are bolded)

4. Discussion and Conclusions

Few studies have previously validated all of the tibiofemoral forces and moments. The presented subject-specific models improve predictions in most of the joint axes. Unexpectedly, this improvement was more limited with the patient with a more rotated implant and further adaptations (muscle wrapping, static optimisation cost function...) may be required.

5. References

1. Taylor et al., J Biomech;65:32-39(2017)
2. Dumas et al., J Biomech;113:110117(2020)
3. Delp et al. IEEE Biomed Eng;37:757-767(1990)
4. Trepczynski et al., Sci Rep;9:182(2021)
5. Moisset et al., J Biomech;47:50-58(2014)

2.8

Towards automatic generation of patient-specific knee models for total knee arthroplasty

Elahéh Elyasi¹, Mathieu Bailet¹, Marek Bucki¹, Antoine Perrier^{1,2}

1 TwInsight, Grenoble, France

2 Groupe hospitalier Diaconesses–Croix Saint-Simon, Paris, France

*elahéh.elyasi@twinsight-medical.com

1. Introduction

Over the past three decades, Finite Element (FE) analysis has been used as a non-invasive approach in biomechanics to study the risk factors impacting the knee joint. An FE analysis normally involves three steps of pre-processing, processing and post-processing. The pre-processing step may take several working days to build a subject specific knee model [1]. This acts as an obstacle for using FE analysis in clinical routine. Therefore, we have designed a pipeline using various features from the TwInsight software suite to reduce the pre-processing time. In this paper, we describe this pipeline for Total Knee Arthroplasty (TKA) that uses novel methodologies such as deep learning for automatic tissue segmentation and anatomical inference.

2. Materials and Methods

Imaging data from an atlas subject was used to build a knee biomechanical model that acts as the basis of the pipeline and corresponds to TKA application. To adapt the model for any new subject, the Computed Tomography (CT) scan of the subject is imported to a tool that automates the segmentation of bones using convolutional neural network. The tool has been trained with CT scan images and segmentation masks from a dataset and its neural network architecture is based on the U-Net, designed for biomedical segmentation of 3D images [2,3]. Dice coefficient (a measure of overlap between the ground truth and the algorithm segmentation mask) has been used to evaluate the performance of the tool.

To create the model from automatically segmented bones, an anatomical inference algorithm was used that non-linearly maps the morphology of the atlas knee model to the morphology of the subject's knee. In this process, the insertion sites of all ligament bundles and the anatomical landmarks are also transferred enabling us to produce the subject specific model without requiring additional image acquisitions than the ones used in clinical routine. Following the inference step, the implant is positioned based on the anatomical landmarks to build the TKA model for subject-specific simulation.

3. Results

A schematic of the developed pipeline is shown in Figure 1. The used automatic segmentation tool reduced the segmentation time for lower limb bones from 3 hours (mean segmentation time by an expert depending on the image resolution [4]) to one and a half minutes with a Dice score of 0.96 after training with a minimal dataset of 23 CTs. The anatomical inference of the ligaments and landmarks took less than 5 minutes.

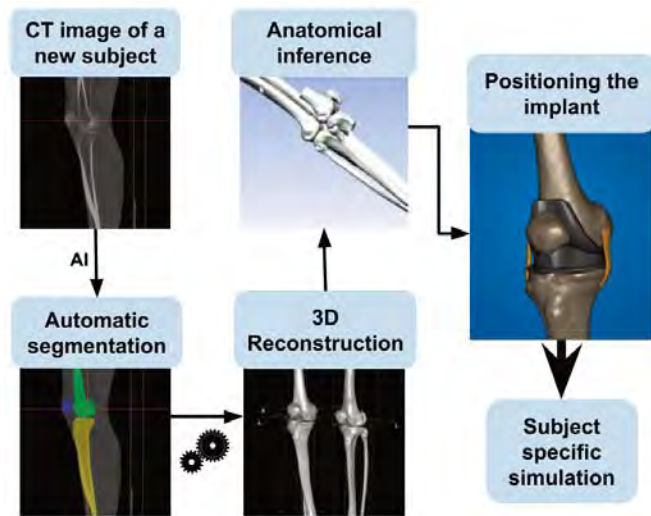


Figure 1: The TwInsight pipeline for automatic generation of subject-specific TKA models.

4. Discussion and Conclusions

Pre-processing is a critical part of performing a FE analysis, and it thus requires to be adapted to a subject-specific modelling framework. The pipeline presented in this abstract successfully enabled us to significantly reduce the required pre-processing time to build TKA models and thus enhance their usability in clinical routine.

5. References

- [1] Cooper RJ, et al. *Med Eng Phys* 2019;74:1–12.
- [2] Çiçek Ö, et al. *Lecture Notes in Computer Science*, 2016;9901 LNCS:424–32.
- [3] Ronneberger O, et al. *Lecture Notes in Computer Science*, 2015;9351:234–41.
- [4] Paz A, et al. *Applied Sciences* 2021;11:11440.

3.1

A physiology-driven model for the generation of a virtual cohort of dyssynchronous heart failure patients

Claudia Alessandra Manetti¹, Nick van Osta¹, Tijmen Koopsen¹, Ahmed Salem Beela¹, Roel Meiburg¹, Tim van Loon¹, Tammo Delhaas¹, Joost Lumens¹

¹ Maastricht University, Biomedical Engineering Department, Netherlands

1. Introduction

Cardiac resynchronization therapy (CRT) improves cardiac performance and heart failure symptoms in appropriately selected patients [1]. Unfortunately, not in all patients the full benefit of CRT is realized. Recent clinical studies [2] demonstrated the potential of deformation imaging for myocardial phenotyping in CRT patients. This study describes the development of an automatic tool for generating a virtual cohort of CRT candidates characterized by realistic myocardial strain traces.

2. Materials and Methods

We used the CircAdapt model of the human heart and circulation to simulate regional myocardial mechanics and global hemodynamics in an 18-segments model of the left ventricle (LV) [3]. A sensitivity analysis with Morris and Saltelli methods was performed to select the model parameters most sensitively determining ventricular strain patterns for patients with electromechanical dyssynchrony and myocardial infarction. The final subset consisted of 40 parameters describing global cardiac pump function, and regional systolic and diastolic tissue properties. To ensure uniformity in the dimensional parameter space, the Sobol low-discrepancy sequence is used [4]. We filtered the resulting cohort with global hemodynamic parameter values and strain indices representative for a CRT cohort, found in literature, guidelines, and clinical data. Simulations were divided in two groups based on the mean value of systolic stretch index (SSI) of 5% [2].

3. Results

We constructed a cohort of 4000 virtual patients and based on the filtering 400 were accepted (Fig. 1). The virtual patients with increased LV wall area and less contractile dysfunction were associated with high SSI value (Fig. 2) which relates to a better response to CRT [2].

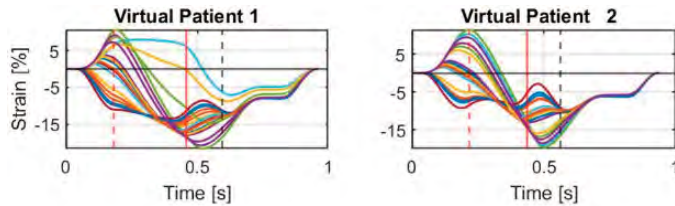


Figure 1. Regional LV strain traces of two virtual patients with mechanical dyssynchrony.

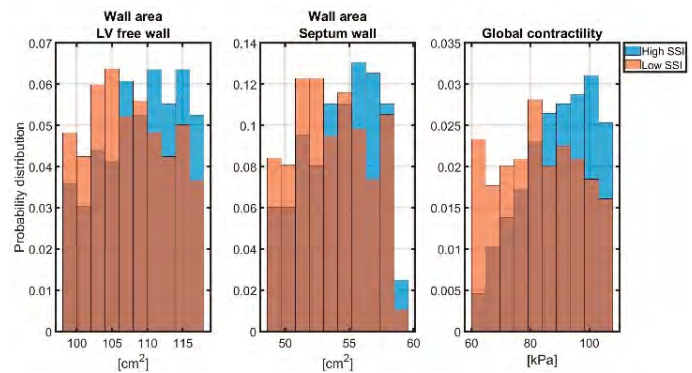


Figure 2. Probability distribution of the subgroup of patients characterized by high SSI (blue) and low SSI (orange). The brown color represents the overlap between the two distributions.

4. Discussion and Conclusions

We developed an automatic tool that generates CRT candidates. This cohort can relate clinical indices to possible substrates. Considering the high invasiveness and high cost of the therapy, in-silico trials can help to explain the differences in myocardial phenotypes between responders and non-responders by revealing the underlying disease substrates.

5. References

1. Ponikowski P. et al, European Heart Journal 2016; 18(8): 891-975
2. Gorcsan III et al, JACC Cardiovasc Imaging (2019);12(9):1741-1752.
3. Lumens J. et al, Ann Biomed Eng 2009; 37:2234–2255
4. Kucherenko S. et al, arXiv - University of Cornell (USA); 2015. JRC98050

Acknowledgements:

This work was supported by the European Union's Horizon 2020 Research and Innovation program under the Marie Skłodowska-Curie grant agreement No. 860745.

3.2

A virtual population approach to support atopic dermatitis clinical trial design and biomarker identification

Igor Faddeenko¹, Simon Arsène¹, Théo Galland¹, Natacha Go¹, Shiny Martis¹, Daniel Smít¹, Riad Kahoul¹, BOISSEL JEAN-PIERRE¹, Aude Chevalier², Lorenz Lehr², Christian Pasquali², Alexander Kulesza¹

1 Novadiscovery, Lyon, France

2 OM Pharma SA, Meyrin, Switzerland

1. Introduction

Disease and response variability are hurdles for new agents in atopic dermatitis (AD). Focus on responding subpopulations reduces the uncertainty of confirmatory trials but requires predictive biomarkers. Systems pharmacology models provide mechanistic detail to complement biomarker programs but are difficult to use for AD trial design. Therefore, we developed in silico clinical trials based on a mechanistic model of skin immunology and Virtual Population of AD patients.

2. Materials and Methods

Four treatment models (emollients, topical corticosteroids (TCS), and the immunomodulator OM-85 [3]) (Fig. 1b) have been interfaced with an skin immune dysregulation and AD severity (i.e SCORAD) model (Figure 1a). Dynamics of immune effectors were informed using published data (for example skin proteomics [4]). Embedded into a trial simulation algorithm, the administration protocol and follow up of particular trials can be simulated.

3. Results

Conducting the in silico trials with a protocol resembling the study of Bodemer et al. [2] and calibrating unknown efficacy-related parameters with the severity time-profiles of this study (Fig 1b), enabled the induction of quantitative links between patient (i.e. baseline) immunological characteristics and differential response to OM-85 vs. TCS. Generalized linear model analysis of baseline patient characteristics suggests five immunological markers (not associated with typical allergy markers such as IgE) predicting the SCORAD response at 6 months (Fig. 1c). When enriching responders in this trial by requiring as eligibility criteria (EC) the values of these 5 markers > median values, the sample size could be reduced by 51.5%. More selective EC do not further decrease the sample size but restrict the eligible number of patients (Fig. 1d).

4. Discussion and Conclusions

We demonstrate that our in silico approach can suggest response biomarkers based on the links established between immunological mechanisms and response profile variability. TCS vs. OM-85 trials similar to Bodemer et al. [2] should sample skin (regulatory) cytokines or pathogens as biomarker candidates for streamlining confirmatory clinical trial study populations.

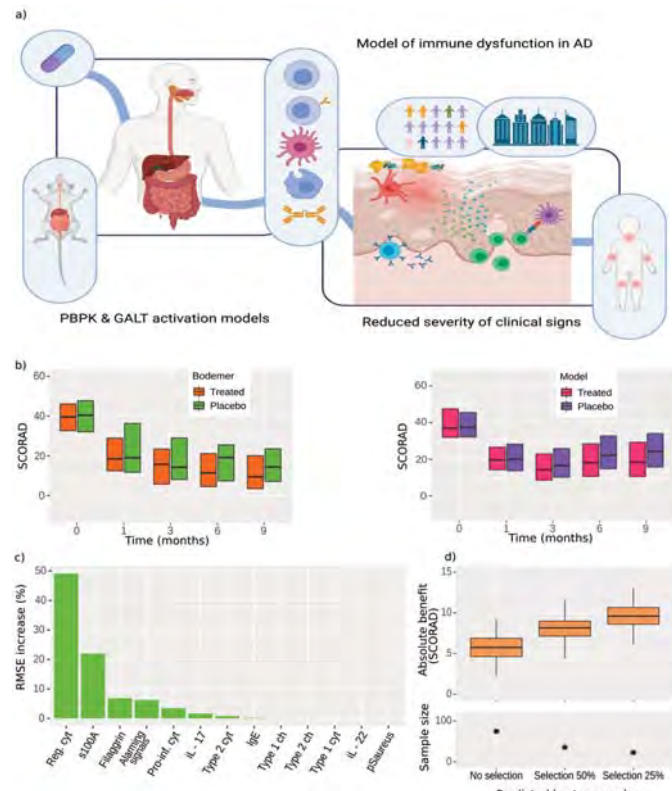


Figure 1: Mechanistic modeling of atopic dermatitis (AD) and treatments: a) Overall model b) SCORAD time profile of the reference trial [1] and the calibrated model. c) Root-mean-square-error increase from dropping a predictive marker in the linear model analysis, e) Absolute benefit and sample size estimates for trials without and with marker based responder enrichment.

5. References

1. Bodemer, Christine, et al. *PloS one* 12.3 (2017): e0161555
2. Lyubchenko, T, et al. *Annals of Allergy, Asthma & Immunology* 126.1 (2021): 46-53.

3.3

An in Silico clinical trial on coronary fractional flow reserve as a replacement for the original clinical trial: A feasibility study

Pjotr Hilhorst¹, Wouter Huberts^{1,2}, Rajarajeswari Ganesan¹, Marcel van 't Veer^{1,3}, Pim Tonino^{1,3}, Frans van de Vosse¹

1 Eindhoven University of Technology, Biomedical Engineering, Eindhoven, Netherlands

2 Maastricht University, Biomedical Engineering, Maastricht, Netherlands

3 Catharina Ziekenhuis, Eindhoven, Netherlands

1. Introduction

In Silico clinical trials have great potential for replacing clinical trials. In this study, we aim to demonstrate the feasibility of conducting in Silico clinical trials by generating virtual patients, and reproducing a clinical trial in which the clinical benefit of fractional flow reserve (FFR) measurements was demonstrated (i.e., the FAME study [1]) for patients suffering from coronary artery disease. Here, we will present the strategy we envision to demonstrate the clinical benefit of the FFR using in Silico trials only. In addition, we will present preliminary results regarding model development.

2. Materials and Methods

An one-dimensional pulse wave propagation model (PWPM) that is capable of computing patient specific FFRs has been developed. Sensitivity analysis will be conducted to prioritize parameters for model personalization. Geometric information will be extracted from angiograms, whereas patient-specific parameters will be estimated by using a machine-learning model that is trained using angiograms, demographics, and pressure losses across stenoses. The latter will be based on FFR measurements or 3D computational fluid dynamic simulations. A synthetically generated training set will be used to assure a large enough dataset and sufficient coverage of the heterogeneity within the population. Secondly, the parameters can be varied to generate virtual patients. In the future, the model output will be transformed into a clinically relevant output (i.e., mortality and morbidity) through a transfer function. Furthermore, the approach will be evaluated on an independent set of real clinical trial data.

3. Results

Pressure and flow waveforms generated with the one-dimensional PWPM can be seen in Figure 1. The aortic pressure is within physiological bounds and the coronary flow shows typical out-of-phase behaviour [2]. Furthermore, a distinct pressure drop can be seen distal from the stenosis. Table 1 shows the computed FFRs at various stenosis severities.

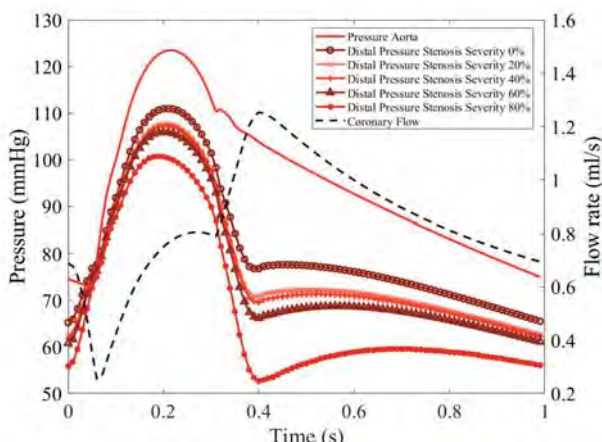


Figure 1: Waveforms at various stenosis severities.

Stenosis Severity [%]	Computed FFR [-]
0	0.86
20	0.82
40	0.81
60	0.79
80	0.71

Table 1: Computed FFR at various stenosis severities.

4. Discussion and Conclusions

The results show that the PWPM can accurately model coronary pathophysiology. The computed FFR values are plausible compared to clinical findings, which typically show an FFR below 0.8 around a stenosis severity of $\geq 50/60\%$ [3]. Overall, it can be concluded that this model is ready for the next step in our devised methodology and can be used as a virtual cohort generator to recreate the FAME1 study in Silico.

5. References

1. Tonino, P.A.L. et al. *N Engl J Med.* 2009; 360(3):213-224.
2. Kim, H.J. et al. *Annals of Biomedical Engineering.* 2010; 38(10), 3195-3209.
3. Kang, S. et al., *Circ Interventions.* 2011. 4(1), 65-71.

Acknowledgements:

We acknowledge the EU's Horizon 2020 research and innovation programme (No: 101016503) for funding.

3.4

Hemodynamics of 1st stage Norwood patient through computer-generated statistical patient cohorts

Canberk Yıldırım¹, Syed Murfad Peer², Berk Ural³, Nurgul Yurtseven⁴, Ahmet Sasmazel⁵, Kerem Pekkan³

¹ Istanbul Bilgi University, Istanbul, Turkey

² Children's National Hospital, Cardiovascular Surgery, Washington, DC, United States

³ Koc University, Mechanical Engineering, Istanbul, Turkey

⁴ Dr. Siyami Ersek Thoracic and Cardiovascular Surgery Training and Research Hospital, Anesthesiology, Istanbul, Turkey

⁵ Dr. Siyami Ersek Thoracic and Cardiovascular Surgery Training and Research Hospital, Cardiovascular Surgery, Istanbul, Turkey

*Kerem Pekkan, PhD; Department of Mechanical Engineering Koc University; Rumelifeneri Campus, Sarıyer, Istanbul, Turkey; Phone: +90 (212) 338 1548; E-mail: kpekkann@ku.edu.tr

1. Introduction

Norwood operation with modified Blalock-Taussig (BT) shunt is a common Stage 1 palliative strategy for hypoplastic left heart syndrome (HLHS) patients [1]. However, early Stage 1 postoperative (PO) period is still associated with high risks of morbidity, mortality and hemodynamic instability [2]. Computational studies aiming to improve the PO performance of Norwood mostly rely on patient-specific cases, since utilizing clinical data is a challenge due to relatively small patient cohorts, financial and ethical considerations [3]. Therefore, in this study, a virtual patient cohort was statistically generated to address these challenges and enable in silico clinical trials targeting early PO period. An established and clinically validated Norwood circulation lumped parameter model (LPM) [4] was utilized to create individual digital patients based on the clinical and published catheterization data. The PO hemodynamics were simulated to help clinical decision making.

2. Materials and Methods

Systemic and pulmonary vascular resistances (SVR and PVR), arterial compliances (Csa and Cpa) and heart rate (HR) were chosen as the continuous random variables (CRV) for statistical analysis. Table 1 shows the data of 1000 digital Norwood patients with normal ejection fraction generated by using our LPM (mean data) and standard deviations (SD) of the CRV in literature and clinical experience.

CRV	Mean (SD)	Range
HR (bpm)	120 (16.35)	100 – 148
SVR (WU)	130 (17.5)	65 – 186
PVR (WU)	19 (2.5)	11.8 – 27.5
Csa (ml/mmHg)	0.08 (0.015)	0.044 – 0.0118
Cpa (ml/mmHg)	0.08 (0.015)	0.049 – 0.0119

Table 1: Generated virtual cohort CRV through the computational model

3. Results

To demonstrate the use of this in silico cohort, 35 digital patients were randomly picked from the cohort, and early PO hemodynamics were simulated for different shunt sizes. Two-sample t-test was used for the comparison, as shown in Table 2. The minimum patient number for statistical significance was also determined as 6.

BT shunt size (n=35)		
	3 mm	3.5 mm
Sys. Flow	0.42 (0.0225)	0.38 (0.024)
Pul. Flow	0.34 (0.031)	0.52 (0.0455)
Aortic Press.	60.65 (4.8)	56.35 (4.1)
Pul. Press.	12.7 (1)	17.1 (1.3)
Venous Press.	6.85 (0.24)	7.3 (0.3)
Pul./Sys. Flow	0.83 (0.1)	1.38 (0.18)

Table 2. Mean (SD) comparison of flows (l/min) and pressures (mmHg) for in silico patients

4. Discussion and Conclusions

In this study, a virtual patient cohort for Norwood physiology was generated first time in literature to the best of our knowledge. The calculated p values for various shunt sizes yield significant differences in mean early PO hemodynamics ($p<0.001$), which agrees well with the clinical data in literature. Therefore, the introduced statistical model generating digital patients has a good potential to provide clinically relevant artificial data in in silico evaluation of the hemodynamics in critical congenital heart defects. This data can also be used in design and development of mechanical circulatory assist therapies for complex circulations [4].

5. References

1. Piskin et al., *J of Biomech*; 50(4) (2017)
2. Mahle et al., *Circulation*; 102 (III) 136-141 (2000)
3. Morrison et al., *Front Med*; 5(241) (2018)
4. Peer et al., *Eur J Cardiothorac Surg* (accepted)

Acknowledgements: ERC-PoC (966765) and Tubitak (1003 118S108) research grants.

3.5

Identification of virtual patient cohorts for in silico clinical trials of cardiopulmonary devices from a database of 331 ECMO patients with diagnosed ARDS

Micha Landoll^{1,2}, Christian Karagiannidis², Stephan Eric Straßmann², Lasse Strudthoff¹, Michael Neidlin¹

¹ Institute of Applied Medical Engineering, Medical Faculty, RWTH Aachen University, Department of Cardiovascular Engineering, Aachen, Germany

² ARDS and ECMO Centre Cologne-Merheim, Kliniken der Stadt Köln, Witten/Herdecke University, Department of Pneumology, Cologne, Germany

1. Introduction

Extracorporeal membrane oxygenation (ECMO) remains a controversial topic in medicine. Existing analyses lack sufficient cohort size or the variety of parameters. Unravelling the intrinsic complexity of ECMO therapy, especially considering the interplay between clinical parameters, device settings and disease state poses a great challenge in biomedical research [1]. In silico clinical trials seem to be a viable approach to increase patient safety and therapy efficacy. Therefore, the identification of virtual patient cohorts from electronic health records (EHR) is necessary [2]. Within this study, we investigate inflammatory phenotypes and often used operating points of ECMO devices using multivariate and heterogeneous clinical data from the intensive care unit (ICU) with Data Science and Machine Learning.

2. Materials and Methods

The analyses included EHR of 331 patients (m: 222, f: 109; Age: mean 53.9 y, standard deviation: 13.2 y; ICU stay: 1-210 d; Mortality: 155, 46.83%) with diagnosed acute respiratory distress syndrome (ARDS) who received ECMO treatment admitted to the ARDS and ECMO Centre Cologne Merheim between 2012 and 2021. The data preprocessing included removing outliers (98% confidence interval), reduction to one daily data point, scaling, mean imputation, and feature selection.

These state descriptions of 7724 ECMO therapy days were used as input in two separate cluster analyses. Four parameters were considered in clustering A to identify inflammatory states while clustering B was focused on technical operating points of ECMO devices and mechanical ventilation (MV). The selection of the input parameters was based on clinical domain knowledge and data availability and quality. The cluster analyses were performed using a k-means algorithm. With random forest regressors and classifiers, we investigated feature importance on mortality, ICU stay length, clinical scores, and cluster membership.

3. Results

The presented data processing pipeline enables data explorative investigations with machine learning of EHR from a large cohort. As shown in Figure 1 four groups of inflammatory phenotypes (A) and five groups of distinct technical parameter settings (B) were identified. The cluster groups A#3 (high lactate and CRP, n=286), A#0 (high LDH and CRP, n=207), B#0 (high pressure and flow settings, n=1971) and B#4 (low FiO₂, n=34) were observed as more critical compared with all others. The feature importance analysis identifies the decisive parameters on cluster membership (see Figure 2) and the descriptions of the therapy days with further examined parameters enriches the characterization.

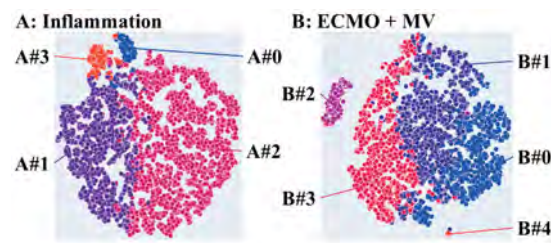


Figure 1: Visualization of cluster groups on t-distributed stochastic neighbor embedding (t-SNE)

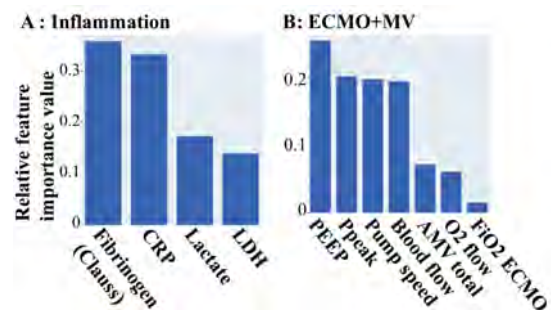


Figure 2: Relative feature importance for cluster membership determined by random forest classifier

4. Discussion and Conclusions

Our pipeline allows the processing and analysis of high-resolution patient data. Thereby virtual cohorts could be identified and described in the context of extracorporeal life support. The descriptions of the cluster groups with further data from EHR demonstrates the differences between the sub cohorts and unravels the heterogeneity of the complex treatment of ARDS on ICU. Based on these findings, we suggest that in silico clinical trials in the context of ECMO need to consider the clinical state of the patient as well as the technical environment during therapy.

5. References

1. Karagiannidis C, Brodie D, Strassmann S, et al., *Intensive Care Medicine*, 42(5):889-896 (2016).
2. Viceconti M et al., *International Journal of Clinical Trials*, 3(2):37-46 (2016).

Acknowledgements:

No funding was received for this study.

3.6

In silico clinical trials for treatment of acute ischemic stroke

Claire Miller¹, Raymond Padmos¹, Sara Bridio², Giulia Luraghi², Praneeta Konduri³, Nerea Arrarte Terreros³, Alfons Hoekstra¹

¹ University of Amsterdam, Computational Science Laboratory, Informatics Institute, Faculty of Science, Amsterdam, Netherlands

² Politecnico di Milano, Laboratory of Biological Structure Mechanics (LaBS), Department of Chemistry, Materials and Chemical Engineering, Milan, Italy

³ Amsterdam UMC, location AMC, Department of Biomedical Engineering and Physics and Department of Radiology and Nuclear Medicine, Amsterdam, Netherlands

1. Introduction

In silico clinical trials (ISCTs) have the potential to reduce the risk, duration, and cost of clinical trials [1]. For example, they could be used to test new therapies in silico to refine populations of interest, or to supplement trial patients with virtual patients.

We have developed an ISCT framework for the treatment of acute ischemic stroke (AIS). AIS occurs when a clot blocks an artery to the brain, reducing blood supply and resulting in brain tissue death. In this abstract we outline our ISCT framework and provide examples of ISCTs we can perform.

2. Materials and Methods

The developed ISCT framework consists of four modules:

1. Generating a cohort of virtual patients: a statistical model is used to generate a cohort of stroke patients who have likely combinations of clinical characteristics.
2. Modelling the treatment and injury due to stroke for each patient: we include models for arterial blood flow to the surface of the brain, perfusion of blood through the brain, brain tissue death, and the two current treatments for AIS: thrombolysis and thrombectomy. This diverse set of models are combined using an event-based modelling approach [2].
3. Predicting patient functional outcome based on the treatment outcome (clot removed or not) and predicted lesion volume from Module 2. This functional outcome is a standard outcome of interest for clinicians in clinical trials for AIS.
4. Assembling trial results and compare different therapies and/or populations.

Full details on model methodologies and the framework are given in [2].

3. Discussion and Conclusions

One outcome of interest in AIS trials is the effectiveness of thrombectomy devices for different subpopulations. Effectiveness is defined here as the recanalization success rate (the percentage of clots successfully removed in the population). For example, we compared treatment outcomes with one device for patients with different clot compositions (high fibrin compared to low fibrin). We found low fibrin clots had a higher recanalization rate than high fibrin clots.

In addition to treatment comparisons, the framework can be used to investigate open questions about stroke. For example, two approaches for improving outcomes for stroke patients are: 1) reduce the timeline between stroke onset and treatment; or 2) increase treatment success rate. We will use the developed framework to investigate which of these approaches will have the greatest effect on population outcome.

5. References

- [1] M. Viceconti, A. Henney, and E. Morley-Fletcher, *Int. J. Clin. Trials*, vol. 3, no. 2, p. 37, May 2016, doi: 10.18203/2349-3259.ijct20161408.
- [2] C. Miller et al., *Comput. Biol. Med.*, vol. 137, p. 104802, Oct. 2021, doi: 10.1016/j.combiomed.2021.104802.

Acknowledgements:

The authors would like to thank the European Horizon 2020 Research and Innovation Programme (Grant no: 777072) for funding this project.

3.7

In silico trial of baroreflex activation therapy for the treatment of diastolic heart failure

John Clemmer¹, W. Andrew Pruitt^{1,2}, Robert L. Hester^{1,2}

1 University of Mississippi Medical Center, Physiology and Biophysics, Jackson, United States
2 HC Simulation, LLC, Canton, United States

1. Introduction

Heart failure (HF) is associated with an increase in sympathetic nerve activity (SNA) and has been shown to be present especially in the heart, but also in the kidney, adrenal glands, and periphery [1]. Patients with higher SNA have worst prognoses, and drugs that block sympathetic overactivation in the heart (β -adrenergic blockers) improve outcomes [2]. Recently, baroreflex activation therapy (BAT) has been approved by the FDA for treatment of HF (reduced ejection fraction) based on its ability to improve HF symptoms, increase ejection fraction, and reduce markers of congestion [3]. However, the benefits of this device in HF associated with preserved ejection fraction (HFpEF) is not entirely clear.

2. Materials and Methods

All simulations were performed using HumMod, a large model of human physiology composed of mathematical relationships derived from experimental and clinical data. HFpEF was modeled by doubling baseline LV stiffness and reducing renal function. β -adrenergic receptors in the heart were allowed to desensitize up to 40% with 3 months of constantly high stimulation. SNA increased with increases in pulmonary venous pressure. BAT was achieved by gradually increasing carotid baroreceptor input into the central nervous system to 40% above normal over the first 2 months in all simulations. This level of baroreceptor afferent input was chosen to produce a ~25 mmHg fall in systolic BP in HFpEF patients treated with BAT [4] and a ~30% decrease in muscle SNA seen in HFrEF patients [5]. 12-month responses to BAT were determined under the following 3 conditions:

- 1) Control: HFpEF alone
- 2) BAT: HFpEF+BAT
- 3) BAT-CSNA: HFpEF+BAT with cardiac SNA clamped at baseline levels
- 4) BAT-RSNA: HFpEF+BAT with renal SNA clamped at baseline levels

3. Results

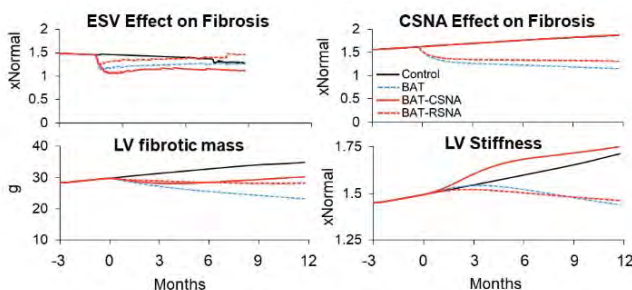


Figure 1: Determinants of LV fibrosis/stiffness

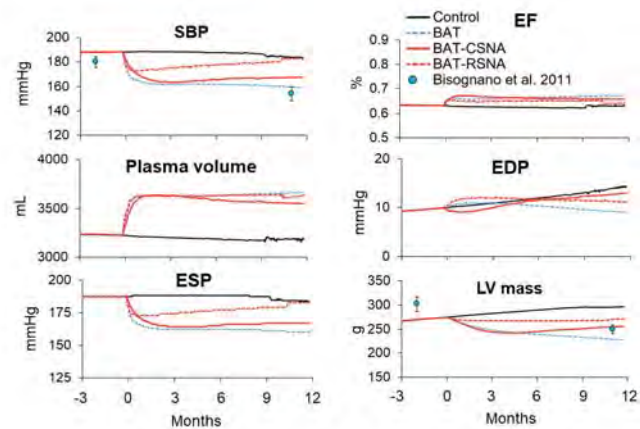


Figure 2: Systemic and cardiac pressures and cardiac function after BAT. SBP and LV mass are compared to clinical data [4](mean \pm SE).

Figure 3. Cardiac and peripheral sympathetic nerve activity and cardiac adrenergic function

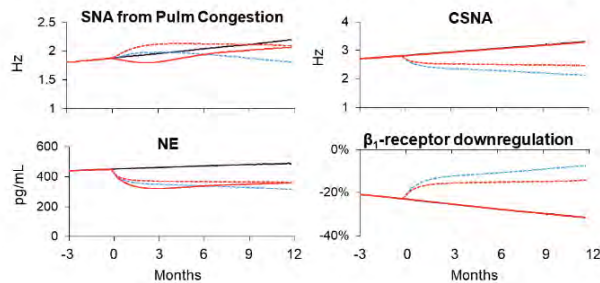


Figure 3: SNA responses

4. Discussion and Conclusions

Clinical trials demonstrate reduced LV mass and BP in hypertensive patients and in patients with hypertensive HFpEF [4]. The direct impacts of cardiac and renal sympathetic overactivation during HFpEF is unknown. Our model of HFpEF was associated with increased LV mass and fibrosis that was reduced with BAT, along with reduced SNA and BP similar to clinical evidence(Figures 1-3). Our results suggest that these beneficial effects may be through the chronic suppression of both cardiac and renal SNA.

5. References

1. Esler et al. Am J Cardiol. 1997;80(11A):7L-14L.
2. Cohn et al. N Engl J Med. 1984;311(13):819-23.
3. Sharif ZI et al. Circ Arrhythm Electrophysiol. 2021;14(4):e009668.
4. Bisognano JD et al. J Am Coll Cardiol. 2011;57(17):1787-8.
5. Dell'Oro R et al. J Hyp. 2017;35(12):2532-6

Acknowledgements:

This work was supported by the National Institute on Minority Health and Health Disparities (R00 MD014738).

4.1

A computational investigation of the fluid dynamic in dialysis catheters for paediatric patients: towards the design optimization.

Claudia Bruno¹, Rayan Moumneh¹, Lynsey Stronach², Emilie Sauvage¹, Ian Simcock², Silvia Schievano^{1,2}, Rukshana Shroff^{1,2}, Claudio Capelli^{1,2}

¹ University College London, Institute of Cardiovascular Science, London, United Kingdom

² Great Ormond Street Hospital for Children, NHS Foundation Trust, London, United Kingdom

Correspondence to Claudia Bruno: c.bruno@ucl.ac.uk

1. Introduction

Central venous lines (CVLs) used for haemodialysis (HD) in children are associated with a high complication rate leading to inadequate HD and line replacement in nearly half of the patients [1]. This project aimed at: i) providing a computational fluid dynamic characterization of CVLs commonly used in children to understand the causes of their complications, and ii) to improve their performance by optimizing their design.

2. Materials and Methods

Four models of CVLs of varying design and sizes (6.5Fr, 8Fr, 10Fr and 14Fr) were recreated starting from microCT scans. Each design presented multiple ports for blood exchange (i.e. tip and side holes). CFD analyses were set up in Ansys Fluent to simulate the CVLs' performance under both ideal and realistic models of superior vena cava and under a variety of working conditions, routinely used in real hospital settings. Haemodynamic features were analysed together with the effect of the catheter insertion inside the vein. CFD findings were then compared to clinical CVLs outcomes from patients ($n=26$ with 57 lines) over the past two years. Anatomical and physiological characteristics of the population of patients of our Centre were used to set up the design optimization process in Ansys DesignXplorer using a Multi-Objective Genetic Algorithm.

3. Results

In all the simulated CVLs, the arterial lumens, where blood is withdrawn from the body, showed the highest stagnation and recirculation areas. The role of arterial tips appeared to be negligible for the blood exchange and the proximal side-holes played a major role for blood aspiration being also subject to the highest levels of shear stress, regardless of the design. Shear stresses >10 Pa were most found in the 8Fr CVL. Longest blood residence time was measured in the 6.5Fr CVL and highest platelet lysis index in the 10Fr. In all the anatomical models, blood velocity increased after catheter insertion (Figure 1a) together with wall shear stresses. Computational data were in accordance with clinical data collected from patients' data. At 90 days, thrombosis-free survival was 35%, 60% and 100% in 8Fr, 10Fr and 14Fr CVLs respectively ($p=0.01$), suggesting that the shear stress is the parameter more strongly related to clinical complications. New optimized designs showed a better haemodynamic performance, reducing shear stress levels and low velocity areas (Figure 1b).

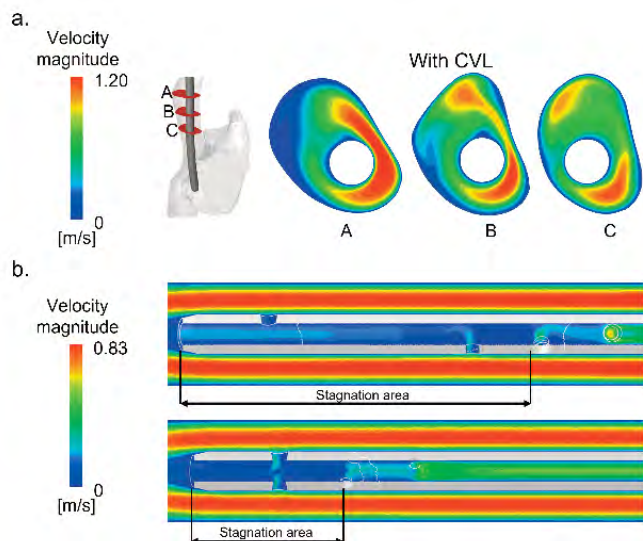


Figure 1: Velocity magnitude contours: a) inside the vein after CVL insertion; b) inside a 6.5Fr model before and after optimization to reduce stagnation areas.

4. Discussion and Conclusions

In this project, we carried out the fluid dynamic characterization of commercially available CVLs for paediatric use to try to explain the associated clinical outcomes. This process guided the optimization of their design.

5. References

- Borzych-Duzalka D et al., 2019

Acknowledgements:

The authors would like to thank Kidney Research UK (Paed_IN_004_20190926).

4.2

Computational Biomechanics as a tool to improve mesh anchoring technique in pelvic organ prolapse repair surgery

Elisabete Silva¹, Margarida Chiote², Sofia Brandão³, Teresa Mascarenhas⁴, António Fernandes²

1 LAETA/INEGI, Biomechanical and Health, Porto, Portugal

2 LAETA/INEGI, Faculty of Engineering, University of Porto, Biomechanical and Health, Porto, Portugal

3 Dep. of Radiology, CHSJ-EPE / Faculty of Medicine, University of Porto

4 Dep. of Obstetrics and Gynecology, CHSJ-EPE / Faculty of Medicine, University of Porto.

1. Introduction

Many surgical procedures to repair pelvic organ prolapse (POP) have been proposed, but their long-term benefits have been poorly evaluated, particularly regarding native tissue repair techniques (with recurrence rates around 29%) [1]. Alternatively, surgeons began to augment native tissue repairs with synthetic meshes. Several post-operative complications such as infections, chronic pain and voiding dysfunction symptoms were previously described, as well as mesh erosion, a phenomenon whereby soft tissues become damaged as a result of contact with the prosthetic mesh. These mesh-related complications prompted the Food and Drug Administration (FDA) to issue safety communications regarding its use [2]. Therefore, the development of innovative tools to increase the biomechanical knowledge associated with POP may be crucial to carry out effective and viable therapeutic procedures.

The main aim of this study is to simulate the effect of the process of the transvaginal reconstructive surgery to reinforce/replace the uterosacral ligaments (USLs), simulating the effect of mesh anchoring technique, and compare the displacement magnitude of the pelvic tissues. Previous studies showed that POP recurrence is common after vaginal mesh implantation that may be related to a strong attachment point for mesh anchorage [3]. The suturing technique with two different anchoring points (simple stitch - a set of four nodes and continuous stitch - a line of nodes) was simulated. The effect of this technique was verified on the pelvic structures, namely the displacement magnitude and supero-inferior displacement of the uterus and vaginal wall.

2. Materials and Methods

A complete pelvic cavity computational model was used (Figure 1 a)). One computational model of the implant was built to mimic the USLs (Figure 1b)) after their total rupture (100% impairment) and with 90% and 50% of impairment. Its mechanical properties were obtained through uniaxial tensile tests performed on a synthetic surgical implant (used for transvaginal POP repair). Also, different anchoring points (simple stitch and continuous stitch) were applied. The Valsalva maneuver was simulated without muscle activation, considering an IAP of 4kPa.

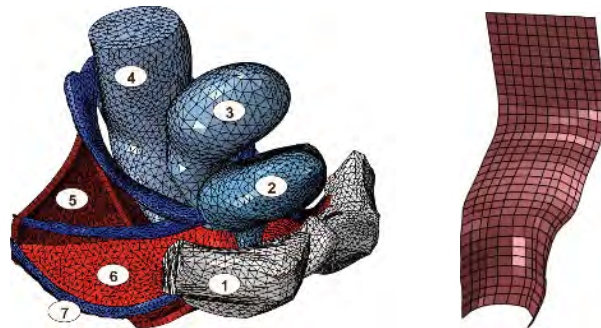


Figure 1: A) 3D computational model. (1) symphysis pubis, (2) bladder, (3) uterus, (4) rectum, (5) levator ani muscle, (6) pelvic fascia, (7) arcus tendineous fasciae pelvis. B) USLs implant.

3. Results

The simple stitch causes a higher supero-inferior displacement of the vagina than the continuous suture for an impairment of 50%, 90% and 100% (total rupture) (Table 1). The simple suture allows more freedom of the implant since it is only fixed in a set a loose point rather than a continuous suture (continuous stitch).

Table 1. Supero-inferior displacement of the vagina, during Valsalva maneuver, after implantation with different anchoring points (simple and continuous suture).

VariableSupero-inferior displacement of the vagina (mm) - USLs Implant			
	Simple	Continuous	Variation (%)
Impairment 50%	7.61	6.92	9%
Impairment 90%	8.78	7.90	10%
Total rupture	10.17	9.25	9%

4. Discussion and Conclusions

The simulations showed that there was a variation of the supero-inferior displacement of the vaginal wall between different anchoring techniques being approximately of 10% for the simulation USLs implant.

5. References

1. Z. Guler and J. P. Roovers. *Biomolecules*, 12: 1, 2022.
2. FDA. <https://www.fda.gov/news-events/press-announcements/fda-takes-action-protect-womens-health-orders-manufacturers-surgical-mesh-intended-transvaginal>, 2019.
3. K. L. Shek et al., *Ultrasound Obstet. Gynecol.*, 42, 699–704, 2013.

Acknowledgements:

The authors gratefully acknowledge funding from project SPINMESH-POCI-01-0145-FEDER-029232, financed through FCT. This work was supported by FCT, through INEGI, under LAETA, project UIDB/50022/2020 and UIDP/50022/2020.

4.3

Exploiting computational modelling to investigate the in-vitro performance of bioresorbable wire-braided stents

Agnese Lucchetti¹, Alissa Zaccaria², Thomas Gries¹, Ted J. Vaughan³

¹ Institut für Textiltechnik of RWTH Aachen University, Aachen, Germany

² Consorzio Intellimech, Bergamo, Italy

³ Biomedical Engineering and Biomechanics Research Centre (BMEC), School of Engineering, College of Science and Engineering, National University of Ireland Galway, Galway, Ireland

1. Introduction

Bioresorbable stents are a promising alternative to permanent metallic devices since they can provide vessel support for the time required and be subsequently naturally degraded. Challenges are still present with polymeric bioresorbable stents since they show lower mechanical properties compared to their metallic counterparts. The use of finite element models allows to obtain a wide understanding of the device mechanical performance in time and cost effective ways. Each model needs to be validated through appropriate comparison with in-vitro test results. This has rarely been carried out for bioresorbable braided stents [1]. The present work aims at building a verified computational model of different in-house manufactured braided polymeric stents with the goal to have a framework allowing further stent optimization.

2. Materials and Methods

Three different braiding patterns, namely 1:1-1, 2:2-1 and 1:1-2 [2] (Fig 1a), were reconstructed with a Matlab code by Zaccaria et. al [3] and imported into Abaqus/Explicit software as meshes of beam elements. Both parallel plate (PP) and radial compression (RC) tests were simulated (Fig 1b). In the tests, the stents were compressed/crimped to reach the 50% of their initial diameter. The mechanical properties of poly-L-lactic acid were determined from tensile testing of single wires. The wire-wire and stent-setup friction coefficients were assigned as a penalty after a fitting process. The computational outcomes were verified by comparison with experimental curves derived from mechanical tests.

3. Results

From the friction coefficient analysis, it could be observed that the curve hysteresis mainly depends on friction between the stent and the plates, while internal friction between the stent wires plays a minor role. A unique friction coefficient was not identifiable for all the three geometries simulated. As showed in Fig 1c-d, a good fitting was found for the parallel plate compression test as well as for the radial test. The force at maximum compression (for PP), radial stiffness, chronic outward force and radial resistive force (for RC) are well represented.

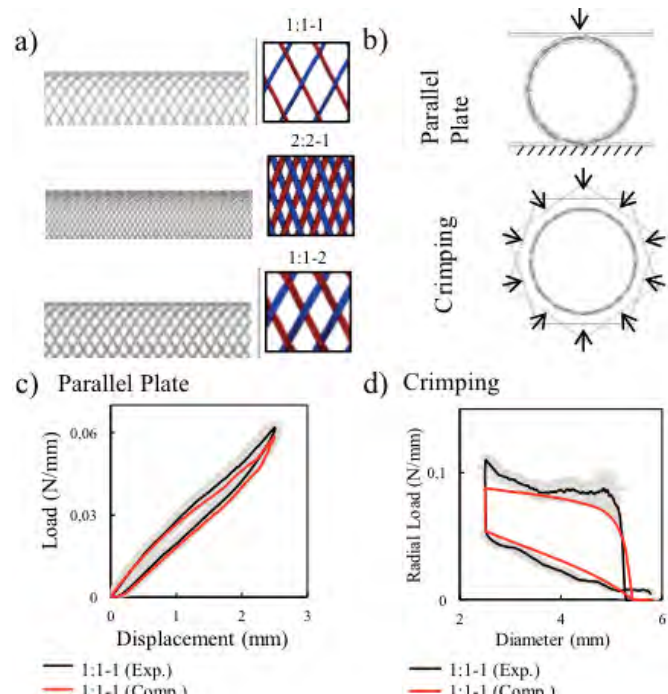


Fig 1: (a) Braiding patterns; (b) parallel plate and crimping test schematics; (c) example of parallel plate and crimping (d) tests results.

4. Discussion and Conclusions

This study developed and experimentally-verified a computational model that could provide an additional insight on the mechanical properties and potentialities of PLLA bioresorbable braided stents. This could be also used as a framework for further mechanical properties optimization to decrease the performance gap between the current bioresorbable braided stents and their metallic counterparts.

5. References

1. Zhao et al, *JMBBM*, 2019.
2. Kyosev, 2015.
3. Zaccaria et al, *J Biomech*, 2020.

Acknowledgements:

This project has received funding from the European Union's Horizon 2020 research and innovation programme under grant agreement No 813869.

4.4

High-fidelity model of the TEVAR procedure: patient-specific cases

Anna Ramella¹, Francesco Migliavacca¹, José Félix Rodriguez Matas¹, Francesca Dedola², Michele Conti³, Frederic Heim⁴, Sara Allievi², Daniele Bissacco², Maurizio Domanin², Santi Trimarchi², Giulia Luraghi¹

1 Politecnico di Milano, Italy

2 Università degli Studi di Milano, Italy

3 Università degli Studi di Pavia, Italy

4 Université de Haute Alsace, France

1. Introduction

Thoracic Endovascular Aortic Repair (TEVAR) is a minimally invasive technique to treat thoracic aorta pathologies, as aneurysm or dissections [1]. Despite its increasing use, many influential factors are still to be understood and require a continuous investigation.

Computational models play a key role in procedural planning and must be reliable [2]. In this work, high-fidelity simulations of the procedure with one commercial stent-graft are developed and used to virtually replicate the deployment in two patients.

2. Materials and Methods

The geometry of one commercial thoracic stent-graft models was discretized with beam (stent) and membrane (graft) elements. Experimental radial crimping tests were performed on the stent-graft to calibrate and then validate the superelastic Nitinol (stent) and the linear elastic fabric PET (graft) material parameters. Pre-stress due to a nominal diameter oversizing of the stent was considered to realize the device model [3]. The stent-graft was experimentally deployed into a 3D silicon aortic phantom under CT scan, and it was virtually reproduced with a finite-element simulation for validation purpose. Finally, the validated model was used to model patient-specific TEVAR cases, in presence of an aneurysm or a dissection.

3. Results

The final configuration of the deployment simulation is depicted in figure 1. A qualitative comparison is managed by superimposing the stent configuration from the simulation (in red) and from the segmentation (in grey). The local Opening Area (OA) for each ring is computed and the error (e_{OA}) between in vitro and in silico is always below 4%. The application of the TEVAR model in two different patients suffering from aneurysm and dissection is shown in figure 2.

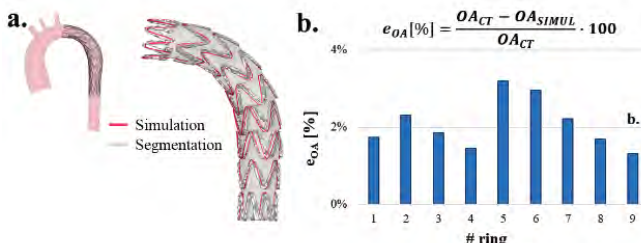


Figure 1: (a.) Deployment simulation result and validation study with qualitative (b.) and quantitative (c.) comparison between in vitro (CT) and in silico TEVAR in terms of opening area (OA).

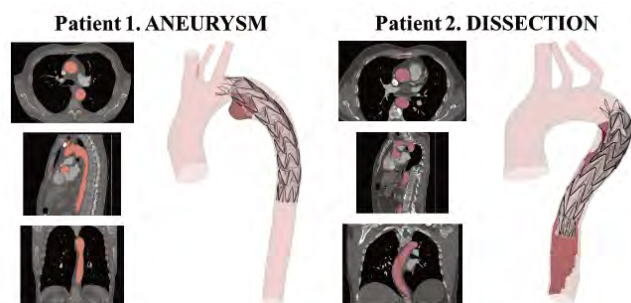


Figure 2: Patient specific TEVAR simulations

4. Discussion and Conclusions

The development of high-fidelity stent-graft numerical simulations can be useful to improve the procedure and/or to design and optimize new devices. The innovative aspects regarding the TEVAR model are the graft material modeled as a fabric material (validated with experimental tests), the real device tracking modeling and the quantitative validation. In conclusion, the development of realistic and accurate TEVAR patient-specific models can be used as a support for clinical decisions before the implantation.

5. References

- Daye et al., *Cardio Diagn & Ther*; 8:S138 (2018).
- Viceconti et al., *Methods*; 185:120-127 (2021).
- Concannon et al., *Biomech Mod Mech*; 20:2373-92 (2021)

Acknowledgements:

This project has received funding from the MIUR FISR-FISR2019_03221 CECOMES.

4.5

On the credibility of finite element modelling of self-expanding nickel-titanium stents: verification and validation activities

Martina Bernini¹, William Ronan¹, Ted Vaughan¹

¹ National University of Ireland, Galway, Biomechanics Research Centre (BMEC), School of Engineering and Informatics, Galway, Ireland

1. Introduction

Finite element (FE) models are widely employed in literature to predict the behaviour of self-expanding Nickel-Titanium (NiTi) stents [1, 2]. Given the increasing complexity of these models, a systematic assessment of their credibility is necessary. In this study, a series of verification and validation (V&V) activities were performed based on the V&V-40 ASME [3] for computational modelling of medical devices. Their relevance towards several contexts of use (COU), namely radial compression response (COU-1), stent deployment in a vessel (COU-2) and fatigue-life prediction (COU-3), was assessed.

2. Materials and Methods

A FE model of the Zilver (Cook® Medical) stent was developed with Abaqus/Explicit (SIMULIA, Dassault Systèmes). An in-built material law [4] was used to describe the superelastic behaviour of NiTi, with parameters calibrated on bench tests on the real devices. V&V activities [3] were performed, ranging from verification, sensitivity analysis and validation with in vitro comparators. Verification activities assessed the influence of spatial and temporal discretization, and element formulation on global and local outputs (forces and stress and strain distributions) for each COU. Sensitivity of model input parameters investigated the effects of a variation of stent geometrical and material parameters on radial performance (COU-1). Validation was assessed for COU-2 with the comparison of stent deployment configuration with in vitro experiments of stent implantation in a straight silicone vessel and in 3D-printed resin geometries of realistic arteries, accounting several testing conditions (e.g., stent sizes).

3. Results

Verification: spatial and temporal discretization showed relevant influence on global and local outputs for COU-1 and COU-3, while minimal effects for COU-2 were found. Sensitivity analysis: effects on global and local outputs for COU-1 were less than input variation on geometry and material parameters. Validation: comparison with in vitro tests demonstrated the capability of predicting qualitatively the configuration of the device, and clinically-relevant metrics within a certain level of accuracy.

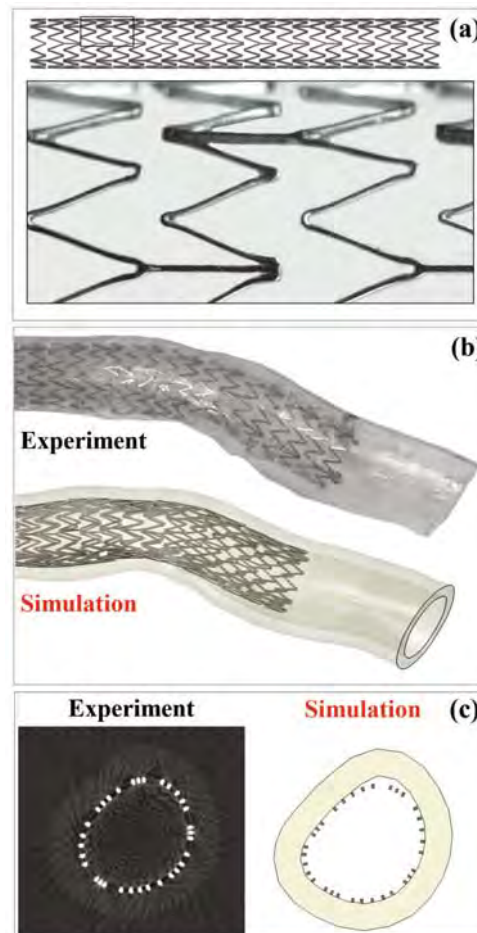


Figure 1. (a) Stent FE model with detail of real device; FE model and in vitro comparator for COU-2 with deployment configuration (b) and cross-section comparison (c).

4. Discussion

V&V activities were addressed for FE modelling of NiTi cardiovascular devices, with attention at their relevance within common COUs. The study offers an example for the development of complex numerical model of similar devices and for guiding the choice of proper verification and validation activities.

5. References

- [1] Gökgöl C et al., *Ann. Biomed. Eng.* 43, (2015).
- [2] Conti M. et al., *Meccanica* 52, (2017)
- [3] ASME, V&V 40 (2018)
- [4] Auricchio F et al., *Comput. Meth. Appl. Mech. Eng.* 146, (1997).

Acknowledgements:

This study is part of the BiolImplant ITN project, which has received funding from the European Union's Horizon 2020 research and innovation programme under grant agreement No 813869.

4.6

Performance assessment of braided venous stent designs through computational modeling

Rene Ubachs¹, Scott Smith², Jake P Mertens², Olaf van der Sluis^{1,3}

1 Philips, Research, Eindhoven, Netherlands

2 Philips, Image Guided Therapy Devices, Maple grove, United States

3 Eindhoven University of Technology, Eindhoven, Netherlands

*Rene.Ubachs@Philips.com, Philips Research, High Tech Campus 34, 5656 AE Eindhoven, The Netherlands

1. Introduction

The application of stents in the venous system is increasing. Where arterial stents have been used and developed for many decades, specific venous stents have not received the same level of attention while their requirements are clearly distinct from arterial stents.

Here, computational modelling has been used to quantify the performance of braided stents for the venous system and develop an optimization tool for their design.

2. Materials and Methods

Explicit finite element models have been created of venous stents which are modelled using beam elements. Beam elements provide an efficient alternative to full 3D solid elements and the braided wire stent geometry is very suited for this approach [1,2]. To avoid unphysical behavior, wire crossovers are modelled with a contact algorithm including friction.

Crush resistance is evaluated using cylinder crush tests resembling May-Thurner syndrome type loading on free stents, Fig. 1, and stents deployed in an artificial vein. Chronic outward force is assessed and conformability is investigated by deploying the stent in a 90 degrees angled tube and assessing wall apposition.

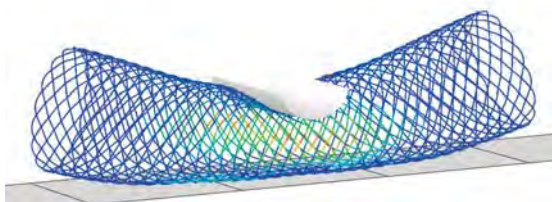


Figure 1: Cylinder compression of an end-looped braided stent.

Based on performance parameters for venous stents, tests have been selected and suitable metrics defined.

The created models have first been validated by comparing with bench test measurements, followed by an investigation of the influence of different design parameters: stent length and diameter, wire diameter and amount, winding angle, end type (open or looped).

3. Results

Wire diameter and winding angle are found to be critical design factors for local crush resistance, while stents with looped ends exhibit significantly higher chronic outward force and better conformability. Friction is observed to play a key role in the deformation behavior of braided stents, Fig. 2 which is also affected by being deployed in a vein, Fig. 3.

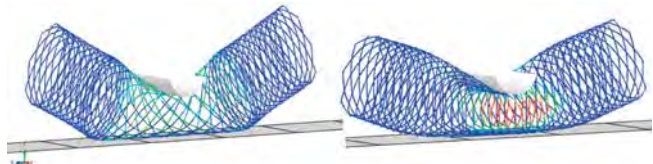


Figure 2: Effect of friction, low (top) vs high (bottom), on stent deformation.

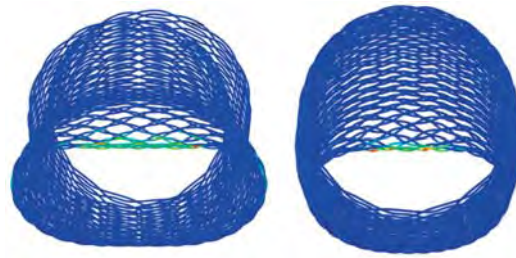


Figure 3: Front view of a cylinder compression test on a stent on bench (left) and a stent-in-vein on bench (right).

4. Discussion and Conclusions

Using validated computational modelling for the evaluation of stent performance provides a significant advantage in creating insight in the stent behavior. The modeling strategy proposed here allows for fast quantified evaluation of design features, facilitating optimal stent design.

5. References

1. Záhora J. et al., *Physiol Res* 56, 2007.
2. Auricchio F. et al., *Med Eng Phys* 33(3), 2011.

4.7

TEE-based Simulation Study on the Influence of Transcatheter Edge-to-Edge Device Position on Diastolic Hemodynamic Parameters

Katharina Vellguth¹, Lars Walczak^{1,2} and Leonid Goubergrits^{1,3},

1 Charité - Universitätsmedizin Berlin, Institute of Computer-assisted Cardiovascular Medicine, Berlin, Germany

2 Fraunhofer MEVIS, Bremen, Germany

3 Einstein Center Digital Future, Berlin, Germany

1. Introduction

Transcatheter edge-to-edge repair (TEER) is the leading treatment strategy for patients with mitral regurgitation (MR) and prohibitive operational risk [1]. Procedure planning is difficult with regard to estimation of residual MR and iatrogenic stenosis and no tools are available to support this to date. The objective of this study is to systematically vary the TEER device position by using virtual therapy based on patient-individual mitral valve geometries and evaluate the effect on diastolic hemodynamic parameters.

2. Materials and Methods

Patient-specific anatomies (10 Patients, age: 57 ± 8 years) of the left ventricle (LV) and mitral valve (MV) were segmented from 3D echocardiography data (TEE) and virtually treated with TEER by means of a position based dynamics approach [2]. The device position was defined as shown in Fig. 1 at lateral, central and medial position, respectively. Patient-specific boundary conditions are adjusted such that conditions of rest and moderate stress are represented. A total of 70 computational fluid dynamics (CFD) simulations were performed on pre- and post-interventional geometries using STAR-CCM+ with patient specific boundary conditions [3].

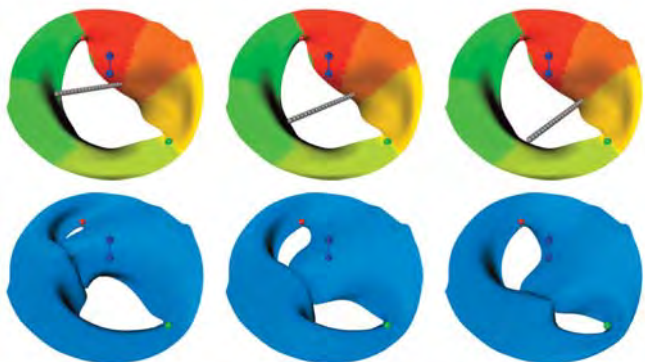


Figure 1: Virtual TEER of patient specific mitral valve geometry at lateral, central and medial position. The systematic placement definition is shown in the upper row while the lower row shows the results after virtual device placement.

3. Results

Simulated maximum velocities (v_{max}) and diastolic mitral pressure gradient (MPG) can be estimated on basis of the peak E-wave blood flow rate and the mitral valve area (MVA) only ($R^2 > 0.7$). Further, central device positions lead to significantly stronger reduction of MVA and correspondingly to a more severe increase in v_{max} and MPG: MVA reduce to 40% of the pre-interventional area for eccentric (lateral and medial) device positions, while central device placing leads to a reduction to 34%.

At rest, v_{max} increase from to 2.20 ± 0.38 m/s after central TEER and to 1.94 ± 0.60 m/s and 1.97 ± 0.32 m/s after lateral and medial device placing. MPG rises from 1.46 ± 0.63 mmHg to 16.30 ± 9.00 mmHg after virtual TEER. Central device positions lead to an approx. 5 mmHg larger increase than eccentric positions.

4. Discussion and Conclusions

The results show, that central TEER device positions lead to a higher risk of iatrogenic stenosis than eccentric positions. However, to obtain successful treatment outcome, individual pathologies and characteristics of the patient's mitral valve must also be taken into account when planning the device position.

The estimation of MPG on basis of blood flow rates and MVA can help to assess the individual risk of iatrogenic stenosis, e.g., regarding borderline cases or when considering the implantation of a second TEER device.

This study was limited by basing on pre-interventional data only. The approach needs to be validated with real post-procedural data after TEER.

5. References

1. Vahanian A. et al. Eur. Heart J. 43 561-632 (2021)
2. Walczak L. et al. Computer Graphics Forum 41 270–287 (2020).
3. Vellguth K. et al. JCARS 13 1795-1805 (2018)

4.8

Developing a SAPIEN-3 TAVI FEM/FSI model considering VVUQ frameworks to establish model credibility

Nils Götzen¹, Tahir Turgut¹, Omar Zahalka¹, Vincent Bouwman¹, Salvatore Pasta²

1 4RealSim Services BV, IJsselstein, Netherlands

2 University of Palermo, Department of Engineering, Palermo, Italy

Corresponding author: Dr.-Ing. Nils Götzen, email: nils@4realsim.com, Groene Dijk 2B, 3401 NJ IJsselstein, The Netherlands

1. Introduction

An FEM/FSI model of the SAPIEN 3 TAVI device was build, following a hierarchical VVUQ approach. This model will be used during later project stages in virtual hydrodynamic assessments and patient-specific in-silico clinical trials. We report on the modelling and simulation strategies while complying with relevant V&V standards [1,2], ISO standards [3], and internal risk-based VVUQ Master Plan with Question of Interest and Context of Use specifications.

2. Materials and Methods

A fully parametric FEM model was developed in Abaqus (Dassault Systèmes, version 2021) for two device sizes (ND23 &26), based on available literature, datasheets, and limited direct measurements. The device comprises all relevant components: the stent frame; the leaflets; the skirt; the balloon delivery system (Fig 1). Modelling simplifications, such as beam-modelling, were introduced where appropriate and sufficiently accurate.

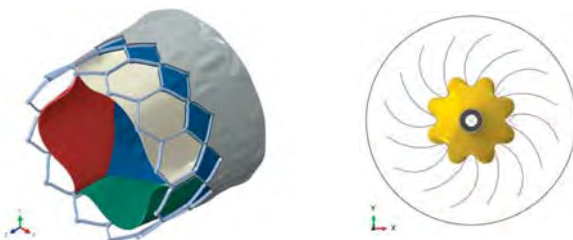


Figure 1: Sapien 3 model and associated balloon delivery system (during simulated folding process).

All individual components and the final assembly underwent a thorough verification processes. Separate model validations were conducted with respect to the different functions of the device components: quasistatic leaflet closing mechanics; and stent crimping/expansion mechanics plus radial stiffness. Due to the limited access to SAPIEN-3 devices/test-data, comparator data were taken from the literature exclusively [4,5].

Extensive UQ and SA considering all key-parameters were conducted using surrogate modelling and Monte Carlo simulations (Fig 2).

3. Results

The fully parametrized model revealed several challenges related to model verifications using explicit solver techniques. The validation was considered successful for stent mechanics, with an relative error of 1.6-8.4% (acceptance level 5.0%), while the error for the leaflet mechanics was significantly above the acceptance limit. SA helped to identify which parameters contributed mostly to the lack of agreement. A model iteration and subsequent UQ/SA will follow.

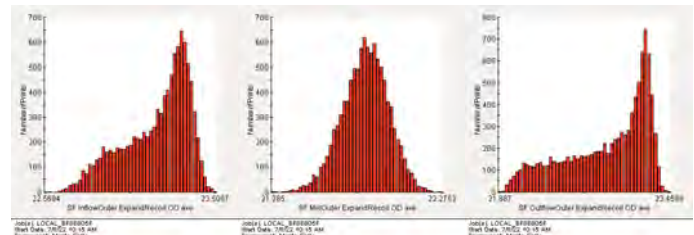


Figure 2: computed probability density functions for the stent frame outer diameters after recoil.

4. Discussion and Conclusions

A model development and validation without having access to all the necessary model & test data is technically impossible. Nevertheless, we demonstrate the added value of conducting a thorough VVUQ program to establish the needed model credibility.

5. References

1. ASME V&V 10-2016
2. ASME, V&V 40-2018
3. ISO 5840-1:2021(E)
4. Abbas M et al., *J Biomech.* 2018;76:27-34
5. Sathananthan J. et al., *JACC: Cardiovascular Interventions*, 2018;11(17):1696-1705

Acknowledgements:

This work is part of the SimInSitu project, which is fully funded by the EU (GA no.: 101017523).

5.1

Definition of intended learning outcomes for in silico trials

Els De Swerdt¹, Jos Vander Sloten², Guy Van Looy³

1 KU Leuven, Division of Biomechanics, Faculty of Engineering Sciences, Sint-Niklaas, Belgium

2 KU Leuven, LRD, Division of Biomechanics, Faculty of Engineering Sciences, Heverlee, Belgium

3 KU Leuven, Faculty of Engineering Sciences, Educational Support, Heverlee, Belgium

Els De Swerdt (els.deswerdt@kuleuven.be)

1. Introduction

Physics-based and/or data-driven computer modeling and simulation (CM&S) gain importance in cardio-vascular, musculoskeletal, immuno-therapeutic, neurological and pharmaceutical applications. Goal of the In Silico World project is to lower barriers in the adoption of in Silico Trials (IST). This paper describes the process how this project is defining Intended Learning Outcomes (ILO) for training and retraining of multiple stakeholder categories.

2. Methods

The education related work package is defining ILO through the organization of ILO workshops. ILO are a statement of what a student will know and be able to do at the end a course module. [1] During the workshop we make use of a Miro board [2] in order to collect training needs and to translate them into draft ILO. The workshop is organized in three parts:

1. Brainwriting of training needs
2. Grouping and prioritization
3. Formulation of ILO



Figure 1: Miro Brainwriting board

Every column of the brainwriting board in figure 1 stands for ONE combination of a stakeholder category and one particular training need. Training needs are being prioritized based on importance on one hand and the difficulty in cognitive process dimension on the other hand (e.g. creation is more challenging than applying or understanding). In order to formulate ILO, we apply a revision of Bloom's Taxonomy of Educational Objectives created by Rex Heer from Iowa State university [3]. A statement of a learning objective contains a verb and an object. The verb refers to the cognitive process, the object describes the type of knowledge the students need to acquire (factual, conceptual, procedural).

3. Formulation of ILO (examples)

1. Biomedical engineering students are able to construct physics-based models. They can specify the purpose, the outcome and use. They reflect critically upon those models. Prior knowledge is finite elements method and/or fluid dynamics.
2. Biomedical engineering students can apply data-driven models. They may contribute in building data-driven models. They should be able to select appropriate AI method. Prior knowledge is relevant about math, linear algebra, programming and neural networks.
3. Biomedical engineering students need to be able to assess credibility by performing verification and validation.
4. Students, academics, industry, hospitals need to be aware of and to comply to ethical and legal requirements.
5. The medical devices and pharma industry management need to judge the effectiveness of IST solutions versus traditional ones. They need to integrate IST solutions into their business.

4. Discussion and Conclusions

ILO definition is an iterative process during which multiple stakeholder groups will be involved. The Miro Brainwriting board is a useful tool to achieve this.

5. References

1. Greensted and Hommel (2014). Intended Learning Outcomes: Friend or Foe? EFMD Global Focus
2. Miro | Online Whiteboard for Visual Collaboration
3. Heer, R. (2012). A Model of Learning Objectives. Iowa State University.

Acknowledgements

The authors acknowledge the EU funded project In Silico World (grant number 101016503).

5.2

C4Bio: Community challenge towards consensus on characterization of biological tissue

Nele Famaey¹, Heleen Fehervary¹, Ali Akyildiz², Karine Bruyère-Garnier³, Yoann Lafon³

¹ KU Leuven, Mechanical Engineering, Heverlee, Belgium

² Erasmus MC, Biomechanics Laboratory, Netherlands

³ Univ Lyon, Univ Gustave Eiffel, Univ Claude Bernard Lyon, LBMC, Lyon, France

1. Introduction

Credible numerical simulations require reliable input parameters, assessed through model calibration evidence [1]. However, the focus of this model calibration evidence currently lies in assessing the quality of fit between the model and the experimental data. Less attention is given to assessing the quality of the experimental data itself. How can a numerical analyst, or e.g. the notified body evaluating an in silico trial, assess the quality and uncertainty of the experimental dataset used to calibrate the model parameters?

Literature abounds with studies on experimental characterization of the material behaviour of various types of biological tissue, but meta-analysis suggests a disconcerting degree of variability in results as well as in methodology. Indeed, there are currently no standards available for testing the material properties of biological tissue, be them mechanical, thermal, electrical or other. Moreover, a quantitative analysis of the degree of methodological variability has, to our knowledge, never been attempted and is an essential step towards proper uncertainty quantification (UQ) in model credibility assessment.

2. Materials and Methods

The Virtual Physiological Human institute together with the Avicenna Alliance and FIBEr are taking the first steps to quantify the degree of methodological variability and work towards a community consensus of methods for biological tissue characterization, in the so-called C4Bio initiative. A pilot testing campaign was initiated in 2021, focusing on uniaxial tensile testing of porcine aorta. In phase 1, expert labs from all around the globe were asked to perform uniaxial tensile tests on the same type of material, using their preferred methodology. To this end, carefully prepared sets of porcine aorta and synthetic material were shipped in dry ice to 25 participants all over the world. In phase 2, we evaluated these results and defined a consensus methodology with all participants. In phase 3, we redistributed the same type of material to the expert labs, who now performed the experiments using the consensus methodology.

3. Results

Statistical analysis of the results showed that in both test rounds, the variability in test results was large, with coefficients of variation in the order of 100%. A slight improvement could be observed in the second round, which had less outliers and decreasing variability for a number of the evaluated output parameters. Further analysis suggests that uncertainty of sample thickness measurement is a major contributing factor to the overall variability.

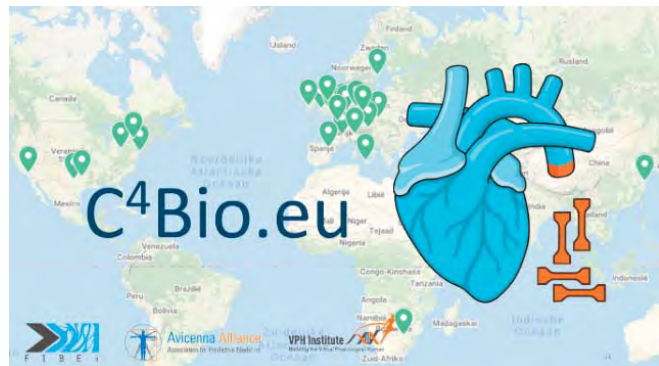


Figure 1: C4Bio around the globe. The green markers indicate the locations of the expert labs participating in the pilot campaign.

4. Discussion and Conclusions

Even for a relatively simple method like uniaxial tensile testing, the methodological variation between expert labs is staggering. Even a consensus protocol only resulted in a slight decrease in variability. This first C4Bio campaign serves as a proof of concept, as well as a wake-up call that credible simulations require credible experimental datasets. Through community effort we should aim to increase the quality and reduce the uncertainty of such datasets to a workable level, for various tissue types and characterization methods.

5. References

- ASME V&V 40 (2018). *Assessing Credibility of Computational Models Through Verification and Validation: Application to Medical Devices*. Washington, DC: Standard, American Society of Mechanical Engineers.

Acknowledgements:

This work was financially supported by the Avicenna Alliance, VPH and FIBEr. We gratefully acknowledge each of the participating labs, who performed the experiments at their own expense, and contributed to the group discussions and consensus protocol. A list of contributors can be found on C4bio.eu.

5.3

Pressure estimation in physiological brain geometry from magnetic resonance elastography data

Felipe Galarce¹, Alfonso Caiazzo¹, Karsten Tavelow¹, Joerg Polzehl¹, Ingolf Sack²

1 Weierstrass-Institut für Angewandte Analysis und Stochastik. Leibniz-Institut im Forschungsverbund Berlin, Berlin, Germany

2 Charité – Universitätsmedizin Berlin, Department of Radiology, Berlin, Germany

1. Introduction

We introduce a numerical framework for the estimation of pressure gradients in the human brain using Magnetic Resonance Elastography (MRE) data. The method relies on a variational data assimilation approach which allows to combine the available observations with an underlying poroelastic tissue model. The approach is designed to handle uncertainty on model parameters, as well as partial availability of measurements. Validation on a physiological human brain geometry using synthetic MRE data is shown, showing the potential of the method to the medical community as a tool to assess the brain function.

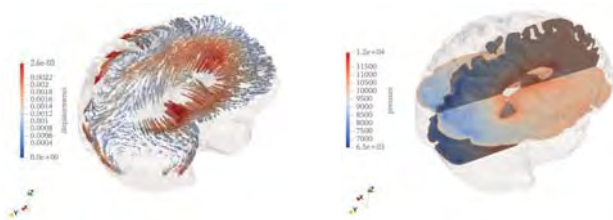


Figure 1: Snapshot of a forward solution: Displacements field on a cross section (left); Pressure view on two cross sections (right).

2. Material and Methods

The core of the data assimilation procedure follows the approach by Maday [1]. Let H be a Hilbert space where the reconstruction is sought. The space is endowed with the inner product $\langle \cdot, \cdot \rangle$ and norm $\|\cdot\|$. The MRE input data is modelled as

$$l_i = \langle u_{\text{true}}, \omega_i \rangle, i=1,\dots,3m,$$

for a set of m voxels. The observation space W is the space spanned by the Riesz representers ω_i , meaning that any observed state u_{true} can be interpreted as the projection: $\Pi_W u_{\text{true}}$.

2.1. Modelling and Simulation

The governing dynamics is based on a linear poroelastic tissue model, following the theory proposed by Biot [2]. The displacement and pressure fields obey the following system of PDEs:

$$\begin{aligned} \alpha \partial_t \epsilon_{ii} + S_e \partial_t p - \frac{\kappa}{\mu} \Delta p &= 0 \\ \rho \partial_{tt} u - \nabla \cdot (\lambda_s \epsilon(u) + \mu_s I \epsilon_{ii}(u)) + \alpha \nabla p &= 0 \end{aligned}$$

where ρ , α , S_e , λ_s , κ , μ_s , T and μ are real model parameters and $\epsilon(u)$ is a linear strain tensor. The equations are solved using finite elements within a physiological brain geometry obtained from medical images (Figure 1).

The governing equations are sampled within a physiological range of parameters to build a manifold of solutions. From this PDE-informed manifold, a reduced space V_n is computed via a Proper Orthogonal Decomposition.

The optimisation algorithm to reconstruct both states by fitting model and measures reads as follows:

$$\begin{aligned} u^* &= \operatorname{argmin}_{u \in H} \|u - \Pi_{V_n} u\| \\ \text{s.t. } l_i &= \langle u, \omega_i \rangle, i = 1, \dots, m. \end{aligned}$$

that holds the property $u^* \in V_n \oplus W \cap V_n^\perp$.

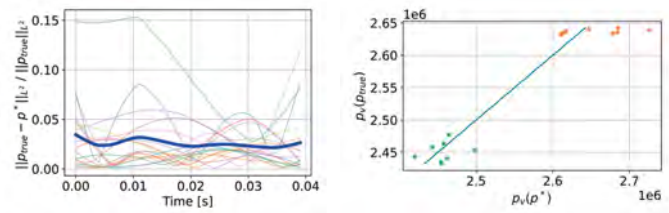


Figure 2: Left: Validation of the accuracy of the pressure reconstruction. Right: Characterization of healthy and pathological cases based on reconstructed ventricular pressure.

4. Results

The data assimilation algorithm is tested on 16 different in silico patients, obtaining an average error below the 5% (Figure 2, left). In addition, the methodology is able to cluster healthy from pathological simulations based on the reconstructed ventricular pressure (Figure 2, right).

5. Discussion and Conclusions

We presented a data assimilation algorithm, trained using a PDE model, for the joint reconstruction of poroelastic displacements and pressures in the human brain. We show preliminary results for the estimation of pressure dependent biomarkers from partial MRE data.

5. References

1. Maday Y, Patera A.T, Penn J.D. and Yano M. *Int. J. Num. Methods Engr.* 2014;102(5):933-965
2. Biot M.A. *The Journal of the Acoustical Society of America*: 1956;28(2)

5.4

Agent-based digital twin simulations of denosumab treatment, discontinuation and placebo scenarios explore the role of osteomorphs

Charles Ledoux¹, Daniele Boaretti¹, Jack Kendall¹, Ralph Müller¹, Caitlyn Collins²

¹ Institute for Biomechanics, Zürich, Switzerland

² Virginia Tech-Wake Forest University School of Biomedical Engineering and Sciences, Blacksburg, United States

Corresponding author: Professor Caitlyn J. Collins, caitlyn.collins@hest.ethz.ch

1. Introduction

Incidence of osteoporosis (OP) is increasing with our aging population. Denosumab, a common treatment for OP, is a monoclonal antibody that binds to RANKL and thus reduces osteoclastogenesis, osteoclast-mediated bone resorption and remodelling rates. Upon cessation of treatment, however, resorption rises quickly to levels even higher than baseline and thus rapid bone loss occurs [1], perhaps due to accumulation of osteoclast precursors during treatment [2]. Further, the recent discovery of osteomorphs, recyclable cells in the marrow resistant to low RANKL concentration, suggests that current OP treatments do not target all the relevant cell-types associated with bone resorption [3]. The goal of the current work is to investigate these cell-cytokine dynamics using patient-derived agent-based models of bone remodelling.

2. Materials and Methods

Starting from 7 micro-CT scans of iliac crest biopsies from postmenopausal women (age: 72 ± 5 years) [4], digital twin simulations were run for 4 years of pbo vs 2 years of denosumab with an additional 2 years of follow-up without treatment and for 3 years of treatment vs placebo using a micro-multiphysics agent-based (micro-MPA) model [4] for comparison with clinical trials [1] and [2], respectively. Briefly, bone and marrow cells (including osteomorphs) are represented as agents on a voxel-based lattice derived directly from the micro-CT data; cells are motile and capable of producing or resorbing tissue and cytokines. Both sets of digital twin simulations were run with and without explicit inclusion of osteomorphs following preclinical data on osteomorph dynamics[3].

3. Results

Bone volume fraction dropped rapidly starting 6 months after the last denosumab injection and stabilized below baseline but above placebo levels by month 48 for the simulated iliac crest micro-MP models with and without osteomorphs, matching in vivo trials. Without osteomorphs, cell numbers were inconsistent with in vivo data; after 3 years of denosumab treatment, the mean ratio of osteoclast precursors in the marrow of the treatment vs placebo cases was 1.84 in clinical patient data [2], 2.43 in simulations w/o osteomorphs and 1.78 in simulations with osteomorphs.

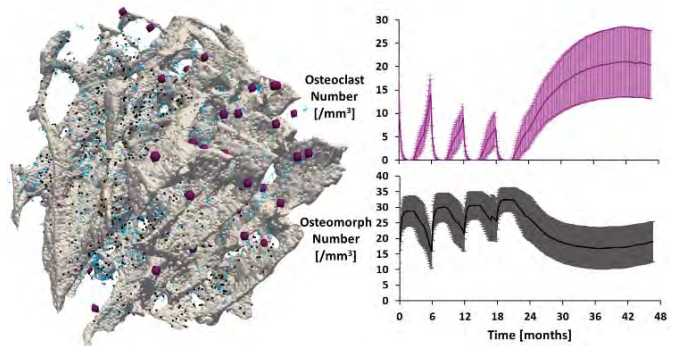


Figure 1: Clasts (violet), clast precursors (blue) and morphs (black) after 3 years of denosumab and clast and morph numbers during 2 years of denosumab followed by 2 years without treatment (right)

4. Discussion and Conclusions

With and without osteomorphs, the digital twin simulations using the micro-MPA model reproduced trends in bone mineral density observed experimentally after withdrawal of denosumab. The accumulation of preosteoclasts more closely matched in vivo measurements when osteomorphs were explicitly included as an additional cell type in the model. These simulations showcase the possible uses of digital twin simulations for hypothesis tests, clinical trial design and personalized treatment.

5. References

1. Bone et al J Clin End & Met 96(4):972-80 (2011)
2. Fontalis et al Bone Reports 13:100457 (2020)
3. McDonald et al. Cell 184(5):1330-1347 (2021)
4. Tourolle et al. JBMR Plus 5(6):e10494 (2021)

Acknowledgements:

Swiss National Supercomputing Centre (s1070) and Euler compute cluster at ETH Zurich.

5.5

Neural network simulation based finite element modeling of heart mechanics

Wenbo Zhang¹, Michael Sacks²

¹ University of Texas at Austin, Oden Institute, Austin, United States
² University of Texas at Austin, Biomedical Engineering, Austin, United States

1. Introduction

Computational modeling has been a major approach for understanding cardiac function in health and disease. The governing equations for the underlying mechanism of biomechanics and electro-mechanics are partial differential equations (PDEs). To develop high-fidelity finite element (FE) models of the heart, structurally informed material models, local myofiber structure and imaging-based geometry are essential. Digital twin approaches have been advocated for a heart models (1). However, high-fidelity simulations remain infeasible to evaluate numerous treatment scenarios in clinically relevant time frames.

To this end, we have recently developed a neural network-finite element approach for simulations of passive myocardium (2). In the present work we demonstrate a first step in translating this approach to the functional heart. We take advantage of the fact that development of ventricular model can be facilitated by the differentiable FEs based on open-source software libraries to backpropagate gradient information to neural networks.

2. Materials and Methods

To train the neural network model we employed a physics-based approach. The active stress generally cannot be derived from a potential, so we cannot use the potential formulation as the passive behavior. To address this challenge, we develop the training algorithm that drives the PDE residuals to zeros. The variations of the virtual work δW with respect to the nodal values of the test function yield the residual force vector R . Our aim is to drive the residual to zero for all instances of the training dataset M . We sample N realizations of the M . This means solving the nonlinear equations corresponding to the stationary equations for the variational problem. We then implemented a differentiable finite element library using Google Jax to streamline the computational pipelines with neural network surrogate model. We consider a prolate spheroidal model of the left ventricle (Figure 1-a). The domain is discretized using unstructured tetrahedron elements. The fiber geometry was based on an approximagine the -60 to 60 degree transmural gradient, and a Fung-type material model with constants taken from the ovine heart used (Figure 1-a). The entire pipeline was then trained against a range of pressure-volume loops (Figure 1-b). To verify our differentiable implementation of finite elements, we utilized the finite element method for verification on the same model.

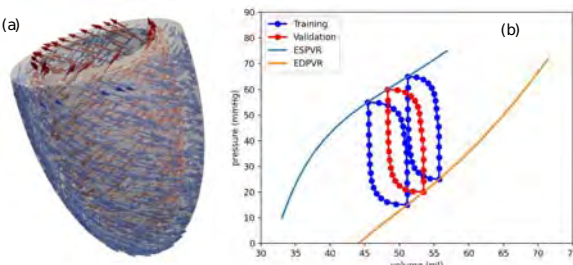


Figure 1: (a) The prolate spheroidal LV model using a Fung-based constitutive model and transmurally varying local fibers. (b) Training EDPVR and ESPVR loops, where the blue points are the training set and the red the predicted validation.

3. Results

The final trained model was able to predict be trained on a range of complete pressure-volume ranges (Figure 1-b, red trace). Moreover, contractile patterns were able to reproduce the finite element 'ground-truth' solution with very high accuracy (mean error < 0.001 mm), as well as key features such as axial torsion (Figure 2).

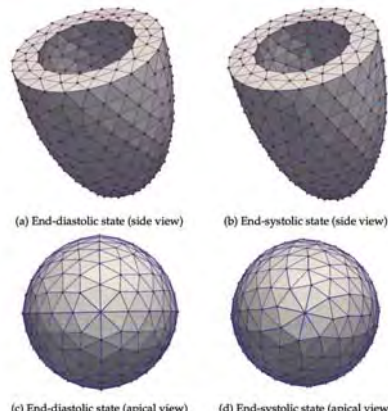


Figure 2: Comparison between the FE solutions (red points) and the neural network predictions (blue wireframes) of the deformed states of the prolate spheroidal model at the end-diastolic state and end-systolic state. Note that the active contraction induced the torsion effects (see apical views in c,d).

4. Discussion and Conclusions

We have developed a novel differentiable neural network surrogate model for the organ-level modeling of the heart. We verified our implementation with widely used finite element library and obtained excellent matches. The present surrogate modeling method is extensible to incorporate advanced material models of myocardium and geometries of the real heart.

5. References

1. S.A Niederer, M.S. Sacks, M. Girolami, K. Willcox, *Nature Comp. Sci.*, Vol 1(5), 2021.
2. W. Zhang, D. Li, T. Bui, and M.S. Sacks, *CMAME*, 2022 (in-press).

5.6

Validation of a Synthetic Cohort of Aortic Stenosis Patients

Jan Brüning¹, Pavlo Yevtushenko¹, Leonid Goubergrits¹

¹ Charité - Universitätsmedizin Berlin, Institute for Computer-Assisted Cardiovascular Medicine, Berlin, Germany

1. Introduction

Image-based modelling for diagnosis and treatment planning for aortic stenosis became increasingly relevant in cardiovascular research. In theory, the method allows non-invasive calculation of diagnostic parameters. Furthermore, prediction of hemodynamic outcome after different treatment strategies is feasible. This approach might help to identify optimal treatment strategies for a patient as well as support development of novel implantable devices.

A relevant problem for translation into clinical or industrial application is the lack of available data sets due to data privacy regulations. A promising approach to mitigate this problem is the generation of synthetic data. This type of data can be shared freely, supporting reproducibility studies and comparison of different in-silico approaches.

However, synthetic data must be validated by demonstrating, that the data matches the cohort it is intended to mimic. In this study, we generated synthetic data of aortic stenosis patients. The data set includes general demographics, functional parameters, and geometries of the aorta and the aortic valve. Peak-systolic hemodynamics of the real patients as well as the synthetic data set was calculated and compared against each other.

2. Materials and Methods

A sample of 101 patients with moderate to severe aortic stenosis was investigated in this study. Using computed tomography image data, the anatomy of the aortic root and ascending aorta was reconstructed. Different geometric parameters as for example AVA, the diameters of the aortic annulus and the sinotubular junction were evaluated.

Using copulas [1], multivariate joint distributions for several demographic, functional and anatomic parameters were identified. Then, a randomized sample of synthetic patients mimicking these distributions was generated. Using a parameterized model, synthetic geometries matching the randomized parameters were generated.

Using computational fluid dynamics, the peak-systolic hemodynamics were calculated. Different parameters as for example pressure gradients, the peak-systolic velocity, and the wall shear stresses in the ascending aorta were calculated for the real and synthetic patients. Agreement between real and synthetic data will be evaluated using descriptive statistics, equivalency tests, and visual inspection of generated surface geometries.

3. Results

Deviations between the randomized parameter values and the synthetic surface geometries were observed. Generated surface geometries matched the parameter distributions of the real patient data. Surface geometries were considered to be plausible by experts. Evaluation of the peak-systolic hemodynamics is still ongoing. If final validation of the synthetic cohorts is successful, the generated data set will be made available.

4. References

1. Nelsen RB. *An Introduction to Copulas*. Springer, New York (1999)

Acknowledgements:

This project has received funding from the European Union's H2020 research and innovation programme under grant agreement N° 101017578. www.simcor-h2020.eu

6.1

Analysis of functionally graded and uniform scaffolds based on mechano-biology and cell diffusion

Mervenaz Sahin¹, Ahmet Fatih Tabak², Gullu Kiziltas Sendur^{3,4}

1 Faculty of Engineering, Materials Science and NanoEngineering, Sabanci University, Turkey

2 Faculty of Engineering, Mechatronics Engineering, Kadir Has University, Istanbul, Turkey

3 Faculty of Engineering, Mechatronics Engineering, Sabanci University, Istanbul, Turkey

4 Sabanci University Nanotechnology Research and Application Center, Istanbul, Turkey

Correspondence author: msahin@sabanciuniv.edu

1. Introduction

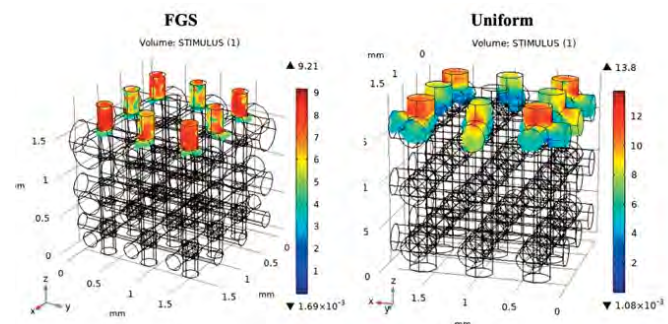
Bone scaffolds are temporary structures that stimulate bone formation by providing the necessary environment for cells to enhance regeneration [1]. Optimized scaffolds with specific porosity, pore size, interconnectivity, and microstructure in addition to material properties are desired to obtain effective healing. A special class of scaffolds mimicking host tissue are functionally graded scaffolds (FGS) proven to meet these requirements leading to effective bone regeneration [2,3]. Different from existing studies in literature, we demonstrate the design of poroelastic FGS based on mechano-biology (MB) simulations using Finite Element Analysis (FEA) incorporating cell diffusion.

2. Materials and Methods

3D scaffold geometries with interconnected pores were modeled as poroelastic materials. Solid mechanics and Darcy's Law modules were coupled via Poroelasticity Multiphysics module in COMSOL software and integrated to the Transport of diluted species module to incorporate cell diffusion. Simulations of the integrated analysis model were conducted via COMSOL with MATLAB scripting environment to allow for iterative updates of the material properties based on cell differentiation and the corresponding MB stimulus (S), which depends on the fluid velocity and octahedral shear strain [4]. Pore diameters of the FGS were assigned between 0.2–0.5 mm while a medium pore size was assigned to the uniform scaffold.

3. Results

Both uniform and FGS structures were analyzed under same cell seeding conditions. Results indicate that the FGS structure induces more bone formation (69.135%) compared to the scaffold with uniform pores (65.279%). Results based on the developed integrated poroelastic model are consistent with results obtained in the work of Boccaccio et al. [5], where under pure compressive loading and including MB, but without considering MSC diffusion, bone formation was slightly higher than in uniform pore scaffolds. Bone formation ability of FGS seem to be further enhanced as suggested by the proposed model incorporating cell diffusion.



4. Discussion and Conclusions

Initial results of MB based analysis including cell diffusion show that tissue differentiation occurs under fluid flow and compressive pressure and FGS geometries seem to support more enhanced bone formation. This analysis model should prove useful to further study the performance of various FGS structures and has the potential to be used in optimization studies for patient specific scaffolds.

5. References

1. Fonseca DR et al, *Biomater. Sci.*, 6:1569-1579 (2018)
2. Hollister S.J. et al, *Biomaterials*, 23: 4095-4103 (2002)
3. Liu F et al, *Materials & Design*, 160: 849-860 (2018)
4. Prendergast PJ et al, *J Biomech*, 30(6):539–48 (1997)
5. Boccaccio A, et al., *PLoS ONE* 11(1):e0146935 (2016)

Acknowledgements:

This work was supported by TUBITAK (The Scientific and Technological Research Council of Turkey) Support Program for Scientific and Technological Research Project Grant, 119M470.

6.2

Inverse calculation of multiscale bone composition out of DXA images

Javier Giráldez¹, Carlos Ruiz Wills¹, Jerome Noailly¹

1 Universitat Pompeu Fabra (UPF), BCN MedTech., Barcelona, Spain, jerome.noailly@upf.edu

1. Introduction

Dual-energy absorptiometry (DXA) is used to diagnose osteoporosis but cannot quantify the relative effects of bone properties at different scales and has limited capacity to predict fragile fracture. Multiscale homogenization theories exploit the universality of bone properties at the nanoscale, to extrapolate extracellular and macroscale tissue properties out of composition and computed tomography (CT) data [1]. In this study, a reverse engineering method is proposed to obtain descriptors of the multiscale composition of bone out of DXA information.

2. Materials and Methods

A genetic algorithm (GA) was used to calculate the following bone properties: vascular porosity (ϕ_{vas}), lacunar porosity (ϕ_{lac}), extracellular density (ρ_{ec}) and volume fractions of hydroxyapatite (f_{HA}), water (f_{H2O}) and organic matter (f_{org}). Properties were determined, according to two models that follow the concept of bone multiscale homogenization [1]:

$$\rho_{macro} = \phi_{vas} * \rho_{H2O} + (1 - \phi_{vas}) * \rho_{ev}$$

$$\rho_{ev} = \phi_{iac} * \rho_{H2O} + (1 - \phi_{iac}) * \rho_{ec}$$

$$\rho_{ec} = f_{H2O} * \rho_{H2O} + f_{org} * \rho_{org} + f_{HA} * \rho_{HA}$$

In a 6-variable model, the GA was constrained with universal relationships between f_{H2O} , f_{HA} , f_{org} and ρ_{ec} at the micro-scale [2] (Fig. 1). A ρ_{macro} was calculated and used as design variable, being compared to an apparent bone density, $\rho_{macroApp}$, calculated out of an ash density, ρ_{AshApp} :

$$\rho_{MacroApp} = 3.69 * \rho_{AshApp} - 0.26$$

$$Fitness = (1 - \frac{\rho_{macro}}{\rho_{MacroApp}})^2$$

ρ_{AshApp} values were extrapolated from DXA images through equivalent CT-based densities provided by the software 3D Shaper® [3]:

$$\rho_{AshApp} = (\rho_{Oct} + 0.05) / 0.98$$

In a 3-variable model, ϕ_{lac} , ϕ_{vas} and ρ_{ec} were directly optimized though the relationship they are expected to share with the Ash density [4]:

$$\rho_{Ash} = (1 - \phi_{vas}) * (1 - \phi_{lac}) * \rho_{ec}$$

$$Fitness = (1 - (\rho_{Ash} / \rho_{AshApp}))^2$$

Then, volume fractions were calculated according to their relationship with ρ_{ec} (Fig.1).

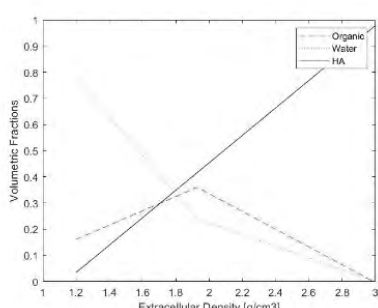


Fig 1. f_{HA} , $f_{(H_2O)}$, and f_{Org} in extracellular bone matrix, as a function of ρ_{ec} . Femur Human range highlighted [2].

3. Results

The 6-variable model with constrained equations could not reach physiological bone properties. However, the 3-variable model with ρ_{Ash} as a design variable led to fitness values of the order of 10-10 and to ρ_{ec} values between 1.85 and 1.95 g.cm⁻³ (Fig.2), within the range of values reported for human bones (Fig. 1).

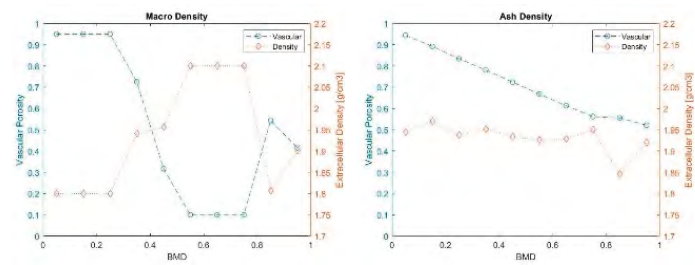


Fig 2. 3-variable model optimized over a full range of bone mineral density (BMD) with ρ_{macro} (left) and ρ_{Ash} (right).

4. Discussion and Conclusions

For the first time, bone multiscale properties were back-calculated out of DXA data. The apparent success of the 3-variable model reveals that the apparent bone density is not a good design variable, especially when BMD values are low (below 0.6 g.cm⁻³). This new approach can enhance the information traditionally extracted from medical images. It opens the door to monitor the effect of different osteoporosis treatments on bone composition, and map mechanical properties, without needing any phenomenological relationship between bone stiffness and density [1].

5. References

- Blanchard et al Int. J. Numer. Meth. Biomed. Engng., 2016
- Vuong et al J Thero Biol, 287, 2011
- Ruiz Wills et al, Bone, 2019
- Schileo et al J Biomech, 41, 2008

6. Acknowledgements

Funds from Spanish Government (ANDAMIO-RTC2019-007413-1, RYC-2015-18888) are acknowledged

6.3

Modelling the mechano-inflammatory regulation of chondrocyte in early osteoarthritis

Maria Segarra-Queralt¹, Gemma Piella¹, Jerome Noailly¹

¹IBCN MedTech, Universitat Pompeu Fabra, Barcelona, Spain

*Corresponding author information: jerome.noailly@upf.edu

1. Introduction

Articular cartilage (AC) chondrocytes (CC) respond to mechanical loads through a process known as mechanotransduction (MT). Modest loads are vital for AC homeostasis, whereas injurious loads promote AC degradation and inflammation, which influence the onset of osteoarthritis (OA). Network-based models (NBM) can integrate large amount of biological information about CC metabolism [1], in contrast to tissue-scale mechanobiology models [2]. NBM allow us to predict steady states (SS) according to imposed nodal initial conditions (representing CC microenvironments), which informs about CC activity. A NBM was developed as a dynamical system, including mechano-sensors, signaling pathways, and inflammatory processes.

2. Materials and methods

44 peer-reviewed articles from indexed journals were retained to map MT paths, which led to an interactome of 118 nodes and 358 edges (simplified in Fig.1). It was converted into a system of ordinary differential equations following [3]. SS were achieved according to different initial conditions: physio-osmotic (PO), inflammation (INF), static compression (SC), and tensile strain (TS). A qualitative evaluation was done against literature to analyze whether the model could predict CC activity changes. Finally, a sensitivity analysis was performed based on a factorial design of treatments (analyzed through an ANOVA test ($\alpha=0.05$) for each node of the network).

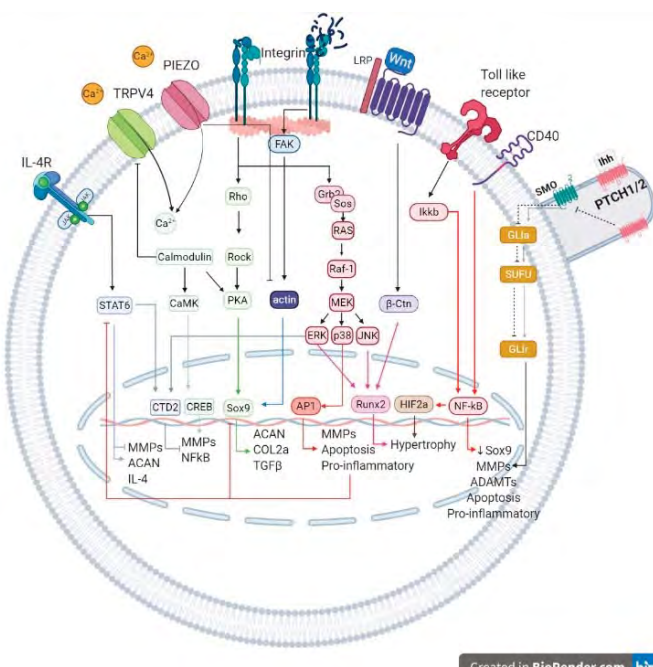


Figure 1. Simplified MT interactome.

3. Results

Under PO initial condition (Fig.2 green) anti-INF and structural proteins have higher activation rates than pro-INF or degrading enzymes. When injurious conditions are tested (INF (pink), SC (blue), or TS (purple)) a different SS profile can be seen: pro-INF and degrading enzymes have high expression rates, but not anti-INF and structural proteins. Hypertrophy markers (BMP2, MMP12, Runx2) behave similarly to pro-INF nodes. Regarding qualitative evaluation, our model could represent 94% of expected responses. The sensitivity analysis reveals that changes in INF and anti-INF nodes promote the strongest switches in CC metabolism for every node.

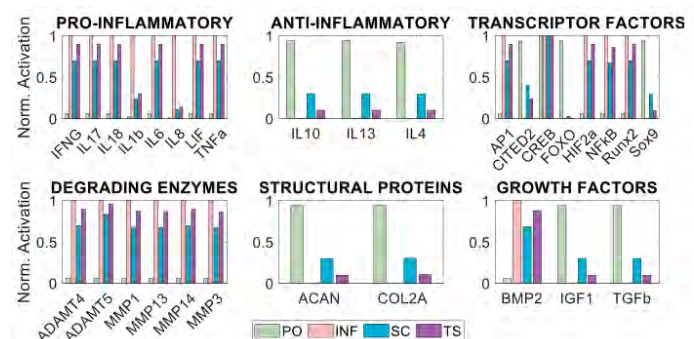


Figure 2. Steady states of different group of nodes under different initial conditions.

4. Discussion and Conclusion

High levels of INF lead to AC destruction, as anabolic factors are inhibited. SC seems less harmful than TS, but both show limited ability to preserve AC integrity, reflecting also the potential deleterious effects of persistent static postures. Sensibility analysis reveals that anti-INF therapies are more likely to stop AC degradation than PO environments. In conclusion, a MT NBM coupled with INF routes is successfully developed, revealing the potential to reflect load-induced chondroprotection or AC degradation in different mechano-chemical-environments.

5. References

1. Segarra-Queralt et al. SciRep. 12;2022 p.38-56
2. MarcR et al. PLoS One 13; 2018p.e0200899
3. Mendoza et al. TheBioMedMod.3;2006.p.3-13.

Acknowledgements

Spanish (RYC-2015-18888) & Catalan Governments (2020-FI_b00680).

6.4

Nucleus pulposus cell network modelling in early intervertebral disc degeneration

SOFIA TSERANIDOU¹, Maria Segarra-Queralt¹, Janet Piñero², Jerome Noailly¹

1 UNIVERSITAT POMPEU FABRA, BCN MEDTECH

2 IMIM

1. Introduction

Intervertebral disc (IVD) degeneration (IDD) involves loss of water, proteoglycans and type-II collagen, in the nucleus pulposus (NP). As biochemical processes are complex, redundant and feedback-looped, IDD remains poorly understood, and numerical [1] and experimental [2,3] models explore its mechanisms. Yet, improved integration of knowledge is needed. Accordingly, a new NP cell (NPC) regulatory network model (RNM) is presented, incorporating critical biochemical interactions in IVD regulation.

2. Methods

A unique corpus of 120 articles was built about the biochemical stimuli in the NP and their activation and/or inhibition effects on the regulation of soluble cytokines, proteases, and structural proteins by NPC. Limited knowledge motivated corpus enrichment through the STRING database, including general protein-protein interactions in *Homo Sapiens* and relevant interactions in chondrocyte regulation (Fig. 1). In the RNM, proteins were represented as nodes that interacted among each other through inhibition and activation edges. Node activations were calculated through ordinary differential equations that semi-quantitatively interpolate Boolean rules, to provide the stable steady states (SSS) of the RNM [4]. Finally, two experimental NPC culture studies [2,3] were simulated to evaluate the model.

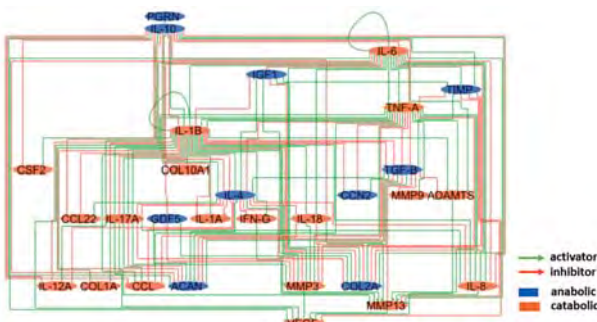


Figure 1: NPC RNM topology after enrichment

3. Results and Discussion

Simulations revealed an anabolic basal SSS of the RNM (light blue bars in Fig. 2). According to experimental measurements [2,3], initial activation of IL-17A strongly enhanced COL1A, while it significantly inactivated anabolic nodes. In contrast, initial activation of GDF5 led to highest expressions of ACAN, COL2A, important growth factors and anti-inflammatory cytokines that play an important anabolic role in the IVD. Interestingly, the increase of MMP-13 activation by IL-17A stimulation was very low, which seems to be supported by evidence that this protease does not play a clear role in IDD [5].

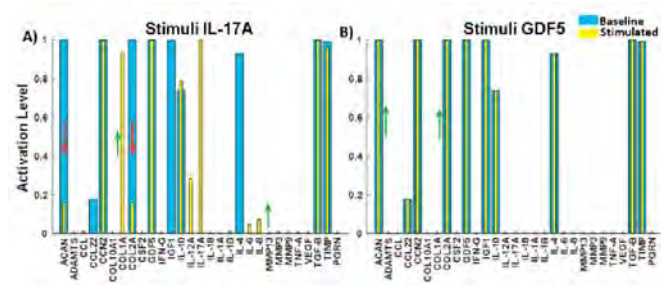


Figure 2: Baseline (blue) & stimulated (yellow) SSS of the NPC RNM with IL-17A (A) and GDF5 (B).

Further experiments with IL-4 and TGF-B did not show any changes in the anabolic state of the network at baseline. IL-1B initial activation significantly increased the activation of ADAMTs, the primary enzymes that cleave proteoglycans in IDD, whereas the activation of MMP3, believed to increase in advanced stages of IDD [5], remained low in the RNM.

Despite, the relatively limited amount of knowledge about IDD, compared to other diseases, e.g., osteoarthritis, an enriched RNM was built and successfully assessed against independent experiments. This RNM in IDD stands for a unique model to further integrate mechano-regulation and biochemical factors, including and dose-dependent NPC activity [1].

5. References

1. Baumgartner L. et al, *Front Bioeng* 10:9:734258, 2021
2. Yao, Zhixiao et al, *Inflammation* 39: 1997–2007, 2016
3. Chujo, Takehide et al, *Spine* 1;31(25):2909-17, 2006
4. Mendoza et al, *Theor Biol Med Model*, 3:1-13, 2006.
5. Vo et al, *Spine J.* 13:331-41, 2013

Acknowledgements:

Funding from the Spanish Government (RYC-2015-18888) the European Commission (Disc4All-MSCA-2020-ITN-ETN-955735

6.5

Open source computational model to investigate patient-device interaction during extracorporeal life support

Jan-Niklas Thiel¹, Ana Martins Costa², Katharina Maria Sander¹, Bettina Wiegmann^{3,4,5}, Michael Neidlin¹, Jutta Arens^{1,2}

¹ Institute of Applied Medical Engineering, Medical Faculty, RWTH Aachen University, Department of Cardiovascular Engineering, Aachen, Germany

² University of Twente, Engineering Organ Support Technologies group, Department of Biomechanical Engineering, Enschede, Netherlands

³ Department for Cardiothoracic, Transplantation and Vascular Surgery, Hannover Medical School, Hannover, Germany

⁴ Lower Saxony Center for Biomedical Engineering, Implant Research and Development; Hannover Medical School, Hannover, Germany

⁵ German Center for Lung Research, BREATH, Hannover Medical School, Hannover, Germany

1. Introduction

Extracorporeal membrane oxygenation (ECMO) is a technique used in intensive care medicine for providing prolonged support for cardiac and/or respiratory failure [1]. Although lifesaving, ECMO is very costly and clinical treatment is cumbersome, time-consuming, has high complication rates, and requires high specialization [2]. Consequently, a comprehensive analysis of patient-device interaction is essential to better understand the cardiopulmonary physiology of patients connected to extracorporeal circuits and thus make patient outcomes more reliable and reproducible [3].

For this reason, this study focuses on the development of a cardiopulmonary model of a patient under extracorporeal life support to investigate its effect on human hemodynamics and tissue gas exchange.

2. Materials and Methods

A state-of-the-art cardiovascular model from Neidlin et al. has been extended by a pulmonary system that includes lung mechanics with an autoregulatory system, as well as gas exchange and gas transfer between both lungs and tissues in the human body [4]. An ECMO system with an external pump, oxygenator, and additional cannulae was implemented. This model was fitted to an ARDS patient with Influenza A Pneumonia (f, 28y, sedated) using Bayesian optimization to select optimal machine learning hyperparameters. Veno-venous ECMO (VV-ECMO) was applied to analyze hemodynamics and tissue gas exchange. Blood was both drained and reinfused at the right atrium.

3. Results

To investigate the influence of different operating points of VV-ECMO on the hemodynamics of the patient's circulatory system, the pV loops of the right ventricle are shown in Fig. 1 for different rotational speeds. Right ventricular end-diastolic volume increases for 2500 rpm and drops below the reference value when the flow rate of the ECMO system is increased. The same applies to the cardiac output as a result of increased ECMO flow. ECMO flows were 0.80 L/min for 2500 rpm, 1.96 L/min for 4000 rpm and 4.16 L/min for 6000 rpm.

Arterial blood leaving the left ventricle for a healthy person has an O₂ concentration of 196 mL O₂/L blood and a CO₂ concentration of 479 mL CO₂/L blood, which corresponds to values observed in clinical practice.

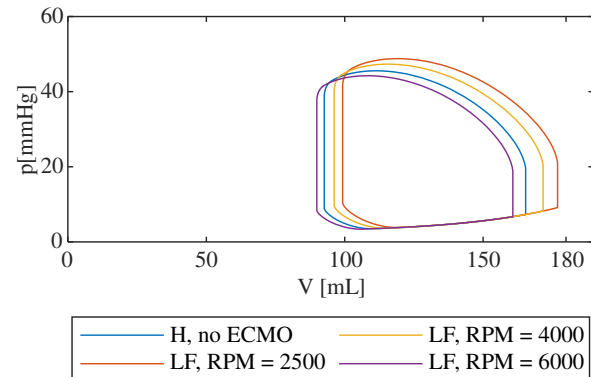


Figure 1: pV loops of the right ventricle for different operating points of the ECMO system; H=Healthy; LF=Lung failure.

For the previously described ARDS patient, O₂ concentration decreases by 60 % and CO₂ increases by 21 % without ECMO therapy. When ECMO is used and the rotational speed is increased up to 6000 rpm, the O₂ concentration can be increased by 179 % and the CO₂ concentration can be decreased by 20 % again.

4. Discussion and Conclusions

The application to VV-ECMO demonstrates the potential of this model and highlights the impact of external devices on the human circulatory system. The presented model can be applied to different pathological scenarios as well as to different ECMO strategies using clinical data. Because patients undergoing ECMO are often at high risk for acute kidney injury, the next step will be to investigate the effects of additional continuous renal replacement therapies on human hemodynamics. We make this modular platform available to the scientific community as an open-source repository.

5. References

1. Ratnani I et al., *Methodist DeBakey Cardiovasc J*, 14(2):110-119 (2018).
2. Patel B et al., *J Thorac Dis*, 11(14):1698-1707 (2019).
3. Colasanti S et al., *Artif Organs*, 45(4):399-410 (2021).
4. Neidlin M et al., *J Biomech*, 49(13):2718-2725 (2016).

Acknowledgements:

This project is funded by the DFG SPP2014 "Towards the Artificial Lung" - PN: 447746988.

6.6

Use of a mechanistic model of chronic viral hepatitis B to investigate the dynamics and variability of serum viral markers in response to drug treatments

Anne Schneider¹, Solène Porte¹, Solène Granjeon-Noriot¹, Lara Bruezière¹

1 Novadiscovery, LYON, France

1. Introduction

Chronic hepatitis B (CHB) is a major public health issue threatening the life of 296M people worldwide [1]. However, with current treatment options functional cure rates (defined as loss of serum HBsAg) are low. Testing and predicting a new drug's efficacy is challenging as CHB pathophysiology involves numerous intertwined mechanisms related to viral replication and host immune response, resulting in a high inter-patient variability. To investigate serum viral markers' (SVM) dynamics and variability in response to CHB treatments, we built an original mechanistic model. Simulations were run with entecavir (ETV) and peginterferon alfa-2a (IFN) monotherapies, currently standard of care, and results were calibrated with published data. With a global sensitivity analysis (SA) main mechanisms contributing to the variability in SVM were identified.

2. Materials and Methods

We developed an ODE-based mechanistic model (Fig. 1) that simulates SVM dynamics in response to ETV and IFN monotherapies and accounts for the HBV replication cycle (RC), immune system (IS) response, drugs' pharmacokinetics and mechanisms of action, based on published data. Model parameter ranges were estimated to reproduce observed SVM's inter-patient variability. We performed a global SA on SVM at the beginning of treatment (BOT) and on SVM changes at end of treatment (EOT) after ETV and IFN monotherapies and assessed the sensitivity index of model parameters to identify main explanatory factors of inter-patient variability.

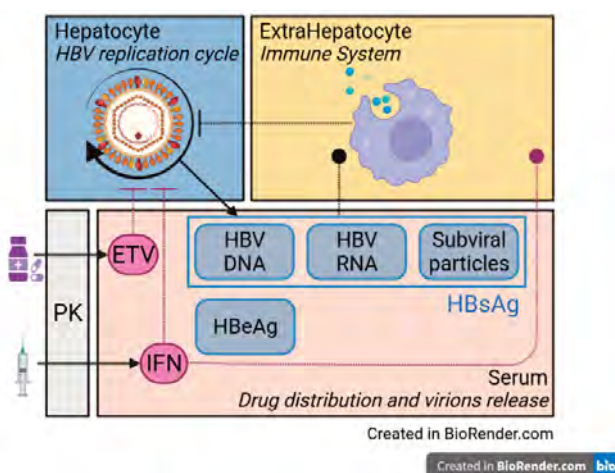


Figure 1: Simplified model structure. SVM are based on ETV and IFN posologies, HBV RC and IS.

3. Results

The model reproduced SVM levels (including HBV DNA and HBsAg) at BOT and SVM changes at EOT after ETV and IFN monotherapies as reported in the literature [2] with respect to mean values and distributions. A global SA conducted on SVM showed highest sensitivity for HBV RC related parameters at BOT. Variability of SVM changes at EOT after ETV treatment could be explained primarily with parameters related to HBV RC and IS and after IFN treatment with HBV RC, IS and treatment related parameters (TRP) (see Fig. 2, serum HBV DNA).

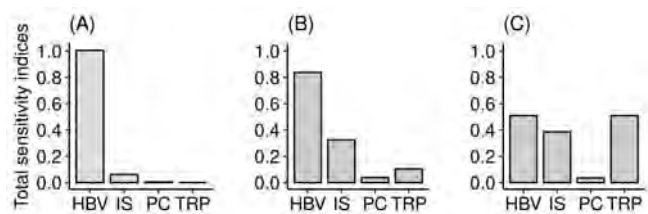


Figure 2: Summed contributions, expressed as total sensitivity indices [3], of parameters related to HBV RC, IS, patients characteristics (PC) and TRP, on the variability of serum HBV DNA at BOT (A) and changes at EOT after ETV (B) and IFN (C) treatment.

4. Discussion and Conclusions

This original ODE-based mechanistic CHB model was used to simulate dynamics and inter-patient variability of SVM routinely measured to track patients' treatment response, including HBsAg. The model reproduced SVM response at baseline and under treatment. SA results showed a high contribution of IS-related parameters on SVM response to treatment and a strong difference between ETV and IFN. Our model offers the potential to dissect mechanisms of the IS and explore new treatment targets and modalities. With this model, the effects of new drug candidates and their combinations can be investigated in silico with a virtual population at the patient-level accounting for inter-patient variability.

5. References

1. Global Hepatitis Report 2017. Geneva: World Health Organization. License: CC BY-NC-SA 3.0 IGO (2017)
2. Yu XQ et al., J Clin Microbiol. 2020;58(9):e00075-20(2010)
3. Saltelli A et al., Comput. Phys. Comm. 2010;181(2):pp.259-270 (2010)

Acknowledgements:

This study was supported by Enyo Pharma SA, Lyon, France.

7.1

Can a transformer architecture match convolutional neural networks for segmentation of anatomic structures in 3D computed tomography?

Gonçalo Almeida¹, João Manuel R.S. Tavares²

1 INEGI - Institute of Science and Innovation in Mechanical and Industrial Engineering, Porto, Portugal

2 Faculty of Engineering - University of Porto, Department of Mechanical Engineering, Porto, Portugal

1. Introduction

Image segmentation applied to medical imaging is a longstanding computer vision problem. Deep learning has been applied successfully for some time, and the most recent advance is the emergence of a network architecture initially applied to natural language processing: transformers. At its core is the multi-headed self-attention mechanism, which compares all variables in the input sample, learning the relations between them in a fully automated method [1]. Unlike convolutional neural networks (CNN), there is no *a priori* imposition of any spatial relation between regions of the input images. Recently, the Swin Unet was presented [2], which applies the self-attention method together with shifted windows [3] to the encoder-decoder Unet tailored for medical image segmentation [4].

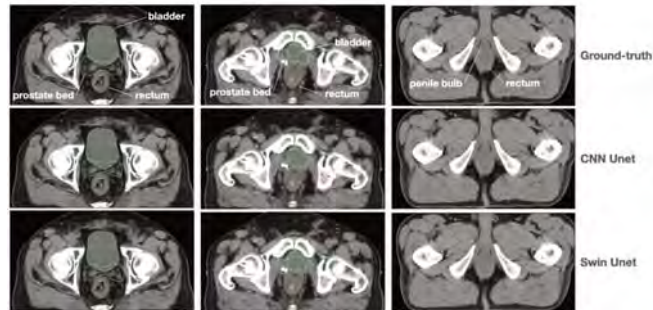


Figure 1: Examples of both neural networks' segmentations of three patients.

2. Materials and Methods

The used dataset is composed of 775 computed tomography (CT) scans of prostate cancer patients who had the prostate surgically removed before undergoing radiation therapy. The scans are the planning CTs used as part of their treatment. The anatomic structures segmented are the prostate surgical bed, which is the region from which the prostate had been previously removed, i.e., the radiation therapy target, and the surrounding normal tissues: bladder, rectum, and penile bulb. The scans were preprocessed so that voxel intensities match window-level and window-width of 35 and 350, using the same standard as radiologists when analyzing CTs of this anatomical region. The images were also resampled to isometric resolution of 1 mm³ voxels. A training/testing split of 700/75 samples was used. The manual segmentation performed by medical experts was used as ground-truth.

Two different models were trained: a CNN Unet, [4] and a Swin-Unet [2], both adapted for fully three-dimensional processing. The 3D volumes had size of 224 on each side. The training was performed for 150 epochs on an Nvidia DGX Station with V100 32GB GPUs.

3. Results

Using the volumetric Dice coefficient, the average across all structures and all test patients was 75.13% and 74.23% for the CNN-Unet and the Swin-Unet, respectively. However, looking at the different organs separately, the Swin-Unet outperforms in the prostate bed (68.71% vs 72.72%), and is very close in the larger organs (bladder: 96.25% vs 96.02%; rectum: 85.13% vs 84.25%), with a larger difference in the bulb (50.43% vs 43.95%). Using boundary distance metrics, the results are very close with a slight edge for the Swin-Unet: average 8.27 mm vs 7.54 mm in the 95% Hausdorff distance and 2.05 mm vs 1.90 mm in the Average Boundary Distance.

4. Discussion and Conclusions

A recent trend has been emerging in the Deep Learning field where there is a convergence of the techniques that were typically applied to different problems and different data types. The obtained results help corroborate this thesis, that transformer networks can be used for computer vision tasks with good outcomes. With more research and further improvements on both architectures, it is possible that a better solution lies with some mixture of both approaches.

5. References

1. Vaswani, A., et al. (2017). Attention is All you Need. *Advances in neural information processing systems (NIPS)*, 30.
 2. Cao, H., et al. (2021). Swin-Unet: Unet-like Pure Transformer for Medical Image Segmentation. *ArXiv*, abs/2105.05537.
 3. Liu, Z., et al. (2021). Swin Transformer: Hierarchical Vision Transformer using Shifted Windows. *2021 ICCV 2021*, 9992-10002.
 4. Ronneberger, O., et al. (2015). U-Net: Convolutional Networks for Biomedical Image Segmentation. *MICCAI 2015*, pp. 234-241. Springer
- a Instituto de Ciéncia e Inovação em Engenharia Mecânica e Engenharia Industrial, Faculdade de Engenharia, Universidade do Porto, Porto, Portugal
- b Instituto de Ciéncia e Inovação em Engenharia Mecânica e Engenharia Industrial, Departamento de Engenharia Mecânica, Faculdade de Engenharia, Universidade do Porto, Porto, Portugal

7.2

Dynamic analysis of pelvic mobility using Magnetic Resonance Images

Pauline Lecomte-Grosbras¹, Jean-François Witz², Olivier Mayeur³, Lisan Morsinkhof⁴, Michel Cosson⁵, Rubod Chrystele⁶, Franck Simonis⁷, Anique Bellos-Grob⁸

- 1 Centrale Lille, LaMcube, Villeneuve d'Ascq Cedex, France
- 2 CNRS, LaMcube, Villeneuve d'Ascq, France
- 3 Centrale Lille, LaMcube, Villeneuve d'Ascq, France
- 4 University of Twente, Magnetic Detection and Imaging (MD&I), Enschede, Netherlands
- 5 CHU-Lille, LaMcube, Villeneuve d'Ascq, France
- 6 CHU-Lille, LaMcube, Villeneuve d'Ascq, France
- 7 Twente university, Magnetic Detection and Imaging (MD&I), Enschede, Netherlands
- 8 Twente University, Multi Modality Medical Imaging (M3I), Enschede, Netherlands

1. Introduction

Imaging has become an important complementary tool in the assessment of pelvic floor disorders. Magnetic resonance imaging (MRI) can simultaneously evaluate all the compartments of the pelvic floor [1]. Pelvic organ mobility is defined as the displacement of pelvic organs between rest and maximal straining. Mobility of pelvic organs is essential to ensure physiological functioning. Indirectly, modified pelvic mobility is a sign of pathology.

The study of pelvic organ mobility can help to better understand the biomechanics of pelvic system in the physiological case as well as in the case of pelvic pathologies leading to hypo or hyper mobility (such as endometriosis or prolapse) [2]. Quantitative measurement of mobility could also be used to evaluate or compare the effectiveness of pelvic surgeries and treatments [3-4] in different position from supine to upright [5]. This study proposes a protocol to quantify pelvic mobility in order to better understand the physiological biomechanics of pelvic system as well as a method to evaluate pathologies and treatments.

2. Materials and Methods

MR images allow to observe the patient's 3D volume by capturing several 2D slices with a chosen thickness while the patient remains motionless. To visualise the motion of the organs, it is also possible to perform 2D dynamic observations by observing a fixed plane and capturing images at a chosen temporal frequency during defecography or valsalva manoeuvre. MRI examinations are usually performed in the supine position, but some equipment offers the possibility of performing acquisitions in upright position. It is then possible to analyse the movement of organs under the effect of gravity in upright position in 2D and 3D. Image registration using Elastix software and the protocol proposed by [2] has been applied to analyse dynamic MRI, on different patients: a young volunteer without pelvic pathology [2], a patient after surgery [3] and a prolapse patient in both supine and upright position [5].

3. Results

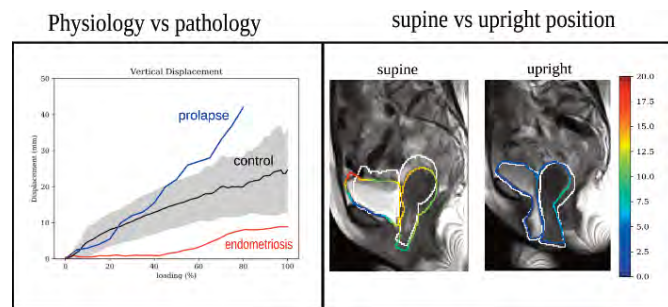


Figure 1: Quantification of pelvic mobility using dynamic MRI. Left: absolute displacement during a defecography in three cases; Right: example of displacement field measured on same patient in supine and upright position

The displacement fields allow to evaluate physiological mobilities and to assess the impact of a pathology on functional mobility as shown on Fig. 1 on two cases of prolapse and endometriosis. A comparison between displacement fields from MRI performed in upright and supine position shows important differences in mobility [5]. Furthermore, the study by van IJsselmuizen [3] shows small differences in post-surgical mobility regardless of the surgical technique used.

4. Discussion and Conclusions

Image registration allows quantitative displacement measurements to compare mobilities and evaluate the effectiveness of treatments and surgeries. The differences measured in the supine and upright position illustrates our interest in upright measurements, which are more representative of the daily situation. This measurement method could be applied in 3D for even more complete analyses and shows multiple possibilities for a more complete and personalised diagnosis (prolapse, endometriosis). It also allows for a more quantitative evaluation of surgical techniques by comparing post-surgical mobilities with physiological mobilities or even quantify, optimise and personalise medical devices such as pessaries.

5. References

1. Kobi M. et al, JMRI, 47 (2018)
2. Lecomte-Grosbras P. et al, Strains 51 (2015)
3. van IJsselmuizen M.N. et al, IUJ, 31 (2020)
4. Hong C.X. IUJ, 33 (2022)
5. Morsinkhof L.M. et al, ISMRM (2021)

7.3

iTwin4Face: A Digital Twin of the Human Face for Enhancing Facial Paralysis Grading and Rehabilitation Precision

Tan-Nhu NGUYEN^{1,2}, Abbass BALLIT^{1,3}, Tien-Tuan DAO¹

¹ Centrale Lille Institut, UMR CNRS 9013 Laboratoire de Mécanique, Multiphysique, Multiéchelle (LaMcube) , Villeneuve-d'Ascq, France

² University of Technology of Compiègne, Biomechanics and Bio-Engineering, Compiègne, France

³ University of Technology of Compiègne, Biomechanics and BioEngineering, Compiègne, France

1. Introduction

Facial palsy negatively affects both the professional and personal life qualities of involved patients. Classical facial rehabilitation strategies can recover facial mimics into their normal and symmetrical movements and appearances [1]. However, there are a lack of objective, quantitative, and in-vivo facial texture and muscle activation bio-feedbacks for personalizing rehabilitation programs and diagnosing recovery progress. The objective of our work is to develop a digital twin of the human face for capturing facial mimics and muscle strains in real-time for providing bio-feedbacks and personalizing the facial rehabilitation movements.

2. Materials and Methods

A patient-specific 3D geometrical model generation process was developed to capture the external shape of the face and then animate it in real-time conditions by using two stereo-cameras and a data fusion process (Fig. 1). The skull component was generated using a statistical shape learning algorithm [2]. Then, a facial muscle network was generated [3]. A real-time interactive animation interface for capturing facial mimics, computing muscle strains, and evaluating geometrical asymmetries of facial mimics was developed using the system of systems approach. Finally, rehabilitation-oriented serious games with different difficulty levels were designed and implemented for training slow motions and symmetrical movements of facial mimics.

3. Results

Fig. 1 shows the data capture, 3D model generation, and facial movement (symmetrical and asymmetrical) detection and tracking processes in real-time (24 FPS). The serious games for training zygomatic muscles with slow motions and symmetrical movements are illustrated in Fig. 2.

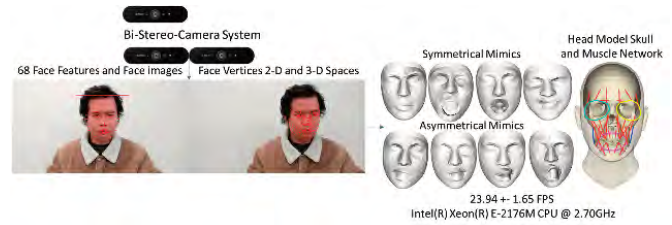


Figure 1. Symmetrical and asymmetrical facial mimics are detected by two stereo camera systems in real-time.

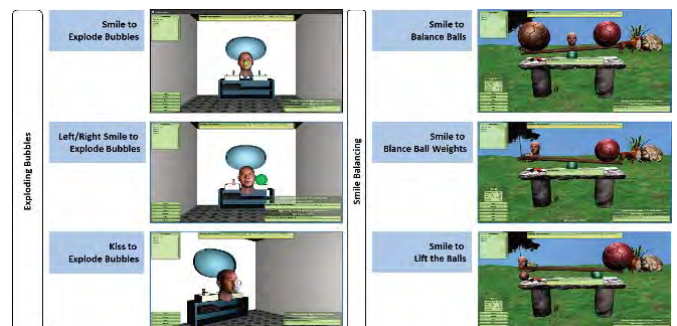


Figure 2. Serious games for facial mimic rehabilitation

4. Discussion and Conclusions

This work has opened new challenges for estimating internal biomechanical bio-feedbacks based on external shape and motions. Moreover, new serious games have been proposed for patient-specific facial rehabilitation for facial palsy and face transplantation patients. In perspective, fast soft-tissue deformations will be integrated using our recent development of a novel HyperMSM formulation [4] and deep learning-based methods for enhancing real-time biofeedback.

5. References

1. Khalifian et al., *Lancet* 384(9960): 2153–2163, 2014
2. Nguyen et al. *Medical & Biological Engineering & Computing* 59(6), 1235-1244, 2020
3. Nguyen et al., *Comput. Methods Programs Biomed.* 200:105846, 2021
4. Ballit et al., *Comput. Methods Programs Biomed.* 216:106659, 2022.

Acknowledgments:

The authors would like to thank Labex, Hauts-de-France region, and SATT LUTECH for funding.

7.4

Modelling the fetal face growth from 3D US

Raphael Sivera¹, Anna Clark², Andrea Dall'Asta³, Christoph C. Lees², Silvia Schievano¹

1 University College London, London, United Kingdom

2 Imperial Healthcare NHS Trust, Queen Charlotte's & Chelsea Hospital, London, United Kingdom

3 University Hospital of Parma, Parma, Italy

*corresponding author: r.sivera@ucl.ac.uk

1. Introduction

Objective quantification of the fetal face morphology has the potential to improve the clinical stratification of risk factors associated with fetal growth restriction (FGR). Statistical shape analyses (SSA) are however hindered by the large differences associated with the growth of the fetuses. We aimed to evaluate the use of a model to correct for overall growth and to propose a comprehensive model of the longitudinal changes.

2. Materials and Methods

3D surface meshes were extracted from US volumes through semi-automatic segmentation [1]. Meshes were then rescaled according to an estimated growth curve such that the average size was constant over time. A statistical shape model[2] consisting of a mean shape and individual deformations (parametrized by shape vectors), was finally estimated. Relations between age, diagnosis, and shape vectors were evaluated by a hypothesis testing approach that combines a local measure of the effect and a permutation-based scheme for a corrected single p-value.

Our population consisted of 181 fetal faces (25 FGR) between 24 and 34 gestation weeks.

3. Results

The estimated growth curve was compatible with tabulated head circumference values[3].

We identified additional differences in facial development linked to gestational age around the midface (Fig 1.1). Their amplitude and "direction" is shown using the divergence of the infinitesimal deformation field (Fig 1.2). These differences translate to fuller cheeks and more pronounced nasal arch in later gestations. The amplitude of this effect corresponds to 4% of the average growth. Significant differences were also associated with FGR diagnosis (Fig 1.3-4) with a similar midface pattern but more differences on the forehead.

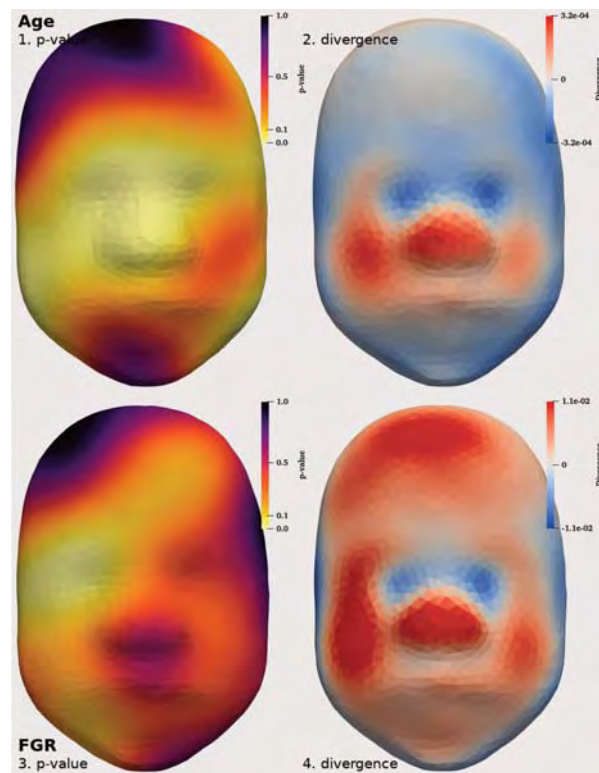


Figure 1: Effect of gestational age (top) and FGR diagnosis (bottom) on the face. Left: result of the statistical testing. P-values are shown on the mesh but are estimated at the deformation control points. Yellow=significant effect. Purple=no visible effect. Right: Amplitude of the local volume change. For age, faster expansion in red (slower in blue). For FGR smaller region in red (bigger in blue).

4. Discussion and Conclusions

We highlighted local facial growth variation during the 3rd semester of fetal development. This work stresses the importance of a model of the longitudinal growth to be able to explore more subtle variations of clinical interest.

5. References

1. Clark et al., R.Soc.OpenSci 7.11:201342, 2020.
2. Durrleman et al., NeuroImage 101:p35-49, 2014.
3. Kiserud et al. PLoS med. 14.1:e1002220, 2017.

Acknowledgements:

This work was supported by the NIHR Imperial BRC and the EPSRC EP/N02124X/1.

7.5

Super-resolution of 4D-Flow MRI in the left ventricle using physics-informed neural networks

Fergus Shone¹, Zeike A. Taylor¹, Alejandro F. Frangi¹, Erica Dall'Armellina², Peter Jimack³

1 University of Leeds, CISTIB, School of Computing, Sir William Bragg Building, Leeds, United Kingdom

2 University of Leeds, LICAMM, University of Leeds, Leeds, United Kingdom

3 University of Leeds, School of Computing, Sir William Bragg Building, Leeds, United Kingdom

1. Introduction

4D-Flow magnetic resonance imaging (MRI) provides unique means of studying cardiac flow and its role in progression of cardiopathies. However, low spatial resolution (1.5 – 3 mm³) and artifacts such as acquisition noise hamper its clinical impact, by making e.g. sensitive flow derivatives difficult to calculate accurately. It is hypothesised that such complex haemodynamic parameters are of clinical relevance in e.g. adverse left ventricular remodelling [1,2]. A predictive tool for capturing such features could potentially enable earlier-stage risk stratification.

2. Materials and Methods

To address the aforementioned shortcomings, we propose a physics-informed neural network (PINN) [3] for flow super-resolution and de-noising. Physical loss constraints consist of the Navier-Stokes equations and no slip condition on the endocardial boundary. Adaptive SIREN activation functions are used. An outline of the PINN architecture is shown in Fig. 1.

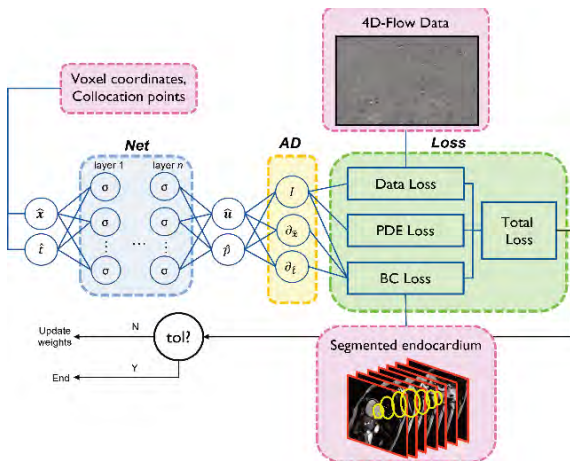


Figure 1: Basic outline of the PINN architecture and how each data component is used.

The model was tested on a synthetic example using a 2D idealised ventricle. High-res ground truth flow data were acquired using CFD, then spatially down-sampled by a factor of 16 and temporally by 2. The PINN was then used to recover the high-res result.

3. Results

Example flow results are presented in Fig. 2. Error values are reported in table 1.

4. Discussion and Conclusions

Preliminary results show good agreement between prediction and ground truth. However, solid conclusions cannot be drawn until the model has been thoroughly tested with more complex synthetic cases and real patient data.

Predicted variable	nRMSE
x-velocity	0.081
y-velocity	0.062
pressure	0.057

Table 1: Normalised root mean squared error (nRMSE) values for each predicted variable.

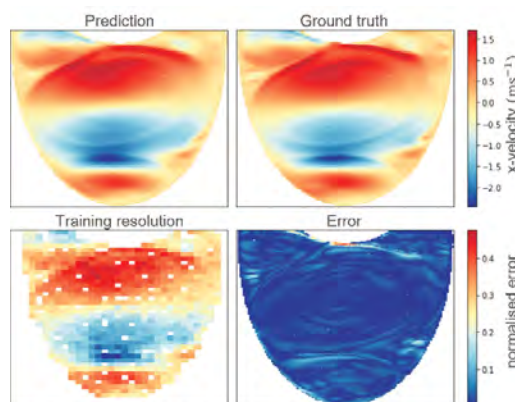


Figure 2: Contours of flow x-velocity and normalised error at one time step.

5. References

1. Filomena, D, et al. *ESC Heart Failure* 9: 496-505, 2022
2. Elbaz, M.S.M, et al. *J Cardiovasc Magn Reson* 2014
3. Raissi, M, et al., *J Comp Phys* 378: 686-707, 2019

Acknowledgements:

The authors gratefully acknowledge funding support from EPSRC (EP/L014823/1) and RAEEng (LTRF2021\17115; CiET1819\19).

7.6

Virtual Reality for Teaching and Treating Congenital Heart Disease

Endrit Pajaziti¹, Jess Ma¹, Silvia Schievano¹, Andrew Cook¹, Claudio Capelli¹

¹ University College London, Institute of Cardiovascular Science

*Corresponding author: endrit.pajaziti.13@ucl.ac.uk

1. Introduction

Congenital heart disease (CHD) affects almost 1% of newborns. Complex surgical repair for severe CHD holds a high risk for adverse developmental outcomes. The treatment path therefore requires a personalised approach when pathologies are complex. In these cases, understanding the patient 3D anatomy and spatial relationships between structures is a challenge. Virtual Reality (VR) offers an immersive experience to inspect image-based 3D anatomy [1, 2]. This study reports a single centre experience in assessing the benefit of using VR in educational and clinical settings.

2. Materials and Methods

We have designed a novel VR application (i.e. VheaRts) specifically for CHD models. The application was created using the software Unity3D and for the Oculus Rift/Quest headsets. There are 10+ tools which include 3D slicing, ultrasound emulation and distance measuring. Multiplayer functionalities were implemented to allow several users to connect the same VR room online. For education, 20 models of patient-specific hearts with lesions were generated through segmentation of magnetic resonance (MR) or computed tomography (CT) images. Models used for education were also labelled in order to aid students. Group learning was evaluated. For clinical applications, the users were able to import new patient-specific cases and analyse anatomical features pre-operatively. The use of VheaRts for planning a range of surgical procedures was assessed at our Centre over the period 2020-2022.

3. Results

3.1 VR for Medical Education

VR was implemented into educational courses at UCL and at GOSH. From 2018 – 2020, 58 healthcare professionals attended a cardiac morphology course at UCL which included a session with VR. Attendees were from very mixed clinical backgrounds. Over 89% found VR useful (4/5) or very useful (5/5) for learning complex cardiac anatomy. The VR app was implemented in UCL undergraduate and postgraduate cardiovascular science courses in the period 2020-2022, reaching over 100 students. During the COVID-19 pandemic, VR headsets were sent to students in order to conduct virtual anatomy labs remotely.

3.2 VR for Pre-Operative Planning

Over 50 clinical cases were assessed with VR. The average age of the patients was 3.65 ± 4.70 years. Double outlet right ventricle was the most common diagnosis, and presence of ventricular septal defect the most common associated lesion. The patients were treated successfully with no major complications. Clinicians who used VheaRts ($n=6$, 17.5 years of experience) strongly agreed that VR allowed for better understanding of the spatial relationships between structures. The most significant advantages were recorded to be visualisation and slicing tools. VR was considered more useful than 3D printing.



Figure 1: A labelled healthy fetal heart model (from a specimen) being inspected in VR using a slicer.

4. Discussion and Conclusions

We have developed and trialled a VR application. Feedback showed how anatomical understanding and surgical preparedness can be improved with the use of VR.

5. References

1. H Brun et al. 2018
2. Milano E et al., 2019

8.2

Device induced deformation, damage, and puncture of arterial porcine tissue

Mathieu Oude Vrielink¹, Bertus van de Wetering², Peter Timmermans¹, Marco Stijnen², Olaf van der Sluis^{1,3}

¹ Philips Research, Eindhoven, Netherlands

² LifeTec Group, Eindhoven, Netherlands

³ Eindhoven University of Technology, Eindhoven, Netherlands

*p.h.m.timmermans@philips.com, Philips Research, High Tech Campus 34, 5656 AE Eindhoven

1. Introduction

An aspect of intravascular medical procedures is the navigation to optimally position the device, while avoiding tissue damage. If the conditions under which tissue damage occurs are known, this can be used to improve the device design. In vascular surgery, knowledge of a threshold force to prevent tissue damage helps to improve patient safety during the procedure. In this study, the threshold force at which a medical device punctures a vessel wall is measured. The measured force and device geometry are used to analyse local deformations and stress values using a finite element model. The tissue is described using the model developed and characterized in [1]. The purpose of this study is to find a relation between device geometry and the threshold force to avoid tissue damage for use in device design optimization.

2. Materials and Methods

The experimental set-up consists of a displacement-controlled holder for the medical device. A porcine artery is pre-strained to physiological conditions, with a soft substrate as support to mimic surrounding tissue. The force exerted by the device is measured. Fig. 1 shows a schematic of the set-up and the artery.

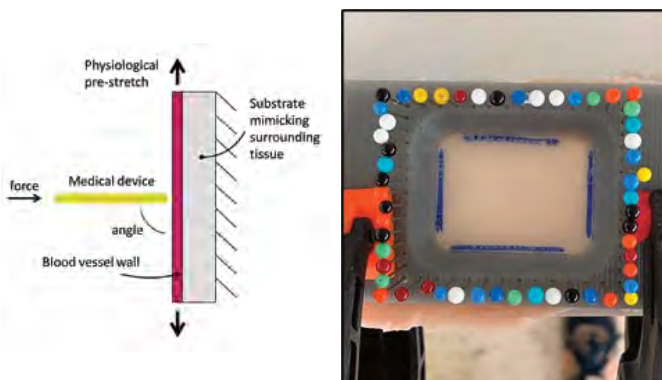


Figure 1: Test set-up and clamped porcine artery.

The arterial tissue model developed in [1] is implemented into a finite element code through a user subroutine. It includes the observed loading/unloading hysteresis in arterial tissue using an internal damage variable.

3. Results

The experimentally obtained force as a function of time (at constant speed) in Fig. 2. is in qualitative agreement with results obtained in [2]. The threshold force at which the tissue is punctured by the medical device can be extracted. The local stress and internal damage levels at the threshold force for an unstressed vessel wall on a substrate can be analysed with a 2D plane strain FEM model (Fig. 2).

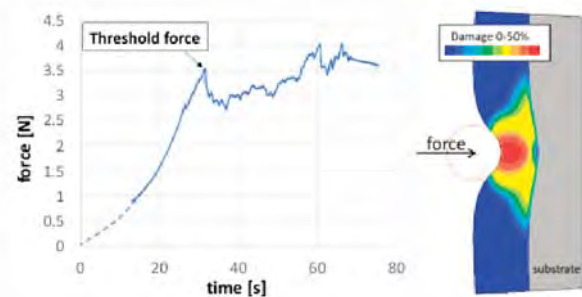


Figure 2: Measured force and calculated damage variable for a cylinder indenting a medial layer.

4. Discussion and Conclusions

An experimental and numerical procedure have been developed to analyse device-induced tissue damage. As a next step, device tip geometries, substrates and angles of approach will be varied. Results will be used to optimize device design for minimal risk on tissue damage.

5. References

1. Weisbecker et al., *J.Mech.Behavior.Biom.Mater.*; 12:93-106 (2012).
2. Gasser et al., *J.Biomech.*; 42:626-633 (2009).

Acknowledgements:

The authors thank the partial support by the ITEA3 UPSIM project (N°19006), funded by BMBF, FFG, RVO and IFD.

8.3

Digital twins of electrical stimulation devices for tissue engineering applications

Julius Zimmermann¹, Lam Vien Che¹, Ursula van Rienen¹

¹ University of Rostock, Institute of General Electrical Engineering, Rostock, Germany
julius.zimmermann@uni-rostock.de

1. Introduction

Electrical stimulation (ES) is considered for tissue engineering applications including bone and cartilage regeneration [1]. The ES signals are delivered by electrodes in direct contact or separated by an insulating layer (capacitive coupling (CC)). While direct contact ES can lead to electrochemical reactions, CC does not. For previously considered CCES devices, the insulation impedance is dominant. Thus, impedance measurements cannot access the properties of the cell culture [2]. This makes the development of a digital twin (DT) of CC devices impossible. Nevertheless, DTs can be realised for direct contact devices coupling numerical simulations and impedance spectroscopy [3].

In this contribution, we suggest modifying the material of the insulating layer to make the development of a DT for CCES feasible.

2. Materials and Methods

The DT consists of a model of the ES device, impedance recordings and means to update the model upon data recordings [3,4]. The model of the device comprises a 3D geometry and the electroquasistatic equation solved by the finite element method [2,3]. The model is mapped on an equivalent circuit (EC) representation, which is also used to analyse the impedance recordings. EC parameter changes update the model of the device. We consider the same device as in [2]. Instead of glass cover slips, 1 mm-thick barium titanate (BTO) disks with a permittivity of 5,000 are considered [5]. A sensitivity analysis is performed as in [2].

3. Results

Due to the large permittivity of the BTO disks, the impedance depends on the medium conductivity at frequencies accessible by impedance analysers (Fig. 1). The field strength at relevant frequencies is about hundred times larger than with cover slips.

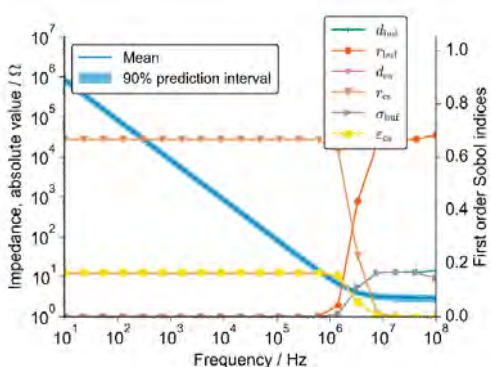


Figure 1: Impedance and 1st order Sobol indices indicating the sensitivity of the impedance w.r.t. the model parameters (see [2] for details).

4. Discussion and Conclusions

With the modification, a DT of the CC device becomes feasible. Hence, monitoring the medium conductivity and thus its temperature are possible [3]. Furthermore, a reliable estimate of the field becomes available. The decreased impedance and thus higher field save energy. The BTO disks are commercially available. We plan to demonstrate the experimental implementation of the device and its DT.

5. References

- Thrivikraman G et al., *Biomaterials*, 150:60-86 (2018).
- Zimmermann J et al., *Molecules*; 25(20):4750 (2020).
- Zimmermann J et al., *Front. Bioeng. Biotechnol.*, 9: 765516 (2021).
- Wright L and Davidson S. *Adv. Model. Simul. Eng. Sci.*, 7:13 (2020).
- Carstensen E et al., *IEEE Trans. Biomed. Eng.*, BME-31(8):557-558 (1984).

Acknowledgements:

Funded by the Deutsche Forschungs-gemeinschaft – SFB 1270/2 - 299150580.

8.4

Hardware Density Reduction Aviods T3 PJF In Adult Spine Surgery: FE Simulation

Morteza RASOULIGANDOMANI¹, Alex del Arco², Ferran Pellisé³, Miguel González Ballester⁴, Fabio Galbusera⁵, Jérôme Noailly¹

¹ Pompeu Fabra University Poblenou Campus, DTIC, Barcelona, Spain

² Hospital del Mar, Barcelona, Spain

³ Hospital Universitari Vall d'Hebron, Barcelona, Spain

⁴ Pompeu Fabra University Poblenou Campus, Barcelona, Spain

⁵ Schulthess Klinik, Zürich, Switzerland

Corresponding author: Morteza Rasouligandomani, University Pompeu Fabra, Email: morteza.rasouli@upf.edu

Introduction

Proximal Junctional Failure (PJF) is a severe post-operative complication (61.7%) [1]. Since lumbar osteotomy provoke complications (34.8%), surgeons avoid lumbar correction for T10 PJF and might extend T10 to T3 even with high Global Alignment and Proportion (GAP) [2]. These may lead to PJF but Hardware Density (HD) may stabilize the biomechanical loads at adjacent Upper Instrumented Vertebra (UIV). Hence, this study aims to explore effect of HD to avoid T3 PJF with severe GAP score. A patient-specific model with iliac/T3 fixations was generated using Statistical Shape Model (SSM) and mesh morphing techniques. UIV+1 disk Fibre Strain (FS) and screw Pull-out Forces (SPF) were assessed for different HDs.

Materials and Methods

42 pre-operated patients are selected: age 50-75, Pelvic inclination>20°, SVA>5cm, PJF. Modelling Pipeline is shown in Figure 1. 3D surfaces were obtained using sterEOS software. Principal Component Analysis (PCA) allowed to learn the main modes of SSM.

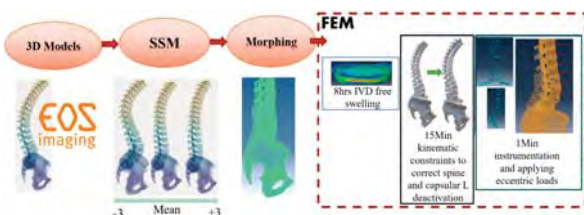


Figure 1: Modeling and FEM pipeline

Out of an independent database, a T10PJF patient whose Hardware was extended to T3, with GAP11, was selected (Figure 2). The SSM led to a 3D model of this patient spine that was further used as a target to morph (combination of Thin-Plate Spline and Coherent Point Drift [3]) a structured finite element (FE) model [4].



Figure 2: T3PJF patient (76 y.o.)

Material properties and boundary conditions are introduced in Table 1. FS at UIV/UIV+1 was assessed and trade-off between FS and SPF selected optimal scenarios.

Material properties	Intervertebral disc	Vertebras	Ligaments
	Anisotropic hyperelastic model [4]	Linear elastic [5]	Hypoelastic model [6]
Boundary Conditions	Eccentric load in vertebra center; Sacrum is fixed		

Results and Discussion

FS at UIV/UIV+1 is compared to average control values [7]. Results showed that reducing HD to 1, 2, 3 vertebrae left, led to 41%, 58% and 70% FS reduction, respectively (Figure 3).

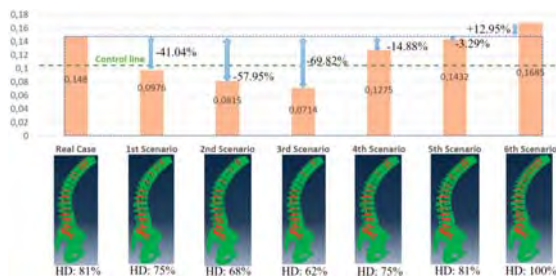


Figure 3: Maximum principal fibre strain at T3/T2

However, HD reduction increased SPF (e.g., 34%, between 3rd scenario and real case, Figure 4). While forces were well below the threshold for healthy bone, 2nd and 3rd scenarios were rejected in case of osteoporotic bone.

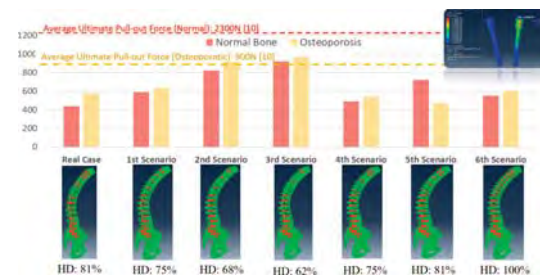


Figure 4: Pull-out Force (N) on UIV screw

Trade-off between FS and SPF showed that for osteoporotic bone, 1st scenario and for healthy bone 1st, 2nd and 3rd scenarios might avoid PJF. This study showed the possible high value of personalized FE simulations to explore HD reduction as a mean to reduce the risk of PJF.

References

- Hyun SJ, et al, Korean J Spine, 14(4), 2017
- Yilgor C, et al, The Spine J, 17(10), 2017
- Rasouli, M, et al, 26th ESB congress, 2021
- Malandrino, A, et al, Front. Bioeng., 2015
- Galbusera, F, et al, Med. Eng., 2011
- Noailly, J, et al, Eur. Spine J., 2012
- Rasouli, M, et al, ESB Cap.Esp, 2021

Acknowledgements

Funds received from DTIC-UPF, IMIM, IRCCS Istituto Ortopedico Galeazzi & Spanish Government (RYC-2015-18888, MDM-2015-0502).

8.5

In silico modelling of cancer cell response to cold helium plasma jet and chemotherapy

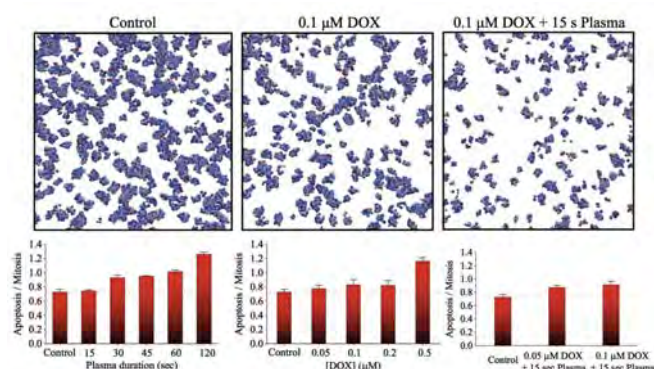
Kristaq Gazeli^{1,2}, Eleftherios Ioannou³, Myrianthi Hadjicharalambous³, Odhisea Gazeli², Constantinos Lazarou², Charalambos Anastassiou², **Vasileios Vavourakis**^{3,4}, Georgios E. Georghiou²

¹ Centre National de la Recherche Scientifique, Laboratoire des Sciences des Procédés et des Matériaux – LSPM, France

² University of Cyprus, Department of Electrical & Computer Engineering, Cyprus

³ University of Cyprus, Department of Mechanical & Manufacturing Engineering, Cyprus

⁴ University College London, Department of Medical Physics & Biomedical Engineering, United Kingdom



1. Introduction

The study of atmospheric pressure plasma jets (APPJ) interacting with living biological tissue offers novel prospects in cancer treatment. Most efforts on APPJ and neoplasia focus on in vitro and in vivo models. However, we present an in silico approach to simulate cancer cell response to APPJ and cytotoxics.

2. Materials and Methods

The in silico approach employs agent-based modelling [1], where cancer cells are modelled as individual agents that can undergo mitosis, apoptosis, growth and migration. For the in vitro, melanoma cells (B16F10) are incubated in RPMI-1640 medium, and their viability is assessed after their treatment [2]. Three cancer-cell treatment scenarios are tested: (i) doxorubicin at concentrations: $[DOX]=0.05\text{--}0.5\mu\text{M}$, (ii) RPMI is subjected to APPJ, duration of plasma treatment: $d_{\text{Plasma}}=15\text{--}120\text{s}$ and then plasma-conditioned RPMI (PC-RPMI) is put in contact with the cells, (iii) DOX-treated cells ($0.05\mu\text{M}$ or $0.1\mu\text{M}$) are exposed to APPJ for 15 seconds. Simulations are used to evaluate cell population (N_c) development, and probability values for apoptosis (%Ap) and mitosis (%Mi).

3. Results

At $d_{\text{Plasma}}=15\text{s}$, treating melanoma cells with PC-RPMI practically did not affect N_c and apoptosis-to-mitosis probability ratio ($r_{\text{A-M}}$) compared to the Control, while $[DOX]=0.05\mu\text{M}$ resulted to ~ 1.4 times smaller N_c and $\sim 7\%$ larger $r_{\text{A-M}}$ than the control. Increasing d_{Plasma} and $[DOX]$ to 120s and $0.5\mu\text{M}$ respectively, N_c declined by approximately 20 and 22 times, while the simulated $r_{\text{A-M}}$ increased by 73% and 59% with respect to control. Combined treatment $[DOX]=0.1\mu\text{M}$ with $d_{\text{Plasma}}=15\text{s}$, resulted in 2.25 and ~ 4 times smaller N_c compared to DOX and PC-RPMI effects alone.

4. Discussion and Conclusions

The in silico agree with the in vitro data. Our model reveals that PC-RPMI enhances %Ap, and reduces N_c with increasing d_{Plasma} . DOX suppresses %Mi and assists %Ap with increasing [DOX], while combined use of DOX and APPJ is more toxic to the cancer cells than DOX or PC-RPMI alone. Such models are complementary to in vitro and can be useful in plasma medicine for predicting responses of neoplasia to APPJ or/and cancer drugs.

5. References

- Breitwieser et al., *Bioinformatics* 1–8 (2021).
- Pefani-Antimisiari et al., *Scientific Reports* 11, 14788 (2021).

Acknowledgements:

We thank the Research & Innovation Foundation (OPPORTUNITY/0916/MSCA/0023) and UCY for using the HPC facilities.

8.6

In silico rational design of Antibodies: from Molecular Modeling to Deep Learning approaches

Anne Goupli¹

¹ BIOVIA, Science Council, Vélizy-Villacoublay, France

1. Introduction

Biologics, and especially antibodies, are promising therapeutics. They are expected to show higher subtype selectivity and less off-target activity than small molecules. G protein-coupled receptors (GPCRs) being the main drug targets, there is a need for antibodies modulating these receptors. The metabotropic glutamate receptors, or mGluRs, are members of the group C family of GPCRs and perform a variety of functions in the central and peripheral nervous systems. We will describe how molecular modeling tools were used to build tri-dimensional model of nanobodies binding to different mGluRs and to suggest mutations that were validated experimentally. Several Deep Learning algorithms are now available and we also examined how these algorithms complement state of the art molecular modeling tools.

2. Materials and Methods

Tri-dimensional models for nanobodies were built using homology modelling (Modeler). Models for mGluR were also built with Modeler when no experimental structures were available. ZDOCK, which is a protein-protein docking algorithm, was used to predict how the nanobodies interact with the mGluRs. With ZDOCK many poses are generated and the best scoring pose was selected (Figure 1). Because we are performing rigid docking, the poses needed to be relaxed with explicit solvent molecular dynamics simulations for several nanoseconds. The interactions were then analysed for the duration of the simulation to understand which residues are the most important for binding and selectivity (Figure 2). Virtual mutagenesis was then used to suggest the mutations that were then validated experimentally to confirm the epitope (Figure 3).

Deep learning algorithms were used at a second stage and we will illustrate with some examples how they can complement traditional molecular modelling.

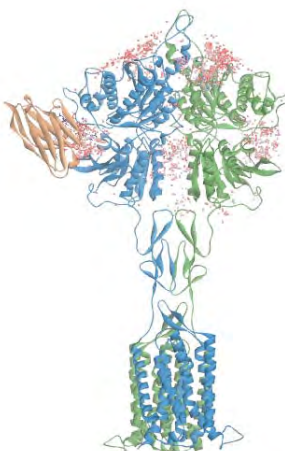


Figure 1: Homology model of a nanobody docked to a mGluR receptor. Best pose is represented in orange. Other dots represent possible poses.

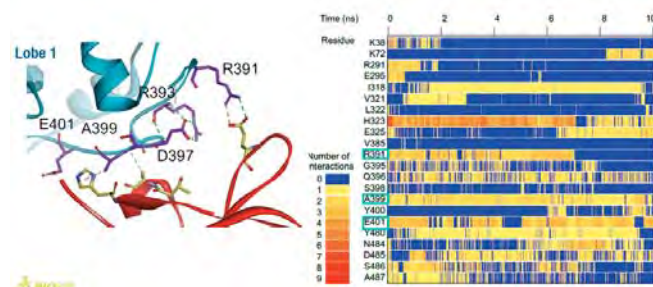


Figure 2: Analysis of the binding interface during simulation to identify key residues

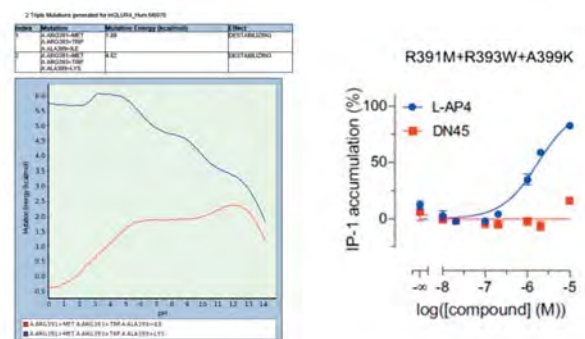


Figure 3: Virtual mutagenesis left. Experimental results right.

3. Results and Discussion

Molecular modelling was shown to be quite helpful in understanding biological experiment results, but also to design new experiments. The identification of the epitope was very accurate and validated experimentally. The mutations that we suggested could not have been proposed without having a tri-dimensional models coupled to atomistic simulations. Deep learning approaches as starting to provide also some very interesting predictions.

10.1

A cardiovascular modelling approach for non-invasive estimation of chamber pressure and diagnosis of heart disease

Sinclair McGaffin¹, Finbar Argus², Martyn Nash², Gonzalo Maso Talou², Debbie Zhao², Matthew Savage¹

1 University of Auckland, Grafton Campus, Medical and Health Sciences, Auckland, New Zealand

2 The University of Auckland, Auckland Bioengineering Institute, University of Auckland, Auckland, New Zealand

farg967@aucklanduni.ac.nz

1. Introduction

Accurate, non-invasive estimation of heart chamber pressures and transvalvular pressure drops provide information on patient condition and improve disease diagnosis and prognosis. These variables help provide clinical information about disease severity, heart valve function, ventricular and atrial dynamics and often are considered in preoperative and intraoperative care. Computational cardiovascular system (CVS) models can be used to fill the hemodynamic information gap that non-invasive cardiac assessments do not always capture. We present a pipeline consisting of a computational lumped parameter model of the CVS and an automatic parameter identification process that fits the model towards clinically available brachial pressure and echocardiogram measurements. This pipeline is designed to add to an echocardiogram study enabling near-immediate estimations of patient chamber pressures.

2. Materials and Methods

Brachial artery cuff pressure and echocardiogram measurements were obtained from patients presenting for routine cardiac catheterisation. Chamber volumes (m³) via the biplane method of disks and peak velocities (m/s) from pulsed-wave Doppler (PWD) were estimated. A time-varying orifice model of the valves was used to predict flow [1], which was converted to a velocity approximation to coincide with the measured PWD peak-velocity. A parallel genetic algorithm fit the computational model parameters to minimise the error between predicted and measured chamber volumes, brachial pressure, and valve peak velocities [2].

3. Results

This pipeline predicts blood pressure and volume in all four chambers and transvalvular flows. When provided with inputs from non-invasive clinical data, the model produces relevant clinical outputs capturing patient hemodynamic status. The preliminary training accuracies for model prediction vs echocardiogram and systemic pressure measured values for the first exemplar participant were: left ventricle max volume [1.01%], left ventricle min volume [0.32%], left atrium max volume [14.58%], left atrium min volume [13.39%], mitral valve peak E-wave velocity [17.01 %], aortic valve peak velocity [6.67%], systemic systolic pressure [0.32%], systemic diastolic pressure [0.64%].

4. Discussion and Conclusions

This pipeline demonstrates the potential for a patient-specific model to be an accurate and clinically comprehensive tool assisting patients' hemodynamic assessment. Future work will explore validation against invasive pressure measurements.

5. References

1. Mynard JP, Davidson MR, Penny DJ, Smolich J. A simple, versatile valve model for use in lumped parameter and one-dimensional cardiovascular models. *International Journal for Numerical Methods in Biomedical Engineering*. 2012 Jun;28(6-7):626-41.
2. Pironet A et al., Practical identifiability analysis of a minimal cardiovascular system model. *Computer methods and programs in biomedicine*. 2019 Apr 1;171:53-65.

Acknowledgements:

The authors acknowledge the help of Dr Nicola Edwards, ADHB, New Zealand.

10.2

A one-dimensional patient-specific model of the hemodynamics in the microvascular network of the retina using multimodal imaging

Laureline Julien^{1,2}, Michel Paques^{2,3}, José-Maria Fullana¹

1 Institut Jean le Rond d'Alembert - CNRS - Sorbonne Université, FCIH, Paris, France

2 Institute Vision - Sorbonne University, Paris, France

3 Centre Hospitalier National d'Ophtalmologie des Quinze-Vingts, Centre d'Investigation Clinique 1423; INSERM; Sorbonne Université, Paris, France

*laureline.julien@dalembert.upmc.fr

1. Introduction

In cardiovascular disorders the microvascular network of the retina may undergo hemodynamics and morphological perturbations. The severity of these disorders can produce a rapid alteration of the vision. Focal stenoses may affect the network according to their characteristics (severity, length). Because the study of clinic data alone is not sufficient to understand the consequence of local perturbations, we propose here a modelisation. We develop a 1D patient-specific retina model of arterial microcirculation and to use it to study the hemodynamics impacts of focal stenoses. Our model is based on conservation laws, and on multimodal imaging. The model simulates the blood flow from the central retina artery (CRA) to the terminal smallest arterioles.

2. Materials and Methods

The 1D microcirculatory model developed gives us the area and the flow rate deduced from Navier-Stokes equations integrated over the section [1]. For the apparent viscosity we use the Kiani model [2] who take into account the Fåhræus-Lindqvist effect [3]. The core viscosity is defined with the Cross model [4].

The morphological data : vessel diameters, positions and lengths are extracted by segmentation of confocal Scanning Laser Ophthalmoscope and Adaptive Optics Ophthalmoscope images. Those data allow us to build the geometry imposed of the simulation. Doppler Ultrasound (DU) gives us quantitative data of flow rate $Q_{in}(t)$ that is imposed at the input of the network.

3. Results

The study case is a patient affected by a stenosis of the left carotid artery. We choose the network of the right eye as a healthy model. Blood flow in vessels resulting from the simulation is in Fig. 1. For the pathological simulations we applied a stenosis (Fig. 1). We perform simulations for different degrees of stenosis.

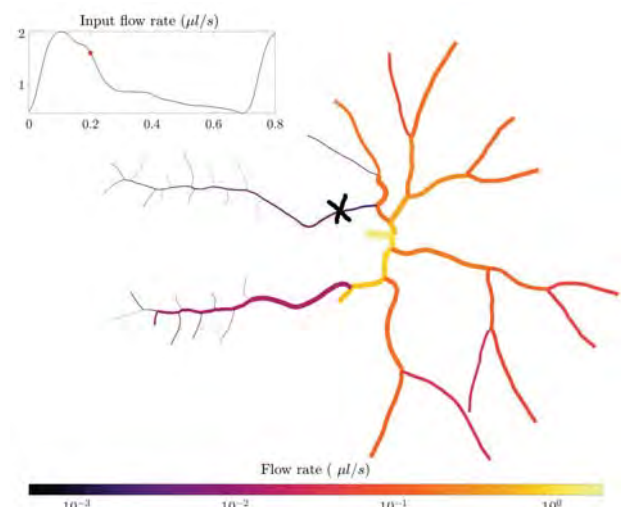


Figure 1: Flow rate snapshot obtained with the model without stenosis. Top-left: the flow $Q_{in}(t)$, red dot indicates the position on the cardiac cycle. The black cross is the position of the stenosis.

4. Discussion and Conclusions

We compare simulations with and without stenosis. Upstream of the stenosis differences are observed only after a certain degree of stenosis: an average increase in flow and a slight phase shift of the flow wave. For downstream vessels the flow is strongly reduced with a strong correlation with the degree of stenosis. In addition the waves show a characteristic delay.

5. References

1. Ghigo A, Lagrée P-Y, Fullana J-M. *Journal of non-newtonian Fluid Mechanics*. 253:36–49 (2018).
2. Kiani M, Hudetz A. *Biorheology*. 28:65–73 (1990).
3. Cross M. *Journal of Colloid Science*. 20:417–437 (1965).
4. Fåhræus R, Lindqvist T. *American Journal of Physiology-Legacy Content*. 96:3:562–568 (1931).

Acknowledgements :

The authors would like to thank M. Atlan, S. Bonnin, C. Chaumette and F. Rossant.

10.3

ADAVN: An anatomically detailed arterial and venous network model

Lucas Omar Müller¹, Sansuke Mario Watanabe², Eleuterio Francisco Toro³, Raul Antonio Feijóo⁴, Pablo Javier Blanco⁴

1 University of Trento, Department of Mathematics, Trento, Italy

2 Universidade Federal do Agreste de Pernambuco

3 University of Trento, Laboratory of Applied Mathematics, DICAM

4 Laboratório Nacional de Computação Científica

1. Introduction

The task of improving our understanding of systemic haemodynamics from the perspective of closed-loop systems has traditionally been faced using lumped-parameter models [1] or strong simplifications of such models where physical and physiological understanding is replaced by experimentally observed relations [2]. Recently, efforts have been made to improve the level of description of systemic haemodynamics by constructing models that account for arterial and venous networks described using one-dimensional (1D) blood flow models [3,4,5]. Here we present work regarding a step forward in this direction. We present a first version of an Anatomically Detailed Arterial and venous Network (ADAVN) model, which builds on the existing arterial counterpart [6] and focuses on venous districts of cerebral and coronary circulation.

2. Materials and Methods

Blood flow in arteries and veins is modelled using a 1D blood flow model. The present stage of development can be seen in Fig. 1. The arterial model consists of 2142 vessels, 28 specific organs and 116 vascular territories. The venous model consists of 168 vessels draining blood from: head, trunk and limbs. Special attention is given to the cerebral venous vasculature, with 77 vessels and 44 venous inlets. The model is closed-loop, including the heart, pulmonary circulation, venous valves and Starling resistors. The resulting model is discretized using a state-of-the art algorithm where PDEs are solved using a finite-volume type local time stepping high order scheme [7].

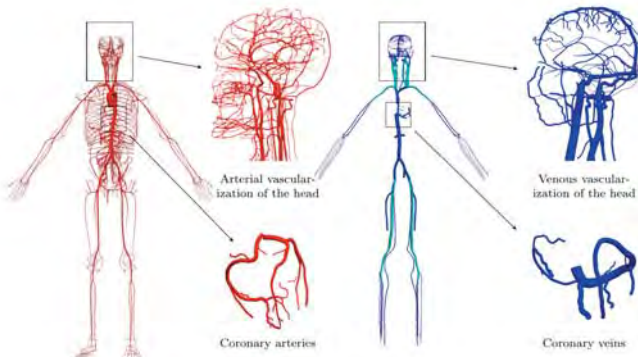


Figure 1: Overview of ADAVN model arterial and venous networks with detail of cerebral and coronary circulation.

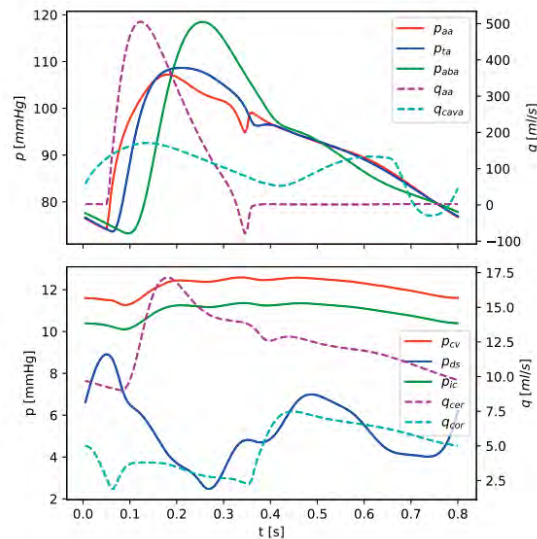


Figure 1: Exemplary pressure and flow waveforms obtained with the ADAVN model.

3. Results and discussion

Some of the main features to observe are: the typical biphasic venous return, the systolic cerebral arterial flow, the diastolic coronary arterial flow and the pressure in cerebral venous circulation.

In this presentation we will illustrate the capacity of the model to reproduce main cardiovascular indexes and discuss several relevant aspects, namely: extensive conventional sensitivity analysis; left ventricular-arterial coupling; implications of closed-loop character of model when matching common experiments to characterise the cardiovascular system (mean circulatory filling pressure, total vascular compliance, etc).

4. References

1. Heldt et al. *J Appl Physiol*, 92(3):1239–1254, 2002.
2. Guyton et al. *Annu Rev Physiol*, 34(1):13–44, 1972.
3. Müller et al. *Int J Numer Meth Bio*, 30(7):681–724, 2014.
4. Toro et al. *Int J Numer Meth Bio*, 38(1):e3532, 2022.
5. Mynard et al. *Ann Biomed Eng*, 43(6):1443–1460, 2015.
6. Blanco et al. *IEEE Trans Bio-Med Eng*, 62:736–753, 2015.
7. Müller et al. *Int J Numer Meth Bio*, 32(10):e02761, 2016.

10.4

Blood flow simulations for understanding sickle cell disease across age

Weiqiang Liu¹, Lazaros Papamanolis¹, Christian Kassasseyea², Suzanne Verlhac³, Pablo Bartolucci², Irene Vignon-Clementel¹

1 Inria Saclay Île-De-France, Palaiseau, France

2 Henri-Mondor University Hospital, Créteil, France

3 Hôpital Robert Debré, Paris, France

1. Introduction

Sickle cell disease (SCD) is a blood disorder that can lead to stenosis in cerebral arteries and eventually stroke. The main identified risk factor for developing cerebral vasculopathy (CV) is accelerations of cerebral arterial velocities with a critical time-mean of maximum velocity (TMMV) of 200 cm/s on transcranial Doppler [1]. However, it is still unclear why only some early childhood SCD patients reach critical TMMV and developed CV. We propose a computational fluid dynamics simulation pipeline and investigate how hemodynamics change over age in SCD.

2. Materials and Methods

The intracranial internal carotid artery (ICA) with its terminal branches was segmented from MRI images for 9 patients from 3 to 13 years old: 4 patients under 5 (UF) and 5 patients over 5 (OF) years old. Blood flow was modelled using the 3D Navier-Stokes equations, assuming that blood is an incompressible Newtonian fluid. Blood flow simulations were run with inlet flow rates varying from 5 to 15 mL/s. Pulsatile flow was assigned as an inlet boundary condition and a “no slip” condition was imposed on the wall. TMMV was calculated over five regions of interest (ROIs), as shown in Fig. 1. A Windkessel boundary condition model was applied at the two outlets of the terminal branches.

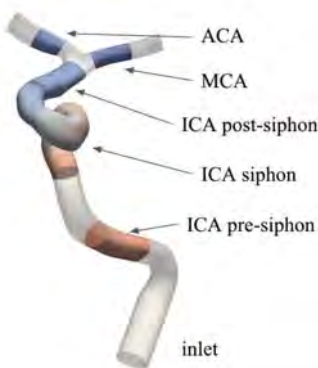


Figure 1: Regions of interest in segmented geometry.

3. Results

Simulation results for one case (5y) show that the critical TMMV is reached at the siphon region for a flow rate of 10 mL/s (Fig. 2). Similarly for all cases, as flowrate is increased, critical TMMV values appear first in the siphon or post-siphon regions.

When comparing TMMV results between age groups (Fig. 3), for the same inlet flow rate, children in the UF group reach higher TMMV values compared to the OF group, and with more variability. As a result, patients in the UF group tend to reach critical TMMV at lower inlet flow rates compared to the OF group.

4. Discussion and Conclusions

Results demonstrate that SCD patients in early childhood (UF group) are more likely to reach pathologically high cerebral velocities, putting them

at an increased risk of stroke: critical TMMV values can be achieved for lower flow rates compared to older patients (OF group). This is potentially due to a combination of hyperflow and geometrical features, such as diameter, tortuosity and curvature, which will be explored in future work.

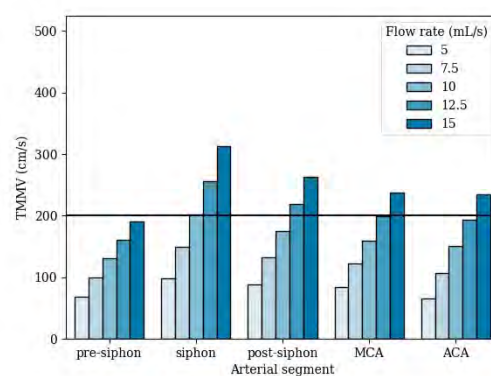


Figure 2: Simulated TMMV with varying inlet flow rates in ROIs of a 5 year-old patient. The straight horizontal line represents the critical risk threshold.

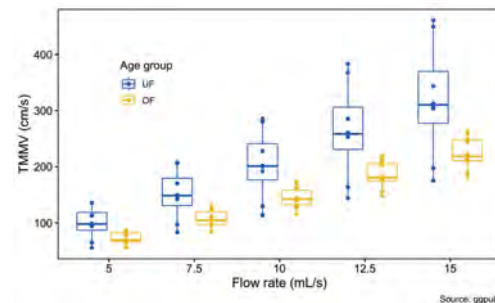


Figure 3: Simulated TMMV in the siphon region for varying inlet flow rates for UF (left) and OF (right) age groups.

5. References

1. Bernaudin, Françoise, et al. *Blood*, Am. J. Hematol. (2011)

10.5

Distinguishing hypertensive renal injury from diabetic nephropathy using MR imaging and computational modelling of renal blood flow

Ning Wang^{1,2}, Kanishka Sharma³, Steven P Sourbron^{1,3}, Alberto Marzo^{1,2}

1 INSIGNEO Institute for *in silico* medicine, The University of Sheffield, Sheffield, United Kingdom

2 The University of Sheffield, Department of Mechanical Engineering, Sheffield, United Kingdom

3 The University of Sheffield, Department of Infection, Immunity and Cardiovascular Disease, Sheffield, United Kingdom

Ning Wang, The University of Sheffield, Sheffield, South Yorkshire, UK, nwang37@sheffield.ac.uk

1. Introduction

Hypertension and diabetes are common comorbidities that independently cause chronic kidney disease (CKD) and show similar characteristics. It is not currently possible to distinguish between these two pathologies non-invasively, which ultimately impacts the disease prediction and management strategies. Our hypothesis is that a mechanistic model of the renal circulation can be used to identify biomarkers of interest that can then be used to distinguish these two etiologies, non-invasively, using ultrasound (US) or phase-contrast magnetic resonance imaging (PC-MRI) data.

2. Materials and Methods

Starting from a verified and validated 1D circulation software (openBF), which includes a representation of the relationship between transmural pressure and wall elasticity, we extended the model to include a comprehensive renal network and validated it using data from the literature [1], as shown in Fig. 1. We modelled differential changes induced by the two pathologies on blood viscosity, lumen radius, wall thickness, peripheral resistance, and vessel compliance, [1,2]. Resistive index (RI, Fig. 2) was used to quantify changes in the blood velocity waveform as a potential biomarker to differentiate between these two diseases. RI for two diseases will be validated by the results from US.

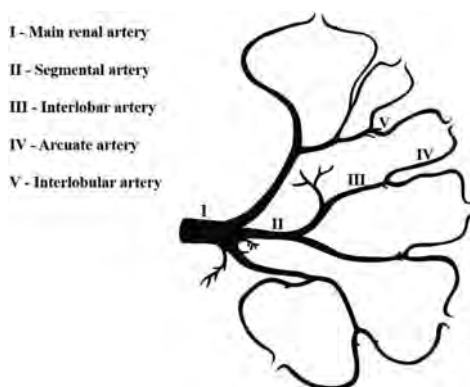


Figure 1: Illustration of the modelled renal network.

3. Results

Early results illustrate the potential differential impact that hypertension and diabetes have on RI. As shown in Fig. 2, our study show that hypertension and diabetes may increase RI by about 18% and 8%, respectively, along various renal vessels.

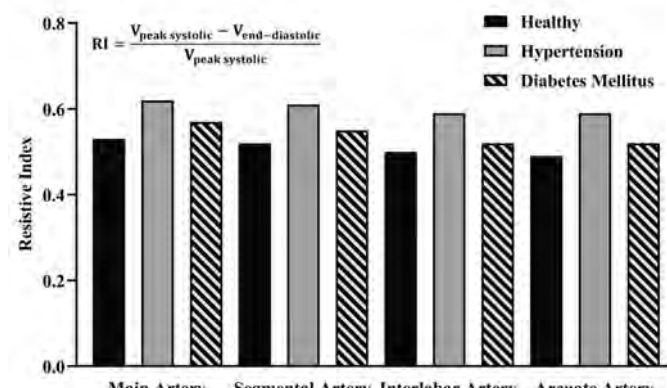


Figure 2: RI predicted in healthy, hypertensive, and diabetic individuals along various renal vessels.

4. Discussion and Conclusions

Our results show that RI could be considered as a potentially effective biomarker to distinguish early hypertension from diabetes. Clinical data is available to support a 19% increase in RI in early-stage hypertensive patients [3]. Data for middle or end stage diabetes show an RI increase of 20% in diabetic patients [4].

5. References

1. Hardigan T et al., *Comp. Physiol.*; 311(3):466-477 (2016).
2. Laurent S et al., *Circ. Res.*; 116(6):1007-1021 (2014).
3. Toledo C et al., *Hypertension*; 66(2): 382-388 (2015).
4. Ohta Y et al., *J. Hypertens.*; 23(10):1905-1911 (2005).

Acknowledgements:

The authors would like to thank University of Sheffield Research Scholarship (Faculty of Engineering) for supporting this work. The study received support from the iBEAt study, part of the BEAt-DKD project.

10.6

High-rate atrial pacing to reduce left heart filling pressures: a combined computational-clinical study

Tim van Loon¹, Pam Boerdonk¹, Kevin Sack², Richard Cornelussen³, Troy Jackson², Tammo Delhaas¹, Dominik Linz⁴, Justin Luermans⁴, Kevin Vernooy⁴, Joost Lumens¹

¹ Maastricht University, Biomedical Engineering, Maastricht, Netherlands

² Medtronic, Minneapolis, United States

³ Medtronic Bakken Research Center, Maastricht, Netherlands

⁴ Maastricht University, Cardiology, Maastricht, Netherlands

Corresponding address: t.vanloon@maastrichtuniversity.nl

1. Introduction

In heart failure patients, reduction of increased left heart filling pressures (e.g., mean left atrial pressure (mLAP)) improves symptoms, quality of life, and reduces mortality [1]. However, limited management options are available to this date [2]. In this combined in silico-clinical study, we explore the potential of high-rate atrial pacing to reduce left heart filling pressures.

2. Materials and Methods

The theoretical basis was explored in the CircAdapt computational model of the heart and circulation by simulating reduced left ventricular (LV) compliance [3]. Previous studies have observed interpatient variability of atrioventricular conduction (AV) delay in response to atrial pacing [4]. Hence, we simulated increasing pacing rates with various AV delays. In each simulation, homeostatic pressure-flow regulation was enabled to maintain cardiac output and mean arterial pressure.

Following the computational results, a clinical pilot study was designed and conducted in 29 paroxysmal atrial fibrillation (AF) patients undergoing pulmonary vein isolation (PVI) during sinus rhythm. In each patient, LA pacing rate was gradually increased from intrinsic- to Wenckebach rhythm with 10bpm increments. LAP was continuously monitored by a fluid-filled transseptal catheter.

3. Results

Computational modelling demonstrated a parabolic relationship between atrial pacing rate and mLAP, which was highly dependent on AV delay (Figure-top).

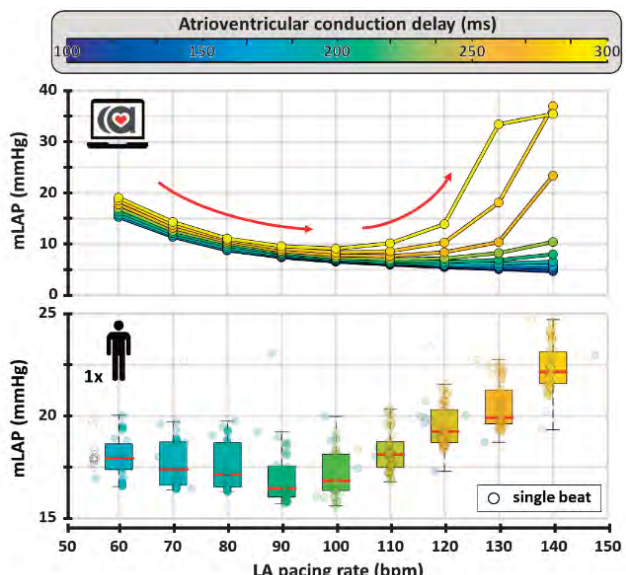


Figure. Modelled (top) and measured (bottom) response of mLAP to high-rate atrial pacing. Colours indicate AV delay.

An example beat-to-beat analysis of a single patient shows the same behaviour as proposed by the simulations (Figure-bottom).

In the total population, compared to the intrinsic rate, an intermediate rate increase (60[60;70], median[IQR], to 90[70;100]bpm) reduced mLAP (16[14;20] to 14[10;17]mmHg, $p<0.05$), whereas a high rate increase (130[120;140]bpm) increased mLAP (26[21;28]mmHg, $p<0.05$).

4. Discussion and Conclusions

Computational modelling results hypothesized the potential of atrial pacing to reduce left heart filling pressures. From these in silico observations, a clinical study was designed whose results supported our hypothesis. However, interpatient variability of response to high-rate pacing was observed, which may originate from varying AV delays.

5. References

1. Holland, D.J., Prasad, S., Marwick, T., *Circ Cardiovasc Imaging*. 2010;3, 149-156.
2. McDonagh, T.A. et al., *Eur Heart J*. 2021;42(36), 3599-3726.
3. Van Loon, T. et al., *Eur Heart J – Digital Health*. 2020;1(1), 40-50.
4. Kyriacou, A. et al., *Pacing Clin Electrophysiol*. 2018;41, 959-966.

Acknowledgements:

Supported by the Dutch Organization for Scientific Research (NWO-ZonMw, VIDI grant 016.176.340 to J.L.), the Dutch Heart Foundation (ERA-CVD JTC2018 grant 2018T094; Dr. Dekker Program grant 2015T082 to J.L.).

10.7

Impact of Image Segmentation Variability on Hemodynamic Prediction of Flow Quantities in AAA

Marc Horner¹, Antonio Martínez^{2,3}, Daan Jongerius⁴, Leonardo Geronzi², Eirini Kardampiki², Marco Evangelos Biancolini²

1 ANSYS, Inc., United States

2 University of Rome, Rome, Italy

3 ANSYS, Inc., Lyon, France

4 Eindhoven University of Technology, Eindhoven, Netherlands

1. Introduction

Abdominal aortic aneurysms (AAA) are a disease whose progression is difficult to predict, which means conservative estimates are often used when deciding treatment options. There are clinical guidelines to assess the severity of the AAA[1]. However, these guidelines are not always sufficient in the prediction of AAA rupture. Computational fluid dynamics (CFD) can be used to compute various hemodynamic factors, such as wall shear stress (WSS), pressure and velocity fields in the AAA, which may be used to assist with the risk assessment.

Variability in the shape of the AAA lumen may arise during segmentation of the lumen wall from the medical image data. The resulting variation in local geometrical factors, such as the diameter and curvature, may impact the rupture prediction. Therefore, this study aims to estimate the effect of geometric uncertainty due to the segmentation process on WSS and wall pressure predictions.

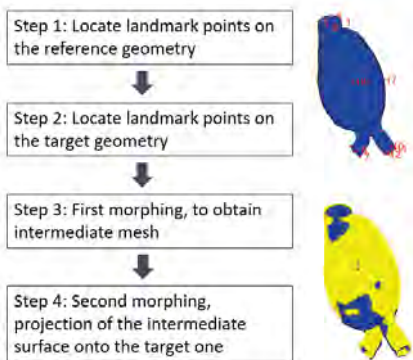


Figure 1: Summary of the morphing workflow.

2. Materials and Methods

Raw CT-data was segmented by several independent research groups and a total of 12 segmentations were obtained. A principal component analysis (PCA) is performed to obtain a statistical shape model (SSM), which provides information on the importance of shape variations. This SSM is used as reference mesh and is morphed onto the other segmented geometries to obtain iso-topological meshes of the different geometries. Figure 1 shows the morphing workflow, which is performed using RBF Morph™[2]. Steady-state CFD analyses are performed for all meshes to determine the uncertainty in WSS and pressure.

3. Results

The smallest, middle and largest volumes are highlighted in this section (Fig. 2,3). The uncertainty in results for the population of AAA segmentations will be computed and its relative effect on WSS and pressure quantified.

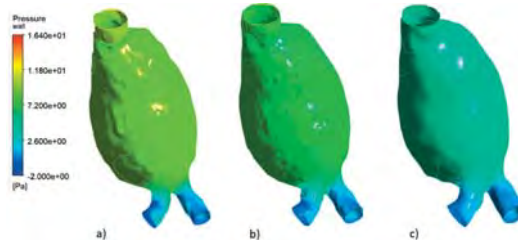


Figure 2: Pressure at the wall for smallest (a), middle (b) and largest luminal volume (c).

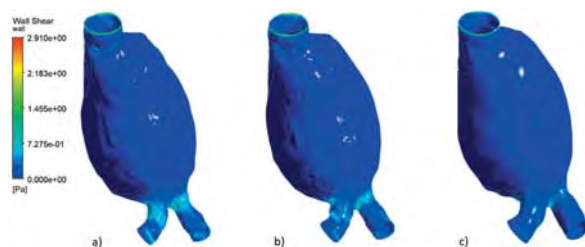


Figure 3: WSS at the wall for smallest (a), middle (b) and largest luminal volume (c).

4. Discussion and Conclusions

The main aim of this study is to utilize SSM of segmented AAA to investigate the influence shape variations have on hemodynamic quantities computed with the use of CFD simulations.

Acknowledgements

This project has received funding from the European Union's Horizon 2020 research and innovation programme under the Marie Skłodowska-Curie grant agreement No 859836.

5. References

1. Roger et al, Circulation (2012) 125:e2–e220
2. Biancolini, Fast radial basis functions for engineering applications, Springer (2017)

10.8

Sensitivity analysis on the modeling parameters of a cardiovascular model simulating partial hepatectomy

Lorenzo Sala¹, Nicolas Golsé², Alexandre Joosten², Eric Vibert², Irene Vignon-Clementel¹

¹ Inria Saclay Île-de-France, Palaiseau, France

² University of Paris-Saclay, Inserm, Physiopathogenèse et traitement des maladie du foie, Gif-sur-Yvette, France

1. Introduction

Hepatocellular carcinoma (HCC) is the most common primary liver cancer; every year in Europe HCC is accounting for around 47000 deaths. At early stages a treatment option is partial hepatectomy (HPX), which consists in the partial removal of the liver. Despite the recent progresses in clinical and surgical techniques, the understanding of the hemodynamics variations during this procedure is an open challenge in medicine, in particular related to the post-hepatectomy liver failure (PHLF), which remains the leading cause of postoperative death.

2. Materials and Methods

Exploiting the electric analogy to fluid flow, our team has developed a lumped parameter mathematical model (Fig. 1), simulating the hemodynamics response during. In a recent study [1], the authors employed this mathematical model using patient-specific clinical measurements to predict the risk of PHLF by estimating the postoperative portal vein pressure (Ppv) and the portacaval gradient (PCG), two major risk factors of PHLF.

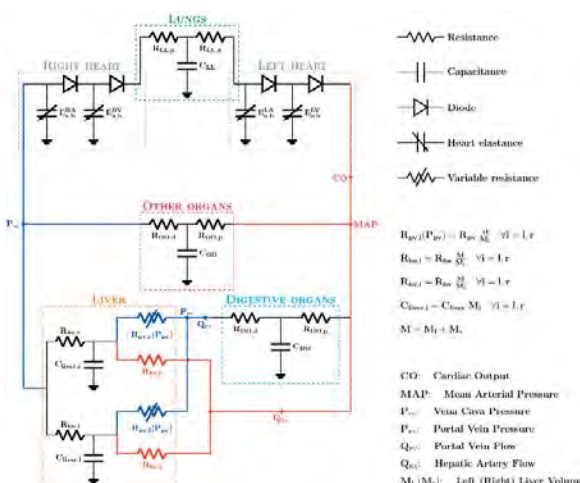


Figure 1: schematic of the cardiovascular model simulating partial hepatectomy.

In this work we propose a sensitivity analysis based on Sobol' indices [2] to investigate the influence on the main clinical outputs caused by the uncertainties of the modelling parameters that have been considered constant in [1]. In particular, the analysis hinges on 9 modeling input parameters sampled with uniform distributions: the modeling coefficient that partitions the liver pressure between portal and hepatic veins (aliver), the liver capacitance (Cliver), the coefficients representing the portal vein resistance non-linearity (Kpv, bpv, cpv), the total pulmonary resistance (RLL), the pulmonary capacitance (CLL), the digestive organs capacitance (CDO), and the other organs capacitance (COO). The computational pipeline is composed by a parameter calibration step completed with the CMA-ES (Covariance Matrix Adaptation Evolution Strategy) [3] followed by the patient-specific simulation of the virtual HPX.

3. Results

Sobol' indices are reported in Fig. 2 for pre-operative and post-operative Ppv and PCG, evaluated over several exemplary virtual patients. The numerical results suggest that the most influential inputs are aliver, RLL, and bpv.

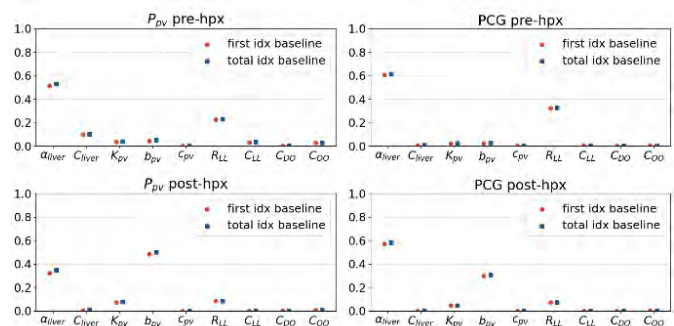


Figure 2: Computed Sobol' indices for pre-operative and post-operative Ppv and PCG.

4. Discussion and Conclusions

The results show that the contribution of some parameters selected for this study is negligible with respect to the considered clinical outputs. Thus, their values can be considered as constants without losing in accuracy and without the need of complex or invasive evaluations. Moreover, the most influential parameters need now to be integrated in the uncertainty quantification study comprehensive of patient-specific clinical measurements.

5. References

- Golsé N et al. *Journal of Hepatology*, 74(3): p 661-669 (2021).
- Saltelli A et al. *Technometrics*, 41(1): p 39-56 (1999).
- Hansen N, Ostermeier A. *Evolutionary Computation*, 9(2): p 159-195 (2001).

Acknowledgements:

Financial support: European Research Council (Grant no: 864313).

11.1

A 3D finite-element analysis of residual limb biomechanics in transfemoral subjects

Animesh Ranjan^{1,2}, Okan Avci¹, Oliver Röhrle^{1,2}

1 Fraunhofer Institute for Manufacturing Engineering and Automation, Biomechatronic Systems, Stuttgart, Germany

2 Institute for Modelling and Simulation of Biomechanical Systems (CBB), Stuttgart, Germany

1. Introduction

Prosthetic socket development for transfemoral amputees is a cumbersome and complex process. As each case presents the orthopaedic surgeon and socket designer with unique, subject-specific scenarios, crucial aspects such as muscle physiology, soft-tissue mechanics and residual limb biomechanics are mostly ignored, often resulting in several design iterations and increased patient discomfort. Investigating post-surgery residual limb biomechanics using computational models would provide deeper insights into efficient prosthesis design.

The current study aims at illustrating a quick and efficient, imaging-based simulation workflow for generating subject-specific, residual limb Finite Element (FE)-Models using unsupervised image segmentation techniques. Numerical optimization methods were used to predict pre-stretch values of individual muscle flexors and extensors, based on measured range of motion. Consequently, findings of socket-tissue interaction and soft tissue deformation in single-, double-limb support phase and muscle activation-driven limb motion are presented.

2. Materials and Methods

We use non-linear image deformation techniques to generate detailed FE-Models, based on subject-specific, Magnetic Resonance (MR) imaging sequences. Fibre tractography was employed to model anisotropy within soft tissue using Diffusion-MR imaging. The constitutive model for muscles and tendons was based on a 3D continuum-mechanical model by Röhrle et al. [1], implemented as a user material subroutine in LS-Dyna. Consequently, a combined 3D FE-model with socket-residual limb setup was simulated to determine the resulting soft tissue deformations in amputated musculature during various stages of the standing phase and due to activation of hip flexors and extensors, along with their estimated pre-stretches.

3. Results

The current study provides useful physiological information about soft tissue deformation due to interaction with prosthetic sockets in standing phase and during muscle activation-driven limb motion.

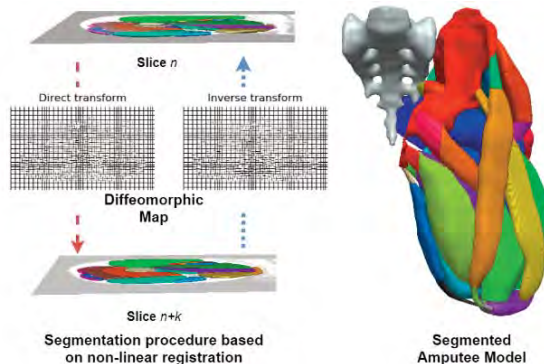


Figure 1: Unsupervised, image segmentation algorithm for segmentation of soft and hard-tissues.

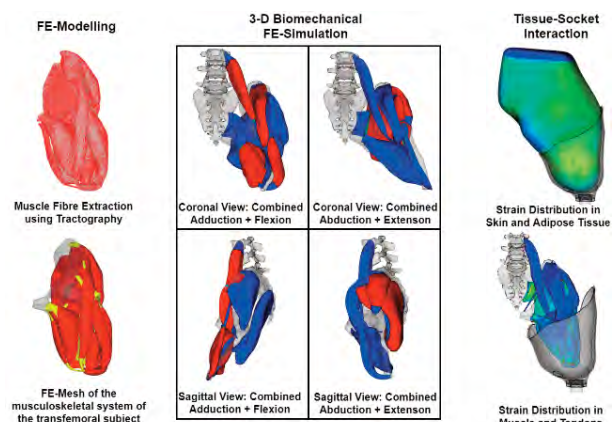


Figure 2: The 3D, FE-model and the biomechanical simulations to predict soft-tissue deformation.

4. Discussion and Conclusions

The current study provides a deeper understanding on the role of muscular physiology in the resulting residual limb biomechanics. As a result, the presented findings could be extended beyond socket development towards efficient surgical planning to ensure effective stabilization and interaction with prosthetic sockets.

5. References

- Röhrle, O., Sprenger, M., and Schmitt, S. (2017). A two-muscle, continuum-mechanical forward simulation of the upper limb. *Biomechan. Model. Mechanobiol.* 16, 743–762.

Acknowledgements:

The research leading to these results has received funding from the Bundesministerium für Bildung und Forschung (BMBF) Grant Agreement No. 02P19C093 (Patch-2-Patient).

11.2

A fully regulated hybrid in silico - in vitro cardiorespiratory simulator for comprehensive testing of cardiac assist devices.

Libera Fresiello¹, Krzysztof Zieliński², Maria Rocchi³, Bart Meyns³, Christopher Hayward⁴, Kavitha Muthiah⁴, Dirk Donker¹

¹ University of Twente, Cardiovascular and Respiratory Physiology group, Enschede, Netherlands

² Polish Academy of Sciences, Nalecz Institute of Biocybernetics and Biomedical Engineering, Warsaw, Poland

³ Katholieke Universiteit Leuven, Cardiovascular Sciences, Cardiac Surgery, Leuven, Belgium

⁴ St. Vincent's Hospital, Department of Cardiology, Sidney, Australia

Corresponding author: Asst. Prof. Libera Fresiello, Technohal 3181, 7500 AE Enschede, the Netherlands, phone: +31 53 489 43 57, email: libera.fresiello@gmail.com

1. Introduction

Simulators are expected to facilitate medical device (MD) development and deployment into the medical field. This is important for FDA class III cardiovascular MDs for which extensive testing is required before market approval. We present here a hybrid in silico – in vitro cardiorespiratory simulator as a sophisticated and versatile test bench for these MDs.

2. Materials and Methods

The simulator includes a closed-loop in silico lumped parameters model of the cardiovascular system, ventilation and respiration.

Ventilation, heart and vessels are regulated by dedicated controls. The in vitro system consists of four active hydraulic chambers developed at the IBIB-PAS, that can mimic the pressure/flow in anatomical sites of interest. They act as interfaces to which MDs are connected and tested. For the present work, a Medtronic HeartWare™ HVAD™ was connected between two hydraulic chambers, one reproducing the left ventricle and the other the aorta. The two chambers exchange pressure/flow data in real time with rest of the cardiorespiratory system in silico (Fig.1).

The simulator was tuned to an average end-stage heart failure patient at rest and HVAD was activated at 2620 rpm. Then, body O₂ consumption was manually increased by +422 mL/min to simulate bicycle exercise and the simulator was left to evolve.

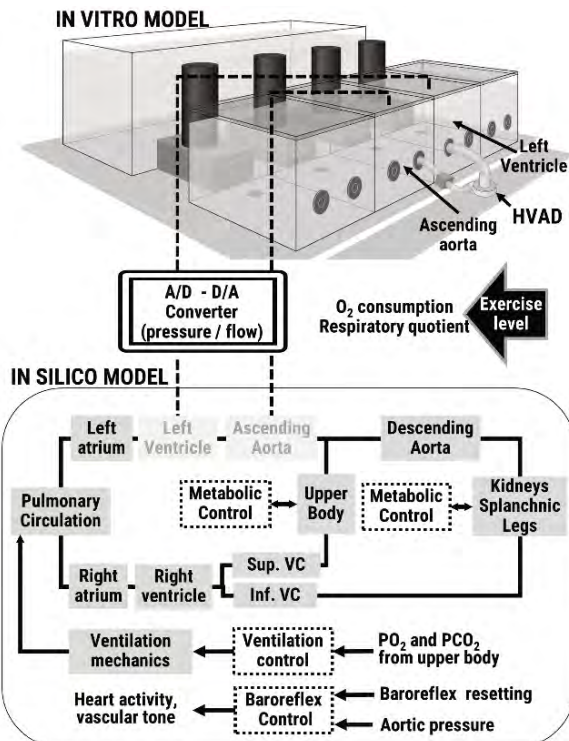


Figure. 1 Schematic overview of the in vitro-in silico simulator with an HVAD.

3. Results

As O₂ consumption is increased, the simulator automatically reacts thanks to its control systems. It predicts the dynamic response to exercise in terms of increase in cardiac output +1.4 L/min, heart rate +18 bpm, ventilation +12 L/min and main hemodynamics, in agreement with [1]. The HVAD reacts to this by changing its performance (flow +1.3 L/min).

4. Discussion and Conclusions

This is, to authors' knowledge, the first closed-loop and fully controlled cardiorespiratory simulator interacting with a real MD. This mixed in silico – in vitro simulation environment offers clear advantages when testing MDs: the in vitro system enables to assess the performance of a real MD (instead of a surrogate model), the in silico system offers a high fidelity model suitable to simulate complex and diversified clinical scenarios. The HVAD was a proof of concept, but the simulator is adaptable to any class III cardiac MD.

5. References

1. Muthiah, K. et al. *The Journal of heart and lung transplantation* 34(4), 522–529 (2015).

11.3

A paradigm shift in decomposing motor units: In silico trials show superiority of magnetomyography over electromyography

Thomas Klotz¹, Francesco Negro², Lena Lehmann¹, Oliver Röhrle¹

¹ University of Stuttgart, Institut for Modelling and Simulation of Biomechanical Systems, Stuttgart, Germany

² University of Brescia, Department of Clinical and Experimental Sciences, Brescia, Italy

1. Introduction

Studying motor units (MUs) is essential for understanding motor control, neuromuscular disorders, and driving human-machine interfaces. Individual MU firings are currently estimated in vivo by decomposing electromyographic (EMG) signals. Due to our body's electric properties, the separability of the individual MU sources is limited [1]. Unlike electrical signals, magnetic fields pass through biological tissues without distortion. This and the emerging technology of quantum sensors make magnetomyography (MMG) a highly promising methodology [2]. However, the full potential of MMG for providing novel insights on neuromuscular physiology has yet to be explored. We investigate if MMG can push the limits of non-invasive MU decompositions. This is achieved by performing in silico trials.

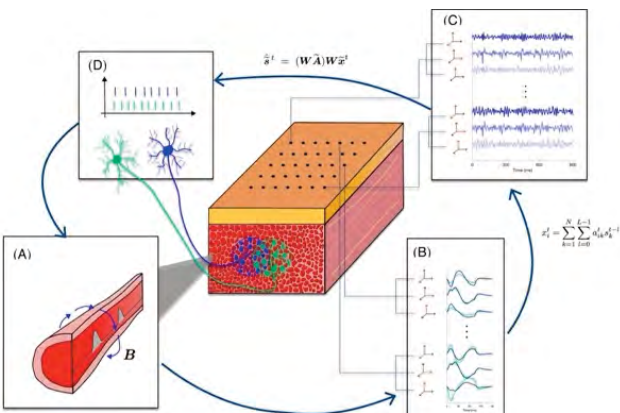


Figure 1: The concept of using MMG as a window into the central nervous system: (A) Active muscles induce magnetic fields and (B) are amplifiers of a MU pool. Hence, deconvolving signals from the muscle (C) yields the MU spike trains (D).

2. Materials and Methods

We use a computational model [3] to simulate the EMG and MMG signals for a population of virtual muscles. To obtain upper bound accuracy estimates for the separability of EMG and MMG we integrate the knowledge on the forward mixing model into a state-of-the art decomposition algorithm [4]. That is, (i) extending the EMG/MMG signal, (ii) whiten the extended signal and (iii) correlating the pre-processed signal with the whitened mixing matrix.

3. Results

Our in silico trials demonstrate the superiority of MMG over EMG for estimating the firing times of individual MUs during voluntary contractions. Decomposing MMG instead of MMG increases the number of separable MUs by 84%. Importantly, MMG decomposition is less biased to detect superficial MUs and hence, provides a more representative view on neuromuscular physiology. Further, the in silico experiments demonstrate that representing a 3D vector field is the most important feature for explaining the MMG's superior separability.

4. Discussion and Conclusions

The presented simulations provide new insights on methods for studying the neuromuscular system in vivo not easily feasible experimentally and hence, guidance for revolutionizing biomedical applications.

5. References

1. Merletti R and Farina D, John Wiley & Sons (2016).
2. Zuo S. et al., *Adv. Mater. Technol.*, 5(6): 2000185 (2020).
3. Klotz T et al, *Biomech. Model. Mechanobiol.*, doi:10.1007/s10237-022-01572-7 (2022).
4. Negro F et al., *J. Neural Eng.*; 13:026027 (2016).

Acknowledgements:

The research was partially funded by the Deutsche Forschungsgemeinschaft (DFG, German Research Foundation) under Germany's Excellence Strategy – EXC 2075-390740016 and through BMBF 3DFoot under contract numbers 01EC1907B

11.4

AI-powered modeling approaches to predict the efficacy of new therapies for autoimmune diseases

Philippe Moingeon¹, Graham Ball², Vincent Hurez³, Emiko Desvaux⁴, Sandra Hubert⁴, Christina Friedrich³, Dimitrios Zafeiris⁵, Mike Reed⁶, Simon Hayworth⁵, Audrey Aussy⁷, Perrine Soret⁷, Jacques Olivier Pers⁸, Sylvain Foulard⁷, Glenn Gauderat⁴, Mickael Guedj⁷, Laurence Laigle⁷

1 Servier, Yvelines, Suresnes, France

2 Intellomx, R and D, Nottingham, United Kingdom

3 Rosa, R and D, San Carlos, United States

4 Servier, R and D, Suresnes, France

5 Intellomx, Nottingham, United Kingdom

6 Rosa, San Carlos, United States

7 Servier, Suresnes, France

8 Université Brest, Brest, France

1. Introduction:

Autoimmune diseases such as primary Sjögren's syndrome (pSS) and Systemic Lupus Erythematosus (SLE) still require better therapies to address unmet medical needs. To this aim, various models of pSS and SLE are generated by integrating molecular profiling data obtained from large cohorts of patients with artificial intelligence (AI) and machine learning (ML). We report the development of such models in order to document patient heterogeneity, identify therapeutic targets and simulate in silico the efficacy of drug candidates for autoimmune diseases.

2. Methods:

Multomics profiling data of whole blood samples from 304 pSS patients and 330 matched controls from the PRECISEADs IMI cohort were used to stratify patients by hierarchical and k-means clustering [1]. A parallel modeling of pSS based on Artificial Neural Networks (ANN) data mining and ANN Inference (ANNi) [4] was undertaken on transcriptomics data in the blood and in salivary glands [2]. A quantitative system pharmacology (QSP) PhysioPD Platform of SLE was developed and qualified using the Model Qualification Method [3] to assess the efficacy of the pan-neutralizing anti-interferon (IFN)-1 S95021 monoclonal antibody. This model encompasses quantitative data related to keratinocytes, immune cell subsets and biological mediators in the blood, skin and lymph nodes. It also integrates components of the Cutaneous LE Disease Area and Severity Index (CLASI) based on published responses to existing or investigational drugs.

3. Results:

The integrated analysis of multomics profiling data led to the identification of 4 clusters of pSS patients. Gene enrichment analyses further revealed distinct patterns of immune dysregulation across clusters [1]. ML approaches allowed identification of classifiers to sort patients in either one of those clusters. Using ANN-based network inference, pSS was represented in the blood and in salivary glands as an interactome of dysregulated genes when compared with the homeostatic state of non-Sjögren controls. This model identified previously undescribed molecular drivers as candidate therapeutic targets for drug discovery, while confirming the relevance of type I IFN in the pathophysiology of pSS. Further simulations were conducted through computational perturbations of the interactome to assess in silico the benefit of targeting selected molecular hubs to treat pSS.

The mechanistic QSP model of cutaneous lupus yielded simulations of the CLASI score responses which matched published clinical trial data with existing drugs. The model further predicted the efficacy of the S95021 antibody in cutaneous lupus. A 492-virtual patient cohort was created to

identify SLE patient phenotypes that would benefit the most from S95021. QSP modeling provided evidence on candidate biomarkers to predict those foreseen responders, as well as insights on optimal dosing regimens to enhance S95021 clinical efficacy.

4. Discussion and conclusions:

The use of AI and ML allows integration of massive and multimodal molecular profiling data from large cohorts of patients, thus yielding various models of complex autoimmune diseases. Together with QSP simulation of virtual patients, such models are powerful tools to inform drug development and support precision medicine strategies. As such, they provide supportive data to document both drug efficacy and safety, while increasing significantly the probability of success of confirmatory real-world clinical studies.

5. References:

1. Moingeon P et al. *Drug Discov Today*; 27:215-222 (2022).
2. Soret P et al. *Nature Commun*; 12: 3523-3541 (2021).
3. Friedrich, C.M. et al. *CPT Pharmacometrics Syst Pharmacol*; 5(2): 43-53 (2016).
4. Tong Dong L et al. *Frontiers Immunol*; 11: DOI 10.3389/fimmu.2020.00380 (2022)

6. Acknowledgements:

These studies were funded by Servier.

11.5

Effect of flow diverter deployment variability on velocity reduction in intracranial aneurysms

Benjamin Csippa¹, Gábor Závodszky², Levente Sándor¹, Márton Németh¹, István Szikora³, György Paál¹

¹ Budapest University of Technology and Economics, Department of Hydrodynamic Systems, Budapest, Hungary

² University of Amsterdam, Informatics Institute, Amsterdam, Netherlands

³ National Institute of Mental Health, Neurology and Neurosurgery, Department of Neurointerventions, Budapest, Hungary

1. Introduction

In Silico trials on the treatment of intracranial aneurysms have a great potential to at least partially replace traditional clinical trials. Furthermore, as stated by [1], such trials could extend the knowledge compared to what can be gathered from a clinical trial since a large number of scenarios can be evaluated. A statistically powerful trial would have to address multiple layers of data uncertainty or variability to ensure that a proper virtual population is tested. Here, one aspect of such a layer is analysed, namely the variability of the flow diverters and their effect on the flow field inside the aneurysm sack.

2. Materials and Methods

Five patient-specific aneurysm geometries were selected for this computational study. The mechanical and hydrodynamic resistance properties of flow diverter (FD) devices from two manufacturers were measured previously in various deployment scenarios [2]. Here, FD data are selected for nominal (parent artery diameter is the same as the FD nominal diameter) and oversized (larger stent in smaller parent artery) scenarios.

Deployment simulation was carried out using the finite difference method. Stents are modelled as an interconnected spring network and their parameters were calibrated by mechanical measurements. Fluid simulations were based on the lattice-Boltzmann method in which the FD is modelled as a homogeneous porous material, set according to the Darcy-Forcheimer law. Pulsatile boundary condition was set on the inlet and Murray's law was applied on the outlets. In total, 85 simulations were performed, and later automatically post-processed. Velocity reduction is defined as the relative difference of the temporal and spatial sac average velocity between the non-stented and stented scenario.

3. Results

Figure 1. shows the velocity reduction as the function of the linear resistance coefficient. The colours represent the different cases and the different symbols – triangle and x – the nominal and oversized cases, respectively. The horizontal dashed line presents the cut-off value of 35% velocity reduction, which according to [1] is defined to be a successful outcome in terms of aneurysm occlusion.

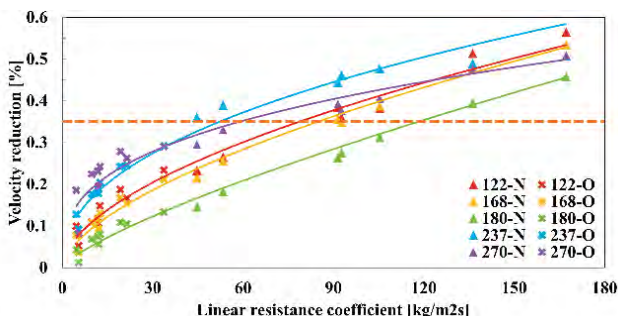


Figure 1: Five aneurysm cases (colours). Velocity reduction for 16 FD deployment scenarios. The triangle and "x" symbols represent the nominal and oversized scenarios.

4. Discussion and Conclusions

Strong power law relationships were found between the linear resistance coefficients and velocity reductions for all cases ($R^2 = 0.92-0.99$). However, the velocity reduction and the quadratic resistance coefficient do not reveal any relationship. Therefore, it seems that the peri-aneurysm velocity range is mostly affected by the linear coefficient.

Trying multiple scenarios for all of aneurysm cases showed that the 35% cut-off value was reached only with the nominal deployments. Still, in some cases the oversized deployments also reached almost 30% reduction, implying that "low-profile stenting" could be feasible.

In an in-silico trial additional information can be obtained compared to a traditional clinical trial. Analysing various deployment scenarios for a given aneurysm gives an estimation of the applicability range based on the velocity reduction. Furthermore, the connection between aneurysm morphology and deployment scenarios is a good candidate for uncertainty quantification in the near future with a sufficient number of cases.

5. References

1. Sarrami-Foroushani, A. et al., *Nature communications*, 12(1), pp.1-12 (2021).
2. Gyürki, D. et al., *Clinical Neuroradiology* (2021).

Acknowledgements:

We acknowledge the EU's Horizon 2020 research and innovation programme (*In Silico World*) (No: 101016503) for funding.

11.6

Modelling endogenous tissue restoration using a homogenized constrained mixture theory

Thibault Vervenne¹, Lauranne Maes¹, Amber Hendrickx², Stéphane Avril³, Felipe Sempértegui³, Nele Famaey¹

¹ KU Leuven, Department of Mechanical Engineering, Leuven, Belgium

² KU Leuven, Department of Cardiac Surgery, Leuven, Belgium

³ Mines Saint-Etienne, Université de Lyon, Université Jean Monnet, INSERM, Saint-Étienne, France

*Corresponding author. KU Leuven, Biomechanics Section, Celestijnenlaan 300, box 2422, 3001, Leuven, Belgium. E-mail address: thibault.vervenne@kuleuven.be (T. Vervenne).

1. Introduction

Endogenous Tissue Restoration (ETR) is a new therapeutic approach, enabling the patient's own body to restore a new blood vessel or heart valve. With ETR, the natural healing system develops tissue that pervades a biodegradable scaffold, forming a fully functional blood vessel or heart valve. ETR is enabled by biodegradable polymers, and a transformation process takes place from a synthetic scaffold into remodelled tissue. ETR modelling can be used to predict this acute and long-term response of in-situ tissue engineered devices.

2. Materials and Methods

A homogenized constrained mixture theory (HCMT) approach is used for ETR model development. The HCMT considers a mixture of material constituents that are constrained to deform together from an arbitrary reference configuration to the current configuration with deformation gradient F . Eq. 1. From the reference configuration towards a stress-free state, growth first leads to an inelastic deformation F_g defining changes in mass. Secondly, an inelastic remodelling deformation F_r^i represents mass exchange, i.e. change in microstructure, of each constituent i . Finally, an elastic deformation F_e^i maps the deformation from its individual stress-free state to the current configuration of the mixture. The considered constituents are elastin, collagen, smooth muscle cells and graft material [1]. A UMAT is used to simulate the ETR process with the finite element (FE) software Abaqus.

$$F = F_g F_r^i F_e^i$$

Credibility of the model will be assessed according to the ASME V&V 40 methodology. Analytical code and calculation verification will be performed. Simulated ETR results will be validated against ovine experimental data by comparison in terms geometry from imaging, First Piola-Kirchhoff stresses from mechanical testing, constituent fractions from histology, and gene upregulation from RNA-sequencing.

3. Results

Factors driving the evolving mass turnover of constituents in a cylindrical FE model include the loss of polymeric graft on the one side, and the mass production and mass degradation of inflammation-driven and mechanobiologically-mediated remodelling on the other side (Fig. 1a). Fig. 1b depicts the evolving vessel diameter and wall thickness during the ETR simulation.

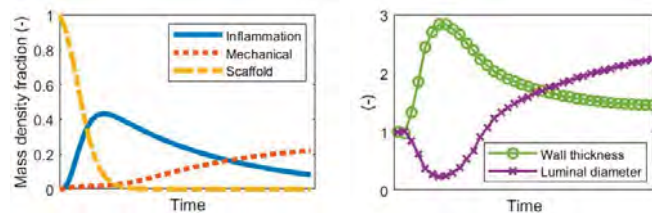


Figure 1: (a) Simulated collagen remodelling and scaffold degradation. (b) Resulting geometry.

4. Discussion and Conclusions

The FE model simulates a combined scaffold-degradation and tissue-restoration process, with a spontaneous reversal of vessel narrowing and thickening [2]. It is hypothesized that transient inflammatory neotissue turnover initiates natural and long-term mechanical remodelling. Additional animal trial data (Fig. 2), together with risk assessments and uncertainty quantification, will contribute to the successful completion of an in-silico clinical trial.

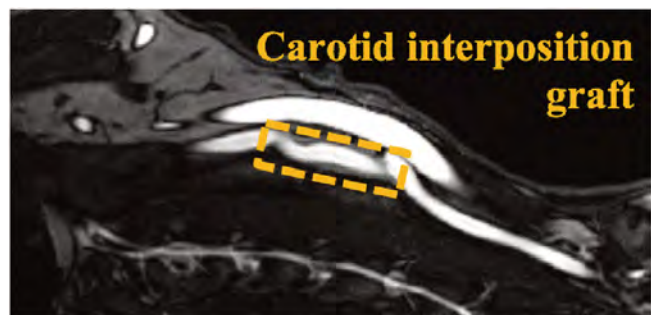


Figure 2: follow-up MRI angiography of scaffold.

5. References

1. Cyron CJ et al, *Biomech Model Mechanobiol*; 15:1389-1403 (2016).
2. Drews JD et al, *Sci Transl Med*; 12:6919 (2020).

Acknowledgements:

The authors would like to thank the European Commission and its Horizon 2020 funding program (Grant ID: 101017523) for providing financial support to the SimInSitu project.

11.7

Pathway activation models for deep brain stimulation in rodents

Jan Philipp Payonk¹, Ursula van Rienen^{1,2,3}, Revathi Appali^{1,3}

¹ University of Rostock, Institute of General Electrical Engineering, Rostock, Germany

² University of Rostock, Department of Ageing of Individuals and Society, Rostock, Germany

³ University of Rostock, Department Life, Light & Matter, Rostock, Germany

jan.payonk@uni-rostock.de

1. Introduction

Deep Brain Stimulation (DBS) is an effective treatment option for different brain disorders. Since the mechanisms of action of DBS are not fully understood, research in animal models is essential to enhance our knowledge. For this purpose, in-silico studies assist animal research by modeling the brain and the DBS electrodes. To get precise models, the imaging and the analysis of these images are crucial. Since modern equipment enables high-quality images of rodent brains, the field of pathway activation modeling is evolving. In this study, we derive white matter fiber tracts from images of the rodent brain to generate pathway activation models (PAM) and investigate the activation for different stimulation settings.

2. Materials and Methods

Our studies include two different open-source toolboxes to generate comprehensive and reliable computational models, including our in-house open-source software platform OSS-DBS [1]. Here we use the finite element method (FEM) to solve the so-called electro-quasistatic equation

in a specific domain (Ω), to simulate the distribution of the electric field in the rodent's brain. Further, we use the open-source Matlab software package Lead-DBS [2] as a comprehensive electrode reconstruction and visualization tool.

A simple computation of active pathways can be done by calculating the volume of tissue activated (VTA) and marking all intersected fibers as active. We derive our models with a more complex method by solving the cable equation for all fibers in the vicinity of the stimulation electrode (Fig. 1).

3. Results

Based on the activation calculations done in OSS-DBS on the rodent brain model, we can visualize the activated fibers or fiber bundles for different stimulation settings.

We intend to compare our results with different electrode positions in rodent brains. The overarching goal is to compare the results with the experimental data.

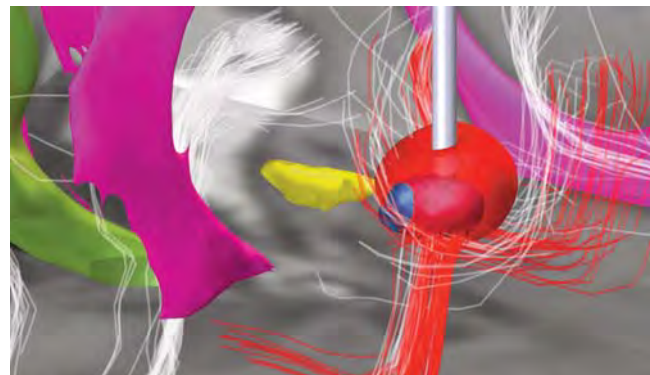


Figure 1: PAM for a rat model using the Johnson rat atlas [3]. Simulation shows active pathways (red) and inactive pathways (white) induced by EPN (blue) stimulation.

4. Discussion and Conclusions

Since DBS is used for numerous motor- and non-motor diseases, it is essential to understand the brain's connectivity. PAM supersede VTA calculations by employing anatomical information to get more realistic simulations. Hence PAM for rodents are of significant interest for further DBS research.

5. References

1. Butenko K et al, *PLoS Computational Biology*. 16(7): 1-18. (2020).
2. Horn A et al, *NeuroImage* 184: 293-316. (2019).
3. Johnson GA et al, *NeuroImage* 62: 1848-1856. (2012).

Acknowledgments:

Funded by Deutsche Forschungsgemeinschaft (DFG, German Research Foundation) - SFB 1270/2 – 299150580.

11.8

Towards in silico trials to assess the performance of thrombectomy devices

Sara Bridio¹, Giulia Luraghi¹, Praneeta Konduri^{2,3}, Nerea Arrarte Terreros^{2,3}, Henk Marquering^{2,3}, Charles Majoie³, José Félix Rodriguez Matas¹, Francesco Migliavacca¹

¹ Politecnico di Milano, Laboratory of Biological Structure Mechanics (LaBS), Department of Chemistry, Materials and Chemical Engineering, Milano, Italy

² Amsterdam UMC, locatie AMC, Department of Biomedical Engineering and Physics, Amsterdam, Netherlands

³ Amsterdam UMC, locatie AMC, Department of Radiology and Nuclear Medicine, Amsterdam, Netherlands

1. Introduction

Several randomized clinical trials proved the efficacy of stent-retriever thrombectomy as a treatment for acute ischemic stroke due to large vessel occlusions [1]. The introduction of new devices into the market would benefit from the use of in silico trials based on high-fidelity computational simulations of the clinical procedure [2] to reduce times and costs of the usual clinical trials. In this work, an in silico methodology is implemented to compare the performance of two commercial devices in patient-specific vascular models.

2. Materials and Methods

An automatic procedure was implemented to reconstruct 100 patient-specific vascular models from images of stroke patients collected from the MR CLEAN registry [3] (Fig.1). Thrombi of different lengths and compositions following literature distributions [4,5] were placed in the middle cerebral artery (MCA) of each model. The models were used to run validated finite-element simulations of the thrombectomy procedure [2] (Fig.2a), with two different stent-retrievers for each virtual patient (Stent A and Stent B). The stent was optimally placed with respect to the occlusion following clinical guidelines [6]. The performance of the two devices was assessed by comparing the outcomes of the simulations: a procedure is considered to have a positive outcome if the thrombus is removed from the vessel, negative otherwise.

3. Results

With the Stent A, 96 out of 100 simulations had an admissible outcome (4 of them had numerical instability), and of these 13 (14%) had a negative outcome. With the Stent B also 96 out of 100 simulations had an admissible outcome, and 10 of them (10%) had a negative outcome. The causes for negative outcomes were either the thrombus was lost at the bifurcation or in the carotid siphon. The Stent B has a dual-layer design that ensured a stronger engagement of the thrombus during retrieval (Fig.2b).

4. Discussion and Conclusions

A set of 96 high-fidelity simulations of the thrombectomy procedure was used to assess the performance of two commercial devices. The high success rate was mainly due to the optimal stent positioning. Future analyses can consider non-optimal conditions. This methodology can be used for the assessment of the performance of new thrombectomy devices.



Figure 1: Examples of reconstructed patient-specific vasculatures.

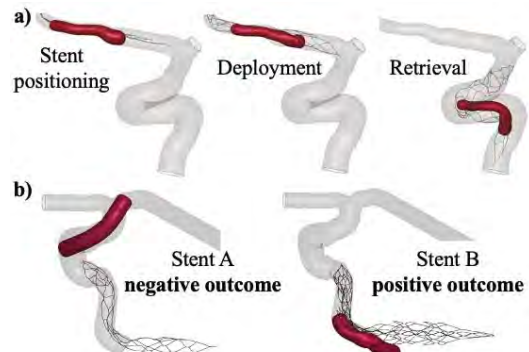


Figure 2: a) Steps of the thrombectomy simulation; b) example of different performance of the two devices for the same virtual patient.

5. References

1. Goyal et al., Lancet; 387:1723-31 (2016).
2. Luraghi et al., J Biomech; 126:110622 (2021).
3. Jansen et al., BMJ; 360 (2018).
4. Boodt et al., Stroke; 51:1727-35 (2020).
5. Duffy et al., Stroke; 50:1156-63 (2019).
6. Ospel et al., Exp Rev Med Dev; 16:955-63 (2019).

Acknowledgements:

This project has received funding from the European Union's Horizon 2020 research and innovation programme under grant agreement No 777072 and from the MIUR FISR-FISR2019_03221 CECOMES.

12.1

A 1D co-axial model for coupled blood-CSF flow simulations in cerebral vascular-perivascular networks

Beatrice Ghitti¹, Eleuterio F. Toro², Francesco Costanzo³, Bianca Maria Laudenzi¹, Sagar Buch⁴, E. Mark Haacke^{5,6}, Lucas O. Müller¹

¹ University of Trento, Department of Mathematics, Trento, Italy

² University of Trento, Laboratory of Applied Mathematics, DICAM, Trento, Italy

³ The Pennsylvania State University, Center for Neural Engineering, University Park, PA, United States

⁴ Wayne State University, Department of Neurology, Detroit, MI, United States

⁵ Wayne State University, Department of Radiology, Detroit, MI, United States

1. Introduction

The brain parenchyma lacks a conventional lymphatic system for waste clearance, while the “glymphatic circulation hypothesis” remains controversial [1]. Even if flow of cerebrospinal fluid (CSF) in perivascular spaces (PVS) surrounding cerebral arterial vessels is widely accepted as a key mechanism for brain solute transport and clearance, the nature and driving forces of CSF flow and solute transport remain unclear. Mathematical modelling and fluid dynamics simulations represent a valuable complementary tool to experimental approaches in understanding the mechanisms driving fluid flow and solute transport in PVS, see for instance [2,3,4].

2. Materials and Methods

In this work, departing from [5], we present a one-dimensional (1D) co-axial model for computing the CSF flow within the PVS coupled to the blood flow dynamics. The model consists of two flexible co-axial tubes, the inner representing the arterial vessel and the outer being the surrounding CSF-filled PVS. The geometrical and mechanical characterization of both domains and corresponding fluids is addressed. As commonly done for blood flow, suitable coupling conditions are also derived and applied to couple multiple 1D PVS domains and simulate the blood-CSF flow dynamics in networks.

3D models based on the incompressible Navier-Stokes equations become very expensive, computationally, when simulating large 3D networks of vessels and PVS. Therefore, we adopted a 1D co-axial model, which is still able to accurately predict fluid flow and pressure in both cerebral vessels and PVS, but at a much lower computational cost. Furthermore, in most published models ([3,4] for instance), only the fluid dynamics in the PVS is simulated, whereas the blood vessel's wall movement is simply prescribed at the inner boundary of the PVS. Our proposed modelling approach allows to couple and simultaneously describe both blood and CSF flow dynamics, to study the full interaction between vascular and perivascular flow and deformation.

3. Results and Discussion

In this contribution, we will show the results obtained by applying the proposed model to solve increasingly large vascular-perivascular networks. Results from a single vessel-PVS configuration and a simple bifurcation will be compared to available experimental and computational data. Then, blood-CSF flow simulations will be performed on real cerebral arterial networks of superficial/cortical arteries reconstructed from in-vivo MRI data, as the one shown in Fig. 1. Different scenarios will be tested and investigated, such as the potential role of arterial pulsations and pressure gradients as driving forces for CSF flow through the PVS.



Figure 1: 3D rendering of a cerebral arterio-venous network reconstructed from in-vivo high-resolution MRI data in human brain. Blue: venous territory of left septal veins; Red: matching arterial network of superficial/cortical arteries.

4. Conclusions

The proposed 1D co-axial model sets the basis for an efficient computational and modelling framework for simulations of the coupled blood-CSF flow dynamics in increasingly large networks of cerebral vessels and PVS and to explore and investigate current hypotheses about the nature, mechanisms and driving forces of CSF flow and solute transport through PVS and their role in brain waste clearance.

5. References

1. Hladky SB, Barrand MA. *Fluids Barriers CNS*. 2022; 19(1):9.
2. Martinac AD, Bilston LE. *Biomech Model Mechanobiol*. 2019; 19(3):781-800.
3. Kedaresetti RT et al. *Sci Rep*. 2020; 10(1):10102.
4. Daversin-Catty C et al. *arXiv*:2111.12451. 2021.
5. Toro EF et al. *J Biomech Eng*. 2019; 141(1):011004.

12.2

A chemotaxis model of peritoneal adhesions

Madge Martin¹, Thibault Lemaire²

1 CNRS, Univ Paris Est Creteil, Univ Gustave Eiffel, UMR 8208, MSME, Creteil, France

2 Univ Paris Est Creteil, Univ Gustave Eiffel, UMR 8208, MSME, Creteil, France

*madge.martin@u-pec.fr

1. Introduction

Peritoneal adhesions are pathological fibrotic connections forming between organ surfaces. They typically follow a surgical procedure of the thorax, abdomen or pelvis, or result from inflammatory diseases such as Crohn's or endometriosis. Adhesions can cause small bowel obstruction, chronic pain or infertility.

During the process of tissue repair after insult, a fibrin exudate is formed [1,2]. Mesothelial cells (MC) ensure the fibrin breakdown by secreting enzymes such as tissue plasminogen activator (tPA). However, adhesion promoting factors such as hypoxia or necrosis impair the fibrinolytic activity of the protective lining. Fibroblasts (FB) stemming from migration or MC phenotype transition build extracellular matrix and collagen to form long-lasting adhesions [2]. So far, there is no model available to study adhesion formation despite the lack of answer to this clinical problem.

2. Materials and Methods

We propose here a model of adhesion formation representing in 2D the volume B between the peritoneal serosa ∂B_p and the tissue boundary ∂B_t , where the following mechanisms occur: (i) the formation of the fibrin exudate upon tissue insult, and (ii) FB-mediated fibrosis. To this end, we implemented in Comsol Multiphysics 5.4 a system of differential equations depicting the time- and space-dependent evolution of four variables: the fibrin, collagen and tPA levels and FB concentration.

Fibrin (F_n), tPA (t_{PA}) and FB (b) evolutions are represented by an interdependent system of partial differential equations accounting from fibrin-mediated chemotaxis of FB (sensitivity χ), which evolve as follows in the volume B:

$$\frac{\partial}{\partial t} \begin{bmatrix} b \\ F_n \\ t_{PA} \end{bmatrix} = \nabla \cdot \begin{bmatrix} \mu_{Fb} \nabla b - \chi b \nabla F_n & b \\ D^{Fn} \nabla F_n & -d \cdot F_n \\ D^{tPA} \nabla t_{PA} & t_{PA} \end{bmatrix}$$

where $d = [a_b, d_{Fn}, d_{tPA}]$ accounts for FB apoptosis A_b , fibrin (d_{Fn}) and tPA degradation (d_{tPA}). The time-derivative of the collagen content c is defined as a linear function of FB activity and collagen degradation.

Constant fibrin ϕ_{Fn} and FB ϕ_b fluxes are imposed on the injury site. Outside the injury, a fibrinolytic tPA flux ϕ_{tPA} is set to a constant flux ϕ_{tPA}^0 to account for the action of MCs and decreased to $\phi_{tPA} = (\phi_{tPA}^0)/100$ for an adhesive (pathological) repair.

3. Results

Figure 1 highlights FB seeding into the fibrin exudate, producing collagen, therefore connecting the tissue and serosa boundaries. The black and white lines mark the bounds of the collagen-rich volumes in adhesive and healthy repairs, respectively (threshold $c \geq 100 \mu\text{g}/\text{mg}$, representing dense adhesions as per histological data [2]). In the case of a healthy regeneration, the inhibition of fibrin by tPA-mediated fibrinolysis prevents formation of the dense connective tissue bond (white line).

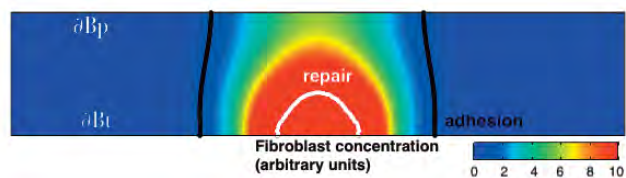


Figure 1: Fibroblast concentration 10 days after tissue trauma, resulting in an adhesive bond (black) or repair (white) depending on fibrinolytic activity.

4. Discussion and Conclusions

This is the first attempt to quantify the mechanisms of adhesion formation. We successfully depicted the main events following tissue trauma. Future work will investigate the next remodelling steps, in particular involving innervation and in vivo mechanical stimulation.

5. References

1. Brochhausen et al., *J Gastrointest Surg*; 16(6):1256-1274 (2012).
2. Binnebösel M et al., *Langenbecks Arch Surg*; 393:59-66 (2008).

12.3

A mechanistic model of 3rd generation tyrosine kinase inhibitor on lung adenocarcinoma evolution

MARTIN BASTIEN¹, Nicoletta Ceres¹, Hippolyte Darré¹, Guillaume Bouchard¹, Riad Kahoul¹, Raphaël Toueg², Lucile Lefevre², Jacques Cadranel³, Nicolas Girard⁴, Jean-Louis Palgen¹, Claudio Monteiro¹, Adèle L'Hostis¹

1 Novadiscovery, Lyon, France

2 Janssen-Cilag France, Issy-les-Moulineaux, France

3 Service de Pneumologie, Hôpital Tenon, Assistance Publique-Hôpitaux de Paris (AP-HP) and Université Pierre-et-Marie-Curie (Paris 6), Paris, France., France

4 Respiratory Medicine Department, Hospices Civils de Lyon, Lyon, France; Claude Bernard University Lyon 1, Lyon, France, France

1. Introduction

16,4% of lung adenocarcinomas are caused by a mutation in the Epidermal Growth Factor Receptor (EGFR) as reported in the Epidemiological Strategy and Medical Economics (ESME) database[1], resulting in the constitutive activation of downstream pathways, and eventually in cell proliferation and progression. Most common mutations occur on exons 19 and 21 of the protein, but 3,9% of them emerge from insertions in the exon 20[1]. While some tyrosine kinase inhibitors (TKIs) have been developed to target EGFR+ mutations, exon 20 insertions are known to be resistant to many of them[2]. 3rd generation TKIs can show a partial activity on exon 20 insertions, but the extent of this activity remains to be characterized[2]. Based on an in silico approach, we investigate here the impact of TKIs on tumor size according to EGFR mutations.

2. Materials and Methods

We built a mechanistic model including tumor size evolution according to patient individual characteristics and a full physiologically-based pharmacokinetics/pharmacodynamic (PBPK/PD) model of 3rd generation TKIs. This model notably allows exploration of the impact of TKIs on tumor size according to the EGFR mutation and the co-mutations present.

3. Results

The model successfully reproduced biological behaviors (i.e pharmacokinetics and tumor size evolution) observed in mice and humans. As expected, while common EGFR mutations (exon 19 and 21) were more sensitive to 3rd generation TKI than exon 20 insertion mutations, response variability was observed based on the consideration of mutations.

4. Discussion and Conclusions

This model paves the way to a further exploration of the efficacy of treatment on given patients, based upon individual characteristics. It moves us closer to an effective, rational approach to personalized medicine.

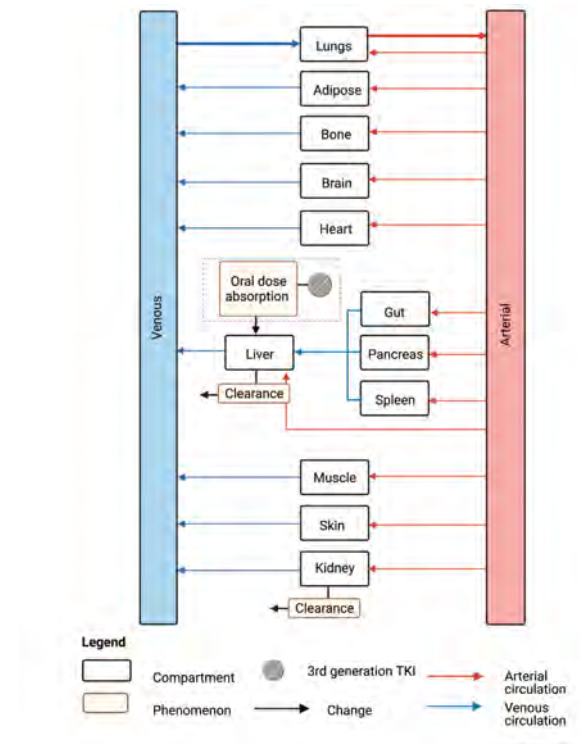


Figure 1: Schematic representation of part of the model, representing 3rd generation TKI PBPK model from absorption (dotted line rectangle), distribution in major organs, liver metabolism and systemic elimination through liver and kidney.

5. References

- Chouiad C. et al. "A Real-World Study of Patients with Advanced Non-squamous Non-small Cell Lung Cancer with EGFR Exon 20 Insertion: Clinical Characteristics and Outcomes", Targeted Oncology, 2021
- Vyse, S., & Huang, P. H. (2019). "Targeting EGFR exon 20 insertion mutations in non-small cell lung cancer. Signal transduction and targeted therapy", 4, 5

Acknowledgements:

The authors would like to thank Janssen-Cilag France for the support to the project.

12.4

Age and sex informed uncertainty quantification of a 1D-model of the common carotid artery

Friederike Schäfer¹, Jacob Sturdy¹, Leif Rune Hellevik¹

¹ Norwegian University of Science and Technology, Department of Structural Engineering, Trondheim, Norway

1. Introduction

Lifestyle, ageing, and diet change the material properties of arteries [1-3]. Abnormal alterations can lead to cardiovascular diseases like calcification and aneurysm formation. It is recognized that the local arterial stiffness can be a marker for these diseases, but it cannot be directly measured in humans [4].

Through inverse modelling it is possible to estimate material properties from non-invasive measurements. Since the inverse problem estimation depends on the behaviour of the direct model, it is necessary to explore the model's sensitivity to uncertain input parameters. In this work, we aim to quantify the uncertainty of the direct model's output due to population variations in different age and sex groups. Additionally, we determine the model parameters resulting in the greatest output variability.

2. Materials and Methods

The common carotid artery is represented in a 1D model. The interaction between the blood flow and the arterial wall is described with the linear elastic tube law relating the pressure to the area. The boundary conditions are a prescribed flow rate at the inlet and a three-element Windkessel model at the outlet.

Polynomial chaos expansion is applied to quantify the uncertainty due to population variations in model parameters for different age groups. Furthermore, we investigated if there are differences in terms of model output variability due to gender. Computing the main and total sensitivity indices gives insights into the most sensitive parameters.

3. Results

Results suggest that the variations of the input parameters associated with each sex lead to the same ranking in the sensitivity analysis for each age group. Variations in the arterial compliance of the Windkessel model seem to have greater influence on model output variability in young adults than in elderly.

4. Discussion and Conclusions

This work showed that the computed pressure, flow rate and area at the mid-point of the artery segment are most sensitive to uncertainties in the material parameters. This high sensitivity to stiffness is a necessary condition for inference of stiffness through an inverse problem, however, it is not a sufficient condition. This work supports the feasibility of developing an inverse method for estimating local arterial stiffness of the carotid artery.

5. References

1. Chirinos AJ. et al., *J. Am. Coll. Cardiol.*, 74: 1237–1263 (2019).
2. G. Parati G, Salvi P, *Blood Pressure and Arterial Wall Mechanics in Cardiovascular Diseases*; Springer, 2014. p. 163–173.
3. van de Vosse F, Stergiopoulos N., *Annu Rev Fluid Mech*, 43: 467–499 (2011).
4. Alastruey J et al., *J Biomech*, 44:12 (2011).

Acknowledgements:

The authors would like to thank the Polish National Science Center GRIEG programme, (Grant no: UMO-2019/34/H/ST8/00624) for providing financial support to this project.

12.5

Clinical testing of a non-invasive method for lung compliance estimation during pressure support ventilation

Rob S.P. Warnaar¹, Eline Mos-Oppersma¹, Alexander D. Cornet², Dirk W. Donker^{1,3}

¹ University of Twente, Cardiovascular and Respiratory Physiology Group, TechMed Centre, Enschede, Netherlands

² Medisch Spectrum Twente, Department of Intensive Care Medicine, Enschede, Netherlands

³ University Medical Centre Utrecht, Department of Intensive Care Medicine, Utrecht, Netherlands

Rob Warnaar, Technical Medical Centre, University of Twente, Technohal 3184, P.O. box 217, 7500 AE Enschede, the Netherlands, phone: +31 53 489 96 52, email: r.s.p.warnaar@utwente.nl

Introduction

Comprehensive quantification of respiratory system mechanics during pressure support ventilation (PSV) classically requires invasive measurements or interruptions of spontaneous breathing. This limits broad clinical applicability of these methods for lung compliance optimisation during PSV. Therefore, we present a non-invasive approach for individualised PEEP titration based on dynamic lung compliance measurements at the bedside.

Objective

This study focuses on the sensitivity of a non-invasive method for bedside quantification of dynamic lung compliance in response to PEEP interventions in patients receiving PSV.

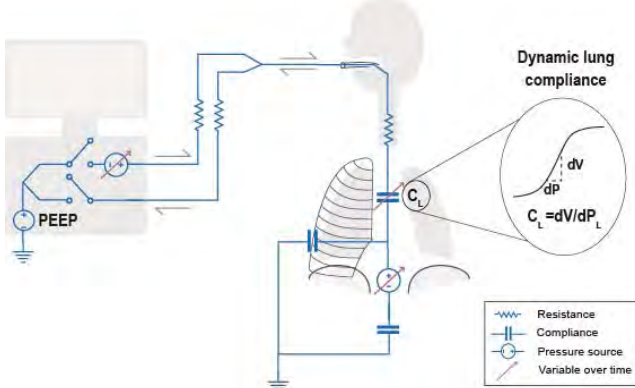


Figure 1: Mechanically ventilated patient represented as an electrical analogue.

Methods

A patient was ventilated in PSV mode applying 4 different PEEP levels: 3, 5, 7, and 9 cmH₂O as part of a clinical study. The study protocol was approved by the regional ethics committee. Pressure, flow and volume traces were extracted from the ventilator. The time constant (airway resistance * respiratory system compliance = RAW * CRS) was estimated as the linearised slope of the expiratory flow-volume, assuming a single compartment model (Fig 1). The airway resistance was determined as the time derivative of the airway pressure divided by the time derivative of the flow, both around zero flow at end-inspiration. CRS per breath was calculated as the RC-time over the median airway resistance over all breaths.

Results

The calculated CRS at each PEEP level are shown in Fig 2. Individualised titration of PEEP was possible using the proposed method, as the PEEP level for maximal lung compliance can be discriminated.

Discussion & Conclusion

We demonstrate that this method allows for non-invasive, individualised PEEP titration during PSV ventilation in a clinical case. This approach has great potential for future bedside use, and therefore deserves further clinical testing, aiming to optimise pressure support ventilation, and promote patient-ventilator synchrony and weaning.

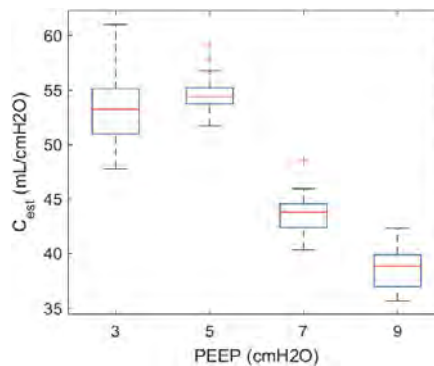


Figure 2: Calculated respiratory system compliance (CRS) at four PEEP levels in one patient.

12.6

Combining machine learning and mathematical modeling in the estimation of T1 relaxation time from cardiac magnetic resonance imaging data

Kateřina Škardová¹, Radek Galabov^{1,2}, Kateřina Fricková¹, Tomáš Pevný³, Jaroslav Tintěra², Tomáš Oberhuber¹, Radomír Chabinicok^{4,5}

1 FNSPE, CTU, Prague, Czech Republic

2 Institute for Clinical and Experimental Medicine, Prague, Czech Republic

3 FEE, CTU, Prague, Czech Republic

4 UT Southwestern Medical Center, Dallas, United States

5 FNSPE, CTU, Prague, Czech Republic

Corresponding author: Kateřina Škardová, Katerina.Skardova@fjfi.cvut.cz

1. Introduction

Biophysical models allow estimating material parameters representing the physical properties of the tissue (e.g. passive myocardial stiffness or contractility using cine or tagged MRI). In this work, we propose a two-stage method for estimating T1 relaxation time from the Modified Look-Locker Inversion recovery (MOLLI) image series, by combining a biophysical model of tissue nuclear magnetic resonance relaxation, neural network (NN), and numerical optimization (NO). The proposed method is evaluated on synthetic data (generated by model); specially-designed MRI phantom experiment; and in vivo patient data. The validation data were acquired on both, 1.5 and 3T MRI systems.

2. Materials and Methods

The model – Bloch simulator – is based on the mathematical description of the relaxation process given by the Bloch equations. Recently, several ways of estimating T1 by optimizing the parameters of Bloch simulator, using separately NO [1] or NN [2], have been pursued. In the proposed method, we combine these two approaches. In our work, the Bloch simulator operates with two sets of parameters: measurement-specific parameters c and tissue-specific parameters p . First, the Bloch simulator $F(c,p)$ provides training data for the NN used in the first stage. Subsequently, the generic model F is turned into a patient- and measurement-specific regime $F^*(p)$ by inputting the known measurement-specific parameters c . In the second stage, the specified model is used to fine-tune the estimated parameters by NO, while using the NN-based estimate as an initial guess.

3. Results

In the phantom study, the proposed method provided results comparable to the MR scanner on 1.5T and results closer to pseudo-ground truth in 7 out of 8 phantoms on 3T. The NO stage improved the accuracy and decreased the variation of T1 obtained by the NN stage.

In the in vivo study, blood, and myocardial T1 obtained by the proposed method was higher than the scanner value in most pre-contrast cases. For an example of the T1 maps from the in vivo study, see Figure 1.

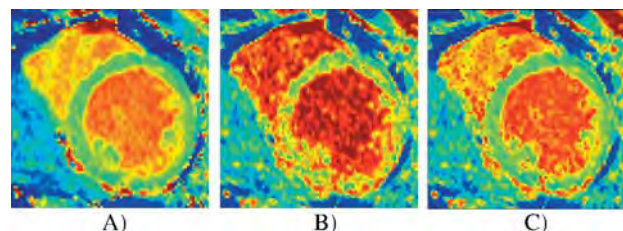


Figure 1: Example of myocardial T1 maps obtained by the MR scanner (A), the first stage (B), and the second stage (C) of the proposed method.

4. Discussion and Conclusions

The NN initialization has the potential to substantially increase the efficiency of the subsequent NO, particularly if the NN is trained beforehand and not for individual patients. The method can be used also in other problems of coupling between in vivo imaging and modeling, particularly when estimating tissue and functional parameters.

5. References

1. J. Shao, et al., *JMRI* 43.2 (2016): 414-425.
2. J. Shao, et al., *MRM* 84.5 (2020): 2831-2845.

Acknowledgements:

This work was supported by MEYS of the Czech Republic under the OP RDE grants no. CZ.2.11/0/0/16_019/0000778, CZ.2.11/0/0/16_019/0000765, by Ministry of Health of the Czech Republic project no. NV19-08-00071 and by Institutional Support MHCZ-DRO IN 00023001, by the Inria France UTSW Medical Center Dallas Associated Team TOFMOD.

12.7

Computational insights on the roles of Dll4-Notch and uPARAP in lymphangiogenic sprouts

Sophie Bekisz¹, Marine Gautier², Thomas Mead^{3 4}, Katie Bentley^{3 4 5}, Agnès Noël², Liesbet Geris^{1 6}

1 ULiège, Biomechanics Research Unit, GLGA In Silico Medicine, Liège, Belgium

2 ULiège, Laboratory of Biology of Tumor and Development, GLGA Cancer, Liège, Belgium

3 Francis Crick Institute, Cellular Adaptive Behaviour Lab, United Kingdom

4 King's College London, Department of Informatics, United Kingdom

5 Harvard Medical School, Center for Vascular Biology Research, Beth Israel Deaconess Medical Center, Department of Pathology, United States

6 KU Leuven, Skeletal Biology and Engineering Research Center, Belgium

*sophie.bekisz@uliege.be

1. Introduction

(Lymph-) Angiogenesis is the formation of new lymphatic/blood vessels by lymph/blood endothelial cells (LECs, BECs) sprouting from pre-existing vessels. Angiogenic sprouts consist of highly motile leading tip cells and a heterogeneous mix of more active and inactive following stalk cells. This heterogeneity of tip and stalk cell motility is governed by a lateral inhibition mediated by the Dll4-Notch pathway. However, much remains unclear on the adaptability of this central tip and stalk cell selection pathway during lymphangiogenic sprouting [1].

This study first investigates the presence and activation of the Dll4-Notch pathway in lymphatics. The possible conservation of the Dll4-Notch regulation of endothelial motile states in lymphatic vessels is then studied. After, using both experiments and adaptation of a well-established computer model of Notch tip selection [3,4], we explore whether a modulator of hyperbranched lymphangiogenesis and VEGFR-2/-3 hetero/homodimer formation [2] – uPARAP - is Notch regulated and thus heterogeneously expressed in more motile LECs.

2. Materials and Methods

In vitro: Cells used are LECs, transfected or not with siRNAs targeting uPARAP. Monolayers of LECs are cultured in various conditions (DAPT treatment, VEGF-C stimulation, Dll4 coating). DAPT is a γ-secretase inhibitor, blocking Notch signaling. Protein modulations are assessed by Western blotting. LEC spheroids embedded in type-1 collagen matrix are cultured in the previously cited conditions. Spheroid images are acquired through confocal microscopy and quantified by computer assisted methods. In silico: The hierarchical agent-based model used here was previously validated as predictive of new *in vivo* mechanisms to explore Notch lateral inhibition and tip cell selection during angiogenesis [3,4]. This *in silico* framework is being adapted to lymphangiogenesis, by including lymphatic-specific players (e.g. uPARAP) and integrating ODEs of lymphatic receptor trafficking.

3. Results

The changes in LEC protein expression levels were similar to previously reported results in BECs. Indeed, increased Dll4 and decreased VEGFR-2 and -3 levels are found after VEGF-C stimulation. In contrast, both receptors levels are increased in DAPT treated cells. Dll4 coating logically activates Notch pathway. Spheroids (Fig 1.) treated with VEGF-C or DAPT both display migration and sprouts. Combination of VEGF-C and DAPT appears to lead to spheroids with longer and larger sprouts (quantification in progress). uPARAP silencing seems to counteract the effect of DAPT on LEC spheroids, highlighting a potential but unexpected role of uPARAP in Dll4-Notch pathway.

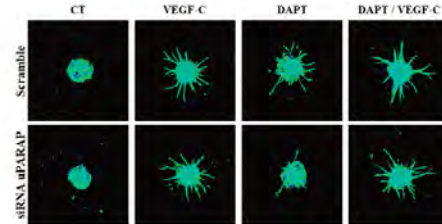


Figure 1: Representative binary images of LEC spheroids in various conditions.

4. Discussion and Conclusions

The Dll4-Notch pathway appears to be activated and to regulate sprouting in LECs similar to BECs. uPARAP silencing has been proven to induce hyperbranched sprouts [2]. Surprisingly, uPARAP silencing leads to a reduction of cell sprouting in the presence of DAPT. Several potential links between uPARAP, Dll4 and Notch, including feedback loops, can be easily implemented in the adapted agent-based computational model [3,4], which then could return the best possible scenarios for induction of abrogation of lymphangiogenic process.

5. References

1. Zheng W. et al., *Blood*, 2011. 10.1182/blood2010-11-317800 2. Durré T. et al., *Nat. Commun.*, 2018. 10.1038/s41467-018-07514-1 3. Bentley K. et al., *Phil. Trans. R. Soc. B*. 2017. 10.1098/rstb.2015.0522. 4. Bentley K. et al., *Plos Comput. Biol.*, 2009. 10.1371/journal.pcbi.1000549

Acknowledgements:

This project received funding from the European Research Council under the European Union's Horizon 2020 research and innovation programme (FP/2014-2020)/ERC (n. 772418) and from the ULiège (A.R.C. "NovLYMPATHIC"). Sophie Bekisz is a FRIA grantee of the Fonds de la Recherche Scientifique-FNRS.

12.8

Model-based personalized anemia therapy: A clinical implementation

Doris Helene Fuertinger¹, David Jörg¹, Sabrina Casper¹, Peter Kotanko^{2,3}

1 Fresenius Medical Care, Biomedical Modeling and Simulation, Bad Homburg, Germany

2 Renal Research Institute, New York, United States

3 Icahn School of Medicine at Mount Sinai, Nephrology, New York, United States

Correspondence: D. H. Fuertinger, doris.fuertinger@fmc-ag.com

1. Introduction

Most patients suffering from end-stage kidney disease develop anemia. Its clinical management poses significant challenges due to highly variable individual disease characteristics. Treatment is further complicated by long-time delays between drug administration and the manifestation of its effects in clinically observable parameters. In this study we present a model-based, fully personalized dose recommendation tool and discuss its implementation and acceptance in a clinical setting.

2. Materials and Methods

A comprehensive mathematical model describing the production of red blood cells and the effect of erythropoiesis stimulating agents (ESA) was introduced in Ref. [1]. A custom parameter estimation methodology was developed to adapt the resulting system of hyperbolic partial differential equations (PDE) to individual patients using routine clinical data. For each patient a set of key parameters was estimated and updated in regular intervals to account for potential changes in individual disease characteristics. A nonlinear model predictive controller (MPC) designed around the PDE model was adapted to a long-acting ESA, similar to the framework presented in Ref. [2]. The parameter estimation technique and the MPC were designed to be robust against noisy and missing data and uncertainties in the individualized model, respectively.

3. Results

The dose recommendation tool as depicted in Fig. 1 was used in a randomized controlled clinical trial. Model parameters and controller output were updated on a bi-weekly basis for each patient. Dose recommendations could be successfully calculated in over 90% of the cases. Reasons for failure to produce a recommendation included (listed in order of occurrence): insufficient coverage with clinical data, model adaptation failures, high predictive uncertainty in the MPC. Acceptance of dose recommendations by the clinical staff was high (~95%).

4. Discussion and Conclusions

Model-based treatment strategies provide a tool to support physicians in tailoring medical treatments to individual patients, particularly in diseases that are challenging to treat. In the example of anemia therapy the use of such a technology led to improved patient outcomes at decreased medication costs.

5. References

1. Fuertinger DH et al. *J Math Biol*; 66, 1209-1240 (2013).
2. Rogg S et al. *J Math Biol*; 79(6-7):2281-2313 (2019).
3. Caiazzo A et al., ICCS 2009 conference: Springer; 2009. p. 705-14

Acknowledgements:

The authors would like to thank the Clinical Research Team, Data Science Team and Clinical Staff of the Renal Research Institute for their significant contributions and support in conducting the clinical study.

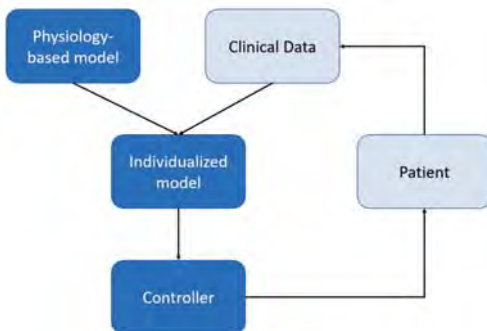


Figure 1: Schematic of the framework to determine individualized dosing recommendations.

13.1

A method for evaluating the performance of a novel percutaneous Left Ventricular Assist Device and optimizing it's design

Bar Vinder¹, Idit Avrahami¹, Chen Hajaj²

1 Ariel University, Mechanical Engineering, Ari'el, Israel

2 Ariel University, Industrial Engineering and Management, Ari'el, Israel

1. Introduction

A novel percutaneous Left Ventricular Assist Device (p-LVAD) based on an axial impeller is designed to treat patients with acute heart failure (see Figure 1a). The device includes an axial impeller with a radial outlet port. The novel design is intended to reduce known complications of the assist device, including blood damage and thrombus formation due to the high rotational speed of the impeller. Experiments were conducted to estimate the VAD performance, and machine learning (ML) algorithms were used to optimize the pump configuration. The suggested design is based on modifying the impeller's hub design and thus improving pump performance and reducing the rotational speed required for sufficient flow and pressure conditions.

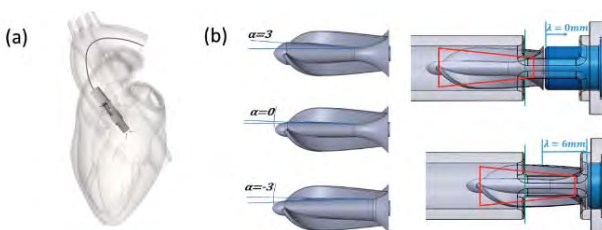


Figure 1 – (a) a schematic description of the p-LVAD model, (b) definition of hub angle (1) and offsets (2).

2. Materials and Methods

In the study, an experimental system was built to evaluate the pump performance as a function of the impeller's hub convergence angle (α) and the offset between the impeller and the outlet window (λ) (see Figure 1b). These two parameters define together the configuration and division between the axial and the centrifugal areas of the impeller. To investigate the effect of the pump's geometry, 5 different impeller designs (of 6mm blades diameter) were examined with 3 different hub angles ($\alpha = (-3)^\circ$ to 3°) and 5 different offsets ($\lambda = 0$ to 6 mm). Flow rate, pressure head, and motor rotation speed were measured for different system loads to analyse the pump's performance. The experiments used water-glycerol solution to simulate the blood viscosity. Each design was tested at 24 varying load resistance and rotational speeds. A machine-learning algorithm was developed to analyse the data, predict the pump performance related to its impeller geometric, and optimize the pump design.

3. Results

Results show pump performance improvement and rotation speed reduction for impellers with a higher hub angle ($\alpha = 2^\circ$ - 3°). In addition, for the specific work condition, there is a correlation between the hub angle and the offset (see Figure 2a). Those results are based on the ML predictions, the adjusted prediction model shows residual errors of up to 10% for 97% of all data from the experiments performed (see Figure 2b).

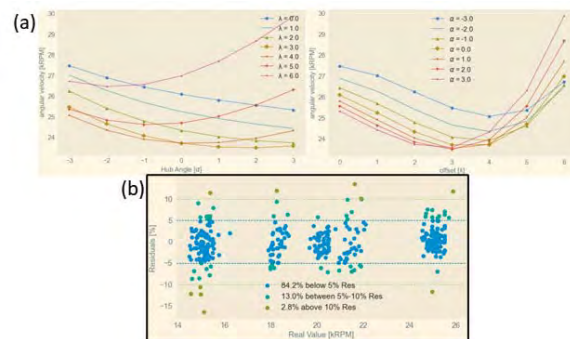


Figure 2 – (a) Result example for a specific working condition (1 L/min, 60 mmHg), (b) ML prediction results

4. Discussion and Conclusions

Our results show that the rotational speed can be reduced by 6-10% by changing the geometry for the same pressure and flow conditions. In this study, we show that changing the combination of hub angle and window offset may improve the pump's performance. Based on the results obtained, we conclude that expanding the impeller hub at the inlet, the blade's area is reduced and thus a larger length of the impeller blade is required to collect sufficient fluid volume to drive the flow.

Acknowledgments:

This work was conducted in Ariel Biomechanics Center (ABMC) at Ariel University. This research was supported by the Ministry of Science & Technology, Israel.

13.2

A newborn digital twin for cardiovascular modelling in early life

Robyn May¹, Finbar Argus¹, Tom Gentles², Frank Bloomfield³, Gonzalo Maso Talou¹, Soroush Safaei¹

¹ University of Auckland, Auckland Bioengineering Institute, Auckland, New Zealand

² Auckland District Health Board, Auckland, New Zealand

³ University of Auckland, Liggins Institute, Auckland, New Zealand

*Corresponding author: Robyn May, r.may@auckland.ac.nz

1. Introduction

Preterm birth (defined as birth before 37 completed weeks of gestation) and low birth weight (defined as weight less than 2500g at birth) are a worldwide burden. These babies are at increased cardiovascular risk in adulthood; they also frequently have cardiovascular instability after birth and are at risk of short-term morbidities that may impact the developing cardiovascular system. We hypothesise that factors related to early growth and remodelling of the cardiovascular system predict later cardiovascular structure and function. We aim to develop anatomical computational models of the cardiovascular system for newborns, which are readily personalisable and expressive enough to model preterm and term scenarios.

2. Materials and Methods

A 0D closed-loop model simulates blood pressure and flows in the newborn cardiovascular system using bond graph methodology. Bond graph vessel segments representing the large thoracic arteries are parameterised by geometric data (length and radius) allometrically scaled from an adult cardiovascular model [1]. The lumped parameter components (including peripheral vascular beds, venous and pulmonary circulation) are optimised using a reduced order unscented Kalman filter. In a single-centre observational, prospective ultrasound study in term and late-preterm (34+0–36+6 weeks' gestation) newborns, we collected anatomical data on cardiovascular geometry to personalise the model for each participant – creating a newborn clinical digital twin. Participants were assessed at birth and three weeks of age (term-equivalent age for the late-preterms) to quantify growth and developmental trends. Blood flow predictions were validated against Doppler measurements.

3. Results

For the full term neonatal cardiovascular system, computed haemodynamic variables are in agreement with the physiological ranges from the literature: systemic blood pressure 78/33 mmHg (normal $73 \pm 11/45 \pm 12$ mmHg) with a mean of 45 mmHg (normal 58 ± 12 mmHg); aortic peak flow velocity 55 cm/s (normal 88 ± 12 cm/s). The predicted abdominal aorta blood flow waveform is qualitatively similar to an empirical Doppler waveform (see Figure 1).

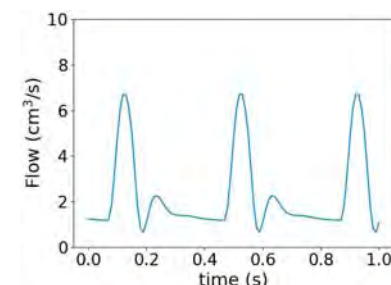
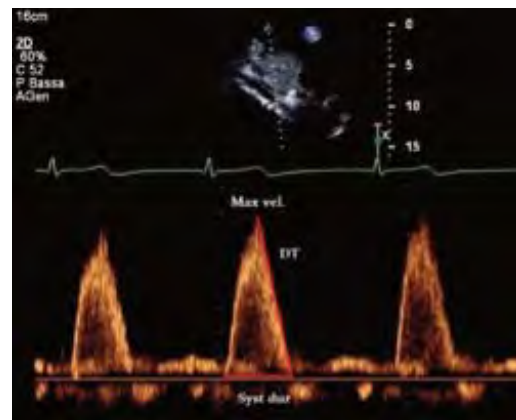


Figure 1: (Top) Abdominal aorta pulsed-wave Doppler flow measurement and (bottom) simulated flow in the abdominal aorta.

4. Discussion and Conclusions

These models could be directly applicable in clinical practice to provide valuable haemodynamic data for diagnosis and surgical planning. Additionally, this approach provides new opportunities to study mechanisms of cardiovascular remodelling related to prematurity with lifelong consequences.

5. References

1. Safaei, S., Blanco, P.J., Müller, L.O., Hellevik, L.R. and Hunter P.J. (2018). Bond graph model of cerebral circulation: Toward clinically feasible systemic blood flow simulations. *Frontiers in Physiology* 9.MAR, pp. 1–15. DOI: 10.3389/fphys.2018.00148.

Acknowledgements:

This project is supported by an Auckland Medical Research Foundation Doctoral Scholarship.

13.3

Deep learning framework for cardiac electrophysiology model error correction

Victoriya Kashtanova^{1,2}, Maxime Sermesant^{*1,2}, Ibrahim Ayed^{3,4}, Patrick Gallinari^{3,5},

1 Inria, Université Côte d'Azur, Nice, France

2 3IA Côte d'Azur, Sophia Antipolis, France

3 Sorbonne University, Paris, France

4 Theresis lab, Thales, France

5 Criteo AI Lab, Paris, France

*maxime.sermesant@inria.fr

1. Introduction

Even though biophysically detailed cardiac electrophysiology (EP) models (such as [1]) can accurately reproduce electrical behaviour of cardiac cells, these models are complex and computationally expensive, and have many hidden variables which are impossible to measure, making model parameters difficult to personalise. The phenomenological models (such as [2]), simplified models, have fewer parameters and are therefore useful for rapid computational modelling. However, they are less realistic and need a complementary mechanism to fit them to the measured data.

We propose a Deep Learning framework (APHYN-EP), based on a fast “low-fidelity” phenomenological model, to model the cardiac electrophysiology dynamics at lower cost. We demonstrate that this framework is able to reproduce with good precision the dynamics simulated by the Ten Tusscher-Noble-Noble-Panfilov ionic model [1].

2. Learning Framework

To learn cardiac electrophysiology dynamics (X_t) we solve an optimization problem via APHYN-EP framework. This framework combines a physical model (F_p) representing an incomplete description of the underlying phenomenon and a neural network (F_a) which will complement the physical model by capturing the information that cannot be modeled by the physics component.

$$\begin{aligned} & \min_{F_p \in \Phi_p, F_a \in \Phi_a} \|F_a\| \text{ subject to} \\ & \forall X \in \Omega, \forall t, \frac{dX_t}{dt} = F(X_t) = (F_p + F_a)(X_t) \end{aligned}$$

As an incomplete physical model, we use the two-variable Mitchell-Schaeffer model [2], for the data-driven part we use a Residual Network (ResNet) [3].

3. Results

We present here qualitative results on the forecast over 5 ms after assimilating only one first frame of dynamics (see Fig. 1). Table 1 shows the mean-squared error (MSE) results for our framework for different forecasting horizons on validation data samples comparison two baseline models corresponding to the two components of our model, each trained and tested alone.

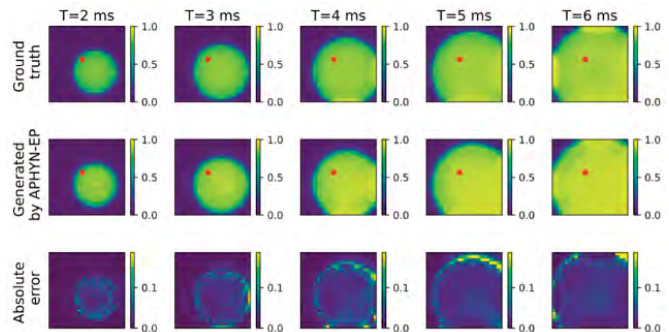


Figure 1: APHYN-EP predicted dynamics for the transmembrane potential diffusion.

	MSE (6 ms)	MSE (50 ms)
APHYN-EP	0.0057	0.002
Phys. mod. only	0.0093	0.0085
Resnet only	0.0195	9.9212

Table 1: MSE of normalised transmembrane potential forecasting per time-step for different forecasting horizons.

4. Discussion and Conclusion

We presented the APHYN-EP framework for modelling complex cardiac EP dynamics via a surrogate model combining simplified physics and deep neural networks. Such framework opens possibilities to introduce prior knowledge in deep learning approaches through explicit equations and to correct model errors from data.

5. References

1. Ten Tusscher KHWJ, Noble D, Noble PJ, Panfilov AV. A model for human ventricular tissue. *Am J Physiol Heart Circ Physiol*;286:H1573–H1589 (2004).
2. Mitchell CC, Schaeffer DG. A two-current model for the dynamics of cardiac membrane. *Bull Math Biol*; 65(5):767–793 (2003).
3. He K, Zhang X, Ren S, Sun J. Deep residual learning for image recognition. In IEEE conf. CVPR 2016: 770–778 (2016).

13.4

Dynamic response of cerebrovascular networks to fluctuations in arterial blood pressure

Stephen Payne¹, YUAN CHUNG CHOU¹

¹ National Taiwan University, Institute of Applied Mechanics, Taiwan

1. Introduction

The cerebral vasculature is a highly complex system of blood vessels ranging across multiple length scales. It plays a critical role in maintaining a tight balance between demand and supply of oxygen, with the mechanisms that act to maintain cerebral blood flow (CBF) approximately constant in response to short-term changes in arterial blood pressure (ABP) termed dynamic cerebral autoregulation (dCA) [1]. However, the different components of the dCA response remain controversial, partly because of the complexity of the different generations of vessels, and the large vessels are typically simulated by a simple lumped compartment. We thus propose a new approach to examine the response of the larger vessels to ABP changes to help in disentangling the different components of autoregulation.

2. Materials and Methods

We take the vessel data from the study by Wright et al. [2]. This contains a detailed study of the large vessels in the brains of 61 individual subjects. To calculate the dynamic response of each vessel we adapt the model proposed by Flores et al. [3]. This is based on a simplified Womersley flow coupled with continuity and a pressure-area relationship. We assume constant compliance and derive a frequency domain expression for the flow passing through a single vessel in terms of the mean of the inlet and outlet flows and the dynamic pressure gradient.

This enables us to solve for fluctuations in CBF in response to fluctuations in ABP, giving a dynamic conductance for each large vessel. This transfer function, given in Equation 1 as a fraction of static conductance, is dependent upon just two characteristic angular frequencies, based on the Womersley number, $\alpha = R_0 \sqrt{\omega/v}$, and a product of flow resistance and wall compliance, $\kappa = \sqrt{i\omega RC}$:

$$\frac{G}{G_0} = \frac{4\kappa}{i\alpha^2} \left[1 - \frac{2J_1(\alpha t^{3/2})}{\alpha t^{3/2} J_0(\alpha t^{3/2})} \right] \left(\frac{2+e^\kappa+e^{-\kappa}}{e^\kappa-e^{-\kappa}} \right)$$

In the limit as frequency tends to zero, this tends to unity, as would be expected. Using the same solution procedure as for static flows, a matrix formulation can thus be derived to solve the dynamic flows in any large network. We use the geometric parameters provided by [2] and the wall properties given in [3]. We then assume typical values of inlet pressure of 100 mmHg with a dynamic component of 10 mmHg and a constant outlet pressure of 40 mmHg.

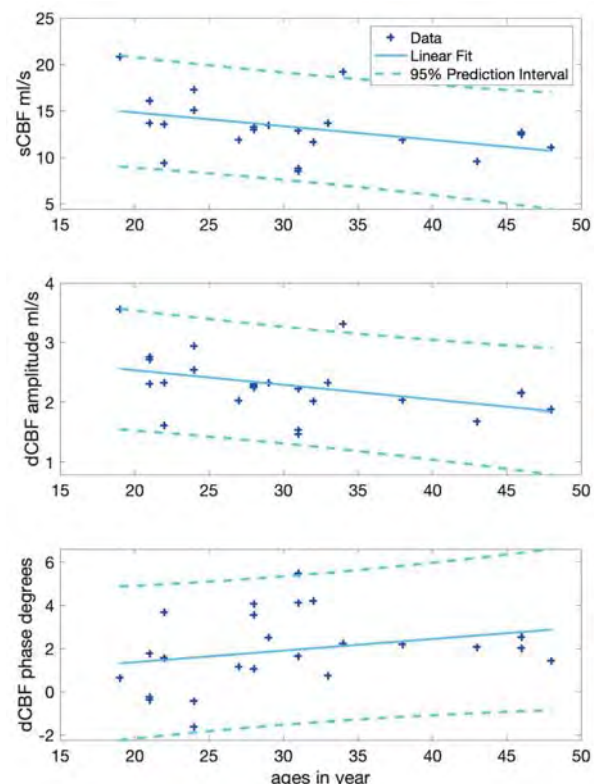


Figure 1: Changes in static (sCBF) and dynamic (dCBF) components of CBF against age for men.

3. Results

The static and dynamic responses for male subjects are shown in Figure 1 (results for women are very similar). Dynamic responses are very similar to the static responses with minimal phase shift, indicating that the dynamic components are in quasi steady-state.

4. Discussion and Conclusions

The results here show that the dynamic components can be well approximated by the static model. This indicates that perturbations within the large vasculature can be taken to be transmitted rapidly through to the inlet to the microcirculation, with important implications for the control of cerebral blood flow.

5. References

1. Payne SJ. *Cerebral Autoregulation*. Springer (2016).
2. Wright SN et al, *Neuroimage*; 82:170-81 (2013).
3. Flores J et al, *Ann Biomed Eng*; 44:3047-68 (2016).

Acknowledgements:

We thank the Ministry of Education, Taiwan, for the award of a Yushan scholarship to SJP.

13.5

Effect of septal and left bundle branch pacing on right ventricular function: a model study

Roel Meiburg¹, Jesse H.J. Rijks², Achmed S. Beela¹, Tammo Delhaas¹, Justin G.L.M. Luermans², Luuk I.B. Heckman³, Frits W. Prinzen³, Kevin Vernooy², Joost Lumens¹

¹ Cardiovascular Research Institute Maastricht (CARIM), Biomedical Engineering, Maastricht, Netherlands

² Cardiovascular Research Institute Maastricht (CARIM), Cardiology, Maastricht, Netherlands

³ Cardiovascular Research Institute Maastricht (CARIM), Physiology, Maastricht, Netherlands

*Correspondence: r.meiburg@maastrichtuniversity.nl

1. Introduction

Cardiac resynchronisation therapy (CRT) has shown to reduce mortality in patients suffering from heart failure and conduction disease [1]. However, CRT still leads to non-physiological electrical and mechanical activation of the heart, inspiring research into alternative pacing strategies, such as left bundle branch (LBB) and left ventricular (LV) septal pacing which are considered to be more physiological [2]. Regardless of the pacing strategy, strong emphasis is placed on LV function, e.g. LV ejection fraction. Right ventricular (RV) function is underappreciated, while it is often a strong predictor of outcome in heart failure with and without CRT [4]. In this study we aim to better quantify the effect of prevailing pacing strategies on the electrical and haemodynamic performance of the right ventricle.

2. Materials and Methods

To simulate CRT in the heart, cardiac electrical activation maps were generated on a realistic 3D biventricular geometry using a graph-based formulation of the Eikonal model. The geometry was segmented and activation times for each segment were calculated, as shown in Fig. 1. These were then used to inform the CircAdapt model of cardiovascular mechanics and haemodynamics to calculate the effect of the different pacing strategies on RV function.

3. Results

Simulated electrical activation maps show a good agreement with clinical measurements. LV septum and LBBpacing strategies improved simulated RV function, but lead to markedly different local mechanical behaviour, despite comparable electrical activation. LBBpacing resulted in higher pre-stretch in the RV than LV septal pacing (10% vs 4%), as well as a more heterogeneous distribution of RV segmental work.

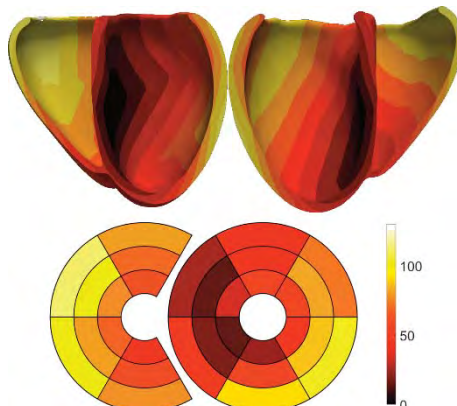


Figure 1: Top - 3D simulation of electrical activation following septal pacing. Bottom – mean activation time of each cardiac segment, which is used to inform the CircAdapt model.

4. Discussion and Conclusions

We present a modelling framework that is able to predict the acute mechanical and haemodynamic response of both ventricles to different pacing strategies. This approach is computationally cheap compared to full 3D models, while providing results on a spatial resolution similar to data currently available in the clinical setting. The low computational cost allows for a comprehensive sensitivity analysis on the different pacing strategies, such as AV-delay, lead location as well as patient variability. Current results assume reduced contractility of the myocardium without impaired electrical conductivity, which may not be physiological. Finally, the model is currently unable to predict long-term outcome, i.e., reverse remodelling, for which more research is needed.

5. References

1. Cazeau S. et al, *N Engl J Med.* 2001; 344(12):873-880.
2. Rademakers LM et al, *JACC: Clin Electrophysiol.* 2016; 2(4): 413-422.
3. Ghio S. et al, *Am J Cardiol.* 2000; 85:837-842.

13.6

Extreme scale excitation-contraction modelling of the heart: from small molecule-protein interaction to full heart mechanics for drug testing in hypertrophic cardiomyopathy

Jazmin Aguado-Sierra¹, Adria Quintanas-Corominas¹, Constantine Butakoff², Danica Prodanovic³, Momcilo Prodanovic^{3,4}, Milos Ivanovic³, Boban Stojanovic³, Nenad Filipovic^{3,4}, Srboljub Mijailovic⁵, Mariano Vazquez^{1,2}

1 Barcelona Supercomputing Center - Centre Nacional de Supercomputació, Barcelona, Spain

2 ELEM Biotech, Barcelona, Spain

3 BIOIRC, Bioengineering Research and Development Center, Kragujevac, Serbia

4 University of Kragujevac, Kragujevac, Serbia

5 Illinois Institute of Technology, Department of Biology, Chicago, United States

Corresponding author: Jazmin Aguado-Sierra, jazmin.aguado@bsc.es.

1. Introduction

Modelling the human cardiac contraction parting from detailed dynamics of the cardiac muscle twitch is highly complex due to its extreme scale nature. In this work we describe the coupling strategy and results from combining computational models that integrate experimental data at multiple scales, from the level of single molecular interactions between contractile proteins and small molecules, with 3D explicit stochastic model Muscle Simulation Code (MUSICO)1,2, to macro changes observed at the whole heart through finite element solver Alya3. MUSICO can model protein-protein interactions and Ca²⁺ regulation in cardiac muscle and is employed to parameterise the MP surrogate model. It is new sliding filament model based on a solution of ODEs that provides the active tension and instantaneous stiffness along the cardiac muscle fibers. The objective of this model is to understand how changes at the molecular scale in contractile proteins associated to hypertrophic cardiomyopathy (HCM) result in detrimental effects in the overall heart function. The model was then employed to assess the effect of Mavacamten.

2. Materials and Methods

The methodology employed to solve the electro-mechanic model at the full heart level is described in Fig 1. The anatomy is coupled to a 3-element windkessel model that describes the aortic and pulmonary arterial pressures.

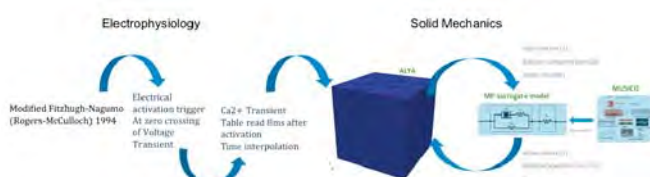


Figure 1: Methodology employed to solve the biventricular electro-mechanical model.

3. Results

Results of the electro-mechanic behaviour are shown in Fig. 2. Pressure-volume loops for both the right and left ventricles were also computed.

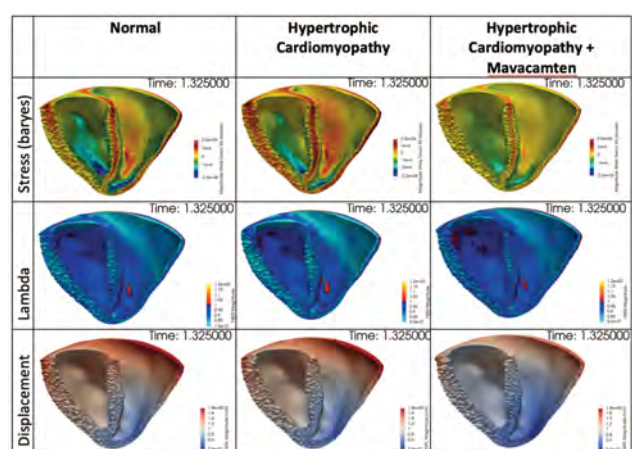


Figure 2: Results at baseline, with HCM phenotype and after the administration of mavacamten.

4. Discussion and Conclusions

The methodology employed has enabled us to model the response of a human heart with a hypertrophic cardiomyopathy phenotype and it can predict the effect of drugs like Mavacamten. These models reside within the SilicoFCM platform. (<https://silicofcm.eu/>)

5. References

1. Mijailovich SM et al; *J Gen Physiol.* Dec. 2016; 148(6):459–488.
2. Mijailovich SM, et al. *J Gen Physiol.* 2021 Mar 1;153(3):e202012604. doi: 10.1085/jgp.202012604.
3. Vazquez M, et al. *J Comput Sci.* 2016;14:15–27.

Acknowledgements:

This work was supported by the European Union's Horizon 2020 under grant agreement 777204. RYC-2017-22532. PTQ2018-010290. Neotec project EXP - 00123159 / SNEO-20191113. Rep. of Serbia Contracts No. 451-03-68/2022-14/200378. This article reflects only the author's view. The European Commission is not responsible for any use that may be made of the information the article contains.

13.7

Generation of a digital aortic valve twin for transcatheter aortic valve implantation

Marcos Loureiro-Ga¹, Cesar Veiga², G. Fdez-Manin³, Laura Busto², Victor Jimenez⁴, Jose A Baz⁴, Andres Iñiguez⁴

¹ Galicia Sur Health Research Institute (IIS Galicia Sur), SERGAS-UVIGO, Spain, Cardiology, Vigo, Spain

² Galicia Sur Health Research Institute (IIS Galicia Sur), SERGAS-UVIGO, Spain

³ University of Vigo, Department of Applied Mathematics II, Spain

⁴ Cardiology Department, Complexo Hospitalario Universitario de Vigo (CHUVI), Spain

1. Introduction

Trans-catheter aortic valve implantation (TAVI) allows the delivery of an artificial valve in the proper position using a catheter instead of an open-heart operation. This procedure has shown to improve survival in high and intermediate risk patients [1]. Although TAVI has a high success rate with few surgical complications, it still carries certain risks such as incorrect device sizing or paravalvular regurgitation, among others.

Our work intends to establish a work pipeline to create a digital aortic valve (AV) twin where different devices can be tested.

2. Materials and Methods

CT of a patient who is proposed to undergo a TAVI is segmented using Philips software to obtain the 3D anatomy reconstruction of the native AV; the digital twin of the patient.

A library of TAVI devices is created. Ideally, geometries should be provided by the device suppliers, but it was not the case. Using a reverse engineering process, we reconstructed different sizes balloon-expandable (BE) and self-expandable (SE) commercial devices as shown in Fig. 1.

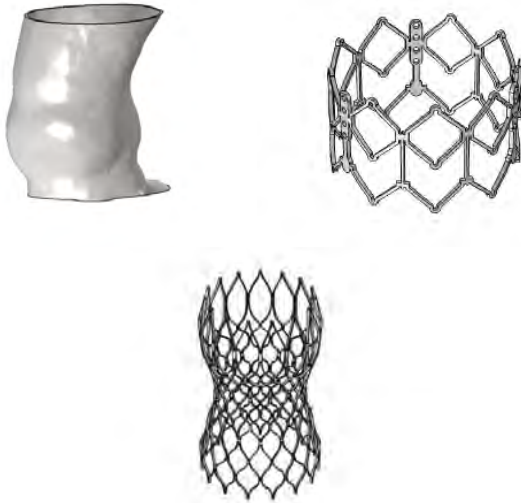


Figure 1: Left: result of a CT segmentation to create the AV digital twin. Centre: balloon-expandable TAVI device reconstruction. Right: self-expandable TAVI device reconstruction.

Using the finite element method (FEM), several biomechanical simulations can be performed implanting various types-sizes TAVIs within the AV digital twin. Different materials appear such as aortic tissue, chromium-cobalt alloy in AE devices and a shape memory alloy (nitinol) in SE devices. Hence a proper material characterization is necessary involving different mechanics problems such as cobalt-chromium [2] and nitinol [3].

3. Results

Several results will be presented considering different TAVI devices, material parameters and patients.

4. Discussion and Conclusions

A work pipeline creating a digital AV twin to test different TAVI devices was presented.

Results of the study could provide new and valuable information for clinical decisions. Further studies are being carried on to evaluate more parameters and SE devices.

5. References

1. Vandvik et al. BMJ, 354:i5085, 2016. <https://doi.org/10.1136/bmj.i5085>
2. Loureiro-Ga et al. Comp Meth in Biomech & Biomed Eng, 2021. <https://doi.org/10.1080/10255842.2021.1906233>
3. Nappi et al. Bioengineering 2021. <https://doi.org/10.3390/bioengineering8050052>

13.8

Non-parametric statistical shape modelling for in silico trials of TAVI

Sabine Verstraeten¹, Damián Suasso de Lima de Prado², Martijn Hoeijmakers³, Frans van de Vosse⁴, Wouter Huberts^{4,5}

- 1 Eindhoven University of Technology, Biomedical Engineering, Eindhoven, Netherlands
- 1 Eindhoven University of Technology, Biomedical Engineering, Eindhoven, Netherlands
- 3 ANSYS Utrecht, Netherlands
- 1 Eindhoven University of Technology, Biomedical Engineering, Eindhoven, Netherlands
- 5 Maastricht University, Biomedical Engineering, Netherlands

1. Introduction

In silico clinical trials are a promising method to increase efficacy and safety of trans-catheter aortic valve implantation (TAVI) devices. Synthetic aortic stenosis (AS) valve geometries for in silico trials can be created by using a Statistical Shape Model (SSM). SSM methods used in previous studies [1], have two disadvantages: (1) They require consistent inter-patient topology; (2) These methods do not consider the relation between shape features and outputs of interest. By considering output related features, the geometries may be described with fewer parameters. Therefore, the aim of this study was to set up a non-parametric SSM for AS valve geometries and take into account the output of interest: the pressure drop across the aortic valve (Δp).

2. Materials and Methods

A data set of 74 aortic valve meshes (EurValve project) and the corresponding Δp resulting from a Computational Fluid Dynamics model [1], were used to train the SSM model [2]. The first step was to obtain deformation vectors, located at fixed grid points for each patient, that deform a template geometry to a patient specific geometry, using the open-source software called "Deformetrica" [3]. The second step was to obtain the main directions of shape variance (shape modes) within these sets of vectors, that are most correlated to Δp , by using Partial Least Square regression [2]. Synthetic and original meshes could be (re)constructed using the template geometry and the resulting shape modes.

3. Results

In Figure 1 the mean distance between the original shape and the shapes reconstructed by using respectively zero, one, and seven shape modes, are visualized on the template geometry.

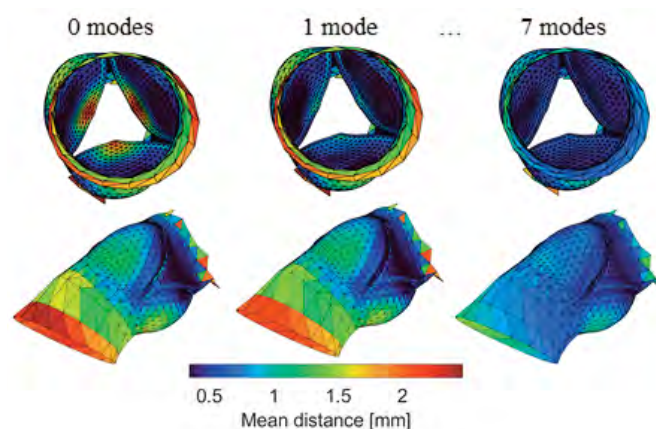


Figure 1: mean distance between original shape and shape reconstructed with 0, 1, and 7 shape modes.

The mean \pm std distance between the original and the template shape (zero shape modes) is 0.83 ± 0.36 mm. The distance decreases with increasing number of shape modes included. After including seven modes, the distance was reduced to 0.62 ± 0.22 mm, and 95% of the total shape variation was captured.

4. Discussion and Conclusions

The results demonstrate that this non-parametric SSM can accurately reconstruct the real geometries by only using seven pressure drop related shape modes. The SSM is now ready to be used to construct realistic, synthetic, stenosed aortic valve geometries for in silico trials of TAVI.

5. References

- Hoeijmakers MJMM et al., *Int. J. Numer. Methods Biomed. Eng.* vol. 36, p. e3387 (2020).
- Bruse JL et al., *BMC Med. Imaging*, vol. 16, no. 1 (2016)
- Bóne A et al., *LNCS*, vol. 11167, pp. 3–13 (2018)

Acknowledgements:

We acknowledge the European Union's Horizon 2020 research and innovation programme (grant agreement No 101017578) for their financial support.

14.1

A GPU-accelerated model of neuroblastoma to predict disease outcome and find drug targets

Kenneth Wertheim^{1,2}, Robert Chisholm¹, Paul Richmond¹, Dawn Walker^{1,2}

1 The University of Sheffield, Department of Computer Science, Sheffield, United Kingdom

2 The University of Sheffield, Insigneo Institute for *in silico* Medicine, Sheffield, United Kingdom

Correspondence email address: k.wertheim@sheffield.ac.uk.

1. Introduction

Neuroblastoma is the most common extra-cranial solid tumour in children; around half of all cases are high-risk and may relapse despite intensive multimodal treatment, whereupon the five-year survival rate drops below 10 % [1]. We developed the first multicellular model of neuroblastoma as a part of the PRIMAGE project [2] and tested hypotheses regarding clonal evolution and therapeutic combinations on hundreds of thousands of cellular agents, simulated on GPUs.

2. Materials and Methods

Our model comprises a continuous automaton (CA) representing the microenvironment inside the tumour, autonomous neuroblast and Schwann cell agents, and a centre-based mechanical model. Cell cycling, apoptosis, and necrosis are the agents' major behaviours, which depend on the CA's inputs and the agents' own attributes. For example, the neuroblasts promote proliferation in Schwann cells. The mechanical model resolves cell-cell overlap. The initial conditions are set to match patient-specific data, including the tumour's histology and mutations (such as MYCN amplification: a strong predictor of adverse outcomes). We devised a calibration pipeline based on Latin hypercube sampling and experimental/clinical observations. As the stochastic model has 20 fitting parameters, we ran the costly simulations within the Flexible Large Scale Agent Modelling Environment for the GPU (FLAMEGPU) [3]. After calibration, we simulated the tumour's evolution over months in 1200 randomly generated conditions defined by the macroscopic properties and clonal composition of the tumour. Macroscopically, we considered the tumour's oxygen level, cellularity, enrichment in Schwann cells, and degree of differentiation. Microscopically, we considered 24 clinically observed clones with unique combinations of mutations. From the 1200 conditions, we selected one favouring tumour progression and simulated the effects of inhibiting selected gene products in the neuroblasts.

3. Results

With hundreds of thousands of agents in the system, it took around a minute to complete hundreds of one-hour time steps. Calibration took around 40 days. Our results—after exploratory analysis, clustering, and dimensionality reduction—show that the tumour's macroscopic properties predict the disease outcome better than its clonal composition. While a lack of oxygen leads to regression, differentiation into healthy neurons occurs when there are enough Schwann cells. The macroscopic properties promoting progression select the MYCN-amplified clone too. The perturbation studies' results show that the intracellular mechanisms are non-linearly linked: inhibiting a gene product may disrupt DNA repair but oddly prevent apoptosis.

4. Discussion and Conclusions

Our results agree with clinical observations of heterogeneous neuroblastoma tumours [4]. Once integrated with the PRIMAGE platform, the model can facilitate patient-specific prediction of disease outcome and unravel the non-linear dynamics of neuroblastoma to find drug targets. The dynamics of up to 10 million cells can be simulated and the successor to FLAMEGPU is constantly being improved on.

5. References

- Morena L et al., *European Journal of Cancer* 136: 52-68 (2020).
- Marti-Bonmatí L et al., *European Radiology Experimental* 4(1): 1-11 (2020).
- Richmond P et al., *Briefings in Bioinformatics* 11(3): 334-347 (2010).
- Berbegall AP et al., *British Journal of Cancer* 118(11): 1502-1512 (2018).

Acknowledgements:

We thank other PRIMAGE partners and the EU's Horizon 2020 research and innovation programme (grant agreement 826494). PR is grateful for an EPSRC grant (EP/N018869/1).

14.2

An interconnected multi-level mechanistic model of the human brain

Nicolas Sundqvist¹, Henrik Podéus¹, Malin Ejneby Silverå¹, Maria Engström², Sebastian Sten², Salvador Dura-Bernal³, Soroush Safaei⁴, Gunnar Cedersund¹

- 1 Linköping University, Department of biomedical Engineering, Linköping, Sweden
 2 Linköping University, Department of Health, Medicine and Caring Sciences, Linköping, Sweden
 3 State University of New York, Department of Physiology and Pharmacology, United States
 4 University of Auckland, Auckland Bioengineering Institute, New Zealand

Correspondence: Gunnar Cedersund, gunnar.cedersund@liu.se, Phone: +46-702-512323.

1. Introduction

In the pursuit of gaining a more comprehensive understanding of the brain, we aim to expand and integrate a set of existing and newly developed mechanistic models that describe different aspects of the neuronal and hemodynamic functions of the brain. The goal is to have an interconnected multi-level, multi-scale model that can explain mechanisms on different levels of the cerebral physiology. Starting at the level of ion channel kinetics (Fig 1B), where neuronal homeostasis can be explored, and zooming out to large intraneuronal signalling networks (Fig 1A), including descriptions of how such signalling activity; i) affect the metabolic control (Fig 1D), and ii) the hemodynamic control of cerebral tissue (Fig 1C), allowing changes in local vessels connect to a global whole body vessel tree (Fig 1E).

2. Materials and Methods

The interconnected model of the brain is constructed using ordinary differential equations (ODEs) and incorporate these equations with large scale neuronal network modelling structures (NEURON and NetPyNE) [1, 2]. The interconnected model utilizes both qualitative and quantitative information from a wide variety of experimental measurements, such as measurement of action potentials (AP) (Fig 1F), magnetic resonance spectroscopy (MRS) (Fig 1G), functional magnetic resonance imaging (fMRI) (Fig 1H), as well as electrophysiological measurements, both on an ion channel level and a cell population level in the form of local field potential (LFP) (Fig 1I), multi-unit activity (MUA) and electro-encephalography (EEG) measurements.

3. Results

The interconnected model can currently offer a detailed mechanistic description of the neurovascular coupling [3], with connections to metabolic responses [4] and neuronal network activity is in development. Further, a versatile ion channel structure and a mechanistic interpretation of neuron facilitation are being integrated.

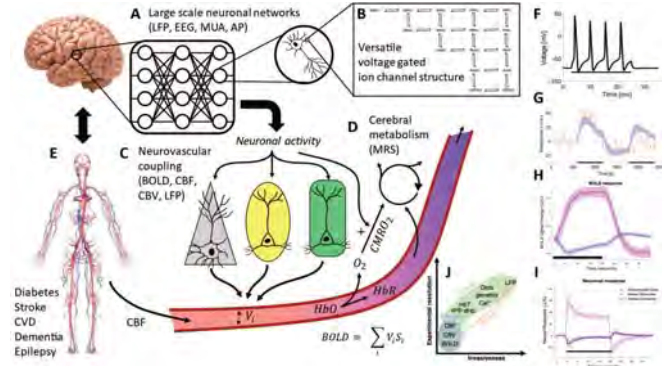


Figure 1: Overview of the interconnected model (A-E) and some of the current sub-model capabilities (F-J).

4. Discussion and Conclusions

By integrating these aspects, we aim to achieve a model that can offer a detailed intracellular description that also reflects the physiological structure of the human brain. The model framework could be used to study and predict different diseases and physiological alterations, such as if facilitation of neurons can cause epilepsy, how Alzheimer's disease affects the signalling patterns between neuron populations, and how stroke affects the cerebral tissue. Such an interconnected model would also allow for qualitative information to be gained from multi-species measurements (Fig 1J).

5. References

- [1] Carnevale, N. T., & Hines, M. L. (2006). *The NEURON book*. Cambridge University Press.
- [2] Dura-Bernal et al (2021). NetPyNE, a tool for data-driven multiscale modeling of brain circuits. *eLife* 2019;8:e44494.
- [3] Sten S (2021). A multi-data based quantitative model for the neurovascular coupling in the brain. *bioRxiv*.
- [4] Sundqvist N (2022) Mechanistic model for human brain metabolism and the neurovascular coupling *bioRxiv*.

Acknowledgements:

This work was supported by the Swedish Research Council, CENIIT, the Swedish Foundation for Strategic Research, SciLifeLab, PRECISE4Q, the Swedish Fund for Research without Animal Experiments, VINNOVA, the Swedish Brain Foundation, NIH, and NSF.

14.3

Assessing the accuracy and efficiency of a binning strategy on a multiscale tumours' growth model

Vinicius Varella^{1,2}, Marek Kasztelnik³, Barbara Quintela⁴, Marco Viceconti^{1,2}

1 Alma Mater Studiorum - Università di Bologna, Department of Industrial Engineering, Bologna, Italy

2 Rizzoli Orthopedic Institute, Medical Technology Lab, Bologna, Italy

3 ACC Cyfronet AGH, Kraków, Poland

4 Universidade Federal de Juiz de Fora, Departamento de Ciencia da Computação, Juiz de Fora, Brazil

1. Introduction

In silico models' applications are frequently used to represent multiscale phenomena. However, These applications tend to be computationally requiring, even using an HPC System.

Therefore, binning techniques are developed aiming to reduce the computational cost making the lost of accuracy in the solutions as minimum as possible. The main goal of this study is to assess the error caused by a specific implementation of the two processes (particularisation / homogenisation) of a binning strategy, in a multiscale model of growth for neuroblastoma tumours.

2. Materials and Methods

The study was leaded on an idealised tumour model, small enough to permit a solution without binning application.

This idealised tumour model considers the cancer to be a spherical solid tumour of 5mm in diameter. The initial oxygen concentration is distributed to change linearly along the radius having 1 mL at the outer skins and 0 mL at the centre. The ratio between cancer cells volume and the total volume, called cellularity, is assumed as a constant value during the whole simulation.

The idealised tumour was run by the multiscale model to simulate the tumour growth for a period of two weeks, without treatment. We used a first prototype implementation of the PRIMAGE multiscale model for predicting the growth of neuroblastoma tumours [1], which is now under development. This prototype orchestrates three component models.

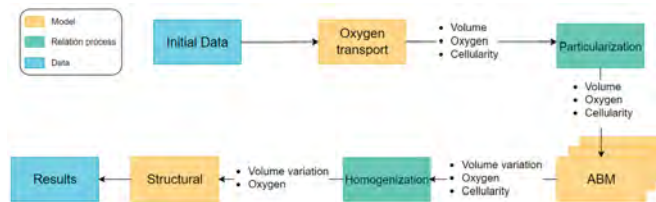


Figure 1: PRIMAGE prototype topology

The volume of the whole tumour at time zero, is decomposed in 4,4k 4-node linear tetraedrons finite elements. In theory, each tissue-scale model (ABM) should be run for each FE, even so, for real tumours this is not possible given the possible sizes of the mesh. Hence, a relation model is joined to the orchestration to manage the particularisation/homogenisation process.

The particularisation process algorithm selects one variable to order the elements and groups them in sets of the same size (bin). The biggest value of each bin is selected to run the tissue model. The homogenisation use all the results obtained by the tissue model and estimates the values (oxygen and volume) for the elements that were not run, using a linear approach on the order the elements were sorted previously.

3. Results

We got the solution with no particularisation and compared to several executions using different levels of particularisation. Thus, the bigger is the particularisation level, less values are being estimated.

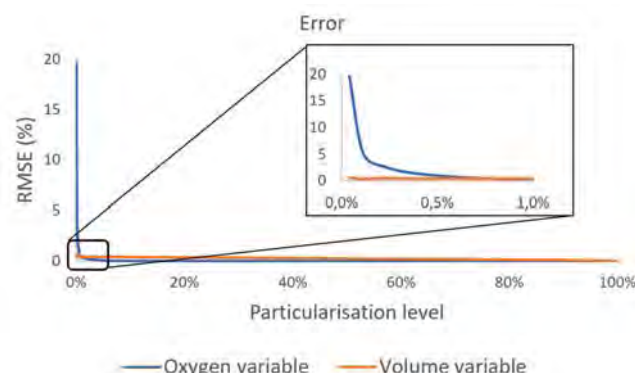


Figure 2: Error doing the particularisation by the oxygen variable

4. Discussion and Conclusions

The best result was obtained doing a particularisation by oxygen concentration. With less than 1% of elements sampled, we obtained an error smaller than 1% for both variables and the computational cost decreased almost 100 times.

5. References

1. Martí-Bonmatí L, et al. PRIMAGE project: predictive in silico multiscale analytics to support childhood cancer personalised evaluation empowered by imaging biomarkers. European radiology experimental 2020; 4(1): 1–11.

Acknowledgements:

This study was supported by the European Commission (topic SC1-DTH-07-2018, grant ID 826494) and the by PLGrid Infrastructure.

14.4

Calibration and validation of a multiscale model to study the role of mechanics and inflammation in osteoarthritis

Satanik Mukherjee^{1,2}, Raphaelle Lesage^{1,2}, Liesbet Geris^{1,2,3}

1 KU Leuven, Prometheus, Division of Skeletal tissue Engineering, Leuven, Belgium

2 KU Leuven, Biomechanics Section, Leuven, Belgium

3 University of Liege, GIGA In silico medicine, Liege, Belgium

1. Introduction

Osteoarthritis (OA), is a highly prevalent degenerative joint disease affecting 1 in 8 adults worldwide. OA is suspected to be triggered by multiple factors, with abnormal mechanics and inflammation being most prominent. In silico multiscale approaches coupling finite element (FE) models at multiple length scales with systems biology models can provide unique insights to unravel the complex interplay between mechanics and pro-inflammatory cytokines in the initiation and progression of OA. However, to obtain credible insights from such multiscale models, they need to be calibrated and validated with respect to in vitro experimental data. This paper aims to develop a multiscale model of articular cartilage and calibrate it with respect to in vitro experiments in literature [1].

2. Materials and Methods

The multiscale in silico model developed for articular cartilage (Fig. 1) consists of: Tissue-level FE model of a bovine cartilage disc of 1 mm thick and 3 mm diameter (mimicking the in vitro experimental setup [1]). Cartilage is modelled as a fibril reinforced poroviscoelastic material [2], subject to dynamic compression of 10%, 20% and 30% strains (0.5 Hz frequency).

Cell-level FE model, consisting of a chondrocyte, pericellular matrix (PCM) and extracellular matrix (ECM). The maximum compressive and shear strains obtained from simulations of the tissue-level model are used as input boundary conditions for cell-level model.

Intracellular model, which is an additive, semi-quantitative regulatory network for chondrocyte mechanotransduction and inflammation developed using a combination of knowledge-based and inference-based approach. The forces sensed by cells in the cell-level FE model are used as an input to perturb the regulatory pathways. To calibrate the multiscale model with respect to the relevant gene expressions (COL2, ACAN, ADAMTS5) measured in experiments [1], a Genetic Algorithm (GA) is used.

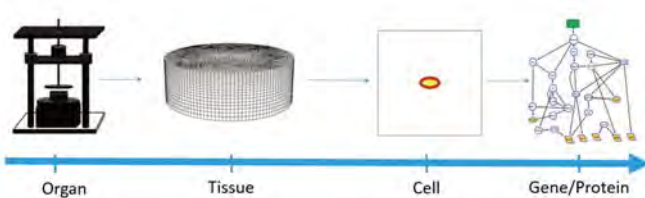


Figure 1: Multiscale model of in vitro setup

3. Results

Simulations of the multiscale model with a combination of different levels inflammatory cytokines and mechanical loading (using a full factorial design) reveals that loss of ECM components (COL2 and Proteoglycan) is triggered more by cytokines as compared to mechanical loading (Fig.2). Matrix degrading enzymes (MMP13 and ADAMTS5) are also more sensitive to the cytokines as compared to mechanical load. Experimental and simulated gene expressions of COL2 and ACAN are also closely correlated to each other.

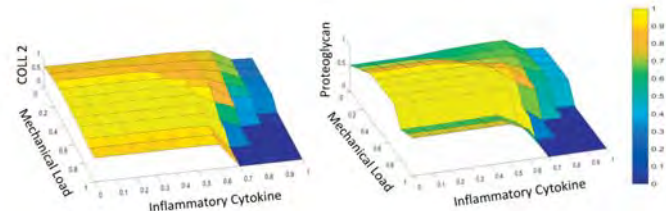


Figure 2: Effect of cytokine and mechanical stimulation on ECM proteins.

4. Discussion and Conclusions

The developed multiscale model captures the combinatorial effect of mechanics and inflammation in the etiology of OA. The model can be further extended to an in vivo case, such as the knee joint, to study the initiation and progression of OA in a clinical setting.

5. References

- [1] Li et.al., Osteo. Cart., 2013, 21(12):1933-4.
- [2] Wilson et. al., J. Biomech., 2005, 38, 1195.

Acknowledgements:

We acknowledge funding from the European Commission (MSCA 721432 & ERC CoG 772418).

14.5

Data-driven multiscale model of macaque auditory thalamocortical circuits

Erica Griffith^{1,2}, Salvador Dura-Bernal^{1,2}, Annamaria Barczak², Monica N O'Connell², Tammy McGinnis², William Lytton^{1,3}, Peter Lakatos^{2,4}, Samuel Neymotin^{2,4}

1 SUNY Downstate Medical Center, Brooklyn, United States

2 Nathan S. Kline Institute for Psychiatric Research, Orangeburg, United States

3 Kings County Hospital Center, Brooklyn, NY, United States

4 NYU Langone Medical Center, New York, NY, United States

1. Introduction

We developed a biophysically-detailed model of the macaque auditory thalamocortical circuit pathway, including primary auditory cortex (A1), medial geniculate body (MGB) and thalamic reticular nuclei (TRN).

2. Materials and Methods

We simulated A1 as a 6-layered cortical column with a depth of 2000 μm and 200 μm diameter. The modeled A1 column included multiple populations of neurons, consisting of 4 excitatory and 4 inhibitory types, with a total of over 12k neurons and 30M synapses. Neuron densities, classes, laminar locations, morphology and biophysics were derived from published experimental data.

The simulated thalamic structures, MGB and TRN, were reciprocally connected to the modeled A1 column, mimicking anatomical connectivity at long-range, local and dendritic scales. The MGB included models of locally-projecting thalamic interneurons, along with core and matrix thalamocortical neurons with layer-specific projections to A1.

The A1 column, MGB, and TRN were modeled using the NEURON simulator [1] and the NetPyNE multiscale modeling tool [2]. Simulation runs and model optimization were conducted on the Google Cloud supercomputing platform.

3. Results

The model generated cell type and layer-specific firing rates consistent with experimentally observed ranges, and accurately simulated the corresponding local field potentials (LFPs), current source density (CSD), and electroencephalogram (EEG) signals. Laminar CSD patterns during spontaneous activity, and in response to speech input, were similar to those recorded experimentally. Physiological oscillations emerged spontaneously across frequency bands, without external rhythmic inputs, and were comparable to those recorded *in vivo* (Fig. 1).

We used the model to unravel the contributions of distinct cell-type and layer-specific neuronal populations to the oscillation events detected in CSD, and to explore how these contributions related to population firing patterns.

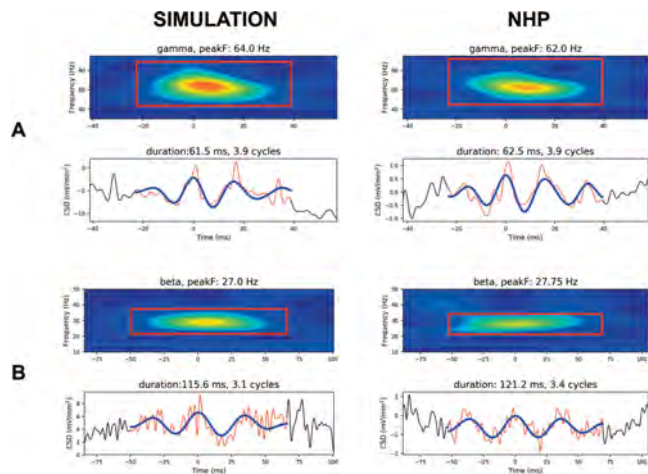


Figure 1: Examples of similar oscillation events detected in CSD recorded from simulations (left) and non-human primates (right), in the (A) gamma and (B) beta frequency bands. These examples demonstrate the model's ability to reproduce physiologically realistic oscillation events.

4. Discussion and Conclusions

Overall, the computational model provides a quantitative theoretical framework to integrate and interpret a wide range of experimental data in auditory circuits. It also constitutes a powerful tool to evaluate hypotheses and make predictions about the cellular and network mechanisms underlying common experimental measurements, including MUA, LFP and EEG signals.

5. References

- Carnevale NT, Hines ML. *The Neuron Book*. Cambridge University Press (2006).
- Dura-Bernal S et al., *eLife* 2019;8:e44494 (2019).

Acknowledgements:

The authors would like to thank the NIH (R01DC012947-06A1, U24EB028998, U01EB017695), the NSF (ECAS 1904444), the NY State DOH (01-C32250GG-3450000), and the Army Research Office (W911NF-19-1-0402) for providing financial support to this project.

14.6

Demand-driven multiscale modelling of myocardial perfusion in the (a)synchronous heart

Anneloes Munneke¹, Joost Lumens¹, Theo Arts¹, Tammo Delhaas¹

¹ CARIM, Biomedical Engineering, Maastricht, Netherlands

*Corresponding Author: a.munneke@maastrichtuniversity.nl

1. Introduction

Asynchronous activation affects cardiac mechanics and myocardial perfusion. Although the tight coupling between myocardial oxygen demand and supply has been recognized for many years, clinical and experimental observations in asynchronous activation are conflicting, and our understanding of the underlying mechanisms remains limited.

2. Materials and Methods

A multi-scale modelling framework for cardiac-to-coronary coupling [1] was constructed to investigate the interaction between myocardial oxygen demand and supply under regulated and fully dilated coronary flow conditions in (a)synchronously activated hearts. Regional fiber stress - fiber strain area was used to estimate regional oxygen demand [2]. Regional coronary flow was regulated with a vasodilator signal based on regional demand, mimicking coronary autoregulation. Coronary flow reserve was calculated as the ratio of hyperaemic to resting peak coronary flow velocity.

3. Results

The model predicts the following: (1) Coronary flow reserve (CFR) is not homogeneously distributed in the synchronously activated heart, decreasing distally, particularly in the posterior descending branch of the right coronary artery; (2) Myocardial demand and supply are decreased in early activated regions and increased in late activated regions; (3) Regional hyperaemic flow was not influenced by dyssynchrony, resulting in increased CFR when demand decreases, and vice versa (Fig. 1).

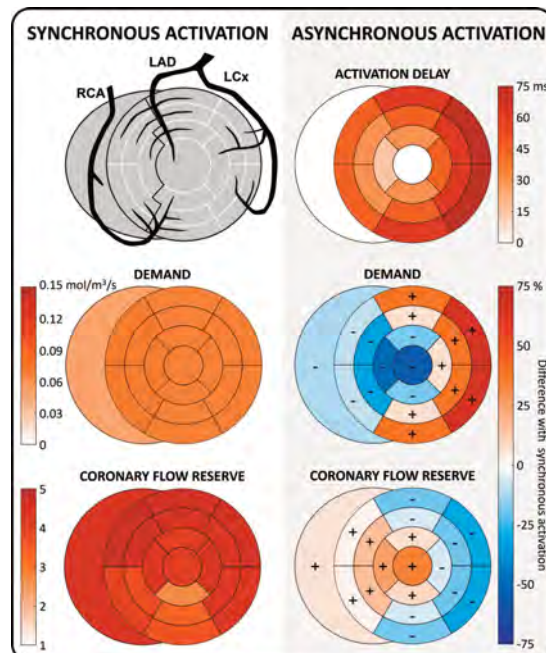


Figure 1: Map of coronary territories (top left), demand (middle left) and coronary flow reserve (bottom left) during synchronous activation, as well as activation delay (top right), and the difference in demand (middle right) and coronary flow reserve (bottom right) with asynchronous activation compared to synchronous activation. LAD: left anterior descending, LCx: left circumflex, RCA: right coronary artery.

4. Discussion and Conclusions

These findings provide theoretical evidence for explaining some clinical and experimental observations, such as reduced CFR in the posterior descending branch compared to the left anterior descending under synchronous activation [3] and septal hypoperfusion in left bundle branch block [4]. Specifically, these findings suggest that septal hypoperfusion in acute dyssynchrony is not an indication of septal ischemia, instead it is caused by autoregulation in response to a reduction in demand, resulting in a higher CFR. In conclusion, we present a new powerful modelling platform capable of simulating coronary hemodynamics with autoregulation under various pathophysiological conditions.

5. References

1. Munneke AG et al., *Front Physiol*;183: 2022.
2. Delhaas T et al., *J Physiol*;477(3):481-496, 1994.
3. Voci P et al., *Am J Cardiol*; 90(9):988-991, 2002.
4. Vernooy K et al., *Eur Heart J*; 26(1): 91-98, 2005.

6. Acknowledgements

Financial support by the Netherlands Organisation for Scientific Research Research (NWO-ZonMw, VIDI grant 016.176.340) and the Dutch Heart Foundation (grant 2015T082).

14.7

Electromechanical Remodelling During Heart Failure in Dilated Cardiomyopathy: a Systematic *in silico* Investigation

Tobias Gerach¹, Axel Loewe¹

¹ Karlsruhe Institute of Technology (KIT), Institute of Biomedical Engineering, Karlsruhe, Germany

*Corresponding author. Email: publications@ibt.kit.edu

1. Introduction

Dilated cardiomyopathy (DCM) is a common cardiac disease and accompanied by an increasing loss of heart function. DCM is characterized by structural (dilation of the ventricles) and functional (impaired contractility) abnormalities and can eventually lead to heart failure (HF) and life-threatening arrhythmias. Different pathomechanisms are known to be involved in the development of DCM. However, the individual role of each mechanism in the development of severe HF is yet to be defined. While the effect of both electrical and mechanical remodelling on cellular tension development has been studied individually, there is a need to elucidate the interplay of both effects. Therefore, we present a model of cardiac electromechanics (EM) to study the impact of remodelling.

2. Materials and Methods

As a baseline, we use an EM model of a human cardiomyocyte consisting of the ionic model in [1] and the tension model in [2]. Mechanical [3] and electrical [4] remodelling were introduced both individually and in combination. To assess the potential impact of the distinctly remodelled cardiomyocytes on DCM and HF, the time courses of intracellular calcium $[Ca^{2+}]_i$, calcium bound to troponin C, and cellular active tension development T_a were analysed.

3. Results

When mechanical remodelling is considered, cardiomyocytes present an increased sensitivity to calcium and a reduced half activation point. As a result, more calcium can bind to troponin C leading to increased crossbridge formation and higher active tension. Electrophysiological remodelling has an overall detrimental effect on the cell. Due to the reduced intracellular calcium concentration, the affinity of calcium to bind to troponin C is reduced as well, resulting in a decrease of active tension. Combining both types of remodelling leads to an overall reduction in tension development compared to the control model.

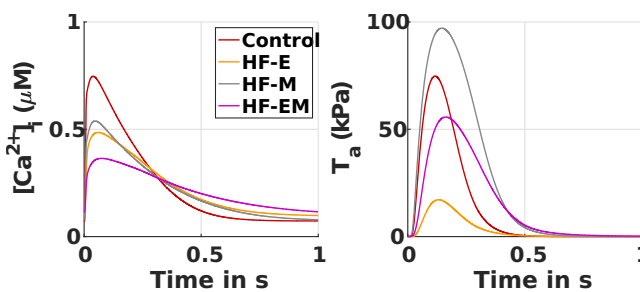


Figure 1: $[Ca^{2+}]_i$ and T_a for the control model and electrical (HF-E), mechanical (HF-M) and electromechanical (HF-EM) remodelling due to HF.

4. Discussion and Conclusions

Electromechanically altered cardiomyocytes contribute to the HF phenotype in DCM due to inhibited tension development. Future investigations will have to verify whether the cellular remodelling is sufficient to reproduce clinically observed biomarkers in patients with DCM in multiscale models.

5. References

1. O'Hara et al. „Simulation of the undiseased human cardiac ventricular action potential: model formulation and experimental validation“. In: PLoS Comput. Biol., 2011
2. Land et al. „A model of cardiac contraction based on novel measurements of tension development in human cardiomyocytes“. In: J. Mol. Cell. Cardiol., 2017
3. Bollen et al. „Myofilament remodeling and function is more impaired in peripartum cardiomyopathy compared with dilated cardiomyopathy and ischemic heart disease“. In: Am. J. Clin. Pathol., 2017
4. Gomez et al. „Electrophysiological and structural remodeling in heart failure modulate arrhythmogenesis. 1d simulation study“. In: PLoS One, 2014

Acknowledgements:

This research was funded by the Deutsche Forschungsgemeinschaft (DFG, German Research Foundation) – Project-ID 258734477 – SFB 1173 and LO 2093/6-1.

14.8

Multiscale mathematical modelling of nanoparticle distribution in a realistic tumour following direct injection

George Caddy¹, Xiao Yun Xu¹, Justin Stebbing¹, Gareth Wakefield²

1 Imperial College London, Department of Chemical Engineering & Department of Surgery and Cancer, United Kingdom

2 Xerion Healthcare Ltd, United Kingdom

yun.xu@imperial.ac.uk

1. Introduction

Cancer is one of the leading causes of death worldwide, with radiotherapy being the most common treatment method. Radiotherapy involves using high energy particles or waves to kill cancerous cells [1]. Improving the efficiency of radiation therapy is an area of keen interest. Radio-sensitizing nanoparticles can be directly injected to increase the efficacy of radiotherapy. However, the exact distribution of nanoparticles within the tumour post-injection remains unclear, only that it will be heterogeneous [2]. Mathematical modelling can help to overcome this problem.

2. Materials and Methods

The computational model consists of a particle tracking model, which calculates the rate of particle deposition onto the cell surface. A nanofluid convection model, that solves for the fluid pressure and velocity. Finally, a nanoparticle transport model which calculates the spatiotemporal concentration of nanoparticles within the tumour. The tumour geometry is reconstructed from micro-CT images of a FaDu tumour and the needle dimensions are that of a 26s gauge needle. The influence of injection locations and nanoparticle surface charge is investigated.

3. Results

Figure 1 shows the nanoparticle (NP) concentration along a cut-plane of the tumour for different NP surface charges, 0mV and -20mV. The distribution of NP within the tumour is significantly increased for negatively charged particles when compared with uncharged particles. When the needle is placed at the end of the tumour, the volumes containing a NP concentration greater than 25% of the inlet concentration, are 0.1139mm³ and 43.466mm³ for the surface charges of 0 and -20mV. The effect of injection location on NP distribution was also investigated, with the needle placed centrally the particle volumes for the are 0.11376mm³ and 38.305mm³.

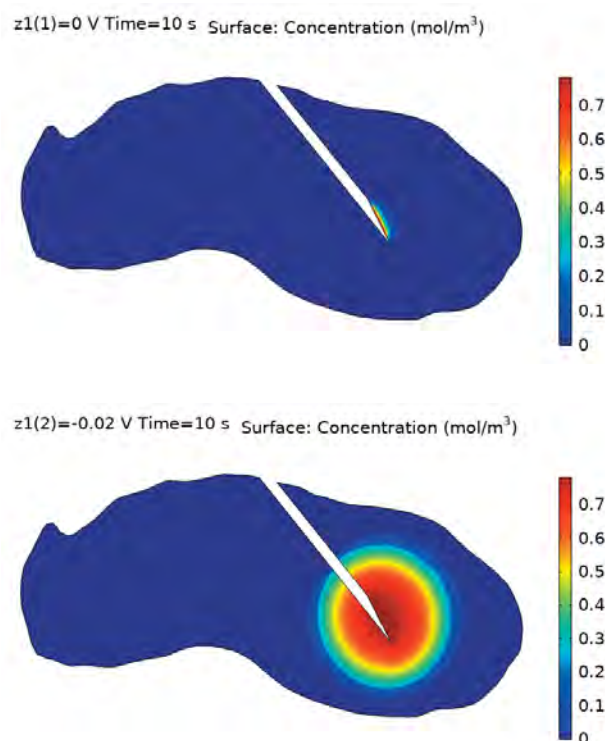


Figure 1: NP concentration at the end of injection for differing particle surface charges; a) -20 mV, b) 0 mV.

4. Discussion and Conclusions

When particles have a negative surface charge a repulsive electrostatic force is created between them and the negatively charged cells, negatively charged NP creates, preventing particle deposition onto cells and therefore allowing particles to travel further from the injection location.

Moving the injection location to the centre causes a reduction in the NP volume within the tumour due to spill-over beyond the tumour boundary. Not only will this compromise the efficacy of the radiotherapy it may also increase damage to the surrounding healthy cells.

5. References

1. Kwatra, D. *Trans Cancer Research* 2013, 2, 330–342.
2. Su, D. *Med & Bio Eng & Comp* 2010, 48, 853–863.

Acknowledgements

This study is support by an EPSRC CASE scholarship and Xerion Healthcare.

15.1

A computer modelling approach to investigate the role of extrinsic and intrinsic mechanical signals on sprouting angiogenesis

Chiara Dazzi¹, Julia Mehl¹, Georg Duda¹, Sara Checa¹

¹ Berlin Institute of Health, Charité - Universitätsmedizin Berlin, Julius Wolff Institute of Biomechanics and Musculoskeletal Regeneration, Berlin, Germany

1. Introduction

Angiogenesis is the process by which new blood vessels sprout off from existing vasculature. Sprouting angiogenesis is essential to many physiological processes but also the regeneration of bone and other tissues. Insufficient re-vascularization may result in delayed or non-healing after bone injury. During sprouting, endothelial cells (ECs) are known to be sensitive and respond to local mechanical stimuli. ECs interact mechanically with outer-vascular stromal cells (SCs) through cell internally generated traction forces (intrinsic loads). In addition, externally applied mechanical loads (extrinsic loads) impact the surrounding tissue deformations and affect sprout patterning [1]. How these two distinct mechanical cues impact angiogenesis remains largely unknown. Here we aim to investigate the relative role of extrinsic and intrinsic mechanical signals on sprout patterning, using a computer modelling approach.

2. Materials and Methods

In silico multi-scale models of the mechano-regulation of sprouting angiogenesis and SCs organization were developed to represent two different experimental setups: 1) the healing region of a mouse osteotomy subjected to physiological loading and stabilized with a rigid or a semirigid fixator [2] and 2) a gelatin substrate subjected to uniaxial stretching [1]. Finite element models at the tissue scale, to compute mechanical strains, were coupled to agent-based models at the cell scale, describing ECs and SCs activity in response to local mechanical signals (e.g. durotaxis). Based on current literature, the influence of mechanical signals on cell migration, orientation and vessel growth was implemented using rule-based approaches. Comparison of model predictions to two different experimental setups allowed to evaluate the validity of the current mechano-biological understanding (reflected by the implemented rules).

3. Results

Vessels were predicted to gradually align towards the direction perpendicular to the bone long-axis while approaching the osteotomy gap, thereby minimizing the shear experienced by the sprouts. This prediction matched the alignment found in the ex vivo samples (Fig.1). Furthermore, under reduced mechanical stability (semirigid fixator) a lack of sprouts was observed at the core of the osteotomy that was also predicted by the in silico analyses (Fig.1).

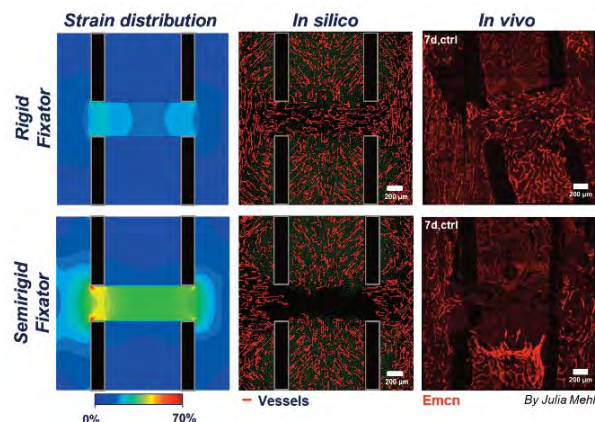


Figure 1: Healing region 7 days post-fracture.

Analogous mechanics-based rules were able to predict a preferential orientation of vessels in the in vitro setting.

4. Discussion and Conclusions

Our mechanics-driven angiogenesis model was able to predict and explain the sprout patterning found both in vivo and in vitro, giving confidence to the mechano-biological rules implemented. Future studies, however, need to further extend the model by including the influence of known biological factors on the process to investigate additional mechano-biological interactions.

5. References

1. Rosenfeld D et al, Proc Natl Acad Sci USA; 12:3215-20 (2016).
2. Borgiani E et al, J Bone Miner Res.; 10:1923-37 (2019).

Acknowledgements:

This work was supported by grant CRC 1444 from the DFG.

15.2

A mechanobiological approach of growth plate morphological evolution

Diego Quexada^{1,2}, Olfa Trabelsi¹, Diego Garzón Alvarado², Marie-Christine Ho Ba Tho¹

1 Université de technologie de Compiègne, Oise, Compiègne, France

2 Universidad Nacional de Colombia, Numerical Methods and Modeling Research Group (GNUM), Bogota, Colombia

1. Introduction

Longitudinal growth of long bones takes place mainly in the growth plate or epiphyseal plate. This zone is composed mostly of hyaline cartilage, which is 70% water with a matrix of collagen fibers and proteoglycans macromolecules [1]. In the developmental stages, the growth plate acts as a mold at both ends of each bone where a primary ossification center is formed. The growth plate is divided into three main zones: reserve, proliferating, and hypertrophic. The apparition of secondary ossification centers at the epiphyses of long bones, induce its radial growth. Changes in the morphology of the growth plate, i.e., in shape, density, and cellular distribution, take place during each developmental stage, which have been attributed to genetic causes, as well as mechanical factors. In this work, a computational model of the evolution of the epiphyseal plate using a new constituent law is presented. This model can be of real use in the clinical field to determine how different loading conditions may influence the changes in growth plate topology.

2. Materials and Methods

In this work, a 2D dynamical simulation on the growth plate morphology and surrounding trabecular tissue is defined by adding a linking relationship between the acceleration \ddot{u} which depends on the mechanical properties of different zones in the growth plate, and the stress distribution σ as described in equation (1).

$$\nabla \sigma = p u \quad (1)$$

The epiphyseal plate topology is achieved at different stages in development, taking into account the stress variations due to changes in the mechanical loading and shape evolution. The finite element method (FEM) is used to solve the dynamic problem in a proximal femur and calcaneus. A function for the mechanical loading dependent on age is implemented to better approximate the boundary conditions.

3. Results

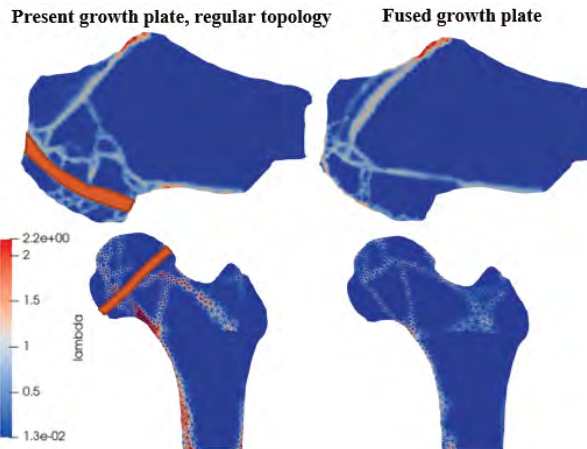


Figure 1: Growth plate presence affecting trabecular formation.

Our model shows how main trabecular group distribution depends on the presence of the growth plate, as seen in figure 1.

4. Discussion and Conclusions

This work can be coupled with biological models that give information on how different paracrine and autocrine regulators act on the growth plate, such as in the work proposed by different authors [3][4]. Furthermore, the proposed mechanobiological approach could help to better understand how diseases affecting the growth plate, such as slipped capital femoral epiphysis (SCFE) or Gaucher's disease, can progress over time and how it occurs for prevention.

5. References

- [1] Nguyen D. J. et al. *Radiographics*, vol. 37, no. 6, pp. 1791–1812, 2017.
- [2] J. M. Guevara, M. A. Moncayo. et al. *vol. 118, no. 1, pp. 59–68, 2015.*
- [3] S. V. Komarova. et al. "Bone, vol. 33, no. 2, pp. 206–215, 2003.
- [4] P. Pivonka et al, *Bone*, vol. 43, no. 2, pp. 249–263, 2008.

Acknowledgements:

The authors acknowledge the financial support of Universidad Nacional de Colombia and Université de technologie de Compiègne.

15.3

Agent-based models for vocal fold regenerative biomaterials: a parameter optimization study

Grace Yu¹, Michael Döllinger², Nicole Li-Jessen³

1 Mayo Clinic, Alix School of Medicine, Rochester, United States

2 University of Erlangen-Nuremberg, Otorhinolaryngology Head & Neck Surgery, Erlangen, Germany

3 McGill University, School of Communication Sciences and Disorders, Montreal, Canada

1. Introduction

Tissue engineering therapeutics have been harnessed for severe vocal fold (VF) defects. However, any slight variations in material physio-chemical properties could affect VF cellular responses [1]. Computational models have been proposed to aid tissue-specific biomaterial design. Our team developed an agent-based model of VF biomaterials (ABM-B) to numerically simulate cell-material and cell-cell interactions for hyaluronan-based hydrogels [2]. High-fidelity biological ABMs are non-linear and high dimensional [3]. A proper optimization method is required for effective parameter calibration. The primary goal of this study was to evaluate four distinct parameter optimization methods for ABM-B.

2. Materials and Methods

ABM-B was written in C++ and executed on compute nodes on Compute Canada. The virtual biomaterial world was set as $0.6 \times 0.6 \times 0.6 \text{ mm}^3$ and seeded with 125 fibroblast cell agents initially. Model inputs were material compositions including hyaluronic acid, gelatin, and PEGDA concentrations. Outputs included mechanical properties of materials, cell viability, as well as concentrations of cytokines (TNF-alpha, TGF-beta, FGF, IL-6, and IL-8) and extracellular matrix proteins (collagen, hyaluronic acid, and elastin).

Sensitivity analysis with Random Forest was performed on 82 agent-rule parameters, whose quantitative values were not reported in literature. Parameter optimization was performed on the three most influential parameters. The objective function is defined in (1), where E is error, F is the number of fibroblasts, C is the amount of collagen, and the subscripts s and e refer to simulated and experimental outputs respectively.

$$E = (F_s - F_e)^2 + (C_s - C_e)^2 \quad (1)$$

Nelder-Mead (NM), Broyden-Fletcher-Goldfarb-Shanno (BFGS), conjugate gradient (CG), and Powell, which are designed to solve unconstrained optimization problems, were employed. Optimization results were verified with a parameter with known values, namely, the half-life of IL-6, which is 1.7 ± 0.6 hours (mean \pm SD) [4].

3. Results

All optimization methods reached the known parameter value within the standard deviation. The error was observed to decrease with NM optimization but not as apparently with BFGS, CG, or Powell methods (Figure 1).

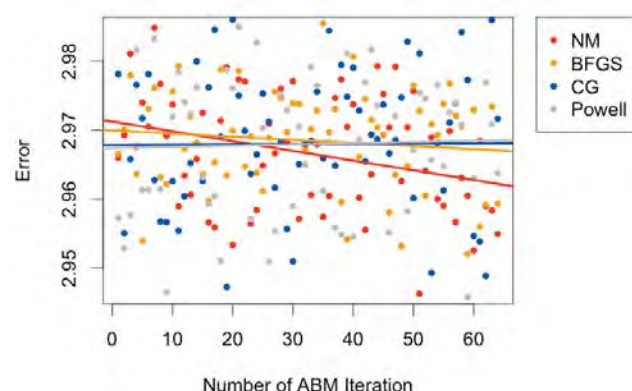


Figure 1. Computed error during NM, BFGS, CG, and Powell optimization methods for each iteration.

4. Discussion and Conclusions

NM was noted to have best reduced the error for the ABM-B. Work is ongoing to expand the model with additional cell types and material compositions, which will allow us to explore a wider scope of biomaterial designs that would otherwise be infeasible with empirical in vitro or in vivo experiments.

5. References

- [1] Coburn PT et al. *Journal of Biomedical Materials Research Part A* 109(8) (2021) 1337-1352.
- [2] Shung C. McGill University, 2017.
- [3] Granato B. et al. ECAI 2020, IOS Press2020, pp. 2905-2906.
- [4] Waage A et al *Journal of Experimental Medicine* 169(1) (1989) 333-338.

Acknowledgements:

This project is supported by the National Sciences and Engineering Research Council of Canada (RGPIN-2018-03843 and ALLRP 548623-19), Compute Canada and Canada Research Chair research stipend (N.L.J.). The presented content is solely the responsibility of the authors and does not necessarily represent the official views of the above funding agencies.

15.4

An in silico framework for virtual optimization of tissue engineering cartilage repair approaches

Seyed Ali Elahi^{1,2}, Petri Tanska³, Rami K. Korhonen³, Rik Lories⁴, Nele Famaey², Ilse Jonkers¹

1 KU Leuven, Department of Movement Sciences, Leuven, Belgium

2 KU Leuven, Mechanical Engineering Department, Leuven, Belgium

3 University of Eastern Finland, Department of Applied Physics, Kuopio, Finland

4 KU Leuven, Department of Development and Regeneration, Leuven, Belgium

1. Introduction

Tissue engineering (TE) approaches aim at repairing large cartilage defects by implanting chondrocyte-laden hydrogel constructs or scaffolds. The chondrocyte is the unique cell type within cartilage and is responsible for synthesizing extracellular matrix (ECM). Successful in-vitro cartilage synthesis in these chondrocyte-seeded constructs is known to be promoted by mechanical stimulation using bioreactors [1]. However, the mechanical quality of the neo-formed cartilage is still inferior to the one of native cartilage tissue. Here, we present an in silico finite element (FE)-based multi-scale modelling framework for virtual optimization of TE treatments that allows evaluating the regenerative capacity of cell-seeded hydrogels with different mechanical characteristics to optimise the loading protocol.

2. Materials and Methods

An FE model of a cylindrical cartilage explant with radius and height of 1.5 mm including a cylindrical defect in the middle of the explant with radius and height of 1 mm was created in Abaqus. Explant was modelled as a fibril reinforced poro-viscoelastic swelling material [2]. The defect was filled with a hydrogel construct modelled as a poro-hyperelastic material [3]. Following a free swelling step, a load-unload cycle with deformation amplitude of 0.1 mm and frequency of 1 Hz was imposed to the explant-construct compound. The following model results were evaluated as regulatory parameters, in agreement with previous experimental works: (i) distance from open construct surface, affecting nutrients delivery to the cells; (ii) fluid velocity, enhancing the nutrient delivery to the cells through fluid flow and increasing the exudation of small proteins and degradation; (iii) dissipated energy, stimulating the ECM production during a load-unload cycle; and (iv) maximum shear strain, causing ECM degradation. All parameters were normalized between 0 and 1 based on thresholds obtained from literature. An objective function (OF) was then formulated to be maximized for maximum regeneration within the construct:

$$OF = d + FV + DE - MSS \quad (1)$$

where, d, FV, DE and MSS are the normalized parameters reflecting the distance from open construct surface, fluid velocity, dissipated energy and maximum shear strain, respectively. The in silico framework was used to evaluate the regenerative capacity of two constructs: Alginate 2.2% and pHema hydrogels.

3. Results

Fig. 1 shows the value of OF over the hydrogel constructs.

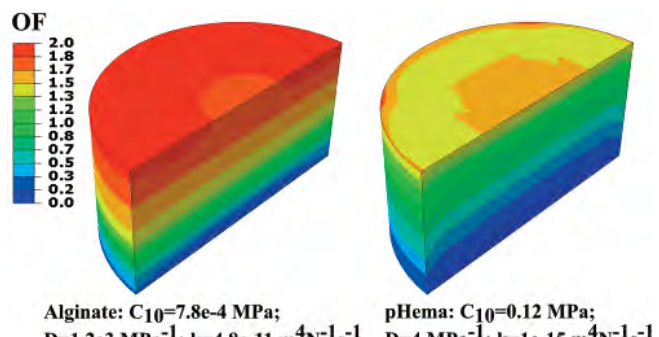


Figure 1: Transverse section of the constructs. C10 and D are the constants of Neohookean hyperelastic material model and k is the permeability. Colour map shows the value of OF (Eq. 1) over the construct after the load-unload cycle.

4. Discussion and Conclusions

The result shows that regeneration potential is superior for the Alginate hydrogel but decreases remote from the hydrogel surface. In the pHema the decreased fluid velocity limits the regenerative capacity already close to the hydrogel surface. In the next step, we aim to use the developed in silico framework to optimize our bioreactor TE protocols by evaluating OF for different loading protocols, construct properties and defect shapes.

5. References

1. Wimmer M et al., *J Biomech*; 42:424-429 (2009).
2. Elahi SA et al., *Front Bioeng Biotech*; 9 (2021).
3. Elahi SA et al., *J Mech Behav Biomed Mater*; 124 (2021).

Acknowledgements:

This work was supported by Marie Skłodowska Curie Individual Fellowship (CREATION project: MSCA-IF-2019-893771) and KU Leuven Happy Joints project (C14/18/077).

15.5

Computational modelling of the mechanical competition within an epithelial cell monolayer under infection

Raúl Aparicio-Yuste^{1,2}, Marie Muenkel², Effie E. Bastounis², María J. Gómez-Benito¹

1 Multiscale in Mechanical and Biological Engineering (M2BE), Mechanical Engineering, University of Zaragoza, Zaragoza, Spain

2 Interfaculty Institute of Microbiology and Infection Medicine, University of Tübingen, Tübingen, Germany

1. Introduction

Listeria monocytogenes (L.m.) is an intracellular bacterial pathogen whose primary site of infection is the intestinal epithelium, lined by a single monolayer of cells. In vitro infection of host epithelial cells triggers a cell mechanical competition between uninfected surrounding cells (winners) against L.m.-infected cells (losers). This competition leads to the squeezing and extrusion of infected cell domains (mounds). It is essential to better understand the mechanisms that L.m. uses to disseminate in the tissue and how host cells respond to infection to restrict infection spread via infected cell extrusion.

2. Materials and Methods

In vitro models have provided insight on infection processes and how L.m. hijacks the host cell cytoskeleton to promote its spread through tissues. However, in silico models can complement the process of understanding this infection process.

We present a three-dimensional computational model that considers a cell monolayer and its extracellular matrix (ECM), describing the mechanical interplay between cells and the ECM under bacterial infection. To do so, we implement a Finite Element Model that considers cell-cell interactions and cell-ECM focal adhesions. The parameters of our model are based on our experimental observations. The number of infected cells in our model is fixed, thus there is no replication or intercellular spread of L.m..

We aim to investigate the role of ECM stiffness in driving the infection process. We consider soft, stiff and glass ECMs with different elastic moduli. Moreover, we also investigate how the size of the infection focus impacts the formation of infection mounds. Lastly, we analyse the influence of the relative stiffness ratio of winners versus losers (RE) on host cell displacements and infected cells' squeezing.

3. Results

Our model predicts that an increased ECM stiffness leads to larger cell displacements, infected cell squeezing and thus promotes mounding. Moreover, a smaller infection focus or a larger RE both enhance infection infected cell squeezing and thus mounding. Our in silico results were confirmed experimentally.

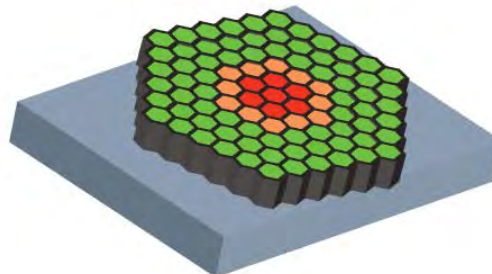


Figure 1: Cell monolayer and the underlying ECM where cells reside. Infected cells (centre) are softer than uninfected surrounding cells.

4. Discussion and Conclusions

We show that (extra)-cellular mechanics play a major role in regulating the cell competition that arises during infection. A better exploration of the biophysical parameters involved will not only assist us on understanding infection processes but also cell competitions that arise during cancer and development.

5. References

1. Bastounis EE et al., *Developmental Cell*; 56, 443–460.e11 (2021).
2. Pentecost M, Otto G. et al., *PLOS Pathogens* 2, 1-12 (2006).
3. Ortega FE, Koslover EF et al., *eLife* 8 (2019)

Acknowledgements:

The authors would like to thank the Spanish Ministry of Universities (FPU20/05274) and the European Union's Horizon 2020 research and innovation programme (826494).

15.6

Design and manufacturing of 3D printed porous scaffolds for critical size bone defects: Three clinical cases

Beat Schmutz^{1,2,3}, Christoph Lahr¹, Marie Luise Wille^{1,2,4}, Dietmar Hutmacher^{1,2,3,4,5}, Boris Holzapfel⁶

1 Queensland University of Technology, School of Mechanical, Medical, and Process Engineering; Faculty of Engineering, Kelvin Grove, QLD, Australia

2 ARC Training Centre for Multiscale 3D Imaging, Modelling and Manufacturing, QUT, Brisbane, Australia

3 Jamieson Trauma Institute, Brisbane, Australia

4 Max Planck Queensland Centre for the Materials Science of Extracellular Matrices, Brisbane, Australia

5 ARC Training Centre in Additive Biomanufacturing, QUT, Brisbane, Australia

6 Musculoskeletal University Centre Munich - Ludwig Maximilians University Munich, Germany

1. Introduction

Scaffold-guided tissue regeneration is a novel method for treating critical sized bone defects. It involves the surgical implantation of a 3D printed bioresorbable scaffold with autologous bone graft, leading to bone regeneration over a period of time [1,2]. Our team has collaborated on three clinical cases that have successfully proven this technique to be effective.

2. Materials and Methods

Case#1: Osteosarcoma patient with 15 cm tibial midshaft osteotomy to be stabilised with an intramedullary nail (IMN). Case#2: Trauma patient with 12 cm distal tibial shaft defect with an IMN in-situ. Case#3: Giant cell tumour patient with 6 cm clavicle defect after resection to be stabilised with a fixation plate.

For Case#1 & 2, modular porous scaffolds of interconnecting hollow cylinders were designed. For pre-op planning of Case#1, optimal nail fit, and position were simulated with our Nail Fit Tool [3]. For Case#3, using the mirrored intact contralateral bone as template, an anatomically shaped solid scaffold with 5 mm holes and end pins was designed (Fig. 1).

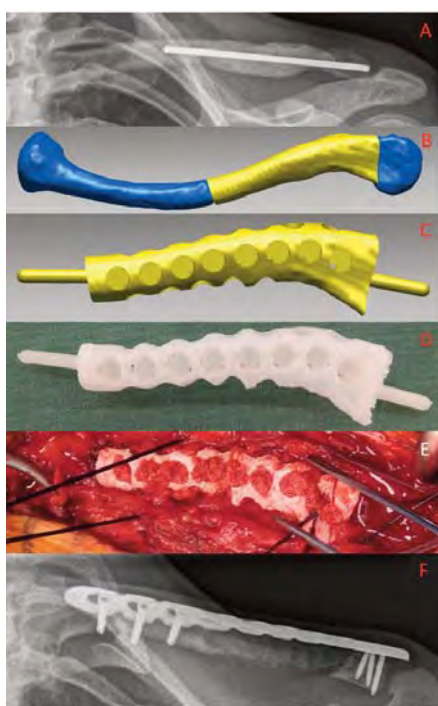


Figure 1: Case#3. (A) Pre-implant x-ray of defect bridged with bone cement and stabilised with pin. (B) Anatomical defect model. (C) Scaffold model. (D) Printed prototype. (E) Filled with bone graft in-situ. (F) 8 months post-op x-ray.

For each case, 3D bone models were reconstructed (Amira) from patient CT scans. The scaffolds were designed with reverse engineering software (Rapidform). Prototypes were 3D printed in-house in polylactic acid using fused filament fabrication (FFF). Final scaffolds were printed (FFF) in medical grade polycaprolactone-tricalcium phosphate by our commercial partner.

3. Results

All three scaffolds have been successfully implanted. The patients have recovered well, showing active bone remodelling and progressive ossification on x-ray follow-ups (Fig. 1).

4. Discussion and Conclusions

Key findings from these cases are: 1) With currently available software applications, bone segmentation in the presence of bone cement and metal artefacts is very time consuming, further, they do not enable efficient design of patient-specific scaffolds. 2) Greater design flexibility in macro pore size (>4 mm) and distribution is required. 3) Close collaboration between surgical, design and manufacturing teams is crucial to design iterations, timeline, and surgical outcome. To address identified limitations, we are working on an integrated platform for development and manufacturing of Voronoi scaffold designs [4].

5. References

1. Henkel et al., *Bone Research*; 1:216-248 (2013).
2. Henkel et al., *Bone*; 153:116163 (2021).
3. Amarathunga et al., *Proc Inst Mech Eng H*; 228:1227–34 (2014).
4. Herath et al., *Mater. Des.*; 212:110224 (2021).

Acknowledgements:

This work was supported by: Max Planck Queensland Centre for the Materials Science of Extracellular Matrices; Australian Research Council Training Centre (ARC ITTC) in Additive Biomanufacturing (IC160100026); ARC ITTC for Multiscale 3D Imaging, Modelling, and Manufacturing (IC180100008).

15.7

In silico investigation of the mechanobiological influence of fixation devices on mandibular fracture healing

Vincenzo Orassi¹, Carsten Rendenbach², Sara Checa¹

1 Berlin Institute of Health at Charité – Universitätsmedizin Berlin, Julius Wolff Institute, Berlin, Germany

2 Department of Oral and Maxillofacial Surgery, Charité – Universitätsmedizin, Berlin, Germany

Correspondence: Sara Checa, sara.checa@bih-charite.de

1. Introduction

Mandibular fracture fixation is commonly performed using titanium fixation devices. However, disadvantages such as imaging artifacts, the need for plate removal, as well as the excessive stiffness of titanium promoted the research of alternative materials, e.g. biodegradable magnesium alloys [1]. However, whether the latter can mechanobiologically support mandibular bone healing remains unknown.

This study aims to investigate the biomechanical conditions induced by already established and alternative fixation devices within the callus region in a mandibular body fracture and their effect on the bone healing process.

2. Materials and Methods

3D finite element models (FEMs) of a mandibular body fracture fixated with two parallel miniplates made of titanium, magnesium alloy WE43, or PLA were developed (Fig. 1a). Physiological post-operative boundary conditions were applied to determine the biomechanical conditions within the healing region.

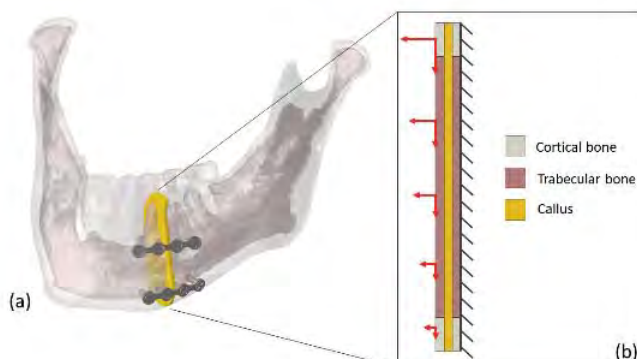


Figure 1: (a) 3D and (b) simplified 2D FEMs.

In addition, a bone healing computer model was developed to investigate the mechanobiological interactions during bone regeneration. Iteratively, a 2D FEM of the healing region (Fig. 1b) was coupled with a 2D agent-based model (ABM), in which cellular activities, such as differentiation, proliferation, migration, and apoptosis, were simulated according to mechanoregulation rules [2].

3. Results

Initial strains within the callus region induced by titanium, magnesium, and PLA fixation were in the range of 0.9-1.1%, 1.8-3.0%, and 11.4-13.7%, respectively. At week 4, new bone deposition was predicted using titanium and magnesium plates, while fibrous tissue formation was predicted using PLA plates (Fig. 2).

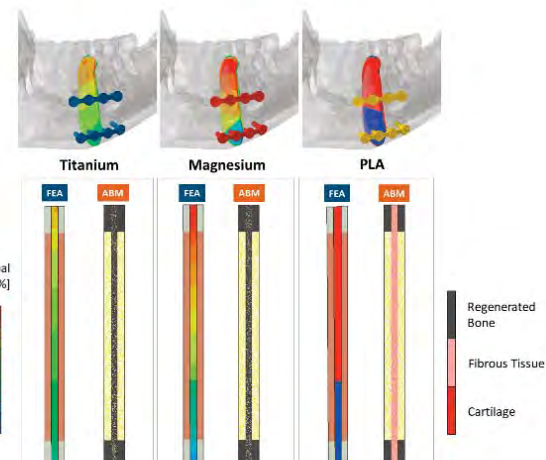


Figure 2: FE biomechanical analysis and ABM healing prediction for the three materials.

4. Discussion and Conclusions

In this study, a bone regeneration model was developed to investigate the potential of magnesium for fracture fixation devices in the mandible. Results suggest that magnesium devices are able to support the healing process despite slightly inferior fixation stability. Future studies will further develop the dynamic mandibular bone healing model to optimize fixation devices.

5. References

- Rendenbach et al., Mater. Sci. Eng.; C 129: 112380 (2021).
- Claes LE, Heigle CA., J. Biomech.; 32.3: 255-266 (1999).

Acknowledgements:

European Union (EU) Horizon 2020, project InterLynk (grant agreement: H2020-NMBP-TR-IND-2020, project ID: 953169).

15.9

OMIBONE: OMics-driven computer model of Bone regeNeration for personalized medicene

Mahdi Jaber^{1,2}, **Johannes Schmidt**³, **Tanja Laske**⁴, **Sara Checa**^{2,5}

- 1 Julius Wolff Institute at BIH, Charité - Universitätsmedizin Berlin, Germany, Berlin, Germany
- 2 BIH Center for Regenerative Therapie, Charité - Universitätsmedizin Berlin, Germany, Berlin, Germany
- 3 Fraunhofer Institute for Cell Therapy and Immunology IZI, Leipzig, Germany
- 4 Institute for Computational Systems Biology, University of Hamburg, Hamburg, Germany
- 1 Julius Wolff Institute at BIH, Charité - Universitätsmedizin Berlin, Germany, Berlin, Germany

1. Introduction

The treatment of bone defects mostly depends on clinical imaging with some references to patients' physiology and medical history [1], but lacks details about the patient-specific healing potential. Omics provide quantifiable biological indication for patients' intrinsic bone regenerative capacity. Proteomics has been explored for biological characterisation of bone healing processes as well as for various bone diseases [2]. Computer models informed by such data have the potential to turn simulations into a predictive tool of individualized healing outcome, providing a new perspective for the design of personalized therapies. Although several computer models of bone regeneration have been developed and partially validated [3], they ignore the patient-specific blueprint. Here, we present OMIBONE, a computer modelling framework that is enriched by patient-specific omics to predict individualized healing outcome.

2. Materials and Methods

OMIBONE follows a computational approach using a previously described computer model for bone regeneration [3], which we extended to incorporate proteomics. The computer model combines finite element (FE) analysis, to determine the mechanical environment within the fracture, and an agent-based model (ABM) to characterize biological processes taking place during bone regeneration [3]. Within OMIBONE, we develop a systematic approach to derive cellular activity rates from subcellular information extracted by the expression levels of the proteins involved in the regeneration process. In detail, the cellular activity rates within the ABM are determined as a function of protein expression levels and time dependent variables. The associated functions of the proteins that are involved in a particular cellular activity are extracted using the Database STRING. We evaluated OMIBONE for its prediction potential using the time-resolved post-surgical proteomics profile together with the corresponding X-ray-based healing progression from a fracture stabilized with an intramedullary pin [2].

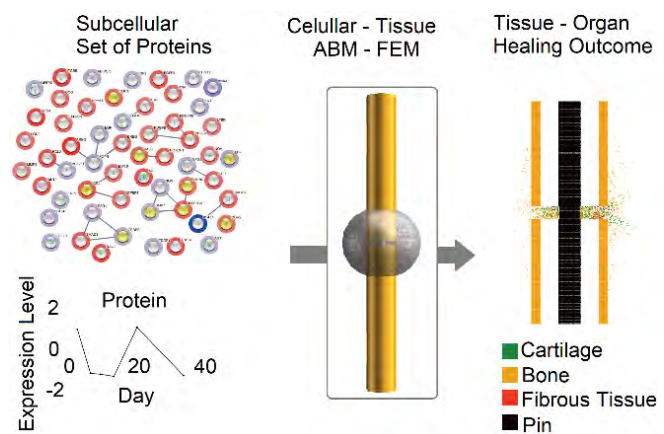


Figure 1: OMIBONE framework: from subcellular protein levels, to prediction of cellular activity to prediction of tissue formation during the regeneration process and healing outcome

3. Results

Computer model predictions of tissue formation during healing agree well with experimental data. The model predicts bone bridging after 2 weeks (Fig1). Omics-derived cellular activity rates show large variations over the course of healing which relates to specific molecular processes at different stages of the healing progression.

4. Discussion and Conclusions

Here, we propose a novel model that considers the intrinsic bone regenerative capacity for individual patients. Future work will focus on validating the model and transferring it to the clinic.

5. References

1. Wiss, D.A. and W.B. Stetson, *JAAOS* 4(5): p. 249-257, 1996.
2. Hussein Al et al., *J Orthop Res*;36(4):1153-1163, 2018.
3. Checa S et al., *J Biomech*. 44(7):1237-45, 2011.

Acknowledgements:

This project is funded by the Federal Ministry of Education and Research (BMBF: research grant [01ZX1910]).

16.1

A correlation study between morphological parameters and hemodynamics indices: an integrated deep learning and statistical shape modeling approach.

Martino Andrea Scarpolini^{1,2}, Marilena Mazzoli^{1,3}, Katia Capellini^{1,3}, Simona Celi¹

1 Fondazione Toscana G. Monasterio, Bio-Engineering, Massa, Italy

2 University of Rome "Tor Vergata", Industrial Engineering, Roma, Italy

3 University of Pisa, Pisa, Italy

email: mascarpolini@monasterio.it

1. Introduction

Deep Learning (DL) has been demonstrated to be an efficient tool to estimate hemodynamic indices in several cardiovascular districts [1]. Recently, the adoption of statistical shape (SS) analysis has been proposed to quantitatively assess geometric variability in several anatomical structures [2]. In this context a critical issue is represented by the inclusion of supra-aortic branches into the SS analysis. Nevertheless, they are fundamental to impose realistic boundary conditions.

In this work, we present a surface-based Statistical Shape Model (SSM) of the thoracic aorta, including supra-aortic branches, combined with DL tools to investigate the correlation between morphological parameters and hemodynamic indices.

2. Materials and Methods

A set of 80 patient-specific 3d surface models of aortas with point-wise correspondence has been created using a specific code for non-rigid registration. The implemented algorithm minimizes the Chamfer distance between surfaces using a modified gradient descent algorithm, as described in [3]. By using the SSM, 800 virtual geometries have been generated. Hemodynamic variables have been estimated through transient Computational Fluid Dynamics (CFD) simulations with RCR Windkessel boundary conditions performed in OpenFOAM. A large-scale CFD dataset of hemodynamic indices (TAWSS, OSI, etc.) was created from this data to train two different neural networks (NNs). The first one with an architecture based on fully connected layers, while the second one is based on layers from graph DL [4]. The correlation between the distribution of hemodynamic variables and the shape parameters associated with each geometry (modes of the SSM) is studied and compared between CFD data and DL predictions.

3. Results

A statistical shape model of the thoracic aorta was successively built with 22 modes representing 99% of the variability of the original dataset (Fig. 1). The trained NNs can predict different hemodynamic variables with errors below 15%. In Table 1, we show the results of the correlation study for CFD data and DL predictions.

4. Discussion and Conclusions

This work shows the capabilities of the combined use of SSMs and DL tool for health care. A quantitatively assessment of the aorta geometry including supra-aortic branches was feasible together with the computation of hemodynamic variables in real-time. Moreover, we show that morphological features extracted by the SSM are highly correlated with hemodynamic indices.

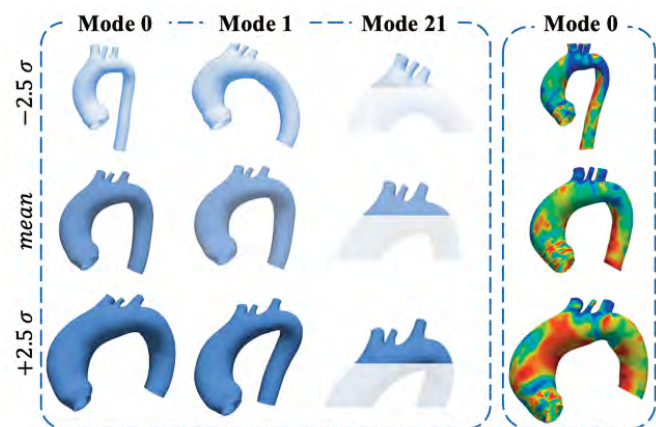


Figure 1: Example of SSM results for Mode 0, 1 and 21 (left) and DL's OSI maps (right) for Mode 0.

	TAWSS	WSS	RRT	ECAP	OSI
mean	-0.96	-0.97	0.96	0.95	0.79
max	-0.82	-0.93	-0.13	0.70	0.39
min	-0.89	-0.83	0.83	0.79	-0.13

Table 1: Results of the correlation study between hemodynamic indices (CFD) and SSM's mode 0. The Pearson correlation coefficient is computed for mean, maximum and minimum values of each hemodynamic field.

5. References

1. Ferez XM et al., *Front. in Physiology* (2021): 834
2. JL Bruse et al., *BMC med imag* 16.1 (2016): 1-19.
3. Nicolet B et al., 2021, *ACM TOG*, 40(6), pp.1-13.
4. Scarpolini MA et al., *ESB2021* p. 185

Acknowledgements:

This project has received funding from the Marie Skłodowska Curie grant agreement No 859836.

16.2

A framework of decision support system for facial rehabilitation based on reinforcement learning coupled with finite element model

Duc-Phong NGUYEN¹, Marie-Christine Ho Ba Tho¹, Tien-Tuan DAO²

1 Université de technologie de Compiègne, CNRS, Biomechanics and Bioengineering, Compiègne, France

2 University of Lille, CNRS, Centrale Lille, UMR 9013 - LaMcube - Laboratoire de Mécanique, Multiphysique, Multiéchelle, Lille, Lille, France

1. Introduction

Patients with facial palsy or those who have had a facial transplant have an asymmetric face and abnormal facial motion due to altered facial muscle functions and nerve damage [1]. The recovery of a symmetric face with balanced functionalities requires a complex rehabilitation process. Thus, understanding of facial motion mechanism helps the involved patients to recover symmetrical movements and normal facial expressions [2]. However, the predictive capacity of current solutions is still limited to explore the facial motion patterns with emerging properties. The present study aims to couple the reinforcement learning and the finite element modeling for better exploring facial motion learning and prediction.



Figure 2: Face animation for symmetry-oriented motion.



Figure 3: Face animation for smile-oriented motion.

2. Materials and Methods

A novel modeling workflow was developed with two main components such as a reinforcement learning agent and a finite element modeling of the face. A physically-based model of the face within the Artisynth modeling platform was used [3]. An information exchange protocol was proposed to manage the information between reinforcement learning and rigid multi-bodies dynamics simulation. Two reinforcement learning algorithms (deep deterministic policy gradient (DDPG) (Fig. 1) and Twin-delayed DDPG (TD3)) were used and implemented to drive the simulations of symmetry-oriented and smile movements. Numerical outcomes were compared to experimental observations using the Bosphorus database.

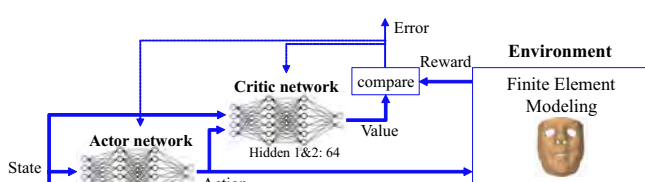


Figure 1: The network architecture of DDPG.

3. Results

As result, reinforcement learning agent spent 100 episodes of random interaction in the environment, and then can find the optimal policy after more than 300 episodes of training. Regarding the symmetry-oriented motion (Fig. 2), the muscle excitations predicted help to increase the value of reward from $R = -2.06$ to $R = -0.23$, which counts for $\sim 89\%$ improvement of the symmetry value of the face. For smile-oriented motion (Fig. 3), two points at the edge of the mouth move up 0.35 cm, which is within the range of movements estimated from the Bosphorus database (0.4 ± 0.32 cm).

4. Discussion and Conclusions

The present study explored the muscle excitation patterns by coupling reinforcement learning with a finite element model of the face. We developed, for the first time, a novel coupling scheme to integrate the finite element simulation into the reinforcement learning for facial motion learning. As perspectives, this present workflow will be applied for facial palsy and facial transplantation patients to guide and optimize the functional rehabilitation program.

5. References

1. Robinson et al. *Operative Techniques in Otolaryngology-Head and Neck Surgery* 23.4 (2012): 288-296.
2. Nguyen et al. *Computer Methods and Programs in Biomedicine* 200 (2021): 105846.
3. Stavness et al. *3D multiscale physiological human*. Springer, London, 2014. 253-274

Acknowledgements:

This work was financially supported by Sorbonne Center for Artificial Intelligence (SCAI).

16.3

An image-based machine learning and morphometric pipeline for the prediction of liver resection complexity

Omar Ali^{1 2 3 4}, Alexandre Bone¹, Caterina Accardo⁵, Omar Belkouchi⁵, Marc-Michel Rohe¹, Eric Vibert^{3 4 5}, Irene Vignon-Clementel²

1 Guerbet, Villepinte, France

2 Inria, Palaiseau, France

3 Inserm, Villejuif, France

4 University of Paris-Saclay, Gif-sur-Yvette, France

5 Hôpital Paul-Brousse Ap-Hp, Villejuif, France

1. Introduction

The preoperative assessment of liver resection complexity (LRC) is necessary to avoid the risk of postoperative complications. We introduce CoRe, an end-to-end automated pipeline for the prediction of LRC from preoperative CT scans. The segmentations of the liver anatomy are first generated using deep learning models, followed by a robust liver vessel pruning algorithm to define the hepatic central zone (HCZ), and a machine learning model to finally predict the LRC.

2. Materials and Methods

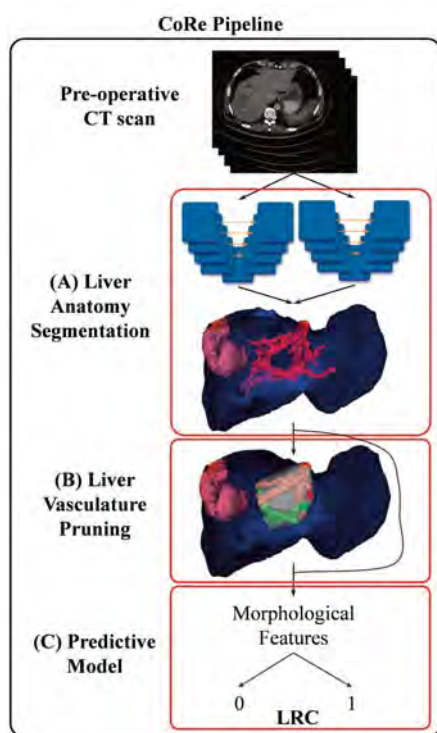


Figure 1: CoRe Pipeline. (A) Liver anatomy segmentation, (blue): liver, (red): vessels, (orange): lesions. (B) Pruning algorithm to define HCZ (white). (C) LRC prediction using features from (A) and (B).

Two independent 3D convolutional neural networks are trained to segment the liver and lesions on one hand, and the portal and hepatic venous vessels on the other hand [1]. The vessel segmentation mask is converted to a graph with branches and edges after reducing it to a skeleton [2-4]. Two distinct venous structures compose most of the liver vascularization: the portal and the hepatic trees. The entry points of each tree are identified by

successively eroding the vessel segmentation mask and keeping the centroids of the two most persistent connected components. The vessel branches are then exploited and robustly pruned beyond the third vascular bifurcation. The convex volume around the pruned vessels defines the HCZ, the region where surgical resections are assumed to be difficult. The liver volume, number of lesions and volume of lesions are the first features extracted from the raw segmentations, and complemented by a newly proposed feature FHCZ, defined to be the normalized volume of occupancy of the lesion when inside the HCZ, and the opposite of the normalized minimal distance to the pruned vessels when outside the HCZ. A logistic regression model is finally trained with these features to predict the LRC.

3. Results

The dice metric used to evaluate the overall segmentation scores reaches 96.0%, 70.6% and 79.1% for the liver, lesions, and hepatic vessels respectively. The results of the ablation study (Table 1) evaluate the importance of every feature and show that the best configuration to predict the LRC combines FHCZ with the volume and number of lesions. This configuration achieves an accuracy, F1 score and AUC of 0.77, 0.75 and 0.84 respectively.

F _{HCZ}	N _{Les}	V _{Les}	V _{Le}	Acc	F1	AUC
✓	✓	✓	✓	0.74	0.71	0.84
✗	✓	✓	✓	0.70	0.68	0.78
✓	✗	✓	✓	0.76	0.73	0.79
✓	✓	✗	✓	0.73	0.71	0.82
✓	✓	✓	✗	0.77	0.75	0.84
✗	✓	✓	✗	0.72	0.70	0.77
✓	✗	✓	✗	0.73	0.70	0.79
✓	✓	✗	✗	0.78	0.78	0.81
✗	✓	✗	✗	0.66	0.60	0.65
✓	✗	✗	✗	0.66	0.65	0.73

Table 1: Ablation study results

4. Discussion and Conclusions

The results highlight the importance of analysing the position of the lesions inside the liver with respect to the HCZ and the major vessels.

5. References

- Isensee F. et al, *Nat Methods*; 18:203-211 (2021).
- Selle D. et al, *IEE-TMI*; 21:1344-1357 (2002).
- Lee T.C. et al, *CVGIP*; 56:462–478 (1994).
- Nunez-Iglesias J. et al, *PeerJ*; 6:e4312 (2018).

Acknowledgements:

Work supported by Guerbet and Île-de-France.

16.4

Artificial intelligence based in silico models for the prediction of resilience related psychological, psychiatric and functional trajectories in women with early breast cancer

Eleni Kolokotroni¹, Paula Poikonen-Saksela², Evangelos Karademas³, Haridimos Kondylakis⁴, Ruth Pat-Horenczyk⁵, Chariklia Tziraki⁶, Ketti Mazzocco⁷, Isabel Manica⁸, Berta Sousa⁸, Fatima Cardoso⁸, Albino O-Maia⁹, **Georgios Stamatakos¹**

¹ National Technical University of Athens, Institute of Communication and Computer Systems, Athens, Greece

² University of Helsinki, Helsinki University Hospital, Finland

³ University of Crete, Department of Psychology, Rethymnon, Greece

⁴ Foundation for Research and Technology–Hellas, Heraklion, Greece

⁵ Hebrew University of Jerusalem, School of Social Work and Social Welfare, Jerusalem, Israel

⁶ Hebrew University of Jerusalem, Jerusalem, Israel

⁷ Istituto Europeo di Oncologia, Milano, Italy

⁸ Champalimaud Foundation, Champalimaud Clinical Centre, Breast Unit, Lisbon, Portugal

⁹ Champalimaud Foundation, Champalimaud Research & Clinical Centre, Lisbon, Portugal

1. Introduction

Coping with breast cancer has been acknowledged as a major socio-economic challenge. There is a growing need for novel in silico approaches to predict and enhance the resilience of women to the variety of stressful experiences and practical challenges related to breast cancer [1,2,3]. In this context, a prospective clinical study has been deployed in four major clinical centres in EU (Finland, Italy and Portugal) and Israel within the framework of the EU funded project BOUNCE (www.bounce-project.eu). Exploitation of the data generated by the study has led to the development of a large number of artificial intelligence (AI) based in silico models for the prediction of resilience related psychological, psychiatric and functional parameter trajectories in women with early breast cancer. Numerous factors including clinical, biological, psychological, functional and socio-demographic data have been considered as potential determinants and predictors of the resilience related trajectories.

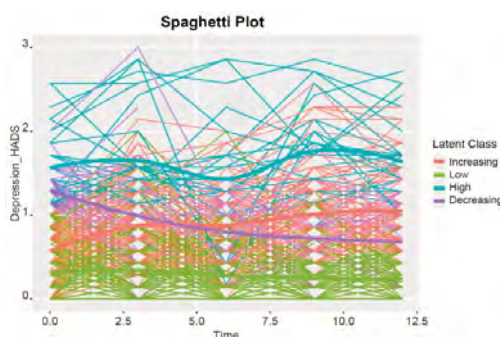


Figure 1. HADS (Hospital Anxiety and Depression Scale) depression trajectories. Each thin line connects the responses for the same patient over time. Thick lines are the mean HADS depression score at each time point (in months) for the four classes identified by the latent-class model.

2. Materials and Methods

The study refers to 558 patients and consists of trajectory clustering and predictive modelling. Trajectory clustering aims to identify clusters of patients that follow similar patterns of change in psychological outcomes across multiple time points. Here, five time points are considered (month 0, 3, 6, 9, 12). Latent-class mixed-effects regression analysis has been used. Predictive modelling is a classification problem where the classes to predict are the trajectory clusters identified in the previous step. A supervised learning based workflow has been applied (including handling of missing values and class imbalance) to identify features of importance and to

construct classification models. Feature importance has been assessed with a random forest specific metric. Model performance is evaluated based on a) nested cross validation, b) leave one hospital out cross validation: "build the models on data from three hospitals and evaluate performance on the left-out hospital". The key psychological outcomes considered are HADS (Hospital Anxiety and Depression Scale) Depression, HADS Anxiety and C30 General Health/QoL (Quality of Life).

3. Results

Indicative results for depression are given in Fig. 1. The trajectory model that best describes data consists of four latent classes (low & increasing for depression score ≤ 1 , decreasing & high for score > 1) (Fig1). A random forest that classifies patients with initial low depression (HADS score ≤ 1) between low and increasing trajectories has been constructed. Acceptable to good performance has been demonstrated under different validation schemes (Table 1). Apart from scales related to emotions (depression, anxiety, emotional function, distress), coping with cancer, optimism, negative affect at baseline and negative affect, fatigued and helpless at month 3 are important explanatory variables.

Table 1. Performance of a Random Forest Classifier.

	Nested cv	Leave the Portuguese hospital out	Leave the Israeli hospital out
Sensitivity	0.71	0.87	0.72
Specificity	0.88	0.83	0.74
ROC	0.88	0.92	0.81
F1	0.70	0.75	0.64

4. Discussion and Conclusions

The results have ensured a good level of model credibility and support the design of targeted interventions early after diagnosis according to a patient's predicted psychological progress.

5. References

- Chatzidimitriou E. et al, VPH2020 Book of Abstracts, 597-598 (2020).
- Karademas E.C et al, Psycho-Oncology, 30(9), 1555-1562 (2021).
- Poikonen-Saksela P, Kolokotroni E et al., Scientific Reports, Nature Publishing Group, 12, 2112 (2022).

Acknowledgements:

This project has received funding from the EU under grant agreement No 777167 (BOUNCE).

16.5

Automatic segmentation of the human pelvis organs using a generative adversarial network and MRI data

Duyen Nguyen-Le¹, Olivier Mayeur¹, Jean-François Witz¹, Pauline Lecomte-Grosbras¹, Michel Cosson^{1,2}, Chrystèle Rubod^{1,2}, Tien-Tuan DAO¹

¹ Univ. Lille, CNRS, Centrale Lille, UMR 9013, LaMcube - Laboratoire de Mécanique, Multiphysique, Multiéchelle, Villeneuve d'Ascq, France

² Service de Chirurgie gynécologique - CHU Lille, Lille, France

1. Introduction

Deep learning has been intensively used to perform the medical image analysis tasks such as classification, detection, reconstruction and segmentation [1]. However, the application of deep learning on the multi-organ segmentation of the female pelvis system has not been well investigated. The precise segmentation of pelvic organs from MRI scan is significantly important to the personalized treatment of genital prolapse and patient-specific modelling. It is clearly that the MRI segmentation is challenging due to the noisy characters and the large anatomical variations. In this work, we propose a state-of-the-art neural network (i.e. a generative adversarial network (GAN)) to segment female pelvic organs (bladder, vagina and rectum) from MRI scans.

2. Materials and Methods

MRI images of 10 female patients were acquired in a previous study [2]. T2-weighted MRI images were used. The ground truth images were manually segmented using Slicer 3D software. In this present study, the GAN model (Fig. 1) [3], was employed. This model consists of two neural networks (NN): a generative U-Net model (G) to generate data, and a discriminator model (D) using the fully convolutional NN to estimate the likelihood of a sample that could be originated from the training dataset. The implemented network includes 600 epochs with learning rate of 2e-4 and Adam optimizer. Dice similarity coefficient (DSC) was used as evaluation indicator.

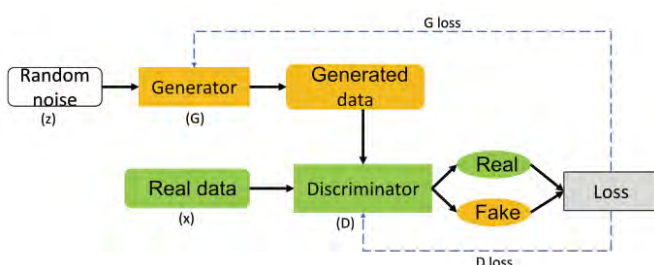


Figure 1: The GAN architecture used in this study.

3. Results

The average DSC is 98% for all segmented organs. Fig. 2 describes some comparisons between ground truth images and GAN segmented results. In addition, an extension in Slicer 3D was also developed to perform automatically the pelvic organ segmentation. The segmentation time is a few seconds for a subject.

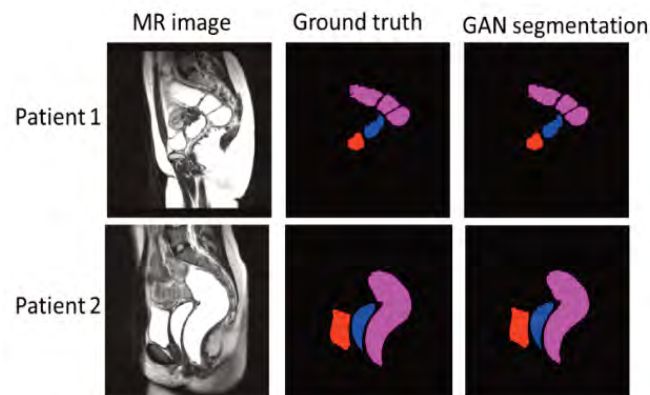


Figure 2: Some segmentations by the GAN model in comparison with ground truth data (manual segmentation) from MRI images.

4. Discussion and Conclusions

The use of the GAN model leads to very good segmentation accuracy of the female pelvic organs (bladder, vagina and rectum). As perspective, this novel segmentation workflow will be integrated into a patient-specific modelling platform of the pelvis system for prolapse treatment planning.

5. References

1. Xue et al. Neuroinform; 16:383-392(2018).
2. Jiang et al., Strain; 55:(2019).
3. Goodfellow et al., NIPS 27th conference: MIT Press; 2014. p. 2672-80.

Acknowledgements:

The authors would like to thank the Métropole Européenne de Lille (MEL) and ISITE ULNE (R-TALENT-20-009-DAO) for funding.

16.6

Predicting miRNA-mRNA interactions with graph neural networks

Jan Przybyszewski¹, Maciej Malawski¹, Sabina Licholai²

1 Sano Centre for Computational Medicine, Kraków, Poland

2 Division of Molecular Biology and Clinical Genetics, Faculty of Medicine, Jagiellonian University Medical College, Kraków, Poland

Jan Przybyszewski, Sano Centre for Computational Medicine, e-mail: j.przybyszewski@sanoscience.org

1. Introduction

Micro RNAs (miRNAs) are short, non-coding ribonucleic acid (RNA) molecules. Each type of miRNA is able to bind to several different types of messenger RNAs (mRNAs) forming a RNA-induced silencing complex (RISC). RISC plays a key role in the RNA interference phenomenon [1], where RNA molecules repress translation of other RNAs. The research shows, that many pathogenic processes are regulated by miRNAs, which indicates their impact on disease development [2]. Knowing which mRNAs are targeted by certain miRNAs can be invaluable for early disease diagnosis, as well as when designing personalized treatment methods. We propose a novel approach, considering target prediction as a graph classification problem, where two input sequences are processed by a graph neural network (GNN) classifier, yielding interaction probabilities. Moreover, we apply a novel encoding method, based on word2vec [3].

2. Materials and Methods

We processed pairs of miRNA and mRNA sequences, originally encoded using standard nucleic acid notation. We divided each sequence into 3-grams and use 16-dimensional word2vec embeddings to represent nucleotide triplets in a numerical form. The embeddings were obtained by training two word2vec models, separately for miRNA and mRNA sequences. To model the graph structure of the miRNA-mRNA complex, we used a graph representation. We first aligned the encoded sequences using their starting elements and then connected the closest neighbours between and within them with bidirectional edges. This resulted in an undirected input graph, as depicted in Fig. 1. The input graph was then fed to a GNN classifier.

3. Results

We tested our approach on the dataset used by a state-of-the-art method from the field – miTAR [4]. The results show that when using the word2vec method instead of a standard one-hot encoding, the classifier obtained F1 score higher by as much as 0.143 on the independent test dataset. Moreover, our method had comparable performance to the miTAR, even yielding a better accuracy score on one of the test datasets.

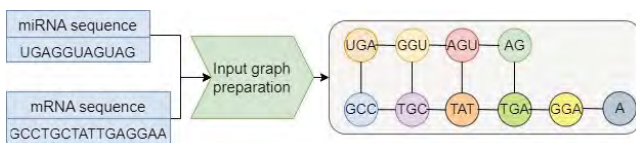


Figure 1: Input graph preparation process, in which 3-grams (1-grams or 2-grams for nucleotides remaining after division by 3) form an input graph.

4. Discussion and Conclusions

In this work, we evaluated the use of a new encoding method for interaction prediction, based on word2vec, together with a GNN classifier. We proved that this encoding approach can significantly boost model's performance. Moreover, we established that graph representation is suitable for the problem - our model obtained results comparable with the state-of-the-art miTAR method.

5. References

1. Gregory J Hannon. RNA interference. *Nature*, 418(6894):244–251, 2002
2. Robin MW Colpaert and Martina Calore. MicroRNAs in cardiac diseases. *Cells*, 8(7):737, 2019.
3. Ehsaneddin Asgari and Mohammad RK Mofrad. Continuous distributed representation of biological sequences for deep proteomics and genomics. *PloS one*, 10(11):e0141287, 2015.
4. Tongjun Gu, Xiwu Zhao, William Bradley Barbazuk, and Ji-Hyun Lee. MiTAR: a hybrid deep learning-based approach for predicting miRNA targets. *BMC bioinformatics*, 22(1):1–16, 2021

Acknowledgements:

This work was supported by the EU H2020 grant "Sano" No 857533; and by the project "Sano" carried out within the International Research Agendas Programme of the Foundation for Polish Science, co-financed by the European Regional Development Fund.

16.7

Towards the development of deep generative model for tree-structured geometries

Rajarajeswari Ganesan¹, Pjotr Hilhorst¹, Marcel van 't Veer^{1,2}, Pim Tonino², Frans van de Vosse¹, Wouter Huberts^{1,3}

1 Eindhoven University of Technology, Biomedical Engineering, Eindhoven, Netherlands

2 Catharina Hospital, Cardiology, Eindhoven, Netherlands

3 CARIM School for Cardiovascular Diseases, Maastricht University, Biomedical Engineering, Maastricht, Netherlands

Introduction:

In Silico Trials show a promising future to fully or partially replace human clinical trials aiming for assessing the safety, efficacy, and reliability of medical devices/interventions as well as drugs. The major challenge for human clinical trials is to include sufficient patients that realistically mimic the heterogeneity in the population. To overcome this challenge, a deep generative model (DGM) for the generation of synthetic geometries can be developed. However, the DGMs also require enormous amounts of data during training. In this study, we demonstrate a method that is able to create a representative training set for Geometry-Aware[1] Variational Autoencoders(GA-VAE) development (>1000) by using one single CT scan of a real patient. Initially, we focus on coronary arteries, but our approach is more widely applicable to other tree-like structures.

Method:

The training dataset is produced by changing anatomical parameters such as bifurcation angle, vessel diameters and curvature within the physiological range together with healthy and stenosed arteries using MorphMan [1].This physiological range has been decided based on the meta-analysis of anatomical studies conducted on different ethnicities, gender, age, and health conditions. The Forest Plot gives weightage to each study based on its precision and the sample size. From the forest plot, statistically significant ranges of anatomical details such as diameter and bifurcation angles have been determined. These ranges are in accordance with age and gender for patient-specific analysis. This entire training dataset has been generated by discrete geometry manipulation.

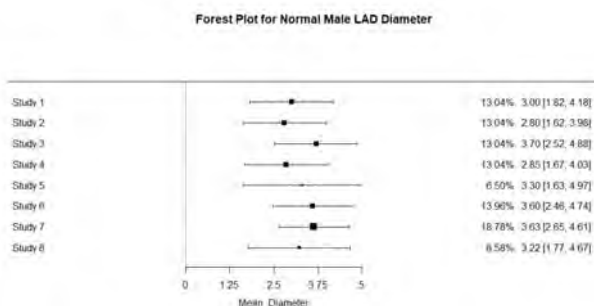


Fig.1: Forest Plot for statistically significant anatomical range

Anatomical Parameters (Diameter)	Attributes for age range (25-75 yrs.)	Range
Left Anterior Descending Artery (LAD)	Male, Healthy Female, Healthy	2.68-3.892 mm 2.69-3.677 mm
Left Circumflex Artery (LCx)	Male, Healthy Female, Healthy	2.48-3.73 mm 2.47-3.45 mm
Right Coronary Artery (RCA)	Male, Healthy Female, Healthy	2.81-4.02 mm 2.54-3.65 mm

Table.1: Statistically Significant Ranges for coronary artery diameters with attributes

In addition to variation of a single parameter, two or three parameters such as angle and diameter are also varied for creating diversified geometries.

Results:

This resulting database consists of healthy patients, patients with stenosis (moderate and severe stenosis) with the additional synthetic patient-specific attributes (Age, Gender etc.).

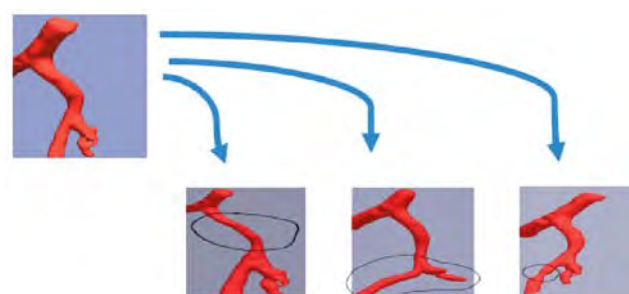


Fig.2: Training Database with anatomical variations.

Discussion:

In future, the GA-VAE will be developed using this synthetic database for coronary arteries and other tree-structured geometries.

References:

- Chadebec, C., Mantoux, C., & Allassonnière, S. (2020). Geometry-aware Hamiltonian variational autoencoder arXiv:2010.11518.
- Kjeldsberg et al., (2019). morphMan: Automated manipulation of vascular geometries. Journal of Open Source Software, <https://doi.org/10.21105/joss.01065>

Acknowledgements:

We acknowledge the EU's Horizon 2020 research and innovation programme (No: 101016503(*In Silico World*) for funding.

16.8

An artificial neural network to predict 3D human posture during one- and two-handed load-handling tasks

Mahdi Mohseni¹, Sadra Zargarzadeh¹, Navid Arjmand¹

¹ Sharif University of Technology, Mechanical Engineering, Tehran, Iran

*Professor, Sharif University of Technology, Tehran, 11155-9567, Iran. Email: arjmand@sharif.edu

1. Introduction

Human body posture is required to be determined for the assessment of musculoskeletal risk injuries during occupational activities [1]. The traditional motion analysis methods to measure body posture is time-consuming and limited to equipped laboratories [2,3]. Therefore, posture prediction methods are presented as alternatives. When developed based on in vivo measured kinematics data, posture-prediction approaches have shown appropriate accuracy in predicting anatomical joint angles during lifting activities [4]. We recently developed an artificial neural network (ANN), trained based on in vivo posture data, to predict 3D body joint coordinates (15 joints) during two-handed activities [5-7]. The present study aims to develop a new comprehensive ANN to predict whole-body 3D posture (coordinates of 41 landmarks required to drive musculoskeletal models) during one- and two-handed static load-handling activities from various load positions performed using different lifting techniques (stoop, squat, and semi-squat).

2. Methods

Ten healthy male subjects with body mass index (BMI) between 18 and 26 kg/m² reached fifteen different positions, i.e., 30, 45, and 60 cm in anterior and/or lateral directions (with respect to the mid-point between ankles) at seven different heights, i.e., 0, 30, 60, 90, 120, 150, and 180 cm from the floor using one or two hands and using different lifting techniques (full-squat, semi-squat, and stoop). In total, each individual performed 204 activities. The motion data of 41 skin markers (39 full-body plug-in gait markers + two markers on T12 and S1 vertebrae) were recorded using a 10-camera Vicon motion capture system. After data post-processing, the data of markers in 1805 lifting tasks were available to develop the model.

According to our previous ANN [7], seven input parameters were introduced to train the posture-prediction ANN: the 3D position of the hand(s), body height and weight, lifting technique, and handling technique, i.e., one- or two-handed. 3D coordinate of the 41 skin markers (123 coordinates) were outputs of the ANN. A feed-forward ANN with one hidden layer was trained using a back-propagation learning algorithm using 70% of the dataset as training data, 15% as the validation data, and the remaining 15% to test the accuracy of the ANN. The number of neurons in the hidden layer was obtained using trial-and-error to reach the best accuracy.

3. Results

The ANN model was trained using 17 neurons in the hidden layer. The training process stopped after 71 iterations to avoid overtraining. The developed ANN was able to accurately predict the 3D coordinates of 41 body markers (RMSE= 3.8 cm, normalized (to range of data) RMSE of 7.6%, and R²= 0.992).

4. Discussion and Conclusions

Results showed that the ANN model was accurate to predict the 3D whole-body posture during one- and two-handed lifting activities. The dataset will be expanded by collecting additional motion data from more individuals in the same BMI range so that ANNs with multiple hidden layers (deep neural networks) can be developed.

5. References

1. Dreischarf M et al., *Journal of Biomechanics*, 49, 833–845 (2016).
2. Ghasemi M, Arjmand N, *Journal of Biomechanics*, 123, 110539 (2021).
3. Asadi F, Arjmand N, *Journal of Biomechanics*, 112, 110043 (2020).
4. Gholipour A, Arjmand N, *Journal of Biomechanics*, 49, 2946–2952 (2016).
5. Aghazadeh et al., *Journal of Biomechanics*, 102, 109332 (2020).
6. Mohseni et al., CMBBE 2021 conference: Bone, Germany, p. 47 (2021).
7. Mohseni et al., *Journal of Biomechanics*, 131, 110921 (2022).

17.1

Validation of Internal Parameters of Adolescent Idiopathic Scoliosis Evaluated using ScolioSIM Solution - Preliminary Results

Sasa Cukovic¹, Christoph Heidt², Daniel Studer², Gabriel Huwyler², Vanja Lukovic³, William R. Taylor¹

1 Swiss Federal Institute of Technology - ETH Zurich, Institute for Biomechanics, Laboratory for Movement Biomechanics, Zurich, Switzerland

2 University Children's Hospital Basel, Pediatric Orthopaedic Department, Basel, Switzerland

3 University of Kragujevac, Faculty of Technical Sciences, Čačak, Serbia

1. Introduction

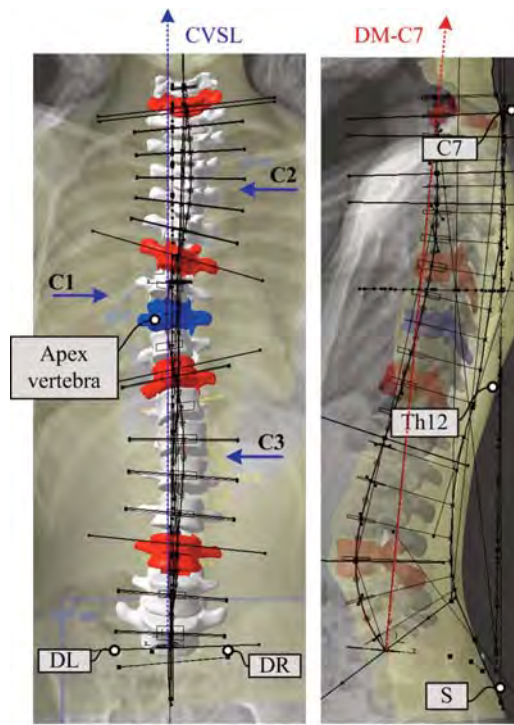
Non-ionizing investigation of Adolescent Idiopathic Scoliosis (AIS), which is one of the most prevalent spinal deformities in adolescents, remains insufficiently developed and tested. However, the ability to monitor AIS progression without ionizing methods would support decreasing the long-term risk of developing malignancies associated with the exposure to multiple X-ray imaging. New technologies in optical 3D digitalisation and artificial intelligence allow better precision in prediction of the internal spinal alignment, and thus extraction of reliable intrinsic parameters of AIS. Here, preliminary results in comparing the main clinical parameters generated with the ScolioSIM simulator from surface [1] with those evaluated by clinical experts from X-ray images in daily practise are presented.

2. Materials and Methods

In this study, the back surfaces of eighteen AIS patients (12 females and 6 males, age: 12.1 ± 1.8 years, (mean \pm SD)) aged between 9 and 15 years old, were optically digitalised. On bi-planar radiographic images the most relevant clinical parameters such as Cobb angle, height, weight were collected (primary Cobb: $21 \pm 12.6^\circ$, height: 1.6 ± 0.1 m, weight 46.8 ± 16.6 kg). Using the ScolioSIM simulator, the internal spinal alignment, back 3D surface and asymmetry curves, parameters of the deformity were calculated, and patient-specific deformity models were generated. These two modalities were manually fused over five markers (DL DR, C7, T12, S) visible on optical surface digitalised with Artec Eva 3D optical scanner and radiographic images (EOS system) and then diagnostic results were compared (Fig. 1).

3. Results

The internal spinal alignment is approximated by the 5th degree of B-Spline which is proved enough to describe the curve's deformity [3]. Calculation of inflection points was done automatically in both, frontal and sagittal planes, thus avoiding subjective estimation of the observers. In the case presented on Fig. 1 ScolioSIM generated the following Cobb angles: C1: 28.7° , C2: 22.7° , and C3: 18.1° . Similar values were evaluated from X-ray images by clinical expert: C1: 26.5° , C2: 21.4° , and C3: 16.5° . Presented values are within the clinically acceptable error range of $\pm 5^\circ$ for Cobb angle.



Legend:

DM-C7: Local spinal axis; CVSL: Central vertical spinal line; C7: 7th cervical vertebra; Th12: 12th thoracic vertebra; DL: dimple left; DR: dimple right; S: sacrum; C1: primary Cobb angle; C2: second Cobb angle; C3: third Cobb angle.

Figure 1: Comparison of Cobb angles extracted by observer and ScolioSIM

4. Discussion and Conclusions

Traditionally, AIS is diagnosed and monitored on X-ray images using Cobb technique. This technique is highly dependent on expertise of observers and it has a high inter and intra observer variability (often hard to identify end vertebra for referencing), thus Cobb angle values often differs [2]. Compared to diagnosis evaluated by clinical experts, ScolioSIM tool showed better precision in extracting main Cobb angles, and measures were within acceptable $\pm 5^\circ$.

5. References

1. S. Cukovic et al, BIBE 2019 conference: IEEE Proceedings; 2019, pp. 316-320.
2. B. S. Richards et al, Spine. 2003;28(11), pp. 1148–1156 (2003).
3. S. Cukovic et al, BIBE 2018 conference: IEEE Proceedings; 2018 pp. 284–287, 2018.

Acknowledgements:

This project has received funding from the EU's Horizon 2020 research and innovation programme under the Marie Skłodowska-Curie grant agreement No 892729.

17.2

Development of a fully-parametric thoracolumbar spine model with articulated rib cage

Alice Pereo¹, Alice Pezzinga¹, Luigi La Barbera^{1,2}

1 Politecnico di Milano, Chemistry, Materials and Chemical Engineering "Giulio Natta", Milan, Italy

2 IRCCS Istituto Ortopedico Galeazzi, Italy

1. Introduction

Spine pathophysiology is based on detailed patient-specific in silico biomechanical models, often including few functional spinal units (FSUs), which can be hardly generalized. Fully-parametric spine models easy-to-adapt to any patient promises to be a more efficient strategy to scale up biomechanical problems by including entire populations featuring a desired range of spinal morphologies and alignments. The present study aimed at: i) developing a fully-parametric thoracolumbar spine model based on few independent parameters, ii) calibrating the kinematic response of a representative thoracic FSU assigning adequate mechanical properties to subcomponents.

2. Materials and Methods

Regression analysis and CAD model. Mean anatomical data describing 38 dependent parameters for each vertebra [1,2], were best-fitted with a third order polynomial regression line where the posterior height of the vertebral bodies (VBHP) was assumed as the only independent parameter. The regression equations were implemented in Solidworks 2020, where the morphology of each vertebra was fully defined. T1-T12 thoracic kyphosis (TK), L1-L5 lumbar lordosis (LL), and sacral slope (SS) were added as additional independent parameters [3], to allow describing the desired sagittal alignment (Figure 1). Rib cage description relied on average values [4,5].



Figure 1: Developed parametric model representing the average spine of a healthy adult (a), and meshed T6-T7-R7 FSU model including the costovertebral joint and ribs (c).

Calibration of T6-T7-R7 FSU FE model. One FSU was meshed in Abaqus 2020. A backward stepwise reduction approach was adopted and FSU components were sequentially added to the model calibrating the mechanical properties of each component by comparison with the available in vitro kinematic data (RoM, range of motion) for FSU [6], FSU+left rib [7], and FSU+ribs+sternum [8].

3. Results

Regression analysis and CAD model. Each dependent parameter was predicted with a RMSE much lower than the mean experimental dispersion (8 vs. 20%). Calibration of T7-T8-R7 FSU. Calibration of tissues' properties ensured an accurate description of the kinematics behaviour in each loading direction (Figure 2).

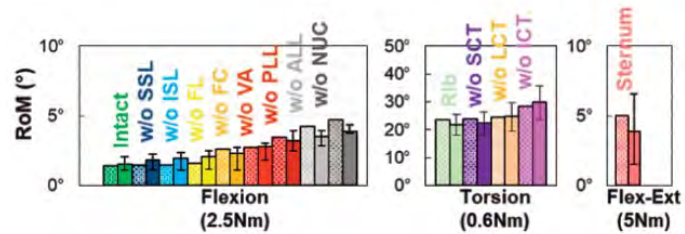


Figure 2: RoMs examples of the T6-T7-R7 FSU calibrated using a backward stepwise reduction approach.

4. Discussion and Conclusions

The regression analysis ensured an accurate description of each vertebra with one independent parameter (VBHP). The additional independent parameters (TK, LL, SS), widely used in clinical practice, allow to describe any global sagittal alignment, both physiological and pathological. The few independent parameters adopted make the proposed parametric model much simpler than any other available to date. The accurate calibration of T6-T7-R7 FSU's RoM, demonstrated that also mechanical properties can be promptly implemented to study FSU biomechanics.

5. References

7. Panjabi et al, Spine, 16(8):888-901, 1991.
8. Panjabi et al, Spine, 17(3):299-306, 1992.
9. Pesenti, Clin Orthop RelatRes, 476(8):1603, 2018.
10. Holcombe et al, J. Anat, 231(2):229-427, 2017.
11. Selthofer et al, Coll Antropol, 30(1):43-47, 2006.
12. Wilke et al, Eur Spine J, 29(1):179-185, 2020.
13. Lemosse et al, Eur Spine J, 7(1):16-23, 1998.
14. Liebsch et al, Spine J, 20(3):488-498, 2020.

Acknowledgements:

This work was funded by MIUR FISR-FISR2019_03221 CECOMES.

17.3

A poro-aniso-hyperelastic model coupled with solute transfer model for in-silico study of intervertebral disc degeneration, a high-performance computing application.

Dimitrios Lialis¹, Mariano Vazquez¹, Beatriz Eguzkitza¹, Eva Casoni¹, Jerome Noailly²

¹ Barcelona Supercomputing Center - Centre Nacional de Supercomputació, CASE, Barcelona, Spain

² Pompeu Fabra University Poblenou Campus, Barcelona, Spain

1. Introduction

The main objectives of the current work are the design of a poromechanical Finite Element (FE) solver and coupling with a solute transfer FE solver, within an HPC framework. Alya, the multi-physics, highly scalable and parallelizable F.E. solver developed by the CASE group of BSC, is employed. This endeavour targets the study of the intervertebral disc (IVD) and its degeneration[1]. IVD degeneration is likely dictated by intricate spatio-temporal events whose simulation is computationally expensive, hence large-scale computing infrastructures would be imperative for in-silico cohort simulations.

2. Methods

The physical domain of this complex problem is subdivided into two models, the poro-mechanical part and the solute transport part. IVDs are known to exhibit poro-aniso-hyper-elastic behaviour. Thus, for the poromechanical simulations, a Modified Neo-Hookean material model is being employed. This accounts for the compressibility of the total IVD matrix, while respecting the incompressibility of both the solid and the fluid grains [2]. The anisotropy is related to the presence of collagen fibres (I, II), for which a modified Holzapfel – Gasser – Ogden model is used [3]. The poromechanical effects in the porous IVD tissues are modelled using Darcy's law. The fluid pressure also includes the contribution of Donnan osmosis [2].

The poromechanical scheme is solved in a two-way coupling setup. The mesh deformations affect the fluid flux and the permeability of the porous model, while the fluid pressure is accounted for in the calculation of the mechanical stress[4].

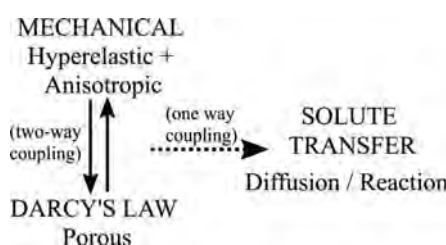


Figure 1: Schematic description of the solution scheme.

Coupled with the poromechanical model, the diffusion of certain solutes (oxygen, lactate and glucose) is solved. A one-way coupling between the poromechanical and the solute transport solvers is considered, as volumetric mesh deformations affect both the diffusion coefficient and the solute concentrations. The incompatibility between the stationary domain, in which Darcy's law and solute diffusion are being solved, with the highly deformable hyper-elastic domain is resolved through a proper set of Piola-Kirchoff transformations. Boundary and load conditions are elected aiming to simulate a normal day consisting of 8h sleep, 8h moderate and 8h high activity.

3. Results

The preliminary results mainly focus on the poromechanical solver, as it was considered the basis for the simulation. Figure 2 shows the stress distribution along the anteroposterior plane of the IVD under physiological swelling. The domains of the IVD are evident through the stress distribution [5], yet the pore pressure seems heavily affected by the boundary conditions, leaving room for further investigation.

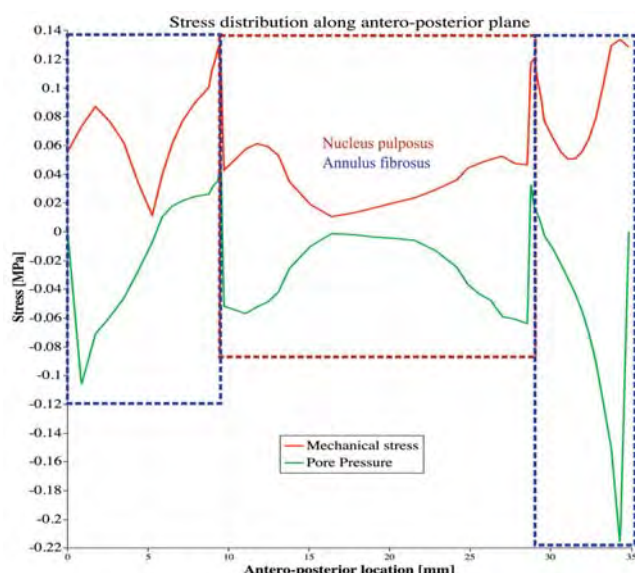


Figure 2: Preliminary results regarding the stress distribution along the IVD.

4. Discussion and Conclusions

The employed model is believed to offer a full description of the IVD and capture a wide spectrum of the mechanics observed in it. The results are pending a comparison against simulations performed by commercial software as well as verification against real life results.

5. References

- [1] C. R. Wills et. al., *J. Mech. Phys. Solids*, vol. 90, pp. 108–123, May 2016
- [2] Y. Schroeder et. al., *Eur. Spine J.*, vol. 15, no. S3, pp. 361–371, Aug. 2006
- [3] D. R. Nolan et. al., *J. Mech. Behav. Biomed. Mater.*, vol. 39, pp. 48–60, Nov. 2014
- [4] A. Grillo et. al., *Theor. Appl. Mech.*, vol. 41, no. 4, pp. 283–322, 2014
- [5] C. Ruiz, et. al., *J. Mech. Behav. Biomed. Mater.*, vol. 26, pp. 1–10, Oct. 2013

Acknowledgements:

Funds from the European Commission (H2020-MSCA-ITN-ETN-2020 GA: 955735) are acknowledged.

17.4

The effect of tibiofemoral joint morphology on contact mechanics under simulated gait conditions: A finite element modelling study.

Rosti Readioff¹, Blake McCall¹, Gavin Day¹, V. Nagitha Wijayathunga¹, Jiacheng Yao¹, Ruth Wilcox¹, Marlène Mengoni¹, Alison Jones¹

¹ The University of Leeds, Institute of Medical and Biological Engineering, School of Mechanical Engineering, Leeds, United Kingdom

*Rosti Readioff, School of Mechanical Engineering, University of Leeds, Leeds, UK. r.readioff@leeds.ac.uk

1. Introduction

One of the risk factors accelerating knee joint osteoarthritis is increased joint contact pressure. The distribution of knee joint contact pressure is dependent on joint morphology [1] which is subject-specific [2]. The literature lacks detailed investigation on the effect of inter-subject variation of knee joint morphology on joint kinematics and contact mechanics. Therefore, this study developed subject-specific finite element (FE) computer models, representing the human tibiofemoral joint, to investigate the influence of degenerated joint morphology on kinematics and contact mechanics of the joint under a simulated gait.

2. Materials and Methods

Two cadaveric tibiofemoral joints were tested experimentally under cyclic walking gait conditions [3] and FE models were developed from three-dimensional images. Magnetic resonance (MR) images were used to manually segment knee menisci, while computed tomography (CT) images were used to segment the femur, tibia, and articular cartilage. The tibiofemoral joint components were aligned using landmarks to replicate the experimental alignment and segmented geometries were exported as FE tetrahedral meshes. FE models with menisci (intact knee) and without menisci (full double-meniscectomy knee) were generated. Boundary conditions and spring stiffness profiles [3] matching the experimental knee simulation were replicated on the subject-specific FE models. Model kinematics were validated against experimental results at seven points in the simulated gait cycle. Subsequently, an initial assessment was made of the inter-subject variation of contact mechanics of degenerated knee joints.

3. Results

The subject-specific FE model kinematics were compared to the simulated gait kinematics in matched cadaveric tissue. The FE were able to replicate the changes in kinematics between gait cycle points. The results showed inter-subject variation patterns in the kinematics (Fig. 1a) and contact mechanics behaviours (Fig. 1b).

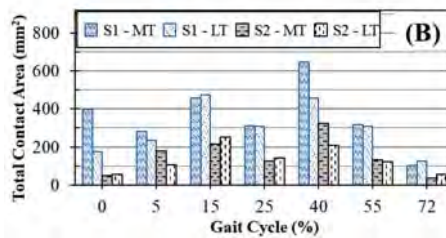
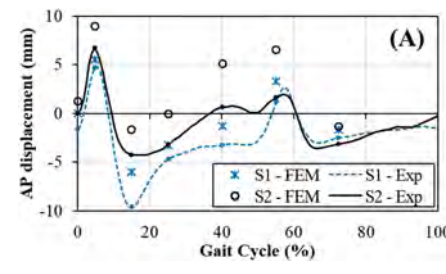


Figure 1: Comparison of two double meniscectomy joints (S1 and S2) and (A) their experimental (Exp) and numerical (FE) results showing anterior-posterior (AP) displacements of the tibia relative to the femur. (B) The total contact area of the medial (MT) and lateral (LT) tibial plateau.

4. Discussion and Conclusions

This study showed subject-specific variation in tibiofemoral joint kinematics and contact mechanics under simulated gait cycles. A parametric study with changed parameters, including forces and joint angles, will provide further evaluation of the inter-subject variation of contact mechanics and kinematics.

5. References

1. Fregly et al., *J Orthop Res*, 2012. 2. Dargel et al., *Knee Surg Sports Traumatol Arthrosc*, 2009 3. Liu et al., *PLOS ONE*, 2020.

Acknowledgements:

This project was funded by the EPSRC (Grant no: EP/P001076/1).

17.5

Prevention of asymmetric maxillary expansion via simulation - evaluation of clinical outcome

Eric Quadrat¹, Alexander Pugachev¹, Lars Bonitz²

1 CADFEM Medical GmbH, Grafing bei München, Germany

2 Klinikum Dortmund gGmbH, Dortmund, Germany

1. Introduction

Asymmetrical widening of the maxilla occurs in up to 50% of patients who have undergone Surgically Assisted Rapid Maxillary Expansion (SARME) [1]. The indications of asymmetrical expansion can be detected in various anatomical directions within the clinical context, and the required corrections often imply additional surgical interventions or dental compensation.

A simulation-based approach was developed for preoperative planning of SARME to identify an optimal osteotomy resulting in a symmetric expansion [2]. The patient-specific approach is based on sampling osteotomy configurations from a specified feasible region and evaluating each configuration by means of finite element analysis. Furthermore, the differentiation between the bone and dental movements would provide an important information about the long-term outcome of the treatment. This work presents a novel vector-based measurement method for the detailed evaluation of SARME.

2. Materials and Methods

Pre-operative and post-distraction CT data of 17 SARME patients were analysed retrospectively. The maxilla and the teeth were segmented using a semi-automatic protocol. The post-distraction geometry was registered to the respective pre-operative geometry. A set of landmarks was placed on the interdental bone and teeth parts to describe the geometry in a way suitable for the comparison. The evaluation of SARME is based on measuring and analyzing the distances between the corresponding pre-operative and post-distraction landmarks.

3. Results

The evaluation method allows for studying the post-distraction movement of bone and dental parts in all spatial directions individually. The deviations between the left and right sides of a skull are served as criterion of the expansion asymmetry. The post-distraction movements are differentiated into the specific regions (palatal and labial/buccal for bone, apical and occlusal/incisal for teeth) to separate the effects of the treatment.

Fig. 1 illustrates the landmark and vector data gathered for a single patient representing the maxilla and the teeth.

Fig. 2 summarizes the results of the evaluation. The deviations demonstrate differences in the expansion in the bone regions, as well as the effect of dental compensation. The results are also presented as local distances and deviations in coronal, sagittal, and axial planes.

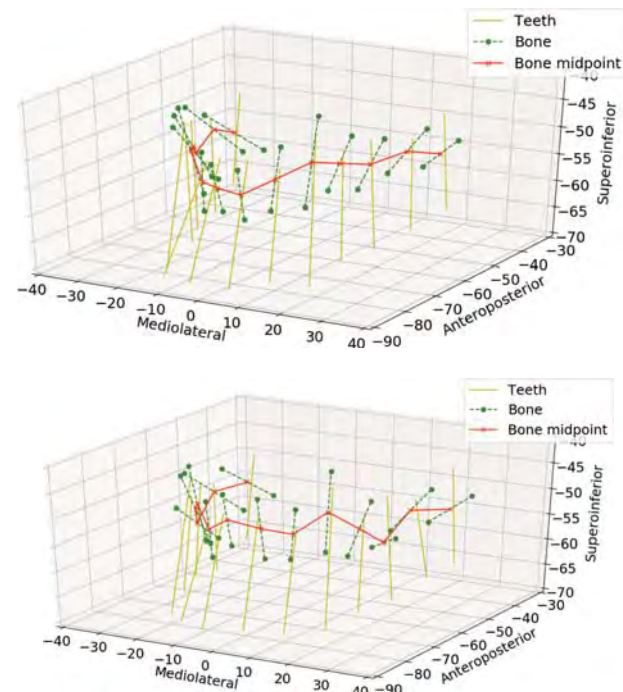


Figure 1: Spatial representation of maxilla and teeth (top – pre-operative, bottom – post-distraction).

4. Discussion and Conclusions

The developed evaluation methodology proved to be useful tool for the detailed analysis and quantification of post-operative bone and dental movements. Furthermore, the approach applied to 17 SARME patients confirmed the advantage of the simulation-based planning in obtaining symmetrical lateral expansion. The approach is not limited to SARME and could be also applied to other rapid palatal expansion techniques.

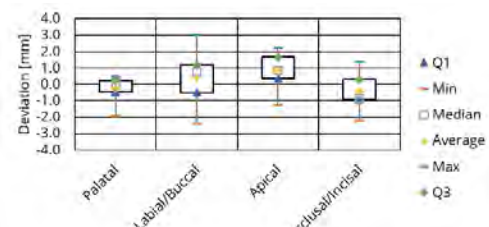


Figure 2: Quantification of pre-operative and post-distraction left-right symmetry.

5. References

1. Huizinga MP et al. *J Craniomaxillofac Surg* 46, 1329-1335 (2018). <https://doi.org/10.1016/j.jcms.2018.05.021>.
2. Chhatwani S et al. *Clin Oral Invest* 25, 6717-6728 (2021). <https://doi.org/10.1007/s00784-021-03958-w>.

18.1

Cytokine Profiling in Cultured Endometrial Cells after Hormonal Treatment

Mark Gavriel^{1,2}, Ariel J. Jaffa², Dan Grisaru², David Elad¹

1 Tel Aviv University, Biomedical Engineering, Tel Aviv-Yafo, Israel

2 Tel Aviv University, Scackler Faculty of Medicine, Tel Aviv-Yafo, Israel

1. Introduction

The human endometrium-myometrium interface (EMI) is the uterine inner barrier without a separatis layer. It is composed of endometrial epithelial cells (EEC) and endometrial stromal cells (ESC) in the endometrium and myometrial smooth muscle cells (MSMC) in the myometrium. The EMI undergoes structural remodeling during the menstruation cycle which are essential for human reproduction. Recently, we co-cultured a layer-by-layer in vitro model of EEC, ESC and MSMC on a synthetic membrane for mechanobiology experiments [1]. We also treated the model with progesterone and 17-β-estradiol in order to mimic the in vivo receptive uterus [2]. In the present study we analyzed the cytokines profile in a single layer of EEC during the phases of hormonal treatment.

2. Materials and Methods

We cultured commercial EEC (RL95-2, ATCC® CRL-1671™) in a 24-wellplate. Then, we applied an hormonal stimuli protocol with 17-β-estradiol and progesterone in time dependent concentration according to the human physiology that mimics the menstrual cycle. The hormonal protocol is schematically described in Figure 1. We collected cell supernatant samples of control, pre-ovulation, ovulation and post-ovulation phases for analysis of the secreted proteins and cytokines. The cytokine profiling was performed using the Proteome Profiler Human XL Cytokine Array Kit (R&D Systems, Inc., USA) that can detect 105 human soluble cytokines. The relative quantification of all the cytokines was performed using xMAP – LUMINEX.

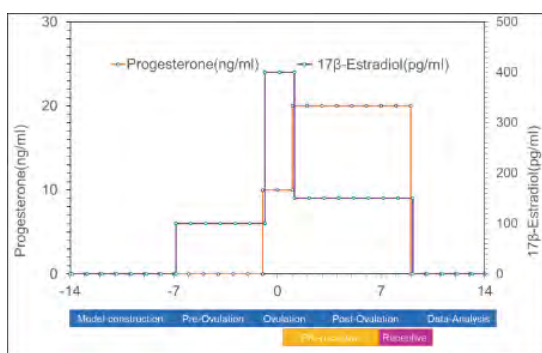


Figure 1: Protocol of hormonal treatment with 17-β-estradiol and progesterone.

3. Results

We conducted a fishing expedition with the 4 membranes of the Proteome Profiler. We processed the images, quantified the spots intensity and normalized these values by the negative control and reference spots at the membrane corners, as shown in Figure 2 a,b,c. Analyses of the relative quantities that reflected changes higher than 5% of the control points of the kit revealed the results shown in Figure 2 d,e.

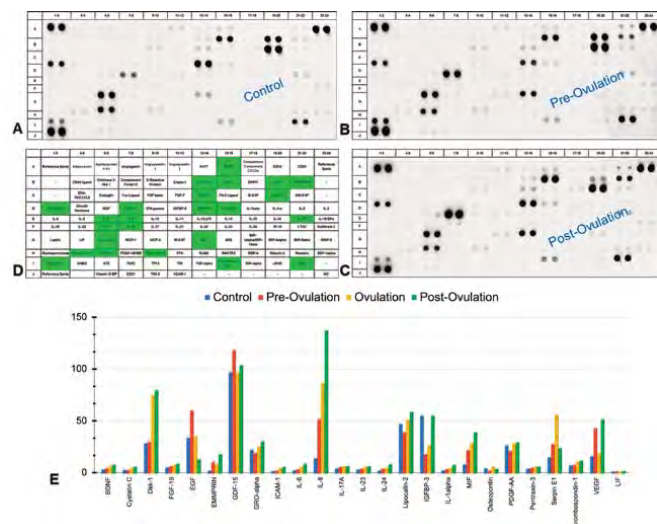


Figure 2: Cytokine profiling of cultured EEC during the phases of the hormonal treatment. The membranes for control (a), Pre-ovulation (b), Post-ovulation (c), cytokines with significant changes (d), and cytokines variations (e).

4. Discussion and Conclusions

The results clearly demonstrated significant changes in cytokine levels for inflammation and angiogenesis pathways. Analysis of tissue-engineered models of the uterine wall will enable deeper investigation of molecular and biomechanical aspects of early reproductive stages during the window of implantation or developments of pathologies.

5. References

- Elad D et al. *APL Bioengineering* 4, 026107 (2020).
- Kuperman T, Gavriel M et al. *Biomech Model Mechanobiol* 19, 1629–1639 (2020).

18.2

Effect of Fetal Membrane Adhesion on Stretch in the Fetal Membrane and Cervix

Erin Louwagie¹, Mirella Mourad², Michael House³, Ronald Wapner², Kristin Myers¹

¹ Columbia University, Mechanical Engineering, New York, United States

² Columbia University Irving Medical Center, Obstetrics and Gynecology, New York, United States

³ Tufts Medical Center, Obstetrics and Gynecology, Boston, United States

1. Introduction

Preterm birth (PTB), defined as delivery before 37 weeks gestation, globally affects 1 in 10 births [1]. The current gold standard for predicting PTB is the sonographic measurement of cervical length, though this method has only a moderate ability to predict PTB [2]. A second test to assess the risk of preterm birth is measurement of foetal fibronectin (fFN) present in the cervicovaginal fluid, because fFN is believed to adhere the foetal membranes to the intrauterine wall [3]. This research aims to elucidate how the intrauterine load is shared between the foetal membranes, uterus, and cervix in pregnancies destined to deliver at-term and preterm. This work investigates how the amount of foetal membrane adhesion to the intrauterine wall affects stretch in the foetal membrane and cervix in computational simulations of pregnancy.

2. Materials and Methods

Ultrasonic maternal uterine and cervical dimensions and in-vivo cervical aspiration stiffness (Pregnolia AG, Switzerland) were measured between 16-24 weeks gestation. Measurements were taken in two clinical patient cohorts, one at high-risk (sonographic cervical length \leq 2cm) and one at low-risk for PTB, at Columbia University Irving Medical Center. We present here results from patients in the high-risk cohort who delivered extremely preterm (23 weeks gestation), late preterm (36 weeks gestation) and at-term (39 weeks gestation). Using our established parametric modelling methods [4], we built a solid model of each patient's abdomen and discretized the geometry into elements (Hypermesh, Altair, Troy, MI). We assigned all reproductive tissues material properties based on existing data, with cervical fibre stiffness determined through inverse finite element analysis (FEA) of the in-vivo aspiration procedure. Physiologically inspired loading, contact, and boundary conditions were applied. Starting from a fully tied contact between the foetal membrane and the uterus and cervix, we ran iterative models allowing more of the foetal membrane to slide on the uterus and cervix. A closed and long cervix was considered reference configuration. FEA was run in FEBio Studio v1.3.0 [5].

3. Results

Figure 1 shows maximum 1st principal stretch in the foetal membrane (a), cervical internal os (opening of cervix into the uterus), and uterocervical junction (b) versus percentage membrane tied (PMT) to the uterus and cervix. As the PMT decreases, stretch in the foetal membrane increases, with the highest magnitude stretches found in the patient who delivered extremely preterm. The stretch at the internal os is greater than at the uterocervical junction at almost all PMT adhesion levels, excepting the patient who delivered extremely preterm, for which the opposite is true.

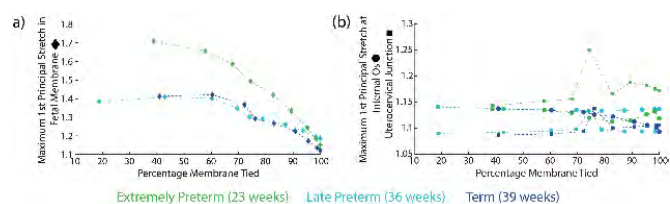


Figure 1: Maximum 1st principal stretch in the foetal membrane (a) and cervical internal os (●) and uterocervical junction (■) (b) as PMT varies for patients who delivered extremely preterm (green), late preterm (cyan), and at-term (blue).

4. Discussion and Conclusions

The adhesion of the foetal membrane to the uterus and cervix affects the levels of stretch experienced in the foetal membranes, cervical internal os, and uterocervical junction. This work could shed light on how the intrauterine pressure load is distributed between the cervix and foetal membranes with loss of fFN.

5. References

- WHO, "Preterm Birth", 2018.
- Berghella V, *Contemp Ob/Gyn*, 49:26-34 (2004).
- Abbott D et al, *Obstet Gynecol*, 125(5):1168-1176 (2015).
- Louwagie E et al, *PLOS ONE*, 16(1):e0242118 (2021).
- Maas S et al., *J Biomech Eng*, 134(1):011005 (2012).

Acknowledgements:

This work is supported by the Eunice Kennedy Shriver National Institute of Child Health & Human Development of the National Institutes of Health under award number 1R01HD091153 -01. The content is solely the responsibility of the authors and does not necessarily represent the official views of the National Institutes of Health.

18.3

Mechanobiology of a multi-cell co-culture model of the endometrium-myometrium interface

Yael Shlomo¹, Mark Gavriel^{1,2}, Ariel Jaffa², Dan Grisaru², David Elad¹

1 Tel Aviv University, Biomedical Engineering, Tel Aviv, Israel

2 Tel Aviv University, Sackler Faculty of Medicine, Tel Aviv, Israel

1. Introduction

The non-pregnant uterus is characterized by spontaneous myometrial contractions that induce intra-uterine peristaltic flows [1]. The human endometrium-myometrium interface (EMI) is composed of endometrial epithelial cells (EEC), endometrial stromal cells (ESC) and myometrial smooth muscle cells (MSMC) without a separating layer. Many in vitro models were developed to study molecular aspects of the EMI. Recently, we developed a layer-by-layer co-culture of the EMI and exposed it to peristaltic wall shear stresses (WSS) [2]. In the present study we developed a new EMI model by co-culture of all the cells together and exposed it to steady WSS.

2. Materials and Methods

In nature, tissue development is the outcome of spontaneous organization of different layers of cells due to cellular and molecular signals. Accordingly, we seeded an equal mixture of EEC (RL95-2, ATCC), ESC (T0533, ABM) and MSMC (ATCC® PCS-460-11™) at once on the collagen coated PTFE membrane using our multi-purpose wells. Immunofluorescence staining with specific antibodies was used to validate the barrier model. Then, we exposed the in vitro model to steady WSS of 0.5 and 0.7 dyne/cm² for 10 minutes.

3. Results

Preliminary results demonstrated that the 3 different cells have arranged into three different layers similar to the results of the seeding layer-by-layer model [2]. The overall barrier model is a three-dimensional (3D) structure as can be depicted in Figure 1a. Further confirmation for the multi-layer model of the EMI is shown in the projection of the different cells and Z-section in Figure 1b. The confocal images clearly show that the barrier thickness was 50920 µm whereas the EEC layer was approximately 25910 µm and the MSMC layer was 1595 µm. We also conducted mechanobiology experiments in which we exposed the new in vitro model to WSS. Examination of confocal images revealed cellular alterations in both layers of EEC and MSMC.

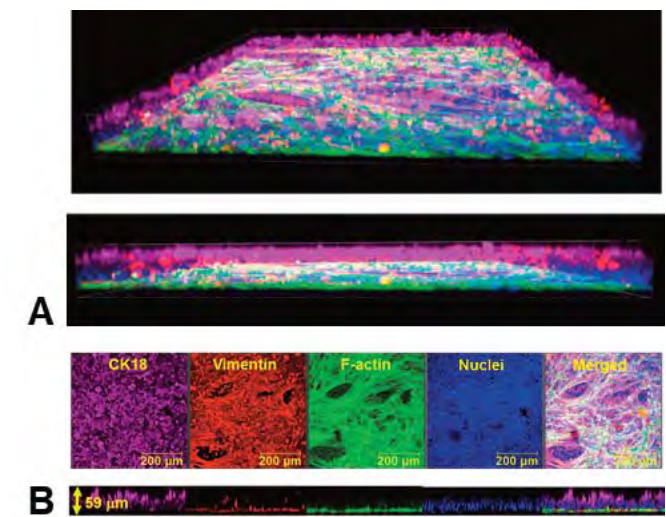


Figure 1: Confocal images of the EMI model cultured of a mixture of EEC, ESC and MSMC: a) Three-dimensional plot, b) Projection of all sections and Z-sections. The cells were stained with non-specific reagent for F-actin Cytopainter Phalloidin - iFlour 488 Reagent ab176753, for EEC conjugated antibody: Anti-Cytokeratin 18 antibody AB-ab206269 [EPR1626] Alexa Fluor® 647 1:100 in 1% BSA, for ESC conjugated Anti-Vimentin antibody [EPR3776] AB-ab202504 (Alexa Fluor® 568) 1:500 in 1% BSA, and DAPI nucleic acid staining (D9542) for the nuclei.

4. Discussion and Conclusions

We successfully developed a complex in vitro 3D model of the EMI with cellular layers that mimic the in vivo structure. Seeding all the cells together revealed that the EMI layers evolved biologically. In addition, application of WSS on the outer layer of the EEC also affected the inner layer of the MSMC. This new in vitro model may be implemented in studies of reproduction physiology and pathophysiology.

5. References

1. Myers K, Elad, D. Wiley Interdiscip Rev: Syst Biol Med 9, e1388 (2017).
2. Elad D et al. APL Bioengineering 4, 026107 (2020).

18.4

Patient-Specific Simulation of Childbirth - A parametric model linked to medical images

Z. Csatl¹, G. Dufaye¹, J-F. Witz¹, P. Lecomte-Grosbras¹, C. Rubod², M. Cosson², O. Mayeur¹

1. Univ. Lille, CNRS, Centrale Lille, UMR 9013- LaMcube - F-59000 Lille, France

2. Service de chirurgie gynécologique - CHU Lille - F-59000 Lille, France

1. Introduction

The patient-specific approach is more and more common in healthcare in order to help doctors in their medical decision. Previous works on pelvic organ prolapse and childbirth [1] considered only the levator ani muscle (LAM) and the surrounding ligaments. The mature techniques now allow to tackle a major societal issue: the risks associated with childbirth [2]. The study presented here can simulate patient-specific childbirth to analyze the deformations that occur on the pelvic floor during delivery according to size of the baby's head and cephalic presentation. The analysis of all these results will bring a better understanding of the phenomena involved on those different configurations.

2. The patient-specific model of pregnant woman

Our highly automated workflow enables personalized childbirth simulations to be carried out quickly. The two main novelties of our work are i) the complete modeling of the perineum with all the muscles, and ii) the creation of a geometry, which is directly suitable for simulation. Our model, shown in Fig. 1, represents the different parts of the perineum muscles and the Levator Ani Muscles (LAM). The generation of this model is based on previous work performed by our team to create a complete muscular model for the simulation of childbirth [3, 4].

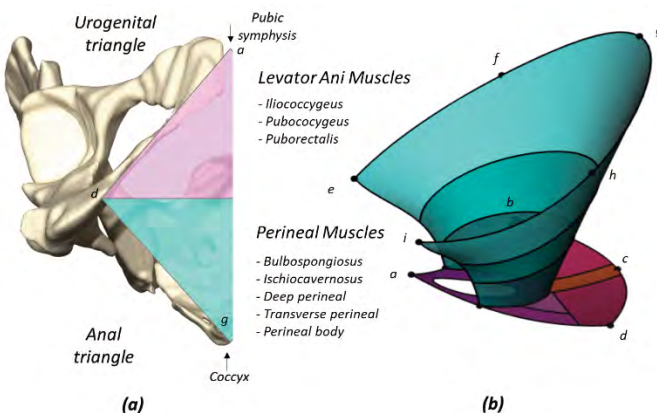
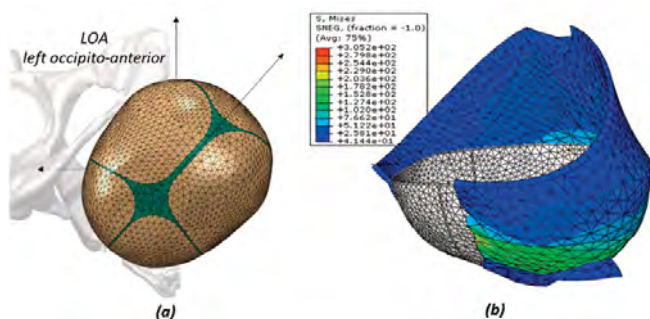


Figure 1: (a) Anal and Urogenital triangles, (b) Simplified geometrical model with nine control points.

This model is fully parametric, which provides high degree of automation: the geometry can be recreated in a matter of seconds for a new patient. Another salient feature of our model is that it contains only nine control points (Fig. 1b, a to i), allowing us to identify the muscle attachment zones that will define the anatomical extrema of our model. To identify the nine control points on CT images, a plugin has been written for 3D Slicer [5]. This plugin, soon to be available in a public repository on GitHub, also supports the visualization of the fetal head with respect to the weeks of gestation, and the users can perform relevant statistical analyses. The geometry has been created without user intervention by harnessing the Python interface to FreeCAD, a cross-platform 3D parametric modeller.

3. Results

Thanks to this parametrized geometry, our approach does not require the segmentation of the anatomical structures of the pelvic region. The advantage of this method is that it is compatible with finite element simulations (Abaqus/CAE 6.12-2 software). For the numerical simulations, we assign mechanical properties from preliminary works referenced in the literature [6, 7]. An isotropic hyperelastic behavior of Yeoh type was considered as a first approximation. These simulations are performed for several head sizes and cephalic presentations, which the user can vary in order to analyze stress on the mother's pelvic floor. The head is also a parameterized model, deformable with the consideration of bone and fontanel plates. The FE analysis demonstrates that our method is applicable as a personalized injury-prevention tool for delivery.



4. Discussion and Conclusions

Due to the hierarchical build of the geometry, it is easy to add new elements to the existing geometry. In the future, if it turns out that muscles and ligaments are not sufficient, we can apply this parametric idea for bones as well. Such a tool is useful to identify the highly stressed areas following the cephalic presentations and the kinematics of the head. This research performed on the whole sustainable structure will help us to take into account the high stress-induced damages. Investigating soft-tissue injury is the next step to adapted obstetric decisions.

5. References

- [1] MP. Parente et al., *Am J Obstet Gynecol*, 203(3):217.e1–217.e6, 2010.
- [2] X. Fritel, *Eur J Obstet Gyn Reprod Biol*; 198:62–67, 2016.
- [3] J. Lepage et al. *Int Urogynecol J*; 26(4):497–504. 2014.
- [4] O. Mayeur et al. *Computational Biomechanics for Medicine*, Springer, Cham, pp.135-146. 2017.
- [5] A. Fedorov et al., *Magn. Reson. Im.*, 30(9):1323–1341, 12.
- [6] L. Havelková et al., *Int. Urogynecol J* 31:1315–1324, 2020.
- [7] M. E. T. Silva, et al., *CMBBE*, 20:8, 842-852, 2017.

Acknowledgements:

These results are part of the StartAIRR Mater project, financed by I-SITE Université Lille Nord-Europe and the Haut-de-France region.

18.5

Pelvic Organ Prolapse: Pre-Operative Evaluation of Surgical Techniques thanks to Numerical Simulation

Olivier Mayeur¹, Zhifan Jiang², Michel COSSON^{2,3}, Guillaume DUFAYE², Jean-François WITZ², Pauline Lecomte-Grosbras², Mathias BRIEU⁴

1 Univ. Lille, CNRS, Centrale Lille, UMR 9013- LaMcube, Villeneuve-d'Ascq, France

2 Univ. Lille, CNRS, Centrale Lille, UMR 9013- LaMcube

3 Service de chirurgie gynécologique CHU Lille

4 California State Univ., Los Angeles, USA, Dpt. Mech. Engg, Los Angeles, United States

1. Introduction

Curing Pelvic Organ Prolapse (POP) is a treatment that mainly requires surgery, while its failure rate remains high [1, 2]. In this context, numerical simulation using the Finite Element (FE) method can help to reduce recurrence by analyzing the mobility of the pelvic system and understanding the phenomena involved in this complex equilibrium [3, 4]. Several studies in the literature interested in the understanding of the POP by taking into account these hypermobility, conditioned by geometrical and mechanical aspects [5, 6]. However, few studies have focused on the surgical correction of the pathologies which are not specifically adapted to the patient [7]. In order to analyze the organ's mobility and to generate models of pelvic system, many studies use medical imaging, and more precisely image registration techniques [8]. This work was performed in this context by using FE method to analyze the impact of different surgical techniques on the POP cure and to develop a pre-operative evaluation tool that may help to select the best treatment for each patient.

2. Materials and Methods

The Patient-specific models are generated by surface reconstruction according to the already published technique [8]. The mechanical properties are then implemented on these FE models as well as the loading conditions to correspond to a physiological mobility, correlated with dynamic MRIs. From these models (Fig1), we adapt anatomical structures and mechanical properties to create hyper-mobility of the organs [9].

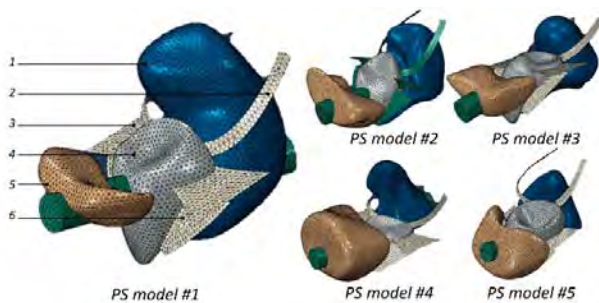


Figure 1: Patient-specific models of the pelvic system with 1. Rectum, 2. Uterosacral ligaments, 3. Cardinal ligaments, 4. Vagina, 5. Bladder and 6. Paravaginal ligaments.

This work is done in a semi-automatic way and allows us to obtain data for FE simulation (ABAQUS 13.1 solver, Dassault System). The 9 different surgical techniques (Sacropexy, Sacrospinofixation, Richter, McCall, Campbell, etc.) could be compared according to several parameters such as installation of the prosthesis, size of the mesh, mechanical properties, etc. The analysis of mobility following this correction allows us to quantify significant differences in mobility according to POP-Q score [10,11].

3. Results

The analysis of POP-Q points (C, Aa, Ba) on the FE results allows a refine analysis of the simulation in connection with a clinical diagnosis.

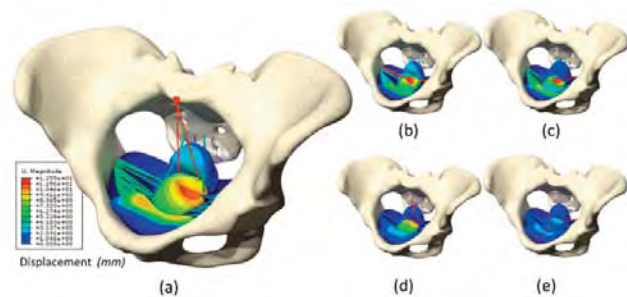


Figure 2: Mobility magnitude (in mm) of a specific patient, illustration of different surgical techniques with (a) Posterior Sacropexy, (b) Bilateral SSF, (c) Right Post SSF Richter, (d) McCall, (e) Campbell.

Figure 2 illustrates the results we obtain for a patient-specific model to which five different surgical techniques were applied. It can be observed that displacement of the organs, as well as strains and stresses distributions, vary in terms of intensity and location with respect to the surgical techniques considered. Preliminary results applied on 2 patients reveal different choices of techniques to limit the POP-Q score. A clinical study, with pre and post-operative data, is currently underway to validate this method and provide valuable assistance in the specific treatment of patients.

4. Discussion and Conclusions

The approach used is a semi-automated method that allows a comparative analysis to be carried out for a patient in one hour using MRI data. This numerical methodology provides relevant information that allows to discriminate, for each patient, the most efficient surgical techniques. This allows to optimize the treatment with respect to the patient-specific anatomy and may help to define the most suitable surgical for every patient.

5. References

1. Samuelsson E, Am J Obstet Gynecol 180:299-305, 1999.
2. Olsen AL. et al., Obstet. Gynecol., 89:501-506, 1997.
3. DeLancey JOL. Am. J. Obstet. & Gynecol., 166t, 1992.
4. Gordon MT. et al., Interface Focus, 9: 20190022, 2019.
5. Mayeur O, Biomed. Simulation, 8789: 220-227, 2014.
6. Mayeur O, Annals of Biomed Eng, 44(1):202-212, 2016.
7. Jeanditgautier E, Int Urogynecol J 27 : 951-957, 2016.
8. Jiang Z. et al., Strain. 55.10.1111/str.12305, 2019.
9. Lamblin G. et al., Arch. Gyneco. Obstet., 294, 2017.
10. DeLancey JOL., Am. J. Obst. & Gynecol., 187: 93-98, 2002.
11. Bump RC., Am. J. Obstet. & Gynecol., 175: 10-17, 1996.

Acknowledgement

The authors would like to thank SATT-Nord for funding part of the work presented in this research.

19.1

Computer modelling and simulation in clinics: mapping usage and opinions for advancing in silico medicine

Raphaëlle Lesage¹, Michiel Van Oudheusden², Martina Contin¹, Silvia Schievano³, Liesbet Geris^{1,4}, Claudio Capelli³

1 VPH institute, Heverlee, Belgium

2 Center for Sociological research, KU Leuven, Leuven, Belgium

3 University College London & Great Ormond Street Hospital, London, United Kingdom

4 KU Leuven, Biomechanics, Leuven, Belgium

1. Introduction

In silico medicine is the application of computer modelling and simulation (CM&S) in the study, diagnosis, treatment or prevention of a disease. Incredible advances in the research have been realised to use CM&S for aiding clinical applications. Nevertheless, the spread of CM&S in clinical practice is not always reflected timely and accurately in the literature. How advanced is the translation of CM&S in clinics? Which are the factors limiting the diffusion of CM&S in healthcare? A clear view on the current awareness, actual usage and opinions from the clinicians is needed to identify the real barriers and opportunities for the future of in silico medicine. The aim of this study was capturing the current state of CM&S in clinics to identify potential opportunities, strengths and barriers for the advance of in silico medicine.

2. Materials and Methods

An online survey made of 25 questions was designed by authors and reviewed by the VPHi Board of Directors. It assessed: levels of awareness and familiarity with silico concepts, experiences in clinics, opinions on barriers and opportunities to use in silico medicine for patients' care. Data were collected through SurveyMonkey [1] using VPHi communication channels, engagement with clinical societies, hospitals and individual contacts, between December 2020 and March 2021. Statistical analyses were done with R [2].

3. Results

163 responses were collected from all over the world (majority in Europe). Clinicians were mostly aged between 35 and 64 years old, with heterogeneous experiences (from junior doctors to head of unit) and areas of expertise (e.g. 48% cardiology, 13% musculoskeletal, 8% General surgery, 5% paediatrics). The CM&S terms 'Personalised medicine' and 'Patient-specific modelling' were the most known within the respondents. 'In silico clinical trials' and 'Digital Twin' were the least known. The familiarity with different methods (e.g. finite element analysis, AI) depended on the medical specialty, highlighting possible cultural and background differences. Figure 1 shows the applications of CM&S in clinics. 50% of the respondents who used CM&S in clinics did so to plan interventions. However, the usage frequency is still scarce. A well-recognized strength associated to CM&S was the increased trust in planning procedures. Overall, the level of trust for CM&S was high and not proportional to awareness level. We also identified potential barriers such as access to computing resources, perception that CM&S is slow, low accuracy of the results. However, clinicians do see a role for CM&S expertise in their team in the future.

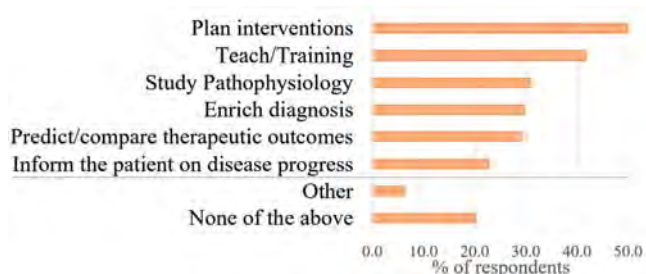


Figure 1: Applications of CM&S by clinicians

4. Discussion and Conclusions

This survey offers a snapshot of the current situation in the clinics. Although the sample size and representativity could be increased, the results provide the community with actionable data and lessons to build a responsible future for in silico medicine. New iterations and follow-up engagement activities are planned to involve the medical community and accelerate uptake of CM&S tools.

5. References

1. <https://www.surveymonkey.co.uk/r/9ZTBW87>
2. R Core Team (2018). R: A language and environment for statistical computing. R Foundation for Statistical Computing, Vienna, Austria. URL <https://www.R-project.org/>.

Acknowledgements:

The authors would like to thank the European Union's Horizon 2020 research and innovation programme (Grant No. 101016496, 101017578 and 101016503) for providing financial support to this project and G. Bassetti for the graphical designs and illustrations.

19.2

Artificial Retinal Microvascular Networks: Virtual Populations for In Silico Trials

Rémi Hernandez^{1,2}, Wahbi El-Bouri^{1,2}

1 University of Liverpool, Liverpool Centre for Cardiovascular Science, Liverpool, United Kingdom

2 University of Liverpool, Department of Cardiovascular and Metabolic Medicine, Liverpool, United Kingdom

*Corresponding author: w.el-bouri@liverpool.ac.uk

1. Introduction

Defects in the oxygen supply to the retina are a common cause of several retinal diseases. The inner retinal vasculature can be imaged noninvasively with optical coherence tomography angiography (OCTA) and numerous biomarkers have been suggested for each disease. We propose here a method to generate microvascular networks that can be used to create populations of retinas, differentiated by a handful of vascular indices.

2. Materials and Methods

From en-face OCTA images, several large vessels are segmented. These vessels are embedded in a 3x3mm² square with a 0.4 mm² representing the macula and the foveal avascular zone (FAZ). The vessels are linked to a root vessel lying outside the macula to form a single root tree, Figure 1. A two-stage constructive constraint optimisation (CCO) algorithm is used to sprout a microvascular tree from the segmented vessels [1].

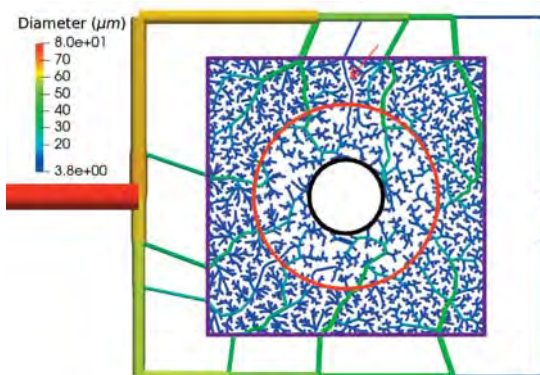


Figure 1: An example output network. The inner black circle defines the FAZ. The red circle makes the boundary between the two growth stages. The arrow points to a vessel that does not branch.

Vascular indices proposed in [2] are used to characterise the resulting networks. Fractal dimension and mean inter-capillary distance are computed using a box counting method and distance-transform method.

3. Results

Figure 1 shows a typical output network. Table 1 compares some of the vascular indices to the values for healthy subjects reported in the literature [2,3,4,5]. Fractal dimension, average inter-capillary distance and vessel skeleton agree closely with experimental measurements. Metrics involving vessel diameters are all below the literature values.

	VAD	VCI	VSD	FD	ICD
Chu	0.51	>10 ⁴	0.01		
Others	0.48			1.68	0.02
This work	0.21	3388	0.02	1.65	0.02

Table 1: Validation of the generated networks against reported values. VDI: vessel diameter index; VCI: vessel complexity index; VSD: vessel skeleton density; FD: fractal dimension; ICD: mean inter-capillary distance.

4. Discussion and Conclusions

Our method generates microvascular networks that match reported values for certain metrics. Overestimation of some measured metrics is likely due to over-segmentation of images, and hence further validation is required.

The method presented here can be used to generate populations of retinal microvascular networks that can be used for in silico modelling of retinal pathologies.

5. References

1. Talou G. D. M. et al., *Scientific Reports* 2021
2. Chu Z et al., *Journal of Biomedical Optics* 2016
3. Alam M. et al., *Retina* 2020
4. Masters B.R. et al., *Ann. Rev. Biom. Eng.* 2004
5. Liu K. et al., *Exper. Biol. and Medicine* 2021

19.3

In silico clinical trials to investigate the effect of trunk morphology on lumbar belt efficacy using representative virtual patients

AICHA ERRABITY^{1,2}, Fanette Chassagne¹, Rebecca Bonnaire³, Woo Suck Han¹, Romain Pannetier², Paul Calmels⁴, Jérôme Molimard¹

1 Mines Saint-Etienne, Univ Lyon, Univ Jean Monnet, INSERM, U 1059 Sainbiose, Centre CIS, Saint-Etienne France

2 ThuaSne, BP243, 92307 Levallois-Perret cedex, France

3 Institut Clément Ader (ICA), Université de Toulouse, CNRS, IMT Mines Albi, INSA, ISAE-SUPAERO, UPS Campus Jarlard, F-81013 Albi, France

4 Hôpital Nord, CHU de Saint-Etienne, France

Corresponding author: Aicha.errabity@emse.fr

1. Introduction

Lumbar belts are one of several therapeutic strategies proposed for Low Back Pain. Few studies have been conducted on their efficacy, most of which have studied their analgesic and subjective effects and some limited biomechanical parameters, through clinical trials. However, clinical trials remain expensive, and patient inclusion criteria are often strict and challenging. In silico clinical trials are a good alternative as they reduce the size of the clinical trial cohort needed to obtain the required statistical results, using a representative virtual patient. A previous in silico clinical study was conducted on a limited cohort of patients for lumbar belt efficacy [1]. One important finding suggested an association between belt efficacy and morphological indicators (BMI). However, more morphologies in the overweight category were needed to improve the statistical results. In this new work, we propose to complement these in silico trials using a virtual set of automatically generated trunk morphologies using a proper orthogonal decomposition POD, already succeeded in generating artificially realistic geometries [2].

2. Materials and Methods

The trunk morphologies of 13 experimental patients, were recorded using a 3D line scanner (Orten, France). They were all pre-processed and used to create a POD base as proposed by [2]. Then, 24 new trunks were generated, and the morphological indicator considered was the waist-to-hip ratio (WHR) as defined by [3].

An in silico clinical trial for the efficacy of a commercial lumbar belt, using the 37 morphologies, was performed. The interface pressure applied to the trunk was calculated using a semi-analytical model based on Laplace's law [1]. The bending moment at the center of the back curvature (the global moment of the resultant forces), considered a measure of the effectiveness of the belt [1] was used to evaluate the belt efficacy.

3. Results

Most of the generated geometries fit into the overweight category (WHR > 0.90) [3], which allows to complete the real patient cohort of [1].

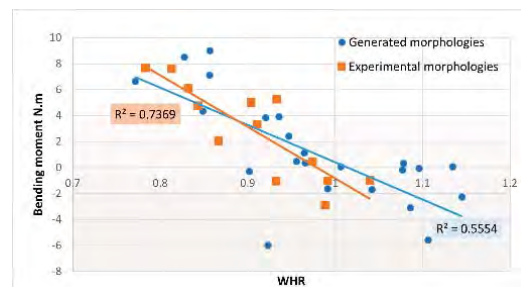


Figure 1: Bending moment in function of WHR

Bending moment was presented as a function of WHR for each cohort (figure 1). A Pearson correlation test was performed and showed a significant influence of WHR on bending moment; it decreased when WHR increased and reached negative values when WHR > 1. Then, the belt has a lordosing instead of a delordosing effect which might increase the patient's pain.

4. Discussion and Conclusions

The results confirmed the negative correlation between the belt efficacy and patient morphology (WHR). Furthermore, a similar trend was found in the results obtained with in silico and experimental trunks. This validates the implementation of POD for the trunk generation.

5. References

1. Molimard, J. et al, *PLoS One*.14(3): 212681(2019).
2. CHASSAGNE, F. et al, *IEEE Transaction on Biomedical Engineering*, 65(2): 449-457 (2017).
3. Leyk, D. et al, *Befragung von mehr als*, 10:609-14(2008).

19.4

Validation of a comprehensive in silico clinical trial for a humeral replacement

Philippe Favre¹, Adam Henderson², Christine Mueri², Ghislain Maquer², Mehul Dharia³, Rodney Summers³, Maged Awadalla³, Jeff Bischoff³

1 Zimmer Biomet, Research , Zug, Switzerland

2 Zimmer Biomet, Research , Winterthur, Switzerland

3 Zimmer Biomet, Research , Warsaw, IN, United States

1. Introduction

Clinical data is required to satisfy regulatory requirements [1], and may be enriched with in silico clinical trials (ISCT). Yet, there are currently no published guidelines available for validating an ISCT. Our objective is thus to present an example of model validation applied to an orthopaedic implant.

2. Materials and Methods

Four biomechanical risks were identified for a humeral replacement, balancing the severity and probability of the patient risk, the impact of implant design on the risk, and the technical feasibility of evaluating the risk via ISCT. For each risk, a model credibility plan identified a benchtop comparator and, when available, a clinical comparator to ensure that the physics and clinical observations are captured by the model. Computational models were then developed to specifically simulate each benchtop/clinical condition, and the prediction credibility was evaluated against their respective comparators.

The 4 risks and corresponding comparators are:

Scapular notching - A study comparing simulated and experimentally determined range of motion provided sufficient credibility for benchtop validation [2]. A clinical study [3] showed a clear relationship between the clinical occurrence of notching and anatomical features and implant position.

Humeral loosening - A benchtop test was performed to assess the humeral stem stability in foam bone. A clinical study [4] showed a significant impact of proximal stem roughness on occurrence of radiolucencies.

Stress shielding - A previous study [5] comparing simulated and experimentally determined bone strain provided sufficient credibility for benchtop validation. A clinical study [6] showed a statistically significant influence of relative stem size on stress shielding.

Head-adapter dissociation - Benchtop pull-off and torque-off tests were performed at multiple assembly loads. No clinical observations were available for clinical validation due to the novelty of the adapter design.

3. Results

All models were able to predict the observed behaviour consistent with applicable benchtop and clinical comparator measurements. The credibility for model validation was achieved for each patient risk.

4. Discussion and Conclusions

To our knowledge, this is the first comprehensive validation of the most relevant biomechanical risks associated with an orthopaedic implant, in the frame of an ISCT. The proposed approach established the models validity by relying on benchtop and clinical data, going beyond existing standards that generally consider benchtop testing as the sole comparator. With these validated computer models, simulations can be conducted across a virtual population, supplying simulation data to enrich clinical data.

5. References

1. Favre et al., *Ann Biomed Eng.* 2021;49(12):3213-3226.
2. Roche et al., *JSES* 2009; 18:734-41
3. Simovitch et al. *J Bone Joint Surg Am.* 2007;89: 588-600.
4. Morwood et al., *JSES* 2017;26:1246-52.
5. Eberle et al., *Med Eng Phys.* 2013;35: 875-83.
6. Nagels et al., *JSES* 2003;12:35-9.

Validation comparator		
	Benchtop	Clinical
Scapular notching	Literature	Literature
Humeral loosening	Internal test	Literature
Stress shielding	Literature	Literature
Adapter dissociation	Internal test	N/A

Table 1: Validation activities for each patient risk

19.5

v-Patients: The web-based end-to-end virtual trial solution for medical device developers

Simon Sonntag¹, Gloria Zörnack¹, Bence Rochlitz¹, Diogo F. Almeida¹, Wen-Yang Chu¹

¹ Virtonomy GmbH, München, Germany

+sonntag@virtonomy.io, Paul-Heyse-Strasse 6, 80336 München, Germany

1. Introduction

Demand for new and more effective medical devices is increasing. Simultaneously, development costs are rising in terms of time to market and profitability due to higher complexity of regulatory requirements. The introduction of technology-enabled device testing alternatives addresses these issues by refining and reducing the need for animal and human testing, while making the process cost-effective, fast and safe. A transition strongly supported by FDA.

2. Materials and Methods

Virtonomy has created the first digital twin web-based technology v-Patients enabling medical device manufacturers to perform end-to-end in silico testing in the web-browser in a collaborative framework. Combining deep learning, statistical analytics, high-performance computing, simulation and Virtual Reality, this approach progressively replaces pre-clinical and clinical evidence with digital evidence throughout the whole development lifecycle, from concept to regulatory approval.

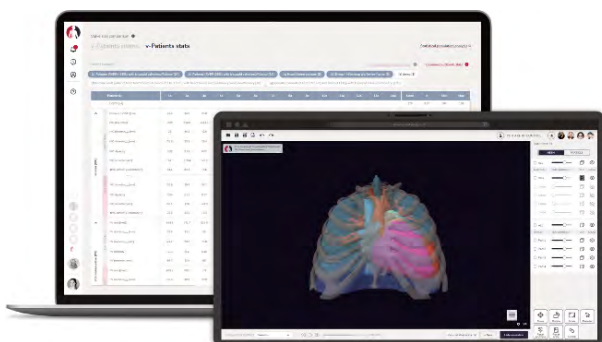


Figure 1: Virtonomy's digital twin end-to-end web-based technology v-Patients

In a first step, the user can create the virtual patient population addressing the target device cohort using our extensive real-world evidence database of thousands of humans and animals. Detailed criteria allow for a proper selection of the target population based on anatomical variation, demographic diversity, pathological conditions etc.

The virtual patient cohort is linked to a statistical population analysis, forming a library of body variations. This allows evaluating the proper target sub-population cohort, define inclusion/exclusion criteria, assess worst-case scenarios, increase evaluation confidence and more. Subsequently, the implant or product family can be simulated (solid, fluid, FSI) in the virtual patient to investigate how the blood-tissue-device interaction may affect the performance and safety. This enables identifying potential for design optimization and material selection by conducting parameter analyses. All in an easy-to-use web environment.

Based on the anatomy, statistical and simulation results, regulatory compliant digital evidence is finally created that can be submitted to regulatory authorities substituting in vitro and in vivo evidence where possible.

3. Results

v-Patients is already successfully applied during the design and approval process of novel ventricular assist devices, total artificial hearts, heart valve repair and replacement devices as well as a pacemakers. The virtual studies are used to verify design decisions, estimate worst-case scenarios of sizes and variants, identify suitable animal models, perform virtual tests on a large number of patients and to determine and justify anatomical and morphological eligibility criteria for sub-population selection.

4. Discussion and Conclusions

Our virtual studies have proven to give results that may not have been possible with conventional approaches, reduce the risky and expensive trial-and-error process, and increase evaluation confidence to ensure product safety prior to clinical trials.

20.1

Machine self-semantic learning of cancer disease: a case study on brain tumour early progression

Anna Drożdż¹, Kamil Woźniak¹, Caitriona McInerney², Seyed Mehdi Jafarnejad², Kevin Prise², Veronica J. Spence², Jose Sousa¹

1 *ano – Centre for Computational Personalised Medicine, Personal Health Data Science, Kraków, Poland*

2 *Patrick G. Johnston Centre for Cancer Research - Queen's University, Belfast, United Kingdom*

1. Introduction

It is anticipated that artificial intelligence (AI) will revolutionise healthcare, as big data provide AI with context data, a foundation of human knowledge. Currently, AI mainly uses deep learning (DL), however, most of the models produced this way emerge from some type of human training. The proposed AI semantic space learning model builds upon the understanding that learning is a process of relating representations of the world to goals [1,2]. Semantic learning brings together statistical learning and complex networks providing an explicit meta-modelling approach to create a decision-making point [2,3]. Additionally, it supports flexible complexity for profiling inference and learning. Here we applied this framework to perform a case-study to assess brain tumour (astrocytoma) progression indicators.

2. Materials and Methods

Gene expression data of astrocytoma Grade II (55 patient) and III (57 patient) tumours were obtained from REMBRANDT repository [4]. Data were analysed using two R packages: the simpleaffy for quality control (passed by all samples) and the affy (Robust Multi-array Average algorithm implemented with justRMA function) for background correction, log2 transformation and quantile normalisation. To identify the emergent associations between genes that may be responsible for disease progression, the AI Semantic Learning Engine (AiLLE) was implemented as a complex networks statistical modelling. Post-hoc analyses were performed to determine whether AiLLE learned new knowledge.

3. Results

Generated networks visualized different number of communities for Grade II (4) and Grade III (5) astrocytoma. Next, we separately examined nine RNA binding protein target groups including 879 genes. The top 20 identified for each target group was compared between Grade II and III. A signature of 103 differences to Grade III was identified. Differential gene expression analysis was implemented to determine whether the genes identified by AiLLE were amongst those identified as differentially expressed between grades. Only 43 of the 103 genes were determined to be significantly different using Mann-Whitney statistical tests.

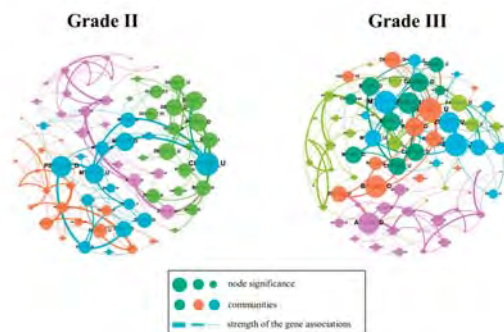


Figure 1: The knowledge graphs for astrocytoma brain tumours gene expression data.

4. Discussion and Conclusions

We developed AI semantic learning framework based on complex networks meta-modelling, capable of learning from data. AiLLE learned new knowledge relating to the biological changes occurring during disease progression. The gene signature of differences identified by AiLLE differed from those identified using traditional methods. The genes identified may have relevance as new therapeutic targets for future clinical trials.

References

1. McCarthy, J., 1981 *Readings in Artificial Intelligence*, 431-450.
2. Damasio, A.R., 1994. *Grosset/Putnam*, 1-352.
3. Damasio, A.R., 1999. *Scientific American*, 281 6, 112-7.
4. Madhavan, S., Zenklusen, J.C., Kotliarov, Y., et al., 2009. *Molecular Cancer Research*, 7, 157-167.

Acknowledgements:

This work was supported by funding from European Union's Horizon 2020 RAI programme (Grant no: 857533) and Brainwaves Northern Ireland (Registry no: NIC103464).

20.2

Model-Based Optimisation Reveals Evolutionary Dynamics Conducive to Effective Therapy for Neuroblastoma

Matteo Italia¹, Kenneth Y. Wertheim², Sabine Taschner-Mandl³, Dawn Walker², Fabio Dercole¹

¹ Politecnico di Milano, Department of Electronic, Information, and Bioengineering, Milano, Italy

² University of Sheffield, Department of Computer Science; Insigneo Institute for in Silico Medicine, Sheffield, United Kingdom

³ St. Anna Children's Cancer Research Institute, Vienna, Austria

*Author to whom any correspondence should be addressed, email: matteo.italia@polimi.it

1. Introduction

Neuroblastoma is the most common extra-cranial solid tumour in children and over half of the high-risk cases relapse despite multi-modal therapy, whereupon survival is rare [1]. As targetable mutations (e.g., in ALK) are selected by chemotherapy and enriched at relapse [2], we propose a new strategy of shrinking the tumour by induction chemotherapy, which is experimentally known to enrich targetable mutations (reduced heterogeneity), before targeting the remaining small and mutated populations. The first strike highly reduces tumor size and sets an evolutionary trap. The second (e.g., ALK inhibitors) exploits the druggable mutations in the vulnerable small populations. Our strategy entails knowing the optimal schedule of drug administration during induction and when to apply the second strike.

2. Materials and Methods

We used ordinary differential equations to model neuroblastoma's clonal evolution induced by cyclophosphamide (CPM) and vincristine (VCR). The model describes the logistic growth of clones with different growth and death rates, as well as phenotypic acclimation to drugs, interclonal mutation, and pharmacokinetics. The parameters were derived from in-vitro experiments. For different initial clonal compositions, we minimised the final population size using a combined gradient descent–genetic algorithm, thus finding the optimal schedule in each case.

3. Results

The one-size-fits-all COJEC induction schedule uses fixed dosages of chemotherapeutic agents in eight two-week cycles [3]. By contrast, our results suggest that using drugs together at the maximum tolerated dosage (MTD) without optimising the number of cycles is only optimal for a fully sensitive tumour. First, in a tumour with VCR-resistant cells too, using just CPM at the MTD will favour the sensitive cells over the VCR-resistant cells, minimising the latter by exploiting clonal evolution. As the sensitive clone becomes increasingly dominant relative to the VCR-resistant clone, increasing the VCR dosage gradually up to the MTD will enhance the overall cytotoxic effect. A lower rate of increase is necessary for a larger VCR-resistant clone. Second, when sensitive and CPM-resistant cells compete, starting with just VCR before administering CPM in later cycles is only optimal when, in the presence of just VCR, the sensitive cells' advantage is bigger than CPM's cytotoxic advantage over VCR. Otherwise, CPM and VCR should both be used at the MTD, with the caveat that there be fewer cycles, which has great implications for timing the second strike. Third, when all clones compete, the optimal schedule is logically the same as in the second case.

4. Discussion and Conclusions

Within the context of our proposed strategy, the results mean that an oncologist would need to know each drug's relative cytotoxicity, the relative fitness of each clone in presence of each drug, and the clonal composition in a patient. The oncologist would customise the second strike according to the mutations enriched by drugs. Our model can absorb such an evolutionary rulebook and patient-specific data generated by emerging technologies such as real-time liquid biopsies to form a decision support system.

5. References

1. Matthay KK et al, *Nature Reviews Disease Primers* 2: 16078 (2016).
2. Schleiermacher G et al, *J Clin Oncol* 32(25): 2727–2734 (2014).
3. Garaventa A et al, *J Clin Oncol* 39(23): 2552–2563 (2021).

20.3

Modeling tumor heterogeneity evolution in lung adenocarcinoma

Claire COUTY¹, Perrine Masson¹, Arnaud Nativel¹, Firas Hammami¹, Angélique Perrillat-Mercerot¹, Matthieu Coudron¹, Evgueni Jacob¹, Lucile Lefevre², Raphaël Toueg², Aurélie Swalduz³, Jean-Louis Palgen¹, Claudio Monteiro¹, Adèle L'Hostis¹

¹ Novadiscovery, Lyon, France

² Janssen Cilag, Issy-les-Moulineaux, France

³ Léon Bérard Center, Department of Medical Oncology, Lyon, France

1. Introduction

Tumor heterogeneity is considered as one of the critical causes of intractability in the treatment of cancers[1]. Intratumor heterogeneity refers to the existence of cellular populations, named cancer subclones, differing in mutational profile resulting in distinct phenotype and therapeutic response. This is difficult to monitor *in vivo*, as it requires multiple biopsies of the tumor at each of several time points over the course of treatment and follow-up.

Modeling is an attractive method to represent and understand intratumor heterogeneity and its consequences on resistance to treatment. The mechanistic modeling case study presented here illustrates the approach for studying tumor heterogeneity in lung cancer to provide clinical support.

Lung cancer is one of the most frequent cancers diagnosed and the leading cause of cancer mortality in the world[2]. In particular, lung cancers with overactive epidermal growth factor receptor mutations (EGFR+) are aggressive, with reduced survival and various mechanisms of treatment resistance linked to intratumor heterogeneity, such as MET amplification, that the model aims to reproduce.

2. Materials and Methods

We developed seven submodels, all based on ordinary differential equations. These are: EGFR-and-C-Met-downstream-pathways, Cell-Cycle-and-Death, Tumor-Growth, Neoangiogenesis, Genomic-profile-of-the-tumor, and Metastases and Pharmacometrics of a 1st generation Tyrosine Kinase Inhibitor (TKI). Submodels are combined together to result in a multiscale model of EGFR+ lung adenocarcinoma, which outputs the tumor size and dynamics of metastases through time. Four submodels are duplicated to represent cancer subclones, characterized by distinct sets of mutations, and thus a corresponding proliferating phenotype. The duplicated submodels are: Cell-Cycle-and-Cell-Death, Neoangiogenesis, EGFR-and-cMET-downstream-pathways and Tumor-Growth.

3. Results

The model follows the proliferating phenotype of each cancer subclone, and shows the emergence of a treatment-resistant subclone after administration of a 1st generation TKI.

Because of the duplication implemented in the model, we are able to follow the prevalence of cancer subclones over time, in the primary tumor as well as in the metastatic sites.

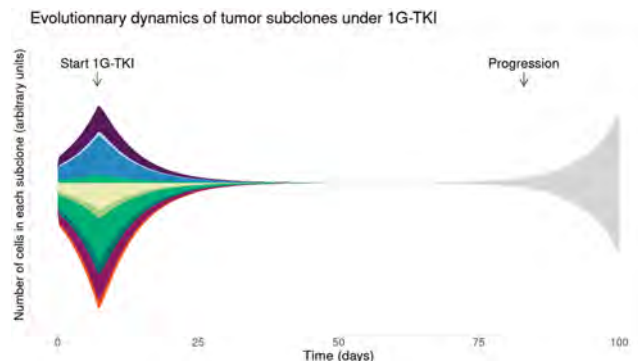


Figure 1: Evolution over time of the cell number in each cancer subclone in the primary tumor. 1st generation TKI (1G-TKI) is administered at $t=7$ d, and each subclone is represented by one color. Subclone represented in light grey grows as it resists treatment and becomes dominant, due to a T790M mutation.

4. Discussion and Conclusions

Modeling allows exploration of how clinical assessment of tumor heterogeneity, via noninvasive methods for example, can support better decision making in the choice of therapeutic strategies and personalised medicine.

5. References

1. S. H. Bradley, M. P. T. Kennedy, and R. D. Neal. "Recognising Lung Cancer in Primary Care". *Adv Ther* 36.1 (2019), pp. 19–30
2. Mimori, Koshi, et al. "Cancer evolution and heterogeneity." *Annals of gastroenterological surgery* 2.5 (2018): 332-338.

Acknowledgements:

The authors would like to thank Janssen-Cilag France for their support.

20.4

Novel antenna for regional microwave hyperthermia cancer treatment

Matouš Brunát¹, David Vrba¹

¹ Czech Technical University in Prague Faculty of Biomedical Engineering, Department of Biomedical Technology, Kladno, Czech Republic
 matous.brunat@fbmi.cvut.cz, david.vrba@fbmi.cvut.cz

1. Introduction

Deep microwave hyperthermia is a complementary cancer treatment that significantly improves patient survival rate. During the treatment, the patient is positioned between multiple antennas, which create an electric field between 70-150 MHz.[1] Electric fields generated by the antennas positively interfere in cancerous tissue, leaving the healthy tissue relatively cold. To achieve such interference, a 3D model of the patient's body is created from a CT scan or MRI. The model is then put between the antennas, meshed, and using numerical simulation optimized for voltage amplitudes and phases for each antenna.

2. Materials and Methods

To heat the tumour, we collaterally heat even healthy tissue around, since the healthy tissue is better at cooling itself than the tumour. This method is used in the system ALBA 4D, which uses waveguides as antennas. Since the waveguide's resonant frequency directly corresponds to its size, it is not ideal for bigger tumours.[2]

We designed a new antenna in COMSOL Multiphysics, which can have any dimensions on selected frequencies. Moreover, we improved key parameters on which the treatment depends. These parameters include effective field size (EFS) and effective penetration depth (EPD).

As a proof of concept, the antenna was built and tested on agar phantom similar to muscle tissue in dielectric parameters. The heated area was screened with an IR camera at a depth of 1 cm.

3. Results

	Waveguide	Our antenna
EFS	65%	78%
EPD	3.2 [cm]	4.3 [cm]

Table 1: Comparison of our antenna and clinically used antenna.

Our prototype dimensions were 42x24 cm, which was selected as optimal for clinical use.

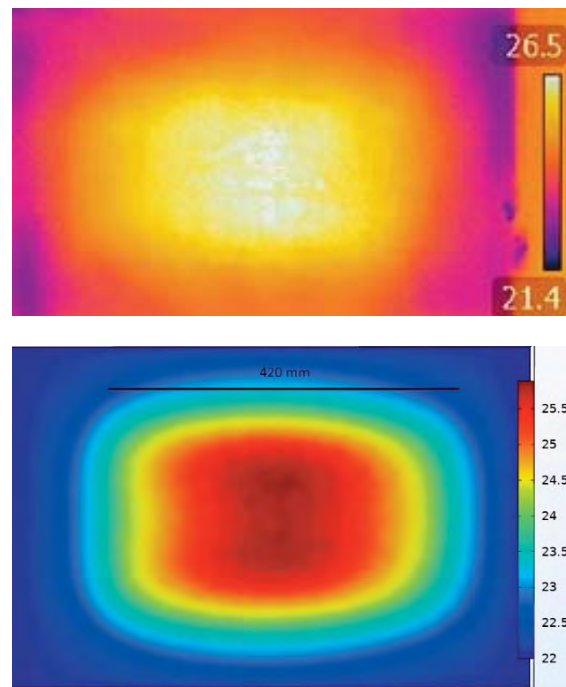


Figure 1: Comparison of our simulation and experiment with the prototype. The heating lasted 15 minutes with 100 watts.

The prototype was tuned for 70 MHz and at that frequency, S11 was -17 dB, which was similar to the simulation at -15 dB.

4. Discussion and Conclusions

Using numerical simulations, we created an antenna with superior parameters over currently used antennas in deep microwave hyperthermia treatment. This antenna has a great potential to become a new industry standard for regional hyperthermia systems.

5. References

1. Fiorentini, Giammaria, et al. "A Narrative Review of Regional Hyperthermia" *integrative Cancer Therapies*, Jan. 2020
2. Maška M et al., "Technical and Clinical Evaluation of the ALBA-4D 70MHz Loco-Regional Hyperthermia System," 2018 48th European Microwave Conference (EuMC), 2018, pp. 328-331

20.5

Virtual instances or avatars of a nephroblastoma digital twin: creating a performance efficient architecture for the clinical adaptation of the Nephroblastoma Oncosimulator

Foteini Panagiotidou¹, Dimosthenis Masouros¹, Marcel Meyerheim², Eleni Georgiadi¹, Norbert Graf², Dimitrios Soudris¹, **Georgios Stamatakos¹**

¹ National Technical University of Athens, Institute of Communication and Computer Systems, School of Electrical and Computer Engineering, Zografos, Greece

² Saarland University, Clinic of Pediatric Oncology and Hematology, Saarland University Hospital, Homburg, Germany

1. Introduction

The Nephroblastoma Oncosimulator (NO) is a digital twin for Wilms tumour that is based on a mechanistic multiscale simulation model of tumour growth and response to treatment. It exploits the patient's imaging, cellular, molecular and clinical data [1,2]. The NO maps the patient's imaging and other data into a 3D discretization mesh and by applying biological laws and rules predicts the tumour evolution over time [1,2]. Its main purposes are to customize treatment based on the patient's individual data and to conduct in silico clinical trials. Two of the major challenges that need to be addressed before the utilization of the NO in clinical practice are i) the assignment of appropriate values to the model parameters for each in silico execution of the model and ii) the model execution efficiency.

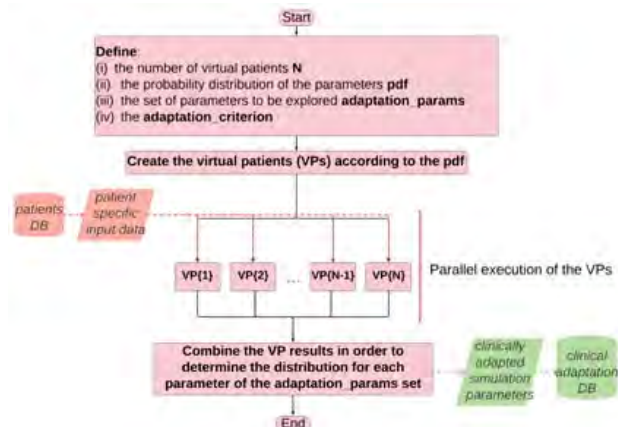
2. Materials and Methods

In order to adequately represent the actual patient in the virtual space, a set of in silico executions with each model parameter being assigned different values from an appropriate parameter distribution is conducted. This is dictated by the need to account for the multifaceted uncertainties in the estimation of the digital twin model parameter values. In this way, numerous virtual instances or avatars of the patient or virtual patients are created for each actual patient. This virtual patient strategy was utilized in order to clinically adapt the value of the key parameter of cell kill probability (CKP) for three nephroblastoma patients of distinct histological profiles and respective risk groups. More specifically, for each actual patient, N virtual patients (VPs) are created. For each VP, the CKP parameter value is independently adjusted until the estimated final tumour volume matches the actual final tumour volume (Fig 1). In order to enhance the overall execution performance, i) the trade-off between the simulation execution cost and the simulation resolution is investigated [2] and ii) the time demanding portions of the execution are identified using the Valgrind profiling tool [3] and parallelized using the OpenMP API software [4].

3. Results

The execution performance was primarily improved by adjusting the simulation resolution through the increase of the 3D mesh voxel size. More specifically, tripling the voxel size caused the execution time to be reduced by 97%, without the corresponding resolution reduction notably affecting the outputs. The OpenMP parallelization introduced a speedup of 16%-24%, since only the simulation on the cellular scale could be parallelized due to data dependencies and considering the bottleneck imposed according to Amdahl's law [5]. The algorithm of Fig 1 was tested for $N=20$ and $N=200$. As expected, increasing the number of VPs led to a more representative sample for the model parameters and to more clinically refined results. The inferred CKP mean values, which are summarized in Table 1, are in agreement with clinical experience in the sense that as the patient risk increases the effectiveness of therapy generally decreases [1].

Figure 1: The flowchart of the VPs algorithm that has been utilized in order to adapt the



CKP parameter to the clinical data for three distinct nephroblastoma patient groups.

Table 1: Mean CKP values for three patients that represent three distinct risk groups as produced by the algorithm of Fig 1 ($N=200$).

Patient risk	Low	Intermediate	High
CKPMEAN	0.88		0.86 0.49

4. Discussion and Conclusions

A workflow for the efficient creation of many virtual patients or avatars corresponding to a single actual patient has been presented and quantitatively analysed through the nephroblastoma paradigm. The latter could be integrated into decision support systems based on clinical digital twins.

5. References

1. G.Stamatakos et al, IEEE Journal of Biomedical and Health Informatics, 2014, vol. 18, no. 3, pp. 840-854.
2. A.Bucur et al, BMC Medical Informatics and Decision Making 07/2016; 16(S2).
3. <https://valgrind.org/> (visited on 8 Mar. 2022)
4. <https://openmp.org/> (visited on 8 Mar. 2022)
5. G.Amdahl, IEEE Solid-State Circuits Society Newsletter, 2007, vol. 12, no. 3, pp. 19-20.

Acknowledgments

The work was partly funded by the European Commission and the Greek GSRT through the project PersoRad (Ref: ERAPERMED2019-299). The clinical data was provided in anonymized form by Prof. Norbert Graf, University Hospital of Saarland, Germany.

21.1

How exascale supercomputers can help with complex multiphysics models: virtual populations in cardiovascular therapies

Mariano Vazquez^{1,2}

1 ELEM Biotech, Barcelona, Spain

2 Barcelona Supercomputing Center, CASE, Barcelona, Spain

mariano@elem.bio

1. Introduction

In this talk we will describe our efforts to move from a virtual-patient-centric paradigm to a virtual-population-centric one, and at what extent exascale is a decisive factor. We will focus on cardiovascular therapies, particularly in cardiac modelling.

2. Materials and Methods

Not every simulation of the biomedical domain requires supercomputers. However, when multiphysics or multiscale, tightly-coupled, comprehensive simulations are required, supercomputers are a must. Particularly, the fact that these complex simulations can have hundreds or thousands of input parameters requires (a) a smart way of selecting them to do something better than brute force attempts, and (b) the possibility of running at least hundreds of simulations in "human time". (a) means that instead of random combinations, these parameter variations must be defined assuring that each point in the design parameters space must represent a "realizable" patient, modelling a real one (for instance patients with 3 or 4 heart ventricles are not realizable).

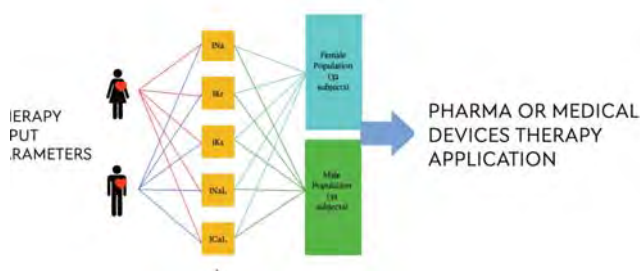


Figure 1: A human cardiac in-silico clinical trial pipeline.

Therefore, our goal will not be to run one massive heroic simulation on a virtual patient but to run hundreds of thousands of them in large meshes, although not so large to occupy, say, more than 10% of a supercomputer.

3. Results

In this talk we will describe how we move to this paradigm using Alya Red, our supercomputer-based multiphysics-multiscale cardiac modelling tool through different application examples.

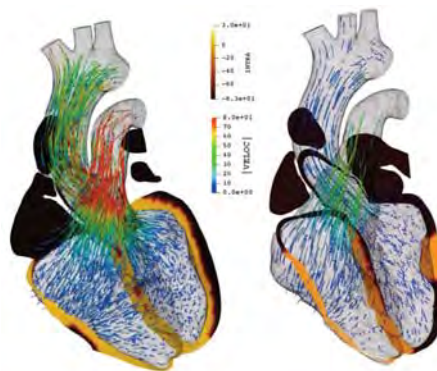


Figure 2: A left bundle branch block (LBBB) patient going through a CRT therapy. Left, the control heart, right, the diseased heart with a pacemaker implanted. Will he/she recover the cardiac function with the implant? Which is the sensitivity to pacemaker position and synchronization?

5. References

1. Santiago, A., Aguado-Sierra, J., Zavala-Aké, M., Doste-Beltran, R., Gómez, S., Arís, R., Cajás, J.C., Casoni, E. and Vázquez, M., 2018. International journal for numerical methods in biomedical engineering, 34(12), p.e3140. (2018).
2. Santiago, A., Butakoff, C., Eguzkitza, B., Gray, R.A., May-Newman, K., Pathmanathan, P., Vu, V. and Vázquez, M., 2022. PLoS computational biology, 18(6), p.e1010141.

Acknowledgements:

The authors would like to thank the European Research Council (CompBioMed2 Grant agreement ID: 823712 and PerMedCoE Grant agreement ID: 951773) and the Spanish Ministerio de Ciencia, Innovación y Universidades / Centro para el Desarrollo Tecnológico Industrial CDTI (EXP - 00123159 / SNEO-20191113 and Ayuda Torres Quevedo PTQ2018-010290) for providing financial support to this project.

21.2

Phase III In Silico Trials of new treatments for osteoporosis using exascale supercomputers

Marco Viceconti^{1,2}, Antonino Amedeo La Mattina^{1,2}, Alessandra Aldieri^{1,2}, Sara Oliviero^{1,2}, Cristina Curreli²

1 Industrial Engineering, Bologna, Italy

2 Alma Mater Studiorum - University of Bologna, Dept. Industrial Engineering, Bologna, Italy

1. Introduction

The clinical evaluation of efficacy for new bone drugs is complex, slow, and expensive, because most regulators require the bone fracture event as primary outcome for the clinical trial. But even at-risk populations show low incidences of fracture events, especially at the hip. Areal Bone Mineral Density (aBMD) measured with Dual X-ray Absorptiometry (DXA) was found correlated with the risk of fracture, but it is not a good predictor of the fracture event; for this reason, regulators accept aBMD only as a secondary outcome [1].

The Bologna Biomechanical Computed Axial Tomography (BoBCAT) is a CT-based patient-specific digital twin model that stratifies fractured and non-fractured patients with an accuracy significantly higher than aBMD [2]. While its use as secondary outcome in place of the aBMD is being evaluated by regulatory agencies, in this work we explore a much more advanced use case, where the technology is used to simulate a whole phase III clinical trial *in silico*.

2. Materials and Methods

BoBCAT couples a stochastic biophysics model of the patient's fall with a patient-specific finite element model to predict if the impact force will produce a hip fracture.

Starting from a collection of 94 patient-specific models, Taylor et al. [3] developed a statistical atlas of the morpho-densitometric variability of the patients' proximal femur. We used such atlas to generate two cohorts of 500 virtual patients, one representing a low-risk population the other a high-risk population.

Using a statistical regression of published clinical data, we developed a stochastic phenomenological disease model that progressively reduces the bone mineral density of each virtual patient, as the simulation time progresses. Using a Markov-Chain Monte Carlo algorithm we simulate a 10-years clinical trial in a placebo arm, as follows:

- Each time step the probability of falling calculates how many times each virtual patient falls in that time interval.
- For each fall, probability of fall conditions calculates the initial conditions of the fall, and the fall model calculates the impact force using height, weight, and soft tissue thickness at the hip.
- The patient-specific finite element model is run to calculate if that impact force intensity and direction will fracture that patient's femur or not; if it does, the patient is excluded from the rest of the simulation, having reached the fracture outcome.
- In all non-fractured patients, the disease model is used to calculate the new bone mineral density distribution as the disease progresses, to be used in the next time step.
- The simulation continues until all the virtual patients fracture or the time reaches the duration of trial (5 or 10 years).

Acknowledgements:

This study was partially supported by the H2020-funded projects CompBioMed2 (grant ID 823712).

21.3

A drop of blood at exascale: new answers that large-scale blood simulations can give in thrombotic and diabetic diseases

Gabor Zavodszky¹

1 University of Amsterdam Music Cognition Group, Computational Science Lab, Amsterdam, Netherlands
 g.zavodszky@uva.nl

1. Introduction

Blood is the single most important fluid in the human body. It has a fundamental role in most healthy and pathologic processes. Yet many of its properties are poorly understood primarily due to its complex cellular nature. Several computational tools are being developed [1] to address this, however, the scale of these simulations (both spatial and time) is rather limited due to high computational requirements.

In the following we present a high-performance cellular blood flow simulation that is targeted at large-scale applications. We present the combination of methods that make these scales feasible and demonstrate its application in a series of diabetic and thrombotic diseases.

2. Materials and Methods

The simulations are based on the open-source HemoCell [2]. This code was demonstrated to scale well above 260,000 CPU cores and therefore it allows the investigation of larger domains efficiently. Recent developments put focus on advanced boundary conditions, such as Lees-Edwards, rotating boundaries, and continuous cell inflows. These enable novel applications, specifically in relation to diabetic blood flows and thrombus formation, and make it possible to replicate complex *in vivo* and *in vitro* setups in the simulations.

3. Results

The most recent results and their connection to the novel developments will be presented, including the effect of the increased rigidity of diabetic red blood cells on platelet margination, the increase in wall shear stress in real retinal microaneurysms as cells are transported, and the effect of curved and stenosed geometries on high shear rate platelet aggregation [3]. Finally, the uncertainty quantification of the most sensitive component, the mechanical model of the cells is presented.

4. Discussion and Conclusions

The presented simulation techniques can successfully reproduce experimental conditions and can complement measurements with additional details that are not available with the current measurement technologies. The presented cases demonstrate how this can efficiently further our understanding on the respective pathologies.

5. References

1. Ye, Ting, et al., *Journal of biomechanics* 49.11 (2016): 2255-2266.
2. Závodszy, Gábor, et al., *Frontiers in physiology* 8 (2017): 563.
3. Spieker, Christian J., et al., *Annals of Biomedical Engineering* 49.12 (2021): 3609-3620.

Acknowledgements:

The authors acknowledge financial support by the European Union Horizon 2020 research and innovation programme under grant agreement no. 675451, the CompBioMed2 project. The use of supercomputer facilities in this work was sponsored by NWO Exakte Wetenschappen (Physical Sciences).

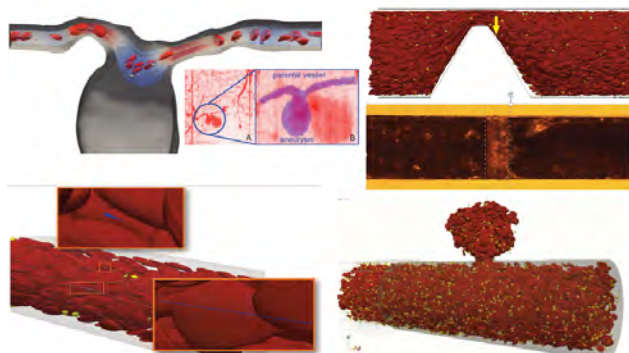


Figure 1: Example cases of a retinal micro-aneurysm circulation, the initiation of a high-shear thrombus, uncoiling of a protein chain in blood, and finally a punctured vessel.

21.4

Finding new cures from old drugs: ensemble Molecular Dynamics with exascale supercomputers enables high-throughput binding affinity for drug repurposing

Peter Coveney¹

1 University College of London, London, United Kingdom

Given the slow pace and substantial costs of new drug discovery and development, together with the urgency of the matter, repurposing of existing drugs for the ongoing disease is an attractive proposition. In a recent study, we use molecular dynamics simulation and an ensemble-based free energy approach to investigate the interactions of a set of existing drugs with the main protease of the SARS-CoV-2 virus. The drug-residue interaction profile elucidates the amino acids crucial to the drug binding while the detailed energetic insights into the nature of binding shed light on possible new routes to future rational drug design. We have coupled the machine learning (ML) and physics-based (PB) ensemble methods into a coherent scientific workflow, bringing together several methods of which some have already been applied in drug discovery while others are relatively new to the field and yet to be adopted. The workflow can be applied to the entire process of early drug discovery stage which involves hit discovery, hit to lead, lead optimization, and evaluation of potential side effects and toxicities. The ensemble computing pattern employs a high throughput "embarrassingly" parallel workload. This workflow is a suite of applications that collectively are able to scale up to exascale machines. We have demonstrated that the innovative, iterative and interactive heterogeneous workflow has the potential to accelerate the drug repurposing and drug discovery processes.

22.1

Whole heart mesh reconstruction for in vitro numerical simulations

Diogo F. Almeida¹, Moritz Jung¹, Yitong Li², André Mourato¹, Wen-Yang Chu¹, Simon Sonntag¹

¹ Virtonomy GmbH, München, Germany

² Technische Universität München, München, Germany

+almeida@virtonomy.io, Paul-Heyse-Strasse 6, 80336 München, Germany

1. Introduction

Whole heart segmentation allows performing patient-specific numerical simulations, improving medical implants' design or planning a cardiovascular intervention. Parallelly, convolutional neural networks have risen to the state-of-the-art approach to computationally reconstruct the segmented anatomy. In the recent years, new network architectures or minor improvements are found in the literature, but these are usually voxel-wise approaches followed by surface reconstruction and post-processing techniques. Because several of the heart analysis or numerical simulations rely on the mesh quality and it's time wise correspondence, having a high resolution, homogeneous, template mesh for each of the heart structures would allow on-the-fly measurements calculation or shape-related statistical analysis, for example. For these reason, we propose an approach based on a graph convolutional neural network to predict deformation on mesh vertices from a pre-defined mesh template to reconstruct multiple anatomical structures in a 4D image volume.

2. Materials and Methods

The mesh reconstruction pipeline [1] consists of three steps to predict the whole-heart meshes from a given medical image: an image encoding module, an image feature sampling module, a deep free-form deformation module that predicts control point displacements to deform the template mesh and a segmentation module that predicts a binary segmentation map to allow additional supervision using ground truth annotations. The training was performed on 106 image-mesh samples for 500 epochs.

By registering a template mesh to the in-image anatomies, node correspondence among each of the heart components. This provides support for several clinical applications, from statistical shape modelling to automatic measurements calculation, just to name a few.

The pipeline can be applied on time-series CT image data that consisted of images from 10 time frames over the cardiac cycle. By tracking a registered point throughout the cardiac cycle, the patient-specific displacement or the strains for a given heart structure or region can be estimated and used for medical device design and functional improvements

3. Results

An example of the mesh reconstruction is depicted in Fig. 1.

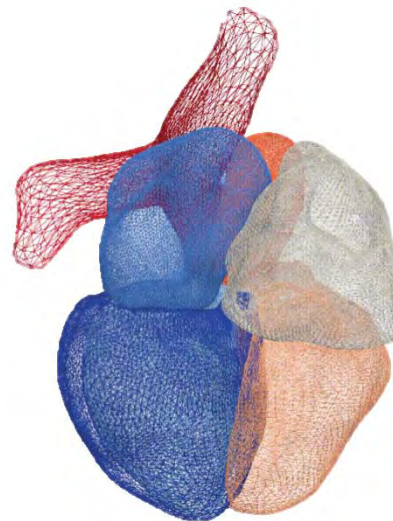


Figure 1: Whole heart mesh reconstruction.

	Myo	LA	LV	RA	RV	AO	PA	WH
DC	0.93	0.95	0.90	0.86	0.89	0.83	0.86	0.86
ASSD	1.26	1.14	0.97	1.28	1.94	1.93	1.98	1.50

Table 1: Dice coefficient and average symmetric surface distance (in mm) of the reconstruction.

4. Discussion and Conclusions

The presented approach has shown to accurately reconstruct whole heart geometries from medical images. Several clinical applications for the presented methodology were also shown.

5. References

1. Kong, F, Shawn CS. Int Conf on Medical Image Computing and Computer-Assisted Intervention.; 550-559 (2021).

22.2

Digital twin predicting diet response before and after long-term fasting

Oscar Arrestam¹, Christian Simonsson^{2,3}, Mattias Ekstedt^{3,4}, Peter Lundberg^{4,5}, Peter Gennemark^{1,6}, Gunnar Cedersund^{2,4}

1 Department of Biomedical Engineering, IMT, Linköping University, Linköping, Sweden, Sweden

2 Biomedical Engineering, IMT, Linköping University, Linköping, Sweden, Sweden

3 Center for Medical Image Science and Visualization, Linköping University, Linköping, Sweden, Sweden

4 Health, Medicine, and Caring Sciences, Linköping University, Linköping, Sweden, Sweden

5 Division of Medical Radiation Physics, at the Department of Health, Medicine and Caring Sciences, Linköping University, Linköping, Sweden, Sweden

6 Drug Metabolism and Pharmacokinetics, Research and Early Development, Cardiovascular, Renal and Metabolism (CVRM), BioPharmaceuticals R&D, AstraZeneca, Gothenburg, Sweden, Sweden

Correspondence: Gunnar Cedersund, Email: gunnar.cedersund@liu.se, +46-702-512323

1. Introduction

Today, there is great interest in diets proposing new combinations of macronutrient compositions and fasting schedules. Unfortunately, available studies measure different sets of variables in different situations of different populations, thus only providing partial and non-connected insights. We lack an approach for integrating all such partial insights into a useful and interconnected big picture. Lately, a new technology has been advocated that potentially can solve this problem: physiologically based digital twins. There are some well-established physiological models, but no available model can deal with changes between different diet compositions and fasting schemes. Herein, in our work, we present such a digital twin that allow us to simulate diet responses on a multi-organ and multi-time scale (minutes to weeks) (Fig 1).

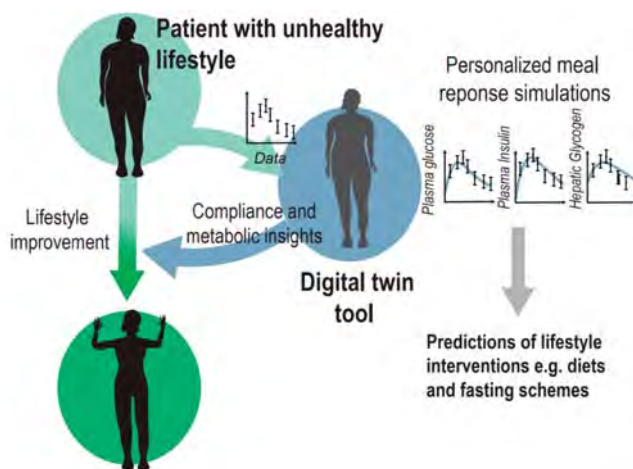


Figure 1: Illustration of patient and digital twin interplay

2. Materials and Methods

Model equations are based on human physiology and parameters were fitted to 4-time continuous and 3 non-time continuous clinical studies simultaneously, including both healthy and diabetic populations. Data from 4 clinical studies - not present in the estimation data - was used to test the new models' capabilities. Furthermore, an individual focused study ($n=3$) was conducted to further test the model's capabilities with a focus to validate protein metabolism combined with long-term fasting (48 h).

3. Results

We have extended the capabilities of our most recent digital twin model [1] which is based on the original Dalla Man model [2], to include: i) intracellular hepatic metabolism, ii) long-term energy regulation, iii) protein metabolism, and iv) prediction personification. The personification is based on person specific information (sex, height, weight, diabetes status) and a data-based calibration. Finally, using the integrated partial insights, 5 common diets: i) LCHF, ii) HCLF, iii) Intermittent fasting, iv) 5:2 diet, and v) SFM, were simulated and compared. Diet simulations qualatively agrees with several previous studies [3,4].

4. Discussion and Conclusions

Our work underlines the potential of digital twins in applications such as health optimization and educational purposes.

5. References

1. Herrgårdh T et al., *Front Physiol.* 2021; 12:619254
2. Dalla Man C et al., *IEEE Trans Biomed Eng.* 2007; 54(10):1740-9.
3. Holmstrup ME et al., *the European e-Journal of Clinical Nutrition and Metabolism.* 2010; 5(6):e277-e80.
4. Paoli A et al., *Nutrients.* 2019;11(4):719.

Acknowledgements:

Swedish Research Council (Grant IDs: 2018-05418, 2018-03319, 2020-04826 and 2014-6157), Knut and Alice Wallenberg Foundation (2020.0182), PRECISE4Q (777107), and VINNOVA (2020-04711).

22.3

Prediction of thrombosis in the arteriovenous grafts

Lotte Piek¹, Mohammad Rezaeimoghaddam¹, Bettine van Willigen¹, Frans van de Vosse¹, Wouter Huberts¹, Maarten Snoeijs²

¹ Department of Biomedical Engineering, Eindhoven University of Technology, the Netherlands

² Department of Vascular Surgery, Maastricht University Medical Center, Maastricht, the Netherlands

1. Introduction

Arteriovenous grafts (AVGs) are an appropriate option for vascular access in certain hemodialysis patients. However, AVG thrombosis due to stenosis near the venous anastomosis is a common complication resulting in graft failure. Computational models are powerful tools that can provide great support and information in medical research. The goal of this study is to obtain a realistic picture of risk factors leading to thrombus formation initiated by pathology in AVGs using computational fluid dynamics (CFD).

2. Materials and Methods

A biochemical model of platelet-fibrin kinetics to predict AVG thrombosis is developed based on our previously validated continuum model [1]. Platelet activation, aggregation, and the coagulation cascade are described by the transport and reaction of biochemical agonists into a series of coupled ordinary differential equations. One of the main proteins involved in thrombogenesis is the von Willebrand Factor (vWF) and its contribution has been recognized as the main mediator of high-shear thrombosis. Hence, a 2D model of the unfolding was created based upon earlier research [2].

In order to obtain clinical relevant results, a 1D wave propagation model coupled with a 0D model of the venous and arterial system in an arm is created. The coupled model is used to compute accurate pressure drop-flow rate due to stenosis for the follow-up data [4]. The pressures and flow rates are used for the boundary conditions of the 3D CFD model. The 3D reconstructed model is obtained from a patient specific AV graft MRI. Finally, a biochemical model of thrombus formation is solved to predict thrombosis.

3. Results

Figure 1 shows the results of the 2D model and was validated with experimental data [3].

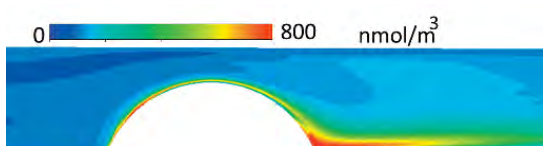


Figure 1: Concentration of unfolded vWF

Schematic of the coupled model and 3D CFD velocity streamlines at peak systolic for 2 weeks post-op and 12 weeks follow-up, are given in Figure 2.

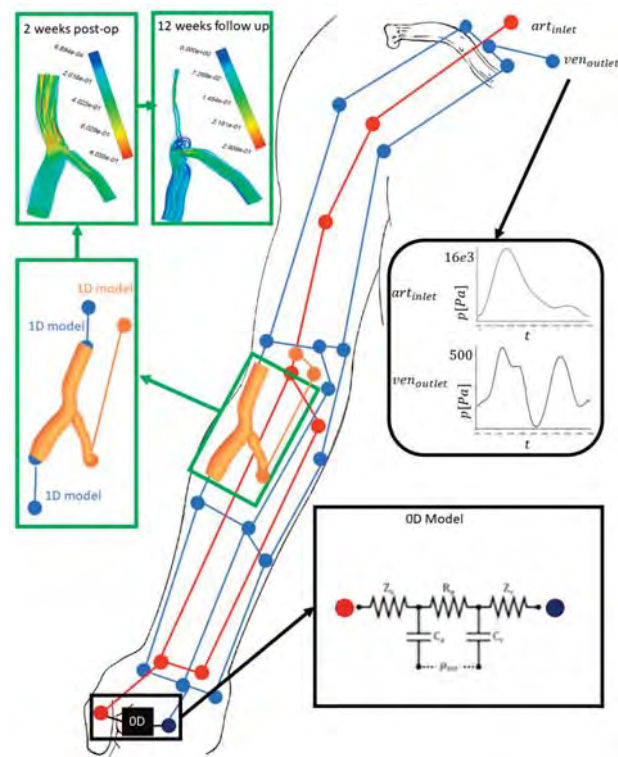


Figure 2: overview of the computational model

The verified thrombus formation model is used to perform simulations on the follow up scans to predict thrombosis. The preliminary results were quite promising (not shown here).

4. Discussion and Conclusions

A unique, multiscale model using 3D CFD and a coupled wave propagation model together with a novel thrombus formation model was proposed. This study would enable us to classify patients regarding the need for immediate medical treatment.

5. References

1. Rezaeimoghaddam et al. *J. Biomech.*, 110915, 2022.
2. Zhussupbekov et al. *Ann Biomed Eng*, 49(9), 2646–2658.
3. Westein et al. *PNAS*, 110(4), 1357–1362.
4. Kroon et al. *Comput. Math. Methods Med.*, . 2012.

Acknowledgements:

This work is supported by RegMed XB, the Vascular Access Society Research Grant and powered by Health~Holland, top sector life sciences & health.

22.4

Prediction of ventricular mechanics based on the degree of pre-operative ventricular outflow tract obstruction: in silico pulmonary valve replacement

Maria Gusseva^{1,2}, Tarique Hussain³, Camille Hancock Friesen⁴, Gerald Greil³, Dominique Chapelle^{1,2}, Radomír Chabiniok^{1,2,3,5}

1 Inria, Palaiseau, France

2 École Polytechnique, Palaiseau, France

3 UT Southwestern Medical Center, Department of Pediatrics, Dallas, United States

4 University of Nebraska Medical Center College of Medicine, Department of Surgery, United States

5 Czech Technical University in Prague, Department of Mathematics, Prague, Czech Republic

Corresponding author: Radomír Chabiniok, MD, PhD; E-mail: radomir.chabiniok@UTSouthwestern.edu

1. Introduction

Biomechanical modeling has been shown to be a promising tool in providing patient-specific mechanical indicators of the myocardium (e.g. myocardial contractility) that are not available in the clinical data [1]. In this work we aim to explore an ability of the biomechanical model to predict a response of the right ventricular (RV) mechanics to in silico pulmonary valve replacement (PVR) in patients with repaired tetralogy of Fallot (rTOF).

2. Materials and Methods

2.1. Patient-specific mechanical properties of the right ventricle and pulmonary circulation

Datasets of 19 rTOF patients undergoing percutaneous PVR and cardiac magnetic resonance were included in this study. Patients data of maximum and minimum pressures and volumes of RVs were used to create patient-specific biomechanical models pre- and post-PVR (PSM_{pre} and PSM_{post}, respectively) [1]. These models (Fig. 1) are defined by the patient-specific parameters of the pulmonary circulation (proximal and distal resistance and capacitances R_{prox}, R_{dist}, C_{prox}, C_{dist}); RV geometry and function (myocardial passive stiffness and active contractility), and mechanics of the RV outflow tract (RVOT forward and backward resistances, R_{for}[^]RVOT and R_{back}[^]RVOT, respectively).

2.2. In silico pulmonary valve replacement

Using PSM_{pre}, assuming the cessation of pulmonary regurgitation from the system and imposing a progressive decrease of the R_{for}[^]RVOT, we recalibrated ventricular contractility for a corresponding decrease in R_{for}[^]RVOT. We built in silico contractility vs. R_{for}[^]RVOT relationships post-PVR [2]. Finally, we confronted in silico contractility against that obtained in actual PSM_{post} in Section 2.1.

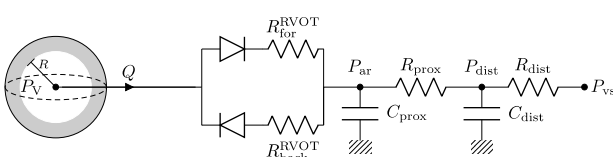


Figure 1: Coupling of the heart with circulation system represented by the system of diodes and 2-stage Windkessel.

3. Results

Predicted in silico contractility vs. R_{for}[^]RVOT relationships were linear for all patients (Fig. 2). The mean (9SD) difference of in silico vs. PSM_{post} contractility was 6.5 (93.0) %.

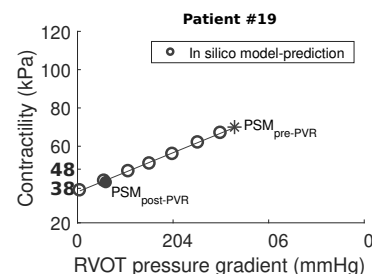


Figure 2: In silico prediction of right ventricular (RV) contractility post-PVR (empty circles) for patient #19. Star and filled circle show values given by patient-specific models pre- and post-PVR, respectively.

4. Discussion and Conclusions

In silico evolution of contractility post-PVR could provide an insight into hypothetical mechanical response of the ventricle based on the degree of pre-operative RVOT obstruction.

5. References

- Gusseva M et al., *Can J Cardiol*; 37, 1789-1807 (2021).
- Gusseva M et al., *Ann Biomed Eng*; 49, 3339-3348 (2021).

22.5

The Impact of Capillary Ageing on In Silico Brains: A Stroke Comparison

Wahbi El-Bouri^{1,2}

¹ University of Liverpool, Liverpool Centre for Cardiovascular Science, Liverpool, United Kingdom

² University of Liverpool, Department of Cardiovascular and Metabolic Medicine, Liverpool, United Kingdom

*Corresponding author: w.el-bouri@liverpool.ac.uk

1. Introduction

Age is the most important non-modifiable risk factor predicting outcomes of stroke and its treatment. To develop successful in silico clinical trials of stroke treatment [1], virtual populations of ageing brains are important. Here, age is introduced as a parameter in the simulation of stroke to determine its impact on lesion size.

2. Materials and Methods

2.1 Healthy and Stroke Scenarios The full-brain perfusion and stroke simulations are developed using the INSIST framework [1]. The porous representation of the microvascular network is used for the simulations [2]. A right middle cerebral artery occlusion (RMCAo) is simulated with a non-porous clot (Fig 1a,1b).

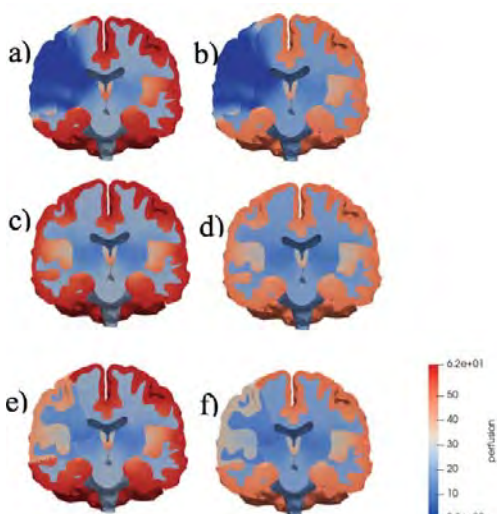


Figure 1: Perfusion maps of a) Middle aged (MA) RMCAo; b) Old RMCAo; c) MA micro-emboli; d) Old micro-emboli; e) MA pericytes; f) Old pericytes

2.2 Micro-emboli post-thrombectomy A micro-emboli shower is released after the clot is removed; the permeability and coupling coefficients of the microcirculation are updated using a previously published model [3].

2.4 Pericyte Contraction Assuming the stroke lasts long enough such that pericytes die and contract, we assume a 10% diameter reduction in capillaries in the focal region of the stroke (defined as < 30% of the original CBF).

2.5 Ageing Using a published model of capillary ageing, the permeability and coupling coefficients are updated to simulate ageing, using a 25% reduction in permeability and coupling coefficients [4].

3. Results

Simulations of the scenarios can be found in Fig 1. On average, older age brains have 20% less flow, yet the stroke lesion size was 10% larger in older brains (Table 1).

	Middle	Old	Old:Middle
Healthy (mL/min)	606	490	0.809
RMCAo (mL/min)	508	412	0.811
<i>Micro-emboli</i>			
(mL/min)	602	488	0.811
Pericytes (mL/min)	578	467	0.808
Stroke lesion volume (mL)	237	260	1.097

Table 1: Comparison of old and middle age for the different scenarios

4. Discussion

A model of the ageing capillary bed is implemented here in a full-brain stroke simulation, demonstrating the impact age has on CBF and stroke. Future work will extend ageing to the arterioles and large blood vessels such that in silico virtual populations of ageing brains are developed.

5. References

- [1] Konduri et al. *Fron. Neurology* 2020
- [2] Józsa et al. *Interface Focus* 2020
- [3] El-Bouri et al. *PLOS Comp. Biol.* 2021
- [4] Graff et al. *Fron. Ageing Neuroscience* 2022

Acknowledgements:

I would like to thank Tamás Józsa, Raymond Padmos, Stephen Payne, Alfons Hoekstra and the rest of the INSIST team.

22.6

Let's talk about sex differences in diabetic kidney

Sangita Swapnasrita¹, Aurélie Carlier¹, Anita Layton²

¹ Department of Cell-Biology Inspired Tissue Engineering, Maastricht University, the Netherlands

² Department of Applied Mathematics, Department of Biology, Cheriton School of Computer Science, and School of Pharmacology, University of Waterloo, Canada

*Corresponding: s.swapnasrita@maastrichtuniversity.nl

1. Introduction

Studies suggest that renal transporters vary sex-specifically along the nephron segments of rodents [1], thus, we hypothesise that the diabetes-induced changes in kidney may exhibit significant sex differences. The goals of this study are to assess the sex-dependent efficacy of an anti-hyperglycemic therapy that inhibits the sodium-glucose cotransporter 2 (SGLT2).

2. Materials and Methods

We developed computational models of kidney, for male and female patients with diabetes [2]. The segmental cell-based transport model is a composite model of one superficial nephron and five juxamedullary nephrons, weighted by their population found in kidney. The model predicts solute concentrations of 15 typical solutes found in kidneys along with fluid flow rates and hydrostatic pressure. We increased the plasma glucose concentration from 5mM in a non-diabetic case by 72% and 300% in (i) moderately (MD) and (ii) severely diabetic (SD) cases respectively. To model SGLT2 inhibition, we reduced SGLT2 activity by 90%.

3. Results

Without drug intervention, glucose excretion was absent in MD patients, similar to non-diabetic patients but increased to 0.6 mol/day in SD patients (Fig. 1, left). In MD, hypertrophy compensates for the increased glucose load. Na⁺ and Cl⁻ excretion was limited in either cases but urine K⁺ concentration increased in both sexes. Under SGLT2 inhibition, the glucose excretion increases up to 0.7 mol/day in MD and up to 2 mol/day in SD (Fig. 1, right). Severe natriuresis is observed in men with sodium excretion increased by 228% but limited in women (68%). The thick ascending limbs in women with higher activity of NKCC2 transporter is able to compensate for the lower Na⁺ absorption in the proximal tubules. Extreme diuresis is seen in all cases.

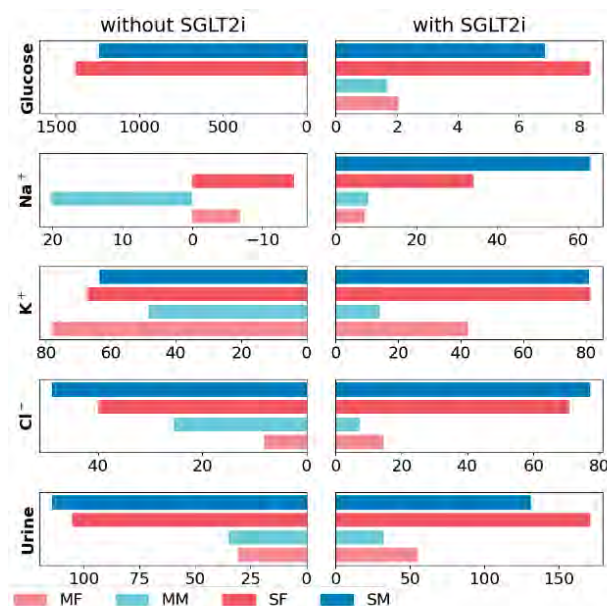


Figure 1: Solute concentrations and urine volume compared to levels in healthy patients. MF/MM: MD diabetic female/male, SF/SM: SD, SGLT2i: SGLT2 inhibition. [3]

4. Discussion and Conclusions

Model simulations suggest that by inducing osmotic diuresis in the proximal tubules, SGLT2 inhibition reduces paracellular transport, eventually leading to diuresis and natriuresis, albeit blunted in women, in part due to their higher distal transport capacity.

5. References

1. Veiras, L.C., et al., *J. Am. Soc. Nephrol.*, 2017. 28(12): p. 3504-3517.
2. Layton, A.T., et al., *PLoS Comput. Biol.*, 2019. 15(2): p. e1006108.
3. Swapnasrita S. et al., *Front. Physiol.*, p.14.

Acknowledgements:

Canada 150 Research Chair program and by the Natural Sciences and Engineering Research Council of Canada, via a Discovery award (RGPIN-2019-03916) The partners of Regenerative Medicine Crossing Borders (RegMed XB).

23.1

Deep Learning for Fast 3D Aortic CFD Simulations

Endrit Pajaziti¹, Claudio Capelli¹, Silvia Schievano¹, Raphael Sivera¹, Javier Montalt Tordera¹, Vivek Muthurangu¹

¹ University College London, Institute of Cardiovascular Science

*Corresponding author: endrit.pajaziti.13@ucl.ac.uk

1. Introduction

The integration of routine computational fluid dynamics (CFD) in clinics is an ongoing challenge due to a multitude of factors. The complexity involved in setting up simulations, along with long processing times and large computing requirements has made them inaccessible for routine clinical use. Machine learning has been proposed as a tool for bypassing these issues [1]. In this study we built models for rapidly inferring full 3D pressure and velocity flow fields on aortic geometries, aiming for results comparable to traditional CFD solvers.

2. Materials and Methods

2.1 Generation of CFD training data

Our training data consisted of 67 aortic arches from patients diagnosed with coarctation of aorta (CoA). Surface meshes were generated via segmentation of cardiac magnetic resonance (CMR) images. A statistical shape model (SSM) was built using the original data. This was used to generate 1650 additional synthetic aortic surfaces. After filtering out inappropriate cases, 1646 total aortic surfaces remained. CFD simulations were performed using Fluent 19.0 (Ansys) on all 1646 subjects. Boundary conditions included a uniform velocity profile of 1.3m/s applied at the inlet, with a 0 gauge pressure outlet. In post-processing, each subject flow field was interpolated onto grids in complete correspondence (27,420 nodes).

2.2 Development of ML model

Principal component analysis (PCA) was used to reduce high dimensionality shape and CFD data into low dimensional representations. This was done to enable neural network training. Two deep, fully-connected neural networks (DNN) were trained to output 3D pressure and velocity fields when presented with a low-dimensional shape vector. Implementation was done on Keras and TensorFlow 2.0. The training set was composed of 1546 subjects. Hyperparameter tuning was conducted with a 5-fold cross validation. A mean average error (MAE) loss function was used. Evaluation was performed on the 100 remaining test subjects. Normalised mean average error (NMAE) was used to assess final model performance.

3. Results

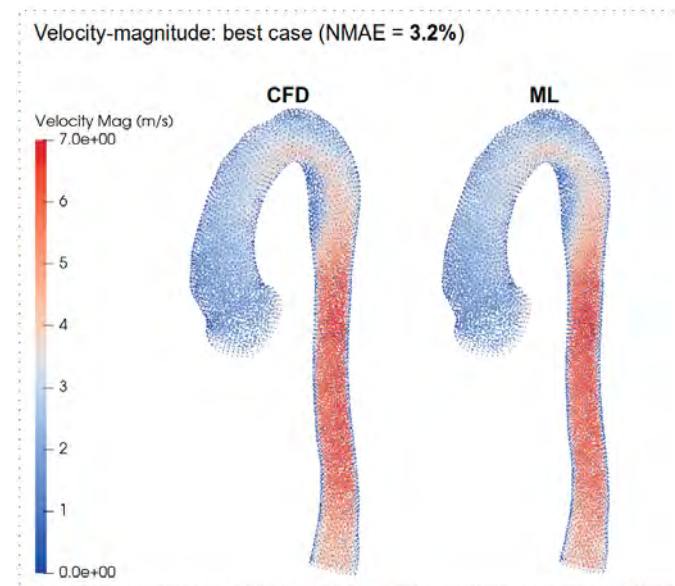


Figure 1: A single comparison between ground truth (CFD) and ML velocity magnitude 3D fields.

Model testing was performed on 100 subjects. Inference time was ~0.07 seconds per prediction. The average error (NMAE) for pressure and velocity was found to be $4.33\% \pm 1.68$ SD and $5.18\% \pm 1.20$ SD, respectively.

4. Discussion and Conclusions

ML has shown to be a suitable approach for creating surrogate models able to reproduce aortic CFD in real-time with a high degree of accuracy. In the future, patient-specific boundary conditions should be implemented in this model for clinical use. This approach could also enable doctors to simulate exercise conditions or potential treatment options non-invasively, contributing towards the vision of a cardiac digital twin.

5. References

1. L. Liang, W. Mao, and W. Sun, *J. Biomech.*, vol. 99, 2020.

23.2

Development of a real-time numerical tool for endovascular navigation by active catheterization

Arif Badrou¹, Nahiène Hamila², Nicolas Tardif¹, Anthony Gravouil¹, Aline Bel-Brunon¹, Nathan Lescanne³, Jérôme Szewczyk³

¹ Univ Lyon, INSA Lyon, CNRS, LaMCoS, UMR5259, Villeurbanne, France

² Ecole Nationale d'Ingénieurs de Brest, ENIB, UMR CNRS 6027, IRDL, Brest, France

³ Basecamp Vascular, Paris, France

Corresponding author: Arif Badrou, arif.badrou@insa-lyon.fr

1. Introduction

In recent years, endovascular therapies have grown significantly. In 20% of cases, the targets are so-called complex and navigation may fail [1]. To overcome these difficulties, a new active guidewire was developed. We have built a finite element model to simulate the navigation of this device into a patient-specific aortic geometry, validated against phantom experimental data. However, simulations are heavy and include many parameters related to tool design and navigation sequences. So, we developed in this work a numerical tool for decision support using a reduction model method named HOPGD (High-Order Proper Generalized Decomposition) [2], based on our model.

2. Materials and Methods

The model implemented in LS-DYNA (ANSYS, Inc.), computes the active guidewire navigation and shows that, besides patient anatomy, navigation depends mostly on 7 parameters. A numerical chart was built, based on HOPGD, to provide in real-time the simulation result for any combination of the 7 mentioned parameters, for a given patient anatomy. For each parameter, minimum and maximum values were chosen after a preliminary sensitivity analysis. 2^7 snapshots, corresponding to the vertices of a hypercube, fed the HOPGD. Here, the quantity of interest was the guidewire position during navigation. So, to evaluate the chart accuracy, we computed the error δ with the L_2 matrix norm as follows:

$$\delta = \frac{\|\mathbf{U} - \mathbf{U}_{red}\|}{\|\mathbf{U}\|}$$

where \mathbf{U} and \mathbf{U}_{red} contain the reference and the HOPGD-computed guidewire position along time, respectively. If $\delta > 5\%$, the snapshots grid was locally refined.

3. Results

A numerical chart was created using the HOPGD method (see Fig.1).

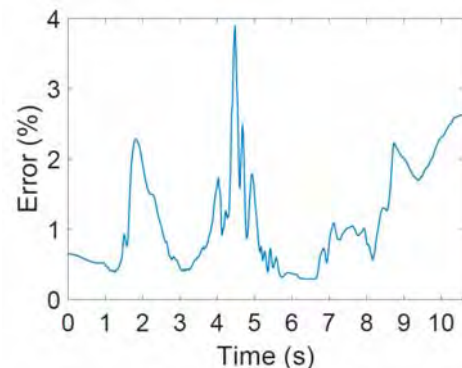
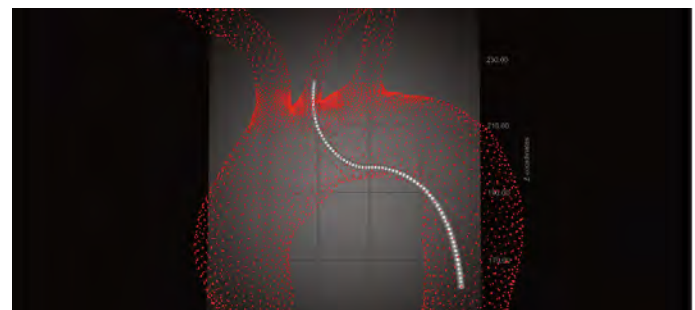


Figure 1: Real-time visualization of the guidewire position in the patient-specific anatomy (left) and error at the hypercube center (right).

432 snapshots were computed. Each snapshot required a simulation time around 3 hours using 2 Xeon 2.30 GHz cores. The reduced model computes the response in 10^{-3} s for each new set of parameters inside the hypercube.

4. Discussion and Conclusions

The obtained numerical chart generates accurate results along the navigation. It could be applied to other families of aortic anatomy to provide guidewire design and navigation indications for any patient.

5. References

1. Madhwal S et al., *J Invasive Cardiol*; 20:200-204 (2008).
2. Lu Y et al., *Int J Numer Methods Eng*; 114(13):1438-1461 (2018).

Acknowledgements:

The French National Research Agency (ANR) partially supported this work through the DEEP project: Devices for augmented Endovascular navigation in complex Pathways (grant n°ANR-18-CE19-0027-01).

23.3

In-silico calibration of thrombosis models using clinical incidence rates of spontaneous thrombosis in intracranial aneurysms

Qiongyao Liu^{1,2}, Yongxing Wang^{1,2}, Ali Foroushani^{1,2}, Michael Macrauld^{1,2}, Christopher Kelly¹, Nishant Ravikumar¹, Zeike A. Taylor¹, Toni Lassila¹, Alejandro F. Frangi^{1,2}, Fengming Lin¹, Yan Yia¹, Tufail Patankar³

1 Centre for Computational Imaging and Simulation Technologies in Biomedicine (CISTIB), School of Computing, Leeds,

2 Leeds Institute for Cardiovascular and Metabolic Medicine (LICAMM), Leeds School of Medicine, Leeds, United Kingdom

3 Leeds General Infirmary, United Kingdom

E-mail: mnqli@leeds.ac.uk

1. Introduction

Thrombus formation in intracranial aneurysms (IAs) plays a crucial role in their treatment by endovascular interventions. In large and giant aneurysms (>10 mm), the presence of spontaneous thrombosis (ST) may further modulate the treatment response. This in-silico study aims to estimate the prevalence of ST and demonstrate how clinical ST incidence data guides computational thrombus formation modelling by identifying plausible ranges of model parameters. We also investigate how ST differs in normo- and hypertensive conditions, modelled as boundary conditions from a Multivariate Gaussian Model (MGM) [1] and a Cerebral Autoregulation System (CARS) [2].

2. Materials and Methods

Through a systematic review, we estimated the clinical ST incidence rate in large and giant aneurysms. Using the ST incidence rate, we performed an in-silico observational study in 109 patients to calibrate two trigger thresholds, residence time (RT) and shear rate (SR), in our model [3]. As shown in Fig. 1, we created an automatic workflow to segment the image data, generate volume meshes, impose boundary conditions and run the simulations on a high-performance computing platform, MULTI-X (<https://multi-x.org>).

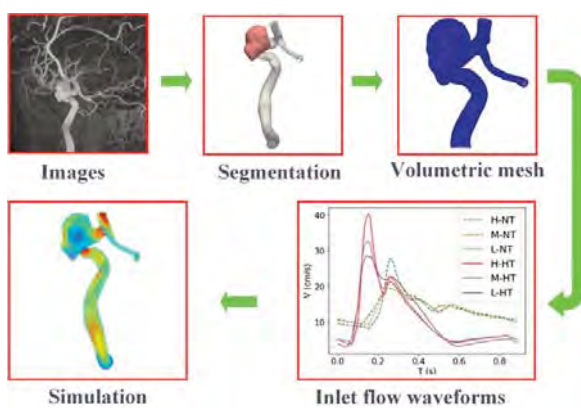


Figure 1: Automatic workflow on MULTI-X.

3. Results

According to our statistical analysis, the clinical ST incidence is $24.10\% \pm 7.94\%$ for large IAs (>10 mm and <25 mm) and $43.33\% \pm 6.08\%$ for giant IAs (≥ 25 mm), with 90% confidence. These statistical ST incidences are used as criteria to calibrate the thrombosis trigger thresholds. The overlap of these parameters at high, mean, and low normotensive flow waveforms, generated by a MGM model, represents the plausible range of thresholds because it indicates where the thresholds are largely independent of the inter-subject flow variability (Fig. 2).

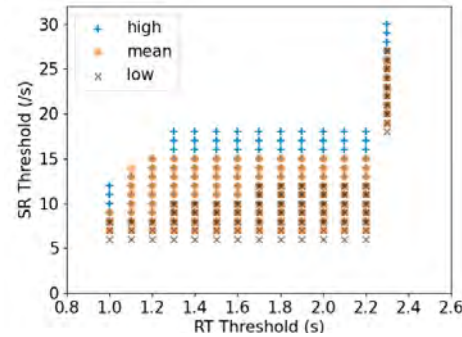


Figure 2: Scatter plot of trigger thresholds by matching the clinical ST incidence rate.

4. Discussion and Conclusions

Our calibrated model predicts that the ST incidence is slightly lower in hypertensive patients than in normotensive patients due to the lower maximum RT and the higher minimum SR in the aneurysm sac caused by hypertension. This study not only collates ST literature and improves our clotting model by providing more accurate threshold parameters, but also reveals that ST may be less common in hypertensive patients with large and giant IAs.

5. References

1. A. Sarrami-Foroushani et al., *J Biomech* 49(16): 3815–3824, 2016.
2. T. Lassila et al., *INT J NUMER METH BIO*, 36(1):e3271, 2020.
3. A. Sarrami-Foroushani et al., *J Biomech* 91: 7–13, 2019.

Acknowledgements:

We acknowledge support from the Royal Academy of Engineering Chair in Emerging Technologies (CiET1819/19).

23.4

In-silico flow diverter performance assessment in posterior communicating artery aneurysms

Michael Macrauld^{1,2}, Shuang Song¹, Ali Sarrami-Foroushani¹, Nishant Ravikumar¹, Christopher Kelly¹, Toni Lassila¹, Zeike Taylor¹, Alejandro Frangi^{1,3}

1 Centre for Computational Imaging and Simulation Technologies in Biomedicine

2 EPSRC Centre for Doctoral Training in Fluid Dynamics

3 Leeds Institute for Cardiovascular and Metabolic Medicine

Corresponding author: scmm@leeds.ac.uk

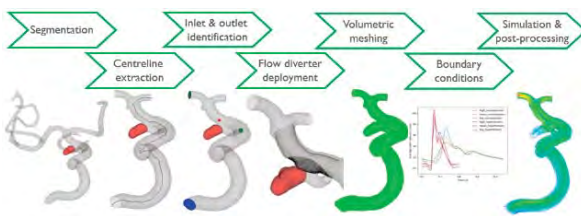
1. Introduction

Posterior communicating artery (PComA) aneurysms account for 25% of all aneurysms [1]. Despite their prevalence, flow diversion (FD) with Pipeline Embolization Devices is not FDA-approved for this subgroup. We performed an in-silico trial (IST) of PComA aneurysm FD, investigating: (i) What is the relationship between FD success and PComA patency [2]? (ii) Which aspect of FD is inhibited in the presence of fetal posterior circulation (FPC) [3]?

2. Materials and Methods

The PComA IST used an automated pipeline, comprising of steps shown in Fig. 1.

Figure 1: Automated in-silico trial pipeline.



An initial cohort of 17 patients was used. For each patient we simulated transient haemodynamics with two physiological states: rest and exercise. FD was assessed through post-treatment reduction in space-and-time-averaged velocity (STAV) in the aneurysm. PComA patency was assessed through post-treatment change in STAV at the PComA outlet and change in pressure drop along the PComA.

3. Results

We use PComA size as a marker for FPC, as in fetal patients the PComA is enlarged. Preliminary results show a weak trend towards greater aneurysm flow reduction and increase in PComA outlet flow post-treatment in smaller PComAs. They also show some correlation between treatment success and PComA patency measures, with greater flow reduction in patients with increase in PComA outlet flow and decrease in PComA pressure drop post-treatment.

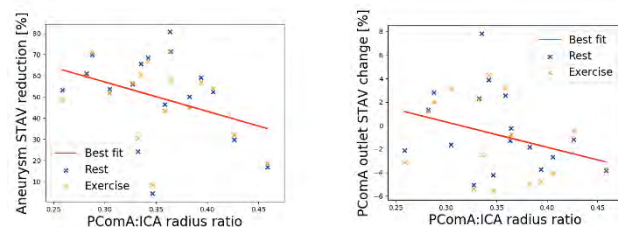


Figure 2: Aneurysm flow reduction (left) and PComA flow change (right) vs PComA size.

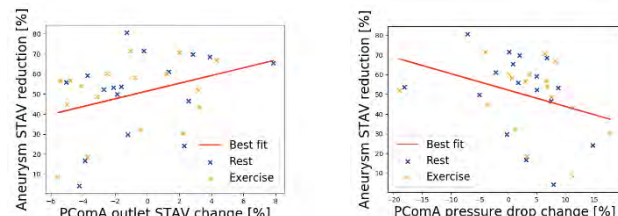


Figure 3: Aneurysm flow reduction vs PComA flow change (left) and pressure drop change (right).

4. Discussion and Conclusions

Larger PComAs demand more flow distally and maintain flow following treatment by PED [3], which is thought to reduce treatment success due to persistent flow through the PED into the aneurysm. We do find worse aneurysm flow reduction in larger PComAs, but conversely, we find larger PComAs are more likely to experience post-treatment flow reduction. We see improved aneurysm flow reduction in cases where PComA outlet flow increased post-treatment and where PComA pressure drop decreased, which conflicts at present.

5. References

1. Golshani, K, et al., *Surg Neurol Int*, 2010.
2. Daou, B, et al., *J Neurosurg*, 126 564-569, 2017.
3. Rinaldo, L, et al., *World Neurosurg*, 127 e1232-e1236, 2019.

Acknowledgements:

We acknowledge support from ANSYS through an Academic Partnership agreement, and funding from EPSRC (EP/L014823/1) and the RAEng (CiET1819/19; LTRF2021/17115).

23.5

Uncertainty Quantification of Hemodynamic Parameters for Cerebral Aneurysm Rupture Risk Assessment

Adriano Schlierf¹, Jan Brüning¹, Samuel Voss², Philipp Berg², Leonid Goubergrits¹

1 Charité - Universitätsmedizin Berlin, Institute for Computer-Assisted Cardiovascular Medicine, Berlin, Germany

2 Otto von Guericke University Magdeburg, Forschungscampus STIMULATE, Magdeburg, Germany

1. Introduction

Cerebral aneurysms are pathologies of the vasculature in the brain, resulting in deformations of the affected vessel. These deformations are associated increased risk of aneurysm rupture and thus subarachnoid haemorrhage, which can be lethal or cause severe neurological impairments. While treatment of aneurysms is feasible, it is also associated with peri- and post-procedural risks. Thus, individualised rupture risk assessment is desired to identify which aneurysm must be treated. Here, image-based reconstruction and modelling became important tools for assessing rupture risk parameters.

During the Multiple Aneurysms AnaTomy CHAllenge (MATCH), five cerebral aneurysms were reconstructed by different research groups [1]. Based on these reconstructions, the uncertainty of different geometric risk parameters was investigated previously [2]. Now, also the uncertainty in hemodynamic risk parameters will be assessed.

2. Materials and Methods

Using the reconstructions performed by 26 groups during MATCH, hemodynamic simulations were performed using STAR-CCM+ [3]. Spatiotemporal pressure, wall shear stress and velocity fields were exported for each aneurysm. Different hemodynamically relevant parameters defined at the aneurysm wall (11), the aneurysm neck (8) and within the aneurysm sac (7) were identified from literature and subsequently evaluated. The correlation between all parameters belonging to each respective group was calculated. Furthermore, the uncertainty range of each parameter was quantified.

3. Results

Correlations between parameters were low unless parameters described similar physical properties. For example, high correlations between mean and maximum pressures in the aneurysm volume but no correlations between pressures and velocities were identified. Almost all parameters featured relatively high relative uncertainty. Parameters with relatively low uncertainty were velocity measures as well as the aneurysmal low shear area, a parameter often associated with aneurysm growth and increased rupture risk.

4. Discussion and Conclusions

Overall, the uncertainty of hemodynamic parameters is larger than that of geometric parameters. As the same simulation approach was used for all aneurysms, the observed uncertainties can directly be attributed to the geometric differences. This uncertainty must be considered as a lower bound, as additional effects of the numerical method will further increase real world uncertainty.

The choice for hemodynamic parameters used for rupture risk assessment in cerebral aneurysms must be based on the discriminatory power of these parameters but also on their relative uncertainty. Independent of the chosen parameters, further standardization for image-based reconstruction and hemodynamic simulation is necessary.

5. References

1. Berg P. et al. *Cardiovasc Eng Technol*; 9(4):565-581 (2018).
2. Goubergrits L. et al. *Biomed Eng Online*; 18(1):35 (2019).
3. Voß S. et al. *PLoS One*; 14(5):e0216813 (2019).

23.6

Coronary flow and ffr prediction: part 1 - numerical modelling and experimental validation

Boris Chernyavsky¹, Alexey Velikorodny¹, D.Sucher¹

1 BioME Science, Paris, France

Corresponding author: B. Chernyavsky, - b.chernyavsky@biome-science.net

1. Introduction

Coronary artery disease and atherosclerotic plaques in the major arteries are one of the leading causes of death worldwide.

We propose an integrated numerical simulation package, which consists of a reduced-order numerical model used to simulate blood flow through a cardiovascular network and an IT solution with graphical interface (see Part II for details) allowing medical professionals to semi-automatically feed the patient-specific CT/MRI scans into the solver and to obtain simulation results in a flexible post-processed format.

2. Materials and Methods

The numerical simulation model uses a set of 1-D conservation equation for the pulsating flow, similar to the ones successfully used in the previous works (e.g. [1]) in this field. The model includes simulation of stenosis of various length, effective obstruction and the blood vessels bifurcations [2]. Validation of numerical model is carried out against experimental results obtained from a controlled experiment using 3D-printed cardiovascular network model (Fig. 1). Utilization of the in-vitro along with in-vivo measurements allows better control and fine-tuning of the model parameters.

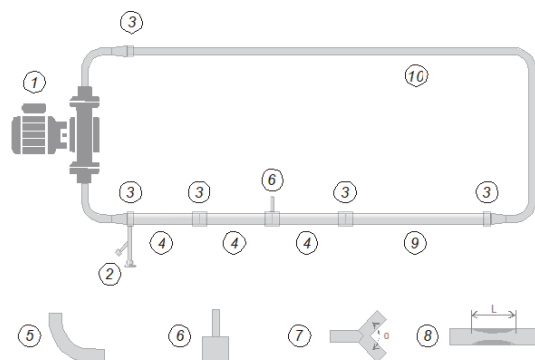


Figure 1: Experimental setup for invitro validation.

3. Results

A series of numerical experiments has been conducted using geometric and inflow data obtained from both invivo measurements and from controlled invitro experiments. Time-resolved and averaged primary (e.g., flow rate and pressure) and derived (e.g., FFR – Fractional Flow Reserve) parameters were obtained and compared against experimental results (Fig. 2), demonstrating reasonable agreement.

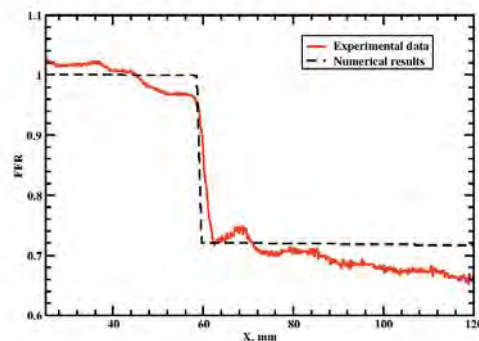


Figure 2: Comparison of measured and calculated FFR along the LAD artery with a plaque.

4. Discussion and Conclusions

Proposed simulation package provides medical professionals with an easy-to-use non-invasive tool for clinical decision making. Present numerical model adequately predicts clinically important parameters. Further improvements can be obtained by introducing modules accounting for additional physical mechanisms.

5. References

- Olufsen M et al, Numerical Simulation and Experimental Validation of Blood Flow in Arteries with Structured-Tree Outflow Conditions, *Ann. Biomed Engg.*, 28(11): 1281-1299 (2000).
- Steele B et al., In Vivo Validation of a One-Dimensional Finite-Element Method for Predicting Blood Flow in Cardiovascular Bypass Grafts, *IEEE Trans Biomed Engg.*; 50(6): 649-656 (2003).

24.1

A Quantitative Imaging Method for Reconstruction of Muscle Architecture using 3D Ultrasound

Annika Sahrmann¹, Geoffrey Handsfield², Oliver Röhrle¹

¹ Institute for Modelling and Simulation of Biomechanical Systems, Stuttgart, Germany

² Auckland Bioengineering Institute, The University Of Auckland, Auckland, New Zealand

*: Corresponding author: sahrmann@imsb.uni-stuttgart.de

1. Introduction

Subject-specific knowledge of a muscle's geometry and its fascicle orientation in 3D are key ingredients for computational models. However, determining these quantities in 3D is typically achieved with Diffusion Tensor Imaging (DTI), which comes with limitations such as long acquisition times. Although ultrasound can overcome some of the limitations, there exist only a few ultrasound studies that focus on fascicle architecture in 3D [1]. In this work, we propose a method for using 3D ultrasound to determine both fascicle and volume information.

2. Materials and Methods

We acquired ultrasound images using a Supersonic Imagine Aixplorer MACH at a 35 Hz frame rate. We used a 3D printed transducer holder for mounting reflective markers. An 8-camera VICON motion capture system recorded at a frame rate of 100 Hz. We triggered the motion capture and the ultrasound system with an Arduino and calibrated the system spatially and temporally.

For validation purpose, we used a custom designed 3D printed phantom consisting of 2 differently oriented groups of nylon wires: 18 parallel wires in a 6x3 arrangement and 2 parallel single wires. All wires are 0.1mm diameter and run from wall to wall. We mounted a marker holder on the phantom to identify the wires' locations.

We repeated this workflow for the tibialis anterior muscle.

3D reconstruction included: 1) determining a reconstruction volume, a nearest neighbour based algorithm for 2) bin filling and 3) hole filling. Based on the segmentation of the 3D reconstruction, the volume is determined.

For enhancing the wire directions on the reconstructed 3D image, we used a method for Multiscale Vessel Enhancement Filtering (MVEF) [2]. We implemented two algorithms for determining the wire directions: 1) we used the directions from the MVEF method; 2) we determined the wire directions by applying a random sample consensus (RANSAC) line detection algorithm.

3. Results

For quantitative analysis, we computed the angle between the two different wire directions and compared them to the reference from the phantom's coordinates (Figure 1A-C). We found a median angle error of less than 1° for the RANSAC algorithm and 2° for the MVEF method. Application on the muscle geometry qualitatively matches the muscle's expected architecture (Figure 1D).

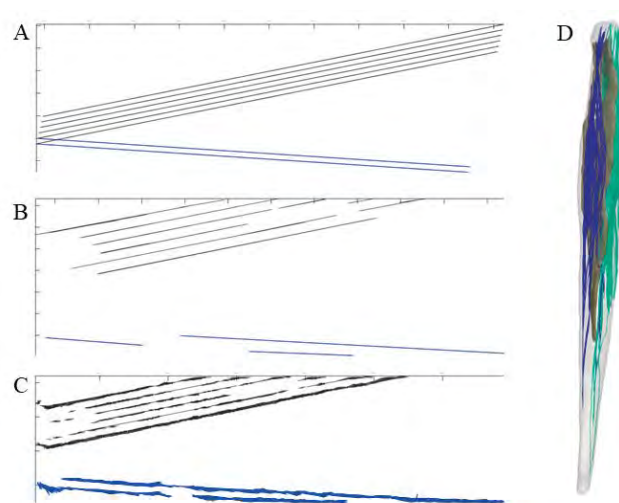


Figure 1: (A) Muscle fascicles on TA from 3D ultrasound images. Phantom wire arrangement in (B) the phantom as reference, the recognized directions from (C) RANSAC and (D) MVEF.

4. Discussion and Conclusions

This work proposes a novel method for determining muscle fascicle arrangement by using ultrasound. In future studies, we will use our method to compute the pennation angle between muscle fascicles and the aponeurosis. We will also compare our results to DTI data.

5. References

1. Rana M, Wakeling JM. *J Biomech*; 44(11):2129-2135 (2011)
2. Frangi et al, MICCAI 1998 conference: Springer, 19989, p. 130-13

Acknowledgements:

This project has received funding from the German Research Foundation (DFG) as part of the International Research Training Group "Soft Tissue Robotics" (GRK 2198).

24.2

The role of muscle pre-stretches in three-dimensional continuum-mechanical musculoskeletal system models.

Oliver Röhrle^{1,2,3}, Okan Avci²

1 University of Stuttgart, Institute for Modelling and Simulation of Biomechanical Systems (IMSB), Stuttgart, Germany

2 Fraunhofer Institute for Manufacturing Engineering and Automation, Stuttgart, Germany

3 University of Stuttgart, Stuttgart Center for Simulation Science (SC SimTech), Stuttgart, Germany

Corresponding author: Oliver Röhrle, Institute of Modeling and Simulation of Biomechanical System, University of Stuttgart, Pfaffenwaldring 5a, roehrle@simtech.uni-stuttgart.de

1. Introduction

The geometrical representation of musculo-skeletal system models is typically obtained by segmenting anatomical images like medical CT, MRI, or DTI, cf. [1]. They can provide highly detailed information on the system structure, but it lacks information on the functional aspect, such as, for example the state of the pre-stretch or the level of activation of a particular muscle. In particular the choice of pre-stretch in musculoskeletal models plays a crucial role.

2. Materials and Methods

A 5-muscle upper limb finite element model, as depicted in Figure 1, is employed to study the impact of the pre-stretch on the overall range of motion. In addition, an optimization criterion will be proposed that leads to optimal pre-stretch values of the respective skeletal muscle will be optimized such that the range of motion of the musculoskeletal system model is maximized.



Figure 1: The 5-muscle finite element upper limb musculoskeletal system model.

The employed constitutive law is similar to the one proposed in [2]. For simplicity, the elbow is considered to be a hinge joint. The sensitivity of the pre-stretch with respect to overall achievable muscle motion is computed and evaluated.

3. Results

The biceps, triceps, and brachialis are, for example, the muscles that influence the overall muscle motion during extension. To reduce the overall computational time of the respective inverse problem, surrogate models are employed. The pre-stretch was able to be determined in such a way, that the range of motion was maximal. The final optimized results show a range of motion that is close to the physiological range of motion. Different activation scenarios will be considered, and the influence on the overall motion will be analysed.

4. Discussion and Conclusions

Deviations from the full range of motion are due to the assumption made with respect to the constrictive law. Improved material parameters would eliminate this problem. The need for appropriate pre-stretches is not only a challenge for continuum-mechanical skeletal muscle modelling frameworks, but also for multibody ones. Despite the significantly large body of literature reporting on multibody musculoskeletal system models, there also seems to be a lack of appropriately determining muscle's pre-stretch. A similar approach can be adopted.

5. References

1. Ramasamy E. et al. *Frontiers in Bioengineering and Biotechnology* 3.12 (2018),
2. Röhrle, O., Sprenger, M., and Schmitt S. *Biomechanics and modeling in mechanobiology* 16.3 (2017), pp. 743–762

Acknowledgements:

The research was partially funded by the Deutsche Forschungsgemeinschaft (DFG, German Research Foundation) under Germany's Excellence Strategy – EXC 2075-390740016 and through BMBF 3DFoot under contract numbers 01EC1907B

24.3

Towards a digital paediatric twin: A statistical shape model for bone shape and clinical bone measurement prediction

Laura Carman¹, Julie Choisne¹, Thor Besier¹, Sue Stott²

1 Auckland Bioengineering Institute, The University Of Auckland, Auckland, New Zealand

2 Faculty of Medical and Health Sciences, University of Auckland, Department of Surgery, Auckland, New Zealand

Correspondence: j.choisne@auckland.ac.nz

1. Introduction

Children are not small adults, yet we often scale down musculoskeletal models developed from an adult database to create paediatric models. About 25% of the world population are aged 15 years and under, this population is not well represented by current digital twins [1].

2. Materials and Methods

Post-mortem CT scans of 333 children (137F, Age: 4-18y, H: 148 ± 24 cm, M: 49 ± 22 kg) were obtained from VIFM (Melbourne, Australia). The pelvis (P), femurs (F) and tibias/fibulas (TF) were segmented. Each bone was fitted and rigidly aligned to a template mesh to achieve nodal correspondence. The shape model was characterized using principal component analysis [2]. Leave one out (LOO) analysis determined the predictive power of the model using demographic (age, height, mass, sex) and bone measurements (thigh and shank length, hip, knee, and ankle width).

Subsequently, bone linear and angular measurements were automatically derived for each participant from bone landmarks. Two-way ANOVA was used to determine the overall influence of age/height and sex on each measurement and significant sex differences for each age/height category.

3. Results

The results from the LOO analysis gave an average RMSE and (DICE score) between the segmented bone and predicted bone of; P: 2.9 ± 1.0 mm (0.77), F: 2.0 ± 0.6 mm (0.89), TF: 1.9 ± 0.5 mm (0.86).

All pelvis measurements showed increasing relationships with both age and height (Figure 1). Femoral and tibial length, epicondylar, condylar and malleolar width, and femoral head diameter, also showed increasing relationships with age and statistically significant sex differences from age 14 onwards.

4. Discussion and Conclusions

Our shape model performs better than linear scaling [2]. The model will next be articulated at the hip and knee with optional inputs of medical imaging and motion capture data.

We developed a method for automatically capturing bone measurements and rotational profiles in children aged 4-18 years. This rich dataset can be used as a resource for researchers and clinicians to understand typical development and form a baseline for comparison to children with atypical bone development.

5. References

1. Osanlouy M et al, *Front. Physiol.* 12; 2021. DOI: 10.3389/fphys.2021.693735
2. Carman L et al, *Sci. Rep.* 2022, 12 (3251).

Acknowledgements:

The University of Auckland Doctoral Scholarship, the Health Research Council of New Zealand, the Aotearoa Fellowship and the Friedlander Foundation.

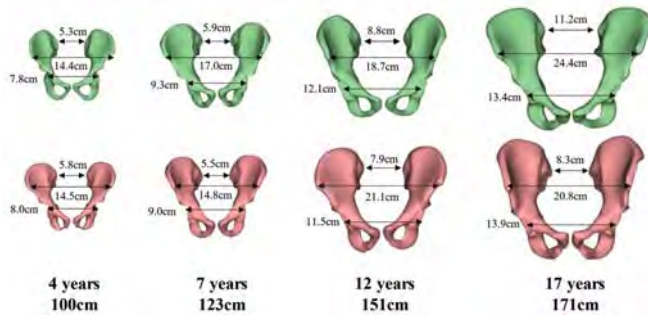


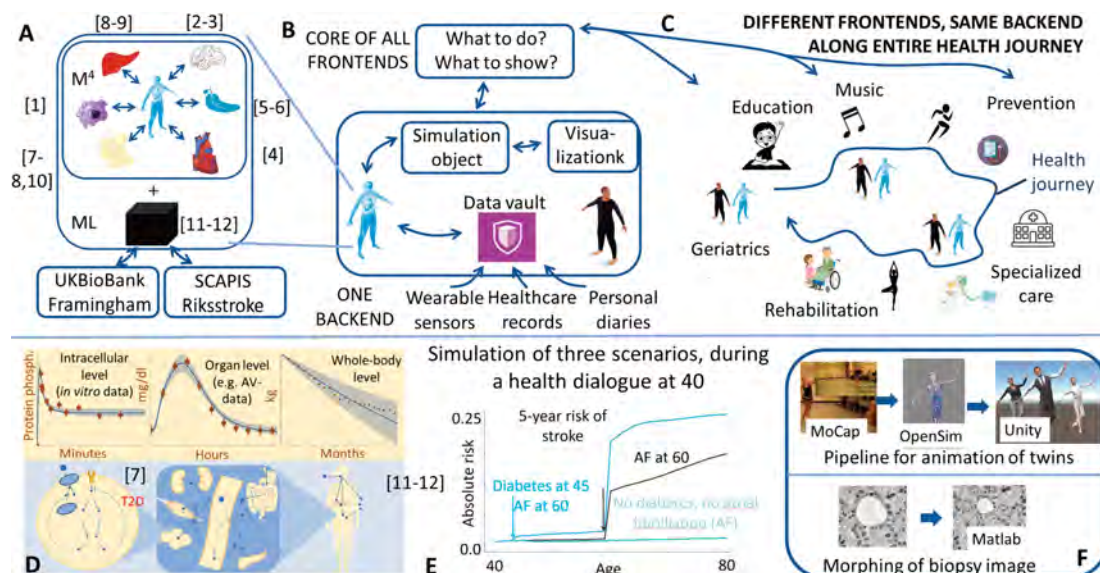
Figure 1: Gender differences (male in red and female in green) in ASIS width, PSIS width, and hip joint centre distance visually of height and aged matched cases.

25.1

M4-health: digital twins that follow you throughout your health journey

Gunnar Cedersund¹

1 Linköping univ, Department of Biomedical Engineering, Linköping, Sweden



1. Introduction

For 20+ years, I have developed and tested mechanistic mathematical models for the main organs in the human body (Fig A)1-12. We have now created a reusable backend (B) to an eHealth platform (C), where the organ-models are interconnected, and where the models can be personalized, and used to simulate scenarios (D-E). The models are Multi-level (intracellular to whole-body), Multi-timescale (seconds to decades), Multi-organ, and Mechanistic (M4).

2. Materials and Methods

The M4-models are developed/simulated using differential-algebraic equations, across various platforms: Matlab, OpenCOR, NEURON, OpenSim, Unreal Engine, INCA, etc. The M4-models are extendable to omics-level network models, and are combined with machine-learning models, to calculate e.g. the risk of a stroke. The backend is written in Python, and can be called from any eHealth-platform.

3. Results

The interconnected M4-model is able to simulate (Fig D, lines) scenarios that agree with data (dots) for all levels and timescales. The omics-level model can simulate diabetes on an phosphoproteome level¹⁰. The digital twins are personalized in appearance (face, proportions, weight, etc), and can be made to move (F). Intrabody images (MRI, microscopy images of biopsies, etc) can visualize both how the organs and cells are now, and how they gradually change, depending on what the digital twin is doing: diet, exercise, medication, etc (F)^{9,11-12}.

4. Discussion and Conclusions

Because of the physiological M4-core (A-B), our model can be re-used across the entire health journey (C): for personalized computer labs in education, for including your digital twins in performances on stage, and for improving communication with your personal trainer at the gym, or with nurses or specialist (hepatologist, cardiologist). The hypothesis is that seeing such scenarios play out, in your own digital twin, will improve the understanding, motivation, and compliance to treatment. In my presentation, I will give examples of how we work with end-users across the different stages of your life journey. Finally, if there is a grand piano, I can show live how dancing digital twins are incorporated in lecture-performances.

5. References

- [1] Nyman et al, *CPT Pharmacometrics Syst Pharmacol*. 2020, 9(12):707-717
- [2] Sten S et al, *Neuroimage*. 2017 158:219-231
- [3] Sten S et al, *bioRxiv*, 2021, 03.25.437053
- [4] Casas B et al, *Front Physiol*, 2018, 9:1515
- [5] Palmér et al, *CPT Pharmacometrics Syst Pharmacol*, 2014, 3:e118
- [6] Cedersund G, M.Sc. Th, DTU, 2001
- [7] Bränmark C et al, *J Biol Chem*. 2013 288(14):9867-80
- [8] Herrgårdh T et al, *Front Physiol*. 2021, 12:619254
- [9] Silfvergren O et al, *bioRxiv*, 2021, 10.1101/2021.11.04.467307
- [10] Lövfors et al, *bioRxiv*, 2022, 10.1101/2022.03.11.483974
- [11] Herrgårdh T et al, *NeuroImage Clin*. 2021, 31:102694
- [12] Herrgårdh T et al, *bioRxiv*, 2022, 10.1101/2022.03.25.485803

Acknowledgements:

I acknowledge support from the VR, ELLIIT, H2020, VINNOVA, SSF; KAW, SciLifeLab, Research without Animal Experiments, SUND.

25.2

Prediction of successful course of vaginal delivery in relation of bony pelvis anatomy and fetal head size using design of experiment

Ludek Hyncik¹, Hana Cechova¹, Linda Havelkova¹, Magdalena Jansova¹, Ladislav Krofta²

1 University of West Bohemia, New Technologies - Research Centre, Pilsen, Czech Republic

2 The Institute for Mother and Child Care, Prague, Czech Republic

1. Introduction

The work contributes to translational medicine from *in silico* to clinical. Using a mathematical biomedical model of a female pelvic floor, the work aims at predicting a successful course of vaginal delivery through the pelvic floor and fetal head dimensions. The prediction is done by a response surface, which interpolates the injury risk value over a domain defined by pre-calculated results.

2. Materials and Methods

The work accommodates a finite element model of a generic female pelvic floor model [1]. Based on the basic bony pelvis measures, particularly anterior-posterior diameter (APD) and transverse diameter (TD), the generic model is scaled to 4 models including their combination. Additionally, the fetal head is also scaled so that the head circumference (HC) corresponds to the 10-percentile and 90-percentile sizes [2]. This leads to additional 2 combinations of the 4 above-mentioned models, so the total number of the computational models is 8. Those 8 models compose 8 corners of a brick defining the response surface (RS) using the statistical method called Design of Experiment (DoE) [3].

For each model, the vaginal delivery process is simulated by a pre-defined trajectory of the fetal head [4]. The injury risk corresponds to the deformation of perineal muscles, so the maximum perineal muscle stretch through the first principal strain, which is independent on material parameters, is monitored.

3. Results

For all design models, the maximum first principal strain appears in the same location at the place connecting the perineal muscle to the perineal body.

The monitored first principal strain serves as the corner values for constructing RS (Fig. 1), which predicts the maximum first principal strain in the perineal muscle over space defined by APD, TD and HC by interpolating among the corner values.

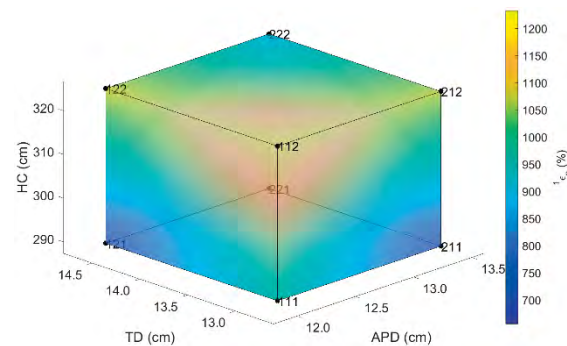


Figure 1: RS as a function of APD, TD and HC.

4. Discussion and Conclusions

DoE was used for assessing the injury risk during vaginal delivery through the maximum strain in the perineal muscle.

Every single computation using costs a considerable time, therefore DoE seems to be a good statistical method for predicting the successful course of vaginal delivery in relation of bony pelvis anatomy and fetal head size.

5. References

1. Cechova H, Kalis V, Havelkova L, et al. *Int Urogynecol J* 32(7), 1997-2003 (2021).
2. Villar J, Cheikh IL, Victora CG, et al. INTERGROWTH-21st Project. *Lancet*, 384(9946):857-68 (2014).
3. Van Schepdael A, Carlier A, Liesbet G. *Sensitivity Analysis by Design of Experiments* (2016).
4. Bamberg C, Rademacher G, Guttler F, et al. *Am J Obstet Gynecol*; 2012, 206:505.e1-6 (2012).

Acknowledgements:

The authors would like to thank the European Regional Development Fund-Project (Grant no: CZ.02.1.01/0.0/0.0/17_048/0007280) and the John H. & Amy Bowles Lawrence Foundation for providing financial support to this project.

25.3

Simulation-based digital twin platform for abdominal aortic aneurysms

Raimon Wintzer¹, Alexander Pugachev¹, Michael W. Gee²

1 CADFEM Medical GmbH, Grafing bei München, Germany

2 Technical University of Munich, Garching bei München, Germany

1. Introduction

A pathological abdominal aortic aneurysm (AAA) is irreversible dilation of the lower aorta that could lead to rupture of the arterial wall and as a result to life threatening internal bleeding. The clinical guidelines for the AAA treatment are based on the maximum diameter of the aneurysm. In case of small-diameter AAA, the patients are advised to undergo regular screenings. This work presents an in-silico platform for enhanced screening of AAA patients using physics-based modelling.

2. Materials and Methods

The developed in-silico platform incorporates a probabilistic framework for the patient-specific rupture risk assessment of AAA [1]. Instead of using deterministic criterion based on ratio between the wall stress and the estimated wall strength, the framework involves efficient computation of the probability of rupture using a Kriging-based surrogate modelling combined with high-fidelity finite element modelling. The probabilistic distributions of unknown mechanical characteristics of the vessel wall are obtained from patient-specific non-invasive properties using a multivariate regression model derived from an available patient data base of aneurysmatic aortic tissue samples and corresponding patient data.

3. Results

The probabilistic approach to the AAA rupture risk assessment was implemented as fully automated in-silico workflow. An automatic 3D reconstruction of AAA geometry from a computed tomography (CT) data was developed using machine learning, see Fig. 1.

The results presented to the physician include the probability of rupture as well as von Mises wall stress. Depending on data availability, the time evolution of rupture risk can be analysed for a particular patient, or the newly obtained patient-specific assessment can be presented within the cohort of other patients, see Fig. 2.

4. Discussion and Conclusions

The developed platform is aimed at the creation of digital twins of AAA patients based on data-driven analysis and biomechanical modelling. Furthermore, the assessment results can be integrated into a clinic's data base and shared in anonymized form with collaborating medical centres to provide additional support to physicians in AAA diagnosis and therapy.

5. References

- Bruder L et al. *PLoS ONE* 15(11) (2020)
<https://doi.org/10.1371/journal.pone.0242097>.

Acknowledgements:

The authors would like to thank the Bavarian Research Foundation (Project no: AZ-1297-17) for providing financial support to this project.



Figure 1: Geometry reconstruction from CT scan and non-invasive clinical data.

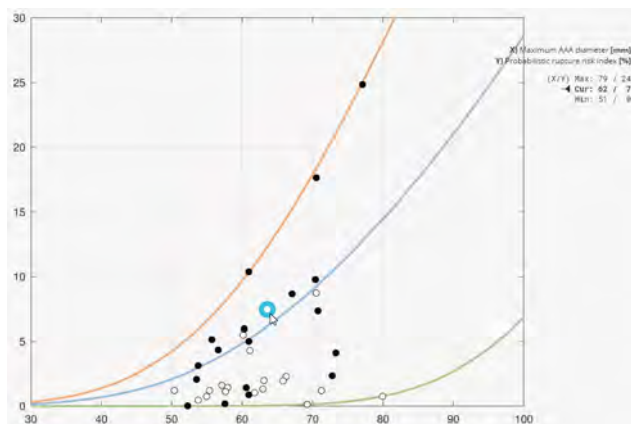


Figure 2: Representation of the patient's rupture risk assessment within the available cohort.

25.4

Toward a deep learning-driven prediction of dynamic soft tissue deformations for a real-time mixed reality simulator of the childbirth processes

Abbass BALLIT¹, Duyen Ngyuen-Le¹, Tan-Nhu NGUYEN¹, Tien-Tuan Dao¹

¹ Univ. Lille, CNRS, Centrale Lille, UMR 9013 - LaMcube - Laboratoire de Mécanique, Multiphysique, Multiéchelle, F-59000 Lille, France

1. Introduction

Accurate and real-time simulation of the soft tissue deformations of the pelvis system is essential for medical interactive applications such as surgical and childbirth simulators. Several state-of-the-art methods have been proposed [1] such as Projective Dynamics (PD), Quasi-Newton, or ADMM. These approaches generally consist of formulating a time-integration scheme providing a compromise between speed and accuracy. Recently, deep learning has been used to estimate skeletal muscle stresses [2]. In this present work, we extended this approach to develop a 3D full-field prediction of dynamic soft-tissue deformations for our real-time mixed-reality obstetric simulator.

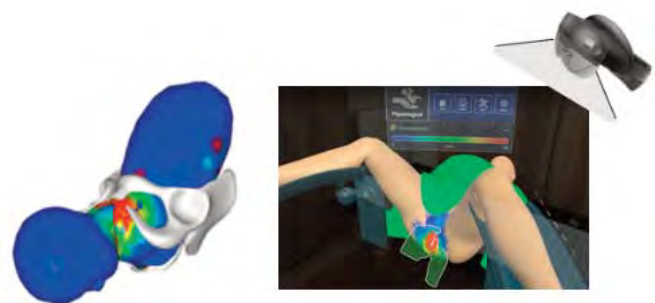


Figure 2: Case study on the baby delivery process using the HyperMSM formulation.

2. Materials and Methods

A dynamic simulation consists of finding the new nodal position vector of the model x_{t+h} , from the current nodal position x_t and velocity v_t , the external nodal forces f_{ext} , and the material properties M :

$$x_{t+h} = \phi(x_t, v_t, f_{ext}, M, h) \quad (\text{Eq.1})$$

To solve the simulation in real-time, a novel simulation workflow was developed (Fig. 1). Firstly, a learning database was built using our novel HyperMSM formulation on the model including the pelvis, the uterus, the floor muscle, and baby body [1] and a probabilistic data generation process.

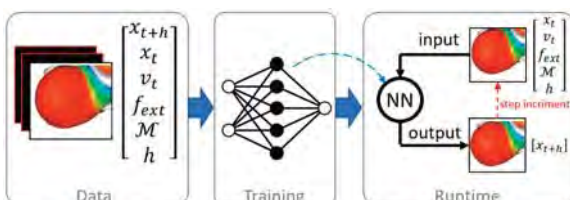


Figure 1: Our proposed data-driven workflow

Then, a long-term memory network (LTMN) was implemented to estimate the displacement, strain, and stress quantities. The comparison with finite element outcomes (Neo-Hookean material for soft tissue models ($C10 = [0.8-200]$ KPa and $D1 = [2-78]$ MPa) was used for validation purposes.

3. Results

Real-time estimation of soft tissue deformation during the baby delivery process and its interaction with the HoloLens device are shown in Fig. 2. The prediction results along a predefined path on the muscle tissue was compared to the FE outcomes (Fig. 3).

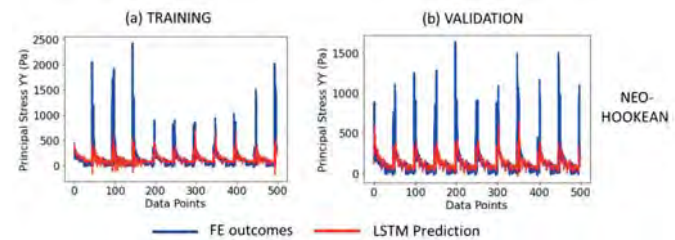


Figure 3: Example of comparison between the LSTM predictions for muscle stress component with Neo-Hookean FE outcomes.

4. Discussion and Conclusions

A novel prediction workflow of the dynamic soft-tissue deformations was proposed. Our workflow allows overcoming the high iteration requirement of the iterative solver like PD solver [1]. Ongoing work relates to the integration of this novel workflow into a real-time mixed-reality simulator of the childbirth processes (physiological and forceps-assisted labors).

5. References

1. Ballit and Dao, *Computer Methods and Programs in Biomedicine*, Vol. 216, 106659, 2022
2. Ballit and Dao. *Medical & Biological Engineering & Computing* 60(4): 1177–118

Acknowledgements:

The authors would like to thank the Métropole Européenne de Lille (MEL) and ISITE ULNE (R-TALENT-20-009-DAO) for funding.

26.1

Multicellular model of effects of cell-to-cell heterogeneity on antiviral timing and potency in an infected patch of epithelial tissue

James Glazier¹, Juliano Ferrari-Gianlupi¹, Tarunendu Mapder², TJ Sego¹, James Sluka¹, Sara Quinney², Morgan Craig³, Robert Stratford²

¹ Indiana University Bloomington, Intelligent Systems Engineering, Bloomington, United States

² Indiana University School of Medicine, Indianapolis, United States

³ University of Montreal, Montréal, Canada

1. Introduction

Computer simulations of within-host infection and response have assisted screening of candidate drug treatments. Non-spatial population models can clarify how dosage and timing influence gross treatment efficacy, but not how cell-to-cell variability affects treatment outcomes. We extend our established CompuCell3D-based [1] multicellular agent-based model (ABM) of infection of lung tissue by SARS-CoV-2 to include pharmacokinetics (PK) and mode of action (MOA) models of remdesivir [2]. We investigate how drug potency, dosing frequency, treatment initiation delay, spatial heterogeneity and variability in cellular uptake and metabolism of remdesivir, affect simulated treatment outcomes.

2. Materials and Methods

Our model of antiviral treatment of COVID-19 integrates a spatio-temporal model of an infected lung tissue patch, a MOA model for the antiviral, and a PK model of the available active metabolite of remdesivir in individual epithelial cells. Infected cells go through an eclipse phase, and a virus releasing phase and then die. Extracellular virus diffuses and decays, exposing other cells, which in turn have a probability of becoming infected. Epithelial cells secrete cytokines after infection or exposure to cytokines. Immune cells recruited into the simulated domain by the cytokines kill infected cells, neutralize virus, and release cytokines. To simulate inter-cell metabolic heterogeneity, each cell has different parameters for drug uptake and clearance. We investigate how different levels of heterogeneity affect predicted treatment efficacy.

3. Results

Heterogeneous drug metabolism decreases efficacy for the same treatment schedule and potency and greater heterogeneity leads to worse outcomes. In simulations without cell-to-cell metabolic heterogeneity, treatment shifts from effective to ineffective for a drug potency multiplier between 25x and 15x, whereas, with heterogeneity, the transition happens between 33x and 20x (a higher dose). This dependence is due to infection being driven by those cells that are least sensitive to the antiviral, which generate the most extracellular virus. With heterogeneity, delaying treatment initiation also reduces treatment efficacy more than it does in the absence of heterogeneity.

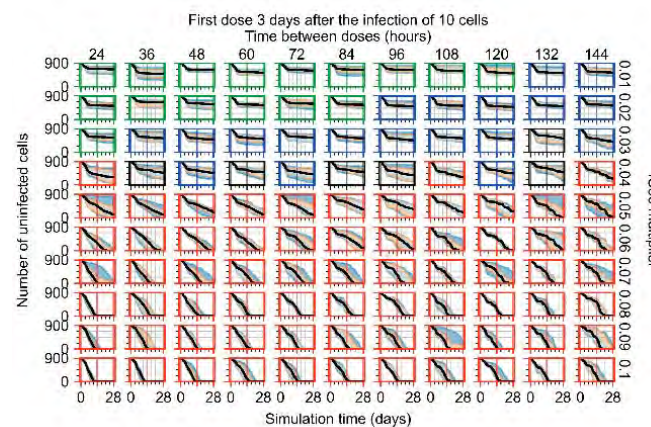


Figure 1: Simulated number of uninfected cells vs time for different dose intervals and potencies in the presence of cell-to-cell heterogeneity in drug metabolism. 20 replicates. Median, black line; the 0th to 100th quantiles are shaded. Rapid clearance: red; slow clearance: blue; partial containment: black; widespread infection: green.

4. Discussion and Conclusions

Higher cell-to-cell variability in cellular antiviral metabolism increases dispersion of outcomes under the same conditions and requires higher antiviral doses to achieve comparable probabilities of control. This increased dispersion may explain some of the ambiguity in clinical trials of antivirals.

Our simulation allows us to probe the roles of distribution, dynamics, and effects of remdesivir within a tissue, which would be difficult to disentangle using only animal and human experimental data, to help translate hypotheses concerning biomedical mechanisms into clinically relevant results. Our modular framework is easily extensible to other tissues, viruses and therapies and to include more realistic models of immune response [3].

5. References

1. <https://compcell3d.org/>
2. Ferrari-Gianlupi J, et al., *Viruses* 14, 10.3390/v14030605 (2022).
3. Sego TJ, et al. *JTB* 532, 10.1016/j.jtbi.2021.110918 (2022).

Acknowledgements:

Funded by NIH U24 EB028887, NIH R01 GM122424, and NSF 1720625, Eli Lilly and Company through the Indiana CTSI, NIH UL1 TR002529, National Center for Advancing Translational Sciences Clinical and Translational Sciences Award, NSERC ALLRP 554923-20 and RGPIN-2018-04546.

26.2

An image-based 3D electrophysiological torso model for simulating maternal and fetal ECG

Julie Uv¹, Lena Myklebust¹, Hannes Welle², Hamid Khoshfekr Rudsari³, Hermenegild Arevalo¹

1 Simula Research Laboratory, Computational Physiology, Oslo, Norway

2 Karlsruhe Institute of Technology, Karlsruhe, Germany

3 Oslo University hospital, Oslo, Norway

1. Introduction

Congenital heart disease (CHD) is a leading cause of infant death [1]. Electrocardiograms (ECG) recorded on the maternal abdomen can non-invasively diagnose CHD. However, extracting the fetal ECG from the maternal abdominal ECG (aECG) is challenging mainly due to low signal-to-noise ratio and limited access to reference data of direct fetal ECG. Here we generate direct fetal and aECG signals through physiological modelling.

2. Materials and Methods

To simulate synthetic aECGs, we incorporated maternal and fetal biventricular hearts into a female torso, constructing a 3D finite element mesh of ~ 17 million nodes. The hearts and torso models are based on CT and MR images respectively [2-5].

Electrophysiological simulations were performed using openCARP [6]. Current propagation through tissue was modelled using the pseudo-bidomain model. Maternal heart membrane kinetics were represented with the Ten Tusscher (TT) model of human ventricular myocytes [7]. In the fetal heart, we used a TT model adapted to match experimental aECG recordings [8].

To model sinus rhythm, we stimulated the endocardium with 500 and 450 ms intervals in the maternal and fetal hearts respectively. To obtain the ECG, we recorded extracellular potentials at 11 torso and one fetal cardiac site (Fig. 1).

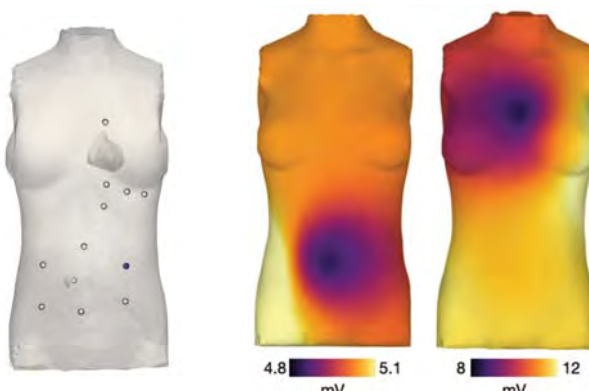


Figure 1: Electrode placement (left). Snapshot of extracellular potential for fetal (middle) and maternal (right) cardiac stimulation.

3. Results

Fig 2 shows maternal aECG and fetal ECG, the prior measured at the coloured electrode in Fig. 1. The simulated signals are consistent with clinical aECGs, showing normal QRST morphologies [9]. The QT interval is ~325 ms, comparable to the clinically measured normal range of 360–460 ms in females. Compared to the abdominal signals, the direct fetal signal has a larger fetal R-peak amplitude, similar to clinical observations [10].

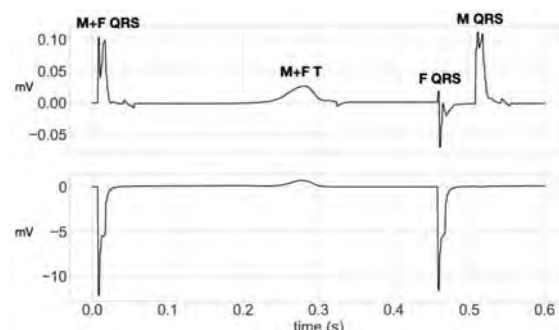


Figure 2: ECG traces for abdominal (top) and (direct) fetal cardiac sites (bottom) with maternal (M) and fetal (F) QRS and T-wave marked.

4. Discussion and Conclusion

Electrophysiological simulations using the torso with maternal and fetal heart model generated abdominal and direct fetal ECGs with realistic features. Further work includes incorporating other torso organs such as lungs, uterus, etc. to more accurately simulate electrical propagation through the torso as well as looking into how fetal CHD can be diagnosed from aECGs.

5. References

1. Nembhard et al., *Ethn Dis*; 18(4), (2008).
2. Martinez-Navarro et al., *Univ of Oxford* (2019).
3. Bibin et al., *IEEE trans BME*; 57(10), (2010).
4. Dahdouh et al., *Phys med and bio*; 59(16), (2014).
5. Daz3D Studio (2000).
6. Plank et al., *Comp meth prog biom*; 208, (2021).
7. ten Tusscher et al., *AJP Heart Circ*, 291 (2006).
8. Pervolaraki et al., *Europace*; 16(5) (2014).
9. Al-Salameh et al., *Acad Press*, 2017.
10. Jezewski et al., *Biom Eng*; 57(5) (2012).

26.3

Hybrid modelling to predict pregnancy complications

Pascalle Wijntjes^{1 2 3}, M. B. van der Hout-van der Jagt^{1 2 3 4}, Wouter Huberts¹, Frans van de Vosse^{1 3}

1 Eindhoven University of Technology, Biomedical Engineering, Eindhoven, Netherlands

2 Máxima MC Veldhoven, Obstetrics and Gynaecology, Veldhoven, Netherlands

3 e/MTIC - Eindhoven MedTech Innovation Center, Eindhoven, Netherlands

4 Eindhoven University of Technology, Electrical Engineering, Eindhoven, Netherlands

1. Introduction

Approximately 10% of all pregnancies are affected by hypertensive disorders, with 3% being affected by the more severe condition of pre-eclampsia [1]. Studies show that multiple pregnancy complications are caused by abnormal placentation [2]. Therefore, it is important to include placental blood circulation as an indicator when stratifying patients at risk for pre-eclampsia.

Existing screening methods are based on maternal characteristics while others include additional biomarkers during pregnancy [3]. However, these approaches have their limitations, as pathophysiological alterations in hemodynamics are not considered. In this study, the feasibility of a hybrid approach that can provide additional pressure data to better stratify the hemodynamic state, is examined.

2. Materials and Methods

The hybrid approach, a Physics-Informed Neural Networks (PINNs) [4], learns the relationship between non-invasive clinical measurements (e.g. flow) and pressure by using a neural network constraint by a priori physiological knowledge.

To train the network and demonstrate its feasibility, in this study, synthetically generated pressure and flow waveforms are used. By altering the physical properties of the blood vessels in an established simulation model [5], we can simulate different pathologies, each resulting in different pressure and flow patterns.

3. Results

Without informing the PINN about the actual blood vessel properties, the model was able to accurately characterize blood pressure given the flow data (see fig. 1.).

4. Discussion and Conclusions

The hybrid modelling technique shows promising results for combining physiology with data and risk factors in situations in which the model parameters are unknown. In future research, this allows us to investigate this approach as an addition to or even as a replacement for the current risk stratification for pre-eclampsia while looking more in-depth into the physiology of the placenta.

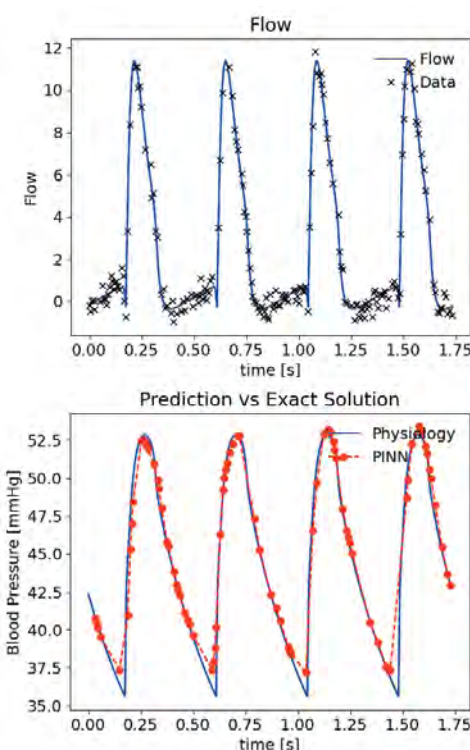


Figure 1: Prediction of blood pressure by our hybrid model (red dots) from synthetical flow data with Gaussian noise (black crosses) shows good agreement with the actual corresponding pressure curve (blue line, bottom figure).

5. References

1. Hutcheon JA et al., *Best Pract Res Clin Ob*, 25(4): 391-403 (2011)
2. Serov A S et al., *J Appl Physiol*, 120(1): 17-28 (2016)
3. Antwi E et al., *PLoS One*, 15(4): e0230955 (2020)
4. Raissi M et al., *J Comput Phys*, 378: 686-707 (2019)
5. Yigit MB et al., *J Biomech*, 48(9): 1662-1670 (2015)

Acknowledgements:

We acknowledge the Eindhoven MedTech Innovation Center (e/MTIC, Grant PICASSO) for funding.

26.4

Modeling a female pelvic floor and foresight biomechanical injuries during vaginal delivery

Rita Moura¹, Dulce Oliveira¹, Marco Parente², Teresa Mascarenhas³, Renato Natal Jorge²

¹ Institute of Science and Innovation in Mechanical and Industrial Engineering, Biomechanics and Health, Porto, Portugal

² Faculty of Engineering of University of Porto, Mechanical Engineering, Porto, Portugal

³ Faculty of Medicine of University of Porto, Obstetrics and Gynecology, Porto, Portugal

*Corresponding author. E-mail: up201404216@edu.fe.up.pt

1. Introduction

Childbirth corresponds to a mechanically and physiological traumatic event. Despite being discussed worldwide, maternal birth trauma continues to affect millions of women and significantly decrease their quality of life [1]. The most common lesions include levator ani avulsions, perineal tears, and obstetric anal sphincter injuries. To improve the knowledge available in this field, computational models can be used to mimic the mechanics of labor. Although there is already considerable work regarding childbirth simulations, a set of sophisticated computational models is a need. The main goal of this work is to develop a finite element model that incorporates both deep and superficial maternal tissues, aiming to simulate the distinct types of lesions that occur during vaginal delivery.

2. Materials and Methods

A 3D finite element model of the pelvic floor muscles was developed based on magnetic resonance images (MRI), medical books, and clinical references. The geometrical model is composed of the levator ani (puborectalis, pubococcygeus, and iliococcygeus), coccygeus muscles, and anal canal. The thickness of the pubovisceral muscle was defined as 6.5 mm, while for the iliococcygeus and coccygeus muscles it was considered 3.6 mm [2, 3]. The mesh is composed of hexahedral solid elements (C3D8H).

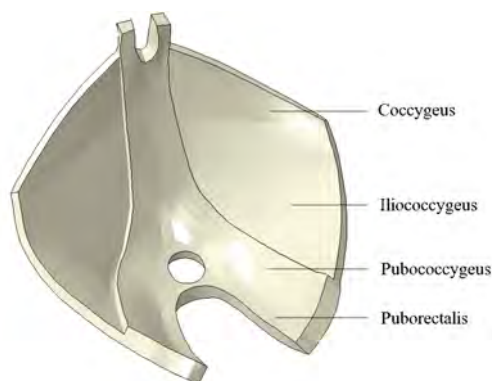


Figure 1: Representation of the female pelvic floor geometrical model.

Regarding the boundary conditions, the nodes corresponding to the extremities of the pelvic floor muscle were fixed. The model was tested using Abaqus Standard® for pressure values corresponding to the intra-abdominal pressure (IAP), which corresponds to 4.0 kPa.

3. Results

Preliminary simulations were performed to analyze the behavior of the muscles. The application of the IAP resulted in a maximum vertical displacement of the pelvic floor muscles of 8.68 mm. The maximum principal stresses were also measured, and it was concluded that the most affected area was the puborectalis muscle, near the anal canal, with a maximum stress of 0.28 MPa.

4. Discussion and Conclusions

During childbirth, the maternal muscles are subjected to mechanical forces that can lead to injuries. The origin and relation between the different lesions are not yet fully understood. The present study corresponds to a first step in the development of a finite element model capable of simulating childbirth and analyzing from a biomechanical perspective the different types of lesions prone to occur.

5. References

1. Dietz, H. et al., *Int Urogynecol J*; 31(11):2311–2315 (2020).
2. Majida, M., et al., *Ultrasound Obstet Gynecol* (2010)
3. Azzam, H et al., *Egypt. J. Radiol. Nucl. Med.* 50, no. 1 (2019)

Acknowledgements:

The authors gratefully acknowledge the support from Portuguese Foundation of Science under the Grant SFRH/BD/05876/2021, the Junior Researcher Contract CEECIND/01522/2020, and the funding of Project UIDB/50022/2020 and Project NORTE-01-0145-FEDER-030062 (SIM4SafeBirth) cofinanced by NORTE2020, through FEDER.

27.1

An agent-based model to simulate DIPG migration in microfluidic devices

Daniel Camacho-Gómez¹, Pedro Enrique Guerrero², Noelia Mendoza², Alberto Schuhmacher², María José Gómez Benito¹, José Manuel García Aznar¹

1 Mechanical Engineering, Zaragoza, Spain

2 Zaragoza, Spain

1. Introduction

Diffuse Intrinsic Pontine Glioma (DIPG) is a fatal childhood brain tumor. The most important hallmark of DIPG is its extreme infiltrative diffuse phenotype. It exhibits a more solid core and an invasive front, composed of single cells and by groups of cells. Moreover, DIPG cells form large, highly diffusive cell aggregates with many branches, and an increase in matrix stiffness produces a dense aggregate of cells [1]. In this work, we aim to reproduce DIPG cell invasion and evaluate the matrix degradation of in vitro experiments in microfluidic devices with a three-dimensional agent-based model.

2. Materials and Methods

We introduce an active migration force to reproduce the invasive characteristics of DIPG cells. Thus, mechanical equilibrium of cells can be obtained from the balance of forces:

$$\sum_{j \in N_c} \mathbf{F}_{cc}^{ij} + \mathbf{F}_{loc}^i + \mathbf{F}_{drag}^i = 0,$$

where \mathbf{F}_{cc}^{ij} is the cell-cell interaction force, \mathbf{F}_{loc}^i is the locomotive active force that cells make to migrate, and \mathbf{F}_{drag}^i is the friction of the cell with the extracellular matrix. We model the extracellular matrix as a continuum similarly to [2]:

$$\frac{\partial e}{\partial t} = -ame, \\ \frac{\partial m}{\partial t} = \beta c - \gamma m,$$

with e the matrix concentration, m the matrix-degrading enzyme concentration, c the cell concentration, a the ECM degradation rate, β the MDE production rate by cells, and the γ the MDE decay rate.

3. Results

First step, we evaluated the individual migration without matrix degradation. For that purpose, we calculated the velocity of the cells and the directionality ratio from in vitro single cell experiments collagen hydrogels with marimastat, a matrix degradation inhibitor. Then, we evaluated degradation of the extracellular matrix through an optimization algorithm to find the degradation parameters that makes that the mean velocity of the simulations matches the experiment in collagen hydrogels without marimastat. Finally, we performed 80 simulations of a moving-single cell in a 2.5 mg/ml collagen concentration matrix with and without marimastat (Fig. 1). When degradation is not blocked, cells degrade the matrix to increase their invasion capability and spread more.

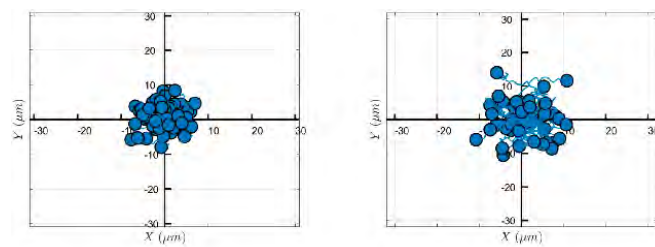


Figure 1: Simulation of cell trajectories in a 2.5 mg/ml collagen concentration matrix without matrix degradation in (a) and with matrix degradation in (b).

4. Discussion and Conclusions

We presented a two-step methodology to estimate from experiments the locomotive forces, the persistence time and the degradation of the matrix to capture cell trajectories without and with matrix degradation. Thus, cells degrade the matrix to increase their invasion capability and modulate the matrix degradation depending on the stiffness of the extracellular matrix.

5. References

1. Wang, C, et al., *Acta Biomaterialia*, 116, pp.201-208.
2. Jeon, J, et al., *Biophys J*. 2010;98(1):37-47.

Acknowledgements:

The authors were supported by PROCANAIID (Grant no: PLEC2021-007709) and by PRIMAGE (Grant no: 826494).

27.2

Calibrating a multiscale model of bone healing with immunofluorescent images

Edoardo Borgiani^{1,2}, Gabriele Nasello², Liesbet Geris^{1,2}

1 U Liege, Biomechanics Research Unit, GIGA in silico medicine, Liege, Belgium

2 KU Leuven, Prometheus, Division of Skeletal Tissue Engineering, Leuven, Belgium

1. Introduction

Bone fracture healing is a complex process. Its complexity is noticeable during the initial inflammatory phase, which starts right after the injury with the activation of the immune response. As in silico technologies are increasingly considered to have a role in developing the next generation of bone healing models [1], we developed a computer model to investigate bone healing from the first hours post-fracture at multiple time- and length-scales. Though currently still being calibrated, we believe that, once fully developed, it will provide clinical added value due to its capacity to explore the mechanical and biological aspects of therapeutic strategies that can enhance bone regeneration from its earliest phases.

2. Materials and Methods

COMMBINI (COmputational Mechano-biological Model of Bone INjury Immunoresponse) is a multiscale in silico model that combines finite element and agent-based models to simulate bone fracture healing mechanical and biological environments, respectively. With this novel approach, the immune cells involved in the inflammatory stage can be simulated as single entities, and their temporal and spatial dynamics can be explored. One calibration strategy compares in silico results with immune-fluorescence images of corresponding time and conditions (Fig. 1).

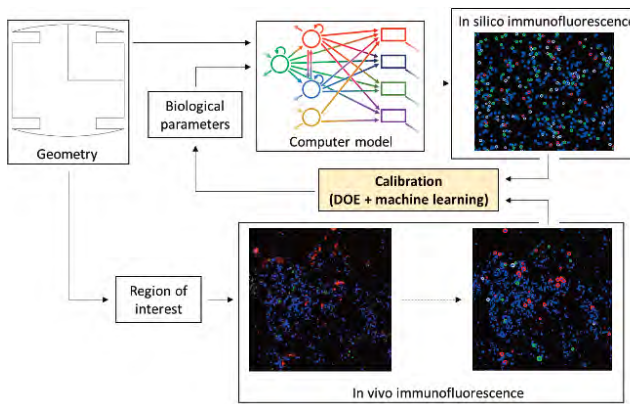


Figure 1: Calibration of the computer model (top) with experimental results (bottom).

In vivo immunofluorescence images from a previous work [2] will be used to obtain quantitative and qualitative information to compare with the simulation results (Fig. 1). These images are processed with DeepCell, a deep learning algorithm for cell segmentation [3]. The segmentation led to the quantification of the different cell types in the bone fracture images. In a first step, a sensitivity analysis was performed with the support of Taguchi's orthogonal arrays [4] applied to design of experiment techniques to identify the most influential parameters of the model. In a second step, said parameters will be calibrated using a genetic algorithm (machine learning).

3. Results

Sensitivity analysis showed that a realistic number of macrophages within the healing region could be obtained if the following parameters are properly calibrated: (a) inactivated macrophages proliferation ratio, (b) macrophages recruitment factor, (c) pro-inflammatory macrophages proliferation ratio (Fig. 2). In detail, while (a) has primary importance during the whole development of the inflammatory stage, the other two are observed to lose (b) or gain (c) their role through time (Fig. 2).

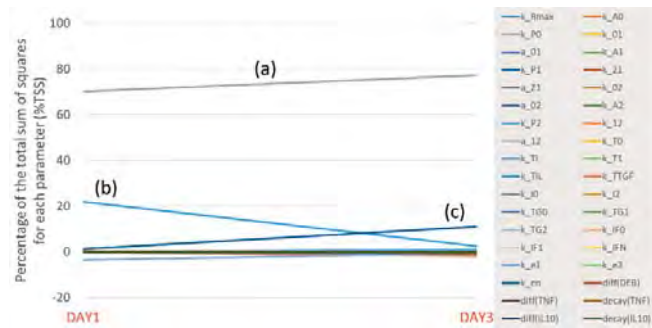


Figure 2: Variation of %TSS relative to the significance of all the model parameters on the overall number of macrophages obtained as output.

4. Discussion and Conclusions

Sensitivity analysis provided useful information to evaluate which parameters to focus on during the calibration phase of the model. This information will be the starting point to train a machine learning algorithm to find the most realistic in silico values to describe the inflammatory stage of bone healing.

5. References

1. Lafuente-Gracia et al., *Front Bioeng Biotechnol* 9:703725 (2021)
2. Schlundt et al., *Bone* 106:78–89(2018)
3. Greenwald et al., *Nat Biotechnol* (2021). doi: 10.1038/s41587-021-01094-0
4. Taguchi et al., *Taguchi's Quality Engineering Handbook*. Wiley (2005)

27.3

Integrated spatial-temporal mathematical model for simulation of fibrotic scar formation

Jieling Zhao^{1,2}, Seddik Hammad^{3,4}, Paul Van Liedekerke¹, Jan Hengstler², Steven Dooley³, Dirk Drasdo^{1,2}

1 Inria Saclay Île-De-France, Palaiseau, France

2 IfADo, Toxicology, Dortmund, Germany

3 Medical Faculty Mannheim Heidelberg University, Medicine II, Mannheim, Germany

4 South Valley University, Forensic Medicine and Toxicology, Qena, Egypt

1. Introduction

Liver fibrosis is characterized by the accumulation of overexpressed extracellular matrix (ECM) proteins as a result of exposure of tissue to repeated damage. There are distinct patterns of fibrosis such as collagen septa (from tissue sections called "fibrotic walls") connecting two central veins due to toxic injury. In the past decade, some computational models using either rule-based models 2D [Dutta-Moscato 2014] or partial differential equations [Lara 2014] of liver fibrosis to study the cellular and molecular mechanisms. Within a 3D single-cell-based model resolving tissue microarchitecture, we now incorporate the collagen fiber mechanics to address fibrosis formation. The same model approach already simulated regeneration after acute liver damage [Hoehme 2010] and tumor initiation [Hoehme 2018] hence fibrosis formation is a further step towards a digital liver twin. The pattern-characterizing parameters in this study were obtained through image analysis of images from animal experiments that were compared to human histopathology. We explored alternative model mechanisms and parameters for a detailed in silico study of possible mechanism on the formation of characteristic fibrotic walls in liver fibrosis.

2. Materials and Methods

2.1 Experiments: Mice were exposed to acute and repeated doses of a hepatotoxic drug. Morphologically, patterns of fibrosis and metabolizing enzymes were analyzed in immunostaining datasets.

2.2 Mathematical model: The hepatocytes are modeled using CBM and DCM model, depending on their localization with regard to the forming fibrotic street [Van Liedekerke 2020]. The fibrotic collagen fibers are represented as semi-flexible springs. The capillary network, CVs and PVs of the liver lobule are modeled as semi-flexible chains of spheres connected by springs.

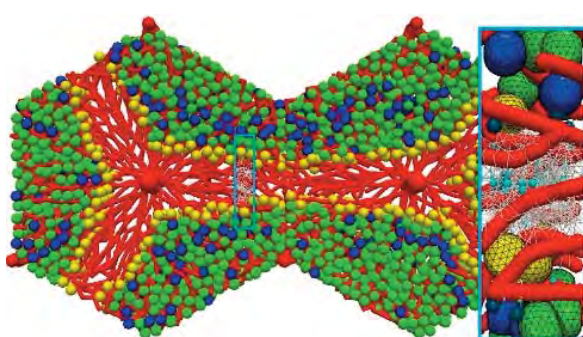


Figure 1: The modeled fibrotic tissue of two liver lobules. Red: sinusoids; Green/Blue/Yellow: quiescent/Proliferating/CYP2E1-expressing hepatocytes; Cyan: HSCs; Dark Blue: macrophages.

3. Results

The in silico fibrosis model is constructed with the spatial distribution of each of the cell type according to corresponding stainings from experimental data (Fig. 1). The simulation of a repeated intoxication generating an interplay of hepatic lesion formation and starting regeneration is run for 3 weeks. After each dose, the drug sensitive hepatocytes were killed. Macrophages and hepatic stellate cells (HSCs) are attracted into the lesion to eliminate the dead cell bodies and generate collagen fibres, respectively. HSCs generate ECM fibres upon activation, macrophages digest dead hepatocytes and collagens. The healthy hepatocytes surrounding the lesion proliferate to replace the dead hepatocytes while deforming the collagen network. In certain parameters windows corresponding to realistic biophysical and cell-kinetic parameters our results show that starting after the second drug dose the collagen fibres are deposited and gradually accumulate. After iterative destruction and partial regeneration cycles over about 3 weeks, the pattern of fibrotic wall is reproduced by our model. We further study how certain perturbations would influence the fibrotic pattern for model validation.

4. Discussion and Conclusions

Our novel collagen model is able to capture the mechanical properties of collagen fibers and cells.

5. References

- Dutta-Moscato J, et al. 2014. A multiscale agent-based in silico model of liver fibrosis progression. *Frontiers in Bioeng. & Biotechnol.* 2:18.
- Lara J, et al. 2014. Computational models of liver fibrosis progression for hepatitis C virus chronic infection. *BMC Bioinformatics.* 15:S5.
- Hoehme S, et al. 2010. Prediction and validation of cell alignment along microvessels as order principle to restore tissue architecture in liver regeneration. *Proc Natl Acad Sci.* 107:10371–10376.
- Hoehme S, et al. 2018. Model prediction and validation of an order mechanism controlling the spatiotemporal phenotype of early hepatocellular carcinoma. *Bull. Math. Biol.* 80: 1134–1171.
- Van Liedekerke P, et al. A quantitative high-resolution computational mechanics cell model for growing and regenerating tissues. *Biomch. & Mod. Mechanobiol.* 19: 189–220.

Acknowledgements:

Funding from BMBF – LiSyM (Germany) and iLite (ANR France) is gratefully acknowledged.

27.4

Quantitatively Comparing Tumor Images to Agent-Based Models for Parameter Fitting

Colin Cess¹, Stacey Finley¹

¹ University of Southern California, Biomedical Engineering, Los Angeles, United States

1. Introduction

Agent-based models (ABMs) of tumors explore how tumors develop temporally and spatially [1]. Despite their predictive power, ABMs are limited in the realm of parameterization. To properly identify unknown parameters, comparison to spatially-resolved images of tumors is required. Here, we developed a novel method to quantitatively compare tumor images to ABM simulations so that parameter fitting can be performed. We test the robustness our method for multiple test ABMs of tumor growth, using model-generated data instead of tumor images to evaluate the accuracy and speed of the method.

2. Materials and Methods

The first step in our method is to convert the training data and the ABM output into the same format. We discretize the locations of cells from the training data and simulations into a series of grids so they can be treated as simplified images. To compare the two, we use a Siamese Neural Network (SNN) [2]. An SNN outputs a vector for each image. The vectors are treated as high-dimensional data points and the distance between the vectors is calculated. The smaller the distance, the more similar the images are. We use a parameter fitting algorithm to minimize this distance. We tested this method with two distinct ABMs that yielded very different morphologies, thus providing different test cases for the method. Figure 1 provides an overview of our method.

3. Results

For both ABMs, we used several parameter sets to produce training data to test the method's robustness. For each parameter set, we could estimate parameters that yielded simulations whose average distance to the training data equaled that of the average distance between training samples. Estimated parameters were reasonably close to the parameters used to produce the training set. Visually, the simulations with the estimated parameters were nearly identical to those of the training data. Equal success was seen with both models for all of the training parameter sets.

4. Discussion and Conclusions

Here we provide, to our knowledge, the first method for quantitatively comparing images to ABM simulations of tumor growth. Our novel method makes the use of tumor images to estimate unknown ABM parameters possible, which we prove using model-generated data.

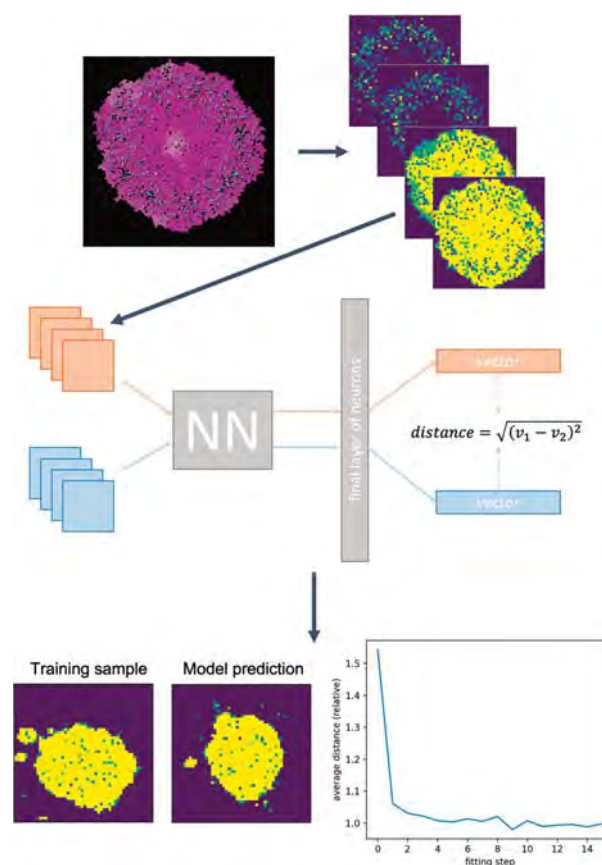
5. References

- Metzcar J et al., *JCO Clinical Cancer Informatics*, 2019;3,1-13 (2019).
- Chicco D. *Methods in Molecular Biology*, vol 2190. (2021).

Acknowledgements:

The authors would like to thank the USC Center for the Computational Modeling of Cancer for providing financial support to this project

Figure 1: Flowchart of method. Continuous cell locations are converted into a series of grids. Pairs of data and simulations are inputted into the SNN. An example of training data and a fitted model simulation, along with the average distance over fitting.



28.1

A 3D in silico model of fracture healing to investigate craniofacial bone defects

Laura Lafuente-Gracia^{1,2}, Mojtaba Barzegari¹, Liesbet Geris^{1,2,3}

¹ Biomechanics section, Department of Mechanical engineering, KU Leuven, Belgium

² Prometheus: Division of Skeletal Tissue Engineering, KU Leuven, Belgium

³ Biomechanics research unit, GIGA in silico medicine, University of Liège, Belgium

1. Introduction

Bone regeneration is a well-coordinated process involving the action and interaction of cells, regulated by a myriad of biochemical and mechanical factors. After fracture, successful healing is usually achieved within weeks. However, fracture severity, anatomical location and host factors can result in delayed healing or non-union. Here, we developed a 3D in silico model of bone regeneration and used it to investigate the influence of a scaffold produced using melt electrowriting (MEW) and coated (or not) with cells or growth factors as treatment strategy in craniofacial bone defects.

2. Methods

In silico model. Following an existing bioregulatory 2D model of bone fracture healing [1] implemented in MATLAB, we developed a 3D model using the open-source software FreeFEM [2]. The model captures biological processes across different time and space scales, simulating osteogenesis and sprouting angiogenesis. At tissue and cellular level, the spatiotemporal evolution of different biochemical factors, cells and extracellular matrices is described using a non-linear system of taxis-diffusion-reaction partial differential equations. At the (intra)cellular level, the developing vasculature is represented with discrete endothelial cells, each of them regulated individually by one ordinary differential equation representing its intracellular module.

Domain. We used our 3D in silico model to investigate two different craniofacial defects: calvarial and mandibular. The corresponding geometrical domains (Fig. 1) represent 10 mm diameter rabbit defects and were generated as finite element (FE) meshes (Fig. 2A) using the open-source software SALOME. Due to symmetry, only one-fourth of the geometrical domain (blue region in Fig.1) was simulated.

Implementation details. The healing progress of the two craniofacial defects was investigated with and without the application of the MEW scaffold. For the calvarial defect, only intramembranous ossification was considered and migration of skeletal progenitor cells (SPCs) was assumed from all domain surfaces (top, bottom and lateral) due to the presence of the periosteum and the dura mater. For the mandibular defect, both intramembranous and endochondral ossification were considered and SPCs migration was assumed only from the lateral surface. The MEW scaffold was incorporated with the addition of initial or boundary conditions representing different burst-release profiles of cells and/or growth factors from the scaffold into the bone defect.

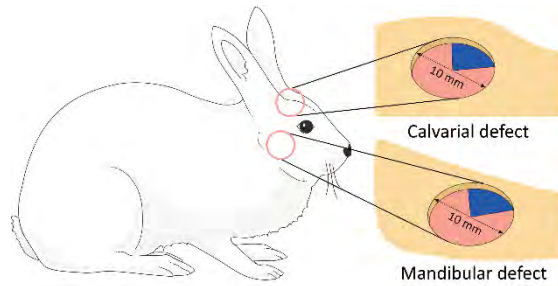


Figure 1: Schematic representation of the 10 mm diameter craniofacial bone defects: calvarial (top) and mandibular (bottom). The blue region indicates the simulated geometrical domain.

3. Results and discussion

The 3D model provided accurate predictions of the bone regeneration outcome and its corresponding biological processes. For instance, Fig. 2B shows SPCs migrations for the mandibular defect case, with subsequent differentiation and differentiation into other cell types; and Fig. 2C presents cartilage formation for the same defect. The additional source of cells and/or GF provided by the MEW scaffold contributed significantly into the healing process (results not shown).

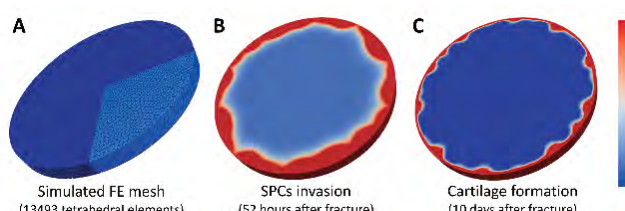


Figure 2: (A) FE mesh representing the defect, highlighting the simulated region. (B) SPCs invasion and (C) cartilage formation for the mandibular defect. Red colour (top) of scale bar indicates the maximum value.

4. Conclusions

We developed a novel 3D in silico model of bone regeneration, allowing a first screening of biomedical applications such as MEW scaffolds to treat non-union occurrences.

5. References

1. Carlier A. et al. *Biofab.* 8(2):025009, 2016.
2. Hecht F. J. *Num Math* 20(3-4):251-266, 2012.

Acknowledgements:

Interreg North-West Europe (BONE, NWE497) and ERC (772418).

28.2

High-performance computational modeling of metallic biomaterials biodegradation; a case-study of a personalized biodegradable porous acetabular implant

Mojtaba Barzegari¹, Fernando Perez Boerema¹, Gábor Závodszyk², Liesbet Geris¹

1 KU Leuven, Department of Mechanical Engineering, Heverlee, Belgium

2 University of Amsterdam, Computational Science Lab, Informatics Institute, Netherlands

1. Introduction

Before we can take advantage of the interesting properties of metallic biodegradable implants, their biodegradation behavior needs to be evaluated and tuned for the target application. One example from orthopedics is tuning the degradation rate of implants to match the rate of bone formation. In silico models can be beneficial in this regard as they can replace resource-consuming *in vitro* or *in vivo* experiments otherwise required. As a case study, in this work, we have developed a computational biodegradation model of a stiffness-optimized patient-specific porous acetabular implant.

2. Materials and Methods

The computational model of the biodegradation process was constructed based on a mechanistic diffusion-reaction model that models the oxidation-reduction reactions occurring during the biodegradation process of metallic materials in simulated body fluid. The finite element method was used to solve the computational model [1]. For building the lattice structure, the in-house developed open-source tool ASLI [2] was used to create a triply periodic minimal surface based infill for the acetabular implant based on the output of a patient-specific topology optimization. The resulting surface mesh, consisting of 5,347,924 faces, was subsequently converted to a volume mesh and embedded in a cubic container that was to act as the environment during the biodegradation simulations. The mesh was refined on the implant/environment interface to increase the numerical accuracy of the model, leading to a final mesh with 45,870,053 elements.

For dealing with a problem of this size and making the model capable of being scaled in large-scale computing systems, the model was implemented making use of the high-performance computing (HPC) techniques available in the FreeFEM language v4.10 and PETSc toolkit v3.16.1 [3]. The simulation was carried out using 2,000 CPU cores with 16.5 TB of available memory. The results, with a total size of 148 GB, were visualized using a parallel ParaView server v5.9.1 running on 128 CPU cores. To obtain the scaling behavior of the model in an HPC environment scaling tests were performed by varying the number of employed CPU cores from 60 to 9,000.

3. Results and Discussion

The generated lattice structure of the implant, infilled by skeletal-gyroid unit cell type, is depicted in Fig. 1A. Biodegradation results show that the acetabular implant degrades faster in the region with higher porosity, i.e. the region with more exposed surface area to the environment (Fig. 1B). Loss of material over time was found to be in line with the values obtained in our previous study [1], showing that scaling the model in an HPC environment does not affect the quantitative predictions made by the model. The scaling tests show that the optimal size for the distributed computing environment is 5,000 CPU cores, above which no significant improvement in the execution time was observed.

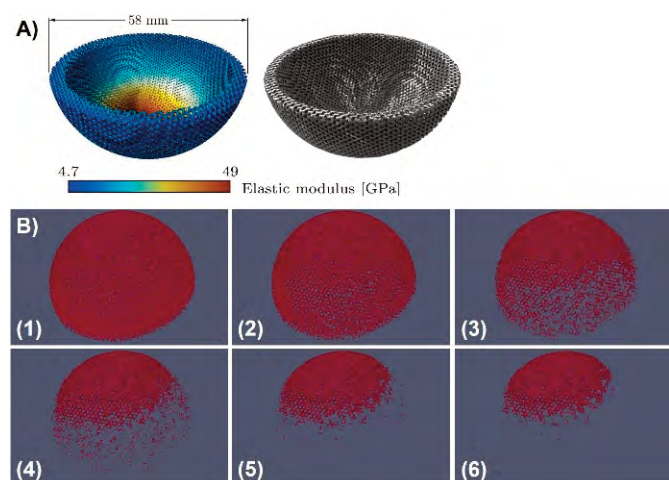


Figure 1: A) acetabular implant infilled by varying volume fraction to match a desired stiffness distribution, B) visualization of the change of morphology of the acetabular implant (time scale not calibrated)

4. Conclusions

In this work, taking advantage of HPC techniques to simulate a large-scale 3D model led to a computational model capable of predicting the biodegradation behavior of an acetabular implant in high resolution. Results demonstrate the potential of the model to act as a tool for assessing and tuning the biodegradation properties of orthopedic implants regardless of shape or complexity.

5. References

1. Barzegari et al. *Corros Sci*;190, 2021.
2. Perez-Boerema et al. *Virtual Phys Prototyp* 2022.
3. Barzegari & Geris *Int J HPC*; 36(2):198, 2022.

Acknowledgments:

Funded by Interreg VA Flanders - Netherlands, (2014TC16RFCB046, Prosperos) & FWO-Vlaanderen (G085018N).

28.3

Modeling osteoporosis to design and optimize pharmacologic therapies comprising multiple drug classes

David Jörg¹, Doris Fuertinger¹, Peter Kotanko^{2,3}

1 Fresenius Medical Care Germany, Biomedical Modeling and Simulation, Bad Homburg, Germany

2 Renal Research Institute, New York, NY, United States

3 Icahn School of Medicine at Mount Sinai, New York, NY, United States

Correspondence: D. J. Jörg, david.joerg@fmc-ag.com

1. Introduction

Osteoporosis-associated bone fractures lead to disabilities, pain and increased mortality [1]. For the treatment of osteoporosis, several drug classes with different mechanisms of action are available. Since only a limited set of dosing regimens can be tested in clinical trials, it is currently unclear whether common medication strategies achieve optimal effect regarding bone density increase and fracture reduction. To explore the vast number of alternative dosing schemes, especially those comprising multiple drug classes, we have developed a parsimonious physiology-based modeling framework of drug interventions for osteoporosis that unifies fundamental mechanisms of bone remodeling and the mechanisms of action of several drug classes [2].

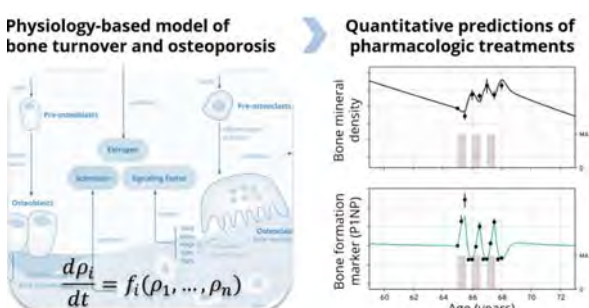


Figure 1: Our model describes the cellular activity, cell fates and intercellular signaling within a "representative bone remodeling unit".

2. Materials and Methods

Our model captures the long-term dynamics of bone formation and resorption [2]. It describes, at a compartmental level, cell fates and cellular activity of osteoblasts, osteoclasts, osteocytes and their progenitor populations as well as important signaling molecules such as estrogen and sclerostin (Fig. 1). Moreover, the model includes the mechanisms of action of several drug classes commonly used for osteoporosis treatment: bisphosphonates, PTH analogs, sclerostin inhibitors and RANKL inhibitors.

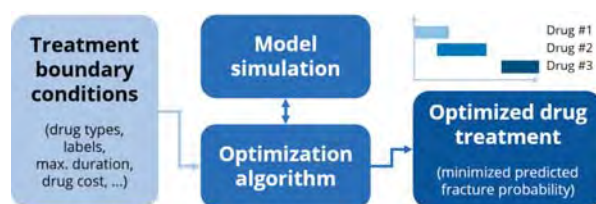


Figure 2: Treatment optimization scheme.

In a second step, we developed an algorithm that finds optimized drug dosing schemes which minimize future fracture probability for given treatment boundary conditions (like drug classes, treatment duration, cost etc.) (Fig. 2).

3. Results

Using published data from a limited set (18) of clinical trials, we calibrated and validated the model, demonstrating its predictive capacity for complex medication scenarios in 60 study arms from 25 clinical studies.

Notably, model-aided treatment optimization yielded novel combination therapies, which in simulations achieved considerably higher bone mineral density gains than those tested in clinical trials so far, while not increasing the total medication load [2].

4. Discussion and Conclusions

Our model results show that there is a large potential to improve osteoporosis treatment by exploiting synergistic interactions between different drugs. Thus, the proposed model can provide a quantitative platform for the development of personalized osteoporosis therapy, taking into account patient-specific pharmacodynamic properties such as individual drug half-lives and drug resistivities.

5. References

1. C. Cooper and S. Ferrari, "IOF Compendium of Osteoporosis." 2019
2. Jörg DJ, Fuertinger DH, Cherif A, Bushinsky DA, Mermelstein A, Raimann JG, Kotanko P. *bioRxiv*. 2021; 10.1101/2021.12.17.473190.

28.4

The PNT-Methodology: a novel high-level top-down network modelling approach applied to the intervertebral disc

Laura Baumgartner¹, Miguel Ángel González Ballester^{1,2}, Jérôme Noailly¹

¹ Universitat Pompeu Fabra, Information and Communication Technologies, Barcelona, Spain

² ICREA, Barcelona, Spain

Laura Baumgartner, laura.baumgartner@upf.edu

1. Introduction

Network models to estimate biological activity are highly sensitive to the topology. Moreover, the capacity to integrate time sensitivity to chronic stimulus exposure is limited. We present a novel network modelling approach to approximate cell activities (CA), including time sensitivities to simulate long time periods. The methodology was developed to estimate CA of intervertebral disc Nucleus Pulposus (NP) cells.

2. Materials and Methods

The system consisted of key relevant stimuli and CA for NP cells. Stimuli were glucose (glc), pH, load magnitude (mag) and frequency (freq). CA were the mRNA expressions (expr) of tissue proteins (Aggrecan (Agg), Collagens Type I & II (Col-I, Col-II)) and proteases (MMP3, ADAMTS4) (Fig.1).

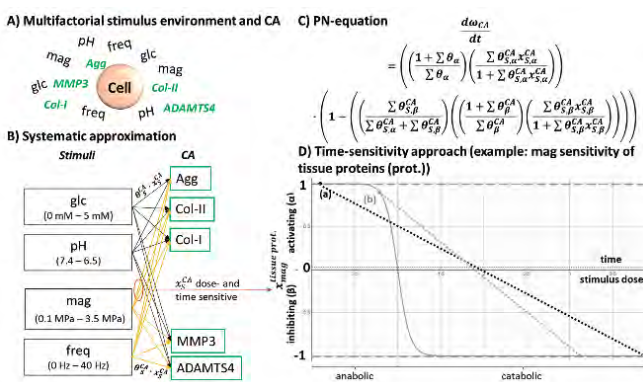


Figure 1: System of interest (A) systematically approached (B) and calculated with the PN-equation (C) including time-dependent effects of load (D).

The cell is considered as a black box and each CA (ω_{CA}) is interpreted as an individual, parallel network (PN), regulated by its surrounding stimuli (Fig.1, B). The relationship between a stimulus and a CA is determined by the sensitivity of the CA to the given stimulus (subscript s) $\llbracket(x)\rrbracket_{S^CA}$ [1] and by the relative impact of the stimulus on the CA (θ_{S^CA})[2]. Time sensitivity was integrated for mechanical load parameters. It reflected a constant adaptation of x_{S^CA} depending on initial, user-defined stimulus doses (Fig.1,D, e.g. doses (a), (b)). PN environments were calculated with the PN-equation (Fig.1,C), characteristic of the time-dependent Parallel Networks (PNT) Methodology. It provided interrelated outputs for each CA, reflected as PN-activity. Six months exposure to microgravity (0.25 MPa [3], 0 Hz) under optimal nutritional conditions (5 mM glc, pH 7.1) are simulated and compared to daily live under gravity (one day: 10h laying down (0.15MPa, 0Hz), 2x4h sitting (0.55MPa, 0Hz) and 3x2h walking (0.60MPa, 1.80Hz)[3]).

3. Results

Results show a constant decrease of Agg and Col-II mRNA expr, whilst protease expr remain low over the first months of exposure (Fig. 2).

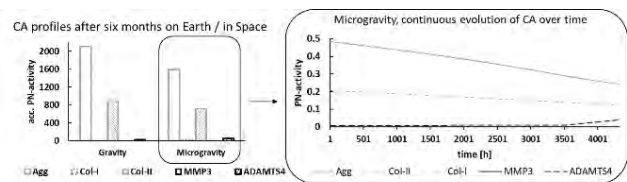


Figure 2: Prediction of CA within an astronaut's NP.

4. Discussion and Conclusions

Exposure to microgravity downregulated tissue proteins, especially Agg, compared to life on Earth, but the process was slow. Among the protease mRNA expr, only ADAMTS4 increased slightly, after several months in Space. These time-dependent outcomes might explain both disc swelling in bedrest studies of few days [4] and disc desiccation in astronauts during long space flights [5]. Relative changes in PN-activity can further inform changes in tissue properties, in multiscale simulations. The PNT-Methodology could uniquely estimate CA over time, for user-defined stimulus conditions.

5. References

- Baumgartner et al, Bioinformatics, 37:1246-53 (2020)
- Baumgartner et al, Front. Bioeng. Biotechnol. 9:1-17 (2021)
- Wilke et al, Spine, 24:755-62 (1999)
- Koy et al, PLoS ONE, 9: e112104 (2014)
- Garcia et al. J Ultrasound Med 37:987-99 (2018)

Acknowledgements:

The authors would like to thank the Spanish Government (RYC-2015-18888), the DTIC-UPF and the European Commission (H2020-MSCA-ITN-ETN-2020-955735)

Poster viewing session 1

Wednesday 7th September, 13:15-14:15

Chairs: Renato Natal Jorge, Laura Lafuente-Gracia

- 1.1 How does spine segment shape affect intradiscal and facets contact pressure? An in-silico study; *Amin Kassab-Bachi, United Kingdom*
- 1.2 Blood flow modeling in patient-specific aneurysm geometry; *Jana Trdlcová, Czech Republic*
- 1.3 Machine self-semantic learning for socio-behavioural factors assessment in dementia progression; *Kamil Woźniak, Poland*
- 1.4 On generating realistic variations of patient specific arterial anatomy; *Jacob Sturdy, Norway*
- 1.5 Response to antihypertensive combination therapy requires a healthy heart: a simulation and Interpretable AI study; *Robert Hester, United States*
- 1.6 Intracranial aneurysm rupture status discrimination and geometric uncertainty; *Jan Brüning, Germany*
- 1.7 Procedural planning using computational fluid dynamics for pulmonary artery stenosis stenting with limited clinical data; *Liam Swanson, United Kingdom*
- 1.8 Computational fluid dynamics modelling of airflow in congenital tracheal defects - in silico modelling for informing and optimizing surgical strategies; *Liam Swanson, United Kingdom*
- 1.9 A model for the human fetal ventricular myocyte (HFVM) electrophysiology; *Adelisa Avezzù, United Kingdom*
- 1.10 Local flow analysis in the iliac vein bifurcation informed by a 0D model of the lower limb circulation; *Magdalena Otta, Poland*
- 1.11 Computed Tomography Based Assessment of Transvalvular Pressure Gradient in Aortic Stenosis; *Benedikt Franke, Germany*
- 1.12 Towards machine learning based pressure drop assessment in aortic stenosis; *Andreea Bianca Popescu, Romania*
- 1.13 Catheter tracking in thrombectomy procedure: a finite element analysis and patient-specific comparison; *Nerea Arrarte Terreros, Netherlands*
- 1.14 Fluid-structure interaction analysis of eccentricity and leaflet rigidity on thrombosis biomarkers in bioprosthetic aortic valve replacements; *David Oks, Spain*
- 1.15 Coupling Agent Based Method and Computational Fluid Dynamics for Plaque Development in the Carotid Artery; *Andjela Blagojević, Serbia*
- 1.16 Multiscale modeling of spreading depolarization and depression in brain slices; *Craig Kelley, United States*
- 1.17 Assessing credibility of an In Silico trial model for the development of new vaccines against tuberculosis; *Cristina Curreli, Italy*

Poster viewing session 2

Wednesday 7th September, 13:15-14:15

Chairs: Claudio Capelli, Sara Bridio

- 2.1 A Mathematical Model describing Cell Shape Evolution and the Impact of Cellular Forces on the Extracellular Matrix during Cell Invasion through a Flexible Channel; *Qiyao Peng, Netherlands*
- 2.2 Early in silico assessment of drug-induced proarrhythmic risk using Drug Safety Suite; *Cristina Vaghi, Italy*
- 2.3 Monitoring age-related penetrance of right ventricular myocardial disease in arrhythmogenic cardiomyopathy using a Digital Twin approach; *Nick van Osta, Netherlands*
- 2.4 Coronary flow and ffr prediction: part 2 - semi-automatic cad/cae system for clinical decision support; *Boris Chernyavsky, France*
- 2.5 A framework for the development of intestinal digital twins integrating machine learning and multiphysics modelling; *Panagiotis Kalozoumis, Greece*
- 2.6 Developing a physiological map as a framework to study chemical-induced liver steatosis; *Luiz Carlos Maia Ladeira, Belgium*
- 2.7 Validation of stress shielding for an in silico clinical trial in support of a regulatory submission; *Philippe Favre, Switzerland*
- 2.8 Reliable digital twin simulation development and execution on the HPC infrastructures; *Marian Bubak, Poland*
- 2.9 From Physiological Map to Ontology Unravelling Kidney Toxicity; *Alessio Gamba, Belgium*
- 2.10 Implementing Public & Patient Involvement (PPI) for in silico medicine.; *Cyrille Thinnies, Ireland*
- 2.11 Computation approach to circularRNA estimation; *Sabina Licholai, Poland*
- 2.12 Systematic engagement with notified bodies to advance in silico trials in Europe; *Simon Sonntag, Germany*
- 2.13 Building a cloud simulation system for reproducible and multi-level cached in-silico trials; *Yves Pares, France*
- 2.14 Clinical trial simulations in oncologic patients using the InSilicoONCO suite; *Chiara Nicolò, Italy*
- 2.15 iSi Health: the KU Leuven institute of physics-based modeling for in silico health; *Erica Beaucage-Gauvreau, Belgium*

Poster viewing session 3

Thursday, September 8th, 12.45-13.45

Chairs: Luděk Hynčík, Mojtaba Barzegari

- 3.1 Automatic Fracture Reduction of Pelvis using Statistical Shape Modelling; *Tabassum Husain, Australia*
- 3.2 Sensitivity analysis of an one-dimensional pulse wave propagation model with correlated input.; *Pjotr Hilhorst, Netherlands*
- 3.3 Identification of the most influential factors on pulmonary artery hemodynamics using variance-based sensitivity analysis; *Hamed Moradi, Netherlands*
- 3.4 Dependency of healing outcomes on biomechanical conditions in postoperative reconstructed mandibles; *Giorgio Biesso, Germany*
- 3.5 Simulating non-Newtonian flow through aortic phantom: comparison between lattice Boltzmann method and magnetic resonance imaging; *Radek Galabov, Czech Republic*
- 3.6 Meshless Simulation of Cell Growth Dependent on Oxygen and Glucose Concentration; *Maria Inês Barbosa, Portugal*
- 3.7 Cell Proliferation Study Using a Discretization Meshless Technique; *Maria Inês Barbosa, Portugal*
- 3.8 v-Patients Simulation: Smoothed Particle Hydrodynamics for Simulating Implant - Tissue Interaction; *Bence Rochlitz, Germany*
- 3.9 Neural-network-based visualization for pervasive continuum-biomechanical simulations; *David Rosin, Germany*
- 3.10 Towards a repository of patient-specific intervertebral discs finite element models; *Estefano Muñoz-Moya, Spain*
- 3.11 Musculoskeletal modeling and simulation of subject specific lower limb joint loads computing during normal and abnormal gait; *Carlos Rodrigues, Portugal*
- 3.12 Effective scaffold design optimization through coupling of complex and simple models for scaffold mediated bone growth; *Mahdi Jaber, Germany*
- 3.13 Subject-specific 3D models to investigate the influence of rehabilitation exercises on Achilles tendon strains; *Alessia Funaro, Belgium*
- 3.14 Image-based simulation of left ventricular hemodynamics: study on mitral regurgitation and left ventricle aneurysm patients; *Lukas Obermeier, Germany*
- 3.15 Epiretinal Membrane Contraction: a Finite Element Analysis; *Margarida Chiote, Portugal*

Poster viewing session 4

Thursday, September 8th, 12.45-13.45

Chairs: Andrew Narracott, Goncalo Almeida

- 4.1 Detection of Pulmonary Hypertension Using Explainable Machine Learning; *Michał K. Grzeszczyk, Poland*
- 4.2 Bayesian history matching to calibrate virtual cohorts of human hearts; *Cristobal Rodero, United Kingdom*
- 4.3 Effect of left ventricular shape on hemodynamics using computational fluid dynamics and non-invasive imaging data; *Sumit Kumar, India*
- 4.4 Modelling Infarct Formation During Acute Ischaemic Stroke Treatment; *Raymond Padmos, Netherlands*
- 4.5 Angiogenesis modelling through a coupled mixed-dimensional haemodynamic/tissue model; *Cameron Apeldoorn, New Zealand*
- 4.6 PPG sensor modelling for cardiovascular parameter estimation; *Xavier Bednarek, France*
- 4.7 Integration of heterogeneous biological data in multiscale mechanistic model calibration; *Jean-Louis Palgen, France*
- 4.8 Multiscale modeling of electrically active bone implants; *Anna Karina Fontes Gomes, Germany*
- 4.9 Measurements of the intraoperative migration of proximal femoral nail in a wide medullary canal; *Krzysztof Zerdzicki, Poland*
- 4.10 Physiomics of right atrial ganglionic plexus neurons predicted from transcriptomics; *Suranjana Gupta, United States*
- 4.11 Transmembrane mucin response in conjunctival epithelial cells exposed to wall shear stresses; *Shir Itah, Israel*
- 4.12 Optimization of 3D-printed breast prosthesis for breast reconstruction; *Xuan-Tien Kévin TRINH, France*
- 4.13 MicroMap: Interactive visualisation of human microbiome metabolism realised via online systematic team empowerment of STEM undergraduates in Ireland.; *Cyrille Thinnies, Ireland*
- 4.14 Estimating Skeletal Muscle Forces in vivo: A Shear Wave Elastography Approach; *Manuela Zimmer, Germany*
- 4.15 Determining the navier slip parameter in the descending aorta using 4d pc-mri data; *Alena Jarolímová, Czech Republic*

P1.1

How does spine segment shape affect intradiscal and facets contact pressure? An in-silico study

Amin Kassab-Bachi^{1,2}, Nishant Ravikumar², Ruth Wilcox¹, Alejandro F. Frangi², Zeike A. Taylor^{1,2}

1 Institute of Medical and Biological Engineering (iMBE), School of Mechanical Engineering, Leeds, United Kingdom

2 Center for Computational Imaging & Simulation Technologies in Biomedicine (CISTIB), School of Computing, Leeds, United Kingdom

Email: mn15akb@leeds.ac.uk

1- Introduction

The relationship between spine segment geometry and biomechanics can inform both patient-specific modelling and cohort studies by quantifying the relative importance of anatomical features. This relationship was studied in [1,2] using idealised geometric models that parameterised key shape features. But, while these features are correlated in real populations, they were varied independently in [1,2], likely producing geometries not in practice found in real cohorts.

We used a principal component analysis-based statistical shape model (SSM) to parameterise the L4/L5 functional spinal unit (FSU) geometry. This model was sampled to generate realistic new geometries, which were used to assess the influence of naturally-occurring shape variations on intradiscal pressure (IDP) and facet joint contact pressure (FCP) under pure axial compression.

2- Materials and Methods

152 L4/L5 FSU geometries were sourced from the MySpine database and used to train an SSM. 500 new geometries were then synthesised via Latin hypercube sampling of the SSM. FEM parameters were propagated from a template model to each instance. Shape features dependence of IDP and FCP were then evaluated through correlation and Shapley value analyses.

3- Results

FE predictions were close to values found in literature [3,4]: mean IDP and FCP were 0.504 MPa (CI:[0.495-0.512]) and 0.77 MPa (CI:[0.69-0.86]), respectively. The first shape mode (SM1) explained 22.6% of shape variation and had the largest correlation with, and contribution to IDP (17%) and FCP (11%). The largest geometric variation in SM1 was in the nucleus pulposus size (Fig. 1).

4- Discussion and Conclusions

Multiple shape features were significantly correlated with IDP/FCP predictions, though their contribution levels varied widely (Fig. 2). The proposed method can produce spinal samples that reflect the shape variability in a real cohort. Furthermore, although individual shape modes (SMs) are independent in the principal component space, each SM normally affects more than one anatomical feature in the Cartesian space. Hence, this parameterisation approach is able, by construction, to capture correlations between anatomical features in real populations and produce plausible new (sampled) geometries.

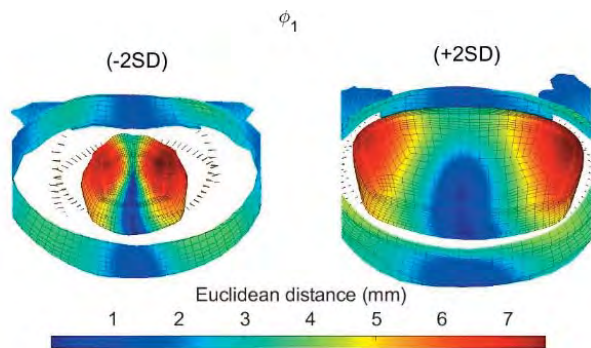


Figure 1: Nucleus shape change in SM1. Heat-map represents Euclidean distance from the mean shape.

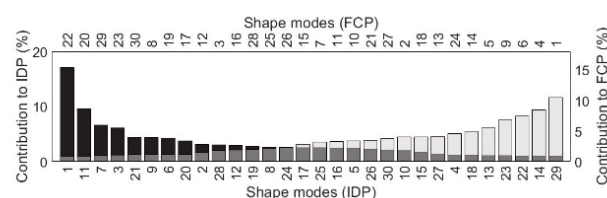


Figure 2: SMs contributions to IDP/FCP.

5- References

1. Niemeyer F, et al. J Biomech 45: 1414-23, 2012.
2. Zander T, et al. J Biomech 53: 185-190, 2017.
3. Dreischaff M, et al. J Biomech 47: 1757-66, 2014.
4. Lorenz M, et al. Spine 8: 122-130, 1983.

Acknowledgements:

The authors gratefully acknowledge funding support from EPSRC (EP/L014823/1) and RAEEng (LTRF2021\17115; CiET1819\19).

P1.2

Blood flow modeling in patient-specific aneurysm geometry

Jana Trdlicová¹, Jaroslav Hron¹

¹ Charles University, Faculty of Mathematics and Physics, Mathematical Institute, Prague, Czech Republic
trdlicova@karlin.mff.cuni.cz, hron@karlin.mff.cuni.cz

1. Introduction

Recent years have seen increasing interest in the use of computational fluid dynamics for modeling blood flow in diseased human vessels such as aneurysms. Patient-specific numerical models represent an encouraging tool that could help optimize clinical management in the future [1], since hemodynamic quantities could be employed as indicators of risk of rupture.

Recent studies on patient-specific blood flow models almost exclusively prescribe the no-slip wall boundary condition (BC), which assumes that blood does not move on the vessel wall. Although easy to implement, there are arguments based on experimental observations that reported evidence of slippage between the solid wall and blood [2]. This phenomenon can be captured by the Navier slip BC, which gives the proportionality between the tangential part of the velocity on the wall and the shear stress using an additional parameter $\theta \in (0,1)$

$$\theta \vec{v}_t + \gamma_*(1 - \theta) (T\vec{n})_t = \vec{0}, \quad (1)$$

where γ_* is a material parameter characterizing the slip, T is the Cauchy stress tensor, the subscripts t,n denote the tangential and normal parts of a vector, respectively.

2. Materials and Methods

The governing equations for blood flow are the Navier–Stokes equations. Prescribing suitable boundary conditions (BC) and constitutive relations, we seek the solution via the finite element method. Blood was modeled as both a Newtonian and a non-Newtonian fluid, and differences in hemodynamics were evaluated. The wall is assumed to be impermeable and rigid. We prescribe Navier slip BC on the vessel wall, a parabolic velocity profile on the inlet part of the boundary, and directional do-nothing BC on the outlet parts. We use the FEniCS module (fenicsproject.org) with a nonlinear solver adopted from the PETSc library, see [2].

3. Results

The results showed that the effect of the non-Newtonian properties of the blood did not have a significant impact on hemodynamics in this geometry. However, variations in the slip parameter considerably change the character of the flow within the aneurysm (Fig. 1) and therefore the hemodynamic quantities also changed significantly – not only in magnitude but also in the site of extreme values. Namely, we observed the wall shear stress, oscillatory shear index (OSI), and a novel hemodynamic quantity oscillatory velocity index (OVI). Interestingly, we showed that, while using the Navier slip BC, OVI appears to be a better hemodynamic quantity than OSI, as it captures, in addition to the information on the wall, the complexity of flow within the aneurysm. Furthermore, for lower slip parameters, the OVI isosurfaces showed a vortex whose center led to the known rupture site (Fig. 1), which was identified by a surgeon.



Figure 1: Isosurfaces of OVI=0.05 for slip parameters 1, 0.9, 0.7, 0.5 from left to right. The aneurysm is shown in a transparent gray color, and the known rupture site is denoted by a circle.

4. Discussion and Conclusions

The novelty of our approach is prescribing the Navier slip BC instead of the common no-slip, which has the potential to more realistically capture the blood flow and help evaluate the risk of rupture in the future. Currently, our goal is to fit the velocity model with measurements to determine the value of the slip parameter.

5. References

- Hu B et al., *Chinese Journal of Academic Radiology*, 4(3):150–159, (2021).
Chabinic R et al., *Applications in Engineering Science*, 6:100038 (2021).

Acknowledgements:

The work was supported by the Ministry of Health of the Czech Republic, grant nr. NV19-04-00270.

P1.3

Machine self-semantic learning for socio-behavioural factors assessment in dementia progression

Kamil Woźniak¹, Anna Drożdż¹, Jose Sousa¹

1 Sano Centre for Computational Medicine, Personal Health Data Science, Kraków, Poland

1. Introduction

Dementia is a complex disease that emerges from a combination of interdependent and personal risk factors, including social behaviour [1]. Machine learning (ML) can model complex interactions, most frequently taking the supervised form and using large data sets. However, relying on pre-labelling is time-consuming, expensive and do not generalize well [2, 3]. Therefore, a learning approach for the dynamics and complexity of the disease techno-social system needs to be able to self-create knowledge representations using different sources and data types.

Here, we present a method for modelling reality and extracting knowledge to identify most relevant socio-behavioural factors for the development of dementia. Obtained results were compared with univariate tests and Bayesian network modelling.

2. Materials and Methods

The data was obtained from the 1st to 6th wave of English Longitudinal Study on Ageing (ELSA). After pre-processing dataset contained 268 participants (134 with dementia) with 27 variables including socio-behavioural assessment and comorbidities. Both groups were characterized with Chi² test (characterization of comorbidities) and t-test (investigation of socio-behavioural differences).

Next, data were pre-processed and then the abstraction was sent to computational intelligence (CI). The knowledge network was structured using betweenness (node size), communities (colour), and weight of the connectivity (edge width).

Finally, data were analysed using Bayesian network modelling with temporal dimensions analysis.

3. Results

Chi² test did not show any significant differences in the prevalence of comorbidities in dementia and control group. Contrarily, knowledge models, which were produced for data sets stratified by gender, revealed an apparent difference in the network structure. Results achieved with self-learning showed that comorbidities and social relation 'profile' (SRP) characteristic are only relevant for females. In comparison, the univariate test presents evidence for the effect of SRP for both genders, while Bayesian network modelling – for interaction between dementia, comorbidities, and SRP,

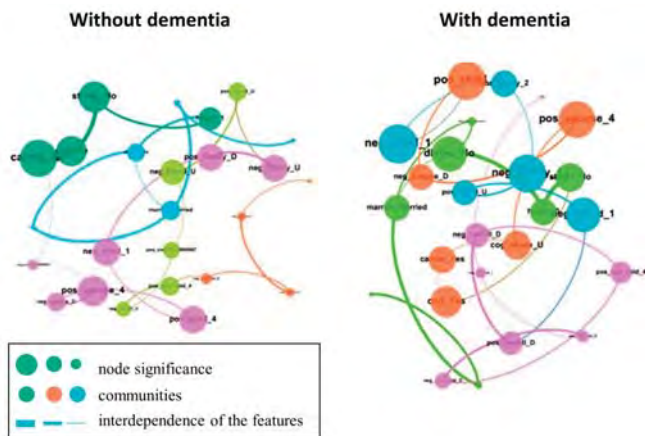


Figure 1: The knowledge graphs generated for the females.

4. Discussion and Conclusions

The presented approach allowed to infer about interactions which are impossible to detect with traditional statistical tests. We indicated social behaviour markers that could be used as measures to understand dementia progression, improve profiling of the disease from the social behaviour perspective and approach the diagnosis from a set of unique angles that are gender-related, creating a systematic understanding of their importance.

5. References

1. Fratiglionio, L., Wang, H.X., Ericsson, K., et al., 2000. *Lancet (London, England)* 355, 1315–1319
 2. Kim, J., Wilhelm, T., 2008. *Phys. A Stat. Mech. its Appl.* 387, 2637–2652.
 3. Zheng, Y., Jin, M., Liu, et al., 2021. *IEEE Trans. Knowl. Data Eng.* 1.

Acknowledgements:

We acknowledge the European Union's Horizon 2020 RAI programme (Grant no: 857533) for providing financial support and ELSA funded by National Institute of Aging (Grant no: R01AG017644).

P1.4**On generating realistic variations of patient specific arterial anatomy****Jacob Sturdy¹**

1 Norwegian University of Science and Technology, Norway

1. Introduction

Personalized cardiovascular simulations signal a transformation in cardiovascular medicine recognized in both medical and engineering research [1-3]. Powerful modelling and simulation frameworks apply our knowledge of the fundamental physics and physiology, yet numerous obstacles remain that prevent wider clinically relevant application of these approaches. In this work we investigate representation of patient specific anatomical variation of arterial bifurcations and propose a method for assessing the consistency generated variations by comparing them with observed anatomy derived from image segmentations. As generation of variations is necessary for realistic assessment of uncertainty in patient specific simulations, evaluations of such generative methods are needed to calibrate predictive uncertainties and to build confidence in the models.

2. Materials and Methods

Uncertainty quantification and sensitivity analysis (UQSA) are essential to verification and validation of models applied in clinical contexts[4]. While a number UQSA methods exist, in general these require a discrete representation of the inputs that are uncertain. Several studies have investigated the role of geometric uncertainty in hemodynamic simulations [5-7]. The representation of geometric uncertainty is typically grossly simplified from the realistic uncertainty for a number of reasons. First, the geometry and its anatomy are in general three dimensional and direct discretization approaches will result a number of uncertain inputs that far exceeds the dimensionality for which computations of UQSA are feasible. Second, indirect discretization approaches rely on some sort of parametrization of the underlying anatomy which in general induces significant biases from the real anatomy. We apply the Karhunen-Loève expansion to arterial bifurcations to discretize the anatomical variation in a manner that accounts for strong spatial correlation of variations. Further, this approach is an efficient way to produce realistic variations to an arbitrary geometry, thus the realizations are free to vary at all points in space without any underlying parametric geometry.

As it is essential to confirm that the approach produces realizations that are consistent with observed variations in anatomy, we develop a generative data model based on this approach and compare the generated data with observed variations in geometries segmented from medical imaging.

3. Results

This approach shows that it is possible to efficiently generate complex variations in geometry that still respect fundamental constraints of smooth variation in the arterial wall and further evaluates the plausibility of these generated geometries by comparison to variations observed in segmentations.

4. Discussion and Conclusions

Anatomical representations derived from medical imaging are uncertain and vary substantially between observers [8]. Approaches like that presented here are essential to account for anatomical variation.

5. References

1. Morris PD, et al. *Heart* 102(1):18–28 (2016)
2. Huberts W et al., *J Comput Sci* 24:68–84 (2018)
3. Hose DR et al., *Med Eng Phys*, 72:38–48 (2019)
4. Steinman DA, Migliavacca F. *Cardiovasc Eng Tech* 9(4):539–43 (2018)
5. Colebank MJ et al., *J R Soc Interface* 16(159): 20190284 (2019)
6. Müller LO et al., *Int J Numer Meth Biomed Engng.* E3246 (2019)
7. Sankaran S et al., *J Biomech*, 49(12):2540–47 (2016)
8. Berg P et al., *Cardiovasc Eng Tech* 9(4):565–81 (2018)

Acknowledgements:

The authors thank the Polish National Science Center GRIEG programme, (Grant no: UMO-2019/34/H/ST8/00624) for providing financial support to this project".

P1.5

Response to antihypertensive combination therapy requires a healthy heart: a simulation and Interpretable AI study

W. Andrew Pruett^{1,2}, John Clemmer¹, Robert L. Hester^{1,2}

¹ University of Mississippi Medical Center, Physiology and Biophysics, Jackson, United States
² HC Simulation, Canton, United States

1. Introduction

The prevalence of hypertension (HTN) in the US and Europe is >30%, rising to 40% in some regions [1]. Because blood pressure (BP) drives tissue perfusion, the body has multiple mechanisms to preserve it. Treating patients with multiple HTN therapies can be effective by affecting multiple axes, but 10% still remain hypertensive ≥ 3 drugs (resistant HTN) [2]. These patients have a high frequency of congestive heart failure (CHF)[3], but the mechanisms are unclear. Also, the factors that predispose patients to CHF and their impact on HTN therapy responses are unknown. Interpretable artificial intelligence (AI) methods may provide causal or predictive explanation for patient specific responses.

2. Materials and Methods

All simulations were performed using HumMod, a large model of human physiology composed of mathematical relationships derived from experimental and clinical data. Obesity/apnea-associated HTN was simulated by increasing chemoreceptor-associated sympathetic nerve (SN) output. A virtual population (VP) was constructed by sampling 21 model coefficients associated with BP during SN activation. These models were steadied and subjected to triple therapy consisting of amlodipine (2.5 mg daily), lisinopril (10 mg daily), and furosemide (12 mg daily). Each therapy was simulated for 1 week before the next was begun, and the patient was steadied with all three drugs for 90 days. A proxy model for patient response was created with gradient boosted trees (RStudio, gbm), and association with the change in BP was tested using individual conditional expectation (RStudio, ICEbox).

3. Results

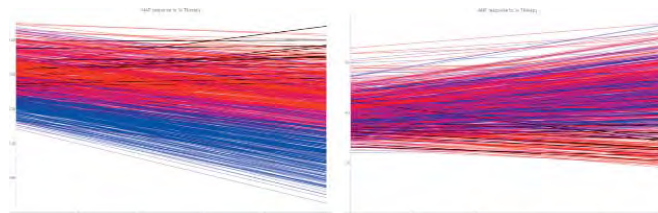


Figure 1: Response to triple therapy. Left, mean BP. Right plasma [ANP] (pg/ml). Black lines denote patients who had <0 mmHg response, Red <10 mmHg, Blue >10 mmHg.

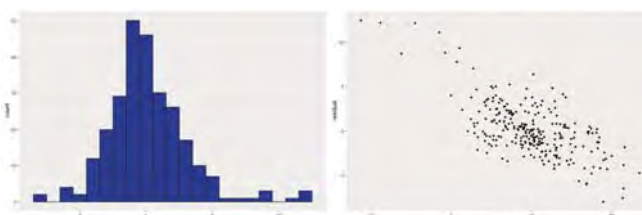


Figure 2: Proxy model fit for BP response. GBM trained on 70% of the VP, fit tested against remaining 30%. Standard deviation of error was < 3.0 mmHg (left), and the error was evenly distributed throughout the range of responses (right).

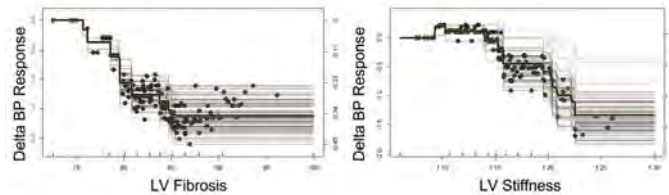


Figure 3: While LV stiffness and fibrosis are not correlated with resistance, increasing diastolic dysfunction in VP leaving all other factors unchanged reduces response to triple therapy.

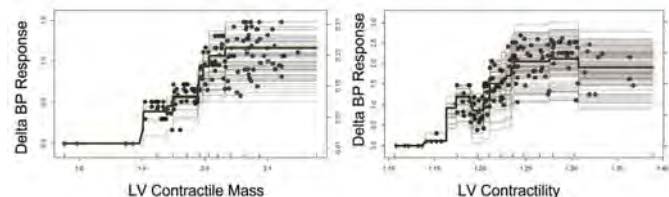


Figure 4: Increasing contractile mass or decreasing contractility while leaving all other factors unchanged are associated with triple therapy resistance.

4. Discussion and Conclusions

Interpretable AI uses a well-fit model to investigate valid states not part of the sampled training and testing data. The virtual population showed worsening diastolic dysfunction (Figure 3) and systolic dysfunction (Figure 4). Together these suggest alternate therapeutic options may need to be explored in patients with indications for HF of either type.

5. References

1. Sahuja et al. *J Hypertens.* 2015; 33(3):644-51.
2. Noubiap et al. *Heart.* 2019; 105:98-105.
3. Cai and Calhoun. *Hypertension.* 2017; 70(1): 5-9.

Acknowledgements:

Supported by NSF SBIR 2110147.

P1.6

Intracranial aneurysm rupture status discrimination and geometric uncertainty

Florian Hellmeier¹, Jan Brüning¹, Leonid Goubergrits^{1,2}

1 Charité – Universitätsmedizin Berlin, Institute of Computer-assisted Cardiovascular Medicine, Berlin, Germany

2 Einstein Center Digital Future, Berlin, Germany

1. Introduction

Incidental unruptured intracranial aneurysms (IA) are not uncommon [1] and managing the risk associated with them remains a clinical challenge. A variety of rupture risk parameters and scores have been developed with generally mixed performance. This presentation compares the discriminative abilities of a set of geometric risk parameters to the uncertainty inherent in their assessment. It also provides information on the correlation between parameters.

2. Materials and Methods

37 geometric risk parameters from four groups (12 size, 6 neck, 9 non-dimensional, and 10 curvature parameters) were calculated for 244 IA geometries from two datasets. Analysis was stratified by anatomical location, based on the PHASES score. Standardized absolute differences (SAD) between the ruptured and unruptured IAs were calculated. Additionally, the ratio of SAD to previously published [2] median relative uncertainty (MRU) values was used to assess parameter robustness. Finally, Pearson's r was calculated to evaluate inter-parameter correlations.

3. Results

Substantial variation of SAD within and across parameter groups was found. Additionally, IA location substantially impacted SAD, with IAs of the posterior anatomical region exhibiting overall higher SAD. Higher-dimensional size parameters tended to exhibit a worse ratio of SAD to MRU than lower-dimensional parameters. Performance of non-dimensional parameters tended to be generally favorable. Correlations between parameters were strongest within parameter groups and generally far less sensitive to anatomical location than SAD.

4. Discussion and Conclusions

The non-dimensional parameter group's overall combination of discriminative performance and robustness indicates better generalization to other datasets compared to other parameter groups. Regarding the correlation analysis, the generally strong correlations between parameters from the same parameter group suggests that parameters within a parameter group often capture similar aspect of IA morphology. It might therefore be sufficient to use a comparatively small set of parameters in any given risk model and still capture most of the relevant morphological information.

5. References

1. Vlak MHM, Algra A, Brandenburg R, Rinkel GJE. Lancet Neurol. 2011;10(7):626-636
2. Goubergrits L et al. Biomed Eng Online. 2019;18(1):35

Acknowledgements:

The authors would like to acknowledge PD Dr.-Ing. Philipp Berg (Laboratory of Fluid Dynamics and Technical Flows, University of Magdeburg) and PD Dr.-Ing. Sylvia Saalfeld (Department of Simulation and Graphics, University of Magdeburg) for providing one of the datasets.

P1.7

Procedural planning using computational fluid dynamics for pulmonary artery stenosis stenting with limited clinical data

Liam Swanson^{1,2}, Emilie Sauvage¹, Hopewell Ntsinjana^{3,4}, Silvia Schievano^{1,2}, Claudio Capelli^{1,2}

1 University College London, Institute of Cardiovascular Science, London, United Kingdom

2 Great Ormond Street Hospital for Children, London, United Kingdom

3 University of the Witwatersrand, Johannesburg, South Africa

4 Nelson Mandela Children's Hospital (NMCH), Paediatric Cardiology, Johannesburg, South Africa

Correspondence to Liam Swanson: liam.swanson.20@ucl.ac.uk

1. Introduction

Congenital heart disease (CHD) is the most common group of congenital malformations and where post-intervention morbidity often requires repeated interventions. Computational fluid dynamics (CFD) can support and optimise procedural planning through enhanced haemodynamic data of the pathological and in silico designed repair scenarios. Patient-specific CFD in CHD is, however, challenged by complex geometries and sparse clinical data available to define the simulation [1]. This research presents a workflow for a patient-specific CFD simulation to optimise right pulmonary artery (RPA) stenting where limited clinical information was available.

2. Materials and Methods

An 11-year-old patient with severe RPA stenosis and minor left pulmonary artery (LPA) stenosis after a truncus arteriosus type II repair was referred to our centres for either unilateral or bilateral PA stenting. The pre-intervention case was simulated using computed tomography (CT) and Doppler echocardiography (Doppler echo) data. The pulmonary trunk graft and branch pulmonary arteries (PA) were segmented, and for which peak systolic flow conditions were simulated. The outlet boundary conditions (BCs) were tuned to reproduce the velocity and pressure gradient measurements within 4%. Flow through virtual reconstructions of four RPA stenting scenarios was simulated to measure the impact on both branch PA pressure gradients. Limited clinical data in turn constrained the definition of outlet BCs. A simplified, linear model of RPA flow rate splits for increasing stent diameters was produced and used to define RPA flow rate proportions at each stent diameter.

3. Results

The CFD results showed recirculation distal to the RPA stenosis, in the trunk graft and LPA. RPA pressure gradients reduced from pre-procedural 140.9 mmHg to 42.9, 31.9, 29.6 and 21.9 mmHg when stented to 6, 8, 10 and 12 mm respectively (Figure 1). In reality, the internal diameter of the implanted RPA stent was 7mm which lead to a maximum pressure gradient of 32.8 mmHg – measured through doppler echo. This falls inbetween the estimates of the 6 and 8 mm simulations.

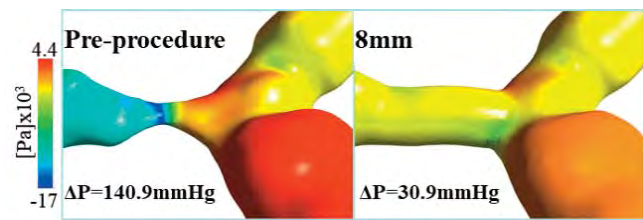


Figure 1: Pressure fields of the pre-procedural and 8mm stented RPA show favourable pressure reduction after stenting.

4. Discussion and Conclusions

Patient-specific CFD analysis using routinely collected and sparse clinical data replicated baseline flow conditions and optimised the stenting of the RPA. Post-repair pressure gradients were in the region of those calculated by the simplified CFD model. In many instances, complex and accurate computational models are simply infeasible in scenarios where routinely collected data only allows simple models. This study shows that even simple models can add value in the clinic.

5. References

- Marsden, A. L. & Feinstein, J. A. *Current Opinion in Pediatrics* (2015).

Acknowledgements:

The authors are thankful for the support from the British Heart Foundation and First Rand Laurie Dippenaar Scholarship.

P1.8

Computational fluid dynamics modelling of airflow in congenital tracheal defects - in silico modelling for informing and optimizing surgical strategies

Liam Swanson^{1,2}, Emilie Sauvage¹, Madhavan Ramaswamy², Arun Beeman², Nagarajan Muthialu², Silvia Schievano^{1,2}, Claudio Capelli^{1,2}

1 University College London, Institute of Cardiovascular Science, London, United Kingdom

2 Great Ormond Street Hospital for Children, London, United Kingdom

*Correspondence to Liam Swanson: liam.swanson.20@ucl.ac.uk

1. Introduction

Rare congenital tracheal abnormalities that cause airflow obstruction include isolated tracheal stenosis, tracheal stenosis with a left pulmonary artery (LPA) sling, with tracheal bronchus or with vascular rings. The available clinical investigations have limited functional data to inform the decision in offering interventional treatments. Computational Fluid Dynamics (CFD) modelling of air flow in pre- and post-repair configurations of the trachea provides access to new metrics in the clinic [1]. This study presents a methodology for CFD modelling of airflow in pre-intervention and virtually generated post-intervention geometries of patients suffering from these congenital tracheal abnormalities to inform and optimize treatment.

2. Materials and Methods

A collection of 7, anonymized, computed tomography image datasets of patients previously investigated for LPA slings, vascular rings, tracheal bronchus or isolated tracheal stenosis was retrospectively obtained, with patient consent. The 3D trachea geometries were segmented and processed to extract centerlines and prepare the inlet and outlet planes. The post-surgery geometries were designed, in conjunction with clinicians, using the GIBBON toolbox [2]. CFD analysis was conducted in Fluent v19.2 (ANSYS Inc.) package. A steady velocity condition was imposed at the inlet and zero pressure at the outlets. The inlet velocity was calculated based on the respiratory rate and values of tidal volumes derived from literature.

3. Results

CFD simulations were successfully run to visualize velocity and pressure fields and in turn calculate flow rates in each bronchus, pressure gradients across the obstruction and energy loss in the system. The vascular ring repair, shown in Figure 1 showed a 67% improvement in pressure gradient and energy loss after obstruction relief while flow rates reached a new distribution where flow to the right bronchus increased closer to what is expected – from 49.6% to 57.5%.

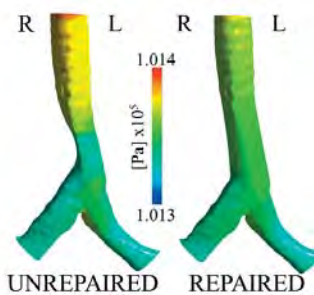


Figure 1: Pressure fields of the pre- and post-procedural scenarios show improved pressure gradients across the stenosed area. R=Right, L=Left.

4. Discussion and Conclusions

Clinicians have limited functional data to enlighten their decision in the surgical repair of congenitally malformed trachea. The methodology here presented can virtually simulate flow in pre- and post-repair scenarios in several different malformations but is however limited to simplified boundary conditions as a result of a lack of patient-specific data. The comparison shows value in using CFD modelling for collecting/harvesting new fluid dynamics metrics and supplement the clinical decision-making process as shown by these results.

4. References

1. S. Qi et al., *J. Med. Syst.*, 2018.
2. Moerman, K. JOSS, 2018

Acknowledgements:

Thanks goes to the British Heart Foundation, First Rand Laurie Dippenaar Scholarship and Action Medical Research for their support.

P1.9

A model for the human fetal ventricular myocyte (HFVM) electrophysiology

Adelisa Avezzù¹, Stefano Longobardi¹, Franka Schultz², Anita Alvarez Laviada³, Tharni Vasavan⁴, Julia Gorelik⁵, Catherine Williamson⁶, Steven Niederer¹

¹ King's College London, Biomedical engineering and imaging sciences, London, United Kingdom

² Imperial College London, Electrophysiology and molecular medicine, London, United Kingdom

³ Imperial College London, London, United Kingdom

⁴ King's College London, Department of Women & Children's Health, London, United Kingdom

⁵ National Heart and Lung Institute, London, United Kingdom

⁶ King's College London, Women & Children's Health, London, United Kingdom

1. Introduction

In this study we developed the first biophysical model of human fetal ventricular cardiac myocyte (HFVM) electrophysiology, based on and validated against human fetal data only. The model represents a pragmatic initial framework for integrating available data, identifying areas of uncertainty and to facilitate future experimental designs.

2. Materials and Methods

The fetal model is based on the Ten Tusscher and Panfilov model for the human adult ventricular myocyte (TT2) [1]. All the membrane transporters and buffering proteins in the adult cell model are assumed to be present in the fetal myocyte model, with dynamics remained unchanged between the adult and fetal and differences been explained by changes in proteins density. In addition to the ion channels in the TT2 model we also introduced the T-type calcium channel and the funny current. Cell volume, membrane capacitance, internal compartments distribution and heart rate in the fetal myocyte model are adapted to fetal measurements. Voltage-clamp current recordings were available to constrain the T-type calcium channel. Fluorescence measurements of calcium transient and fetal action potential (AP) data from literature were used to constrain intracellular dynamics and membrane potential. The parameters fit was performed using Bayesian history matching and model surrogate fast evaluating emulators. Ion channels gene mRNA expression data of human foetal ventricles were used as reference values for channels conductance and proteins density. The model was validated against literature AP data from self-contracting fetal myocytes and APD data from fetal myocytes paced at different frequencies.

3. Results

The HFVM model aims to represent healthy human fetal ventricular myocyte electrophysiology at 10 gestational weeks (gw). Characteristic of HFVM model are shown in table 1.

	HFVM	TT2
Time period [ms]	353	1000
RMP [mV]	-82.56	-85.42
Vmax [mV]	32.06	32.49
Vamp [mV]	114.63	117.91
APD [ms]	200	308
Carest [nM]	100.05	104.65
Camax [nM]	220.86	907.17
Caamp [nM]	120.81	802.51
CaD [ms]	326	457

Table 1: Comparison between AP and Ca transient of HFVM and TT2 models.

4. Discussion and Conclusions

The AP morphology of the HFVM model is in agreement with AP data of human fetal ventricular myocytes aged 7 to 12 gw, exhibiting a shorter APD and a more positive RMP than the adult ventricular myocyte, as well as hyperpolarisation at the end of phase 3 of the cardiac cycle due to the presence of funny current in the fetal ventricular myocyte which is absent in the adult ventricular myocyte. APD is shorter at lower pacing frequencies in accordance with the behaviour of human fetal ventricular myocytes in the experiments, while in adult myocytes APD tend to increase as the frequency decreases until reaching a stability. Calcium transient of the fetal model has similar morphology to the one measured in fetal rats, both for shape and amplitude, with much lower amplitude than in adult in agreement with the poor function of sarcoplasmic reticulum at early fetal stage. This model provide an important step forward in the investigation of fetal arrhythmia and other fetal diseases related to pregnancy and in the understanding of human fetal heart electrophysiology of which poor is known so far. This HFVM model intends to serve as a base for future models of the human fetal myocytes later in gestation as well as neonatal

5. References

1. Ten Tusscher KH, Panfilov AV. Am J Physiol Heart Circ; 291(3):H1088-H1100 (2006).
2. Longobardi S et al., Phil. Trans. R. Soc. A; 378(2173):2019.0334 (2020).

Acknowledgements:

The project is funded by the department of women & children's health of King's college London in collaboration with CEMRG research group.

P1.10

Local flow analysis in the iliac vein bifurcation informed by a 0D model of the lower limb circulation

Magdalena Otta^{1,2,3}, Ian Halliday^{1,3}, Janice Tsui^{4,5}, Chung Lim^{4,5}, Zbigniew Struzik^{2,6,7}, Andrew Narracott^{1,8}

1 The University of Sheffield, Infection, Immunity and Cardiovascular Disease, Sheffield, United Kingdom

2 Sano Centre for Computational Personalised Medicine, Modelling and Simulation Team, Kraków, Poland

3 Insigneo Institute for *in silico* medicine, The University of Sheffield, Sheffield, United Kingdom

4 Royal Free London NHS Foundation Trust, London, United Kingdom

5 University College London, London, United Kingdom

6 The University of Tokyo, Graduate School of Education, Bunkyo City, Japan

7 The University of Warsaw, Faculty of Physics, Warsaw, Poland

8 Insigneo Institute for *in silico* medicine, Sheffield, United Kingdom

Corresponding author: motta1@sheffield.ac.uk

1. Introduction

Post-thrombotic syndrome (PTS) is a common long-term complication of deep vein thrombosis (DVT) of the lower limb. Because of variable clinical presentation, clinical decision-making in PTS treatment lacks supporting evidence. The influence of variation in venous anatomy on treatment outcomes is yet to be discovered.

2. Materials and Methods

A steady state, 0D model was developed to characterise blood circulation in the complex venous anatomy of the lower limb. Assessment of local and global sensitivity analysis of blood flow to variability in venous anatomy was performed as described in [1], using anatomical data reported in [2]. A 3D steady-state CFD model of idealised bifurcation geometry was created in ANSYS Fluent to investigate local flow characteristics in the internal, external, and common iliac veins - a likely site for thrombus development. Blood properties were defined using constant viscosity 0.0035 Pa s and constant density 1050 kg m⁻³. Flow in the external and internal iliac veins was taken from the 0D model (525 and 111 ml/min respectively) and applied as mass flow boundary conditions at the inlet of each vessel. The pressure at the outlet of the common iliac vein was set to 0 Pa. The velocity distribution of the flow field and the wall shear stress (WSS) were analysed.

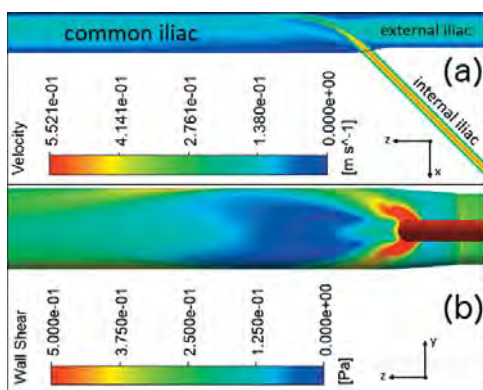


Figure 1: (a) Velocity distribution (b) WSS distribution in the common iliac - scale adjusted to highlight low WSS region.

3. Results

Velocity distribution on a plane through the centre of the vessels and WSS in the common iliac vein are shown in Fig. 1. The internal iliac vein presents the highest velocity resulting in a pronounced jet extending inside the common iliac vein. Consequently, low WSS is observed in that region.

4. Discussion and Conclusions

Regions of low shear stress have been associated with abnormal vascular response, potentially leading to thrombosis. This study has identified such a region in the common iliac vein, close to the bifurcation. These results are dependent on the assumptions made in the 0D approach. Repeating the analysis under different assumptions in the 0D model, e.g., including other output metrics in addition to the flow, could help to assess this. Future work will include a sensitivity analysis of the coupled 0D-3D network, to investigate the influence of anatomical variation on the local flow. Including capillary resistance in this analysis may have a significant effect on WSS distribution. Such analysis of the local flow distribution has the potential to guide clinical decisions for patient-specific interventions to reduce thrombosis risk.

5. References

1. Otta, M. et al., accepted for ICCS 2022 conference; London, UK, June 2022
2. Müller, L. and Toro, E. *Int J Numer Method Biomed Eng*, 30(7):681-725 (2014)

Acknowledgements:

This study is supported by the European Union's Horizon 2020 research and innovation programme under grant agreement Sano No 857533 and carried out within the International Research Agendas programme of the Foundation for Polish Science, co-financed by the European Union under the European Regional Development Fund.

P1.11

Computed Tomography Based Assessment of Transvalvular Pressure Gradient in Aortic Stenosis

Benedikt Franke¹, Jan Brüning¹, Pavlo Yevtushenko¹, Leonid Goubergrits^{1,3}, Marie Schafstedde^{1,2}

¹ Institute for Imaging Science and Computational Modelling in Cardiovascular Medicine, Charité – Universitätsmedizin Berlin, Berlin, Germany.

² Department of Congenital Heart Disease, German Heart Center Berlin, Berlin, Germany.

³ Einstein Center Digital Future, Berlin, Germany

1. Introduction

Aortic valve stenosis (AS) is the most common heart valve disease. Grading of AS severity is primarily based on the echocardiography measured maximum flow velocity across the aortic valve. Computed tomography (CT) is only used for intervention-planning but not for functional diagnosis.

The objective of this study was to introduce a method for transvalvular pressure gradient (TPG) assessment using aortic flow rates (Q) and aortic valve area (AVA), both measured from CT images.

2. Materials and Methods

Patient-specific anatomies of the left ventricle (LV), the aortic valve, and the aorta ascendens (Aa) were segmented from cardiac CT images from clinical routine, using an approach described earlier [1]. AVA was determined by measuring the aortic valve orifice area during peak-systole, whereas Q was quantified based on volumetric assessment of the LV.

Simulations were performed for each anatomy using STAR-CCM+ to calculate hemodynamics. TPG_{CT} was calculated as the difference of the area-averaged pressure in the LV and the Aa.

A reduced order model for calculation of TPG based on Q and AVA, which was introduced earlier [2], was fitted to the data. For validation, invasively measured TPG_{catheter} was calculated from pressure measurements in the LV and Aa. Altogether, 84 data sets of patients with AS were used to compare TPG_{CT} against TPG_{catheter}.

3. Results

Adjustment of the model's parameters resulted in the following expression:

$$TPG_{CT} = 185.5 \cdot Q^{1.483} \cdot AVA^{-1.385}$$

Here, TPG_{CT} is in mmHg, Q in l/s and AVA in cm².

TPG_{catheter} and TPG_{CT} were 50.6 ± 28.0 mmHg and 48.0 ± 26 mmHg, respectively ($p = 0.56$). Bland-Altman analysis revealed good agreement between both methods with a mean difference in TPG of 2.6 mmHg and a standard deviation of 19.3 mmHg. Both methods showed good correlation with $r = 0.72$ ($p < 0.001$).

4. Discussion and Conclusions

The results show that CT-based estimation of TPG performs well compared against invasive cardiac catheterization. The method is easy to apply and complements the current diagnostic capabilities of cardiac CT by providing additional functional hemodynamic information.

Error analysis revealed that heart rate between CT and catheterization, limited temporal resolution of the CT-Images, and the presence of MI promote errors in the model's prediction. In the future, intra- and interobserver errors will be investigated.

5. References

1. Weese J. et al. *Med Phys* 44 2281-2292 (2017).
2. Franke B. et al. *Biol Eng Comput* 58 1667-1679 (2020).

P1.12

Towards machine learning based pressure drop assessment in aortic stenosis

Andreea Bianca Popescu^{1,2}, **Cosmin Ioan Nita**², **Costin Florian Ciusdel**^{1,2}, **Lucian Mihai Itu**^{1,2}

1 Siemens SRL, Advanta, Brașov, Romania

2 Transilvania University of Brasov, Brasov, Romania

1. Introduction

Aortic stenosis occurs when the aortic valve does not fully open during systole, which reduces or blocks blood flow to the systemic circulation. The treatment depends on the severity of the stenosis, which is assessed based on the trans-valvular peak pressure drop. Clinically, the pressure drop is routinely estimated analytically, which may lead to sub-optimal results because certain hemodynamic aspects are not fully captured (pressure recovery, turbulence) [1]. A promising solution is based on the use of a machine learning (ML) model to estimate the pressure drop based on certain patient-specific characteristics. Although an ML-based solution could provide the desired results in real-time, training an accurate model requires a large database of invasively measured pressure drops, which is difficult and costly to set up.

2. Materials and Methods

Our approach is to train the ML model with ground truth values computed using a high-fidelity computational fluid dynamics (CFD) model. The first step is to create a parameterizable anatomical model of the aortic valve. Meshes are then constructed based on this anatomy. The difference between inlet and outlet pressure is calculated after performing simulations for various aorta and valve dimensions, and inlet flow values, all set based on population level characteristics. Thus, a dataset that maps valve and blood flow characteristics to pressure drop is obtained. The open-source CFD software OpenFOAM [2] was employed for the dataset generation.

3. Results

In the following we present first experiments, using three adjustable parameters that influence the pressure drop: vessel diameter (D), percentage area reduction (Ar) and inlet flow (q).

D [cm]	Ar [%]	q [ml/s]	Δp [mmHg]
4	59.44	376.5	1.82
2	56.23	93.9	2.08
6	44.78	847.2	0.60
4	60.31	125.5	0.24

Table 1: CFD-based pressure drop estimation.

Steady-state simulations, corresponding to peak systole, were run. The turbulent flow in the proximity of the valve is visible in Fig. 1 (b), where the velocities are displayed.

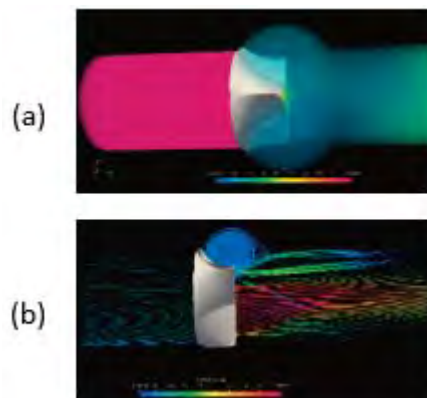


Figure 1: ParaView visualisation: (a) pressure, (b) velocity.

4. Discussion and Conclusions

The data generation process for training an ML model can be readily automated by employing Python scripts and an open-source CFD solver. The next step is to build a substantial collection of different geometries and run the flow simulations. As a result, a dataset will be constructed, enabling ML model training for pressure drop estimation in aortic stenosis.

5. References

1. Hoeijmakers, M. et al., *J Biomech Eng*. 2022 Mar 1;144(3):031010. doi: 10.1115/1.4052459.
2. Weller, H. et al., *Comp Physics*, Vol. 12, Issue 6, Nov. 1998 pp. 620–631. doi: <https://doi.org/10.1063/1.168744>.

Acknowledgements:

This work was supported by a grant of the Romanian National Authority for Scientific Research and Innovation, CCCDI – UEFISCDI, project number ERANET-PERMED-HeartMed, within PNCDI III.

P1.13

Catheter tracking in thrombectomy procedure: a finite element analysis and patient-specific comparison

Silvia Renon¹, Francesca Zucchelli¹, Nerea Arrarte Terreros², Sara Bridio¹, Francesco Migliavacca¹, José Félix Rodriguez Matas¹, Praneeta Konduri², Aad van der Lugt³, Wim van Zwam⁴, Henk Marquering², Charles Majoie², Giulia Luraghi¹

¹ Politecnico di Milano, Italy

² Amsterdam UMC, location AMC, Netherlands

³ Erasmus MC, Netherlands

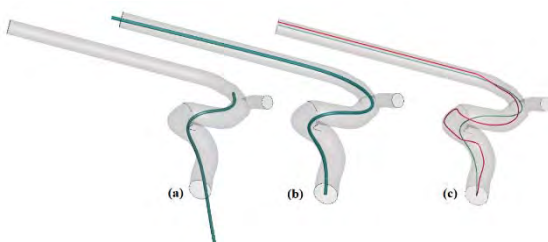
⁴ Maastricht UMC, Netherlands

1. Introduction

Mechanical thrombectomy (MT) is the standard of care for acute ischemic stroke (AIS) in which the occluding thrombus is removed using stent-retrievers and/or aspiration devices. MT success can be influenced by multiple factors, such as the thrombus-device interaction [1]. Accurate and realistic in silico models of MT can aid in the understanding of retrieval failure. Accordingly, the aim of this work is to develop an improved computational model to mimic the microcatheter tracking during MT compared to previous centreline-based techniques [2,3]. Additionally, we compare the catheter positioning with patient-specific digital subtraction angiography (DSA) images to visually assess the performance of the implemented in silico model.

2. Materials and Methods

The patient-specific anterior circulation vessels were segmented from computed tomography angiography (CTA) images as described in [4]. The CTA and DSA scans were provided by the Dutch AIS MR CLEAN Registry database. The vessels were modelled as rigid, and the catheter as a linear elastic cylindrical beam [2]. Catheter tracking was performed in a one-step insertion simulation: the catheter tip advanced along the vessel centreline



while the catheter body was free to interact with the vessel wall.

Figure 1: (a) Catheter tip follows the vessel centreline; (b) Catheter relaxes against vessel walls; (c) Catheter comparison: (red) centreline based technique, (blue) new technique

3. Results

The catheter tracking simulation steps are depicted in Fig.1. A qualitative comparison between in silico and in vivo catheter/stent tracking is shown in Fig.2.



Figure 2: Left: in silico results of microcatheter positioning; Right: DSA image showing the stent/microcatheter positioning.

4. Discussion and Conclusions

Patient-specific analysis of DSA images showed that the presented method more accurately resembles the microcatheter (and therefore, stent) positioning in the vessel, compared to centreline tracking techniques. The development of a computational method to simulate a realistic catheter insertion can be used to have an improved understanding of MT failure.

5. References

1. Belachew et al., AJNR; 42(12) (2021)
2. Wang et al., J Card Surg; 34(8): 690-699 (2019).
3. Luraghi et al., J Biomech; 126:110622 (2021).
4. Moerman et al., J Biomech; 133:110896 (2022)

Acknowledgements:

This project has received funding from the EU's Horizon 2020 research and innovation programme under grant agreement No 777072. The MR CLEAN registry is partially funded by unrestricted grants from the Applied Scientific Institute for Neuromodulation, Erasmus MC, Amsterdam UMC and Maastricht UMC.

P1.14

Fluid-structure interaction analysis of eccentricity and leaflet rigidity on thrombosis biomarkers in bioprosthetic aortic valve replacements

David Oks¹, Cristóbal Samaniego¹, Mariano Vázquez², Guillaume Houzeaux¹, Hadrien Calmet¹, Constantine Butakoff²

¹ Barcelona Supercomputing Center - Centre Nacional de Supercomputació, CASE, Barcelona, Spain

² ELEM Biotech, Barcelona, Spain

1. Introduction

A Fluid-Structure Interaction (FSI) computational model is implemented and used to study the effect of aortic annulus eccentricity on the performance, thrombogenic and calcification risk of cardiac bioprostheses.

2. Materials and Methods

The FSI model is based on an immersed boundary method implemented in Alya, a high-performance computing multi-physics simulation software. The leaflet rigidity and the aortic annulus eccentricity are the two controlled variables considered in this study. We analyze the effect of these two variables on Quantities of Interest (QoI) associated to valve performance, thrombogenic and leaflet calcification risk. Regions of peak Residence Time (RT) and Shear Rate (SR) are considered as the biomarkers indicative of thrombogenic risk. RT is the total time that a fluid parcel has spent inside a control volume, computed as:

$$\partial_t T_R + \nabla \cdot (u T_R) = 1 \quad (1)$$

with u the fluid velocity. Shear rate, a Galilean invariant, also associated with thrombosis is computed as the squared root of the second invariant of the strain symmetric tensor Q_S :

$$\dot{\gamma} = \sqrt{Q_S}$$

To evaluate valve bioprosthesis performance the Geometric Orifice Area (GOA) and Transvalvular Pressure Gradients (TPG) are evaluated, as described in the ISO 5840-3 standard [1]. Finally, the leaflet structural von Mises stresses (VMS) are taken as indicators of leaflet calcification.

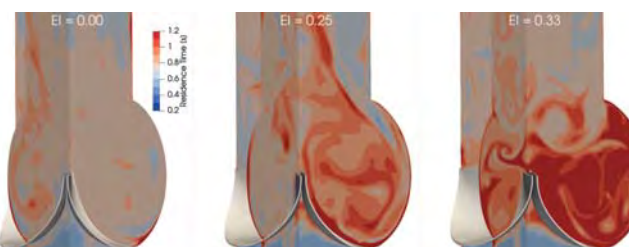


Figure 1: Residence time in diastole for a cardiac output of 5l/min and increasing eccentricity indices from left to right: 0, 0.25 and 0.33.

3. Results

EOA and TPG, showed good agreement with respect to the experimental work of Sigüenza et al. [2]. We observed that increasing leaflet Young modulus decreases the EOA while increasing the absolute TPG. Moreover, increasing rigidities produced an increase in peak thrombogenically risky regions, associated to long residence times and high shear strains. By increasing annulus eccentricities, EOAs are observed to decrease while TPGs are observed to increase, as observed in Kütting et al. [3]. On the other hand, as eccentricity is increased, the regions of peak RT and SR are both intensified, increasing the risk of thrombus formation. Finally, it is observed that peak leaflet VMS increase with stronger eccentricities, enhancing the leaflet calcification risk.

4. Discussion and Conclusions

The decrease of EOA and increase in TPG with increasing annulus eccentricity is reproduced, indicating a larger load on the left ventricle, potentially increasing risk of left ventricle hypertrophy and eventually cardiac failure. Moreover extreme eccentricities were observed to enhance thrombogenic risk. This computational work provides a first in its kind, showing the potential of FSI simulations in optimizing bioprostheses design.

5. References

1. Cardiovascular Implants - Cardiac Valve Prostheses - Part 3: Heart valve substitutes implanted by transcatheeter techniques - ISO 5840-3:2013(E) standard, International Organization for Standardization; Geneva, CH: 2013.
2. Sigüenza et al. Int J for Num Meth in Biomed Engng 2018; 34(4): e2945. cmn.2945 doi: 10.1002/cnm.2945
3. Kütting et al. J Biomech. 2014; 47(5): 957-65. doi: 10.1016/j.biomech.2014.01.024

Acknowledgements:

This project has received funding from the European Union's Horizon 2020 research innovation programme under the Marie Skłodowska-Curie grant agreement No. 713673. Authors would like to extend their gratitude to Alfonso Santiago and Vi Vu for the discussions regarding QoIs associated to thrombogenic risk.

P1.15

Coupling Agent Based Method and Computational Fluid Dynamics for Plaque Development in the Carotid Artery

Nenad Filipovic^{1,2}, Andjela Blagojević², Smiljana Djorovic², Branko Arsic³, Tijana Djukic¹

1 Bioengineering Research and Development center, BIOIRC, Kragujevac, Serbia

2 University of Kragujevac, Faculty of Mechanical Engineering, Kragujevac, Serbia

3 University of Kragujevac, Faculty of Science, Kragujevac, Serbia

smiljana@kg.ac.rs

1. Introduction

Atherosclerosis is a progressive disease characterized in particular by the accumulation of lipids and fibrous elements in artery walls [1]. It is characterized by dysfunction of endothelium, vasculitis and accumulation of lipid, cholesterol and cell elements inside blood vessel wall. This process develops in arterial walls with discrete nature between cells, molecular biomarkers, which indicate that discrete modelling approach like Agent Based Model (ABM) can be used for simulation of complex process for plaque development. We here concentrate for carotid artery plaque development.

2. Materials and Methods

Beside agents, the agent-based simulations require a domain where the agents will live and exhibit their behavior. Deep learning technique was implemented for segmentation from Ultrasound images. The automatic carotid artery (lumen and wall) segmentation has been done using SegNet and U-Net based deep convolutional networks.

The initial geometry for ABM was a 2D circular cross-section composed by 3 concentric layers - tunica intima, media and adventitia with the internal and external elastic laminae - IEL and EEL.

3. Results

Blood flow through a curve blood vessel with stenosis was modeled using 3D finite element method (FEM). Fluid dynamics computation is performed by PAK solver, giving velocity and pressure field, as well as wall shear stress distribution [2]. ABM method was applied on the arterial wall taken into account cell mitosis and ECM production in the intima including lipid cells.



Figure 1: Curved artery example with coupled ABM and CFD

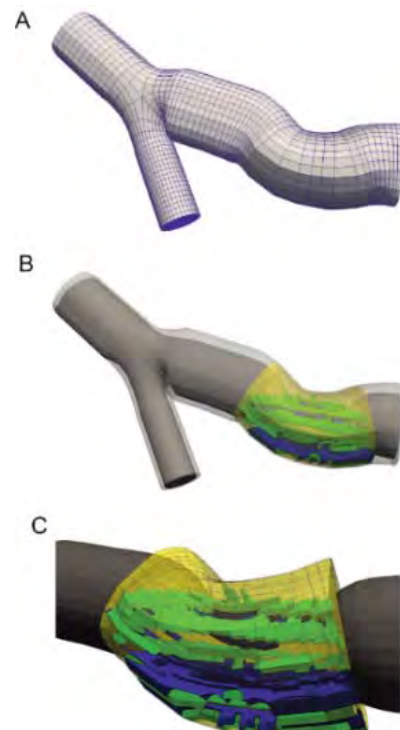


Figure 2: Carotid artery example with coupled ABM and CFD finite element. A – Full model, B – Transparent model with colored plaque components, C – Augmented part with the FE elements defined as plaque

Curved and carotid artery example with coupled ABM and CFD finite element has been presented in Figs. 1 and 2.

4. Discussion and Conclusions

Specific carotid artery patient from US was modeled with coupled FEM and ABM method. First results show good agreement between proposed method and clinical measurements in the follow up 3D US image reconstruction.

5. References

1. Libby P Inflammation in atherosclerosis. *Nature* 420:868–874. (2002)
2. Filipovic ND, Zivic M, Obradovic M, Djukic T, Markovic ZS, Rosic M, Numerical and experimental LDL transport through arterial wall, *Microfluidics and nanofluidics*, Vol.16, No.3, pp 455-464, ISSN 1613-4982, (2014).

Acknowledgements:

The research presented in this study was part of the project that has received funding from the European Union's Horizon 2020 research and innovation programme under grant agreement No. 755320-2 - TAXINOMISIS.

P1.16

Multiscale modeling of spreading depolarization and depression in brain slices

Craig Kelley¹, Adam Newton¹, Sabina Hrabetova¹, Robert McDougal², William Lytton¹

¹ SUNY Downstate Medical Center, United States

² Yale University, New Haven, United States

1. Introduction

Spreading depolarization (SD) is a slow-moving wave of neuronal depolarization accompanied by a breakdown of ion homeostasis, followed by long periods of neuronal silence (spreading depression), and associated with several neurological conditions. We developed multiscale computer models of SD in brain slices using the NEURON simulator, which demonstrated the importance of extracellular space (ECS) in SD speed, exhibited spreading ischemia in response to SD, and predicted depth dependent SD propagation in perfused slices.

2. Materials and Methods

We developed models of brain slices using the NEURON simulator: 36,000-72,000 neurons (2 voltage-gated ion channels, 3 leak channels, and 3 ion exchangers/pumps) were embedded in the ECS of a brain slice with ion and O₂ diffusion and equilibration with a surrounding bath. Glia and neurons cleared excess K⁺ from ECS via Na⁺/K⁺ pumps. SD was initiated by elevating K⁺ concentration to 20-70 mM in a 100-300 μm diameter volume at the center of the slice.

3. Results

Our model reproduced a number of the properties of SD observed in brain slices, including wave speeds (2-5 mm/min), firing rates, SD's all-or-none nature, and a [K⁺] threshold of ~20 mM [1,2,3]. Incorporating effects of hypoxia and propionate increased SD speed by 25-30%, which was mediated by ECS shrinkage. Our model allows making the following predictions: 1. SD can be inhibited by enlarging ECS volume; 2. SD velocity will be greater in areas with greater neuronal density, volume, or larger/more dendrites; 3. SD is all-or-none: initiating K⁺ bolus properties do not impact SD speed; 4. Slice thickness influences SD due to relative hypoxia in the slice core, exacerbated by SD in a pathological cycle; 5. Higher spike rates and faster spread will be observed in the core than the periphery of perfused slice during SD.

3. Discussion & Conclusions

We are expanding the framework to simulate SD in models which are digital twins of human and mouse brain slices whose cell types, positions, morphology, and connectivity have been determined through electron microscopy.

4. Acknowledgements

This work was funded by NIMH R01MH086638 and NSF Internet2 E-CAS 1904444.

5. References

1. Hrabe, J, and Hrabetova S. *Biophysical Journal* 117 (10): 1783-94. (2019)
2. Lemaire Let al. *PLoS Computational Biology* 17 (7): e1009239. (2021)
3. Andrew, RD, et al. *J of Cereb. Blood Flow and Metabolism*: 37 (5): 1735-47 (2017).

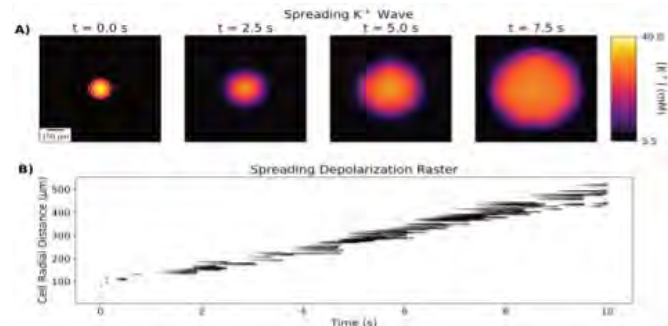


Figure 1. Spreading K⁺ and depolarization waves in perfused slice. A. [K⁺]_{ECS} averaged across slice depth (400 μm) at 4 time points during SD. B. Spike raster plot of 250 randomly-selected neurons (out of 1e36c3) during SD.

P1.17

Assessing credibility of an In Silico trial model for the development of new vaccines against tuberculosis

Cristina Curreli^{1,2}, Valentina Di Salvatore³, Giulia Russo^{3,4}, Francesco Pappalardo³, and Marco Viceconti^{1,2}

1 Department of Industrial Engineering, Alma Mater Studiorum - University of Bologna (IT)

2 Medical Technology Lab, IRCCS Istituto Ortopedico Rizzoli, Bologna (IT)

3 Department of Drug Sciences, University of Catania (IT)

4 Mimesis srl, Catania (IT)

1. Introduction

Tuberculosis (TB) is considered one of the leading causes of death in several developing countries. Therapeutic vaccines promise to drastically reduce the duration of the treatment and are considered today a promising solution to prevent the recurrence of the disease. However, the clinical evaluation of these new therapies is slow and prohibitively expensive. In Silico Trials can be used to accelerate medical product development and reduce the cost of the clinical experimentations. One specific application of this modelling and simulation-based approaches is the assessment of the optimal drug dose to be used in the clinical study. Recently, the Universal Immune System Simulator of pulmonary TB (UISS-TB) [1] has been extended to predict the dose-response of the RUTI therapeutic vaccine and to suggest the design of phase II and phase III clinical trials. One fundamental aspect that must be properly investigated before using such methods in clinical practice is model credibility assessment. A risk-informed framework for UISS-TB model credibility evaluation was introduced in [2]; however, a description of all the activities and evidences has never been reported. The aim of this work is to propose a detailed model credibility assessment plan that can be used as evidence for qualification of the method to a regulator authority.

2. Materials and Methods

The standard ASME V&V40 for medical devices was used to guide the development of credibility requirements [3]. Based on the intended context of use (CoU) of the model and the derived model risk assessment, the credibility goals and factors were then properly selected, including verification and validation (V&V) activities. Typical tests needed to quantify and reduce the numerical errors associated with the agent based model were considered for the calculation verification workflow [4]. The data observed in the phase II clinical trial where three different doses (5, 25 and 50 µg) of RUTI vaccine were evaluated in term of safety, tolerability and immunogenicity were used as validation comparator. The credibility evidences were also classified according the guidelines recently published in the draft guidance document by FDA.

3. Results

The main result of this work is the definition of the all the credibility factors that can be used to demonstrate the accuracy of the model prediction related to the specified CoU. Solution verification activities include both determinist and stochastic model verification, while among validation studies we identified typical uncertainty quantification analyses on input parameters and assessment of outputs results. Some other evidence (e.g., population based evidence and emergent model behavior) were also considered to demonstrate the credibility of our agent based model.

4. Discussion and Conclusions

Based on the planned activities and first validation results, an adequacy assessment study allowed us to positively answer to the question "Will the credibility evidence be sufficient to support using the model for the COU given the risk assessment?". This work provides the basis for the Qualification Advice request that will be submitted soon to the European Medicine Agency.

5. References

1. Pappalardo F et al, *In: 2010:649–650.*
2. Musuamba FT et al, *CPT: pharmacometrics & systems pharmacology 2021.*
3. ASME V&V40-2018.
4. Curreli C et al, *IJNMBE, 2021.*

Acknowledgements:

This study was supported by the European Commission through the H2020 project "STriTuVaD (grant ID 777123).

P2.1

A Mathematical Model describing Cell Shape Evolution and the Impact of Cellular Forces on the Extracellular Matrix during Cell Invasion through a Flexible Channel

Qiyao Peng^{1 2 3}, Fred Vermolen^{2 3}, Daphne Weihs⁴

1 Leiden University, Mathematical Institute, Leiden, Netherlands

2 Hasselt University, Computational Mathematics Group, Discipline group Mathematics and Statistics, Faculty of Science, Diepenbeek, Belgium

3 Delft University of Technology (TU Delft), Delft Institute of Applied Mathematics, Delft, Netherlands

4 Technion - Israel Institute of Technology, Faculty of Biomedical Engineering, Haifa, Israel

1. Introduction

Cell geometry influences cellular activities like cell mobility and adhesion to the direct environment. The shape of a motile cell is determined by its boundaries, which dynamically varies with a local balance between retraction and protrusion. For cancer cell metastasis, cancer cells need to deform to adapt to obstacles during invasion and they are observed to apply traction forces on their immediate environment. Hence, a lot of research has been done on cell penetration the micro-tubes to mimic the tissue-like environment where cells are allowed to transmigrate through cavities.

2. Materials and Methods

We extended the phenomenological model [1] to simulate cell shape evolution during cell migration: The cell membrane is split into line segments by nodal points, and each point is connected to the cell center and the neighboring points by springs to maintain the cell cytoskeleton. A cell is divided into head and tail part with different properties. Together with other mechanics, the displacement of the nodal point is determined. Hence, the cell shape evolves over time.

We consider a series of cells that penetrate through a flexible narrow channel (the width is narrower than the cell size), sequentially, of which the walls are plastically deformable due to the cellular traction forces.

3. Results

We consider two circumstances: (1) the next cell enters the channel when the previous one has left completely, i.e. there is no mechanical contact between the cells; (2) cells enter the channel following each other, and the mechanical contact may take place. There is significant reduction in transmigration time of the subsequent cells in Case (1), whereas in Case (2) there is less significant reduction. For both cases, we fix the initial positions of the first cell and other settings of the model as much as possible. It can be seen that for Case (2), the first cell might benefit from the second cell exerting the pushing force when they have mechanical contact. To investigate further regarding how the subsequent cells can benefit from the leading cell, Monte Carlo simulations will be conducted.

Table 1: Duration time of cell transmigrating the channel

Duration Time (min)	1st Cell	2nd Cell	3rd Cell
Case (1)	85.47	66.85	61.39
Case (2)	76.51	75.95	N.A.

4. Discussion and Conclusions

We extended our model in [1] to make it more realistic and investigate how the subsequent cells can benefit from the leading cell when they need to penetrate through a channel which is much smaller than the cell size. We conclude that cells collaborate by opening up the channel in the substrate, such that the other cells transmigrate more easily and faster.

5. References

[1] Peng Q, Vermolen FJ, Weihs D. *Biomechanics and Modeling in Mechanobiology* 20(4):1459-1475(2021).

P2.2

Early in silico assessment of drug-induced proarrhythmic risk using Drug Safety Suite

Hiroshi Matsukawa¹, Mao Yamaguchi¹, Koji Nakano¹, Masaru Tsuboi¹, Chiara Nicolò², Fianne Sips², Cristina Vaghi², Roberta Bursi²

¹ Higashimatsuyama Laboratories, Drug Safety Testing Center Co., Ltd. (DSTC)

² R&D Division, In SilicoTrials Technologies S.p.A.

1. Introduction

The Comprehensive in vitro Proarrhythmia Assay (CiPA) initiative was established to improve the accuracy of torsadogenic risk predictions by combining in vitro experiments with modelling and simulation. To this end, we launched the Drug Safety Suite - a collection of three web-based products (QT/TdP Risk Screen, STrihPS and CiPA in Silico) to perform an early assessment of pro-arrhythmic risk. This study illustrates how this Suite can complement in vitro safety testing, improving the accuracy of cardiac safety assessments.

2. Materials and Methods

The Drug Safety Suite was run on eight drugs with known cardiac risk (bepridil, dofetilide, astemizole, chlorpromazine, cisapride, ranolazine, verapamil, and flecainide). For each compound, hERG kinetics data following the Milnes protocol and cardiac channel data for hERG, hCav1.2, and peak/late hNav1.5 were manually obtained at DSTC. These data were used as input parameters to run each product according to their requisites. QT/TdP Risk Screen was run to classify each compound as clinically safe or unsafe based on the CredibleMeds classification criteria [1], [2]. CiPA In Silico was run to deliver the drug-specific safety marker qNet following FDA standards [3], [4]. STrihPS was run to estimate safety markers in a population of human iPS cells-derived cardiomyocytes [5], [6].

3. Results

For this original data, QT/TdP Risk Screen, CiPA In Silico and STrihPS classifications were generally in good agreement with the drug's known torsadogenic risk and previous publications.

The combined use of the three tools could improve cardiac risk predictions. For instance, flecainide's qNet value was predicted by CiPA In Silico close to the discrimination threshold and with a degree of uncertainty that resulted in an inconclusive classification. Predictions obtained with the other two tools, confirmed flecainide as a high-risk drug.

4. Discussion and Conclusions

This study has shown how the Drug Safety Suite can complement in vitro experiments to assess the potential proarrhythmic risk of compounds in early preclinical screening. The three tools performed well individually, but when used in combination complemented and strengthened each other's outcomes. The Suite is available on the secure and user-friendly InSilicoTrials.com platform. Runtime of the products varies from seconds to a few hours, making the predictions in real time highly efficient.

5. References

- [1] J. Llopis-Lorente et al, *J. Chem. Inf. Model.*, vol. 60, no. 10, pp. 5172–5187, Oct. 2020
- [2] www.crediblemeds.org
- [3] K. C. Chang et al, *Front. Physiol.*, vol. 8, p. 917, Nov. 2017
- [4] Z. Li et al, *Clin. Pharmacol. Ther.*, vol. 105, no. 2, pp. 466–475, Feb. 2019
- [5] M. Paci et al, *Front. Physiol.*, vol. 9, p. 709, Jun. 2018
- [6] M. Paci et al, presented at the 2018 Computing in Cardiology Conference, Dec. 2018

P2.3

Monitoring age-related penetrance of right ventricular myocardial disease in arrhythmogenic cardiomyopathy using a Digital Twin approach

Nick van Osta¹, Feddo Kirkels², Christine Rootwelt-Norberg³, Folkert Asselbergs², Maarten J Cramer², Tammo Delhaas¹, Arco Teske², Kristina Haugaa³, Joost Lumens¹

¹ Maastricht University, Biomedical Engineering, Maastricht, Netherlands

² UMC Utrecht, Department of Cardiology, Utrecht, Netherlands

³ Rikshospitalet, Department of Cardiology, Norway

Corresponding address: n.vanosta@maastrichtuniversity.nl

1. Introduction

Arrhythmogenic cardiomyopathy (AC) is a heritable cardiomyopathy characterized by risk of life-threatening ventricular arrhythmias and fibrofatty replacement of primarily the right ventricular (RV) myocardium [1]. Deformation imaging has been shown to reveal abnormalities in early-disease stage [2] and life-long repeated cardiac imaging of relatives at risk is important to detect penetrant disease. We used a recently developed Digital Twin framework [3] to determine whether structural disease progression occurs in all age groups

2. Materials and Methods

We included 82 early-stage AC patients and genotype positive family members (57% female, age 39 ± 17 years, 10% probands) from a consecutive cohort evaluated at Oslo University Hospital, Rikshospitalet, Norway [4,5]. Patients were divided into three groups based on age at baseline: early presenters (<30 years), mid-life presenters (30–50 years) and late presenters (>50 years). 313 baseline and follow-up echocardiographic assessments were included, mean follow-up was 6.7 ± 3.3 years. We personalized the CircAdapt model to reproduce measured deformation patterns including measurement uncertainty [3]. The resulting Digital Twin revealed regional contractility, compliance, and mechanical activation delay of the RV wall.

3. Results

An example estimation of a single patient is shown in Fig. 1. In the total population, on average, contractility of the basal segment decreased in the first two age-groups ($p=0.005$ and $p=0.022$, respectively). Estimated compliance increased in the apical segment in all age-groups ($p<0.001$). Heterogeneity within the RV free wall increased in all estimated RV tissue properties in the first group.

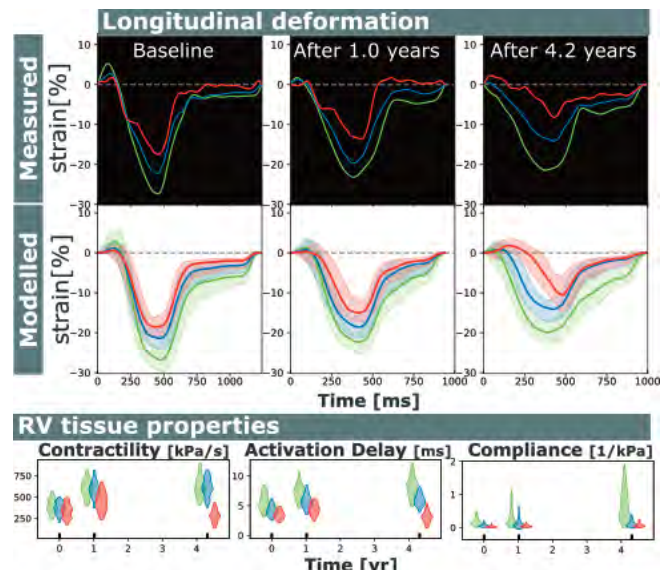


Figure 1. Measured and modelled deformation with corresponding tissue properties at baseline and during follow-up.

4. Discussion and Conclusions

Repetitive Digital Twin simulations of cardiac function in AC patients revealed the development of a myocardial disease substrate affecting contractility, compliance, and activation delay in all age-groups. Therefore, age-tailoring of follow-up intervals for cardiac imaging is not supported by our data.

5. References

- Thiene, G., Nava, A., Corrado, D., Rossi, L. & Pennelli, N. *N. Engl. J. Med.* 318, 129–133 (1988).
- Mast, T. P. et al. *J. Am. Coll. Cardiol.* 68, 2185–2197 (2016).
- Osta, N. van et al. *Front. Physiol.* (2021).
- Chivulescu, M. et al. *Eur. Heart J.* 41, 1401–1410 (2020).
- Rootwelt-Norberg, C. et al. *Europace* 23, 1084–1091 (2021).

Acknowledgements:

Supported by the Netherlands Organisation for Scientific Research (NWO-ZonMw, VIDI grant 016.176.340 to J.L.), the Dutch Heart Foundation (ERA-CVD JTC2018 grant 2018T094; Dr. Dekker Program grant 2015T082 to J.L.). The funders had no role in the study.

P2.4

Coronary flow and ffr prediction: part 2 - semi-automatic cad/cae system for clinical decision support

Boris Chernyavsky¹, Alexey Velikorodny²

¹ BioME Science, France

² BioME Science, Paris, France

Corresponding author: A. Velikorodny, PhD a.velikorodny@biome-science.net

1. Introduction

In the US alone, more than 8.7 million patients go through various non-invasive diagnostic testing for suspected coronary artery disease (CAD) at the expense of \$15 billion annually, [1]. Medical science recent advances allow the application usage for the non-invasive personalized tests to see how a blockage impacts blood flow in the heart or elsewhere. Utilization of coronary computed tomography angiography supplemented by computed fractional flow reserve (FFR) does not only reduce rates of death, but also is cost-effective compared to functional testing of chest pain patients. We have developed a new efficient and robust computational hemodynamic model, (described and validated in PART1). This presentation describes its integration in a Hospital Information System (HIS) along with a semi-automatic vascular segmentation module, all for clinical decision support.

2. Materials and Methods

The source of data for the web-service under development is HIS and PACS server containing CT images. Once the series and parameters are prescribed according to the protocol, the order is sent to proceed through segmentation, hemodynamic modeling and post-processing modules (Fig. 1). A printed form is then created using personal data from hospital PACS server. If another calculation is required a medical professional would proceed with a new order.

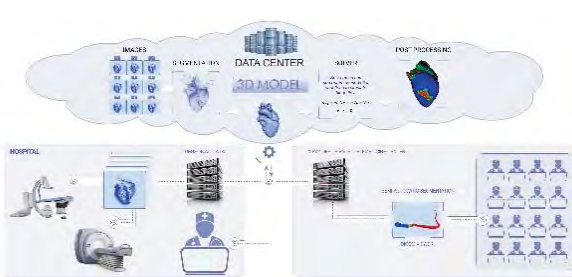


Figure 1: General scheme of system and modules

3. Results

Once the web-service processed all stages without errors, the results arrive back to HIS through data interface within minutes. Fig. 2 shows an example of information presented to medical professional, which can be examined and printed out, including detailed description of coronary vessel(s) and corresponding flow/FFR parameters.

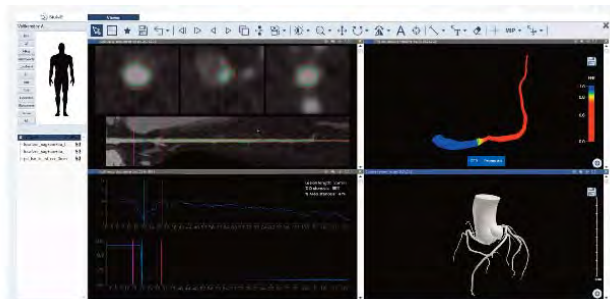


Figure 2: Example of data provided by the web-service: description of coronary vessel(s) & flow/FFR

4. Discussion and Conclusions

Pressure wire-based fractional flow reserve is considered the standard of reference parameter for evaluation of the ischemic potential of coronary stenoses and the expected benefit from revascularization [2]. Our solution for clinics and hospitals is a decision support service providing an efficient and robust manner for non-invasive assessment of lesion-specific ischemia based on segmented CT images and dedicated computational hemodynamic model.

5. References

1. Virani S, et al. American Heart Association Council on Epidemiology and Prevention Statistics Committee and Stroke Statistics Subcommittee. Heart Disease and Stroke Statistics-2021 Update Circulation. 2021 Feb 23;143(8):e254-e743
2. Pijls NHJ, De Bruyne B. Coronary Pressure. Second Edition. Kluwer Academic Publishers, 1999.

P2.5

A framework for the development of intestinal digital twins integrating machine learning and multiphysics modelling

Panagiotis Kalozoumis¹, Georgios Dimas¹, Georgios Triantafyllou¹, Dimitris Iakovidis¹

¹ University of Thessaly, Department of Computer Science and Biomedical Informatics, Lamia, Greece

1. Introduction

Medical devices (MDs) are evaluated through extensive clinical studies, which are costly and time-consuming. In silico clinical trials (ISCTs) with virtual populations can partially replace clinical trials. The function of an organ can be simulated using 3D in silico models, known as digital twins (DTs) [1]. The gastrointestinal tract is a system with complex anatomy, tissue properties and physiology. Most of the available studies have developed intestinal models with oversimplified geometric characteristics [2]. To develop high-fidelity intestinal DTs with near-physiological characteristics, we propose a novel framework integrating machine learning and multiphysics modelling.

2. Materials and Methods

The proposed framework uses real-world data (CT image sequences and motion information), to generate intestinal DTs. First, the CT images are automatically segmented using the active contour method and the intestinal geometries are reconstructed. Then, a multilayer perceptron (MLP) with a WaveShaping (WS) activation function (Eq. 1) is applied to refine the reconstructed 3D patient-specific (PS) models and facilitate the meshing process.

$$WS(x) = \frac{e^{\sin(x)} - e^{-\sin(x)}}{e^{\sin(x)} + e^{-\sin(x)}}$$

This is followed by the setup of a multiphysics simulation model, where the finite element method (FEM) and smooth particle hydrodynamics (SPH) approaches are combined to model the intestinal walls and contents, respectively.

3. Results

A prototype model of the final segment of a PS large intestine was developed. Details of the intestinal wall material properties, mesh quality, and boundary conditions can be found in [1]. The contents were modelled with ~10,000 SPH particles (mass=1.05×10⁻² g; density=1.056 g/cm³). Multiphysics simulations using the developed DT were performed to assess its interaction with a colon capsule endoscope (PillCam™ COLON2, Medtronic). Fig. 1(a) illustrates the intestinal part before and after the application of the MLP-WS. The geometry was significantly refined without losing any anatomical features. In comparison with the state-of-the-art approach proposed in [3], an improvement of 63% was achieved. Fig. 1(b) illustrates indicative results. It shows the initial capsule position, and its position translated by 16.4 mm after two consecutive peristaltic contractions that lasted 2.4 s.

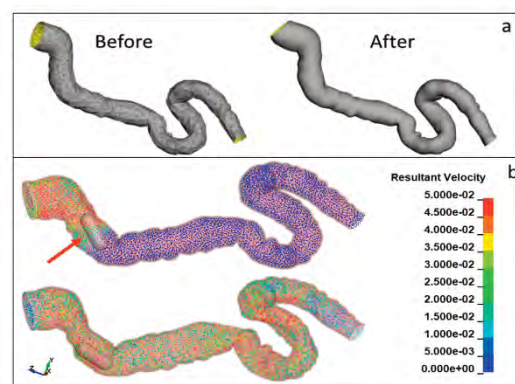


Figure 1: (a) Intestinal geometry before and after the application of the MLP-WS; (b) Peristaltic wave propagation and capsule transit in the intestinal segment after two contractions. The red arrow indicates the capsule location and the SPH particles are coloured according to their velocity (m/s).

4. Discussion and Conclusions

The results show that the proposed framework can provide both quantitative and qualitative data for MD design and optimization. Future work aims at the validation of the generated models against *in vivo* and/or *in vitro* data.

5. References

1. Kalozoumis PG et al., *Digital Twins for Digital Transformation: Innovation in Industry* (2022)
2. Sinnott, MD et al., *Applied Mathematical Modelling*, 44, 143-159 (2017)
3. Sitzmann V et al., *Advances in Neural Inf. Processing Systems* 33:7462–7473 (2020)

Acknowledgements:

Co-financed by Greece and EU (European Regional Development Fund) NSRF 2014-2020, MIS 5047243.

P2.6

Developing a physiological map as a framework to study chemical-induced liver steatosis

Luiz Carlos Maia Ladeira¹, Alessio Gamba¹, Raphaëlle Lesage², Anouk Verhoeven³, Jian Jiang³, Jonas van Ertvelde³, Ramiro Jover⁴, Tamara Vanhaecke³, Vinken Mathieu³, Liesbet Geris^{1,2,5}, Bernard Staumont¹

¹ University of Liège, Giga In Silico Medicine, Liège, Belgium

² KU Leuven, Skeletal Biology and Engineering Research Center, Leuven, Belgium

³ Vrije Universiteit Brussel, Pharmaceutical and Pharmacological Sciences, Brussel, Belgium

⁴ University of Valencia, Departamento Bioquímica y Biología Molecular, Valencia, Spain

⁵ KU Leuven, Biomechanics Section, Department of Mechanical Engineering, Leuven, Belgium

*lcladeira@uliege.be **liesbet.geris@uliege.be

1. Introduction

Physiological maps (PMs) are conceptual constructs that integrate knowledge as mechanistic representations of biological processes [1]. They are indeed a type of pathway model [2], with the main goal of describing a physiological process. PMs can be used qualitatively as a mechanistic background in Adverse Outcome Pathways (AOP) creation and refinement, supporting model rationale, and quantitatively to develop computational models serving different purposes. Here, we developed a liver lipid metabolism PM (LLMPM) to serve as a framework to improve a steatosis AOP network and build an ontology [1] for the study of chemical-induced steatosis.

2. Materials and Methods

We adapted the workflow from the Disease Maps project [3] to construct the LLMPM. First, relevant physiological literature (mainly review papers and book chapters) was curated with the help of domain experts. Then, we listed the fundamental mechanisms to be mapped and screened online databases (e.g. [4]) for previously described pathways. Finally, we integrated pathways and data from literature using the CellDesigner software.

3. Results

Fig. 1 shows a part of the LLMPM we designed. The identified key mechanisms are: fatty acids uptake, fatty acids synthesis, triacylglycerol synthesis, cholesterol synthesis and glycolysis (as input); mitochondrial beta-oxidation, peroxisomal beta-oxidation, microsomal omega-oxidation, ketogenesis, and very-low-density lipoproteins (VLDL) secretion (as output); hormones and transcriptional factors (as regulators). The pathways are represented considering the human genome and proteome.

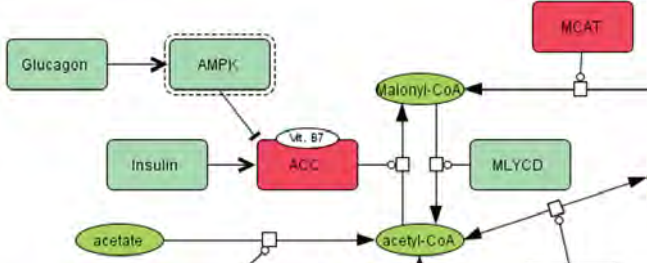


Fig. 1 – Part of the liver lipid metabolism PM, mapping the mechanisms described as pathways using the systems biology graphical notation.

4. Discussion and Conclusions

We built this network considering expert-curated literature and community-developed pathways previously available, focusing on physiological mechanisms. This network needs to be continuously updated if it is to be a dynamic tool serving the community in the aforementioned ways. However, we can already glimpse its usage potential in this early stage. This map is a multi-layered tool that will be developed further to integrate a pathological information represented by AOPs as well as quantitative kinetic and chemical information. In due course, every layer will be integrated to form a chemical-induced disease ontology [1]. Ultimately, such a tool might provide a broader understanding of liver pathways influenced by specific chemicals, with subsequent integration into more complex networks downstream to an initial molecular events, allowing future toxicity prediction and disease modeling.

5. References

1. Vinken, M. et al. *Toxicology*, v. 458, n. June, p. 1–7, (2021).
2. Hanspers, K. et al. *PLoS Computational Biology*, v. 17, n. 8, p. 1–14, (2021).
3. Mazein, A. et al. *npj Systems Biology and Applications*, v. 4, n. 1, (2018).
4. Martens, M. et al. *Nucleic Acids Research*, v. 49, n. D1, p. D613–D621, (2021).

Acknowledgements:

This project has received funding from the European Union's Horizon 2020 research and innovation programme under grant agreement No 963845 (ONTOX project).

P2.7

Validation of stress shielding for an in silico clinical trial in support of a regulatory submission

Christine Mueri¹, Adam Henderson¹, Ghislain Maquer¹, Jeff Bischoff², Philippe Favre³

1 Zimmer Biomet, Research, Winterthur, Switzerland

2 Zimmer Biomet, Research, Warsaw, IN, United States

3 Zimmer Biomet, Research, Zug, Switzerland

1. Introduction

Regulatory requirements for providing clinical data are increasing [1]. Clinical data may be enriched with in silico clinical trials (ISCT), where virtual cohorts of patient-specific computer models predict the clinical performance of a medical device.

There exists no published guideline on how to validate an ISCT for a medical device. Our objective is to present a detailed example of model validation for stress shielding.

2. Materials and Methods

The credibility plan for stress shielding included model verification and validation per the ASME V&V40 with two aspects: A) traditional benchtop validation to ensure the physics are captured correctly; B) clinical validation to ensure the clinical findings are captured correctly, which is the main focus of this study.

For benchtop validation A), a published study [2] comparing simulated and experimentally determined bone strain provides sufficient credibility for benchtop validation, and demonstrated the ability to accurately predict bone strains following the approach to be used here.

The purpose of the clinical validation B) consisted in reproducing the results of a clinical study that reported cortical thinning in the superior lateral cortex of the humerus when a large canal filling stem was implanted [3]. A cohort of 25 virtual humeri was taken from an internal 3D bone database, and virtual surgery was performed, with the same implant as the clinical study (Figure 1A-C). The implanted bones were imported to a finite element (FE) software for meshing, contacts definitions and application of boundary conditions including joint reaction and muscle loads representative of daily usage (Figure 1D-F). Bone material properties were assigned from the bone density information (Figure 1E). Stress shielding was assessed in the same regions as in the clinical study by comparing the change in strain energy density (SED) in the intact bone and after implantation.

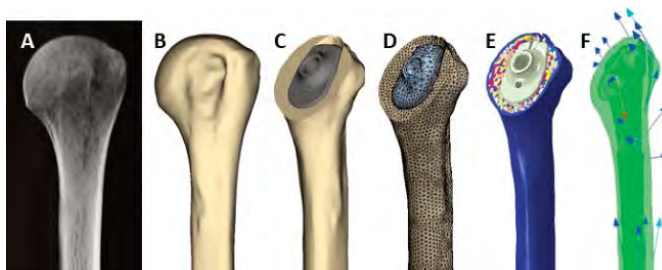


Figure 1: Steps for creation of FE models

3. Results

Reduction in SED between the intact and implanted bone, indicative of stress shielding, was highest in the location of clinically observed stress shielding, and occurred specifically when a large canal filling stem was implanted (Figure 2).

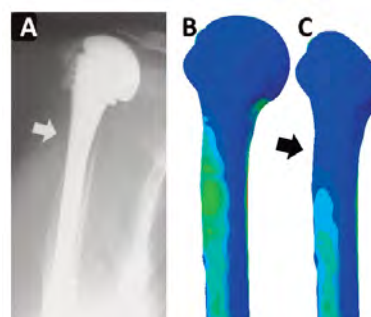


Figure 2: Stress shielding (A) [3] and change in SED between intact (B) and after implantation (C).

4. Discussion and Conclusions

The validity of the modelling approach was established by relying on benchtop and clinical data, extending existing standards that generally consider benchtop testing as the single comparator.

With these validated computer models, simulations for stress shielding can be conducted across a virtual population, supplying simulation data to enrich clinical data and compensate for slow enrolment or loss to follow-up.

5. References

1. Favre et al., Ann Biomed Eng. 2021;49(12):3213-3226.
2. Eberle et al., Med Eng Phys. 2013;35: 875-83
3. Nagels et al., J Shoulder Elbow Surg. 2003;12:35-9.

P2.8

Reliable digital twin simulation development and execution on the HPC infrastructures

Marek Kasztelnik¹, Tomasz Gubała^{1,2}, Piotr Nowakowski^{1,2}, Jan Meizner^{1,2}, Piotr Poleć¹, Maciej Malawski^{1,2}, Marian Bubak^{1,2}

1 ACC Cyfronet AGH, Kraków, Poland

2 Sano Centre for Computational Medicine, Kraków, Poland

Corresponding author: Marek Kasztelnik, email: m.kasztelnik@cyfronet.pl, Nawojki 11, 30-950 Kraków, Poland

1. Introduction

Building simulations for the digital twins is a challenging task. When we add an additional level of complexity connected with the underlying HPC infrastructure and require repeatability, replicability, and reproducibility, the amount of work and knowledge required from researchers increases considerably. To improve this situation the Model Execution Environment (MEE) was created [1]. This environment enables digital twin simulations to be developed in a simple and organized manner, and easily run on the integrated HPC infrastructure. Here, we report on how the environment has been extended and improved by adding support for multiple organizations, advanced versioning of model code and input/output data management.

2. Materials and Methods

The classical way to develop and execute simulation on HPC involves numerous manual steps such as model preparation and local tests, copying model source code and required inputs to HPC, running the simulation (via a queuing system), monitoring progress, and fetching results. Such manual procedure can produce problems, e.g.: files copied to the wrong directory may become inaccessible for group members; model source code may remain unversioned, making it hard to trace results back to a specific model version; new results can overwrite previous results, etc.

3. Results

The enhanced MEE addresses these issues by introducing a complete environment where models and simulations can be designed as pipelines and executed directly on HPC. MEE is integrated with Git repositories, where the source code of the model is hosted. When the computation is launched in MEE, selected versions of models are uploaded to the HPC infrastructure and executed. MEE automatically monitors execution and reports back when the results are ready. Through integration with HPC storage, MEE creates a dedicated structure for each execution (preventing results from being overwritten), and allows for easy upload of inputs and download of results.

4. Discussion and Conclusions

The presented solution was validated during EurValve (<http://www.eurvalve.eu>), and currently supports investigations in PRIMAGE (<https://www.primageproject.eu>) and InSilicoWorld (<https://insilico.world>) projects running human heart and multi-scale tumor complex simulations. It will be further enhanced to match user requirements and progress in distributed computing.

5. References

1. M Bubak, K Czechowicz, T Gubała, DR Hose, M Kasztelnik, M Malawski, J Meizner, P Nowakowski, S Wood The EurValve model execution environment, *Interface Focus* 11 (1), 20200006, 2021

Acknowledgments:

This work was supported by the EU project PRIMAGE H2020-EU.3.1.5.3 826494 and by the PL-Grid Infrastructure (www.plgrid.pl).

P2.9

From Physiological Map to Ontology Unravelling Kidney Toxicity

Alessio Gamba¹, Luiz Carlos Maia Ladeira¹, Raphaëlle Lesage², Daniël Roodzant³, Devon A. Barnes⁴, Manoe J. Janssen⁴, Marc Teunis³, Rosalinde Masereeuw⁴, Liesbet Geris^{1,2,5}, Bernard Staumon¹

¹ University of Liège, Biomechanics Research Unit, GIGA In Silico Medicine, Liège, Belgium

² KU Leuven, Skeletal Biology and Engineering Research Center, Leuven, Belgium

³ Utrecht University of Applied Sciences, Innovative testing in Life Sciences & Chemistry, Utrecht, Netherlands

⁴ Utrecht University, Div. Pharmacology, Utrecht Institute for Pharmaceutical Sciences, Utrecht, Netherlands

⁵ KU Leuven, Biomechanics Section, Department of Mechanical Engineering, Leuven, Belgium

*agamba@uliege.be **liesbet.geris@uliege.be

1. Introduction

In the emerging field of computational toxicology, many predictive tools are available today, covering different toxicological endpoints and providing high accuracy predictions [1]. However, two main issues affect these in silico models. First, models are mainly based on animal-test data, raising ethical concerns and lacking a good correlation when applied to human toxicity. Second, models often cannot explain the biological mechanisms of toxicity, since they are developed solely on the structures of toxic/non-toxic chemicals. To overcome current limitations, we developed a new systems biology approach to build a Physiological Map (PM) based on human data and represented in an online interactive interface.

2. Materials and Methods

The semi-automated method described here is useful to retrieve data in order to build the initial PM, as well as for its validation. An initial manual literature review, with the support of domain experts, is supplemented by computational interrogation of ontologies (e.g. Gene Ontology) creating a network of genes, proteins, molecules, and phenotypes [2]. Then, this automatically generated network can be converted into pathways to add manually to the PM. Ultimately, the PM is represented using the graphical layout of CellDesigner and can be visualized on the web using the MINERVA platform, allowing field experts to review it.

3. Results

We developed several PMs in the frame of the European project ONTOX. The project aims to improve risk assessment in the liver, kidney, and developing brain, avoiding the use of animal tests [3]. We present here the kidney PM, organized in its main compartments: tubular lumen, blood, glomerulus, proximal tubule, the loop of Henle, distal tubule, and collecting duct. We display all the processes involved in filtration, reabsorption and secretion for urine production. The PM shows the normal physiology but it is aimed to study two pathological conditions: kidney cristallopathy and tubular necrosis.

4. Discussion and Conclusions

The method proposed here guides the user through the construction of PM even starting from limited information. The PMs are initially developed as a qualitative and static representation of physiological processes. However, they can be useful for the parallel or subsequent development of adverse outcome pathways. The next step is to add kinetic parameters and transform our PMs into dynamic and quantitative models able to describe different cellular conditions. At the end, all the collected data can be organized in a dictionary of related elements, a structure called ontology in ONTOX project. This represents an exceptional opportunity to improve toxicological predictions and investigate human toxicities from a new perspective.

5. References

- [1] Manganelli, S., et al. (2022) *Meth in Mol Biology*, vol 2425. Humana, New York, NY.
- [2] Gamba, A., et al. (2020), *Sci Rep* 10, 10423.
- [3] Vinken M., et al. (2021), *Toxicology* 458, 152846.

Acknowledgements:

This project received funding from the EUH2020 ONTOX project (no 963845).

P2.10

Implementing Public & Patient Involvement (PPI) for in silico medicine.

Cyrille Thinnes^{1,2,3}, Steven Levine^{2,4}

1 National University of Ireland, Galway, Medicine & Ryan Institute, Galway, Ireland

2 Avicenna Alliance - Association for Predictive Medicine, Belgium

3 Virtual Physiological Human Institute for Integrative Biomedical Research, Belgium

4 Dassault Systèmes, The Living Heart Project, United States

cyrille.thinnes@nuigalway.ie ✉ steven.levine@3ds.com

1. Introduction

Public and Patient Involvement (PPI) generates research carried out with or by (rather than to/about/for) the public, thereby presenting an opportunity for accelerating impactful research outcomes through end-user driven systematic stakeholder involvement [1]. PPI-driven value has generated international momentum primarily in a clinical context, with pre-clinical efforts still lagging behind. There are no concerted international PPI efforts in the in silico medicine space to date – a gap which has now been addressed by the Avicenna Alliance through the creation of the PPI task force of the policy development working group in 2021.

2. Materials and Methods

Following the formation of a diverse, multidisciplinary, and international PPI task force, uniting members from both public and private sectors, we performed internal and external analyses in the PPI context including stakeholder mapping, community broker identification, review of existing resources established by current PPI thought leaders, surveys, and critical assessment of accumulated knowledge relating to relevance of PPI in the in silico medicine context during monthly facilitated task force meetings.

3. Results

The critical assessment of the rich resources of general PPI knowledge and experiences accessible to the task force members and relationship establishment with PPI thought leaders enabled us to craft a pathway to impact in a stepwise approach driven by continuous, collaborative, and iterative learning. First, we will focus internally to raise awareness of PPI within the Avicenna Alliance through establishment of a White Paper focusing on PPI for in silico medicine, which will form the basis for discussion with external stakeholders, including PPI groups, for iterative improvement and establish an in silico medicine guide for implementing PPI across the entire research lifecycle. This guide will then form the basis to shift from a relatively more internal to an external focus, promoting the steadily evolving guide to advocate for PPI implementation in the digital health space through publications, workshops, and establishment of case studies to eventually craft a position to suggest 'best practices' for in silico medicine PPI.

4. Discussion and Conclusions

PPI has gained significant momentum in the health research community over the recent years with demonstrable value to the end user and potential to improve research outcomes. Within the currently underserved area of PPI in the pre-clinical environment, we identified a strategic fit for implementing PPI for in silico medicine, which remains currently unaddressed. Based on our internal and external analyses, we defined a stepwise approach to establish the Avicenna Alliance as a pioneer and leader to drive in silico medicine-specific PPI implementation through co-creation of PPI resources through systematic stakeholder involvement of international thought leaders within the communities of Avicenna Alliance members and beyond to accelerate impactful in silico medicine research for patient benefit.

5. References

1. Crocker JH et al, *Health Expectations* 20.3:519-528 (2017).

Acknowledgements:

We would like to express our gratitude to the work, dedication, and proactive contribution of all the PPI task force members, the policy development working group, and the Avicenna Alliance.

P2.11

Computation approach to circularRNA estimation.

Sabina Lichołai¹

1 Academic Computer Centre CYFRONET AGH

1. Introduction

Circular RNAs are a group of non-coding nucleic acids that, unlike the other molecules in this group, take the form of a circle. This makes them invulnerable to enzymatic degradation by conventional pathways, and thus increases the likelihood of their sustained participation in regulatory pathways and creates the possibility of their use as potential biomarkers for many diseases. Unfortunately, their exact function as well as their interaction model is not fully understood. There are also no suitable tools that would allow efficient estimation of their number and possible function in specific cellular conditions. Therefore, in this work, an attempt has been made to create a comprehensive tool, which using HPC-type infrastructure and models based on machine learning will allow to solve this problem.

2. Materials and Methods

Circular RNAs are a group of non-coding nucleic acids that, unlike the other molecules in this group, take the form of a circle. This makes them invulnerable to enzymatic degradation by conventional pathways, and thus increases the likelihood of their sustained participation in regulatory pathways and creates the possibility of their use as potential biomarkers for many diseases. Unfortunately, their exact function as well as their interaction model is not fully understood. There are also no suitable tools that would allow efficient estimation of their number and possible function in specific cellular conditions. Therefore, in this work, an attempt has been made to create a comprehensive tool, which using HPC-type infrastructure and models based on machine learning will allow to solve this problem.

3. Results

Analysis of the resulting whole-genome transcriptome RNA sequencing yielded a total of 1068 unique circular RNA sequences. Of these, 1055 were previously annotated in publicly available databases. 1007 of the obtained transcripts originated from protein-coding genes. The number of circRNAs for which the number of reads in our cells exceeded 50 reads is 17, and 42 were more abundant in cells than their linear counterparts derived from the same gene.

Then we compared the sequences we obtained with publicly available circular RNA databases. 13 of the transcripts we found were not previously annotated, and 3 of them are located within protein-coding genes. Because function of circular RNAs in endothelial cell biology is not fully elucidated and suggested mechanism is based on selectively binding to the miRNA followed by inhibition their functions, we created a model of how these molecules interact together. As a result, we have shown that using appropriate metrics, we can identify a pool of about 100 molecules (out of 30000) whose expression will be disrupted, and about 80 of these have been confirmed experimentally.

4. Discussion and Conclusions

It is not entirely clear how circular RNA expression is regulated. Unlike linear forms of mRNA, whose expression levels are subject to a variety of regulatory mechanisms, changes in circular RNA levels appear more chaotic. In the present study, we analysed the expression level of circular RNA and compared it with the location or structure of host genes. Under microRNA stimulation, a specific pool of circular RNA molecules underwent altered expression. MicroRNAs inhibit expression at the post-translational level and have their target sites on specific genes. However, there is no correlation or overrepresentation of changes in expression levels of circular RNAs encoded by the host genes on which target genes for specific microRNAs are located. In contrast, we were able to show that the greatest potential for altered expression levels of circular RNAs are molecules whose ratio of host gene genomic length to the number of its exons is lower than the genome-wide average. In the pool of these molecules, we observe an overrepresentation of circular RNAs with altered expression levels. This may indicate that the formation of circular RNAs by backsplicing occurs most easily in long genes, divided by a smaller number of exons.

Acknowledgements:

This research was supported in part by the PLGrid Infrastructure and by the European Union's Horizon 2020 programme under grant Sano No 857533, and Sano project carried out within the International Research Agendas programme of the Foundation for Polish Science, co-financed by the European Union under the European Regional Development Fund.

P2.12

Systematic engagement with notified bodies to advance in silico trials in Europe

Simon Sonntag^{1,2}, Bernard Staumont^{2,3,4}, Liesbet Geris^{2,3,4,5}, Thierry Marchal^{2,6}

1 Virtonomy, Munich, Germany

2 Avicenna Alliance - Association for Predictive Medicine, Belgium

3 University of Liège, Biomechanics Research Unit, GIGA in silico medicine, Liège, Belgium

4 Virtual Physiological Human Institute for Integrative Biomedical Research, Belgium

5 KU Leuven, Biomechanics Section, Leuven, Belgium

6 Ansys Inc., United States

*sonntag@virtonomy.io

1. Introduction

Notified Bodies (NB) are organisations designated by the National Health Authorities to assess the conformity of certain products within the European Union (EU), i.e., medical devices (MD) and in vitro diagnostics (IVD) before granting market access [1]. These independent and impartial bodies carry out tasks related to conformity assessment procedures set out in the applicable legislation. Within the policy development working group of the Avicenna Alliance, the NB task force aims to engage with NBs to increase acceptance of in silico evidence in Europe, provide NBs with guidance documents and offer them assistance in the review process of digital evidence.

2. Materials and Methods

The NB task force of the Avicenna Alliance mapped the various NBs designated under the EU MDR (Regulation 2017/745) [2] and EU IVDR (Regulation 2017/746) [3]. The task force also engaged with NBs and evaluated the perception of in silico evidence among them. The NB task force started discussions with several NBs as well as The European Association for Medical devices of Notified Bodies (Team-NB) to identify gaps and challenges in the acceptance of in silico evidence by NBs. Collaboration with standardisation bodies to develop & harmonise guidance documents is also ongoing.

3. Results

The following key outcomes emerged from the mapping and discussions with NBs, which: (i) are all aware that in silico medicine is a reality; (ii) see the opportunities of in silico testing for the development of MDs, e.g., by bringing MDs faster to the market or by increasing the quality of MDs; (iii) perceive the challenges and opportunities for innovation; (iv) already receive submission dossiers from manufacturers including in silico evidence, however, often as additional material and only occasionally as the main source of evidence.

4. Discussion and Conclusions

The feedback from Team-NB and the NBs allowed the task force to identify the following challenges and action points: (1) one needs to improve the understanding of the state-of-the-art of in silico testing among NBs, for which the task force aims to engage further with NBs (meetings, workshops) to clarify questions and challenges related to the interpretation of digital evidence, training needs and other possible obstacles to the adoption of in silico medicine; (2) the NBs need more guidance documents, such as extensions of (ISO) standards on which the NB task force is currently working on; (3) the trust in in silico evidence and validation can be increased by providing NBs with success stories for regulatory approval using in silico evidence in Europe and the development of a quantifiable measure of success; (4) as the NBs lack resources to tackle submissions with digital evidence, the task force suggests to establish an independent network of experts who could help reducing the workload within NBs.

5. References

1. https://ec.europa.eu/growth/single-market/goods/building-blocks/notified-bodies_en
2. https://ec.europa.eu/growth/tools-databases/nando/index.cfm?fuseaction=directive.notifiedbody&dir_id=34
3. https://ec.europa.eu/growth/tools-databases/nando/index.cfm?fuseaction=directive.notifiedbody&dir_id=35

Acknowledgements:

We would like to thank all the NB task force members, the policy development working group and the Avicenna Alliance for their dedicated work and proactive contribution.

P2.13

Building a cloud simulation system for reproducible and multi-level cached in-silico trials

Yves Pares¹, Matthieu Coudron¹, Louis Philippe¹, Elliott Tixier¹

¹ Novadiscovery, France

1. Introduction

In-silico trials usually involve running a lot of simulations on the same computational systems biology model at one given version, only varying slightly the parameters and initial conditions. One can identify a unitary brick of computation, which we call “atomic job”: solving a specific version of a specific model using a specific set of parameters and initial conditions. An important thing to note is that this atomic job is deterministic: running it twice would produce the exact same results. This important property provides reproducibility, a key aspect of the scientific method. We can use that atomic job as part of many simulations and parameter-space exploration jobs, which are most of the time highly parallelizable. These atomic jobs being deterministic, these high-level jobs can share results and compute time. We aim at presenting here the key aspects of the Jinko.ai platform design, currently developed by NovaDiscovery for trialists and QSP modellers.

2. Materials and Methods

2.1 In-silico trial jobs

An atomic job in the context of in-silico trials consists in solving the differential system (typically ODE-based) derived from a biochemical reaction network and serialising the outputs (typically time series of some species and parameters and scalar quantities of interest derived from them). For computational efficiency, the differential system is optimised using LLVM [1] and solved using Sundials' CVODE [2] library.

2.2 Job distribution

The distributed simulation engine of the Jinko.ai platform is made to provide at-least-once semantics. It is based around three key ideas: (a) a fully symmetric and failure-tolerant “job-borrowing” mechanism that only needs a basic queue system and a relational database, (b) a representation of the various workloads as a hierarchy of deterministic, cached jobs, and (c) content-addressing of input resources, job instances and job results.

(a) implies that besides the queue and persistence layer (which can be provided by common tools like Redis and PostgreSQL databases, but any third-party services ensuring safe concurrent accesses would work), every service deployed is the exact same executable, and all operate at any time along the exact same rules. There is no central scheduler or bookkeeping service. It alleviates a classical issue in job-stealing architectures, where workers take a job from some queue and may die before being able to signal it: an external bookkeeping service is thus needed to track pending jobs and ensure the unfinished ones are put back in the queue, therefore adding the necessity to maintain this extra service.

(b) means that jobs are able to start other jobs (until we reach our terminal jobs) and organise their internal computations as they see fit using a generic workflow framework that keeps track of every resource needed by each intermediate job [4]. This allows us to devise complex schemes that fit either a trial (simulating a set of “virtual patients”), a bayesian exploration algorithm to calibrate the model’s parameters, etc. and run them on our workers with again no need for external schedulers.

(c) is what makes use of the deterministic nature of our jobs: we can identify a computation based on what it will do (using techniques from the world of build systems such as Nix [3]), the resources it will read, etc. with the guarantee that we have a one-to-one mapping between this identifier and the end results. It allows for caching at various levels of granularity, and it allows jobs to share intermediate jobs and results, limiting computation time and storage.

3. References

1. Lattner C et al, "LLVM: A compilation framework for lifelong program..." *Int Symposium on Code Gen and Opt*, IEEE, 2004.
2. Hindmarsh AC et al, *ACM Trans on Math Soft (TOMS)* 31.3 (2005): 363-396.
3. Dolstra E: "The purely functional software deployment model", *PhD th*, Utrecht U, 2006
4. Parès Y et al, "Composing effects into tasks and workflows." *Proc 13th ACM SIGPLAN International Symposium on Haskell*. 2020.

P2.14

Clinical trial simulations in oncologic patients using the InSilicoONCO suite

Chiara Nicolò¹, Cristina Vaghi¹, Marc-Antonio Bisotti¹, Roberta Bursi¹

1 InSilicoTrials Technologies S.p.A.

1. Introduction

Difficult comparison of new drugs with those already available in the market, clinical trials' high costs and failure risk are among the major challenges that pharmaceutical companies encounter while setting up their oncology clinical development programs. To help solve these challenges, InSilicoTrials Technologies has developed PCa GnRH Agonists Simulator and CTx NeuroSim, two products of InSilicoONCO, a growing suite of cloud-based tools to perform clinical trials simulations in virtual oncologic patients. Specifically, PCa GnRH Agonists Simulator simulates testosterone suppression on prostate cancer patients treated with a GnRH agonist; CTx NeuroSim simulates neutropenic effects in patients treated with a chemotherapeutic agent.

2. Materials and Methods

Both PCa GnRH Agonists Simulator and CTx NeuroSim are based on semi-mechanistic computational PK/PD models [1]–[3].

Clinical trial simulation with these tools requires the following inputs:

- Definition of the clinical trial design in terms of population size, dosing regimen, and the treatment duration;
- Specification of the compound pharmacokinetics;
- Specification of the drug-related parameters. Specifically, PCa GnRH Agonists Simulator requires the receptor equilibrium dissociation constant of the GnRH agonist. CTx NeuroSim requires the value of a parameter, IMPdrug, quantifying the drug impact on proliferative hematopoietic stem cells.

3. Results

The pharmacokinetic and pharmacodynamic properties of a number of known drugs are available in the GnRH agonists library of PCa GnRH Agonists Simulator. Here, leuprorelin administered as a sustained release formulation was selected to simulate the testosterone suppression under different schedules over one year to replicate real clinical trials. Results were provided in terms of number of patients reaching testosterone levels under 0.5 ng/ml and were in agreement with clinical findings [4]–[6].

CTx NeuroSim was applied to simulate the neutropenic effects of docetaxel given as 1h infusion of 100 mg/m² on day 1 of a 3-week cycle. An appropriate value for the unknown drug-related parameter, IMPdrug, was obtained by comparing simulation results across different IMPdrug values against synthetic data generated from a published PK/PD model of docetaxel [7]. Simulation results were in agreement with the neutropenia incidence, time to nadir and absolute neutrophil count at nadir observed in a real phase II clinical study of docetaxel [8], providing evidence of the model's capability at predicting neutropenic effects.

4. Discussion and Conclusions

PCa GnRH Agonists Simulator and CTx NeuroSim enable to setup and run in silico clinical trials in a user-friendly way by using a step-by-step integrated workflow. They can be used to explore different clinical trial scenarios, allowing to optimize phase I and II clinical trial design, cutting time and costs of a drug development program for pharmaceutical companies and CROs.

5. References

- [1] E. Romero et al., *J. Pharmacol. Exp. Ther.*, vol. 342, no. 3, pp. 788–798, Sep. 2012
- [2] C. N. Lim and A. H. Salem, *Clin Pharmacokinet*, vol. 54, no. 9, pp. 963–973, Sep. 2015
- [3] V. Mangas-Sanjuan et al., *Pharmacol. Exp. Ther.*, vol. 354, no. 1, pp. 55–64, Jul. 2015
- [4] N. D. Shore et al., *Clin. Ther.*, vol. 41, no. 3, pp. 412–425, Mar. 2019
- [5] A. Spitz et al., *Prostate Cancer Prostatic Dis.*, vol. 15, no. 1, pp. 93–99, Mar. 2012, doi: 10.1038/pcan.2011.50.
- [6] R. Sharifi et al., *Urology*, vol. 51, no. 2, pp. 271–276, Feb. 1998
- [7] C. Kloft et al., *Clin. Cancer Res. Off. J. Am. Assoc. Cancer Res.*, vol. 12, no. 18, pp. 5481–5490, Sep. 2006
- [8] P. M. Ravdin et al., *J. Clin. Oncol. Off. J. Am. Soc. Clin. Oncol.*, vol. 13, no. 12, pp. 2879–2885, Dec. 1995

Acknowledgements:

The cloud-based tools PCa GnRH Agonists Simulator and CTx NeuroSim are results of a collaboration between InSilicoTrials Technologies and the University of Navarra. The authors acknowledge Prof. Troconiz for his contribution to this work.

P2.15

iSi Health: the KU Leuven institute of physics-based modeling for in silico health

Erica Beaucage-Gauvreau¹, Ilse Jonkers², Lennart Scheyns³, Jos Vander Sloten⁴, Karl Meerbergen⁵

1 KU Leuven, iSi Health, Leuven, Belgium

2 KU Leuven, Movement and Rehabilitation Sciences, Leuven, Belgium

3 KU Leuven, Development and Regeneration, Leuven, Belgium

4 KU Leuven, Mechanical Engineering, Leuven, Belgium

5 KU Leuven, Computer Science, Leuven, Belgium

1. Introduction

In silico clinical trials are a promising alternative to conventional approaches to ensure the safety and efficacy of new biomedical products and treatments. In contrast to traditional clinical trials that typically rely on animals or humans, in silico clinical trials are based on physics-based computer modeling and simulation. Computational models replicating the characteristics of patients (virtual patient or digital twin) can be used to test medicinal drugs or medical devices simulated virtually, without causing potential adverse effects to the patient, while also reducing the high costs associated with the development of new treatments. However, in order to ensure the efficacy and safety of these in silico techniques for health, a rigorous framework is needed. To this end, iSi Health: the KU Leuven Institute of Physics-based Modeling for in silico Health was recently established to play a pioneering role in further implementing physics-based simulations for health in the clinical context. iSi Health aims to contribute to five research domains: 1) Development and implementation of modeling and simulation methods (lead principal investigator (PI): G. Samaey); 2) Definition and validation of multi-scale cell-tissue-organ models (lead PI: N. Famaey); 3) Development of socio-econo-legal framework of in silico health (lead PI: L. Marelli); 4) Initiation of clinical translation and integration into health policy and leverage economical valorization (lead PI: F. Weekers); 5) Development of educational, training, and outreach activities (lead PI: J. Vander Sloten).

2. Materials and Methods

The mission of iSi Health is to establish a comprehensive in silico health network, uniting the unique multidisciplinary expertise at KU Leuven and University Hospitals (UZ) Leuven. More specifically, iSi Health will:

- act as a central network hub to foster and facilitate collaborative research activities for its members and to support partnerships with industrial and governmental stakeholders;
- initiate the formulation of good practices for the verification and validation of data-driven and physics-based computational tools;
- launch concerted research activities on the approval, societal acceptance, socioeconomic impact, and legal integration of in silico techniques for health;
- develop educational programmes targeting essential multidisciplinary skills integrating biomedical, medical, and engineering expertise for the workforce of the future;
- accelerate pilot implementation of selected state-of-the-art in silico models ready for accreditation to forge the path for physics-based models of the human system from bench-to-bedside to benefit future patients.



Figure 1: iSi Health: The KU Leuven Institute of Physics-based Modeling for in silico Health.

3. Discussion and Conclusions

Through collaborations between more than 60 KU Leuven and UZ Leuven researchers, and in synergy with established international partners, such as VPH and Avicenna Alliance, iSi Health will target the core challenges currently limiting the clinical implementation of in silico techniques for health. iSi Health will take a leading role in bringing healthcare into the digital era with the implementation of multi-scale, physics-based models to optimize patient-specific therapeutic intervention.

P3.1

Automatic Fracture Reduction of Pelvis using Statistical Shape Modelling

Tabassum Husain^{1,2}, Andrew Razjigaev^{1,2}, Andreas Petersik³, Heiko Gottschling³, Manuel Schröder³, Andrew Fielding^{2,4}, J Paige Little^{1,2}, Beat Schmutz^{1,2}
 5

¹ QUT Gardens Point Campus, School of Mechanical, Medical, and Process Engineering, Faculty of Engineering, Brisbane City, Australia

² ARC Training Centre for Multiscale 3D Imaging, Modelling and Manufacturing, Brisbane City, Australia

³ Stryker Trauma GmbH, Digital Technologies Trauma & Extremities, Schönkirchen, Germany

⁴ QUT Gardens Point Campus, School of Chemistry and Physics, Faculty of Science, Brisbane City, Australia

⁵ Jamieson Trauma Institute, Brisbane City, Australia

1. Introduction

Pre-operative fracture reduction of the pelvis is a challenging task due to the complex bone anatomy. Through the use of a point distribution model (PDM), automatic fracture reduction can be achieved. Due to sexual dimorphism of pelvic bone anatomy, we used a novel approach of creating sex specific PDMs. We applied an automatic fracture reduction method of simultaneous PDM adaptation and registration with the largest pelvic fragment [1]. We evaluated the method with clinical data of 5 female and 5 male fractured pelvises.

2. Material and Methods

The data consisting of 3D segmented bone models for clinical cases and the PDM were taken from Stryker's SOMA database [2].

After initial brute force registration of the combined fragment models with the PDM, subsequent model adaption is achieved using the following steps:

1. Distance based point correspondence is established between the PDM and largest fragment, and then used to adapt the PDM to the fragment [3].
2. The PDM is again registered with the largest fragment using a point registration method.
3. Steps 1-2 are repeated over 500 iterations. All the other fragments are registered with the adapted PDM using an ICP registration resulting in reduction of the fracture fragments.

The registration was quantified by a surface comparison of the registered fragments to the adapted PDM, and compared with the gold-standard contralateral side as template (Fig.1).

3. Results

Use of the mirrored contralateral as a template generated higher quality reductions than the PDM (Table 1). However, using the contralateral side requires manual interaction and will not work for complex bilateral fractures, which can be overcome by using the PDM.

Table 1: PDM and Mirrored contralateral average mean (standard deviation) distance-based differences (mm) and surface area (%) within 2mm and 5mm clinical tolerance thresholds [3].

Template	+Avg	-Avg	≤2mm	≤5mm
PDM	1.67 (0.51)	-2.42 (0.62)	72.53 (8.26)	89.83 (3.54)
Mirrored.	0.52 (0.59)	-2.57 (1.57)	90.16 (8.02)	95.73 (6.17)
p-value	0.0017	0.79	0.0028	0.0045

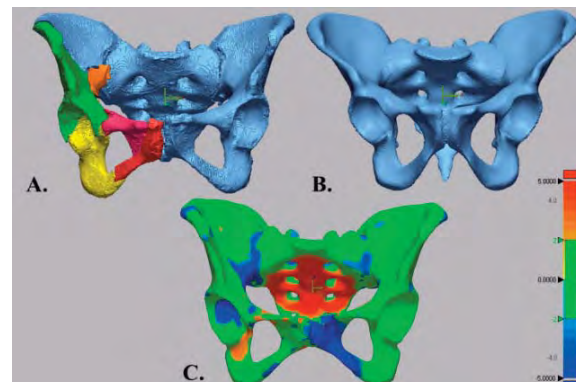


Figure 1: A) Acetabular and pubis fracture solution B) Adapted PDM C) Surface comparison where green regions are under a ±2mm tolerance in a ±5mm colour scale relative to the PDM

4. Discussion and Conclusions

Our approach of automatic fracture reduction achieved clinically acceptable results for most cases. However, discontinuous steps between adjoining fragments (Fig.1A) have shown that local PDM adaptation may be necessary. Our future work will focus on solutions addressing this issue.

5. References

1. Albrecht T, Vetter T; Springer Berlin 2012.
2. Schmidt W, et al. Surg Technol Int. 2018;32:315-324.
3. Zheng G, et al. IEEE Trans Biomed Eng. 2007;54(12):2109-22.

Acknowledgements:

This work was supported by: Australian Research Council Training Centre for Multiscale 3D Imaging, Modelling, and Manufacturing (IC180100008); Stryker Trauma GmbH, Germany.

P3.2

Sensitivity analysis of an one-dimensional pulse wave propagation model with correlated input

Pjotr Hilhorst¹, Sjeng Quicken¹, Frans van de Vosse¹, Wouter Huberts^{1,2}

¹ Eindhoven University of Technology, Biomedical Engineering, Eindhoven, Netherlands

² Maastricht University, Biomedical Engineering, Maastricht, Netherlands

1. Introduction

Patient-specific one-dimensional pulse wave propagation models (PWPM) are highly suited for outcome prediction of clinical interventions. Variance-based sensitivity analysis (SA) can be used for parameter-prioritization of these models based on their contribution to the total output uncertainty. Most variance-based SA approaches assume statistical input independence for the sake of computability while in many cases the inputs are correlated which may affect input importance ranking. This study aimed to compare the importance ranking of a SA with and without considering the correlation between model inputs on an one-dimensional PWPM.

2. Materials and Methods

A vectorial kernel orthogonal greedy algorithm [1] surrogate model-based approach is used to perform the SA of a PWPM. This approach allows for the creation of a kernel function based on a set of inputs and outputs generated with the PWPM. The kernel function relates input variables to an output, thereby drastically speeding up the SA. The correlated SA, based on the work of Li et al. [2], was performed on the surrogate model with and without considering correlated inputs. For validation, the uncorrelated analysis was compared to an established SA method for uncorrelated parameters based on adaptive generalized polynomial chaos expansion (agPCE) [3]. Later, the effects of statistical dependencies on the sensitivity indices (SIs) were investigated by changing the correlation coefficient ρ between the aortic length and diameter from $\rho \rightarrow -1$ to $\rho \rightarrow 1$.

3. Results

The correlated SA implementation method was benchmarked against analytical solutions of well-known functions, such as the Ishigami function. The surrogate-based approach in combination with the method of Li et al. resulted in similar SIs as found with the agPCE method. One surrogate-based model evaluation took about 0.05 milliseconds. Figure 1 shows the computed SI for a subset of input parameters.

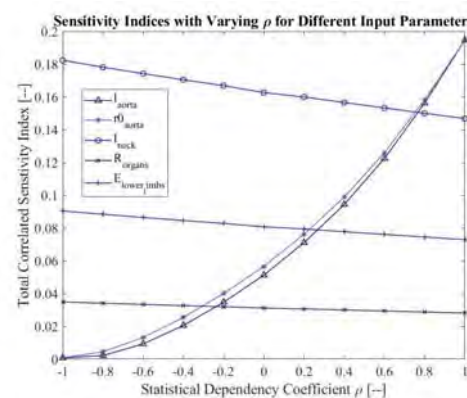


Figure 1: Computed SI for varying ρ

It was found that using a different value for the ρ considerably affects the importance ranking of the correlated input parameters. Moreover, the SIs of non-correlated input parameters were also affected, but to a smaller degree.

4. Discussion and Conclusions

The surrogate model-based approach allowed for a statistically dependent SA at a low computational cost for a relatively complex cardiovascular model. In the future, this method could be applied to more complex models. Including statistical dependency had a large impact on computed SIs. Therefore, when performing SA, it should be verified beforehand if statistical dependency should be considered.

5. References

1. Santin G. et al., *Kernel Methods for Surrogate Modeling*, ArXiv preprint 1907.10556 (2019).
2. Li L. et al., *Aerospace Science and Technology*, 62; (2017).
3. Quicken S. et al., *Journal of Biomechanical Engineering*, 138; (2016).

Acknowledgements:

We acknowledge the EU's Horizon 2020 research and innovation programme (No: 101016503 & 101017578) for funding.

P3.3

Identification of the most influential factors on pulmonary artery hemodynamics using variance-based sensitivity analysis

Hamed Moradi¹, Frans van de Vosse¹, Wouter Huberts^{1,2}

¹ Eindhoven University of Technology, Department of Biomedical Engineering, Eindhoven, Netherlands

² Maastricht University, Biomedical Engineering, CARIM School for Cardiovascular Diseases, Maastricht, Netherlands

1. Introduction

Variance-based sensitivity analysis are useful during model personalization as they can identify which parameters are rewarding to measure patient-specifically, and which parameters can be set to a population value [2].

The variations in parameters that determine the boundary conditions of CFD simulations significantly affect the pressure and velocity fields [1]. In this study, we investigate the effects of these parameters on the hemodynamics in the pulmonary arteries to design our measurement protocol when advancing to patient-specific simulations.

2. Materials and Methods

The variance-based sensitivity analysis attributes each fraction of the total output variance to individual factors and their uncertainty, or to the interactions between input factors [2]. The individual contributions are quantified by the main Sobol index, whereas the interactions are quantified by the difference between the total and main Sobol indices.

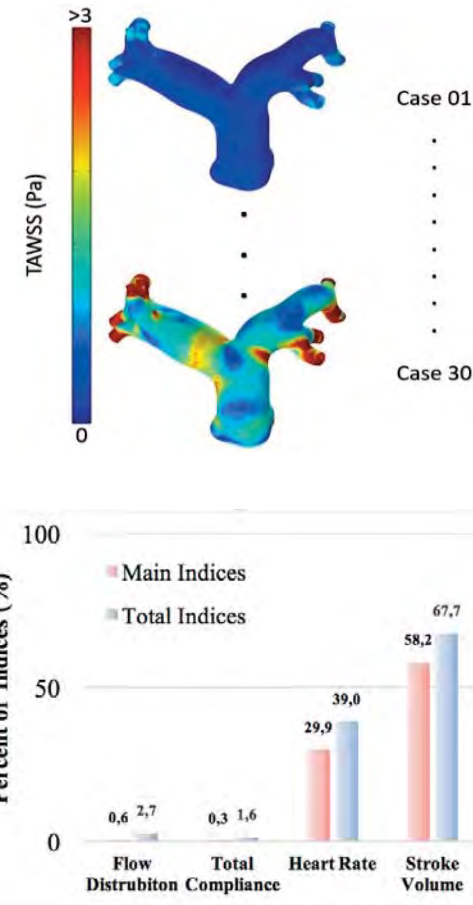
A high main index indicates that measuring this parameter is rewarding. The total index is useful to assess whether a parameter is irrelevant and can be fixed to a constant. To estimate these Sobol indices, an adaptive generalized polynomial chaos expansion method (agPCE) was applied on a 3D-CFD model [3] of the pulmonary artery. Three-element Windkessel models were coupled at the outlets and a typical inlet flow waveform was applied at the inlet. The 3D-transient model was calculated by using COMSOL. The input space for the sensitivity analysis is spanned by four uncertain inputs (Table 1). The input is subsequently sampled within these ranges using the low-discrepancy Sobol sequence via the built-in MATLAB function sobolset. Based on an a priori estimation a database of 30 samples is created.

Table 1: Input parameters and their ranges

Input parameter	Ranges
Q_{RPA} to Q_{LPA} ratio [-]	45-65
Stroke Volume [ml]	50-150
Total Compliance [ml/mmHg]	1-4
Heart Rate [bpm]	60-120

3. Results

An accurate agPCE ($Q_2 > 0.999$) was found for the mean time-averaged wall shear stress (MTAWSS), which was considered as an exemplary output of interest. The Sobol indices derived from the agPCE demonstrate that the percent of main indicate for stroke volume and heart rate is much more than total compliance and flow distribution. (Figure 1, and Figure 2)



4. Discussion and Conclusions

Sensitivity analysis of the boundary condition parameters in pulmonary artery shows that MTAWSS is sensitive to stroke volume and heart rate. Also, it seems that there is not any meaningful sensitivity from total compliance and flow distribution for MTAWSS.

5. References

- Stevens, Raoul, et al. *IEEE Trans on Biomedical Engineering* 67.4 (2019):1030-1039
- Eck, Vinzenz, et al. *International journal for numerical methods in bio eng* 32.8 (2016):e02755
- Quicken, Sjeng, et al. *Journal of bio eng* 138.12(2016)

Acknowledgements:

We acknowledge the European Union's Horizon 2020 research and innovation programme (grant agreement No 101017578) for their financial support.

P3.4

Dependency of healing outcomes on biomechanical conditions in postoperative reconstructed mandibles

Giorgio Biesso^{1,2,3}, **Vincenzo Orassi**^{1,3}, **Clarence Janka**⁴, **Carsten Rendenbach**², **Sara Checa**¹

1 Berlin Institute of Health at Charité – Universitätsmedizin Berlin, Julius Wolff Institute, Berlin, Germany

² Charité – Universitätsmedizin Berlin, Freie Universität Berlin, Humboldt-Universität zu Berlin and Berlin Institute of Health, Department of Oral and Maxillofacial Surgery, Berlin, Germany

3 Berlin-Brandenburg School for Regenerative Therapies, Berlin, Germany

4 Karl Leibinger Medizintechnik GmbH & Co.KG, Tuttlingen, Germany

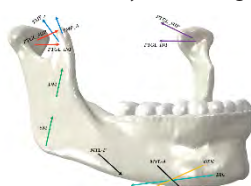
Correspondence: Sara Checa, sara.checa@bih-charite.de

1. Introduction

Optimal reconstruction of mandibular defects is a major clinical challenge. Novel approaches include the use of vascularized autologous bone grafts that are fixated to the mandible with computer-aided design and computer-aided manufacturing (CAD/CAM) plates. However, despite the plates being designed on patients anthropometric characteristics, recent investigations have reported high rates of osseous non-union [1]. Mechanical signals are known to play a role on bone regeneration [2], but they are difficult to measure experimentally. This study aims to investigate through a computational model, whether the healing outcome in reconstructed patients is related to postoperative biomechanical conditions.

2. Materials and Methods

A subject-specific finite element model (FEM) of a reconstructed mandible was developed based on the patient CT imaging data. The individual was treated with a fibula free flap and presented successful healing outcome. The fixation system consisted of a combination of titanium alloy CAD/CAM load-bearing and load-sharing fixation plates (Fig. 1). 14 muscles, modelled as actuators, were added to the FEM through coupling constraints. Insertion points were based on anatomic literature [3]. Individual muscle forces (F_i) were calculated by minimizing the following objective function:



$$\sum_{i=1}^m \left(\frac{F_i}{PCSA_i} \right)^2$$

where PCSAi is the physiological cross-sectional area of the individual muscles. To ensure a proper occlusion, condylar processes were assumed locked in the mandibular fossa. A unilateral clenching task was simulated and the 1st (ϵ_1) and 3rd (ϵ_3) principal strains were evaluated.

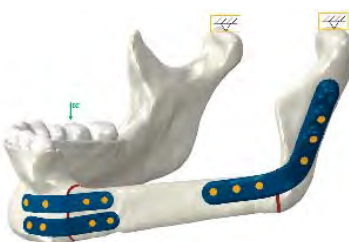


Figure 1: (Left): Muscular vector forces acting on the mandible. (Right): FEM of a reconstructed mandible fixated with CAD/CAM plates and related boundary conditions.

3. Results

For a unilateral biting task of 50N, the average ε_1 within the osteotomy regions was 1.2% (0.002 SD) and the average ε_3 was 0.04% (0.002 SD). Tensile strains were determined in the crestal sides, whereas the inferior regions were mainly under compression. Strain magnitudes for ε_1 and ε_3 were found to be higher on the distal interosseous gap than on the mesial (Fig. 2). 7 of 14 muscles were identified as responsible for the movement, with an average activation level of 20%.

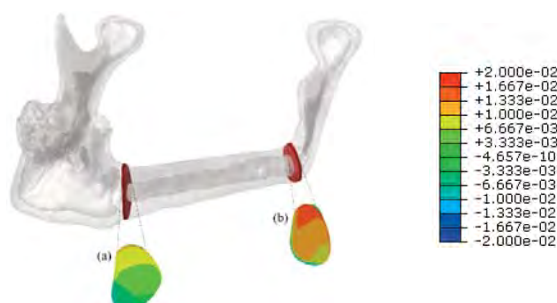


Figure 2: Absolute principal strains within the (a) mesial and (b) distal healing regions.

4. Discussion and Conclusions

A FE model of a reconstructed mandible with a positive clinical outcome was developed. Determined mechanical strains are in the range of those previously reported to promote intramembranous ossification [4]. Future studies are needed to investigate the biomechanical environment present in non-union scenarios.

5. References

Rendenbach et al., J. Oral Maxillofac. Surg., 2018.

Epari et al., Clinical Biomechanics, 2006.

Van Eijden et al. Anatomical Record 1997

Van Eijden et al., *Anatomical Record*, 1999.

Acknowledgements:

The study was funded by the German Research Foundation (CH 1123/10-1).

P3.5

Simulating non-Newtonian flow through aortic phantom: comparison between lattice Boltzmann method and magnetic resonance imaging

Pavel Eichler¹, Radek Galabov^{1,2}, Radek Fučík¹, Kateřina Škardová¹, Tomáš Oberhuber¹, Petr Pauš¹, Jaroslav Tintěra², Radomír Chabiniov^{1,3}

1 FNSPE CTU in Prague, Czech Republic

2 Institute for Clinical and Experimental Medicine, Czech Republic

3 UT Southwestern Medical Center, Dallas, United States

Corresponding author: R. Galabov, radekgalabov@gmail.com

1. Introduction

Currently, various approaches employing computational fluid dynamics in cardiovascular medicine are being explored. However, there persists uncertainty about the applicability of different models to different problems. In this work, we investigated a 3D model of lattice Boltzmann method (LBM) for non-Newtonian fluid in the turbulent regime. The in silico data were compared with velocity data obtained by a magnetic resonance imaging (MRI) scanner.

2. Materials and Methods

Three acrylic plates mimicking different stages of aortic stenosis – mild, moderate and severe – were placed in a rigid straight tube as in [1]. Water and two non-Newtonian fluids containing xanthan gum, GX and SX were circulated through the tube under a constant flow rate. A stack of slices perpendicular to the flow direction was measured by a 2D phase-contrast MRI sequence to obtain velocity data.

The cumulant LBM model proposed in [2] was used. The non-Newtonian behavior of the fluids was modeled by the Careau-Yasuda model for the dynamic viscosity μ_{CY} . In addition, two Newtonian LBM models were also implemented, considering two values of viscosity μ_0 and μ_∞ , appertaining to zero and infinite shear rate, respectively.

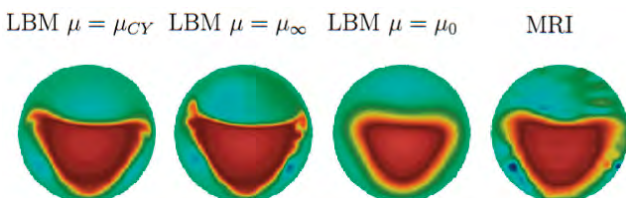


Figure 1: Flow profiles for the mild stenosis as simulated by the LBM models and measured by MRI. A Non-Newtonian fluid was used.

The two sets of velocity data (in silico and in vitro) were compared pointwise and in terms of the total reversed flow per slice.

3. Results

Qualitative match (Fig. 1) and quantitative match (Tab. 1) show promising results in favor of μ_{CY} and μ_∞ models.

Fluid	Data	Mild	Mod.	Sev.
SX	MRI	18	54	83
μ_0		5	25	58
μ_∞		19	54	85
μ_{CY}		15	53	85

Table 1: Maximal negative flow after mild, moderate and severe stenosis in ml/s for one fluid.

4. Discussion and Conclusions

The non-Newtonian LBM model of turbulent blood flow yields results with the accuracy sufficient for clinical practice. If needed, it can be substituted by the computationally faster Newtonian model μ_∞ . Interpretation of the results is limited by the use of constant flow rate. Further detailed quantitative results will be presented.

5. References

1. R. Fučík, et al., MAGMA. 33.5 (2020): 649-662.
2. M. Geier, et al., Comput Math Appl. 70.4 (2015): 507-547.

Acknowledgements:

This work was supported by MEYS of the Czech Republic under the OP RDE grants no. CZ.2.11/0/0/16_019/0000778, CZ.2.11/0/0/16_019/0000765, by Ministry of Health of the Czech Republic project no. NV19-08-00071 and by Institutional Support MHCZ-DRO IN 00023001, by the Inria France-UTSW Medical Center Dallas Associated Team TOFMOD.

P3.6

Meshless Simulation of Cell Growth Dependent on Oxygen and Glucose Concentration

Maria Inês Barbosa¹, Jorge Belinha², Renato Natal Jorge³, Ana Carvalho⁴

1 INEGI - Institute of Science and Innovation in Mechanical and Industrial Engineering, Porto, Portugal

2 ISEP - Instituto Superior de Engenharia do Porto, Porto, Portugal

3 Faculty of Engineering - University of Porto, Porto, Portugal

4 i3S - Instituto de Investigação e Inovação em Saúde da Universidade do Porto, Porto, Portugal

1. Introduction

One of the most important cell features is their capacity for proliferating which leads to their growth and division, through an organized process, which is dependent on oxygen and glucose [1, 2]. However, this process can be compromised and, in some cases, originate tumour cells [3]. Computational models can be used to study cell proliferation and have been proven to be a useful tool that saves money and time [4]. This work studies the influence of different concentrations of oxygen and glucose in the process of proliferation of a healthy and tumorous cell, using a new proposed algorithm.

2. Materials and Methods

The algorithm is based on a phenomenological law proposed by the authors that allows cells to grow iteratively until they double their initial volume and divide. This law is dependent on the concentration of oxygen and glucose so that the cell growth is affected by these parameters. Under adequate values of concentration, the cell grows and divides but, if this condition is not verified, the process of apoptosis can be initiated. To establish the system of equations, the algorithm uses the Radial Point Interpolation Method (RPIM), which is characterized by discretizing the domain using a nodal set, imposing the nodal connectivity by overlapping influence-domains and creating shape functions by combining radial basis and polynomial basis functions [5].

3. Results

The evolution of the cell volume was analysed by combining twenty-five ranges of oxygen and glucose concentrations, both for healthy and tumour cells. Each range represented a different state of oxygen (extreme hyperoxia, hyperoxia, normal oxygen concentration, hypoxia and extreme hypoxia) and glucose (extreme hyperglycaemia, hyperglycaemia, normal glucose, hypoglycaemia and extreme hypoglycaemia for glucose) concentration that differently influence the cell growth. For the two types of cells, the cell grows in almost all combinations of concentration but with different velocity rates. Only in the extreme states, the process of apoptosis occurred.

4. Discussion and Conclusions

The healthy cell grew in 24 h and the tumour cell in 18 h when normal concentrations were considered, which is within the expected time duration interval for a human cell cycle. However, when these concentrations were modified the time needed to achieve division was affected. For hyperoxia, hypoxia, and hypoglycaemia the growth tended to be slower. For the extreme states, the apoptosis process is initiated, and the cell started to die due to the aggressiveness of the medium. The main difference between the two cells were the velocity rates and the effect of hyperglycaemia, which in the tumour cell accelerated the growth process and in the normal cell slowed it down.

5. References

24. Sandal, T., *Molecular aspects of the mammalian cell cycle and cancer. The oncologist*, 2002. 7(1): p. 73-81.
25. Cristini, V. and J. Lowengrub, *Multiscale modeling of cancer: an integrated experimental and mathematical modeling approach*. 2010: Cambridge University Press.
26. Rudden, R.W., *Cancer biology*. 2007: Oxford University Press.
27. Alfieri, R., et al., *Modeling the cell cycle: From deterministic models to hybrid systems*. Biosystems, 2011. 105(1): p. 34-40.
28. Belinha, J. (2014). *Meshless Methods in Biomechanics. Lecture Notes in Computational Vision and Biomechanics* (1. ed.), Springer.

Acknowledgements:

The authors acknowledge the funding provided by Ministério da Ciência, Tecnologia e Ensino Superior - Fundação para a Ciéncia e a Tecnologia (Portugal), under Grant SFRH/BD/146272/2019 and by LAETA, under project UIDB/50022/2020.

P3.7

Cell Proliferation Study Using a Discretization Meshless Technique

Maria Inês Barbosa¹, Jorge Belinha², Renato Natal Jorge³, Ana Carvalho⁴

1 INEGI - Institute of Science and Innovation in Mechanical and Industrial Engineering, Porto, Portugal

2 ISEP - Instituto Superior de Engenharia do Porto, Porto, Portugal

3 Faculty of Engineering - University of Porto, Porto, Portugal

4 i3S - Instituto de Investigação e Inovação em Saúde da Universidade do Porto, Porto, Portugal

1. Introduction

During cell proliferation, cells grow and divide through an extremely regulated and complex process [1, 2]. Nowadays, this process can be studied using computational models; this way it is possible to reduce the time and money spent on experimental analyses [3]. In this work, a new iterative discrete computational model was created based on a novel cell growth phenomenological law and combined with the Radial Point Interpolation Method (RPIM) to simulate cell proliferation. To study its efficiency, which is dependent on the efficiency of the RPIM, an analysis of the optimal number of integration points and nodes per integration cell for each influence-domain was performed.

2. Materials and Methods

As with others numerical methods, the first steps of the RPIM are the creation of the geometry of the problem, and the imposition of the solid domain, its limits, and its boundary conditions. Since it is a meshless method, after these steps, a nodal set discretizes the domain, influence-domains impose the nodal connectivity and a combination of radial basis functions and polynomial basis functions creates the shape functions [4]. Regarding the algorithm, cell growth is initiated after introducing specific input data and establishing the growth law. This growth occurs and continues if the concentrations of oxygen and glucose are higher than 0 and until the cell doubles its volume. When this last parameter is achieved, the process stops and cell divides.

3. Results

To study the efficiency of the model and to optimize it, the optimal number of integration points per integration cell and the optimal number of nodes for each influence-domain were analysed. To do that, several integration schemes and influence-domain sizes were tested, taking into account: the evolution of the growth of the volume of the cell until it divides; the computing time; the average error and; the error/computing time relation. Considering both parameters, in general, higher numbers of points and nodes promoted more accurate analyses but also more time-consuming. Thus, a balance between these two factors is required to obtain a viable analysis.

4. Discussion and Conclusions

To optimize the algorithm performance, the best integration scheme of the RPIM formulation and the optimal number of nodes inside each influence domain were found. By analysing different integration schemes and influence-domain sizes, lower numbers of integration points per integration cell and of nodes for each influence-domain promoted faster simulations but less accurate results. The opposite was verified with higher values. To balance these factors, an integration scheme of 6x6 per integration cell and 7 nodes inside the influence domain was defined as the best option to optimize the algorithm. These were assumed as the calibration values and will be used in future simulations.

5. References

1. Tortora, G.J. and B.H. Derrickson, *Introduction to the human body*. 2017: John Wiley & Sons, Incorporated.
2. Sandal, T., *Molecular aspects of the mammalian cell cycle and cancer*. *The oncologist*, 2002. 7(1): p. 73-81.
3. Alfieri, R., et al., *Modeling the cell cycle: From deterministic models to hybrid systems*. *Biosystems*, 2011. 105(1): p. 34-40.
4. Belinha, J. (2014). *Meshless Methods in Biomechanics*. Lecture Notes in Computational Vision and Biomechanics (1. ed.), Springer.

Acknowledgements:

The authors acknowledge the funding provided by Ministério da Ciência, Tecnologia e Ensino Superior - Fundação para a Ciência e a Tecnologia (Portugal), under Grant SFRH/BD/146272/2019 and by LAETA, under project UIDB/50022/2020.

P3.8

v-Patients Simulation: Smoothed Particle Hydrodynamics for Simulating Implant - Tissue Interaction

Bence Rochlitz¹, John Benjamin¹, Fabien Pean¹, Gloria Zörnack¹, Diogo F. Almeida¹, Wen-Yang Chu¹, Simon Sonntag¹

¹ Virtonomy GmbH, München, Germany

+rochlitz@virtonomy.io, Paul-Heyse-Strasse 6, 80336 München, Germany

1. Introduction

Anatomical simulations raise many challenges that current state-of-the-art simulation methods fail to properly address. These include automatic mesh generation, large deformations, non-linear material models and contacts, and fluid-structure interaction. The simulation setups require deep expert knowledge, a high entry bar for many medical device makers to take advantage of virtual testing. Smoothed Particle Hydrodynamics (SPH) is a novel framework addressing these issues. It enables a solution with low entry requirements, necessary for the wider adoption of simulations in the medical device industry.

2. Materials and Methods

Virtonomy has created the first SPH-based web solution, v-Patients Simulation, that enables medical device manufacturers to perform medical-grade simulations without simulation expertise. This means that quality engineers and CAD developers have sufficient control over the relevant technical aspects but numerical settings are automatically generated. Thus, a wide user group can integrate virtual testing into their daily development. The simulations are customized for the specific product phase, from concept to preparation for clinical studies.

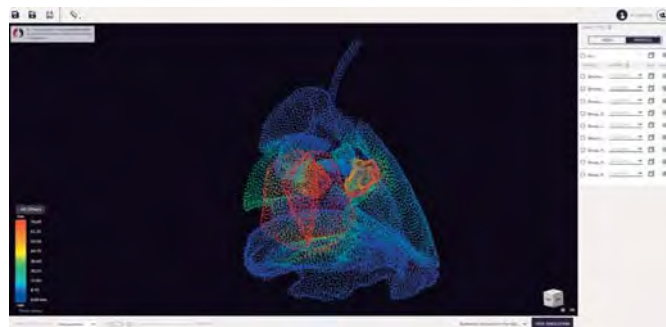


Figure 1: v-Patients Simulation platform

The user can select a patient from the target virtual sub-population, based on clinical data and decide what simulation to perform.

The platform composes a library of simulation use cases tailored for specific medical device types. Each use case relates to a Question of Interest (QoI) and Context of Use (CoU). They include medical implant–tissue interaction simulations, combined with blood flow. The users can also access virtual ISO standard benchtop tests.

Certain simulations are impossible to replicate in reality, without performing in-vivo human experiments. Such models are designed to support the preparation of animal tests and clinical studies. Simulation-based design optimization can mitigate risks and boost success rates.

The tool provides automatic reporting of the simulation results to bridge the time-consuming post-processing step. A software verification report is additionally available to support the regulatory submission. The simulations are linked to a specific device version and patient, such that all design changes can be reasoned.

3. Results

Medical implant–tissue simulations extend the capabilities of virtual 3D implantation using reconstructed CT data. Medical device development can be streamlined using the proper simulation in each product phase. Transfemoral cannula, heart valve repair and replacement, and ventricle assist device designs can be evaluated in a virtual environment.

4. Discussion and Conclusions

Virtonomy's v-Patients Simulation is a crucial step to lower the entry barriers concerning simulation expertise, thereby broadening the adoption of simulations. Finally, it streamlines the preparation for and can mitigate the risk of animal and human trials.

P3.9

Neural-network-based visualization for pervasive continuum-biomechanical simulations

David Rosin^{1,2}, Johannes Kässinger^{2,3}, Xingyao Yu^{2,4}, Okan Avcı⁵, Michael Sedlmair^{2,6}, Kurt Rothermel^{2,3}, Oliver Röhrle^{1,2,5}

1 Institute for Modelling and Simulation of Biomechanical Systems, Continuum Biomechanics and Mechanobiology Research Group, Stuttgart, Germany

2 Stuttgart Center of Simulation Science (SC SimTech), Stuttgart, Germany

3 Institute for Parallel and Distributed Systems, Stuttgart, Germany

4 Visualization Research Center VISUS, Stuttgart, Germany

5 Fraunhofer IPA, Biomechatronic Systems, Stuttgart, Germany

Corresponding author: David Rosin, rosin@imsb.uni-stuttgart.de, Pfaffenwaldring 5a, 70569 Stuttgart, Germany

1. Introduction

Bringing simulation capabilities to resource-poor systems like mobile devices is of growing interest across many research fields. In contrast, continuum-biomechanical simulations are considered resource-intensive, with biophysics-based and anatomically realistic [1] simulations of biomechanical systems requiring substantial compute-time, even on large supercomputers [2]. Yet, the use of sparse grid surrogate-models has since been shown to allow for real-time forward-simulation of a human upper limb model based on continuum-mechanical data [3]. This did however not involve visualizing the model's geometry. The aim of this work is to achieve exactly that, while maintaining real-time performance.

2. Materials and Methods

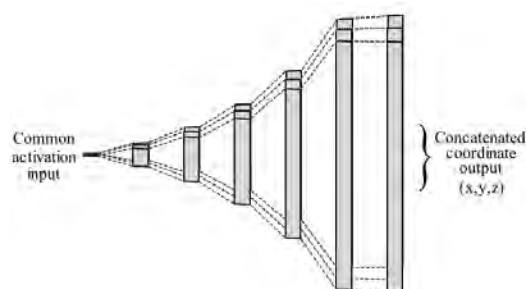


Figure 1: Neural network architecture with five hidden layers of exponentially increasing width.

Building on the results presented in [3], we used a sparse grid surrogate for the surface deformation of the m. biceps brachii to train a deep learning model for real-time visualization. The model takes one activation parameters per muscle in the model as input, and outputs the corresponding surface configuration of the muscle as Cartesian coordinates. Consequently, the neural network architecture devised for this purpose features significantly less inputs than outputs, estimating the position of 2809 mesh-nodes on the biceps surface based on only five activation parameters (see Figure 1). Each sample of these activation levels represents the optimal choice of activation to reach a certain elbow angle, according to the minimal sum of activation, to minimize energy expenditure.

3. Results

The model predicted a randomly chosen test-set of surface configurations within an average error of 0.97 ± 0.16 mm, or 0.57 ± 0.10 %. The model achieved evaluation times of 9.88 ms without and 3.48 ms with GPU-support.

4. Discussion and Conclusions

This model currently only visualizes one of five muscles in the model. Thus, it is beneficial that it is significantly faster than necessary (40 ms), as it remains to be seen how its performance will scale, when introducing additional muscles. Deep learning surrogates thus provide a strong candidate to make continuum-biomechanical simulations accessible for real-time applications.

5. References

1. Ackerman, M. J., *Proceedings of the IEEE*; 86(3):504-511 (1998).
2. Bradley, C.P., Emamy, N., Ertl, T., Göddeke, D., Hessenthaler, A., Klotz, T., ... & Röhrle, O., *Frontiers in physiology*; 9:816 (2018).
3. Valentin, J., Sprenger, M., Pflüger, D., Röhrle, O., *International journal for numerical methods in biomedical engineering*, 34(5):e2965 (2018).

Acknowledgements:

Funded by Deutsche Forschungsgemeinschaft (DFG, German Research Foundation) under Germany's Excellence Strategy - EXC 2075 – 390740016. We acknowledge the support by the Stuttgart Center for Simulation Science (SimTech).

P3.10

Towards a repository of patient-specific intervertebral discs finite element models

Estefano Muñoz-Moya¹, Morteza RASOULIGANDOMANI¹, Carlos Ruiz Wills¹, Gemma Piella¹, Jerome Noailly¹

¹ Universitat Pompeu Fabra, BCN MedTech, Department of Information and Communication Technologies, Barcelona, Spain

1. Introduction

Numerical analysis methods, such as Finite Element Analysis (FEA), have been widely used to study the biomechanics of human tissues and organs. However, patient-specific (PS) model creation usually requires complex procedures that are difficult to automatize in some instances. For example, in spine computational studies, intervertebral disc (IVD) modeling requires structural meshing, as the synchronized mechanical behavior of specific tissue domains needs to be explored under large deformations [1]. Multiple studies related to IVD degeneration (DD) have been carried out using FEA, but a repository of IVD PS models has not yet been created to explore in-depth PS particularities, e.g., as hypothesized in [2]. A significant challenge is the ability to map different tissue regions, such as the Cartilage Endplate (CEP), Annulus Fibrosus (AF), Nucleus Pulposus (NP), and the Transition Zone (TZ) in PS IVD shapes. Such mapping can provide further information about the influence of the CEP on DD combined with the effects of different sets of diffusion distances from the peripheral vasculature to the NP [1]. This work aims to generate a repository of PS finite element meshes of IVD models with the same mesh connectivity and different geometries of the external surface and its internal components for systematic FEA.

2. Materials and Methods

Using T2-weighted magnetic resonance images, 176 PS IVD models were obtained through 3D segmentation, acquired during the European project My Spine (FP7-269909) [3]. Segmentations included the AF and NP. The Bayesian coherent point drift (BCPD) algorithm was used to non-rigidly align the meshes [4]. This code fits a point cloud of a source mesh (template) to a target mesh (segmentations). In this way, a pre-existing structural mesh of an IVD [1] was adapted to the PS models. The external surfaces of the AF and NP were represented by point clouds, which were used as targets. The morphing process of the template was carried out in three stages. First, the AF and the NP surfaces were adapted. Then, the results were merged into a single point cloud, used as a target, for the final fitting of the complete volumetric mesh of the template. The CEPs, not visible in the images, were automatically recreated, with a thickness between 0.7 and 1 mm. The development of the second stage preserved the surface area initially covered in the IVD. Mesh quality of the morphed models and Euclidean distance between the morphed and the target were checked to ensure a good element quality.

3. Results

A repository of 176 PS IVDs finite element meshes with the same connectivity was created following the abovementioned method (Figure 1). Regarding mesh quality, the average criteria limits of all morphed IVDs were: Min and Max angle on Quad Faces (<10 and >160) were less than 0.2 and 0.8 % of the total elements, respectively. The Hex elements that exceeded the Aspect Ratio criteria limit (>10) were less than 6% of the total elements. Quad elements were not impaired under these criteria.

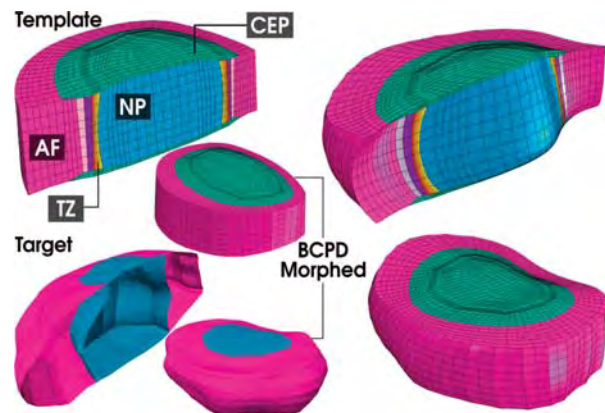


Figure 1: Target, Template, and Morphed disc using Bayesian coherent point drift.

4. Discussion and Conclusions

This repository is a unique set of model collections to explore the effect of multiple geometrical variations on the IVD multiphysics and mechanobiology, including the likely substantial impact of the CEP [2]. Although the template elements tend to deform and impair their mesh quality, they are not close to the CEP. The algorithm can generate PS FE models from any segmented surfaces third parties provide. The database will be used to train a metamodel of FEA outcomes.

5. References

1. Ruiz, C. et al. (2018). *Frontiers in Physiology*.
2. Malandrino, A. et al. (2015). *Front. Bioeng. Biotechnol.*
3. Castro-Mateos I et al. (2014). *Physics in Medicine & Biology*.
4. O. Hirose. (2021). *IEEE*.

Acknowledgements:

Funding by the European Commission (Disc4All-MSCA-2020-ITN-ETN GA: 955735) and the Spanish Government (RYC-2015-1888).

P3.11

Musculoskeletal modeling and simulation of subject specific lower limb joint loads computing during normal and abnormal gait

Carlos Rodrigues^{1,2}, Miguel Correia^{1,2}, João Abrantes³, Marco Rodrigues⁴, Jurandir Nadal⁵

1 Faculdade de Engenharia da Universidade do Porto, Doctoral Program in Biomedical Engineering, Porto, Portugal

2 Institute for Systems and Computer Engineering, Technology and Science, Centre for Biomedical Engineering Research, Porto, Portugal

3 Lusófona University, CICANT (Centre for Research in Applied Communication, Culture, and New Technologies), Lisbon, Portugal

4 Federal University of Pernambuco, Department of Electronic and Systems, Recife, Brazil

5 Federal University of Rio de Janeiro, Biomedical Engineering Program, Rio de Janeiro, Brazil

1. Introduction

Internal joint loads information presents as key issue for musculoskeletal injury and disease prevention, diagnosis, intervention planning and rehabilitation. Direct measurements of internal joint loads can only be performed invasively with inherent difficulties at in vivo measurement during natural daily human activities. For this reason, there is an increasing need for musculoskeletal modelling and simulation (MSK-MS) towards subject specific joint loads computing based on non-invasive measures. Given the importance of gait as a daily natural human activity and the large number of injury and disease risk factors potentially affecting gait, attention was focused on subject specific lower limb joint loads computing during normal and abnormal gait.

2. Materials and Methods

Case study was selected for subject specific analysis of a 40-year-old healthy male with 70 kg mass and 1.86 m height. Reflective adhesive markers were applied at the right and left anterior and posterior superior iliac spines, thigh superior, lateral, and inferior, knee lateral and medial, shank superior, lateral and inferior, ankle lateral and medial, heel and navicular bone, first and fifth metatarsal. Ground reaction forces were acquired with two AMTI force plates at 2000 Hz and trajectories of reflective skin markers on the subject recorded at 100 Hz with an eight-camera Qualisys system during normal gait (NG) at self-selected velocity, stiff-knee gait (SKG) with subject right knee strait during gait at self-selected velocity and slow running (SR) at minimum velocity with a phase of both feet off the ground. Subject specific musculoskeletal analysis was developed using AnyGait v.0.92 configured for the experimental setup, with stick-figure based on static trial and over-determinate kinematic analysis based on dynamic trials during NG, SKG and SR. Stick-figure and Twente Lower Extremity Model (TLEM) were morphed, and inverse dynamics performed using computed joint angles and kinetic boundary conditions [2].

3. Results

Vertical forces computed by musculoskeletal simulation at the hip, the knee, and the ankle normalized to body weight at NG, SKG and SR gait cycles present the distributions of Figure 1 for the right and left joints.

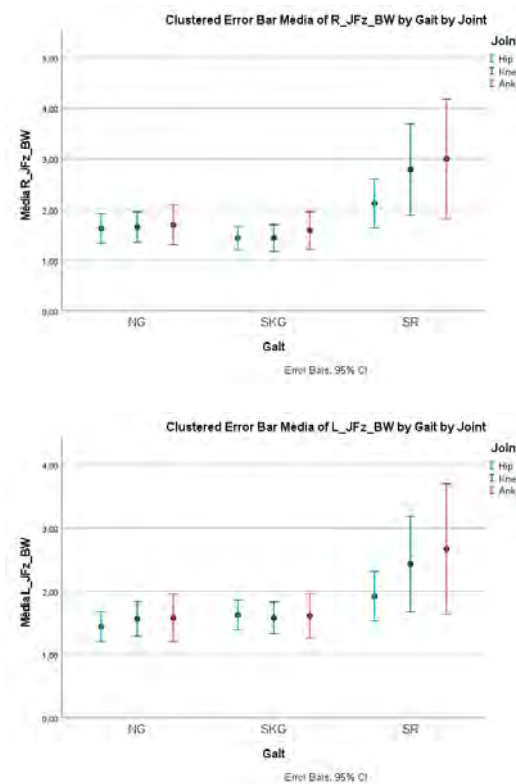


Figure 1: Right and left hip, knee and ankle joint internal vertical force normalized to body weight (JFz/BW) at NG, SKG, SR.

4. Discussion and Conclusions

Computed MSK-MS allowed detection of subject specific differences between JFz/BW distributions at each lower limb joint, side, and NG, SKG and SR gait modes. Comparison of lower limb joint subject specific MSK-MS to direct measurements on different subjects with instrument implant at comparable gait mode [3] conducted to higher magnitude of computed loads in relation to direct measurements on different post-operative patients.

5. References

1. Lund ME et al. Proc Inst Mech Eng H: J Eng. in Medicine;226(2):82-994 (2012).
2. Andersen, MS et al., Dep. Mech. and Manuf. Engineering Aalborg University (2012).
3. Rodrigues C et al., CMBBE 2021 Abstract book; 2021. p. 269.

P3.12

Effective scaffold design optimization through coupling of complex and simple models for scaffold mediated bone growth

Marius Zeinhofer¹, Mahdi Jaber², Sara Checa², Patrick Dondl³

1 Simula Research Laboratory, Departement for numerical analysis and scientific computing, Oslo, Norway

2 Charité-Universitätsmedizin Berlin, Julius Wolff Institute at Berlin Institute of Health, Berlin, Germany

3 Albert-Ludwigs University, Abteilung für angewandte Mathematik, Freiburg, Germany

1. Introduction

Large bone defects constitute a considerable clinical challenge, with a high risk of unsuccessful healing outcome [1]. Currently, treatment strategies based on the implantation of 3D porous scaffolds have shown potential in pre-clinical studies and are being investigated as viable alternatives for existing methods [2]. However, scaffold design is determined by a large number of parameters (e.g. pore size, porosity, architecture, etc), all of them having an effect on healing outcome. To overcome the highly limited experimental trial and error approach, in silico approaches for scaffold design optimization appear as a promising tool. However, in silico optimization of scaffolds is a highly expensive computational task since each tested scaffold configuration needs to be checked in terms of predicted bone regeneration potential.

The aim of this study is to develop a time efficient computational framework for the design optimization of bone scaffolds towards enhanced bone regeneration...

2. Materials and Methods

We couple a previously described, complex model for scaffold-supported bone regeneration [3], based on an hybrid FEM-ABM approach, to a computationally efficient, simple model using locally averaged quantities and homogenized material properties (Fig.1). The complex model acts as a predicator and validator for the simple model. Cellular activities rates such as the cell differentiation, proliferation and migration rates that are needed in the simple model are extracted from the complex model. The simple model is then used for scaffold porosity optimization, a computationally expensive task in the complex model. The optimization in the simple model is formulated as a PDE constrained optimization problem and solved by the finite element method. This approach allows a flexible scaffold porosity optimization, the degrees of freedom in the optimization being the elements in the computational mesh. The optimization can be carried out in a few hours on a usual desktop machine.

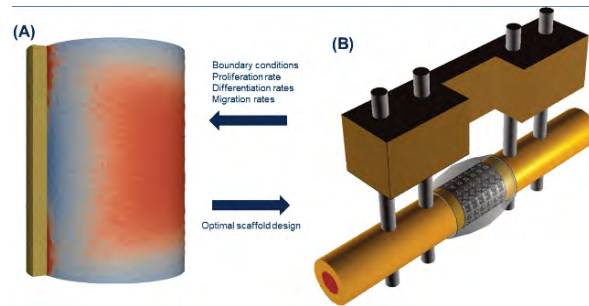


Figure 1: Reduced computational complexity from the complex to the fine model. (A): scaffold density distribution and (B) Geometry of complex model replicating rat femur

3. Results

Initial simulations predict scaffold designs with varied porosity along the healing region and specific designs for different simulated healing potentials.

4. Discussion and Conclusions

We proposed a computationally efficient approach to design bone scaffolds, using a coupling of a complex and a simple model to reduce computational complexity. First numerical results show potential for this approach. Further work will focus on the closer integration of the two models.

5. References

1. A. Nauth et al., *Journal of orthopaedic trauma*, 32:S7–S11, 2018.
2. A. Petersen et al., et al. *aNature communications*, 9(1):1–16, 2018.
3. Perier-Metz et al, *Front. Bioeng. Biotechnol* 2020, 8:585799

Acknowledgements:

This project is funded by the Federal Ministry of Education and Research (BMBF: research grant [01ZX1910])

P3.13

Subject-specific 3D models to investigate the influence of rehabilitation exercises on Achilles tendon strains

Alessia Funaro¹, Vickie Shim², Marion Crouzier¹, Ine Myns¹, Benedict Vanwanseele¹

¹ KU Leuven, Human Movement Biomechanics Research Group, Leuven, Belgium

² University of Auckland, Auckland Bioengineering Institute, Grafton, Auckland, New Zealand

1. Introduction

The strain magnitude is a crucial factor for AT adaptation and an optimal loading dose [1] could facilitate adaptation of the AT. Finite element models aid the investigation of the effects of changes in AT geometry on AT strains. The main aim of this study was to investigate the impact of different rehabilitation exercises on AT strains, including the effect of twist of the sub-tendons.

2. Materials and Methods

A subject-specific geometry of the free AT was obtained from one healthy female participant, using 3D freehand ultrasound. The 3D tendon model was divided in three sub-tendons, each one arising from one of the three Triceps Surae muscles. Three different types of twisted geometries were created according to [2]. Material properties were defined according to [3]. Subject-specific muscles forces were obtained by a combination of 3D motion capture of the participant completing five rehabilitation exercises and musculoskeletal modelling. The muscle forces were used as boundary conditions. The peak and average of the maximum Lagrange strain, in the mid portion of the AT, were calculated to identify the differences between the rehabilitation exercises. The maximum Lagrange strain and location of the peak strain in the whole free AT were simulated to characterize the difference strain patterns between different twist types and exercises.

3. Results

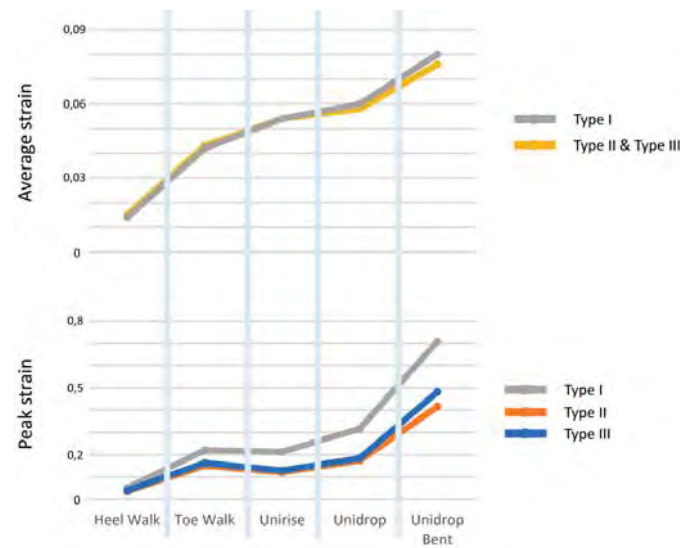
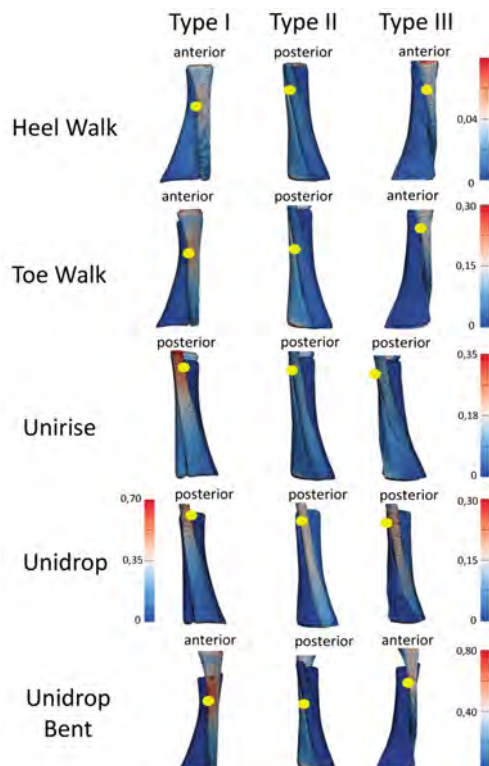


Figure 1: Results for the three types of twist and for all the rehabilitation exercises. On the left, distribution of the maximum Lagrange strain and peak strain (yellow dots). On the right, trend of the peak and average of the maximum Lagrange strain, in the mid-portion of the AT models.

4. Discussion and Conclusions

The AT strains were task-dependent. The least twisted geometry, Type I showed the highest peak strain. Type I is not an optimal geometry and may place individuals more at risk of injury. To gradually increase the tendon strain during the rehabilitation protocols, it is recommended to start from walking on heels to unilateral heel drop with knee bent, as last exercise. The ranking was independent of the AT twist. This study was a first step towards future work to design and prescribe mechanically informed rehabilitation protocols.

5. References

- Wang, T. et al. *J. Orthop. Res.* 33, 1888–1896 (2015).
- Pekala BM, H. P. A. et al. 1–11 (2017).
- Weiss, J. A. et al. *Comput. Methods Appl. Mech. Eng.* 135, 107–128 (1996).

Acknowledgements:

The authors would like to thank the Research Council KU Leuven (Grant no: C24M/20/053) for providing financial support to this project.

P3.14

Image-based simulation of left ventricular hemodynamics: study on mitral regurgitation and left ventricle aneurysm patients

Lukas Obermeier¹, Katharina Vellguth¹, Leonid Goubergrits^{1,2}

¹ Institute for Computer-Assisted Cardiovascular Medicine, Charité - Universitätsmedizin Berlin, Germany

² Einstein Center Digital Future, Berlin, Germany

Correspondence: Lukas Obermeier, Charité - Universitätsmedizin Berlin, Institute of Computer-assisted Cardiovascular Medicine, Augustenburger Pl. 1, 13353 Berlin, Germany

1. Introduction

Hemodynamics inside the left ventricle (LV) can potentially serve as indicator for the manifestation of diseases in early states [1]. Computational fluid dynamics (CFD) can complement medical imaging methods in the investigation of such states, enabling analysis at high spatio-temporal resolutions. Existing image-based LV-CFD models are typically complex and time-consuming, interfering with clinical translations. We propose a moderate complexity numerical framework at quick pre-processing and demonstrate its technical feasibility by analyzing four representative cases (no/severe mitral regurgitation (MR); with/without LV aneurysm).

2. Materials and Methods

Cardiac computed tomography (CCT) image data was used for the segmentation of end-diastolic and end-systolic LVs and both annuli via a semi-automatic in-house tool [2]. A Poisson surface reconstruction algorithm is used to retrieve a triangulation of the end-diastolic LVs. Non-patient-specific left atrial and aortic geometries are attached at the annuli and 2D generic valves are included. The LV deformation field is obtained by creating a nodal correspondence between end-diastolic and end-systolic LVs. It is implicitly scaled to make the ventricular contraction follow a specified volume curve. The 3D incompressible Navier-Stokes equations are solved via a finite volume discretization in STAR-CCM+.

3. Results

In the MR cases, the regurgitating blood interferes with the diastolic inflowing jet, leading to fragmentary formation of commonly observed ring vortices and a decomposing diastolic jet. In the MR cases, an increased specific energy dissipation (SED) is observed in systole. In general, a higher SED is seen in the MR cases. In all cases, regions with poor mixing are visible. Pre-processing takes 6-8 h, solving per cycle 12-14 h (4 nodes at 40 cores).

4. Discussion and Conclusions

These findings in MR patients are in line with MRI investigations [3]. The increased SED in systole may be explained by the regurgitating jet that forms its way through the small regurgitation orifice. The poor mixing and washout endanger blood stasis and thrombus formation.

In terms of complexity, the proposed modelling approach is positioned between 0D models and multi-physics 3D frameworks. Pre-processing times are in range of clinical feasibility. Yet, the model still has simplifications that must be critically reviewed, validated, and potentially adapted. With further improvements, we conclude the proposed approach to have a good potential of becoming clinically usable.

5. References

1. Pedrizzetti G. et al. *Nat Rev Cardiol.*; 11:545–53 (2014).
2. Tautz L. et al. *Int J Comput Assist Radiol Surg.*; 13:1741–54 (2018).
3. Al-Wakeel N. et al. *J Magn Resonan Imag.*; 42:1705–12 (2015).

P3.15

Epiretinal Membrane Contraction: a Finite Element Analysis

Margarida Chiote¹, Elisabete Silva^{2,3}, Manuel Falcão⁴, Marco Parente^{1,2}

¹ Faculty of Engineering - University of Porto, Porto, Portugal

² INEGI - Institute of Science and Innovation in Mechanical and Industrial Engineering, Porto, Portugal

³ LAETA - Associated Laboratory for Energy, Transports and Aeronautics, Portugal

⁴ Faculdade de Medicina da Universidade do Porto - FMUP, Porto, Portugal

1. Introduction

Due to superficial retinal folds, the Epiretinal Membrane (ERM) is a thin film of fibrous tissue that can grow across the macular portion of the retina, causing loss of visual acuity or metamorphopsia (Bu, Kuij, Li, Hooymans, & Los, 2014). The current treatment for this pathology is vitrectomy surgery, which is only done after symptoms have appeared. However, some patients do not show any improvement in their vision following surgery (Xiao, Chen, & al, 2017).

The application of computational methods to a patient-specific biomechanical analysis can help researchers better understand the mechanisms that lead to vitrectomy success or failure. An examination of the retinal displacement owing to the constriction of the epiretinal membrane was performed using medical data from two patients who underwent vitrectomy, one with significant improvements and the other with no improvements.

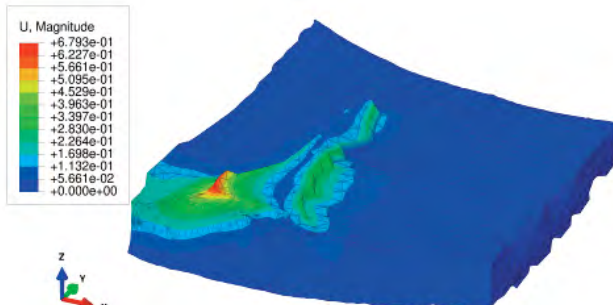
2. Materials and Methods

Two separate patients with two different outcomes were chosen from the University Hospital Centro Hospitalar de São João-EPE (CHSJ_EPE) to test the generated models in real-world circumstances. The first patient's visual acuity improved after the treatment, whereas the second patient's did not.

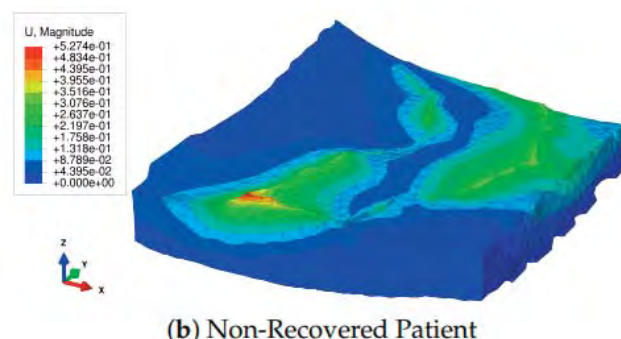
The pre- and post-operative Scanning Laser Ophthalmoscopy (SLO) images for each patient were overlapped in order to get the displacements generated by the ERM contraction experimentally. The displacement field suffered by the retina, directly induced by the presence of the membrane, may be calculated by comparing variations in the position of the blood vessels.

3. Results

For the selected material model, simulation results concerning the displacements are shown in Figure 1 for both patients. By the analysis of these Figures and Table 1, it is possible to conclude that the retina of the Recovered Patient suffered a higher contraction than the retina of the non-recovered Patient.



(a) Recovered Patient



(b) Non-Recovered Patient

Figure 1: Maximum displacements for the Retina and ERM model, [mm].

Table 1: Results for the retina displacements and membrane thickness.

Patient	Horizontal Displacement [mm]	Error [%]	vertical
Displacement [mm]	Error [%]	Final Thickness [mm]	Error [%]
Recovered	0.4151	2.668	0.26481
8.383	0.1439	2.798	
Non-Recovered	0.3506	0.271	0.2603
4.527	0.0723	3.347	

4. Discussion and Conclusions

It was possible to conclude from these two situations that the displacements for the patient who regains vision acuity are substantially higher than for the other patient. One possible explanation is related to the accommodation of the retina in the second patient. Only two extreme circumstances, a fully recovered patient and a non-recovered patient, were used to test the current methods. It would be necessary to apply the current methodology to a larger number of patients, including individuals with varying degrees of recovery, in order to further test it.

5. References

- [1] S.-C. M. Bu, R. Kuij, X.-R. Li, J. M. M. Hooymans e L. I. Los, "IDIOPATHIC EPIRETINAL MEMBRANE," pp. p 2317-2335, 2014.
- [2] W. Xiao, X. Chen e e. al, "Prevalence and risk factors of epiretinal membranes: a systematic review and meta-analysis of population-based studies," BMJ Open, 2017.

Acknowledgements:

This Work was supported by FCT, through INEGI, under LAETA project UIDB/50022/2020 and UIDP/50022/2020.

P4.1

Detection of Pulmonary Hypertension Using Explainable Machine Learning

Michał K. Grzeszczyk¹, Arkadiusz Pajor¹, Angela Lungu², Andrew Swift³, Andrew Narracott^{3,4}, Marian Bubak¹, Rod Hose³, Bartłomiej Snieżynski⁵, Arkadiusz Sitek¹

¹ Sano Centre for Computational Medicine, Cracow, Poland

² Technical University of Cluj-Napoca, Cluj-Napoca, Romania

³ The University of Sheffield, Sheffield, United Kingdom

⁴ Insigneo Institute for *In Silico* Medicine, Sheffield, United Kingdom

⁵ AGH University of Science and Technology, Cracow, Poland

*MK Grzeszczyk, m.grzeszczyk@sanoscience.org

1. Introduction

Pulmonary Hypertension (PH) is a disease characterised by increased mean Pulmonary Artery Pressure in the Main Pulmonary Artery (MPA). We developed non-invasive, Machine Learning (ML) tools for PH diagnosis in the past [1]. While such methods achieve high classification metrics, they suffer from a lack of explainability due to their black-box nature. In this paper, we apply an explainable ML model namely Supersparse Linear Integer Model (FD-RiskSLIM) with the feature discretisation [2,3] to the problem of PH diagnosis from measurements acquired using Magnetic Resonance Imaging (MRI). FD-RiskSLIM is a fully data-driven explainable scoring system. Scoring systems are a popular tool used in medicine. They are, however, created using expert knowledge.

2. Materials and Methods

We use data from 352 patients from ASPIRE Registry (Assessing the Severity of Pulmonary Hypertension In a Pulmonary Hypertension Referral Centre) [4]. The dataset contains 35 measurements (right ventricle (rv) ejection fraction, rv diastolic mass etc.) derived from cardiac MRI and MRI of the MPA. During experiments we apply 5-fold cross-validation. In the course of the algorithm training FD-RiskSLIM described in [3] analyses the training data, selects a small number of points (small integers) which are assigned if the selected feature meets certain conditions. Those conditions are also found in the optimisation process (see Table 1 in the results section for an example of such a system). To use the system, the physician simply sums all points which provide the score. The higher the score the more likely the condition (here the PH). The score can be easily transformed to probability (see [2,3]). We used sensitivity, specificity and Area Under ROC curve (AUC) as metrics of performance and compared it to logistic regression (LR) and XGBoost.

3. Results

The description of the FD-RiskSLIM model that was created based on the training data is presented in Table 1. It achieves sensitivity of 0.88, specificity of 0.87 and AUC of 0.91. The results for XGBoost reach 0.84, 0.92 and 0.89, and for LR are 0.85, 0.93 and 0.90 respectively.

Table 1: Data-derived explainable scoring model for PH detection generated by FD-RiskSLIM for one of the folds.

$164 \leq \text{systolic septal angle (degrees)}$	3 points
$17 \leq \text{lv stroke volume (mL)} < 56$	2 points
$32 \leq \text{rv diastolic mass (g)} \leq 223$	2 points
$138 \leq \text{systolic septal angle (degrees)} < 164$	1 point
$112 \leq \text{diastolic septal angle (degrees)} < 146$	-1 point
$\text{rv end systolic volume (mL)} < 102$	-6 points

4. Discussion and Conclusions

In this paper, we presented an application of the FD-RiskSLIM method to the problem of PH detection based on measurement features derived from MRI. The scoring system presented in table 1 is explainable as it is clear how certain conditions positively or negatively contribute to the score. The number of points also indicates how strong the contribution is. Although the FD-RiskSLIM uses only a small number of features (here 5 out of 35) the classification performance is comparable to state-of-the-art XGBoost and LR models.

5. References

1. M. K. Grzeszczyk et al, ICSS 2022 (accepted).
2. B. Ustun et al, JMLR, 2019.
3. A. Pajor et al, ICSS 2022 (accepted).
4. J. Hurdman et al, Eur Respir J, 2012.

Acknowledgements:

This publication is partly supported by the European Union's Horizon 2020 research and innovation programme under grant agreement Sano No. 857533 and the International Research Agendas programme of the Foundation for Polish Science, co-financed by the European Union under the European Regional Development Fund.

P4.2

Bayesian history matching to calibrate virtual cohorts of human hearts

Cristobal Rodero¹, Stefano Longobardi¹, Christoph Augustin², Marina Strocchi¹, Gernot Plank², Pablo Lamata¹, Steven Niederer¹

1 King's College London, United Kingdom

2 Medical University of Graz, Austria

1. Introduction

Model calibration (MC) is the process of adjusting parameters of a model to maximize the agreement between observed data and simulations. Most MC techniques treat each patient independently, making the methods too expensive for clinical timelines. Surrogate models offer a low-cost alternate to a full model evaluation and can be used for MC.

In this work, we use Gaussian Process Emulators (GPEs) and Bayesian History Matching (BHM) to calibrate cardiac models and show how we can reuse simulations from one subject into another in a pipeline compatible with clinical timelines.

2. Materials and Methods

To represent the anatomy, we use a Statistical Shape Model. We ran electrophysiological (EP) simulations using the reaction-eikonal model. As a result, the model can be represented as a vector of scalars (shape coefficients and EP parameters). We study the use of 14 biomarkers (anatomical and functional measurements) to calibrate the model. We thus train 14 GPEs, one per biomarker.

To fit the models, we followed a BHM strategy [1]. BHM is an iterative method where in each iteration a region of the parameter space is ruled out if the emulation with that set of parameter values produces an “implausible” result. If a set of parameters is unlikely to give a good match, it has a high value of implausibility.

We tested the pipeline using previously reported simulations results [2] as ground truth.

3. Results

We evaluated the initial 14 emulators, training with 280 simulations. The minimum R^2 scores achieved was of 0.99. We also monitored the uncertainty of the emulators obtaining variance quotients (emulator over ground truth) of 1.08, suggesting that the uncertainties of the emulators are comparable to the uncertainties of the ground truth data.

If we compare the GPEs trained using data from previous cases with GPEs trained using data from a new case, we found that 83.61% of the implausible points in the first scenario were also implausible in the second. This could imply that if we already had the simulations for one patient, there is no need of running more simulations for the second patient.

4. Discussion and Conclusions

It is possible to reuse results from previous simulations on unseen subjects to save resources on model calibration. This innovation allows for a reference GPE that could be used in a BHM pipeline for any case, without the need of running more simulations.

5. References

1. Longobardi, S. et al. *Philos. Trans. R. Soc. A Math. Phys. Eng. Sci.* (2020).
2. Rodero, C. et al. *PLOS Comput. Biol.* (2021).

Acknowledgements:

The authors would like to thank the EU (764738), WT (209450/Z/17/Z & 203148/Z/16/Z), BHF (PG/16/75/32383, TG/17/3/33406, RG/20/4/34803 & RE/18/2/34213), NIH (R01-HL152256), ERC (864055) and EPSRC (EP/P01268X/1) for providing financial support.

P4.3

Effect of left ventricular shape on hemodynamics using computational fluid dynamics and non-invasive imaging data

Sumit Kumar¹, Rathish Kumar B.V², Sanjay Kumar Rai¹

¹ Indian Institute of Technology (BHU), Biomedical Engineering, Varanasi, India

² Indian Institute of Technology Kanpur, Mathematics and Statistics, Kanpur, India

1. Introduction

In humans, the left ventricle is primarily responsible for blood pumping during systemic circulation. Furthermore, although the flow inside the LV is highly complicated and multidirectional, the systole and diastole cycles effectively form a flowing continuum regulated by interactions between the LV wall and blood mass. The LV and other cardiac chambers' structure, size, and dynamics, adequate mechanical function of the heart valves, ventricular coupling [1][2] and negative or positive inotropic medications are also factors to consider. The combination of patient medical imaging data with computational fluid dynamics (CFD) modeling of left ventricular (LV) flow has shown considerable promise in providing patient-specific hemodynamic information for heart functional evaluation. To investigate the influence of ventricular size on blood flow dynamics, this work used a combined computational fluid dynamic (CFD) and automated segmentation of the left ventricle approach to model blood flow in the typical left ventricle (LV).

2. Materials and Methods

To build CFD-compatible models for LV flow simulations, the proposed automated system comprises three primary steps: segmentation, mesh creation, and registration [3]. The step-by-step procedure is described below.

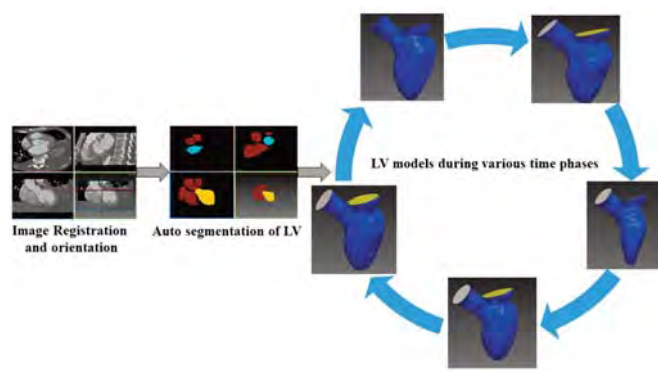


Figure 1: Diagram of the automated model generation outline for LV CFD simulations.

Simvascular, a finite-volume CFD solver, was used to solve the Navier-Stokes equations. The Inflow condition was taken from [2] model.

3. Results

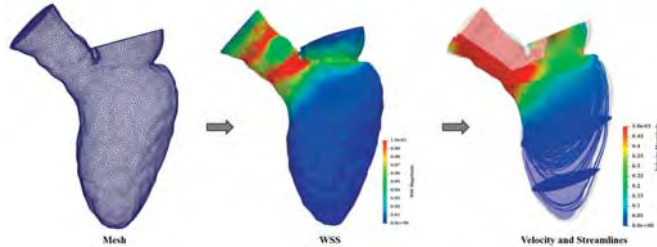


Figure 2: WSS, Velocity, and Streamlines visualization of blood flow during peak filling time

4. Discussion and Conclusions

The left ventricle's shape, as well as the flow from the aorta, plays an important influence in the formation of ventricular blood flow dynamics. To grasp the surgical and ventricular device assistive solution for a patient, a realistic forecast of local blood flow complexity is required. This work establishes a foundation for studying diverse hemodynamic behaviors utilizing CFD and computational modeling techniques. Using WSS, streamlines, velocity, pressure, and vorticity hemodynamic were investigated at various cardiac instant.

5. References

1. L. Ge, M. Ratcliffe, *The Use of Computational Flow Modelling (CFD) to Determine the Effect of Left Ventricular The shape on Blood Flow in the Left Ventricle*, *Annals of Thoracic Surgery*. 87(2009)993–994.
2. J. Adu, L. Yin, H. Zhang, S. Xie, J. Lu, *Simulation of the dynamic flow field in the left ventricle of the heart during diastolic filling*, *AIP Advances*. 10(2020).
3. F. Kong, S.C. Shadden, *Automating Model Generation for Image-Based Cardiac Flow Simulation*, *Journal of Heat Transfer*. 142 (2020) 1–13.

Acknowledgments:

The authors would like to acknowledge simvascular and the ICMR, GOI, for funding and support [ICMR, ID.No.2020-9527].

P4.4

Modelling Infarct Formation During Acute Ischaemic Stroke Treatment

Raymond Padmos¹, Tamás Józsa², Yidan Xue², Stephen Payne³, Alfons Hoekstra¹

¹ University of Amsterdam, Informatics Institute, Amsterdam, Netherlands

² University of Oxford, Department of Engineering Science, Oxford, United Kingdom

³ National Taiwan University, Institute of Applied Mechanics, Taiwan

1. Introduction

Infarct formation during an acute ischemic stroke is a time-dependent process. Time between stroke onset and recanalization and the degree of the collateral circulation determine to a large extent the size of an infarct. The process of infarct formation during acute ischaemic stroke is modelled using a computational mechanistic multi-scale model of cerebral blood flow and cell death.

2. Materials and Methods

Infarct formation is simulated by coupling models for arterial blood flow, tissue perfusion and cell death. Arterial blood flow is simulated using a pressure-dependent one-dimensional resistance network [1]. Tissue perfusion is simulated using a three-compartmental three-dimensional porous media model [2]. Cell death is simulated using a three-state dynamic system model representing the local fraction of healthy, vulnerable, and dead tissue [3]. Tissue perfusion depends on the tissue state, and the rate of cell death depends on tissue perfusion. Infarct formation is simulated for 24 hours with treatment after 1, 3, or 7 hours, representing early, average, and late treatment times respectively. Treatment is simulated as complete recanalization and restoration of flow by setting the surface boundary pressure of the tissue perfusion model to its healthy reference value.

3. Results

An acute ischaemic stroke is simulated by occluding one of the cerebral vessels, e.g., the right middle cerebral artery, in the arterial blood flow model. This causes an immediate decrease in tissue perfusion and starts infarct formation. Infarct volume continues to grow even after successful treatment (full recanalization) as tissue is already progressing to infarction. The final infarct size also depends largely on the degree of collateralization as tissue with higher but still reduced tissue perfusion will take longer to infarct.

4. Discussion and Conclusions

Quantifying the effect of treatment time and the degree of collateralization on infarct volume is critical to better understand the process of infarct formation. Final infarct volume varies significantly between AIS patients [4]. Understanding what causes this large variability is vital to better understand the process of cerebral infarction, and to potentially improve treatment.

The time between stroke onset and recanalization plays an important role in final infarct volume. The multi-scale tissue model presented here is able to reproduce the perfusion and infarct patterns as observed in AIS patients [4].

5. References

1. Padmos, R.M. et al., vol. 12744 LNCS 670–683 (Springer International Publishing, 2021).
2. Józsa, T.I. et al., *Interface Focus* 11, 20190127 (2021)
3. Xue, Y., El-Bouri, W.K., Józsa, T.I. & Payne, S.J., *J. Biomech.* 127, 110705 (2021).
4. Boers, A.M.M. et al., *J. Cereb. Blood Flow Metab.* 37, 3589–3598 (2017).

Acknowledgements:

This project (insist-h2020.eu) has received funding from the European Union's Horizon 2020 research and innovation programme under grant agreement No 777072.

P4.5

Angiogenesis modelling through a coupled mixed-dimensional haemodynamic/tissue model

Cameron Apeldoorn¹, Gonzalo Maso Talou¹, Julian Paton², Soroush Safaei¹

¹ Auckland Bioengineering Institute, The University Of Auckland, Virtual Brain Group, Auckland, New Zealand

² Faculty of Medical and Health Sciences, University of Auckland, Department of Physiology, Auckland, New Zealand

1. Introduction

Angiogenesis is the process through which new blood vessels form from the existing vascular network. It is key to the development and maintenance of the vasculature, recovery from wounds or stroke and in tumoral development. One of the primary drivers of angiogenesis is Vascular Endothelial Growth Factor (VEGF) which is produced in response to tissue hypoxia. We propose a mixed-dimensional formulation (1D vessels in a 3D tissue description) to perform efficient simulations of capillary development accounting for tissue oxygenation, haemodynamics, and vessel adaptation.

2. Methods

To model capillary network development and adaptation, we have identified four major components that must be accounted for. These are the haemodynamics in the vascular network, oxygen-VEGF pathway, angiogenic sprouting and anastomosis mechanisms, and arteriogenesis and pruning adaptation processes.

Firstly, we model the haemodynamics through an initial capillary region, then we calculate oxygen diffusion into the tissue based on vascular wall permeability and tissue properties. Simultaneously, the tissue consumes oxygen based on its metabolic rate and produces VEGF in response to the degree of hypoxia. The VEGF then diffuses back through the tissue to the capillaries. Capillary segments exposed to sufficient levels of VEGF initiate a sprouting process. Sprouts stochastically grow along the VEGF gradient simulating natural movement through the extracellular matrix, and, finally, anastomose with other sprouts and vessels to create new capillary segments. The haemodynamics of the capillary region are then recalculated and an arteriogenesis/pruning update step adjusts the network based on wall shear stress and minimum required flows. This process iterates until the tissue region is sufficiently oxygenated.

3. In-silico Experiments

The model provides a platform for in-silico experiments into the effects of disruptions to metabolic rate, blood oxygenation, blood pressure/flow, or tissue growth on the properties of the capillary network in a tissue region.

Using this methodology, we analyse how the rate of metabolic consumption of oxygen in the tissue affects the resulting capillary networks. We hypothesise that higher metabolic rates result in denser capillary networks and that altering metabolic rate over the course of development will result in corresponding adaptations.

4. Discussion and Conclusions

Performing in-vivo experiments on processes such as capillary network adaptation and development is challenging. A physiological mechanistic model of the processes provides an opportunity to explore the biological mechanisms involved.

Additionally, including haemodynamics enables the adoption of this model as a microscale component of a multiscale simulation of the complete cardiovascular system.

Acknowledgements:

This work was supported by the University of Auckland Doctoral Scholarship program.

P4.6

PPG sensor modelling for cardiovascular parameter estimation

Xavier Bednarek¹, Guillaume Blanquer¹, Mathieu Perriolat¹

¹ Univ. Grenoble Alpes, CEA, LETI, DTBS, LS2P, Grenoble, France

1. Introduction

Photoplethysmography (PPG) is an attractive technology to estimate cardiovascular parameters using wearable devices. However, measurements from commercially available products are cleared as medical grade only for specific measurement conditions.

Understanding vascular dynamics in tissue and sensor physics is crucial to improve the estimation of physiological parameters derived from PPG signals.

We developed the simulation framework (Fig 1) to study perturbations occurring on PPG signals in the daily life.

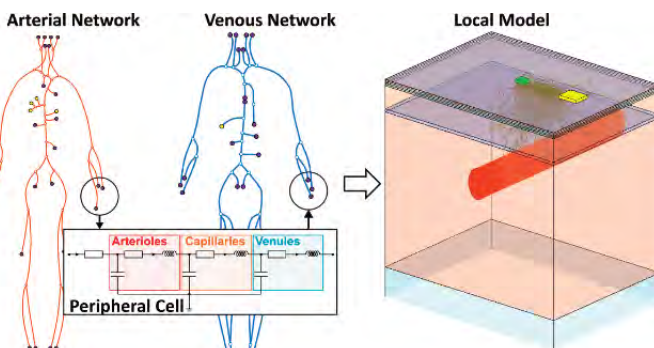


Figure 1: Our framework: general circulation; peripheral cell; local model and PPG sensor.

2. General circulation

The general blood circulation is modeled by the main arteries and veins of the body represented as one-dimensional elements. They are coupled with zero-dimensional cells representing the major organs and peripheral circulations as described in [1, 2]. The model is discretized and solved using finite difference schemes.

This model is placed in an articulated body to handle gravity and inertial effects. They are mandatory to study the perturbations caused by the subject's motion.

3. Local model at the sensor site

The PPG device is placed on the wrist. It is sensitive to the optical properties of the surrounding tissue [3]. They vary over time as cardiovascular activity modifies local perfusion.

To derive the local model, we rely on the cell representing the hand (Fig. 1). It gives the volumes of blood in arterioles, capillaries and venules. The model also includes the radial artery with a time-varying radius.

4. Light interaction with tissues

The PPG sensor works in reflection: it detects the light reflected by the tissues towards the photo-detector. It is modeled by a source and a detector (green and yellow boxes in Fig 1) placed on top of the local model.

Light propagation in tissues is subject to scattering and absorption events. A Monte Carlo simulation evaluates the amount of light backscattered by the local model that hits the detector at each time step.

5. Results

The result shows that the simulated PPG signal matches the real one: the shape presents the systolic phase, the dicrotic notch and the diastolic phase.

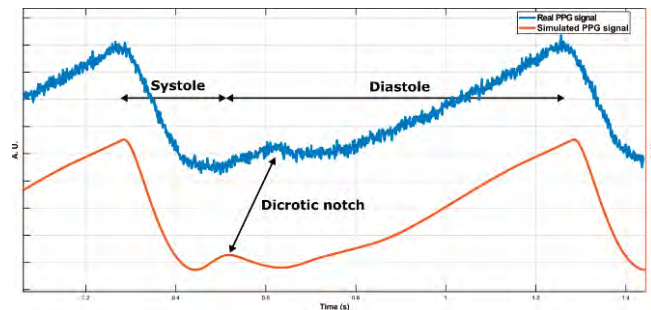


Figure 2: Real and simulated PPG.

6. Discussion and Conclusions

Our multi-physics approach models the multiple circulatory phenomena involved in PPG measurement. Future works will focus on the study of perturbations induced by the motion of the subject.

5. References

1. X. Zhang et al, *Acta Mechanica Sinica*. 2017.
2. L. Müller et al, *Int J Numer Method Biomed Eng*. 2014.
3. Tuchin, *Tissue optics* (SPIE Press, 2007).

Acknowledgements:

This work was supported by the French ANR via Carnot funding and by the French Public Authorities within the IPCEI-nano2022 project.

P4.7

Integration of heterogeneous biological data in multiscale mechanistic model calibration

Jean-Louis Palgen¹, Angélique Perrillat-Mercerot¹, Nicoletta Ceres¹, Emmanuel Peyronnet¹, Matthieu Coudron¹, Jim Bosley¹, Adèle L'Hostis¹, Claudio Monteiro¹

¹ Novadiscovery, Lyon, France

1. Introduction

Mechanistic models can be built using knowledge as the primary information source, with well-established biological and physical laws determining the causal relationships within the model. However, once the causal structure of the knowledge-based model is determined, parameter values must be defined in order to accurately reproduce multi-scaled relevant data^{1,2}. Data available may be scarce, especially in the case of knowledge-based models of pathophysiolgies. Available data may be in an awkward or inconvenient format. As a consequence, determining parameters values and their distributions is particularly challenging. We address this question using the procedure described hereafter.

2. Materials and Methods

We used a step-by-step calibration strategy to overcome the challenges of scarcity and heterogeneity of calibration datasets. We used a covariance matrix adaptation evolution strategy (CMA-ES) optimization, focusing on parameters whose initial values cannot be easily derived from the scientific literature. Final values are estimated with constraints set by relevant data, which represent biological behaviors that the model seeks to reproduce.

3. Results

The stepwise, integrative and iterative approach to multiscale mechanistic model calibration is reported for a pathophysiological lung adenocarcinoma model. We successfully constrained the model to reproduce the relevant biological behaviors observed in vitro, ex vivo and in vivo.

4. Discussion and Conclusions

The step-by-step approach described here allows us to successfully calibrate models based on heterogeneous, complex and scarce data. It can be applied to a wide range of biological models, to help the creation of in silico models supporting drug development.

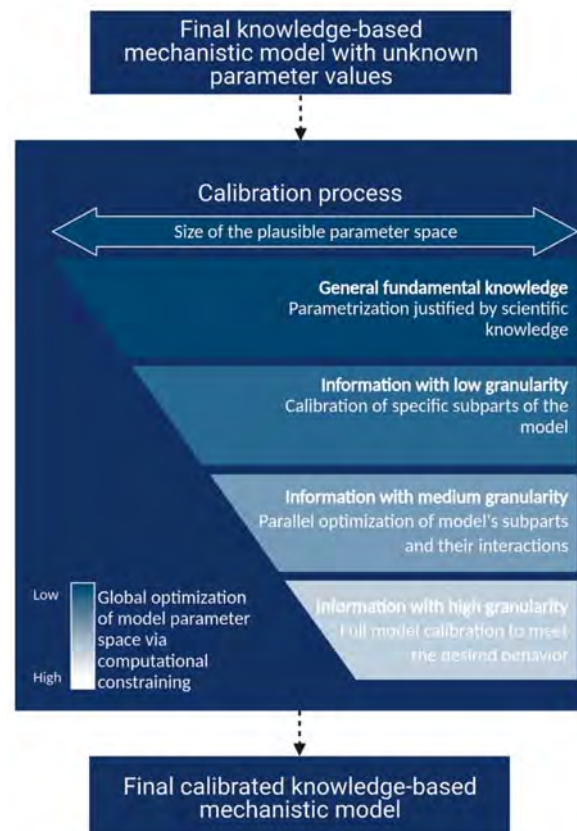


Figure 1: Illustration of the stepwise calibration process of a model with knowledge and data as input. We propose an iterative calibration process where the size of the plausible parameter space decreases at each step, and the effect of the computational constraints applied to the model on the efficiency of the calibration process increases.

5. References

1. Bhattacharya, P., & Viceconti, M. (2017). Multiscale modeling methods in biomechanics. *Wiley interdisciplinary reviews. Syst. biol and med.*, 9(3), e1375.
2. Morrison, T. M., Hariharan, P., Funkhouser, C. M., Afshari, P., Goodin, M., & Horner, M. (2019). Assessing Computational Model Credibility Using a Risk-Based Framework: Application to Hemolysis in Centrifugal Blood Pumps. *ASAIO journal (American Soc. for Art. Int. Organs: 1992)*, 65(4), 349–360.

Acknowledgements:

The authors would like to thank Janssen-Cilag France for their support of the project..

P4.8

Multiscale modeling of electrically active bone implants

Anna Karina Fontes Gomes¹, Ursula van Rienen^{1,2,3}, Revathi Appali^{1,2}

¹ Institute of General Electrical Engineering, Rostock, Germany

² Department of Ageing of Individuals and Society, Interdisciplinary Faculty, Rostock, Germany

³ Department of Life, Light and Matter, Interdisciplinary Faculty, Rostock, Germany

1. Introduction

Electrically active implants such as bone implants have gained importance to regenerate bone and cartilage. In silico models of electrically active implants and their interaction with tissues play a crucial role in understanding the impact of electric fields on the corresponding tissues and improving the functionality of implants. These models range across scales, and the modeling approach can be either bottom-up, top-down, or hybrid.

One way to perform the non-trivial multiscale coupling is the Multiscale Modeling and Simulation Framework (MMSF) [3], providing a structured and well-defined way to exchange information between submodels and connect them. The MMSF uses the Multiscale Modeling Language (MML) [2] to allow the architectural specification of the multiscale simulation.

2. Materials and Methods

The MMSF formalism is composed of four steps: modeling, architecture (theoretical framework), implementation, and execution (computational framework) [1]. Creating the problem's scale separation map (SSM) is essential for the modeling. The SSM is a 2D map with temporal and spatial axes separating the scales of the problem. In the second step, an MML diagram must be designed to define the coupling between the models, the input, outputs, and the coupling topology. Both steps are crucial in developing an efficient computational framework for the multiscale problem, which is constituted by implementing single scale models, scale bridging techniques (SBT), and their execution. The SBT realizes the interaction between submodels of different scales and is implemented using the MML depending on the coupled models and the separation degree of scales. This requires a deep knowledge of models and scales.

3. Results and Discussion

This work will present multiscale modeling of bone remodeling in the open-source software MUSCLE3 [4]. We will first focus on the theoretical consideration of MMSF and discuss the implementation and execution later. We will briefly touch on the challenges in multiscale modeling, such as computational costs versus accuracy in bone remodeling.

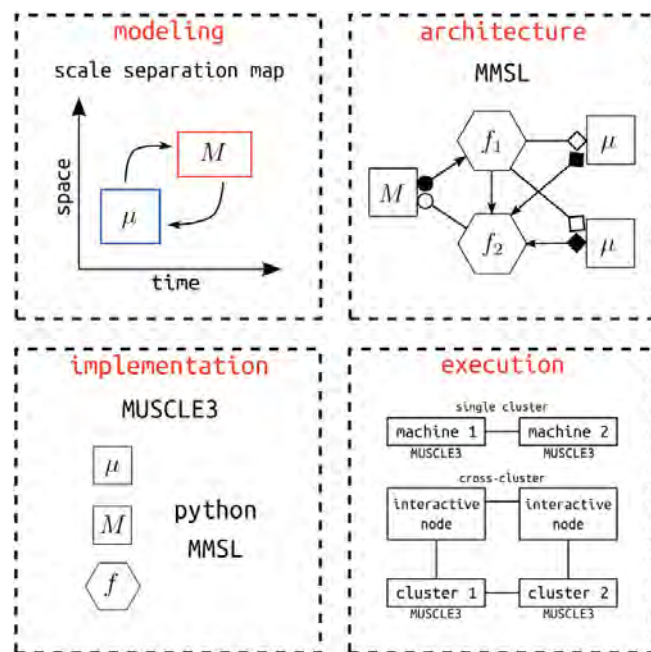


Figure 1: The four steps of the MMSF formalism in MUSCLE3. Modified from [1].

5. References

- Chopard B, Borgdorff J, and Hoekstra AG. A framework for multiscale modelling. *Philosophical Trans of the Royal Society A: Math, Phys and Eng Sciences*, 2014.
- Falcone JL, Chopard B, and Hoekstra A. MML: towards a multiscale modeling language. *Procedia Computer Science*, 1(1):819–826, 2010.
- Hoekstra AG, Lorenz E, Falcone JL, and Chopard B. Towards a complex automata framework for multiscale modeling: Formalism and the scale separation map. *Computational Science – ICCS 2007*, pages 922–930, 2007.
- Veen LE, Hoekstra AG. Easing Multiscale Model Design and Coupling with MUSCLE 3. *Lecture Notes in Computer Science*, vol 12142., 2020.

Acknowledgments:

Funded by the Deutsche Forschungs- gemeinschaft (DFG, German Research Foundation) – SFB 1270/2 - 299150580.

P4.9

Measurements of the intraoperative migration of proximal femoral nail in a wide medullary canal

Krzysztof Zerdzicki¹, Marcin Ceynowa²

¹ Gdańsk University of Technology, Faculty of Civil and Environmental Engineering and BioTechMed Center, Gdańsk, Poland

² Medical University of Gdańsk, Department of Orthopedic Surgery, Gdańsk, Poland

1. Introduction

Cephalomedullary nailing along with dynamic screw plates are regarded favorite methods for fixation of intertrochanteric fractures [1,2]. The surgical technique of intramedullary nails is constantly developed, while the discussion on using the distal locking is still open and its application depends strongly on the stability of the fracture [3]. However, in case of a wide medullary canal, the nail may move from its initial position under the applied force. The aim of the research was to evaluate the lateral migration level of the distal end of the nail based on radiographs of intertrochanteric fracture fixed with cephalomedullary nail.

2. Materials and Methods

There were 43 patients with A1 or A2 fracture types included in the study (34 females and 9 males, mean age 77.8, SD 13.1). The intertrochanteric fractures were fixed during standard surgery with the short Gamma 3 Nail and under fluoroscopic guidance. Before the surgery and six weeks afterwards the radiographs were performed for control purposes. Every pre-, inter- and post-operative radiographs were carefully examined by AutoCAD software. Measurements of the canal width and position of the distal end of a nail was measured and reported at every stage of the operative treatment.

3. Results

The mean medullary canal width on the intraoperative radiograph was 14.4 mm (SD = 1.58). The lateral migration of the distal end of the nail was observed either after compression of the fracture, but before the distal locking device was assembled, after the device was assembled, or during reaming and insertion of the distal screw hole. Mean migration was 0.49 mm (SD = 0.71, range: 0.02 mm – 2.99 mm). The nail migration occurred only in unstable fractures (AO A2 type), with a medullary canal at least 13.7 mm.

4. Discussion and Conclusions

Lateral migration of the nail end can occur in patients with an unstable intertrochanteric fracture type and wide medullary canal. It can occur both intraoperatively before the distal locking screw is inserted and possibly also postoperatively when the distal locking is omitted. This migration may result in a varus angulation of the fracture. However, static locking seems to prevent further dislocation. Additional clinical investigation on this issue is recommended.

5. References

1. Barton TM, Gleeson R, Topliss C, Greenwood R, Harries WJ, Chesser TJS. J Bone Jt Surg - Ser A. 2010;92(4):792–8
2. Bhandari M, Schemitsch E, Jönsson A, Zlowodzki M, Haidukewych GJ. J Orthop Trauma. 2009;23(6):460–4
3. Ciaffa V, Vicenti G, Mori CM, Panella A, Conserva V, Corina G, et al. Injury. 2018;49:S19–25

Acknowledgements:

Financial support of these studies from Gdańsk University of Technology by the DEC-47/2020/IDUB/I.3.3 grant under the ARGENTUM TRIGGERING RESEARCH GRANTS - 'Excellence Initiative - Research University' program is gratefully acknowledged.

P4.10

Physiomics of right atrial ganglionic plexus neurons predicted from transcriptomics

Suranjana Gupta¹, Adam JH Newton¹, Alison Moss², James S. Schwaber², Rajanikanth Vadigepalli², William W. Lytton^{1,3}

1 SUNY Downstate Health Sciences University, Department of Physiology and Pharmacology, Brooklyn, United States

2 Daniel Baugh Institute for Functional Genomics/Computational Biology, Thomas Jefferson University, Department of Pathology, Anatomy and Cell Biology, Philadelphia, United States

3 Kings County Hospital, Department of Neurology, Brooklyn, United States

*Rajanikanth.Vadigepalli@jefferson.edu

1. Introduction

Physiomics follows proteomics follows transcriptomics follows genomics with many a slip from one to the other. Studying the neurons of the right atrial ganglionic plexus (RAGP), a component of the intrinsic cardiac nervous system (ICNS), we found that transcriptomic to electrophysiology translation required tuning due to the many possible proteomic variations.

2. Materials and Methods

Simulations were run using NEURON 8.0 and NetPyNE v1.0.2.

3. Results

We built single-compartment computational models of 405 minipig RAGP principal neurons by incorporating ion channels identified from transcriptomics data via HT-qPCR [1]. The raw data was thresholded based on a cycle threshold value ($\text{ct} < 15$). The 405 cells were reduced to 104 cells with unique ion channel gene combinations. From ~200 genes in the transcriptomics map, we identified 15 genes that encode ion channel proteins: Scna1 (Nav1.1), Kcnc1 (Kv3.1), Kcna1 (Kv1.1), Kcnj3 (GIRK1), HCN1–4, Cacna1a (Cav2.1, P/Q), Cacna1b (Cav2.2, N), Cacna1c (Cav1.2, L), Cacna1d (Cav1.3, L), Cacna1g (Cav3.1, T), Cacna1i (Cav3.3, T). The corresponding Hodgkin-Huxley-based kinetic models were mined from databases obtained via different techniques [2,3]. Simulations were run to shortlist a single model per gene. Substantial difficulties were encountered in identifying adequate models corresponding to specific ion channel types. Some channels had been expressed in oocytes or other foreign cells making their parameters for the same gene discrepant. Further, the genomic identity of the channels did not correspond to their physiological function, making the data hunting challenging. Our neuronal models elicit three distinct firing profiles in response to a current clamp stimulus: phasic (single action potential (AP)), burst (2–5 APs followed by a period of silence during the rest of the stimulus) and tonic (repetitive AP firing throughout the stimulus). We also observe variation in the inter-spike interval of tonically firing cells. Our models also elicit spontaneous activity that surfaces after the termination of the stimulus. Consistent with experimental findings, phasic response is the most dominant response in our neuronal models (~65–72%). The firing frequency of tonically firing cells monotonically increase at a rate of 5–6 Hz per 0.1 nA increase in the stimulus.

4. Discussion and Conclusions

We found that transcriptomics is unable to fully or even largely constrain the choice of ion channel models, or their densities. There is an “incompleteness” regarding the association of genetically identified ion channels with their physiological action. There is a gap in literature associating the genomic identity of ion channels to their physiological function. The ion channels identified by their genes do not specifically correlate to a known physiological behaviour making their implementation in biophysical models extremely challenging.

Furthermore, there is no direct equivalence between the transcriptomics gene expression levels and the channel conductance making it difficult to quantify their contribution while building the model. In order to adequately constrain the model we instead had to rely on physiological measurements, such as *in vitro* measures of firing in response to current clamp input and *in vivo* and *ex vivo* recordings with synaptic input.

5. References

1. Moss, Alison, et al. *Iscience* 24.7 (2021): 102713.
2. Ranjan, Rajnish, et al. *Front neuroinform* 5 (2011):36.
3. McDougal, Robert A., et al. *J of Comp. Neuro.* 42.1 (2017):1-10.

Acknowledgements:

The work has been funded by NIH Common Fund SPARC Program Grant OT2 OD030534.

P4.11

Transmembrane mucin response in conjunctival epithelial cells exposed to wall shear stresses

Shir Itah¹, Mordechai Rosner¹, Dan Grisaru¹, David Elad¹

¹ Tel Aviv University, Tel Aviv, Israel

1. Introduction

The tear film protects the ocular surface and is composed of mucus, aqueous and lipid layers. The inner mucus layer is secreted from goblet cells and transmembrane sources of the human conjunctival epithelial cells (HCEC). The conjunctiva contains two major cell types, goblet cells and stratified squamous cells that discharge different mucins into the tear film. The goblet cells synthesize and secrete the large gel forming MUC5AC and the stratified squamous cell synthesize the membrane spanning mucins MUC1, MUC4, and MUC16 [1]. MUC1 is the smallest one while MUC16 is the largest membrane-bound mucin [2]. The HCEC are continuously subjected to wall shear stresses (WSS) induced by airflows, eyelids movements, as well as wiping and rubbing the eyes. In this study, we cultured primary HCEC and explored the mechanobiology characteristics of mucin secretion and cellular alterations in response to airflow induced WSS perturbations.

2. Materials and Methods

Primary HCEC were isolated from eyelid tissue specimens that were removed during surgical correction of ptosis from patients with healthy conjunctiva tissue. The study was approved by our IRB committee and the donors signed consent forms. The HCEC were seeded on entactin-collagen IV-laminin (ECL) coated synthetic membrane within our custom-designed wells and cultured submerged in the medium. After 3–4 days, the wells were disassembled and the well-bottom with the cultured HCEC was installed in flow chamber for application of WSS on the apical surface of the cells [3]. We exposed the HCEC to steady WSS of 0.5 and 1.0 dyne/cm² for durations of 15 min and 30 min. Cytoskeletal alterations and MUC1 and MUC16 secretions were studied using immunohistochemically fluorescent staining with specific antibodies and enzyme-linked lectin assay (ELLA), respectively.

3. Results

The morphological alterations due to steady WSS obtained in preliminary experiments are shown in Figure 1. The HCEC were exposed to WSS of 0.5 dyne/cm² for 15 min. The exposed cells are depicted in comparison with the unstressed control. Cellular alterations are clearly observed.

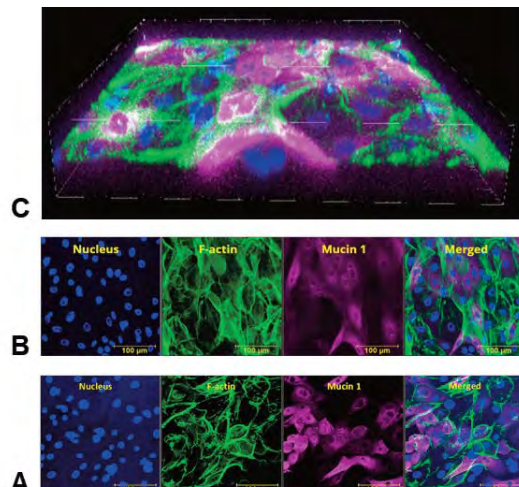


Figure 1: Confocal images of the HCEC in vitro model. A) Projection of unstresses control, b) projection after exposure to WSS of 0.5 dyne/cm² for 15 min, c) 3D image of the stressed HCEC. Immunofluorescence staining: for F-actin Phalloidin - Alexa-Fluor 488 (Ab 176753, Abcam), for MUC1 mucin-specific anti-MUC1 (VU4H5) Alexa Fluor® 647 antibody (sc-7313 AF647, ENCO) and DAPI nucleic acid staining (D9542) for the nuclei. Bar = 100 µm.

4. Discussion and Conclusions

We investigated for the first time an in vitro model of membrane-tethered mucins secretion by HCEC that have been exposed to steady airflow-induced WSS. The results clearly showed that the membrane-tethered MUC1 is secreted and expressed by the HCEC.

5. References

- Ablamowicz AF, Nichols JJ. *Ocul Surf* 14, 331-341 (2016).
- Govindarajan B, Gipson IK. *Exp Eye Res*, 90, 655-663 (2010).
- Sosnovsky et al. *Biomech Model Mechanobiol* 20, 1903-1917 (2021).

P4.12

Optimization of 3D-printed breast prosthesis for breast reconstruction

Xuan-Tien Kévin Trinh¹, Pauline LECOMTE-GROSBRAS¹, Jean-François WITZ¹, Olivier MAYEUR¹, Michel COSSON², Tien-Tuan DAO¹, Jaime DESTOUESSE³

¹ Univ. Lille, CNRS, Centrale Lille, UMR 9013, LaMcube, Lille, France

² Service de Gynécologie médico-chirurgicale, Hôpital Jeanne de Flandre, CHRU de Lille, France

³ Lattice Medical, Lille, France

1. Introduction

Breast cancer concerns 1 in 8 women in the world and is followed in 40% of cases by a mastectomy. Only 14% of women receive reconstructive surgery because of unfavourable clinical issues [1]. The clinical need for adipose tissue engineering in soft tissue defects is in constant increase. In the case of breast reconstruction, tissue engineering chamber (TEC) could be a promising solution to restore large volume of mature and vascularized adipose tissue.

Lattice Medical company aims to bring a new 3D-printed TEC device constituted with bioresorbable materials to be fully absorbed by the body in several weeks. In this context, the TEC mechanical and biological properties over time and the optimal topology need to be assessed.

2. Materials and Methods

We use a numerical approach coupled with experimental observations. Characterization of mechanical properties and degradation kinetics of the polymer reveals an isotropic behaviour in the linear domain, but an anisotropic behaviour for the limits to failure in deformation or stress. At the structural level, the prediction of the mechanical response of the standard geometry prosthesis must be evaluated to meet normative requirements.

Firstly, the purpose is to validate the mechanical resistance of the structure via simulation and compare the calculated deformation field to the measured field over degradation time. Finite element model validated by experimental data is used to simulate the mechanical response.

Then, an open-source python script coupled with abaqus [2] is used to perform a topological optimization, via bidirectional evolutionary structural optimization (BESO) method, of the structure under multiple solicitations and adding the consideration of anisotropic criteria for a mass diminution objective and mechanical properties conservation or improvement.

Finally, the design of a parametric geometric model will allow the customization of the geometry of the prosthesis for a reconstruction that anatomically fits the patient's shape and size breast. The anatomical design is automated by CAD using Catia and/or FreeCAD (Fig. 1).

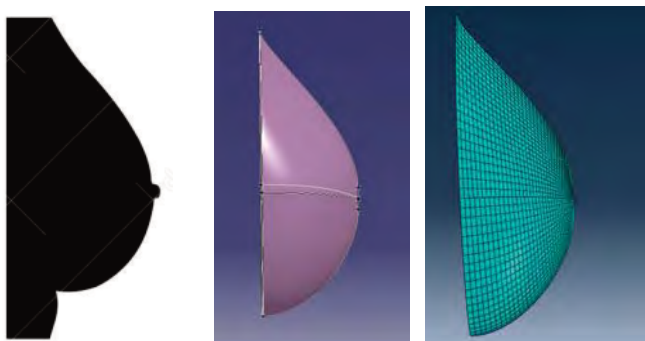


Figure 1: Example of anatomical shape design from parametric breast model

3. Results

After a parameter sensibility analysis, the topological optimization gives new design with far less volume and material (Fig. 2).

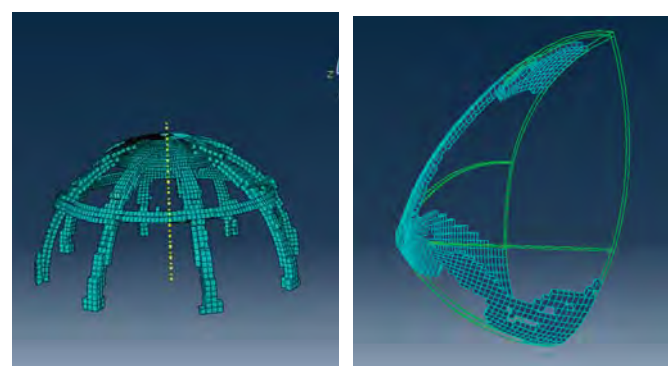


Figure 2: Design from topological optimization of standard shape (left) and anatomical shape (right) bioprosthesis

4. Discussion and Conclusions

The optimization process needs to be improved to consider different loads and to obtain optimal geometries compatible with the growth of biological tissue. Plus, the parametric model needs to be enriched for better automation and to consider the variety of shapes.

5. References

1. Gabriel A, Maxwell GP. Clin Plast Surg. 2015 Oct;42(4):399-404.
2. Zuo Z, Xie YM. Advances in Engineering software. 2015; 85:1-11.

Acknowledgements:

The authors would like to thank the Haut-de-France region, Centrale Lille Institut and Lattice Medical for providing financial support.

P4.13

MicroMap: Interactive visualisation of human microbiome metabolism realised via online systematic team empowerment of STEM undergraduates in Ireland.

Cyrille Thinné¹, Renee Waschkowitz¹, Eoghan Courtney², Eoghan Culligan², Katie Fahy¹, Ruby Ferrazza¹, Ciara Ferris³, Cristina Gonzales², Angeline Lagali³, Rebecca Lane¹, Colm Maye³, Olivia Murphy¹, David Noone¹, Saoirse Ryan¹, Mihaela Bet⁴, Emma Byrne⁴, Maria Corr⁴, Hannah Cummins¹, David Hackett², Ellen Healy², Nina Kulczycka¹, Niall Lang¹, Luke Madden², Lynne McHugh¹, Ivana Pyne¹, Ciara Varley¹, Niamh Harkin¹, Ronan Meade¹, Grace O'Donnell¹, Filippo Martinelli¹, Almut Heinken¹, Ines Thiele¹

¹ National University of Ireland, Galway, Medicine & Ryan Institute, Galway, Ireland

² University College Dublin, Dublin, Ireland

³ University College Cork, Cork, Ireland

⁴ Trinity College Dublin, Dublin, Ireland

cyrille.thinne@nuigalway.ie ines.thiele@nuigalway.ie

1. Introduction

Biocomputational modelling using the AGORA2 resource of human microbiome genome-scale metabolic reconstructions [1] enables predictive and personalised analyses of host-drug-microbiome interactions. A corresponding interface to enable interactive visualisation did not yet exist. We addressed this gap through applying engaged research principles in a systems biomedicine context.

2. Materials and Methods

Based on the AGORA2 resource of 7,209 microbiome genome-scale metabolic reconstructions, the issued metabolites and biochemical reactions were organised and curated to manually draw MicroMap using the CellDesigner software [2] with a city map-inspired design to facilitate intuitive navigation by the biochemically informed user.

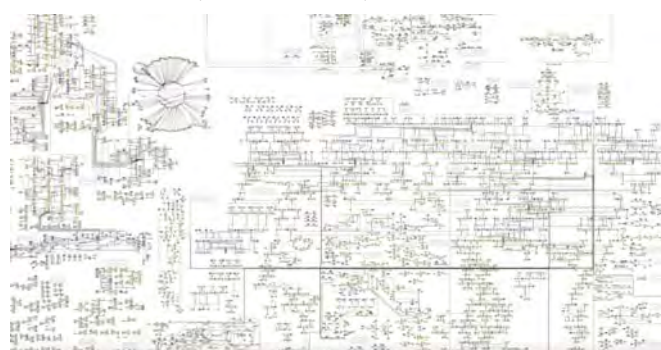


Figure 1: A view of the MicroMap within the Virtual Metabolic Human interface.

The diverse and interdisciplinary teams of undergraduate STEM researchers collaborated in a virtual environment based on systematic team empowerment to conceptualise, design, and implement the map by following principles of engaged research to tackle this challenging project in the midst of the ongoing COVID-19 pandemic while being dispersed across Ireland.

3. Results

We manually drew and curated MicroMap containing 152 reaction classes, 5,098 reactions, and 4,979 metabolites, consistent with the AGORA2 content. MicroMaps is integrated within the Virtual Metabolic Human (VMH, www.vmh.life) to enable content query, custom dataset visualisation, interlinking with other VMH resources, and feedback submission for iterative improvement.

4. Discussion and Conclusions

MicroMap is a manually curated metabolic network map of the human microbiome which enables the interactive visualisation of omics data and flux analysis results in a network context, e.g., via integration with the COBRA Toolbox. MicroMap is integrated within the VMH and therefore seamlessly interconnects with all VMH resources, e.g., the latest human reconstruction Recon3D, in addition to ancillary external resources. MicroMap complements the portfolio of biocomputational tools for studying human-microbiome interactions, such as the gut-brain axis.

5. References

- Heinken A et al, *bioRxiv* 2020.11.09.375451 (2020).
- Funahashi A et al, *BIOSILICO* 1:159-162 (2003).

Acknowledgements:

This work has been supported by the European Research Council (ERC) under the European Union's Horizon 2020 research and innovation programme (grant agreement No 757922).

P4.14

Estimating Skeletal Muscle Forces in vivo: A Shear Wave Elastography Approach

Manuela Zimmer¹, Benedict Kleiser², Justus Marquetand², Filiz Ates¹

¹ Institute of Mechanics, Structural Analysis, and Dynamics of Aerospace Structures, University of Stuttgart, Stuttgart, Germany

² Department of Epileptology, Hertie-Institute for Clinical Brain Research, University of Tübingen, Tübingen, Germany

Corresponding author: Manuela Zimmer, zimmer@isd.uni-stuttgart.de, Pfaffenwaldring 27, D-70569 Stuttgart

1. Introduction

Modelling and simulation of skeletal muscles are essential to understand neuromuscular diseases better and to improve treatment strategies. However model validation with direct muscle force measurements at the respective tendons intra-operatively [e.g. 1] is not straight-forward and not feasible for many scenarios in particular for healthy muscles.

Surface electromyography (sEMG) has been widely used for characterization of muscles, but it lacks the representation of the passive state. Previously, muscle stiffness deduced from shear wave elastography (SWE) was shown to represent muscle mechanics [e.g. 2].

Aiming to investigate the use of a SWE approach in understanding active and passive force production of skeletal muscles, the present study hypothesized that changes in mechanical properties of the biceps brachii muscle (BB) can be detected both in passive state and during isometric ramp contractions. We investigated whether SWE can reveal individual muscle mechanics in relation to joint function which would improve existing muscle models.

2. Materials and Methods

SWE, sEMG of BB, and isometric elbow torque measurements were performed on 14 healthy volunteers (7 males, 28.07 ± 5.06 years). A passive trial, maximum voluntary contractions (MVC) and isometric ramp contractions (up to 25%, 50%, 75% of MVC torque) were performed for five elbow angles (60° , 90° , 120° , 150° , and 180°). BB muscle length was measured using B-mode ultrasound imaging.

3. Results

Muscle length of BB increased with increasing elbow angle ($p < 0.001$). At passive state, elastic modulus of BB deduced from SWE significantly increased with increasing elbow angle ($p < 0.001$) but no significant differences were observed for sEMG root-mean squared amplitude (RMS) ($p > 0.05$). During sub-maximal isometric contractions, both elbow angle and activity level caused significant effects on shear elastic modulus ($p < 0.001$, Fig. 1). However, only the change in activity levels affected sEMG RMS amplitude ($p < 0.001$).

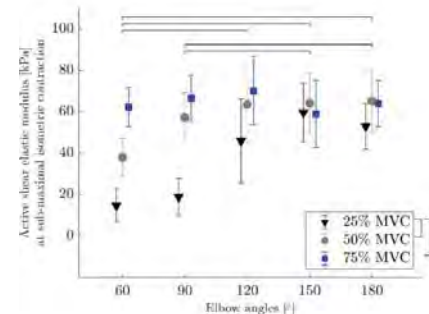


Figure 1: Average active shear elastic modulus at 25%, 50%, and 75% isometric contractions for different elbow angles (60° - 180°).

4. Discussion and Conclusions

The hypothesis posed was supported as SWE is able to characterize passive mechanical muscle properties at tested conditions. During active state, SWE reflected different activity levels while indicating muscle length dependent characteristics. We conclude that SWE describing muscle mechanical characteristics can be developed as an index of muscle force. If validated with experiments [e.g. 1], SWE findings can be used to significantly improve muscle models and simulate the effects of e.g. exercise, neuromuscular diseases, or to monitor treatment effects.

5. References

- Ates F, Temelli Y, Yucesoy CA, Human Movement Science, 2018, 75:103-110
- Ates F et al., Journal of Electromyography and Kinesiology 2015, 25 (4): 703-8

Acknowledgements:

Funded by the Deutsche Forschungsgemeinschaft (DFG – German Research Foundation) GRK 2198 – 277536708.

P4.15

Determining the navier slip parameter in the descending aorta using 4d pc-mri data

Alena Jarolímová¹, Jaroslav Hron¹

¹ Charles University, Faculty of Mathematics and Physics, Mathematical Institute, Prague, Czech Republic
jarolimova@karlin.mff.cuni.cz, hron@karlin.mff.cuni.cz

1. Introduction

The computational simulation of blood flow has been receiving increasing attention due to its potential to provide useful information in clinical practice. The model must be provided with sufficiently precise estimates of material parameters, boundary conditions, and the segmentation of the computational geometry. For that purpose, it is possible to use 4D phase contrast magnetic resonance imaging (4D PC-MRI). However, the resolution and noisiness of the images make it hard to directly determine the required parameters. Therefore, it is feasible to use data assimilation instead.

One of the patient-specific parameters in our model is the amount of slip on the wall. Although no-slip BC is commonly used, there have been studies suggesting that a more general Navier slip BC can provide better agreement with the measured data [2]. The goal of this work is to estimate the slip parameter in the descending aorta based on real patient data.

2. Materials and Methods

Blood can be viewed as an incompressible Newtonian fluid in sufficiently wide arteries. Therefore, we use the Navier-Stokes equations. We prescribe Dirichlet BC for inlet velocity v_{in} and directional do-nothing BC at the outlet. The behaviour of blood on the wall is described using the Navier-slip boundary condition in Eq. 1. For further details on the model, see [2].

$$\theta v_t + \gamma_* (1 - \theta) T_n = 0 \quad (1)$$

We use variational data assimilation [1] to incorporate 4D PC-MRI data into the model. Its main idea is to formulate the problem as a minimization of a functional of the distance between the image data and the model results. The PDE representing the model act as constraint, and the functional is minimized with respect to the control variables, which are θ and v_{in} in our case. The PDE-constrained minimization problem can be solved using an iterative optimization algorithm, where each iteration requires solving the PDE. In the gradient-based algorithm, the adjoint equations are added to the system to compute the gradients at each iteration as well [1].

3. Results

We performed tests with artificial data and geometry, which showed that the method can predict v_{in} and θ reasonably well. We proceed to perform first experiments with the real patient data in 3D on a short part of the descending aorta as shown in Fig. 1.

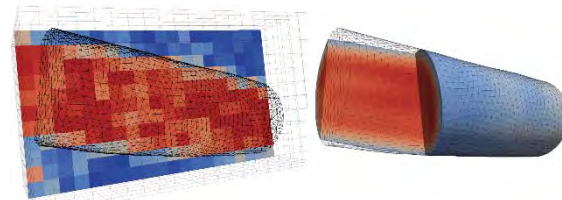


Figure 1: Comparison of the 4D PC-MRI data and the resulting velocity in a short segment of the descending aorta.

4. Discussion and Conclusions

Preliminary results suggest that the optimal θ corresponds to the Navier slip BC rather than the standardly used no-slip BC.

We plan to experiment with larger segments of patient-specific geometry and test the robustness of the algorithm with respect to various initial guesses, as well as the influence of different finite elements and performance of various optimization algorithms.

5. References

1. Bertagna L et al., *Fluid-Structure Interaction and Biomedical Applications*: Springer Basel; 2014. p. 395-477
2. Chabiniok R et al., *Applications in Engineering Science*, 6:100038 (2021).

Acknowledgements:

The work was supported by the Ministry of Health of the Czech Republic, grant nr. NV19-04-00270, and by the Grant Agency of Charles University (project no. 282222).

AUTHOR INDEX

Bold = Presenting author

A. Taylor, Zeike	P1.1, 23.3, 7.5	Bentley, Katie	12.7	Carvalho, Ana	P3.6, P3.7
Abrantes, João	P3.11	Berg, Philipp	23.5	Casoni, Éva	17.3
Accardo, Caterina	16.3	Bernini, Martina	4.5	Casper, Sabrina	12.8
Aguado-Sierra, Jazmin	13.6	Bertoglio, Cristobal	1.7	Cassara, Antonino	2.5
Agur, Anne	300	Besier, Thor	2.1	Cechova, Hana	25.2
Aissaoui, Rachid	2.7	Besier, Thor	24.3	Cedersund, Gunnar	22.2
Akyildiz, Ali	5.2	Besier, Thor	300	Cedersund, Gunnar	14.2
Aldieri, Alessandra	21.2	Bet, Mihaela	P4.13	Cedersund, Gunnar	25.1
Ali, Omar	16.3	Bezy-Wendling, Johanne	278	Celi, Simona	16.1
Allievi, Sara	4.4	Biancolini, Marco Evangelos	10.7	Ceres, Nicoletta	P4.7, 12.3
Almeida, Diogo F.	19.5	Biessو, Giorgio	P3.4	Cess, Colin	27.4
Almeida, Gonçalo	7.1	Bischoff, Jeff	19.4	Ceynowa, Marcin	P4.9
Alvarez Laviada, Anita	P1.9	Bischoff, Jeff	P2.7	Chabiniok, Radomír	12.6
Anastassiou, Charalambos	8.5	Bisotti, Marc-Antonio	P2.14	Chabiniok, Radomír	22.4
Aparicio-Yuste, Raúl	15.5	Bissacco, Daniele	4.4	Chabiniok, Radomír	P3.5
Apeldoorn, Cameron	P4.5	Blagojević, Andjela	P1.15	Chapelle, Dominique	22.4
Appali, Revathi	P4.8, 11.7	Blanco, Pablo javier	10.3	Chaplain, Mark	282
Arens, Jutta	6.5	Blanquer, Guillaume	P4.6	Chassagne, Fanette	19.3
Arevalo, Hermenegild	26.2	Bloomfield, Frank	13.2	Che, Lam Vien	8.3
Argus, Finbar	10.1	Boaretti, Daniele	5.4	Checa, Sara	P3.12
Argus, Finbar	13.2, 10.1	Boerdonk, Pam	10.6	Checa, Sara	P3.4
Arjmand, Navid	16.8	Bone, Alexandre	16.3	Checa, Sara	15.1, 15.9, 15.7
Arrarte Terreros, Nerea	11.8, 3.6, P1.13	Bonitz, Lars	17.5	Chen, Junyi	189
Arrestam, Oscar	22.2	Bonnaire, Rebecca	19.3	Cheng, Leo	2.1
Arsène, Simon	3.2	Borgiani, Edoardo	27.2	Chernyavsky, Boris	23.6, P2.4
Arsic, Branko	P1.15	Bosley, Jim	P4.7	Chevalier, Aude	3.2
Arts, Theo	14.6	Bouchard, Guillaume	12.3	Chiastra, Claudio	1.6
Asselbergs, Folkert	P2.3	Bouwman, Vincent	4.8	Chiote, Margarida	4.2
Ates, Filiz	P4.14	Brandão, Sofia	4.2	Chiote, Margarida	P3.15
Augustin, Christoph	131, P4.2	Bridio, Sara	11.8, 3.6, P1.13	Chisholm, Robert	14.1
Aussy, Audrey	11.4	BRIEU, Mathias	18.5	Choisne, Julie	2.1, 24.3
Avci, Okan	24.2, 11.1, 2.6,	Brinkhuis, Emiel	1.7	CHOU, YUAN CHUNG	13.4
	P3.9	Bruezière, Lara	6.6	Chrystele, Rubod	7.2
Avezzù, Adelisa	P1.9	Brunát, Matouš	20.4	Chu, Wen-Yang	22.1, P3.8
Avrahami, Idit	13.1	Brüning, Jan	P1.6	Chu, Wen-Yang	19.5
Avril, Stéphane	11.6	Brüning, Jan	23.5, 5.6, P1.6	Chumarnaya, Tatiana	390
Awadalla, Maged	19.4	Bruno, Claudia	4.1	Ciusdel, Costin Florian	P1.12
B.V, Rathish Kumar	P4.3	Bruyère-Garnier, Karine	5.2	Clark, Aly	2.1
Babarenda Gamage, Thiranjana Prasad	2.1	Bubak, Marian	P4.1	Clark, Anna	7.4
Badrou, Arif	23.2	Bubak, Marian	P2.8	Clemmer, John	3.7, P1.5
Bailet, Mathieu	2.8	Buch, Sagar	12.1	Collins, Caitlyn	5.4
Ball, Graham	11.4	Bucki, Marek	2.8	Conti, Michele	4.4
BALLIT, Abbass	25.4, 7.3	Budday, Silvia	PT2	Contin, Martina	19.1
Baragona, Marco	168	Budgett, David	2.1	Cook, Andrew	7.6
Barbieri, Fabian	1.8	Burns, Jane	1.5	Cornelussen, Richard	10.6
Barbosa, Maria Inês	P3.6, P3.7	Bursi, Roberta	P2.14	Cornet, Alexander D.	12.5
Barczak, Annamaría	14.5	Bursi, Roberta	P2.2	Corr, Maria	P4.13
Barnes, Devon A.	P2.9	Busto, Laura	13.7	Correia, Miguel	P3.11
Bartolucci, Pablo	10.4	Butakoff, Constantine	P1.14	COSSON, Michel	18.5
Barzegari, Mojtaba	28.1, 28.2	Butakoff, Constantine	13.6	Cosson, Michel	7.2
BASTIEN, MARTIN	12.3	Byrne, Emma	P4.13	Cosson, Michel	16.5
Bastounis, Effie E.	15.5	Caddy, George	14.8	COSSON, Michel	P4.12
Baumgartner, Laura	28.4	Cadrelan, Jacques	12.3	Costanzo, Francesco	12.1
Baz, Jose A	13.7	Caiazzo, Alfonso	5.3, 282	Coudron, Matthieu	20.3, P4.7, P2.13
Bazhutina, Anastasia	390	Calmels, Paul	19.3	Courtney, Eoghan	P4.13
Beaucage-Gauvreau, Erica	P2.15	Calmet, Hadrien	P1.14	COUTY, Claire	20.3
Bednarek, Xavier	P4.6	Calò, Karol	1.3	Coveney, Peter	1.2
Beela, Achmed S.	13.5	Calvo Gallego, José Luis	370	Coveney, Peter	21.4
Beela, Ahmed Salem	3.1	Camacho-Gómez, Daniel	27.1	Craig, Morgan	26.1
Beeman, Arun	P1.8	Capelli, Claudio	23.1, 7.6, P1.7,	Cramer, Maarten J	P2.3
Bekisz, Sophie	12.7		P1.8, 19.1, 4.1	Crespo-Valero, Pedro	2.5
Bel-Brunon, Aline	23.2	Capellini, Katia	16.1	Crispino, Elena	2.3
Belinha, Jorge	P3.6, P3.7	Cardoso, Fatima	16.4	Crouzier, Marion	P3.13
Belkouchi, Omar	16.3	Carlier, Aurélie	22.6	Cruts, Janneke	1.1
bellos-grob, Anique	7.2	Carlier, Aurélie	113	Csippa, Benjamin	11.5
Benjamin, John	P3.8	Carman, Laura	24.3	Cukovic, Sasa	17.1

AUTHOR INDEX

Bold = Presenting author

Culligan, Eoghan	P4.13
Cummins, Hannah	P4.13
Curreli, Cristina	21.2, P1.17
Cutri, Elena	278
Dall'Armellina, Erica	7.5
Dall'Asta, Andrea	7.4
Dao, Tien-Tuan	25.4
DAO, Tien-Tuan	16.5, 7.3, 16.2, P4.12
Darré, Hippolyte	12.3
Day, Gavin	17.4
Dazzi, Chiara	15.1
De Swerdt, Els	5.1
de Vries, Tanja	1.7
Dedola, Francesca	4.4
del Arco, Alex	8.4
Delhaas, Tammo	13.5, P2.3, 14.6, 3.1, 10.6
Dercole, Fabio	20.2
DESTOUESSE, Jaime	P4.12
Desvaux, Emiko	11.4
Dharia, Mehul	19.4
Di Salvatore, Valentina	2.3
Di Salvatore, Valentina	P1.17
Dimas, Georgios	P2.5
Dixon, Alex	2.1
Djorovic, Smiljana	P1.15
Djuric, Tijana	P1.15
Dokuchaev, Arsenii	390
Döllinger, Michael	15.3
Domanin, Maurizio	4.4
Dondl, Patrick	P3.12
Donker, Dirk	11.2
Donker, Dirk	1.4
Donker, Dirk W.	12.5
Dooley, Steven	27.3
Drasdo, Dirk	27.3
Drożdż, Anna	P1.3, 20.1
Duda, Georg	15.1
DUFAYE, Guillaume	18.5
Dumas, Raphaël	2.7
Dura-Bernal, Salvador	14.5
Dura-Bernal, Salvador	14.2
Eager, David	215
Eguzkitza, Beatriz	17.3
Eichler, Pavel	P3.5
Ejneby Silverå, Malin	14.2
Ekstedt, Mattias	22.2
Elad, David	18.3, 18.1, P4.11
Elahi, Seyed Ali	15.4
El-Bouri, Wahbi	22.5, 19.2
Elewelt, Aaldert	168
Eliat, Pierre-Antoine	278
Elyasi, Elaheh	2.8
Engström, Maria	14.2
ERRABITY, AICHA	19.3
F. Almeida, Diogo	22.1, P3.8
F. Frangi, Alejandro	P1.1, 23.3, 7.5
Faddeenkov, Igor	3.2
Fahy, Katie	P4.13
Falcão, Manuel	P3.15
Famaey, Nele	5.2, 11.6, 15.4
Farcito, Silvia	2.5
Favre, Philippe	P2.7, 19.4
Fdez-Manin, G.	13.7
Fehervary, Heleen	5.2
Feijóo, Raul Antonio	10.3
Fernandes, António	4.2
Fernandez, Justin	300
Ferrari-Gianlupi, Juliano	26.1
Ferrazza, Ruby	P4.13
Ferris, Ciara	P4.13
Fielding, Andrew	P3.1
Filipovic, Nenad	13.6
Filipovic, Nenad	P1.15
Finley, Stacey	27.4
Fontes Gomes, Anna Karina	P4.8
Foroushani, Ali	23.3
Fouliard, Sylvain	11.4
Frangi, Alejandro	23.4
Franke, Benedikt	P1.11
Franz, Juliana	1.8
Fresiello, Libera	11.2
Fresiello, Libera	1.4
Fricková, Kateřina	12.6
Friedrich, Christina	11.4
Fučík, Radek	P3.5
Fuertinger, Doris	28.3
Fuertinger, Doris Helene	12.8
Fullana, José-Maria	10.2
Funaro, Alessia	P3.13
Galabov, Radek	P3.5, 12.6
Galabov, Radek	12.6
Galarce, Felipe	5.3
Galbusera, Fabio	8.4
Galland, Théo	3.2
Gallichan, Robert	2.1
Gallo, Diego	1.3
Gallo, Diego	1.6
Gamba, Alessio	P2.9, P2.6
Ganesan, Rajarajeswari	3.3
Ganesan, Rajarajeswari	16.7
García-Aznar, José Manuel	PT1, 27.1
Garzón Alvarado, Diego	15.2
Gauderat, Glenn	11.4
Gautier, Marine	12.7
Gavriel, Mark	18.3
Gavriel, Mark	18.1
Gazeli, Kristaq	8.5
Gazeli, Odhisea	8.5
Gee, Michael W.	25.3
Gennemark, Peter	22.2
Gentles, Tom	13.2
George, Albert Einstein	128, 8.1
Georghiou, Georgios E.	8.5
Georgiadi, Eleni	20.5
Georgiou, Morfo	2.4
Gerach, Tobias	14.7
Gerardo-Giorda, Luca	135
Geris, Liesbet	P2.6, 27.2 , P2.12, 12.7, 28.1, 28.2 P2.9, 27.2, 19.1, 14.4,
Gerondi, Leonardo	10.7
Ghitti, Beatrice	12.1
Gijssen, Frank	1.1
Gillette, Karli	131
Giráldez, Javier	6.2
Giráldez Suárez, Javier	6.2
Girard, Nicolas	12.3
Glazier, James	26.1
Go, Natacha	3.2
Golse, Nicolas	10.8
Gomez, Maria Adelaida	2.3
Gómez Benito, María José	27.1, 15.5
Gonzales, Cristina	P4.13
González Ballester, Miguel	8.4
González Ballester, Miguel Ángel	28.4
Gorelik, Julia	P1.9
Gottschling, Heiko	P3.1
Götzen, Nils	4.8
Goubergrits, Leonid	P1.6
Goubergrits, Leonid	1.8, 23.5
Goubergrits, Leonid	5.6
Goupil, Anne	8.6
Graf, Norbert	20.5
Granjeon-Noriot, Solène	6.6
Gravouil, Anthony	23.2
Greil, Gerald	22.4
Gries, Thomas	4.3
Griffith, Erica	14.5
Grisaru, Dan	P4.11, 18.3, 18.1
Grzeszczyk, Michał K.	P4.1
Gsell, Matthias	131
Guala, Andrea	1.3
Gubała, Tomasz	P2.8
Guedj, Mickael	11.4
Guerrero, Pedro Enrique	27.1
Guitteny, Sacha	2.7
Gupta, Suranjana	P4.10
Gusseva, Maria	22.4
Haacke, E. Mark	12.1
Hackett, David	P4.13
Hadjicharalambous, Myrianthi	2.4, 8.5
Hajaj, Chen	13.1
Halliday, Ian	P1.10
Hamila, Nahïène	23.2
Hammad, Seddik	27.3
Hammami, Firas	20.3
Han, Woo Suck	19.3
Hancock Friesen, Camille	22.4
Handsfield, Geoffrey	24.1
Handsfield, Geoffrey	300
Harkin, Niamh	P4.13
Haugaa, Kristína	P2.3
Havelkova, Linda	25.2
Hayward, Christopher	11.2
Hayworth, Simon	11.4
Healy, Ellen	P4.13
Heckman, Luuk I.B.	13.5
Heidt, Christoph	17.1
Heim, Frederic	4.4
Heinken, Almut	P4.13
Hellevik, Leif Rune	12.4
Hellmeier, Florian	P1.6
Henderson, Adam	P2.7, 19.4
Hendrickx, Amber	11.6
Hengstler, Jan	27.3
Hernandez, Rémi	19.2
Hertwig, Jan	17.5
Hester, Robert L.	3.7, P1.5
Hilhorst, Pjotr	P3.2, 3.3, 16.7
Ho Ba Tho, Marie-Christine	15.2, 16.2
Hoeijmakers, Martijn	13.8
Hoekstra, Alfons	3.6, P4.4
Holzapfel, Boris	15.6
Horner, Marc	10.7
Hose, Rod	P4.1

AUTHOR INDEX

Bold = Presenting author

Hossain, Imam	215	Kazemi, Mousa	300	Liu, Qiongyao	23.3
House, Michael	18.2	Kelley, Craig	P1.16	Liu, Weiqiang	10.4
Houzeaux, Guillaume	P1.14	Kelly, Christopher	23.4	Lloyd, Bryn	2.5
Hrabetova, Sabina	P1.16	Kelly, Christopher	23.3	Lo, Sharp	1.2
Hron, Jaroslav	P1.2, P4.15	Kendall, Jack	5.4	Loewe, Axel	14.7
Hubert, Sandra	11.4	Khamzin, Svyatoslav	390	Longobardi, Stefano	P4.2, P1.9
Huberts, Wouter	P3.3, 13.8, 2.2, 22.3, 26.3, 3.3, P3.2, 16.7	Khoshfekr Rudsari, Hamid	26.2	Lorenzi, Tommaso	282
Hunter, Peter	2.1	Kirkels, Feddo	P2.3	Lories, Rik	15.4
Hurez, Vincent	11.4	Kiziltas Sendur, Gullu	6.1	Loureiro-Ga, Marcos	13.7
Husain, Tabassum	P3.1	Kleiser, Benedict	P4.14	Louwagie, Erin	18.2
Hussain, Tarique	22.4	Klotz, Thomas	11.3	Lucchetti, Agnese	4.3
Hutmacher, Dietmar	15.6	Kolokotroni, Eleni	16.4	Luermans, Justin	10.6
Huwylter, Gabriel	17.1	Konduri, Praneeta	11.8, 3.6, P1.13	Luermans, Justin G.L.M.	13.5
Hyncik, Ludek	25.2	Kondylakis, Haridimos	16.4	Lukovic, Vanja	17.1
Iakovidis, Dimitris	P2.5	Koopsen, Tijmen	3.1	Lumens, Joost	14.6, 3.1, 10.6, P2.3, 13.5
Iñiguez, Andres	13.7	Korhonen, Rami K.	15.4	Lundberg, Peter	22.2
Ioannou, Eleftherios	8.5	Kosinka, Jiri	1.7	Lungu, Angela	P4.1
Ioannou, Eleftherios	2.4	Kotanko, Peter	28.3, 12.8	Luraghi, Giulia	11.8, 4.4, 3.6, P1.13
Issac, Karlos	215	Krofta, Ladislav	25.2	Lyton, William	14.5
Itah, Shir	P4.11	Kulczycka, Nina	P4.13	Lyton, William	P1.16
Italia, Matteo	20.2	Kulesza, Alexander	3.2	Lyton, William W.	P4.10
Itu, Lucian Mihai	P1.12	Kumar, Sumit	P4.3	M, Manisha	241
Ivanovic, Milos	13.6	Kuster, Niels	2.5	Ma, Jess	7.6
Jaber, Mahdi	15.9, P3.12	La Barbera, Luigi	17.2	Macnamara, Cicely	282
Jaber, Mahdi	P3.12	La Mattina, Antonino Amedeo	21.2, 93	Macrauld, Michael	23.3, 23.4
Jackson, Troy	10.6	Lafon, Yoann	5.2	Madden, Luke	P4.13
Jacob, Evgueni	20.3	Lafuente-Gracia, Laura	28.1	Maes, Lauranne	11.6
Jafarnejad, Seyed Mehdi	20.1	Lagali, Angeline	P4.13		
Jaffa, Ariel	18.3	Lahr, Christoph	15.6	Maia Ladeira, Luiz Carlos	P2.6
Jaffa, Ariel J.	18.1	Laigle, Laurence	11.4	Maia Ladeira, Luiz Carlos	P2.9
Janka, Clarence	P3.4	Lakatos, Peter	14.5	Majoie, Charles	11.8
Jansova, Magdalena	25.2	Lamata, Pablo	P4.2	Majoie, Charles	P1.13
Janssen, Manoe J.	P2.9	Landoll, Micha	3.5	Malai, Anastasia	2.4
Jarolimová, Alena	P4.15	Lane, Rebecca	P4.13	Malawski, Maciej	16.6
JEAN-PIERRE, BOISSEL	3.2	Lang, Niall	P4.13	Malawski, Maciej	P2.8
Jiang, Jian	P2.6	LaPointe, Vanessa L. S.	113	Maleki, Avisa	2.3
Jiang, Zifan	18.5	Laske, Tanja	15.9	Malpas, Simon	2.1
Jimack, Peter	7.5	Lassila, Toni	23.3	Manetti, Claudia Alessandra	3.1
Jimenez, Victor	13.7	Lassila, Toni	23.4	Manica, Isabel	16.4
Jones, Alison	17.4	Laudenzi, Bianca Maria	12.1	Manninger, Martin	131
Jongerius, Daan	10.7	Layton, Anita	22.6	Mapder, Tarunendu	26.1
Jonkers, Ilse	15.4, P2.15	Lazarou, Constantinos	8.5	Maquer, Ghislain	P2.7
Joosten, Alexandre	10.8	LECOMTE-GROSBRAS, Pauline	P4.12	Maquer, Ghislain	19.4
Jörg, David	12.8	Lecomte-Grosbras, Pauline	16.5, 7.2	Marchal, Thierry	P2.12
Jörg, David	28.3	Lecomte-Grosbras, Pauline	18.5	Marquering, Henk	11.8
Jover, Ramiro	P2.6	Ledoux, Charles	5.4	Marquering, Henk	P1.13
Józsa, Tamás	P4.4	Lees, Christoph C.	7.4	Marquetand, Justus	P4.14
Julien, Laureline	10.2	Lefevre, Lucile	20.3, 12.3	Marsden, Alison	1.5
Jung, Moritz	22.1	Lehmann, Lena	11.3	Martin, Madge	12.2
Kahn, Andrew	1.5	Lehr, Lorenz	3.2	Martinelli, Filippo	P4.13
Kahoul, Riad	3.2, 12.3	Lemaire, Thibault	12.2	Martínez, Antonio	10.7
Kalozoumis, Panagiotis	P2.5	Leoni, Massimiliano	135	Martínez, Antonio	10.7
Karademas, Evangelos	16.4	Lesage, Raphaëlle	19.1, P2.6, 14.4, P2.9	Martínez Reina, Francisco Javier	370
Karagiannidis, Christian	3.5	Lescanne, Nathan	23.2	Martins Costa, Ana	6.5
Karagöz, Zeynep	113	Levine, Steven	P2.10	Martis, Shiny	3.2
Kardampiki, Eirini	10.7	L'Hostis, Adèle	20.3, P4.7, 12.3	Marzo, Alberto	10.5
Kashtanova, Victoriya	13.3	Li, Yitong	22.1	Mascarenhas, Teresa	4.2, 26.4
Kasner, Mario	1.8	Lialios, Dimitrios	17.3	Masereeuw, Rosalinde	P2.9
Kassab-Bachi, Amin	P1.1	Licholai, Sabina	P2.11	Maso Talou, Gonzalo	10.1
Kassasuya, Christian	10.4	Licholai, Sabina	16.6	Maso Talou, Gonzalo	P4.5, 13.2
Kässinger, Johannes	P3.9	Li-Jessen, Nicole	15.3	Masouros, Dimosthenis	20.5
Kasztelnik, Marek	P2.8, 14.3	Lim, Chung	P1.10	Masson, Perrine	20.3
Katiyar, Vinod	241	Lin, Fengming	23.3	Mathieu, Vinken	P2.6
Katodritis, Nicos	2.4	Linz, Dominik	10.6	Matsukawa, Hiroshi	P2.2
		Little, J Paige	P3.1	May, Robyn	13.2

AUTHOR INDEX

Bold = Presenting author

Maye, Colm	P4.13
MAYEUR, Olivier	P4.12
Mayeur, Olivier	16.5, 7.2, 18.4 , 18.5
Mazzi, Valentina	1.6
Mazzocco, Ketti	16.4
Mazzoli, Marilena	16.1
McCall, Blake	17.4
McCullough, Jon	1.2
McDougal, Robert	P1.16
McGaffin, Sinclair	10.1
McGinnis, Tammy	14.5
McHugh, Lynne	P4.13
McInerney, Caitriona	20.1
Mead, Thomas	12.7
Meade, Ronan	P4.13
Meerbergen, Karl	P2.15
Mehl, Julia	15.1
Meiburg, Roel	13.5 , 3.1
Meizner, Jan	P2.8
Mendoza, Noelia	27.1
Mengoni, Marlène	17.4
Menon, Karthik	1.5
Mertens, Jake P	4.6
Meyerheim, Marcel	20.5
Meyns, Bart	11.2
Migliavacca, Francesco	11.8, 4.4, P1.13
Mijailovic, Srboljub	13.6
Miller, Claire	3.6
Mirjalili, Ali	300
Mohseni, Mahdi	16.8
Moingeon, Philippe	11.4
Molimard, Jérôme	19.3
Montalt Tordera, Javier	23.1
Monteiro, Claudio	20.3, P4.7, 12.3
Moradi, Hamed	P3.3
Morbiducci, Umberto	1.6
Morbiducci, Umberto	1.3
Morel-Corlu, Ewan	278
Morsinkhof, Lisan	7.2
Mos-Oppersma, Eline	12.5
Moss, Alison	P4.10
Moumneh, Rayan	4.1
Moura, Rita	26.4
Mourad, Mirella	18.2
Mourato, André	22.1
Muenkel, Marie	15.5
Mueri, Christine	19.4
Mueri, Christine	P2.7
Mukherjee, Satanik	14.4
Mulder, Marijn	1.4
Müller, Lucas O.	12.1
Müller, Lucas Omar	10.3
Müller, Ralph	5.4
Munneke, Anneloes	14.6
Muñoz-Moya, Estefano	P3.10
Murphy, Olivia	P4.13
Muthiah, Kavitha	11.2
Muthialu, Nagarajan	P1.8
Muthurangu, Vivek	23.1
Myers, Kristin	18.2
Myklebust, Lena	26.2
Mylle, Ine	P3.13
Nadal, Jurandir	P3.11
Nakano, Koji	P2.2
Narracott, Andrew	P4.1, P1.10
Nasello, Gabriele	27.2
Nash, Martyn	2.1
Nash, Martyn	10.1
Natal Jorge, Renato	26.4, P3.6, P3.7
Nativel, Arnaud	20.3
Negro, Francesco	11.3
Neic, Aurel	131
Neidlin, Michael	6.5
Neidlin, Michael	3.5
Németh, Márton	11.5
Neufeld, Esra	2.5
Newton, Adam	P1.16
Newton, Adam JH	P4.10
Newton, Taylor	2.5
Neymotin, Samuel	14.5
NGUYEN, Duc-Phong	16.2
NGUYEN, Tan-Nhu	25.4, 7.3
Nguyen-Le, Duyen	16.5
Nguyen-Le, Duyen	25.4
Nickerson, David	2.1
Nicolò, Chiara	P2.14 , P2.2
Nicoud, Franck	189
Niederer, Steven	P4.2, P1.9
Nielsen, Poul	2.1
Nishida de Assis, Bruno	395
Nita, Cosmin Ioan	P1.12
Noailly, Jerome	6.4, P3.10, 6.3 , 17.3, 6.2
Noailly, Jérôme	28.4
Noailly, Jérôme	8.4
Noël, Agnès	12.7
Noone, David	P4.13
Nowakowski, Piotr	P2.8
Ntsinjana, Hopewell	P1.7
Oberhuber, Tomáš	12.6
Oberhuber, Tomáš	P3.5
Obermeier, Lukas	P3.14
O'Connell, Monica N	14.5
O'Donnell, Grace	P4.13
Oks, David	P1.14
Oliveira, Dulce	26.4
Oliviero, Sara	21.2
O-Maia, Albino	16.4
Orassi, Vincenzo	P3.4, 15.7
Otta, Magdalena	P1.10
Oude Vrielink, Mathieu	8.2
Paál, György	11.5
Padmos, Raymond	3.6 , P4.4
Pajaziti, Endrit	23.1 , 7.6
Pajor, Arkadiusz	P4.1
Palgen, Jean-Louis	20.3, P4.7, 12.3
Panagiotidou, Foteini	20.5
Pannetier, Romain	19.3
Papamanolis, Lazaros	10.4
Pappalardo, Francesco	2.3, P1.17
Paques, Michel	10.2
Parente, Marco	26.4, P3.15
Pares, Yves	P2.13
Pase, Giorgia	1.7
Pasquali, Christian	3.2
Passanha, Fiona	113
Pasta, Salvatore	4.8
Patankar, Tufail	23.3
Pat-Horenczyk, Ruth	16.4
Paton, Julian	P4.5
Pauš, Petr	P3.5
Payne, Stephen	P4.4
Payne, Stephen	13.4
Payonk, Jan Philipp	11.7
Pean, Fabien	P3.8
Peer, Syed Murfad	3.4
Pekkan, Kerem	3.4
Pellisé, Ferran	8.4
Peng, Qiyao	P2.1
Perego, Alice	17.2
Perez Boerema, Fernando	28.2
Perrier, Antoine	2.8
Perrillat-Mercerot, Angélique	20.3, P4.7
Perriolat, Mathieu	P4.6
Pers, Jacques Olivier	11.4
Petersik, Andreas	P3.1
Pevný, Tomáš	12.6
Peyronnet, Emmanuel	P4.7
Pezzinga, Alice	17.2
Philippe, Louis	P2.13
Piek, Lotte	22.3
Piella, Gemma	P3.10, 6.3
Piñero, Janet	6.4
Pivonka, Peter	370
Plank, Gernot	131, P4.2
Podéus, Henrik	14.2
Poikonen-Saksela, Paula	16.4
Poleć, Piotr	P2.8
Polzehl, Joerg	5.3
Popescu, Andreea Bianca	P1.12
Porte, Solène	6.6
Prassl, Anton	131
Prinzen, Frits W.	13.5
Prise, Kevin	20.1
Prodanovic, Danica	13.6
Prodanovic, Momcilo	13.6
Pruett, W. Andrew	3.7, P1.5
Przybyszewski, Jan	16.6
Pugachev, Alexander	25.3 , 17.5
Pyne, Ivana	P4.13
Quadrat, Eric	17.5
Quexada, Diego	15.2
Quicken, Sjeng	P3.2
Quinney, Sara	26.1
Quintanas-Corominas, Adria	13.6
Quintela, Barbara	14.3
R, KOUSHIKA	128, 8.1
R.S. Tavares, João Manuel	7.1
Rai, Sanjay Kumar	P4.3
Ramaswamy, Madhavan	P1.8
Ramella, Anna	4.4
Ramella, Anna	4.4
Ramis-Conde, Ignacio	282
Ranjan, Animesh	11.1 , 2.6
RASOULIGANDOMANI, Morteza	P3.10, 8.4
Ravikumar, Nishant	23.4
Ravikumar, Nishant	P1.1, 23.3
Razjigaev, Andrew	P3.1
Readioff, Rosti	17.4
Reed, Mike	11.4
Reinthalter, Markus	1.8
Rendenbach, Carsten	P3.4, 15.7
Renon, Silvia	P1.13
Rezaeimoghaddam, Mohammad	1.1 , 22.3
Richmond, Paul	14.1
Ricoboni, Laura Teresa	395
Ridolfi, Luca	1.3

AUTHOR INDEX

Bold = Presenting author

Rigobello Battaglion, Leonardo	395	sermesant, maxime	13.3	Taberner, Andrew	2.1
Rijks, Jesse H.J.	13.5	Shakila, Merlin	128, 8.1	Tanska, Petri	15.4
Robeerst, Lars	113	Sharma, Kanishka	10.5	Tardif, Nicolas	23.2
Rocchi, Maria	11.2	Shim, Vickie	P3.13	Taschner-Mandl, Sabine	20.2
Rochlitz, Bence	P3.8	Shimano, Antônio Carlos	395	Tavares, Adriana	PT4
Rochlitz, Bence	19.5	Shlomo, Yael	18.3	Tavelow, Karsten	5.3
Rodero, Cristobal	P4.2	Shone, Fergus	7.5	Tawhai, Merryn	2.1
Rodrigues, Carlos	P3.11	Shroff, Rukshana	4.1	Taylor, William R.	17.1
Rodrigues, Marco	P3.11	Silva, Elisabete	4.2, P3.15	Taylor, Zeike	23.4
Rodriguez Matas, José Félix	11.8, 4.4, P1.13	Simcock, Ian	4.1	Teske, Arco	P2.3
Rohe, Marc-Michel	16.3	Simonis, Franck	7.2	Teunis, Marc	P2.9
Röhrle, Oliver	P3.9	Simonsson, Christian	22.2	Thiel, Jan-Niklas	6.5
Röhrle, Oliver	24.2, 11.1, 11.3, 2.6, 24.1	Sips, Fianne	P2.2	Thiele, Ines	P4.13
Rolland, Yan	278	Sitek, Arkadiusz	P4.1	Thinnes, Cyrille	P2.10, P4.13
Ronan, William	4.5	Sivera, Raphael	23.1	Timmermans, Peter	8.2
Roney, Caroline	131	Sivera, Raphael	7.4	Tintěra, Jaroslav	P3.5
Roodzant, Daniël	P2.9	Škardová, Kateřina	P3.5	Tintěra, Jaroslav	12.6
Rootwelt-Norberg, Christine	P2.3	Škardová, Kateřina	12.6	Tixier, Elliott	P2.13
Rosin, David	P3.9	Sluka, James	26.1	Tokoutsi, Zoi	168
Rosner, Mordechai	P4.11	Smít, Daniel	3.2	Tonino, Pim	16.7, 3.3
Rothermel, Kurt	P3.9	Smith, Scott	4.6	Toro, Eleuterio F.	12.1
Rubod, Chrystèle	16.5	Sniezynski, Bartłomiej	P4.1	Toro, Eleuterio Francisco	10.3
Ruiz Lozano, Rocío	370	Snoeijs, Maarten	22.3	Toueg, Raphaël	20.3, 12.3
Ruiz Wills, Carlos	P3.10	Solovyova, Olga	390	Trabelsi, Olfa	15.2
Russo, Giulia	2.3, P1.17	Song, Shuang	23.4	Trdlicová, Jana	P1.2
Ryan, Saoirse	P4.13	Sonntag, Simon	19.5, 22.1, P3.8, P2.12	Triantafyllou, Georgios	P2.5
Sack, Ingolf	5.3	Soret, Perrine	11.4	Trimarchi, Santi	4.4
Sack, Kevin	10.6	Soudris, Dimitrios	20.5	Trinh, Xuan-Tien Kévin	P4.12
Sacks, Michael	5.5	Sourbron, Steven P	10.5	TSERANIDOU, SOFIA	6.4
Safaei, Soroush	135, P4.5, 13.2	Sousa, Berta	16.4	Tsuboi, Masaru	P2.2
Safaei, Soroush	14.2	Sousa, Jose	P1.3, 20.1	Tsui, Janice	P1.10
SAHIN, Mervenaz	6.1	Spence, Veronica J.	20.1	Turgut, Tahir	4.8
Sahrmann, Annika	24.1	Stamatakos, Georgios	16.4, 20.5	Tziraki, Chariklia	16.4
Saint-Jlmes, Hervé	278	Stamatakos, Georgios	16.4	Ubachs, Rene	4.6
Sala, Lorenzo	10.8	Staumon, Bernard	P2.9	Ural, Berk	3.4
Samaniego, Cristóbal	P1.14	Staumont, Bernard	P2.6, P2.12	Usmanova, Zumrat	183
Sander, Katharina Maria	6.5	Stebbing, Justin	14.8	Uv, Julie	26.2
Sándor, Levente	11.5	Steiner, Melanie	2.5	Vadigepalli, Rajanikanth	P4.10
Sarrami-Foroushani, Ali	23.4	Steinman, David A.	1.3	Vaghi, Cristina	P2.14, P2.2
Sasmazel, Ahmet	3.4	Sten, Sebastian	14.2	Valdez-Jasso, Daniela	PT3
Sauvage, Emilie	4.1	Stijnen, Marco	8.2	van de Vosse, Frans	1.1, P3.3, 13.8, 2.2, 22.3, 26.3, 3.3, 16.7, P3.2
Sauvage, Emilie	P1.7, P1.8	Stojanovic, Boban	13.6	van de Wetering, Bertus	8.2
Savage, Matthew	10.1	Stott, Ngaire Susan	300	van der Hout-van der Jagt, M. B.	2.2, 26.3
Savelli, Giacomo	93	Stott, Sue	24.3	van der Lugt, Aad	P1.13
Scarpolini, Martino Andrea	16.1	Straßmann, Stephan Eric	3.5	van der Sluis, Olaf	4.6, 8.2
Scarsoglio, Stefania	1.3	Stratford, Robert	26.1	van Ertvelde, Jonas	P2.6
Schäfer, Friederike	12.4	Strocchi, Marina	131, P4.2	van Griensven, Martijn	113
Scherr, Daniel	131	Stronach, Lynsey	4.1	Van Liedekerke, Paul	27.3
Scheys, Lennart	P2.15	Strudthoff, Lasse	3.5	van Loon, Tim	10.6, 3.1
Schievano, Silvia	23.1, 7.6, P1.7, P1.8, 4.1, 7.4, 19.1	Struzik, Zbigniew	P1.10	Van Looy, Guy	5.1
Schlief, Adriano	23.5	Studer, Daniel	17.1	van Osta, Nick	P2.3, 3.1
Schmidt, Johannes	15.9	Sturdy, Jacob	P1.4	Van Oudheusden, Michiel	19.1
Schmutz, Beat	P3.1, 15.6	Sturdy, Jacob	12.4	van Rienen, Ursula	11.7
Schneider, Anne	6.6	Suasso de Lima de Prado, Damián	13.8	van Rienen, Ursula	P4.8, 8.3
Schröder, Manuel	P3.1	Summers, Rodney	19.4	van 't Veer, Marcel	3.3, 16.7
Schuhmacher, Alberto	27.1	SUNBULOGLU, Emin	183	van Willigen, Bettine	2.2, 22.3
Schultz, Franka	P1.9	Sundqvist, Nicolás	14.2	Vander Sloten, Jos	P2.15, 5.1
Schwaber, James S.	P4.10	Swalduz, Aurélie	20.3	Vanhaecke, Tamara	P2.6
Sedlmair, Michael	P3.9	Swanson, Liam	P1.7, P1.8	Vanwanseele, Benedicte	P3.13
Segarra-Queralt, Maria	6.4, 6.3	Swapnasrita, Sangita	22.6	Varella, Vinicius	14.3
Sego, TJ	26.1	Swift, Andrew	P4.1	Varley, Ciara	P4.13
Sempértegui, Felipe	11.6	Symeonidou, Chloe	2.4	Vasavan, Tharni	P1.9
Seo, Jongmin	1.5	Szewczyk, Jérôme	23.2	Vaughan, Ted	4.5
		Szikora, István	11.5		
		Tabak, Ahmet Fatih	6.1		

AUTHOR INDEX

Bold = Presenting author

Vaughan, Ted J.	4.3
Vavourakis, Vasileios	2.4, 8.5
Vazquez, Mariano	21.1, 13.6, 17.3, P1.14
Veiga, Cesar	13.7
Velikorodny, Alexey	83, 23.6, 82, P2.4
Vellguth, Katharina	4.7
Verhoeven, Anouk	P2.6
Verlhac, Suzanne	10.4
Vermolen, Fred	P2.1
Vernooy, Kevin	10.6
Vernooy, Kevin	13.5
Verstraeten, Sabine	13.8
Vervenne, Thibault	11.6
Vibert, Eric	10.8, 16.3
Viceconti, Marco	21.2, 93, P1.17, 14.3
Vigmond, Edward	131
Vignon-Clementel, Irene	10.4, 16.3, 10.8
Vinder, Bar	13.1
Vomvas, Dimitrios	2.4
Voss, Samuel	23.5
Vrba, David	20.4
Wakefield, Gareth	14.8
Walker, Dawn	20.2
Walker, Dawn	14.1
Wang, Ning	10.5
Wang, Yongxing	23.3
Wapner, Ronald	18.2
Warnaar, Rob S.P.	12.5
Waschkowitz, Renee	P4.13
Watanabe, Sansuke Mario	10.3
Weihs, Daphne	P2.1
Welle, Hannes	26.2
Wertheim, Kenneth	14.1, 20.2
Wiegmann, Bettina	6.5
Wijayathunga, V. Nagitha	17.4
Wijntjes, Pascale	26.3
Wilcox, Ruth	P1.1, 17.4
Wille, Marie Luise	15.6
Willems, Tineke	1.7
Williamson, Catherine	P1.9
Wills, Carlos Ruiz	6.2
Wintzer, Raimon	25.3
WITZ, Jean-François	18.5
WITZ, Jean-François	P4.12
Witz, Jean-François	16.5, 7.2
Woźniak, Kamil	P1.3, 20.1
Xu, Xiao Yun	14.8
Xue, Yidan	P4.4
Yamaguchi, Mao	P2.2
YAMAK, Fatih	183
Yao, Jiacheng	17.4
Yevtushenko, Pavlo	5.6
Yia, Yan	23.3
Yıldırım, Canberk	3.4
Yıldız, Armağan Can	2.6
Yu, Grace	15.3
Yu, Xingyao	P3.9
Yurtseven, Nurgul	3.4
Zaccaria, Alissa	4.3
Zacharoudiou, Ioannis	1.2
Zafeiris, Dimitrios	11.4
Zahalka, Omar	4.8
Zargarzadeh, Sadra	16.8
Zavodszky, Gabor	21.3, 11.5, 28.2
Zeinhofer, Marius	P3.12
Zerdzicki, Krzysztof	P4.9
Zhang, Wenbo	5.5
Zhao, Debbie	10.1
Zhao, Jieling	27.3
Zhou, Shilei	215
Zhuang, Katie	2.5
Zieliński, Krzysztof	11.2
Zimmer, Manuela	P4.14
Zimmermann, Julius	8.3
Zörnack, Gloria	P3.8
Zörnack, Gloria	19.5
Zubarev, Stepan	390
Zucchelli, Francesca	P1.13
Zwam, Wim van	P1.13